Bing Xiao Zhaoyue Chen Jingwen Xu Lu Cao

# Advanced Attitude Control of Satellite

A Modeling Error Compensation Approach



# Advanced Attitude Control of Satellite

# Advanced Attitude Control of Satellite

A Modeling Error Compensation Approach



Bing Xiao School of Automation Northwestern Polytechnical University Xi'an, Shanxi, China

Jingwen Xu School of Astronautics Northwestern Polytechnical University Xi'an, Shanxi, China Zhaoyue Chen School of Astronautics Beihang University Beijing, China

Lu Cao National Innovation Institute of Defense Technology Chinese Academy of Military Sciences Beijing, China

ISBN 978-981-97-2846-6 ISBN 978-981-97-2847-3 (eBook) https://doi.org/10.1007/978-981-97-2847-3

© The Editor(s) (if applicable) and The Author(s), under exclusive license to Springer Nature Singapore Pte Ltd. 2024

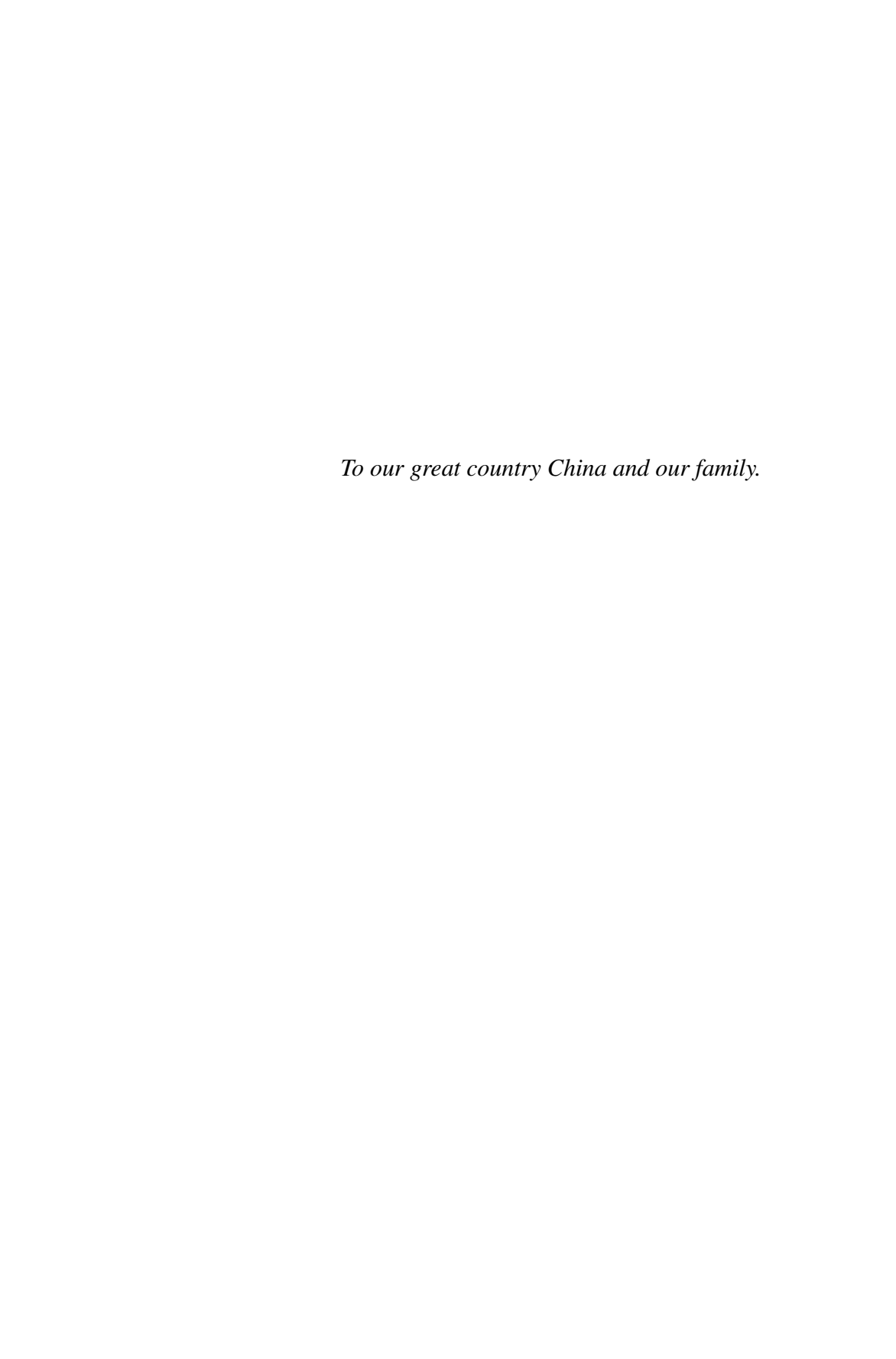
This work is subject to copyright. All rights are solely and exclusively licensed by the Publisher, whether the whole or part of the material is concerned, specifically the rights of translation, reprinting, reuse of illustrations, recitation, broadcasting, reproduction on microfilms or in any other physical way, and transmission or information storage and retrieval, electronic adaptation, computer software, or by similar or dissimilar methodology now known or hereafter developed.

The use of general descriptive names, registered names, trademarks, service marks, etc. in this publication does not imply, even in the absence of a specific statement, that such names are exempt from the relevant protective laws and regulations and therefore free for general use.

The publisher, the authors and the editors are safe to assume that the advice and information in this book are believed to be true and accurate at the date of publication. Neither the publisher nor the authors or the editors give a warranty, expressed or implied, with respect to the material contained herein or for any errors or omissions that may have been made. The publisher remains neutral with regard to jurisdictional claims in published maps and institutional affiliations.

This Springer imprint is published by the registered company Springer Nature Singapore Pte Ltd. The registered company address is: 152 Beach Road, #21-01/04 Gateway East, Singapore 189721, Singapore

If disposing of this product, please recycle the paper.



### **Preface**

There is no doubt that our current and even future lives are highly connected to satellite. We launch satellites to establish the global positioning system to get the precise position of the unmanned vehicles and even the mankind. We launch satellites to achieve Earth observation, weather forecast, fire forecast, video broadcasting, environmental monitoring, etc. Satellite has played an important role in our daily life. To provide such services for mankind, the attitude control system should be developed for satellite. Otherwise, the payloads such as cameras, antennas, etc., will not work perfectly. In the attitude control system design, attitude controller design is one of the most important parts. Although the linear control theory-based controllers including the proportional-integral-derivative control law and its variants have been widely used in satellite attitude control engineering, they are becoming inappropriate for modern satellites demanding high control performance. That is because the dynamics of any satellite is inherently nonlinear in nature. Inspired by the superior performance ensured by nonlinear control theory, many nonlinear attitude control approaches have been proposed for satellites. However, the problem of designing an nonlinear controller to accomplish attitude maneuvers with high control performance is still open.

In addition to the nonlinear dynamics of the satellite attitude system, modeling error is another main hindrance. This inevitably acts on the satellite attitude dynamics. It mostly comes from uncertain and unmodeled inertia, unmeasurable flexible vibration and coupling between the rigid and the flexible part of the satellite, actuator fault, actuator misalignment, and the environmental disturbance torques including the gravity-gradient torque, the aerodynamic torque, the Earth magnetic torque, and the solar radiation pressure torque. Due to the current finite modeling technology, the modeling error is unknown and even time-varying. In practice, if the modeling error is not appropriatly handled and compensated, the attitude control performance will be deteriorated and even the instability of the attitude control system may be resulted. This has led to intense interest in the development of modeling error compensation control approaches, which are supposed to solve this problem.

From the standpoint of rejecting, attenuating, and compensating for modeling error, significant developments have been witnessed for the satellite attitude control

viii Preface

system design in the past two decades. However, there is currently a lack of a unified control framework. Most of the existing methods can compensate for a single type of modeling error only. In addition, many of them do not consider physical and cost limits such as actuator constraint and unmeasurable angular velocity due to gyro failure. On the other hand, fast attitude maneuvering requirement may not be considered during critical phases of the mission in the literature during modeling error compensation. Moreover, the existing robust or adaptive attitude controllers with modeling error accommodated are characterized by severe conservativeness. This will lead to more energy consumption, and thus reduce the lifespan of a satellite. In aerospace engineering, those issues should be addressed simultaneously.

Motivated by the demand for attitude control with the above challenges solved and many existing approaches are unable to achieve this goal, this book attempts to solve the above challenge during satellite attitude control system design. This book focuses on designing advanced compensation control techniques for more types of modeling error with fast, high-accuracy, high-stability, and or velocity-free attitude maneuvering accomplished for satellite. This book first concentrates on developing nonlinear robust solutions to two or more than two types of modeling error compensation attitude control problem of satellite even in the presence of actuator constraint and fault. Its focus comes to design advanced approaches to achieve fast attitude slewing control for satellite with two or more than two types of modeling error compensated adaptively. Finally, three new observer-based approaches are synthesized to accomplish attitude control for satellite, while the modeling error is precisely and fully compensated. The corresponding controller has less and even no conservativeness. Energy is saved when they are applied to perform attitude maneuvering. More specifically, the effectiveness and the superior attitude control performance of those modeling error compensation approaches proposed in this book are verified by numerical simulation and experimental tests via several testbeds on the ground.

The book itself provides the reader with the current state of the art in the nonlinear attitude control area of rigid or flexible satellite with modeling error. Moreover, it also contains the attitude representation, model of satellite attitude system including the attitude kinematics and the attitude dynamics, some fundamental definitions, and lemmas used in nonlinear control theory. Hence, this book can be used as a reference by satellite control engineers and satellite attitude control academic researchers. The book also has readers who are interested in attitude control of other rigid bodies such as unmanned aerial or underwater vehicles. Prerequisites for understanding the book are a sound of knowledge of basic nonlinear control theory especially the Lyapunov stability analysis, rigid body attitude dynamics, basic mathematics, and fundamental physics.

Xi'an, China Beijing, China Xi'an, China Beijing, China February 2024 Bing Xiao Zhaoyue Chen Jingwen Xu Lu Cao

### Acknowledgements

The authors would like to dedicate their gratitude to the person who has supported us along the way. The authors would like to appreciate Prof. Bo Li from Shanghai Maritime University and his students Hui Liu, Xiangyu Zhu, Hongyue Ma, and Ziqi Yang. Without their work in helping with the preparation of the draft of this book, this book would never have been published. The authors are grateful to Prof. Dong Ye from the Harbin Institute of Technology for providing the technical materials of the testbeds in this book and for helping to carry out experimental tests by using those testbeds. Some parts of the research presented in this book are based on the academic collaborations with Prof. Shen Yin from the Norwegian University of Science and Technology, Dr. Mehdi Golestani from Southern University of Science and Technology, and Dr. Haichao Zhang from Northwestern Polytechnical University. Our gratitude also goes to them.

As a special note, the first author would like to express his sincere thanks to all the students with whom he has worked over the past ten years. He is also grateful to his friends Xing Huo, Xiaoxiang Hu, and Yaohong Qu for their encouragement and enthusiastic help. The fourth author would like to dedicate this modest work to his life, academic, and work career's advisor, Prof. Xiaoqian Chen, who is a genius scholar, hardware expert, and research leader, and most importantly, a genuine person, who left us prematurely. Undoubtedly and definitely, all the authors would be forever grateful to their families for their love, more specifically, the smile of their kids.

Most parts of this work would not have been possible without the financial support by the National Natural Science Foundation of China under Grant 11972373 and 12202065, and in part by the National Science and Technology Major Project under Grant J2019-I-0021-0020.

The last thanks go to Rammoban Krishnamurthy and Jing Dou from Springer Nature Singapore Pte Ltd. for their patience throughout this book.

## **Contents**

### **Part I Foundation**

1.1	Introduction
1.2	Attitude Dynamics Modeling Error
	1.2.1 External Disturbance Torques
	1.2.2 Unmodeling Inertia
	1.2.3 Flexible Vibration
	1.2.4 Actuator Fault
	1.2.5 Actuator Misalignment
1.3	External Disturbance Attenuation Control
	1.3.1 Robust Attenuation Control
	1.3.2 Observer-Based Attenuation Control
1.4	Satellite Actuator Fault Tolerant Control
1.5	Satellite Actuator Misalignment Control
1.6	Uncertain Inertia Control of Satellite
1.7	Nonlinear Control with Actuator Constraint
	1.7.1 Methods for General Nonlinear Systems
	1.7.2 Attitude Control with Actuator Constraint
1.8	Angular Velocity-Free Attitude Control
	1.8.1 Observer-Based Velocity-Free Control
	1.8.2 Filter-Based Velocity-Free Control
1.9	Flexible Satellite Attitude Control
1.10	Fast Attitude Control
1.11	Motivation for This Book
1.12	Organization of the Book
1.13	Summary

xii Contents

2	Preli	iminarie	S	35
	2.1	Introdu	action	35
	2.2	Notatio	on	35
	2.3	Mathe	matical Definition	36
	2.4	Prelim	inary Lemmas	37
	2.5	Definit	tion of Reference Frames	38
		2.5.1	Earth-Centered Inertial Frame	39
		2.5.2	Orbit Frame	39
		2.5.3	Body Frame	40
	2.6	Attitud	le Representation	40
		2.6.1	Euler Angles	40
		2.6.2	Unit Quaternion	41
		2.6.3	Modified Rodrigues Parameters	41
	2.7	Model	ing of Satellite Attitude Control System	42
		2.7.1	Attitude Kinematics	42
		2.7.2	Attitude Dynamics	44
	2.8	Attitud	le Control Testbed for Satellite	45
		2.8.1	Three-Axis Non-Air-Bearing Simulator	45
		2.8.2	Single-Axis Air-Bearing Testbed	46
		2.8.3	Three-Axis Air-Bearing Testbed	47
	2.9	Summ	ary	48
	Refe		•	48
Pa	rt II	Modelin	g Error Robust Compensation Attitude Control	
3	Obse	erver.Fr	ee Output Feedback Attitude Control	53
	3.1		action	53
	3.2		ormed Open-Loop Attitude System	54
	3.3		m Statement	55
	3.4		ar Velocity-Free Robust Controller	56
	3.5		ty Proof	58
	3.3	3.5.1	Candidate Lyapunov Function	58
		3.5.2	Stability Analysis	58
		3.5.3	Discussions	61
	3.6		ation Results	61
	3.0	3.6.1	Results of Case #1	62
		3.6.2	Results of Case #2	65
		3.6.3	Quantitative Analysis	67
	3.7		mental Tests	68
	3.7	3.7.1		69
			Experimental Test #1	
		3.7.2	Experimental Test #2	69
	2.0	3.7.3	Quantitative Analysis	72
	3.8		ary	73
		rences .		73

Contents xiii

4	Velo	city-Free Attitude Control with Actuator Constraint	75
	4.1	Introduction	75
	4.2	Attitude Uniformly Ultimately Bounded Control	76
		4.2.1 Flexible Satellite Attitude Tracking System	76
		4.2.2 Problem Formulation	77
		4.2.3 Transformed Attitude Tracking System	77
		4.2.4 Command Filter	78
		4.2.5 Velocity-Free Neural Network Controller	79
		4.2.6 Numerical Example	82
	4.3	$\mathcal{L}_2$ -gain Disturbance Attenuation Attitude Control	84
		4.3.1 Problem Statement	84
		4.3.2 Velocity-Free Filter	85
		4.3.3 $\mathcal{L}_2$ -gain Disturbance Attenuation Controller	85
		4.3.4 Control Input Upper Bound Analysis	89
		4.3.5 Numerical Study	90
	4.4	Summary	93
	Refe	rences	96
5	Velo	city-Free Attitude Fault-Tolerant Control	99
	5.1	Introduction	99
	5.2	Reaction Wheel Faults	101
	5.3	Angular Velocity Measurement Uncertainty	101
	5.4	Problem Formulation	102
	5.5	Transformed System with Reaction Wheel Fault	103
	5.6	Terminal Sliding-Mode Observer	103
	5.7	Velocity-Free Fault-Tolerant Attitude Controller	105
	5.8	Numerical Example	112
		5.8.1 Reaction Wheel Fault Scenarios	113
		5.8.2 Simulation Results	113
		5.8.3 Quantitative Analysis	115
	5.9	Summary	118
	Refe	rences	118
Pa	rt III	<b>Modeling Error Adaptive Compensation Attitude</b>	
		Control	
6	Ado	ptive Attitude Stabilization Control	123
U	6.1		123
		Euler-Lagrange System	123
	6.3		125
	6.4	General Model of Actuator Faults	123
	6.5	Observer-Based State Estimation	120
	0.5	6.5.1 Adaptive State Observer	127
		6.5.2 Effect of System Uncertainties	131
	6.6	Adaptive State Observer-Based Controller	134
	6.7	Application to Microsatellite Attitude Control	137
	0.7	rippinearion to microsatemic ritilluic Control	13/

xiv Contents

		6.7.1	Simulation Results	137
		6.7.2	Experimental Results	140
	6.8	Summa	ary	142
	Refe	rences .		142
7	Five	d-Time (	Optimal Attitude Control	145
′	7.1		iction	145
	7.1		m Statement	146
	7.3		Time Optimal Stabilization Control	148
	7.4		Time Optimal Fault-Tolerant Control	153
	7.5		ical Example	156
	1.5	7.5.1	•	156
		7.5.2		159
	7.6		ary	162
				162
8			-Time Attitude Stabilization Control	165
	8.1		action	165
	8.2		m Statement	166
	8.3		Fixed-Time Stable System	167
	8.4		Time Faster Sliding Mode Surface	169
	8.5		Fixed-Time Attitude Controller	170
	8.6		tion Results	176
	8.7		ary	180
	Refe	rences .		180
Par	t IV		er-Based Modeling Error Compensation Attitude	
		Control		
9	Exte	nded-Sta	ate Observer-Based Attitude Control	185
	9.1	Introdu	action	185
	9.2	Mather	matical Model	186
	9.3	Problei	m Statement	187
	9.4	Extend	led-State Observer for Modeling Error	187
	9.5	Observ	ver-Based Attitude Controller	189
	9.6	Simula	tion Results	192
	9.7	Experi	mental Study	195
	9.8	Summa	ary	198
	Refe	rences .		198
10	Diet	urhance	Observer-Based Attitude Control	201
10	10.1		observer-based Attitude Control	201
	10.1		le Exponential Stabilization Control	201
	10.2	10.2.1	Problem Statement	202
		10.2.1	Disturbance Observer	202
		10.2.2	Estimator for Satellite's Modeling Error	203
		10.4.3	Estimator for satellite's Wodelling Effor	200

Contents xv

		10.2.4	Observer-Based Exponential Controller	206
		10.2.5	Rigid Microsatellite Example	210
	10.3	Attitude	Exponential Tracking Control	216
		10.3.1	Modeling of Actuator Uncertainties	216
		10.3.2	Problem Description	218
		10.3.3	System Transformation	218
		10.3.4	Disturbance Observer for Uncertainties	219
		10.3.5	Observer-Based Resilient Controller	221
		10.3.6	Stability Analysis	222
		10.3.7	Simulation Example	225
	10.4	Summa	ry	231
	Refer	ences		232
11	Unkn	ow Inpu	t Observer-Based Attitude Control	233
	11.1	Introduc	ction	233
	11.2	UIO-Ba	sed Attitude Stabilization Control	234
		11.2.1	General Model of Actuator Uncertainty	234
		11.2.2	Problem Formulation	234
		11.2.3	Main Result	235
		11.2.4	Simulation Results	244
	11.3	UIO-Ba	sed Attitude Tracking Control	251
		11.3.1	System Description	251
		11.3.2	Problem Statement	252
		11.3.3	UIO-Based Exponential Tracking Controller	252
		11.3.4	Rigid-Flexible Coupling Satellite Example	257
	11.4	Summa	ry	263
	Refer	ences		264
12	Conc	lusion .		265
	12.1	Conclus	sion	265
	12.2	Future V	Work	267

# **List of Figures**

Fig. I.I	The component fault analysis of ACS of satellite [18]
Fig. 1.2	The ChinaSat 6C satellite
Fig. 1.3	The configuration of four reaction wheels
Fig. 1.4	The schematic representation of reaction wheel
	misalignment
Fig. 2.1	The Earth-centered inertial, the body, and the orbit
	reference frames
Fig. 2.2	Euler angles
Fig. 2.3	Euler rotation
Fig. 2.4	The non-air-bearing three-degrees-of-freedom testbed
Fig. 2.5	The single-axis attitude air-bearing testbed
Fig. 2.6	The three-axis attitude air-bearing testbed
Fig. 3.1	The attitude tracking error of the controller (3.9) for $u_d$
	in Case #1
Fig. 3.2	The angular velocity tracking error of the controller (3.9)
	for $\boldsymbol{u}_d$ in Case #1
Fig. 3.3	The input torque of the controller (3.9) for $u_d$ in Case #1
Fig. 3.4	The steady-state behavior of the attitude tracking error
	from the controller (3.9) in Case #1
Fig. 3.5	The steady-state behavior of the angular velocity tracking
	error ensured by the controller (3.9) for $\mathbf{u}_d$ , $4\mathbf{u}_d$ , $7\mathbf{u}_d$ ,
	and $10\mathbf{u}_d$ in Case #1
Fig. 3.6	The steady-state behavior of the control torque
	in the presence of $\mathbf{u}_d$ , $4\mathbf{u}_d$ , $7\mathbf{u}_d$ and $10\mathbf{u}_d$ in Case #1
Fig. 3.7	The attitude tracking error ensured by the controller (3.9)
	in Case #2
Fig. 3.8	The angular velocity tracking error from the controller
	(3.9) in Case #2
Fig. 3.9	The tracking error of the attitude from the controller (3.9)
	in Test #1

xviii List of Figures

Fig. 3.10	The angular velocity tracking error from the controller (3.9) in Test #1	70
Fig. 3.11	The input torque demanded by the controller (3.9) in Test	/(
	#1	70
Fig. 3.12	The tracking error of the attitude from the controller (3.9) in Total #2	<b>7</b> 1
Fig. 3.13	in Test #2  The angular velocity tracking error from the controller	7 1
8	(3.9) in Test #2	71
Fig. 3.14	The input torque demanded by the controller (3.9) in Test #2	72
Fig. 4.1	The initial attitude from AVFC and UQOF	91
Fig. 4.2	The steady-state attitude from LAFC and UQOF	92
Fig. 4.3	The initial angular velocity from LAFC and UQOF	93
Fig. 4.4	The steady-state angular velocity from LAFC and UQOF	94
Fig. 4.5	The control input of velocity from LAFC and UQOF	95
Fig. 5.1	The full control architecture of VFAFTTC with actuator	
	faults and angular velocity measurement uncertainty	100
Fig. 5.2	The full control architecture of VFAFTTC with actuator	
	faults and no measurement of angular velocity	100
Fig. 5.3	The attitude tracking error $z_1$ from VFAFTTC	114
Fig. 5.4	The angular velocity estimation error $e_2$ from VFAFTTC	114
Fig. 5.5	The commanded control torque from VFAFTTC	115
Fig. 6.1	The structure of the adaptive SMO-based velocity-free	
	control	124
Fig. 6.2	Four types of actuator faults: a F1; b F2; c F3;	
	and <b>d</b> F4 (the solid line denotes the commanded control	
	of the actuator, while the dashed line denotes the applied	
	control of the actuator)	125
Fig. 6.3	The geometric representation of sets in the proof	
	of Lemma 6.1	129
Fig. 6.4	The observer error $e_1$ from the adaptive SMO	138
Fig. 6.5	The observer error $e_2$ from the adaptive SMO	139
Fig. 6.6	The attitude from the controller (6.36)	139
Fig. 6.7	The angular velocity from the controller (6.36)	139
Fig. 6.8	The commanded control from the controller (6.36)	140
Fig. 6.9	The experimental result of the attitude from the controller	
	(6.36)	141
Fig. 6.10	The initial angular velocity from the controller (6.36)	
	in test	141
Fig. 6.11	The angular velocity's steady-state from the controller	
	(6.36) in test	142
Fig. 7.1	The attitude achieved by PPCADP in Case I	157
Fig. 7.2	The attitude achieved by TADP in Case I	157
Fig. 7.3	The angular velocity achieved by PPCADP and TADP	
	in Case I	157

List of Figures xix

Fig. 7.4	The control achieved by PPCADP and TADP in Case I	158
Fig. 7.5	The estimated weight achieved by PPCADP in Case I	158
Fig. 7.6	$V_{c1}$ achieved by PPCADP and TADP in Case I	158
Fig. 7.7	The attitude achieved by ADPFTC in Case II	160
Fig. 7.8	The attitude achieved by ISMFTC in Case II	160
Fig. 7.9	The velocity achieved by ADPFTC and ISMFTC in Case II	160
Fig. 7.10	The control achieved by ADPFTC and ISMFTC in Case II	161
Fig. 7.11	The estimation error of the estimator (7.32)	161
Fig. 7.12	The estimated weight achieved by ADPFTC in Case II	161
Fig. 7.13	$V_{c2}$ achieved by ADPFTC and ISMFTC in Case II	162
Fig. 8.1	The initial attitude from the controller (8.27)	177
Fig. 8.2	The steady-behavior of the attitude from the controller	
	(8.27)	177
Fig. 8.3	The initial angular velocity from the controller (8.27)	177
Fig. 8.4	The steady-behavior of the velocity from the controller	
	(8.27)	178
Fig. 8.5	The input of the controller (8.27)	178
Fig. 8.6	The flexible vibration from the controller (8.27)	178
Fig. 8.7	The relation between the control accuracy	
	and the convergence time	179
Fig. 9.1	The mechanical structure of the flexible satellite in Chap. 9	186
Fig. 9.2	The estimation error of the lumped modeling error	193
Fig. 9.3	The attitude Euler angles from the controller (9.12)	194
Fig. 9.4	The angular velocity from the controller (9.12)	194
Fig. 9.5	The flexible vibrations from the controller (9.12)	194
Fig. 9.6	The control input of the controller (9.12)	195
Fig. 9.7	The experimental result of the attitude from the controller	
C	(9.12)	196
Fig. 9.8	The experimental result of the angular velocity	
<b>6</b> , 1, 1, 1	from the controller (9.12)	197
Fig. 9.9	The experimental result of the input torque	
8	of the controller (9.12)	197
Fig. 10.1	The attitude from the controller (10.19) in Case #1	211
Fig. 10.2	The angular velocity from the controller (10.19) in Case #1	211
Fig. 10.3	The convergence property from the controller (10.19)	
8	in Case #1	212
Fig. 10.4	The input of the controller (10.19) in Case #1	212
Fig. 10.5	The estimation error from the DO (10.16) in Case #1	212
Fig. 10.6	The convergence property of the DO (10.16) in Case #1	213
Fig. 10.7	The attitude from the controller (10.19) in Case #2	213
Fig. 10.8	The angular velocity from the controller (10.19) in Case #2	214
Fig. 10.9	The estimation error from the DO (10.16) in Case #2	214
Fig. 10.10	The convergence of the attitude from the controller	21 T
5. 10.10	(10.19) in Case #2	214
	(10.12) 111 0400 112 11111111111111111111111111	- I T

xx List of Figures

Fig. 10.11	The convergence of the angular velocity	
_	from the controller (10.19) in Case #2	215
Fig. 10.12	The convergence property of the DO (10.16) in Case #2	215
Fig. 10.13	The input of the controller (10.19) in Case #2	216
Fig. 10.14	The attitude tracking system ensured	
	by the observer-based practically exponential	
	and resilient control approach	219
Fig. 10.15	The estimation error $\Delta f_{e1}$ from the estimator (10.50)	227
Fig. 10.16	The estimation error $\Delta f_{e2}$ from the estimator (10.50)	227
Fig. 10.17	The response of $  \Delta f_{e1}  $ from the estimator (10.50)	228
Fig. 10.18	The response of $  \Delta f_{e2}  $ from the estimator (10.50)	228
Fig. 10.19	The attitude tracking error from the controller (10.58)	228
Fig. 10.20	The angular velocity tracking error from the controller	
O	(10.58)	229
Fig. 10.21	The response of $  \Theta_e  $ from the controller (10.58)	229
Fig. 10.22	The response of $  \dot{\mathbf{\Theta}}_e  $ from the controller (10.58)	229
Fig. 10.23	The attitude tracking error from the controller (10.58)	
U	in test	230
Fig. 10.24	The angular velocity tracking error from the controller	
O	(10.58) in test	231
Fig. 11.1	The closed-loop system from the proposed control in this	
O	Chapter	236
Fig. 11.2	The attitude from (11.31) with normal actuator	245
Fig. 11.3	The angular velocity from (11.31) with normal actuator	245
Fig. 11.4	The torque of the controller (11.31) with normal actuator	245
Fig. 11.5	Norm of the attitude from (11.31) with normal actuators	246
Fig. 11.6	Norm of the angular velocity from (11.31) with normal	
O	actuators	247
Fig. 11.7	The attitude from (11.31) with actuator uncertainty	247
Fig. 11.8	The angular velocity from (11.31) with actuator	
O	uncertainty	248
Fig. 11.9	Norm of the attitude from (11.31) with actuator uncertainty	248
Fig. 11.10	Norm of the angular velocity from (11.31) with actuator	
O	uncertainty	248
Fig. 11.11	The torque of the controller (11.31) with actuator	
O	uncertainty	249
Fig. 11.12	The estimation performance of the estimator (11.20)	250
Fig. 11.13	The estimation error from the estimator (11.20)	250
Fig. 11.14	The diagram of the proposed general control framework	252
Fig. 11.15	The mechanical structure of the rigid-coupling satellite	257
Fig. 11.16	The attitude tracking error from the controller	
<i>G</i> 1-0	(11.49). <b>a</b> Initial response. <b>b</b> Steady-state behavior	
	obtained from the controller. c Steady-state behavior	
	from the controller without the estimator	259

List of Figures xxi

Fig. 11.17	The angular velocity tracking error from the controller	
_	(11.49). <b>a</b> Initial response. <b>b</b> Steady-state behavior	
	obtained from the controller. c Steady-state behavior	
	from the controller without the estimator	260
Fig. 11.18	The uncertainty estimation from the estimator (11.46)	261
Fig. 11.19	The estimation error from the estimator (11.46)	261
Fig. 11.20	The experimental attitude tracking error	
	from the controller (11.49)	262
Fig. 11.21	The experimental angular velocity tracking error	
	the controller (11.49)	262
Fig. 11.22	The input of the controller (11.49) in the experimental test	263

# Part I Foundation

### Chapter 1 Overview



### 1.1 Introduction

The space and universe have always been full of attraction and mystery to the mankind. We have long had the dream and ideal of traveling to space and exploring the universe. The first satellite launched on October 4, 1957 declared that the mankind had entered the space age. The space technology has advanced by leaps and bounds. The development of space technology has shown that the mankind has made great achievements in its journey of the continuous research, exploration, and utilization of space. It brings about important impetus and significant changes in the economic and social developments of mankind. Especially, it can also "impact life on earth through the stimulation of technological development, and generation of scientific knowledge" said by Dr. Ernst Stuhlinger, the associate director for science of NASA Marshall Space Flight Center, in 1970. Of course, space technology is one of the most challenging missions and complex engineering in the world.

Satellite is the fundamental platform of any aerospace mission such as Earth observation, communication, navigation, deep space exploration, etc. For any satellite, an attitude control system (ACS) should be designed. This system is one of the most important subsystems of the satellite. It plays an important role and is an essential part in satellite design. Attitude control should be carried out to accomplish attitude stabilization or tracking maneuvers to ensure that its payloads operate normally. For example, the desired attitude trajectory should be followed to ensure that the camera fixed in the satellite can focus on the interested areas and then take images. The stabilization of attitude is one of the fundamental maneuvers and the primary attitude control tasks that any satellite needs to frequently perform during its mission. It is recognized by aerospace engineers that attitude control determines whether the space missions can be accomplished or not.

Modern space missions are becoming more and more complicated. They ask for more and better requirements for the attitude control performance. More specifically, highly accurate slewing or pointing attitude maneuvers are necessitated. Note that the dynamics of any satellite is inherently nonlinear in nature. Moreover, this 4 1 Overview

nonlinear attitude dynamics is inevitably subject to modeling error. This modeling error will deteriorate the satellite attitude maneuvering performance. It lets the linear control theory-based control methods such as the proportional-integral-derivative (PID) attitude controller and its variants result in an unsatisfactory/inferior performance. That is because the PID controller has a weak capability of handling with such modeling error. To solve this drawback, advanced attitude control schemes are, therefore, imperative for satellites to maintain desirable stability, reliability, and enhanced performance. Inspired by the superior performance ensured by nonlinear control theory [1–3], although significant developments have been witnessed in the nonlinear controller design for satellite attitude stabilization and maneuver tracking objectives [4–7], the problem of attitude control is still open. In particular, from the standpoint of rejecting or attenuating modeling error [8–12], there is currently a lack of a unified attitude control framework.

### 1.2 Attitude Dynamics Modeling Error

Due to the current finite modeling technology, the mathematical model of the satellite attitude system can not be precisely established. The nonlinear attitude dynamics can not be fully described. There exists dynamics modeling error. The external disturbance torques, uncertain inertia, flexible vibration, actuator fault, and actuator misalignment are the five primary modeling error.

### 1.2.1 External Disturbance Torques

The gravity-gradient torque, the aerodynamic torque, the Earth magnetic torque, and the solar radiation pressure torque are the primary environmental and external disturbance. Any non-symmetrical satellite in the orbit is affected by a gravitational torque. This is due to the variation in the Earth's gravitational force over the satellite. Magnetic disturbance torques are induced by the interaction between the satellite's residual magnetic field and the geomagnetic field. The aerodynamic torque results from the satellite's motion through the tenuous upper atmosphere. The air molecule interaction with satellite body will produce such torque on the satellite. It is most effective on satellites orbiting below 400–500 km. The photons from the sun generate a force that produces a torque about the center of the mass of the satellite. This solar radiation pressure has more effect on light objects with relatively high surface. Although there are many mathematical models for those four types of external disturbance torques [13]. They can be not exactly derived. Moreover, in addition to those four torques, there are also some unexpected disturbance torques such as the collision torque due to debris or robotic manipulation. They can not be modeled.

### 1.2.2 Unmodeling Inertia

Once the design of the satellite is finished on the ground, its inertia matrix can be calculated and estimated by using standard equations [13]. This calculated inertia is constantly called the nominal inertia of the satellite. When the satellite is running in the space orbit, its mass properties will be uncertain. It may change due to the motion of onboard payloads such as camera and antennas, rotation of solar arrays, fuel consumption, out-gassing, etc. This leads to the actual inertia of the satellite deviating from the nominal value. Moreover, such deviated inertia is time-varying, uncertain, and unmodeled.

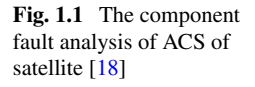
### 1.2.3 Flexible Vibration

To meet ever more demanding mission requirements, there has been a trend for developing satellites with large flexible appendages such as antennas and solar arrays. Those appendages are large, lightweight, and low-stiffness. Such a type of satellite is usually called a flexible satellite. For example, the flexible satellite ETS-VIII has two large deployable reflectors measuring  $17~\text{m}\times19~\text{m}$ , and also a pair of large solar array panels measuring  $19~\text{m}\times2~\text{m}$  [14]. Although the trend towards larger satellites can meet the increasing mission demands, this will inevitably increase the difficulty in their attitude control. This is because the coupling between the structural vibrations of the flexible components and the rigid-body motion can introduce dynamic perturbations to the satellite's attitude. Moreover, when performing rapid attitude maneuvering with high-pointing accuracy demanded by aerospace tasks [15–17], it induces flexible appendages to vibrate. For most flexible satellites, this coupling and the flexible vibration are not measurable. Hence, those two will act on the flexible satellite attitude dynamics as modeling error.

### 1.2.4 Actuator Fault

A satellite's challenging operating conditions increase the possibility of malfunctions in sensors and actuators and faults in the controllers. The analysis of recent satellite accident statistics shows that the fault of the attitude control system accounts for 32%. Moreover, in this percentage, nearly 44% of the faults are caused by actuator faults, as shown in Fig. 1.1. Once a satellite is launched, it is highly unlikely that its hardware can be repaired. Thus, the actuator fault cannot be fixed with replacement parts. When an actuator fault occurs, it will result in an error torque between the nominal torque and the actual torque generated by the satellite's attitude control actuators. This error torque is viewed as the modeling error in the attitude dynamics. It can potentially cause a host of economic, environmental, and safety problems. A recent

6 1 Overview



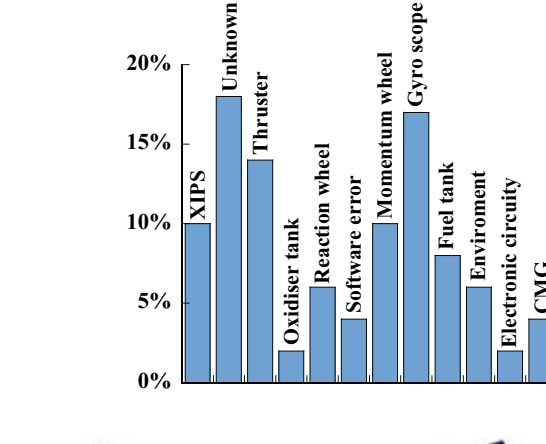


**Fig. 1.2** The ChinaSat 6C satellite



accident occurred with the ChinaSat 6C satellite developed by the China Academy of Space Technology, as shown in Fig. 1.2. This satellite was launched on March 10, 2019. However, faults occurred in its thrusters on December 25, 2023. This led to more energy consumption and a reduction in its lifespan. This incident strongly motivates the development of attitude control systems that ensure an efficient and timely response to maintain stability, reliability, and required performance properties even when components fail.

### 1.2.5 Actuator Misalignment

Actuator misalignment is another type of modeling error in the satellite attitude system. Due to this misalignment, the actual torque acting on the three-axis of the satellite is different from the nominal torque. The extreme case of a backward actuator is especially important. In practice, whether due to finite manufacturing tolerances or warping of the satellite structure during launch, some actuator alignment error exists indeed. Moreover, the satellite's inertia properties are highly coupled to the actuator alignments. Hence, actuator misalignment may cause the onboard attitude controller to fail. This may cause mission performance to degrade and thus pose a significant risk to the successful operation of the satellite.

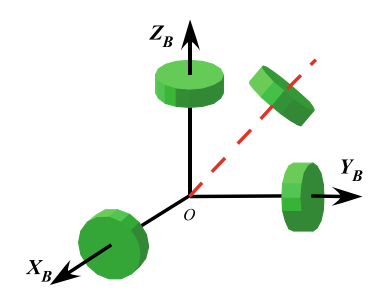


Fig. 1.3 The configuration of four reaction wheels

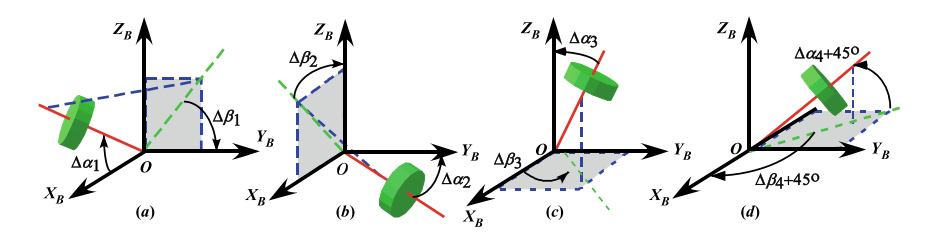


Fig. 1.4 The schematic representation of reaction wheel misalignment

Figure 1.3 shows the mechanical configuration of four reaction wheels used to activate a satellite attitude system. Three wheels are mounted orthogonally, aligned with the satellite body axes, i.e.,  $+X_B$ ,  $+Y_B$ , and  $+Z_B$ , respectively. A fourth, redundant, wheel is mounted skewed at equal angles (54.7 degrees) to each of the body axes, aligned diagonally in the  $+X_B$ ,  $+Y_B$ , and  $+Z_B$  quadrant. This "skew" wheel could be used to provide control power about any of the other axes if one of the orthogonal wheels was to fail. In practice, some alignment errors will exist in this reaction wheel. As an example, actuator alignment error can be mathematically modeled as shown in Fig. 1.4 for this configuration misalignment. The reaction wheel mounted on  $+X_B$  axis is tilted over the nominal direction with constant angles,  $\Delta\alpha_1$  and  $\Delta\beta_1$ ; also the reaction wheels mounted on  $+X_B$  and  $+Y_B$  axis are tilted over the nominal direction with  $\Delta\alpha_2$ ,  $\Delta\beta_2$ ,  $\Delta\alpha_3$ , and  $\Delta\beta_3$ , respectively. While the "skew" wheel is titled over the nominal direction with  $\Delta\alpha_4$  and  $\Delta\beta_4$ .

### 1.3 External Disturbance Attenuation Control

To attenuate the effect of the external disturbance on satellite attitude control performance, many solutions have been developed for satellite [19–22]. In the existing literature on solving the problem, there are two types of approaches. One is to view disturbance torque and uncertain inertia as lumped disturbances/uncertainties, and then design a robust attitude controller [23]. Applying such a robust controller,

8 1 Overview

robustness to disturbance and uncertain inertia is guaranteed [24, 25]. Desired attitude control performance is resulted despite external disturbances, system uncertainties, and even flexible vibrations. The other type to achieve disturbance/uncertainties rejection control is the disturbance observer-based (DOB) control design [26, 27]. For this type, an observer is first designed to estimate disturbance/uncertainties, and the controller is developed by using the observed value to achieve the control objectives with the disturbance accommodated.

### 1.3.1 Robust Attenuation Control

Robust control of external disturbance is widely seen in the literature [28–30]. For instance, the  $\mathcal{H}_{\infty}$  control theory was applied to achieve robust control of external disturbance [31, 32]. In [33], another robust controller was reported to handle external disturbance for the rigid bodies subject to actuator faults and angular velocity constraints. This method was further applied in [34] for satellite attitude tracking with the prescribed performance ensured despite disturbance. In [35], a backstepping-based attitude stabilization controller was designed with external disturbances and constraints in input and measurement solved. The problem of robust disturbance control was also studied in [36]. Only a class of external disturbances with known dynamics was addressed. In [37], the attitude stabilization problem of rigid bodies with external disturbance was solved in the event-triggered framework.

In [38], an adaptive robust tracking controller was presented for robot manipulators. The tracking error was governed to be finite-time stable. In [39], robust cooperative control design of multiple surface vessels was studied, while the vessels were subject to unknown ocean currents and unmodelling dynamics. In [40], the problem of designing a robust tracking controller for rigid body with uncertainty was studied, and it was further investigated in [41] and [42]. The proposed schemes were verified on quadrotors. For surface vessels subject to disturbance uncertainty, a backstepping-based robust trajectory tracking controller was reported in [43]. In [44], a novel controller was developed for aerial robots to achieve attitude trajectory tracking with robustness guaranteed. The proposed law governed the tracking error converging into a small ball, and such error is robust to unknown dynamics. Using the technique of uncertainty and disturbance estimator, a robust tracking control strategy was synthesized for non-affine systems.

In the robust attitude control design, disturbance and uncertainties will not be rejected, and robustness to them is achieved with acceptable attitude control performance. In contrast, another approach to achieve attitude control with good accuracy is to reject disturbance/uncertainties [45–48]. For this type of approach, the magnitude or its upper bound of disturbance torque and uncertainties will be estimated, and then a controller will be designed to compensate for it. To achieve this goal, the adaptive control technique is one widely applied approach [49, 50]. In [51], robust trajectory tracking control was guaranteed for a delta robot. Disturbance rejection was achieved by the adaptive control technique. In [52], an adaptive estimation law

was firstly designed to estimate the parameters of uncertain inertia. By using the estimated information, a nonlinear controller was proposed for the attitude tracking maneuver. In [53], the Chebyshev neural network was adopted to approximate the uncertain dynamics introduced by disturbance and uncertain parameters. Using the approximated value, a terminal sliding mode attitude controller was proposed. In addition to those adaptive controllers, some investigations on attitude control by using adaptive control were also available in [54, 55].

Of particular interest, taking the sliding mode control theory's (SMC) advantages including rapid response and insensitiveness to uncertain parameters or disturbances, this technique has become one of the widely applied tool to design robust attitude controller [56, 57]. In [58], a high-order sliding mode controller was developed. Attitude tracking with high-pointing accuracy was achieved. The proposed controller guaranteed that the system output was robust to disturbance and uncertain inertia. In [59], the problem of attitude tracking control despite disturbance and uncertain inertia was addressed by presenting a sliding mode controller. This problem was also investigated in [60] for satellite attitude stabilization maneuver with actuator output torque constrained. The rejection of disturbance was achieved via the SMC [61].

### 1.3.2 Observer-Based Attenuation Control

The disturbance robust control of satellite is characterized that the developed robust controllers are conservative. In practice, this conservativeness is not desirable for rigid bodies. Motivated by avoiding this drawback, the disturbance-observer-based (DOB) control is a common solution with the disturbance rejection ensured [62–66]. In this solution, a disturbance observer (DO) is preliminarily designed to estimate the external disturbance. Then, a control law is designed by using the estimation of the disturbance to stabilize the closed-loop attitude system [67–70]. A recent review on observer-based uncertainty or disturbance attenuation control design was given in [71]. More specifically, observer-based PID tracking control design was witnessed for uncertain systems in [72, 73]. In [74], a DOB anti-windup controller was presented for hypersonic vehicles. Integrating the DO with the adaptive control theory, a neural-network-based controller was developed for robots with variable stiffness joints and uncertainties [75]. For a class of uncertain stochastic systems, a DOB  $\mathcal{H}_{\infty}$  control law was designed in [76]. Although the disturbances acting on the system were accommodated, the disturbances were required to satisfy an exogenous model. In [77], to handle the external disturbances and uncertainties in the hybrid active-passive heave system, a robust prediction control approach was presented via the DOB technique.

The development of DO plays an important role in the DOB rejection control. To ensure perfect estimation for disturbance, a number of investigations on DO design have been reported. In [78, 79], a high-gain DO was seen to estimate the external disturbance or the uncertainties. However, the high gains would amplify the effect of sensor noise on the system performance. Due to the robustness property of sliding

1 Overview

mode control, sliding mode observer (SMO) [80–82] or high-order sliding mode observer (HOSMO) [83–85] are widely applied in DOB control design with external disturbance compensated.

The extended-state-observer (ESO) is another widely applied technique to accomplish the design of DO [86–88]. For example, the estimation of the mismatched uncertainty was studied in [89]. An ESO was presented in [90] for the quadrotor to estimate the external disturbance due to unknown gust wind. In [91], the trajectory tracking control problem of underwater robots despite external disturbance and uncertainties was studied by including an ESO. In [92], the problem of robust load frequency control of power systems was studied via sliding mode control and ESO. For a class of multi-input-multi-output systems, a generalized ESO was presented in [93]. Moreover, the adaptive ESO (AESO) was another solution to the problem of disturbance or uncertainty estimation [94].

The most existing DO design requires the external disturbance to satisfy some strict conditions. For instance, most ESO are only feasible for the unknown constant disturbance or the disturbance with slow variation [95]. More specifically, because the external disturbance is treated as an extended state in ESO, the external disturbance should be differentiable. On the other hand, it usually requires the SMO or HOSMO to be upper bounded by a known value. In practice, however, the external disturbance may not satisfy these assumptions. The class of the external disturbance handled by the existing DO is limited. Hence, it is of interest to determine observers that can release these constraints or assumptions. Although this is achieved in [95], its result is applicable to linear systems only.

To solve the above drawback [96], viewing disturbance as an unknown input, and then applying the theoretical framework of unknown-input-observer (UIO) [97] is becoming an effective way to estimate disturbances. In [98], the tracking control problem of the linear parameter-varying system was solved by using an unknown input observer. For linear/nonlinear systems, the problem of high-performance control design by using UIO to estimate system uncertainties and disturbances has been extensively investigated [99]. An output feedback bilateral teleoperation approach was designed for robot manipulators [100]. In this approach, UIO was applied to estimate external forces. On the other hand, the problem of observer-based disturbance rejection approach design has also attracted considerable attention in the field of satellite/unmanned aerial vehicle attitude control design in recent years. The result of applying this approach to achieve attitude control can be referred to [101]. In [102], a disturbance observer-based SMC approach was proposed for quadrotor vehicles. A sliding mode observer was presented to estimate external disturbances. The problem of designing observer-based disturbance control for satellite attitude system design was solved in [103].

### 1.4 Satellite Actuator Fault Tolerant Control

The recent incident strongly motivates the development of attitude control systems that ensure an efficient and timely response to maintain stability, reliability, and required performance properties even when components fail [104–106]. In the aerospace industry and academia, fault-tolerant control (FTC) is a widely used scheme to accommodate component failures automatically [107–111]. For satellite attitude fault tolerant control, a lot of FTC approaches have been developed in the past two decades [29, 112–114]. The detailed literature review can be seen in [18].

In this section, some classical attitude FTC schemes are reviewed only. For example, an adaptive FTC was given in [115] to perform the attitude tracking maneuver for satellite. The transient performance was ensured. In [116], a velocity-free FTC by integrating the adaptive and the fuzzy control theory was presented for the satellite. In [117], the FTC problem with prescribed performance guaranteed was studied for satellite attitude tracking maneuvers. In [118], the problems of FTC design ensuring finite-time convergence were investigated for the satellite with actuator faults. In [119], the attitude FTC problem was studied by integrating the iterative learning observer and the control allocation. By a combination of the Lyapunov function and the extended-state observer, an attitude controller was presented in [120] with actuator saturation constraint solved. Using an adaptive extended-state observer, another attitude controller having the capability of handling actuator uncertainty and achieving robustness as well as precise tracking accuracy was proposed in [121]. By estimating the unmeasurable modal variables, a distributed adaptive attitude controller has been reported in [122]. An attitude FTC for satellite with actuator faults was designed by using a fault detection observer [123]. An iterative learning observerbased FTC law was given to solve the attitude stabilization problem [124]. With the development of the intelligent control, the neural network control schemes were proposed to address actuator faults [125, 126].

### 1.5 Satellite Actuator Misalignment Control

There have been several investigations on satellite attitude control in the presence of actuator misalignments [127, 128]. In [129], an adaptive control law was given to accomplish attitude maneuver in the presence of relatively small gimbals' alignment error of variable speed control moment gyros. In [130], a nonlinear model reference adaptive control scheme was tested in the presence of alignment errors up to fifteen degrees. Although an extended Kalman filter was used to develop methods for onorbit actuator alignment calibration, uncertain inertia properties were not taken into account [131]. In another work [132], an adaptive tracking controller was synthesized for Hamiltonian systems. This control law was successfully applied to a satellite with both inertia and actuator uncertainties.

1 Overview

It is worth mentioning that most attitude controllers for actuator alignment were designed in the framework of robust control. A control law was synthesized that the robustness to actuator misalignment was guaranteed. This was reported for the formation flying of satellites in [133]. The misalignment of a specific actuator, i.e., thruster, was addressed by applying the adaptive control theory. This theory was further used in [134–136] to tackle with the misalignment of other actuators such as reaction wheels. In [137, 138], another control theory, i.e., the sliding mode control, was adopted to synthesize attitude controllers for satellites. High-accuracy attitude maneuvers were successfully performed with actuator misalignment accommodated. Other nonlinear control theory-based laws were also available for satellite attitude tracking maneuver [139–144]. The finite-time stability of the attitude tracking system was achieved despite the actuator misalignment.

### 1.6 Uncertain Inertia Control of Satellite

Significant development has been witnessed in the attitude tracking controller design in the presence of uncertain inertia [145–149]. The current approaches to handling system uncertainties are mostly nonlinear control theory based. Attitude controllers are designed to ensure the stability of the closed-loop tracking system in the presence of uncertainties [150, 151]. For example, an angular velocity observer-based attitude tracking solution to the external disturbance rejection problem was reported for satellite [152]. This was achieved by the theory of adaptive control. The bound of the external disturbance is required and should be known. This theory was also applied in [153] to study the attitude tracking control problem. The uncertain inertia and the bias in the measurement of angular velocity were considered. In [154], the coordinated attitude control was investigated, while the satellite was subject to systems uncertainties and attitude constraint. Taking input quantization issue into consideration, robust attitude tracking was achieved for satellite in [155] and [156]. In [157], the attitude tracking control was achieved via attitude output feedback only. Moreover, the finite-time control theory can be applied to develop controllers to achieve fast attitude slewing [158-161]. System stability was achieved after a finite time period. Although the controller design to achieve attitude tracking was discussed well, the system uncertainties were considered only, actuator uncertainties were not handled.

In particular, the adaptive control has been shown to be an effective scheme in the investigations of a wide class of nonlinear systems [162–166], in which there exist unknown parameters. Therefore, adaptive control can be also applied for satellite attitude maneuvering with uncertain inertia. Moreover, by viewing the torque induced by uncertain inertia as external disturbance, then the methods summarized in Sect. 1.3 are appropriate and applicable to achieve attitude control for satellite.

### 1.7 Nonlinear Control with Actuator Constraint

For any linear or nonlinear system in practice, the torque or the force generated by its actuators is finite and bounded due to the physical limitation. All actuators are constrained. Once the required control effort saturates the actuators, the output signals may not achieve the control mission, if the system is not equipped with an appropriate control methodology to dump the saturated actuators. Then, it may lead to control performance deterioration or system instability. Hence, actuator constraint is another key issue that needs to be addressed [167–169].

### 1.7.1 Methods for General Nonlinear Systems

Many results were seen for nonlinear systems to the stability analysis and controller design with actuator constraint [28, 170–172]. For example, a saturation-based fixed-time funnel boundary was proposed in [173] for a class of strict feedback systems with actuator constraint and external disturbances. The corrected signal associated with the actuator constraint error was embedded in the funnel function. For a class of dynamical networks with actuator constraints, a saturated controller was designed to achieve finite-time synchronization [174]. Taking the parametric and the unmodeled uncertainties into consideration for the nonlinear systems, a nested-saturation-function-based control scheme incorporated with a saturated linear ESO was proposed in [175]. For the uncertain nonlinear systems with actuator constraint, an adaptive sliding mode controller by using a barrier function was proposed in [176]. In [177], a dual periodic event-triggered control including saturation-assisted and complemental periodic event-triggers was synthesized to solve the consensus problem for the multi-agent systems (MAS) with actuator constraint.

When a fault occurs in the actuator further, the control system would continue issuing its maneuver that may no longer be achievable by the system. In this case, the required control effort will quickly saturate the actuators while striving to maintain the "healthy" maneuvering performance. It will subsequently destabilize the system. Therefore, actuator constraint should also be accommodated with actuator fault considered simultaneously. In [178], a finite-time fault estimator-based FTC scheme was proposed to address the accurate trajectory-tracking problem of a surface vehicle under actuator constraint and actuator failures. In [179], a smooth function was designed to approximate the controller saturation function and a neural network (NN) to uncertainties and failures for the MAS. For the aircraft control system with actuator constraint and actuator failures, an enhanced anti-disturbance control by utilizing novel auxiliary systems was reported in [180] to avoid and compensate for the actuator constraint.

14 1 Overview

### 1.7.2 Attitude Control with Actuator Constraint

For a satellite attitude control system, its typical actuators are reaction wheel, thruster, and magnetic torquer. Those actuators have a bounded output torque. Actuator constraints are met in satellite. In the past two decades, significant developments are seen in attitude control with actuator constraint [181–190]. One of the most prominent methods is the anti-windup design due to its simple structure [191]. In [191], an anti-windup controller was proposed for large angle attitude control of satellite with actuator saturation. For the attitude tracking control problem with system uncertainties and state constraints, an anti-windup compensator-based robust adaptive controller was designed in [192] to handle actuator constraints. Considering the satellite attitude trajectory tracking control system with external disturbance and actuator constraints, an ESO and anti-windup compensator-based robust finite-time controller was proposed in [193]. For the attitude tracking control problem of a special rigid-flexible-rigid microsatellite with multi-uncertainties and actuator constraints, a robust control system structure including an observer-based compensator and a modified proportional-derivative control law was presented in [194].

In [195], the backstepping technique was applied to the nonlinear flight system in the absence of input constraint first, and then a command filter was employed to compensate for the effect of the control signal rate constraint. In [196], a robust variable structure controller was designed to control the satellite attitude under actuator constraint. An alternative algorithm that applied a positive constant gain within the framework of integrator backstepping-based control design to reduce peak control torque was seen in [197]. A nonlinear adaptive controller including feedback and feed-forward components to handle actuator constraint and linearly parameterized disturbance was reported in [198]. Consider the constraints of input signals and the prescribed performance of the satellite formation control system, an SMC-based fixed-time controller was presented in [199] by incorporating an anti-windup saturation compensator. For the multi-satellite consensus control system under actuator constraint, a novel optimal control law was developed in [200].

Control allocation is another useful method to deal with the actuator constraint issue. A systematic result by using control allocation methods design was available in [201] for satellite. In [202], a saturated proportional-derivative controller combining with a null-space-based optimal control reallocation was presented for the satellite attitude control system.

### 1.8 Angular Velocity-Free Attitude Control

Most controllers for linear or nonlinear systems are developed based on the assumption that precise measurement of the system's full states is available. This assumption is widely used in satellite attitude control system design. The direct and exact measurement of both the attitude and the angular velocity is assumed to be available. How-

ever, the precise measurements of angular velocity are not always satisfied in practice due to either cost limitations or implementation constraints. Some unexpected faults or failures occurring in gyros and other rate sensors also lead to the wrong measurement of velocity. Therefore, towards the implementation-cost optimization issue and sensor fault avoidance, it is highly desirable to design a partial-state feedback attitude controller that does not require the angular velocity measurement.

In the past two decades, the development of attitude control without the measurements of angular velocity has attracted significant attention in the academic and satellite engineering communities. The earliest known result in the field of velocity-free control was presented in [203, 204] through passivity framework. Subsequent extensions to that control design scheme without angular velocity were presented in [205, 206]. In [207], an alternative solution to stabilize attitude by using quaternion only has been proposed based on optimal control technique. Moreover, several other control techniques are also motivated with Lyapunov based techniques [208]. In general, the existing angular velocity-free attitude control approaches can be classified into two types. One is the observer-based control. The other is the filter-based control.

### 1.8.1 Observer-Based Velocity-Free Control

One solution to the attitude control problem without angular velocity is the development of a model-based observer [209, 210] to estimate the angular velocity [211–218]. In this observer-based scheme, angular velocity is estimated with desired estimation accuracy [219–222]. In [116], an adaptive observer by using the fuzzy control technique was developed for the unmeasured angular velocity. Although the velocity estimation error was exponentially stable, external disturbances were not considered. In [223], a smooth angular velocity observer was proposed with the estimation error asymptotically stabilized. However, this was also done in free of external disturbance. In [224], a velocity-free attitude stabilization law was reported with an angular velocity observer. In [225], a hybrid observer was available to exponentially estimate the unmeasured angular velocity for rigid bodies. Although these angular velocity observer-based controllers can achieve attitude maneuvers with attitude output feedback only, their structures are complicated. They require expensive onboard computations. This makes them be not user-friendly for engineering.

If, in addition to unmeasured states, there are parametric uncertainties [226], an observer can be made robust by applying SMC [227]. This observer is called sliding-mode observers (SMOs) [228, 229]. Sliding-mode observers have been proven to be an effective way to estimate unmeasured states [230]. Output feedback control with a sliding mode observer can make use of equivalent control concept [231–233]. In [231], the finite-time output feedback stabilization of a class of second-order systems was discussed. In [232], global finite-time observers were proposed for Lipschitz nonlinear systems. To improve the estimation performance of SMO in the presence

1 Overview

of system uncertainties and disturbances, some other SMO-based design has been discussed, such as high-gain SMO [78, 234, 235] and high-order SMO [236–238].

Almost all of the aforementioned SMO design provides an asymptotic convergence of the observer error. However, finite-time convergence is not ensured. In some applications, it is highly desired a finite-time convergence [239]. For instance, synchronization of chaotic signals is of major importance for walking robots in secure communication or attitude maneuvers of time-critical satellites [240]. For those systems, each step should be done in a finite time. Currently, observer design for states with finite-time convergence has received considerable attention [241]. Many finite-time observer design methods have been proposed for different systems [242]. The high-gain finite-time observer was further pursued using homogeneity concepts in [243]. More recently, there has been another approach to achieve observation in finite time. It is designed by using terminal sliding-mode control technique [244].

### 1.8.2 Filter-Based Velocity-Free Control

An alternative to the angular velocity-free attitude control problem is the filter-based or the auxiliary-based technique [245–247]. This solution is free of any angular velocity observer. In accordance, the controller is synthesized directly to stabilize the attitude system via the Lyapunov stability theory. The first attempt to design such filter-based velocity-free control was made in [248]. The satellite's attitude regulation or tracking maneuvers were achieved in [249–252] via this solution. External disturbances were not addressed. In [253], a velocity-free rotation tracking law was seen by including a filter to compensate for the unmeasured angular velocity. In [254], the velocity-free attitude control issue with actuator and rate constraints was investigated by using the filter-based technique. The robust attitude tracking control problem without measurements of angular velocity was solved in [255] via a quaternion filter. In [256], another velocity-free attitude stabilization control design was reported by applying potential functions. It was not capable of handling disturbances. In [257], the pose tracking control problem without velocity feedback was further investigated. The satellite was assumed to be under no effect of disturbance. In [258], another filter-based velocity-free attitude controller was synthesized to perform the rest-to-rest attitude maneuvering of satellites in the absence of any disturbances.

The filter-based velocity-free control is further examined in [259]. That approach integrates a velocity-generating filter from attitude measurements to design an adaptive attitude tracking controller. Another quaternion-based output feedback control design was reported in [260]. Although that approach does not need the angular velocity and can guarantee the uniformly asymptotical stability of the closed loop system, it is assumed that full knowledge of the inertia matrix and system dynamics is known in advance. In [19], by introducing an auxiliary dynamical system, a velocity-free control scheme for the attitude tracking of rigid satellites is discussed. However, the technique was developed without any external disturbances considered. To treat the external disturbances, an adaptive attitude tracking control approach was

presented in [253] for the rigid satellite. An approximate differentiation filter was introduced to account for the unmeasured angular velocity. In addition, augmentation of an existing controller using the Chebyshev neural network was considered in [261]. The effect of unknown dynamics and external disturbances is carried out by using online neural network approximation. Moreover, the tracking error is shown to be uniformly ultimately bounded even without velocity measurements.

### 1.9 Flexible Satellite Attitude Control

Robust control, exploring various types of techniques, has been frequently considered for attitude control design of flexible satellites in the presence of modeling error with flexible vibration included. In [262], a robust controller was proposed for the flexible mechanical systems and the validity of the design method was confirmed for the flexible satellite attitude control problem. In [263], an extended potential difference controller was developed for a flexible satellite, and robustness to vibrations and external disturbances was achieved. An optimization-based approach was proposed in [264] for the robustness analysis of an attitude and orbit control system for flexible satellites. Simulation studies indicated that the proposed approach appears to have significant potential for improving the industrial flight clearance process for nextgeneration high-performance satellite control systems. In [265], the attitude tracking control problem was investigated by designing a model-based robust controller. Actuator fault, uncertain inertia, and vibrations in flexible appendages were addressed. A robust attitude and vibration control of a flexible satellite was reported in [266] that uses shunted piezoelectric transducers, bonded to the flexible elements in such a way that the vibration energy is transferred to an electric circuit and partially dissipated. In [267], a phase-plane controller was proposed for a flexible satellite (i.e., TacSat-4) attitude control by thrusters. Robustness against structural bending modes less than 1 Hz was ensured.

The majority of the existing robust control schemes for flexible satellites attitude control are proven to be effective only through simulation studies. Of particular interest are the studies carried out in [31] and [32], the designed controllers are intended for experimental verification on ETS-VIII at the end of its mission life. In [31], a two-degrees-of-freedom control based on robust direct velocity and displacement feedback was proposed (instead of the existing classical PID control law) as a candidate controller technology. Optimization algorithms for both the feedback and feedforward controllers described by the linear matrix inequalities in the framework of  $\mathcal{H}_{\infty}$  controller synthesis were proposed. The capability to handle flexible vibrations was verified through simulations. In the follow-up work [32], a linearly interpolated gain scheduling controller was designed for ETS-VIII using its linear parameter-varying model. In a more recent work by the same authors [14], an experimental study was presented in which the on-orbit flight tests of a two-degrees-of-freedom robust controller for ETS-VIII, namely step responses corresponding to the antenna

18 1 Overview

calibration maneuver and impulse responses corresponding to external disturbance can be found.

### 1.10 Fast Attitude Control

Although various controllers are available to perform attitude maneuvers for satellites, most of them stabilize the states of the attitude system as the time approaches infinity. The infinite settling time criterion is not an option during critical phases of the mission. In practice, many missions demand fast attitude maneuvering [268]. To meet this demand, the finite-time stability (FTS) concept is available [269].

Aiming to achieve attitude control within finite-time convergence, attitude control design via SMC has got significant consideration [270]. In [271], the terminal SMC (TSMC) was utilized to achieve finite-time control. However, the TSMC suffers from singularity. To avoid this problem, many non-singular attitude TSMC (NTSMC) approaches have been reported [272]. The implementation of those results necessitates the full knowledge of uncertainties or needs large control gains to attenuate uncertainties. This leads the controllers to be conservative and chattering with rapid energy consumption. As such, the adaptive control theory has been invoked to alleviate chattering [273, 274], whereas their controllers were discontinuous due to the incorporated signum function. To avoid this discontinuity, the signum function was replaced with the hyperbolic tangent or the saturation function in [275]. However, such chattering alleviation is obtained at the cost of control accuracy degradation. Another solution to this problem is the higher order sliding mode-based control while finite-time convergence is ensured [276]. Complicated theoretical analysis and heavy computation were involved. Motivated by solving this challenge and eliminating chattering, this paper will propose a novel continuous adaptive law by estimating the upper bound of uncertainties.

In practice, actuator uncertainty may exist due to aging or malfunction of the actuator's components. Considering this issue and applying the nonsingular TSMC [277], the fast TSMC [278], the backstepping control [279], and the integral backstepping [280], many attitude stabilization controllers are seen to achieve finite-time convergence.

### 1.11 Motivation for This Book

It is obtained from satellite engineering that any satellite has severe modeling error. On the other hand, any satellite is also subject to actuator constraints. The angular velocity measurement may be unavailable further for satellites. Moreover, fast attitude slewing maneuvers are demanded to be performed to accomplish the planned space missions. As a result, the following four challenges are raised in the satellite attitude control, while the preceding reviewed attitude control approaches have

a weak capability of addressing those challenges. Although the results in [281–284], the tracking control approaches proposed for unmanned aerial vehicle [285], robotic manipulator [286], snake robot [287], and nano-positing systems [288], can be referred to solve those challenges, there is not a standard or general solution framework. The following challenges are still open.

- From the standpoint of modeling error compensation control, two or more than two types of modeling error introduced in Sect. 1.2 should be addressed. This problem is widely seen in microsatellites. Most of the existing approaches can handle a single type of modeling error only.
- From the standpoint of attitude control, high-accuracy attitude control should be achieved with two or more than two types of modeling error and actuator constraint simultaneously addressed even without angular velocity measurement. However, most of the attitude control schemes in the literature are not capable of solving this problem.
- The attitude maneuvering should be accomplished during critical phases of the mission with the fast rate even in the presence of two or more than two types of modeling error summarized in Sect. 1.2.
- From the view of saving energy, the modeling error should be compensated with less and even no conservativeness. However, the existing robust or adaptive attitude controllers are characterized by severe conservativeness.

Considering the demand for attitude control with the above four challenges solved and many existing approaches are unable to achieve this goal, this book attempts to solve the above four challenges during satellite attitude control system design. This book focuses on designing advanced compensation control techniques for more types of modeling error with fast, high-accuracy, high-stability, and or velocity-free attitude maneuvering accomplished for satellites.

### 1.12 Organization of the Book

The book is organized into twelve chapters, including three parts on technical results (a totally nine chapters). Part I includes Chaps. 1 and 2 with the overview on modeling error compensation attitude control of satellite and the preliminary knowledge of this book. Part II concentrates on the robust velocity-free solution to two or more than two types of the modeling error compensation attitude control problem of the satellite even in the presence of actuator constraint and fault. Part III focuses on the recent solution to achieve fast attitude slewing control for satellites with two or more than two types of modeling error compensated adaptively. Part IV presents some new observer-based approaches to accomplish attitude control for satellites with less conservativeness, while the modeling error is precisely and fully compensated. The outline of each chapter is listed as follows.

Chapter 1 provides an overview of this book. It gives a description of modeling error acting on the satellite attitude control system. This chapter then briefly intro-

duces a literature review on the recent attitude control approaches for satellites with modeling error. Moreover, the motivation of this book is given in this chapter.

Chapter 2 is a preliminary chapter to provide knowledge for the rest of this book. That knowledge includes the standard notations, definitions, preliminary lemmas, attitude representation methods of satellite, and the mathematical model of satellite attitude control system. This chapter ends with the description of three types of testbeds for attitude control testing on the ground.

Chapter 3 investigates the large-angle velocity-free attitude tracking control problem of rigid satellites with modeling error. An efficient and practical angular velocityfree control strategy with a simple, yet efficient structure is proposed. The attitude tracking maneuver is accomplished with the attitude pointing control performance robustness to modeling error.

Chapter 4 is dedicated to solving the angular velocity-free attitude control problem of satellites with modeling error and actuator constraint. A velocity-free neural network attitude stabilization controller and a disturbance attenuation attitude tracking controller are presented. The effect of the modeling error is attenuated by tunning control gains with great robustness guaranteed.

Chapter 5 is concerned with attitude controller design for satellites without the angular velocity measurements. The velocity-free attitude control problem in the presence of modeling error consists of external disturbance and actuator fault is addressed. Once again, the proposed approach in this chapter is a robust control solution to handle modeling error.

Chapter 6 addresses the velocity-free attenuation control problem of a class of nonlinear systems with modeling error induced by external disturbance and actuator faults. The modeling error is adaptively estimated and compensated. The proposed approach is applicable for satellite attitude stabilization maneuvering despite the modeling error due to uncertain inertia, disturbance, and actuator fault.

Chapter 7 is devoted to prescribed attitude stabilization performance control of satellite with the modeling error including actuator fault and external disturbance. The modeling error is adaptively compensated via reinforcement learning. The attitude of the considered satellite is stabilized by presenting a reinforcement learning-based fixed-time optimal control framework.

Chapter 8 focuses on the rapid attitude control problem of satellites with modeling error including uncertain inertia and external disturbances. A sliding mode-based fixed-time control approach is presented with the modeling error adaptively compensated. It is proved that the states of the satellite attitude system can converge into a small set after a fixed-time even in the presence of modeling error.

Chapter 9 studies the extended state observer-based attitude control for flexible satellites with modeling error induced by external disturbances and unknown vibrations induced by flexible appendages. The modeling error is precisely estimated and fully compensated by the extended state observer. The key feature of this control approach is that its controller has no conservativeness.

Chapter 10 aims to solve the modeling error compensation control problem of the satellite attitude system in the presence of the disturbance observer-based control framework. The drawbacks of the existing disturbance observer requesting the

modeling error to be constant or with a minor rate of change are addressed. This framework lets the attitude maneuvering be accomplished at an exponential rate.

Chapter 11 provides the satellite attitude control system design with a modeling error compensation control approach in the unknown input observer-based framework. A new unknown input observer is presented to estimate modeling error. The developed controller with the output of that observer incorporated can achieve high accuracy pointing control of the satellite.

Chapter 12 is dedicated to ending the book with some concluding remarks on the developed compensation control approaches and to present some future work.

#### 1.13 Summary

The overview of this book is presented in this chapter. The main modeling error of the satellite attitude control system is introduced. The recent works on handling such modeling error with satellite attitude controlled are reviewed. Moreover, the motivation and the organization of this book are detailed given in this chapter.

#### References

- Mao, J., Karimi, H. R., Xiang, Z. (2019) Observer-based adaptive consensus for a class of nonlinear multiagent systems. IEEE Transactions on Systems Man Cybernetics: Systems 49(9): 1893–1900
- Jiang, B., Karimi, H. R., Kao, Y., Gao, C. (2019) Takagi-sugeno model-based sliding mode observer design for finite-time synthesis of semi-markovian jump systems. IEEE Transactions on Systems Man Cybernetics: Systems 49(7): 1505–1515
- 3. Liu, M., Zhang, L., Shi, P., Karimi, H. R. (2014) Robust control of stochastic systems against bounded disturbances with application to flight control. IEEE Transactions on Industral Electronics 61(3): 1504–1515
- Peng, X., Geng, Z., Sun, J. (2020) The specified finite-time distributed observers-based velocity-free attitude synchronization for rigid bodies on SO(3). IEEE Transactions on Systems Man Cybernetics: Systems 50(4): 1610–1621
- Zou, Y., Meng, Z. (2019) Immersion and invariance-based adaptive controller for quadrotor systems. IEEE Transactions on Systems Man Cybernetics: Systems 49(11): 2288–2297
- Chen, M. (2016) Constrained control allocation for overactuated aircraft using a neurodynamic model. IEEE Transactions on Systems Man Cybernetics: Systems 46(12): 1630–1641
- Liu, C., Jiang, B., Zhang, K. (2020) Adaptive fault-tolerant H-infinity output feedback control for lead-wing close formation flight. IEEE Transactions on Systems Man Cybernetics: Systems 50(8): 2804–2814
- 8. Zhong, C. X., Chen, Z. Y., Guo, Y. (2017) Attitude control for flexible spacecraft with disturbance rejection. IEEE Transactions on Aerospace and Electronic Systems 53(1): 101–110
- 9. He, W., Meng, T. T., He, X. Y., Sun, C. Y. (2019) Iterative learning control for a flapping wing micro aerial vehicle under distributed disturbances. IEEE Transactions on Cybernetics 49(4): 1524–1535
- He, W., Yan, Z. C., Sun, C. Y., Chen, Y. N. (2017) Adaptive neural network control of a flapping wing micro aerial vehicle with disturbance observer. IEEE Transactions on Cybernetics 47(10): 3452–3465

 Zhang, Y., Li, M., Zhang, J. R. (2017) Vibration control for rapid attitude stabilization of spacecraft. IEEE Transactions on Aerospace and Electronic Systems 53(3): 1308–1320

- 12. Khanesar, M. A., Kayacan, E., Reyhanoglu, M., Kaynak, O. (2015) Feedback error learning control of magnetic satellites using type-2 fuzzy neural networks with elliptic membership functions. IEEE Transactions on Cybernetics 45(4): 858–868
- 13. Wertz, J. R. (1978) Spacecraft attitude determination and control. Springer Netherlands
- Nagashio, T., Kida, T., Hamada, Y., Ohtani, T. (2014) Robust two-degrees-of-freedom attitude controller design and flight test result for engineering test satellite-VIII spacecraft. IEEE Transactions on Control Systems Technology 22(1): 157–168
- Aoues, S., Cardoso-Ribeiro, F. L., Matignon, D., Alazard, D. (2019) Modeling and control of a rotating flexible spacecraft: A port-Hamiltonian approach. IEEE Transactions on Control Systems Technology 27(1): 355–362
- Chen, T., Shan, J., Wen, H. (2019) Distributed adaptive attitude control for networked underactuated flexible spacecraft. IEEE Transactions on Aerospace and Electronic Systems 55(1): 215–225
- Meng, T., He, W., Yang, H., Liu, J.K., You, W. (2016) Vibration control for a flexible satellite system with output constraints. Nonlinear Dynamics 85(4): 2673–2686
- 18. Hu, Q. L., Xiao, B., Li, B., Zhang, Y. M. (2021) Fault-tolerant attitude control of spacecraft. Elsevier
- Tayebi, A. (2008) Unit quaternion-based output feedback for the attitude tracking problem. IEEE Transactions on Automatic Control 53(6): 1516–1520
- Chunodkar, A. A., Akella, M. R. (2014) Switching angular velocity observer for rigid-body attitude stabilization and tracking control. Journal of Guidance, Control, and Dynamics 37(3): 869–878
- Findlay, E. J., de Ruiter, A., Forbes, J. R., Liu, H. H. T., Damaren, C. J., Lee, J. (2013)
   Magnetic attitude control of a flexible satellite. Journal of Guidance, Control, and Dynamics 36(5): 1522–1527
- Xiao, B., Huo, M. Y., Yang, X. B., Zhang, Y. M. (2015) Fault tolerant attitude stabilization for satellites without rate sensor. IEEE Transactions on Industrial Electronics 62(11): 7191–7202
- 23. Kim, K. S., Kim, Y. (2003) Robust backstepping control for slew maneuver using nonlinear tracking function. IEEE Transactions on Control Systems Technology 11(6): 822–829
- Zanchettin, A. M., Calloni, A., Lovera, M. (2013) Robust magnetic attitude control of satellites. IEEE/ASME Transactions on Mechatronics 18(4): 1259–1268
- Zhao, L., Jia, Y. (2014) Decentralized adaptive attitude synchronization control for spacecraft formation using nonsingular fast terminal sliding mode. Nonlinear Dynamics 78(4): 2779– 2794
- Lee, D. (2017) Nonlinear disturbance observer-based robust control of attitude tracking of rigid spacecraft. Nonlinear Dynamics 88(2): 1317–1328
- 27. Cao, S., Zhao, Y. (2017) Anti-disturbance fault-tolerant attitude control for satellites subject to multiple disturbances and actuator saturation. Nonlinear Dynamics 89(4): 2657–2667
- 28. Chen, M., Sam Ge, S. Z., Ren, B. B. (2011) Adaptive tracking control of uncertain mimo nonlinear systems with input constraints. Automatica 47(3): 452–465
- Shen, Q., Wang, D. W., Zhu, S. Q., Poh, E. K. (2015) Integral-type sliding mode fault-tolerant control for attitude stabilization of spacecraft. IEEE Transactions on Control Systems Technology 23(3): 1131–1138
- Chen, F., Jiang, R., Zhang, K., Jiang, B., Tao, G. (2016) Robust backstepping sliding-mode control and observer-based fault estimation for a quadrotor UAV. IEEE Transactions on Industral Electronics 63(8): 5044–5056
- Nagashio, T., Kida, T. S., Ohtani, T. S., Hamada, Y. S. (2010) Design and implementation of robust symmetric attitude controller for ETS-VIII spacecraft. Control Engineering Practice 18(12): 1440–1451
- 32. Hamada, Y., Ohtani, T., Kida, T., Nagashio, T. (2011) Synthesis of a linearly interpolated gain scheduling controller for large flexible spacecraft ETS-VIII. Control Engineering Practice 19(6): 611–625

33. Shen, Q., Yue, C., Goh, C.H., Wu, B., Wang, D. (2018) Rigid-body attitude stabilization with attitude and angular rate constraints. Automatica 90: 157–163

- 34. Hu, Q., Shao, X., Guo, L. (2018) Adaptive fault-tolerant attitude tracking control of spacecraft with prescribed performance. IEEE/ASME Transactions on Mechatronics 23(1): 331–341
- Sun, L., Zheng, Z. (2017) Disturbance-observer-based robust backstepping attitude stabilization of spacecraft under input saturation and measurement uncertainty. IEEE Transactions on Industral Electronics 64(10): 7994

  –8002
- Ping, Z., Dong, Y., Tang, H., Lu, J. G. (2016) Robust approach for attitude tracking and nonlinear disturbance rejection of rigid body spacecraft. IET Control Theory and Applications 10(17): 2325–2330
- 37. Wu, B., Shen, Q., Cao, X. (2018) Event-triggered attitude control of spacecraft. Advances in Space Research 61(3): 927–934
- 38. Cheng, C. C., Chien, S. H., Shih, F. C. (2010) Design of robust adaptive variable structure tracking controllers with application to rigid robot manipulators. IET Control Theory and Applications 4(9): 1655–1664
- Almeida, J., Silvestre, C., Pascoal, A. (2010) Cooperative control of multiple surface vessels in the presence of ocean currents and parametric model uncertainty. International Journal of Robust and Nonlinear Control 20(14): 1549–1565
- 40. Lee, T. (2013) Robust adaptive attitude tracking on SO(3) with an application to a quadrotor uav. IEEE Transactions on Control Systems Technology 21(5): 1924–1930
- Islam, S., Liu, P. X., ElSaddik, A. (2015) Robust control of four-rotor unmanned aerial vehicle with disturbance uncertainty. IEEE Transactions on Industrial Electronics 62(3): 1563–1571
- Cabecinhas, D., Cunha, R., Silvestre, C. (2015) A globally stabilizing path following controller for rotorcraft with wind disturbance rejection. IEEE Transactions on Control Systems Technology 23(2): 708–714
- Yang, Y., Du, J., Liu, H., Guo, C., Abraham, A. (2014) A trajectory tracking robust controller of surface vessels with disturbance uncertainties. IEEE Transactions on Control Systems Technology 22(4): 1511–1518
- 44. Liu, H., Wang, X., Zhong, Y. (2015) Quaternion-based robust attitude control for uncertain robotic quadrotors. IEEE Transactions on Industrial Informatics 11(2): 406–415
- 45. Feng, Y., Yu, X., Han, F. (2013) High-order terminal sliding-mode observer for parameter estimation of a permanent-magnet synchronous motor. IEEE Transactions on Industral Electronics 60(10): 4272–4280
- Xiao, B., Hu, Q. L., Singhose, W., Huo, X. (2013) Reaction wheel fault compensation and disturbance rejection for spacecraft attitude tracking. Journal of Guidance, Control, and Dynamics 36(6): 1565–1575
- 47. Chen, Z. Y., Huang, J. (2009) Attitude tracking and disturbance rejection of rigid spacecraft by adaptive control. IEEE Transactions on Automatic Control 54(3): 600–605
- 48. Li, Z., Su, C. Y., Wang, L., Chen, Z., Chai, T. (2015) Nonlinear disturbance observer-based control design for a robotic exoskeleton incorporating fuzzy approximation. IEEE Transactions on Industral Electronics 62(9): 5763–5775
- Xiao, B., Hu, Q., Wang, D., Poh, E. K. (2013) Attitude tracking control of rigid spacecraft with actuator misalignment and fault. IEEE Transactions on Control Systems Technology 21(6): 2360–2366
- 50. Pisu, P., Serrani, A. (2007) Attitude tracking with adaptive rejection of rate gyro disturbances. IEEE Transactions on Automatic Control 52(12): 2374–2379
- Castaneda, L. A., Luviano-Juarez, A., Chairez, I. (2015) Robust trajectory tracking of a Delta robot through adaptive active disturbance rejection control. IEEE Transactions on Control Systems Technology 23(4): 1387–1398
- Yoon, H. J., Agrawal, B. N. (2009) Adaptive control of uncertain Hamiltonian multi-input multi-output systems: With application to spacecraft control. IEEE Transactions on Control Systems Technology 17(4): 900–906
- Zou, A. M., Kumar, K. D., Hou, Z. G., Liu, X. (2011) Finite-time attitude tracking control for spacecraft using terminal sliding mode and chebyshev neural network. IEEE Transactions on Systems, Man, and Cybernetics, Part B: Cybernetics 41(4): 950–963

 Xiao, B., Hu, Q. L., Zhang, Y. M. (2012) Adaptive sliding mode fault tolerant attitude tracking control for flexible spacecraft under actuator saturation. IEEE Transactions on Control Systems Technology 20(6): 1605–1612

- 55. Zou, A. M. (2014) Finite-time output feedback attitude tracking control for rigid spacecraft. IEEE Transactions on Control Systems Technology 22(1): 338–345
- Chen, Y. P., Lo, S. C. (1993) Sliding-mode controller design for spacecraft attitude tracking maneuvers. In: 1993 American Control Conference, San Francisco, CA, USA, pp 195–196
- 57. Hui, L., Li, J. (2009) Terminal sliding mode control for spacecraft formation flying. IEEE Transactions on Aerospace and Electronic Systems 45(3): 835–846
- Pukdeboon, C., Zinober, A. S., Thein, M. W. L. (2010) Quasi-continuous higher order slidingmode controllers for spacecraft-attitude-tracking maneuvers. IEEE Transactions on Industrial Electronics 57(4): 1436–1444
- 59. Xia, Y., Zhu, Z., Fu, M., Wang, S. (2011) Attitude tracking of rigid spacecraft with bounded disturbances. IEEE Transactions on Industral Electronics 58(2): 647–659
- Zhu, Z., Xia, Y., Fu, M. (2011) Adaptive sliding mode control for attitude stabilization with actuator saturation. IEEE Transactions on Industral Electronics 58(10): 4898–4907
- 61. Li, B., Hu, Q., Yu, Y., Ma, G. (2017) Observer-based fault-tolerant attitude control for rigid spacecraft. IEEE Transactions on Aerospace and Electronic Systems 53(5): 2572–2582
- 62. Xiao, B., Yang, X. B., Karimi, H. R., Qiu, J. B. (2019) Asymptotic tracking control for a more representative class of uncertain nonlinear systems with mismatched uncertainties. IEEE Transactions on Industrial Electronics 66(12): 9417–9427
- Xiao, B., Yin, S. (2019) Exponential tracking control of robotic manipulators with uncertain dynamics and kinematics. IEEE Transactions on Industrial Informatics 15(2): 689–698
- 64. Yu, X., Li, P., Zhang, Y. (2018) The design of fixed-time observer and finite-time fault-tolerant control for hypersonic gliding vehicles. IEEE Transactions on Industral ElectronicsS 65(5): 4135–4144
- 65. Lathkar, M. S., Shendge, P. D., Phadke, S. B. (2020) Active control of uncertain seat suspension system based on a state and disturbance observer. IEEE Transactions on Systems Man Cybernetics: Systems 50(3): 840–850
- Yu, X., Fu, Y., Li, P., Zhang, Y. (2018) Fault-tolerant aircraft control based on self-constructing fuzzy neural networks and multivariable smc under actuator faults. IEEE Transactions on Fuzzy Systems 26(4): 2324–2335
- 67. Xiao, B., Yin, S., Wu, L. G. (2017) A structure simple controller for satellite attitude tracking maneuver. IEEE Transactions on Industrial Electronics 64(2): 1436–1446
- Xiao, B., Yin, S., Kaynak, O. (2016) Tracking control of robotic manipulators with uncertain kinematics and dynamics. IEEE Transactions on Industrial Electronics 63(10): 6439–6449
- Xiao, B., Yin, S. (2016) Velocity-free fault-tolerant and uncertainty attenuation control for a class of nonlinear systems. IEEE Transactions on Industrial Electronics 63(7): 4400–4411
- 70. Yin, S., Zhu, X., Qiu, J., Gao, H. (2016) State estimation in nonlinear system using sequential evolutionary filter. IEEE Transactions on Industrial Electronics 63(6): 3786–3794
- Chen, W. H., Yang, J., Guo, L., Li, S. (2016) Disturbance-observer-based control and related methods—An overview. IEEE Transactions on Industrial Electronics 63(2): 1083–1095
- Kim, M. J., Chung, W. K. (2015) Disturbance-observer-based pd control of flexible joint robots for asymptotic convergence. IEEE Transactions on Robotics 31(6): 1508–1516
- Cao, Y., Chen, X. B. (2014) Disturbance-observer-based sliding-mode control for a 3-dof nanopositioning stage. IEEE/ASME Transactions on Mechatronics 19(3): 924–931
- An, H., Liu, J., Wang, C., Wu, L. (2016) Disturbance observer-based antiwindup control for air-breathing hypersonic vehicles. IEEE Transactions on Industral Electronics 63(5): 3038– 3049
- Zhang, L., Li, Z., Yang, C. (2017) Adaptive neural network based variable stiffness control of uncertain robotic systems using disturbance observer. IEEE Transactions on Industral Electronics 64(3): 2236–2245
- 76. Liu, Y., Wang, H., Guo, L. (2018) Composite robust  $\mathcal{H}_{\infty}$  control for uncertain stochastic non-llinear systems with state delay via a disturbance observer. IEEE Transactions on Automatic Control 63(12): 4345–4352

77. Li, S., Wei, J., Guo, K., Zhu, W. L. (2017) Nonlinear robust prediction control of hybrid active-passive heave compensator with extended disturbance observer. IEEE Transactions on Industral Electronics 64(8): 6684–6694

- 78. Veluvolu, K. C., Soh, Y. C. (2009) High-gain observers with sliding mode for state and unknown input estimations. IEEE Transactions on Industral Electronics 56(9): 3386–3393
- Mercorelli, P. (2015) A two-stage sliding-mode high-gain observer to reduce uncertainties and disturbances effects for sensorless control in automotive applications. IEEE Transactions on Industral Electronics 62(9): 5929–5940
- Zhang, H., Wang, J. (2016) Adaptive sliding-mode observer design for a selective catalytic reduction system of ground-vehicle diesel engines. IEEE/ASME Transactions on Mechatronics 21(4): 2027–2038
- 81. Ginoya, D., Shendge, P. D., Phadke, S. B. (2014) Sliding mode control for mismatched uncertain systems using an extended disturbance observer. IEEE Transactions on Industral Electronics 61(4): 1983–1992
- 82. Yin, S., Yang, H., Kaynak, O. (2017) Sliding mode observer-based FTC for Markovian jump systems with actuator and sensor faults. IEEE Transactions on Automatic Control 62(7): 3551–3558
- Pilloni, A., Pisano, A., Usai, E. (2015) Observer-based air excess ratio control of a pem fuel cell system via high-order sliding mode. IEEE Transactions on Industral Electronics 62(8): 5236–5246
- 84. Chalanga, A., Kamal, S., Fridman, L. M., Bandyopadhyay, B., Moreno, J. A. (2016) Implementation of super-twisting control: Super-twisting and higher order sliding-mode observer-based approaches. IEEE Transactions on Industral Electronics 63(6): 3677–3685
- Yang, J., Su, J., Li, S., Yu, X. (2014) High-order mismatched disturbance compensation for motion control systems via a continuous dynamic sliding-mode approach. IEEE Transactions on Industrial Informatics 10(1): 604–614
- Yao, Y., J., Jiao, Z., Ma, D. (2014) Extended-state-observer-based output feedback nonlinear robust control of hydraulic systems with backstepping. IEEE Transactions on Industral Electronics 61(11): 6285–6293
- 87. Guo, Q., Zhang, Y., Celler, B. G., Su, S. W. (2016) Backstepping control of electro-hydraulic system based on extended-state-observer with plant dynamics largely unknown. IEEE Transactions on Industral Electronics 63(11): 6909–6920
- 88. Xue, W., Bai, W., Yang, S., Song, K., Huang, Y., Xie, H. (2015) ADRC with adaptive extended state observer and its application to air-fuel ratio control in gasoline engines. IEEE Transactions on Industrial Electronics 62(9): 5847–5857
- 89. Yang, J., Li, S., Yu, X. (2013) Sliding-mode control for systems with mismatched uncertainties via a disturbance observer. IEEE Transactions on Industral Electronics 60(1): 160–169
- Yang, H., Cheng, L., Xia, Y., Yuan, Y. (2018) Active disturbance rejection attitude control for a dual closed-loop quadrotor under gust wind. IEEE Transactions on Control Systems Technology 26(4): 1400–1405
- 91. Cui, R., Chen, L., Yang, C., Chen, M. (2017) Extended state observer-based integral sliding mode control for an underwater robot with unknown disturbances and uncertain nonlinearities. IEEE Transactions on Industral Electronics 64(8): 6785–6795
- Liao, K., Xu, Y. (2018) A robust load frequency control scheme for power systems based on second-order sliding mode and extended disturbance observer. IEEE Transactions on Industrial Informatics 14(7): 3076–3086
- Li, S., Yang, J., Chen, W. H., Chen, X. (2012) Generalized extended state observer based control for systems with mismatched uncertainties. IEEE Transactions on Industrial Electronics 59(12): 4792

  –4802
- Pu, Z., Yuan, R., Yi, J., Tan, X. (2015) A class of adaptive extended state observers for nonlinear disturbed systems. IEEE Transactions on Industral Electronics 62(9): 5858–5869
- Zhang, J., Liu, X., Xia, Y., Zuo, Z., Wang, Y. (2016) Disturbance observer-based integral sliding-mode control for systems with mismatched disturbances. IEEE Transactions on Industral Electronic 63(11): 7040–7048

96. Liu, J., Luo, W., Yang, X., Wu, L. (2016) Robust model-based fault diagnosis for PEM fuel cell air-feed system. IEEE Transactions on Industrial Electronics 63(5): 3261–3270

- 97. Gao, Z., Liu, X., Chen, M. Z. Q. (2016) Unknown input observer-based robust fault estimation for systems corrupted by partially decoupled disturbances. IEEE Transactions on Industral Electronics 63(4): 2537–2547
- 98. Ichalal, D., Mammar, S. (2015) On unknown input observers for LPV systems. IEEE Transactions on Industrial Electronics 62(9): 5870–5880
- Phanomchoeng, G., Rajamani, R. (2014) Real-time estimation of rollover index for tripped rollovers with a novel unknown input nonlinear observer. IEEE/ASME Transactions on Mechatronicsm 19(2): 743–754
- Daly, J. M., Wang, D. W. L. (2014) Time-delayed output feedback bilateral teleoperation with force estimation for n-dof nonlinear manipulators. IEEE Transactions on Control Systems Technology 22(1): 299–306
- 101. Wu, S. N., Sun, X. Y., Sun, Z. W., Wu, X. D. (2010) Sliding-mode control for staring-mode spacecraft using a disturbance observer. Proceedings of the Institution of Mechanical Engineers, Part G: Journal of Aerospace Engineering 224(G2): 215–224
- Besnard, L., Shtessel, Y. B., Landrum, B. (2012) Quadrotor vehicle control via sliding mode controller driven by sliding mode disturbance observer. Journal of the Franklin Institute 349(2): 658–684
- 103. Cong, B. L., Chen, Z., Liu, X. D. (2013) Disturbance observer-based adaptive integral sliding mode control for rigid spacecraft attitude maneuvers. Proceedings of the Institution of Mechanical Engineers, Part G: Journal of Aerospace Engineering 227(10): 1660–1671
- Zhang, Y. M., Jiang, J. (2008) Bibliographical review on reconfigurable fault-tolerant control systems. Annual Reviews in Control 32(2): 229–252
- Yin, S., Huang, Z. H. (2015) Performance monitoring for vehicle suspension system via fuzzy positivistic C-means clustering based on accelerometer measurements. IEEE/ASME Transactions on Mechatronics 20(5): 2613–2620
- Yin, S., Wang, G., Gao, H. J. (2016) Data-driven process monitoring based on modified orthogonal projections to latent structures. IEEE Transactions on Control Systems Technology 24(4): 1480–1487
- Liang, Y. W., Ting, L. W., Lin, L. G. (2012) Study of reliable control via an integral-type sliding mode control scheme. IEEE Transactions on Industrial Electronics 59(8): 3062–3068
- Yin, S., Li, X. W., Gao, H. J., Kaynak, O. (2015) Data-based techniques focused on modern industry: An overview. IEEE Transactions on Industrial Electronics 62(1): 657–667
- Huang, S., Tan, K. K., Lee, T. H. (2012) Fault diagnosis and fault-tolerant control in linear drives using the Kalman filter. IEEE Transactions on Industrial Electronics 59(11): 4285–4292
- Kim, H. S., Lee, H. C. (2011) Fault-tolerant control algorithm for a four-corner closed-loop air suspension system. IEEE Transactions on Industrial Electronics 58(10): 4866–4879
- 111. Yin, S., Zhu, X. P., Kaynak, O. (2015) Improved PLS focused on key-performance-indicatorrelated fault diagnosis. IEEE Transactions on Industrial Electronics 62(3): 1651–1658
- Li, B., Hu, Q., Yang, Y. (2019) Continuous finite-time extended state observer based fault tolerant control for attitude stabilization. Aerospace Science and Technology 84: 204–213
- Shen, Q., Wang, D. W., Zhu, S. Q., Poh, E. K. (2017) Robust control allocation for spacecraft attitude tracking under actuator faults. IEEE Transactions on Control Systems Technology 25(3): 1068–1075
- Chen, M., Tao, G. (2016) Adaptive fault-tolerant control of uncertain nonlinear large-scale systems with unknown dead zone. IEEE Transactions on Cybernetics 46(8): 1851–1862
- Bustan, D., Sani, S. K. H., Pariz, N. (2014) Adaptive fault-tolerant spacecraft attitude control design with transient response control. IEEE/ASME Transactions on Mechatronics 19(4): 1404–1411
- 116. Huo, B. Y., Xia, Y. Q., Yin, L. J., Fu, M. Y. (2017) Fuzzy adaptive fault-tolerant output feedback attitude-tracking control of rigid spacecraft. IEEE Transactions on Systems, Man, and Cybernetics: Systems 47(8): 1898–1908

117. Shao, X., Hu Q., Shi, Y., Jiang, B. (2020) Fault-tolerant prescribed performance attitude tracking control for spacecraft under input saturation. IEEE Transactions on Control Systems Technology 28(2): 574–582

- Gao, J., Fu, Z., Zhang, S. (2019) Adaptive fixed-time attitude tracking control for rigid spacecraft with actuator faults. IEEE Transactions on Industrial Electronics 66(9): 7141–7149
- 119. Hu, Q., Niu, G., Wang, C. (2018) Spacecraft attitude fault-tolerant control based on iterative learning observer and control allocation. Aerospace Science and Technology 75: 245–253
- Li, B., Hu, Q., Ma, G. (2016) Extended state observer based robust attitude control of spacecraft with input saturation. Aerospace Science and Technology 50: 173–182
- Ran, D., Chen, X., de Ruiter, A., Xiao, B. (2018) Adaptive extended-state observer-based fault tolerant attitude control for spacecraft with reaction wheels. Acta Astronautica 145: 501–514
- 122. Chen, T., Shan, J. (2019) Distributed adaptive fault-tolerant attitude tracking of multiple flexible spacecraft on SO(3). Nonlinear Dynamics 95(3): 1827–1839
- 123. Shen, Q., Yue, C., Goh, C. H., Wang, D. (2019) Active fault-tolerant control system design for spacecraft attitude maneuvers with actuator saturation and faults. IEEE Transactions on Industrial Electronics 66(5): 3763–3772
- 124. Zhang, Z. Z., Ye, D., Sun, Z. W. (2019) Observer-based backstepping fault-tolerant control for spacecraft with reaction-wheel failures. In: 2018 the 9th Asia Conference on Mechanical and Aerospace Engineering, Singapore, pp 012012
- 125. He, W., Sun, Y., Yan, Z., Yang, C., Li, Z., Kaynak, O. (2020) Disturbance observer-based neural network control of cooperative multiple manipulators with input saturation. IEEE Transactions on Neural Networks and Learning Systems 31(5): 1735–1746
- 126. Li, Y., Hu, Q., Shao, X. (2022) Neural network-based fault diagnosis for spacecraft with single-gimbal control moment gyros. Chinese Journal of Aeronautics 35(7): 261–273
- 127. Cao X., Wu B. (2017) Robust spacecraft attitude tracking control using hybrid actuators with uncertainties. ACTA Astronautica 136: 1–8
- Tan, X., Hu, Q., Guo, L. (2017) Attitude stabilization control for rigid spacecraft with actuator misalignment and saturation. In: 2017 36th Chinese Control Conference, pp 9454–9459
- 129. Yoon, H., Tsiotras, P. (2005) Adaptive spacecraft attitude tracking control with actuator uncertainties. In: AIAA Guidance, Navigation, and Control Conference and Exhibit, pp 6392
- Scarritt, S. (2008) Nonlinear model reference adaptive control for satellite attitude tracking.
   In: AIAA Guidance, Navigation and Control Conference and Exhibit, pp 7165
- Fosbury, A., Nebelecky, C. (2009) Spacecraft actuator alignment estimation. In: AIAA Guidance, Navigation, and Control Conference, pp 6316
- Yoon, H., Agrawal, B. N. (2009) Adaptive control of uncertain Hamiltonian multi-input multioutput systems: With application to spacecraft control. IEEE Transactions on Control Systems Technology 17(4): 900–906
- 133. Lima, H. C., Bang, H. (2009) Adaptive control for satellite formation flying under thrust misalignment. Acta Astronautica 65(1-2): 112–122
- 134. Zhang, F., Duan, G. (2013) Robust adaptive integrated translation and rotation control of a rigid spacecraft with control saturation and actuator misalignment. Acta Astronautica 86: 167–187
- Zhang, J., Ye, D., Sun, Z., Liu, C. (2018) Extended state observer based robust adaptive control on se(3) for coupled spacecraft tracking maneuver with actuator saturation and misalignment. Acta Astronautica 143: 221–233
- 136. Mercker, T. H., Akella, M. R. (2014) Adaptive estimation and control algorithms for certain independent control axis misalignments. Journal of Guidance, Control, and Dynamics 37(1): 72–85
- Gui, H., Vukovich, G. (2015) Adaptive integral sliding mode control for spacecraft attitude tracking with actuator uncertainty. Journal of the Franklin Institute 352(12): 5832–5852
- Hu, Q., Li, B., Huo, X., Shi, Z. (2013) Spacecraft attitude tracking control under actuator magnitude deviation and misalignment. Aerospace Science and Technology 28(1): 266–280
- Zhang, A. A., Lv, B. C., Zhang, C. Z., She, D. Z. (2017) Finite time fault tolerant attitude control-based observer for a rigid satellite subject to thruster faults. IEEE Access 5: 16808– 16817

 Hu, Q., Li, B., Zhang, A. (2013) Robust finite-time control allocation in spacecraft attitude stabilization under actuator misalignment. Nonlinear Dynamics 73(1-2): 53–71

- Zhang, R., Qiao, J. Z., Li, T., Guo, L. (2014) Robust fault-tolerant control for flexible spacecraft against partial actuator failures. Nonlinear Dynamics 76(3): 1753–1760
- 142. Hu, Q. L., Li, B., Qi, J. T. (2014) Disturbance observer based finite-time attitude control for rigid spacecraft under input saturation. Aerospace Science and Technology 39: 13–21
- 143. Zhang, A., Hu, Q., Friswell, M. I. (2013) Finite-time fault tolerant attitude control for over-activated spacecraft subject to actuator misalignment and faults. IET Control Theory and Applications 7(16): 2007–2020
- 144. Zhang, F., Duan, G. R. (2012) Integrated translational and rotational finite-time maneuver of a rigid spacecraft with actuator misalignment. IET Control Theory and Applications 6(9): 1192–1204
- 145. Arefi, M. M., Jahed-Motlagh, M. R., Karimi, H. R. (2015) Adaptive neural stabilizing controller for a class of mismatched uncertain nonlinear systems by state and output feedback. IEEE Transactions on Cybernetics 45(8): 1587–1596
- 146. Sharma, R., Tewari, A. (2004) Optimal nonlinear tracking of spacecraft attitude maneuvers. IEEE Transactions on Control Systems Technology 12(5): 677–682
- Luo, W. C., Chu, Y. C., Ling, K. V. (2005) Inverse optimal adaptive control for attitude tracking of spacecraft. IEEE Transactions on Automatic Control 50(11): 1639–1654
- Lo, S. C., Chen, Y. P. (1995) Smooth sliding mode control for spacecraft attitude tracking maneuvers. Journal of Guidance, Control, and Dynamics 18(6): 1345–1349
- 149. Hu, Q. L., Cao, J., Zhang, Y. Z. (2009) Robust backstepping sliding mode attitude tracking and vibration damping of flexible spacecraft with actuator dynamics. Journal of Aerospace Engineering 22(2): 139–152
- 150. Zhang, R., Xu, S. (2018) Neural network based terminal sliding-mode control for thrust regulation of a tethered space-tug. Astrodynamics 2(2): 175–185
- Xu, J., Shi, P., Lim, C. C., Cai, C., Zou, Y. (2016) Integrated structural parameter and robust controller design for attitude tracking maneuvers. IEEE/ASME Transactions on Mechatronics 21(5): 2490–2498
- de Ruiter, A. H. J. (2016) Observer-based adaptive spacecraft attitude control with guaranteed performance bounds. IEEE Transactions on Automatic Control 61(10): 3146–3151
- 153. Benallegue, A., Chitour, Y., Tayebi, A. (2018) Adaptive attitude tracking control of rigid body systems with unknown inertia and gyro-bias. IEEE Transactions on Automatic Control 63(11): 3986–3993
- 154. Li, D., Ma, G., Li, C., He, W., Mei, J. (2018) Distributed attitude coordinated control of multiple spacecraft with attitude constraints. IEEE Transactions on Aerospace and Electronic Systems 54(5): 2233–2245
- Sun, H., Hou, L., Zong, G., Yu, X. (2019) Fixed-time attitude tracking control for spacecraft with input quantization. IEEE Transactions on Aerospace and Electronic Systems 55(1): 124– 134
- 156. Wu, B., Cao, X. (2018) Robust attitude tracking control for spacecraft with quantized torques. IEEE Transactions on Aerospace and Electronic Systems 54(2): 1020–1028
- Berkane, S., Abdessameud, A., Tayebi, A. (2018) Hybrid output feedback for attitude tracking on so(3). IEEE Transactions on Automatic Control 63(11): 3956–3963
- Zhao, L., Yu, J., Yu, H. (2018) Adaptive finite-time attitude tracking control for spacecraft with disturbances. IEEE Transactions on Aerospace and Electronic Systems 54(3): 1297–1305
- Xiao, B., Cao, L., Ran, D. (2021) Attitude exponential stabilization control of rigid bodies via disturbance observer. IEEE Transactions on Systems Man Cybernetics: Systems 51(5): 2751–2759
- Bayat, F. (2019) Model predictive sliding control for finite-time three-axis spacecraft attitude tracking. IEEE Transactions on Industrial Electronics 66(10): 7986–7996
- Shi, X. N., Zhou, Z. G., Zhou, D. (2017) Finite-time attitude trajectory tracking control of rigid spacecraft. IEEE Transactions on Aerospace and Electronic Systems 53(6): 2913–2923

 Cai, W. C., Liao, X. H., Song, Y. D. (2008) Indirect robust adaptive fault-tolerant control for attitude tracking of spacecraft. Journal of Guidance, Control, and Dynamics 31(5): 1456–1463

- Junkins, J. L., Akella, M. R., Robinett, R. D. (1997) Nonlinear adaptive control of spacecraft maneuvers. Journal of Guidance, Control, and Dynamics 20(6): 1104–1110
- 164. Ahmed, J., Coppola, V. T., Bernstein, D. S. (1998) Adaptive asymptotic tracking of spacecraft attitude motion with inertia matrix identification. Journal of Guidance, Control, and Dynamics 21(5): 684–691
- Leeghim, H., Choi, Y., Bang, H. (2009) Adaptive attitude control of spacecraft using neural networks. Acta Astronautica 64(7-8): 778–786
- 166. Gennaro, S. (1998) Adaptive robust tracking for flexible spacecraft in presence of disturbances. Journal of Optimization Theory and Applications 98(3): 545–568
- Zou, A. M., de Ruiter, A. H. J., Kumar, K. D. (2017) Finite-time attitude tracking control for rigid spacecraft with control input constraints. IET Control Theory and Applications 11(7): 931–940
- Jiang, B. Y., Hu, Q. L., Friswell, M. I. (2016) Fixed-time attitude control for rigid spacecraft with actuator saturation and faults. IEEE Transactions on Control Systems Technology 24(5): 1892–1898
- Hu, Q. L., Jiang, B. Y., Friswell, M. I. (2014) Robust saturated finite time output feedback attitude stabilization for rigid spacecraft. Journal of Guidance, Control, and Dynamics 37(6): 1914–1929
- Abdessameud, A., Tayebi, A. (2010) On consensus algorithms for double-integrator dynamics without velocity measurements and with input ainaints. Systems & Control Letters 59(12): 812–821
- Gussner, T., Jost, M., Adamy, J. (2012) Controller design for a class of nonlinear systems with input saturation using convex optimization. Systems & Control Letters 61(1): 258–265
- 172. Li, D. W., Xi, Y. G., Lin, Z. L. (2011) An *n*th-step set invariance approach to the analysis and design of discrete-time linear systems subject to actuator saturation. Systems & Control Letters 60(12): 943–951
- Xie, H. X., Jing, Y. W., Dimirovski, G. M., Chen, J. Q. (2023) Adaptive fuzzy prescribed time tracking control for nonlinear systems with input saturation. ISA Transactions 143: 370–384
- 174. Wu, S. C., Li, X. D. (2022) Finite-time synchronization of complex dynamical networks with input saturation. IEEE Transactions on Cybernetics 54(1): 364–372
- 175. Mi, Y. Z., Yao, J. Y. (2023) Adaptive output feedback control of uncertain nonlinear systems with input saturation. International Journal of Robust and Nonlinear Control 33(13): 7623– 7648
- Shao, K., Zheng, J. C., Tang, R. C., Li, X., Man, Z. H., Liang, B. (2022) Barrier function based adaptive sliding mode control for uncertain systems with input saturation. IEEE/ASME Transactions on Mechatronics 27(6): 4258–4268
- 177. Chen, M. S., Yan, H. C., Zhang, H., Fan, S., Shen, H. (2023) Dual periodic event-triggered control for multi-agent systems with input saturation. ISA Transactions 136: 61–74
- 178. Wang, N., Deng, Z. C. (2020) Finite-time fault estimator based fault-tolerance control for a surface vehicle with input saturations. IEEE Transactions on Industrial Informatics 16(2): 1172–1181
- Cheng, S., Cheng, Z. J., Ren, H. R., Lu, R. Q. (2023) Adaptive fault-tolerant containment control for stochastic nonlinear multi-agent systems with input saturation. Optimal Control Applications & Methods 44(3): 1491–1509
- Song, M. S., Zhang, F., Huang, B. X., Huang, P. F. (2023) Enhanced anti-disturbance control for tethered aircraft system under input saturation and actuator faults. Nonlinear Dynamics 111: 21037–21050
- Ma, Z. Q., Sun, G. H. (2017) Adaptive hierarchical sliding mode control with input saturation for attitude regulation of multi-satellite tethered system. Journal of the Astronautical Sciences 64(2): 207–230
- Cheng, Y., Ye, D., Sun, Z. W., Zhang, S. J. (2018) Spacecraft reorientation control in presence of attitude constraint considering input saturation and stochastic disturbance. Acta Astronautica 144: 61–68

 Fan, L. M., Huang, H., Zhou, K. X. (2020) Robust fault-tolerant attitude control for satellite with multiple uncertainties and actuator faults. Chinese Journal of Aeronautics 33(12): 3380– 3394

- Boskovic, J. D., Li, S. M., Mehra, R. K. (2004) Robust tracking control design for spacecraft under control input saturation. Journal of Guidance, Control, and Dynamics 27(4): 627–633
- 185. Hu, Q. L. (2009) Variable structure maneuvering control with time-varying sliding surface and active vibration damping of flexible spacecraft with input saturation. Acta Astronautica 64(11–12): 1085–1108
- Laib, A. (2000) Adaptive output regulation of robot manipulators under actuator constraints.
   IEEE Transactions on Robotics and Automation 16(1): 29–35
- Tsiotras, P., Jihao, L. (2000) Control of underactuated spacecraft with bounded inputs. Automatica 36(8): 1153–1169
- Wallsgrove, R. J., Akella, M. R. (2005) Globally stabilizing saturated attitude control in the presence of bounded unknown disturbances. Journal of Guidance, Control and Dynamics 28(5): 957–963
- Wie, B., Lu, J. B. (1995) Feedback control logic for spacecraft eigenaxis rotations under slew rate and control constraints. Journal of Guidance, Control, and Dynamics 18(6): 1372–1379
- 190. Xiao, B., Hu, Q. L., Ma, G. (2010) Adaptive sliding mode backstepping control for attitude tracking of flexible spacecraft under input saturation and singularity. Proceedings of the Institution of Mechanical Engineers, Part G: Journal of Aerospace Engineering 224(G2): 199–214
- Bang, H., Tahk, M. J., Choi, H. D. (2003) Large angle attitude control of spacecraft with actuator saturation. Control Engineering Practice 11(9): 989–997
- 192. Huang, Y., Jia, Y. M. (2018) Integrated robust adaptive tracking control of non-cooperative fly-around mission subject to input saturation and full state constraints. Aerospace Science and Technology 79: 233–245
- 193. Huang, S. R., Yang, Y. N., Yan, Y., Zhang, S. F., Liu, Z. Y. (2022) Observer-based robust finite-time trajectory tracking control for a stratospheric satellite subject to external disturbance and actuator saturation. International Journal of Aerospace Engineering 2022 2022(5): 1–19
- 194. Fan, L. M., Huang, H., Sun, L., Zhou, K. X. (2019) Robust attitude control for a rigid-flexiblerigid microsatellite with multiple uncertainties and input saturations. Aerospace Science and Technology 95: 105443
- Sonneveldt, L., Chu, Q. P., Mulder, J. A. (2007) Nonlinear flight control design using constrained adaptive backstepping. Journal of Guidance, Control, and Dynamics 30(2): 322–336
- Boskovic, J. D., Li, S. M., Mehra, R. K. (2001) Robust adaptive variable structure control of spacecraft under control input saturation. Journal of Guidance, Control, and Dynamics 24(1): 14–22
- Ali, I., Radice, G., Kim, J. (2010) Backstepping control design with actuator torque bound for spacecraft attitude maneuver. Journal of Guidance, Control, and Dynamics 33(1): 254–259
- De Ruiter, A. H. J. (2010) Adaptive spacecraft attitude tracking control with actuator saturation. Journal of Guidance, Control, and Dynamics 33(5): 1692–1695
- Zhuang, M. L., Tan, L. G., Li, K. H., Song, S. M. (2021) Fixed-time formation control for spacecraft with prescribed performance guarantee under input saturation. Aerospace Science and Technology 119: 107176
- Atallah, M., Okasha, M., Dief, T. N., Jallad, A. H. (2023) Optimal consensus control for multi-satellite assembly in elliptic orbit with input saturation. Acta Astronautica 208: 82–90
- 201. Hu, Q. L., Li, B., Xiao, B., Zhang, Y. M. (2021) Control allocation for spacecraft under actuator faults. Springer Singapore
- Li, B., Hu, Q. L., Qi, J. T. (2015) Null-space-based optimal control reallocation for spacecraft stabilization under input saturation. International Journal of Adaptive Control and Signal Processing 29(6): 705–724
- Egeland, O., Godhavn, J. M. (1994) Passivity-based adaptive attitude control of a rigid spacecraft. IEEE Transactions on Automatic Control 39(4): 842–846

Lizarralde, F., Wen, J. T. (1996) Attitude control without angular velocity measurement: A
passivity approach. IEEE Transactions on Automatic Control 41(3): 468–472

- Costic, B. T., Dawson, D. M., Kapila, V. (2001) Quaternion-based adaptive attitude tracking controller without velocity measurements. Journal of Guidance, Control, and Dynamics 24(6): 1214–1222
- Subbarao, K., Akella, M. R. (2004) Differentiator-free nonlinear proportional-integral controllers for rigid-body attitude stabilization. Journal of Guidance, Control, and Dynamics 27(6): 1092–1096
- Li, S. H., Ding, S. H., Li, Q. (2010) Global set stabilization of the spacecraft attitude control problem based on quaternion. International Journal of Robust and Nonlinear Control 20(1): 84–105
- Schlanbusch, R., Grotli, E. I., Loria, A., Nicklasson, P. J. (2012) Hybrid attitude tracking of rigid bodies without angular velocity measurement. Systems & Control Letters 61(4): 595–601
- Xie, W. F. (2007) Sliding-mode-observer-based adaptive control for servo actuator with friction. IEEE Transactions on Industrial Electronics 54(3): 1517–1527
- Veluvolu, K. C., Soh, Y. C. (2009) Discrete-time sliding-mode state and unknown input estimations for nonlinear systems. IEEE Transactions on Industrial Electronics 56(9): 3443– 3452
- 211. Chen, M., Shao, S. Y., Jiang, B. (2017) Adaptive neural control of uncertain nonlinear systems using disturbance observer. IEEE Transactions on Cybernetics 47(10): 3110–3123
- Hassani, H., Zarei, J., Chadli, M., Qiu, J. B. (2017) Unknown input observer design for interval type-2 t-s fuzzy systems with immeasurable premise variables. IEEE Transactions on Cybernetics 47(9): 2639–2650
- Zou, A. M., Kumar, K. D., Hou, Z. G. (2012) Attitude coordination control for a group of spacecraft without velocity measurements. IEEE Transactions on Control Systems Technology 20(5): 1160–1174
- Chen, C. L. P., Wen, G. X., Liu, Y. J., Liu, Z. (2016) Observer-based adaptive backstepping consensus tracking control for high-order nonlinear semi-strict-feedback multiagent systems. IEEE Transactions on Cybernetics 46(7): 1591–1601
- Jiang, B. P., Karimi, H. R., Kao, Y. G., Gao, C. C. (2020) Adaptive control of nonlinear semimarkovian jump T-S fuzzy systems with immeasurable premise variables via sliding mode observer. IEEE Transactions on Cybernetics 50(2): 810–820
- Benallouch, M., Boutayeb, M., Zasadzinski, M. (2012) Observer design for one-sided Lipschitz discrete-time systems. Systems & Control Letters 61(9): 879–886
- Cao, Y. C., Ren, W., Meng, Z. Y. (2010) Decentralized finite-time sliding mode estimators and their applications in decentralized finite-time formation tracking. Systems & Control Letters 59(9): 522–529
- Farza, M., MSaad, M., Triki, M., Maatoug, T. (2011) High gain observer for a class of non-triangular systems. Systems & Control Letters 60(1): 27–35
- 219. DiGennaro, S. (2002) Output attitude tracking for flexible spacecraft. Automatica 38(10): 1719–1726
- 220. Song, Y. D., Cai, W. C. (2009) Quaternion observer-based model-independent attitude tracking control of spacecraft. Journal of Guidance, Control, and Dynamics 32(5): 1476–1482
- Seo, D., Akella, M. R. (2008) High-performance spacecraft adaptive attitude-tracking control through attracting-manifold design. Journal of Guidance, Control, and Dynamics 31(4): 884– 891
- 222. Seo, D., Akella, M. R. (2007) Separation property for the rigid-body attitude tracking control problem. Journal of Guidance, Control, and Dynamics 30(6): 1569–1576
- Akella, M. R., Thakur, D., Mazenc, F. (2015) Partial Lyapunov strictification: Smooth angular velocity observers for attitude tracking control. Journal of Guidance, Control, and Dynamics 38(3): 442–451
- Sun, S. H., Zhao, L., Jia, Y. M. (2016) Finite-time output feedback attitude stabilisation for rigid spacecraft with input constraints. IET Control Theory and Applications 10(14): 1740– 1750

 Berkane, S., Abdessameud, A., Tayebi, A. (2016) Global exponential angular velocity observer for rigid body systems. In: IEEE 55th Conference on Decision and Control, Las Vegas, NV, USA, pp 4154

–4159

- Yin, S., Shi, P., Yang, H. Y. (2016) Adaptive fuzzy control of strict-feedback nonlinear timedelay systems with unmodeled dynamics. IEEE Transactions on Cybernetics 46(8): 1926– 1938
- Edwards, C., Spurgeon, S.K. (1998) Sliding mode control: Theory and applications. CRC Press London
- Peng, J. Y., Chen, X. B. (2014) Integrated pid-based sliding mode state estimation and control for piezoelectric actuators. IEEE/ASME Transactions on Mechatronics 19(1): 88–99
- Zhang, J. H., Feng, G., Xia, Y. Q. (2014) Design of estimator-based sliding-mode output-feedback controllers for discrete-time systems. IEEE Transactions on Industrial Electronics 61(5): 2432–2440
- Ahmed-Ali, T., Lamnabhi-Lagarrigue, F. (1999) Sliding observer-controller design for uncertain triangular nonlinear systems. IEEE Eransactions on Automatic Control 44(6): 1244–1249
- Orlov, Y., Aoustin, Y., Chevallereau, C. (2011) Finite time stabilization of a perturbed double integrator-Part I: continuous sliding mode-based output feedback synthesis. IEEE Transactions on Automatic Control 56(3): 614–618
- Shen, Y. J., Huang, Y. H., Gu, J. (2011) Global finite-time observers for lipschitz nonlinear systems. IEEE Transactions on Automatic Control 56(2): 418–424
- Daly, J. M., Wang, D. W. L. (2009) Output feedback sliding mode control in the presence of unknown disturbances. Systems & Control Letters 58(3): 188–193
- Hammouri, H., Bornard, G., Busawon, K. (2010) High gain observer for structured multioutput nonlinear systems. IEEE Transactions on Automatic Control 55(4): 987–992
- 235. Kalsi, K., Lian, J. M., Hui, S. F., Zak, S. H. (2010) Sliding-mode observers for systems with unknown inputs: A high-gain approach. Automatica 46(2): 347–353
- 236. Chen, W. T., Saif, M. (2008) Output feedback controller design for a class of mimo nonlinear systems using high-order sliding-mode differentiators with application to a laboratory 3-d crane. IEEE Transactions on Industrial Electronics 55(11): 3985–3997
- Liu, J. X., Laghrouche, S., Wack, M. (2014) Observer-based higher order sliding mode control of power factor in three-phase AC/DC converter for hybrid electric vehicle applications. International Journal of Control 87(6): 1117–1130
- Liu, J., Laghrouche, S., Harmouche, M., Wack, M. (2014) Adaptive-gain second-order sliding mode observer design for switching power converters. Control Engineering Practice 30(SI): 124–131
- 239. He, W., Sam, S. Z. (2015) Dynamic modeling and vibration control of a flexible satellite. IEEE Transactions on Aerospace and Electronic Systems 51(2): 1422–1431
- 240. Gao, H. J., Yang, X. B., Shi, P. (2009) Multi-objective robust  $\mathcal{H}_{\infty}$  control of spacecraft rendezvous. IEEE Transactions on Control Systems Technology 17(4): 794–802
- 241. Du, H. B., Qian, C. J., Yang, S. Z., Li, S. H. (2013) Recursive design of finite-time convergent observers for a class of time-varying nonlinear systems. Automatica 49(2): 601–609
- Davila, J., Fridman, L., Levant, A. (2005) Second-order sliding-mode observer for mechanical systems. IEEE Transactions on Automatic Control 50(11): 1785–1789
- 243. Menard, T., Moulay, E., Perruquetti, W. (2010) A global high-gain finite-time observer. IEEE Transactions on Automatic Control 55(6): 1500–1506
- 244. Tan, C. P., Yu, X. H., Man, Z. H. (2010) Terminal sliding mode observers for a class of nonlinear systems. Automatica 46(8): 1401–1404
- Akella, M. R. (2001) Rigid body attitude tracking without angular velocity feedback. Systems & Control Letters 42(4): 321–326
- He, W., Huang, H. F., Ge, S. S. (2017) Adaptive neural network control of a robotic manipulator with time-varying output constraints. IEEE Transactions on Cybernetics 47(10): 3136–3147
- Schlanbusch, R., Loria, A., Kristiansen, R., Nicklasson, P. J. (2012) PD + based output feedback attitude control of rigid bodies. IEEE Transactions on Automatic Control 57(8): 2146–2152

 Nicosia, S., Tomei, P. (1992) Nonlinear observer and output feedback attitude control of spacecraft. IEEE Transactions on Aerospace and Electronic Systems 28(4): 970–977

- Ailon, A., Segev, R., Arogeti, S. (2004) A simple velocity-free controller for attitude regulation of a spacecraft with delayed feedback. IEEE Transactions on Automatic Control 49(1): 125– 130
- Abdessameud, A., Tayebi, A. (2009) Attitude synchronization of a group of spacecraft without velocity measurements. IEEE Transactions on Aautomatic Control 54(11): 2642–2648
- Tayebi, A., Roberts, A., Benallegue, A. (2013) Inertial vector measurements based velocityfree attitude stabilization. IEEE Transactions on Aautomatic Control 58(11): 2893–2898
- Safaei, F., Namvar, M. (2014) Observer-free control of satellite attitude using a single vector measurement. IEEE Transactions on Aerospace and Electronic Systems 50(3): 2070–2081
- Kristiansen, R., Loria, A., Chaillet, A., Nicklasson, P. J. (2009) Spacecraft relative rotation tracking without angular velocity measurements. Automatica 45(3): 750–756
- Akella, M. R., Valdivia, A., Kotamraju, G. R. (2005) Velocity-free attitude controllers subject to actuator magnitude and rate saturations. Journal of Guidance, Control, and Dynamics 28(4): 659–666
- Mayhew, C. G., Sanfelice, R. G., Teel, A. R. (2011) Quaternion-based hybrid control for robust global attitude tracking. IEEE Transactions on Automatic Control 56(11): 2555–2566
- Berkane, S., Tayebi, A. (2017) Construction of synergistic potential functions on SO(3) with application to velocity-free hybrid attitude stabilization. IEEE Transactions on Automatic Control 62(1): 495–501
- Filipe, N., Valverde, A., Tsiotras, P. (2016) Pose tracking without linear and angular-velocity feedback using dual quaternions. IEEE Transactions on Aerospace and Electronic Systems 52(1): 411–422
- Shen, Q., Yue, C. F., Goh, C.H. (2017) Velocity-free attitude reorientation of a flexible spacecraft with attitude constraints. Journal of Guidance, Control, and Dynamics 40(5): 1289–1295
- 259. Wong, H., Queiroz, M. S., Kapila, V. (2001) Adaptive tracking control using synthesized velocity from attitude measurements. Automatica 37(6): 947–953
- Kristiansen, R., Nicklasson, P. J., Gravdahl, J. T. (2009) Satellite attitude control by quaternion-based backstepping. IEEE Transactions on Control Systems Technology 17(1): 227–232
- Zou, A. M., Kumar, K. D. (2010) Adaptive attitude control of spacecraft without velocity measurements using chebyshev neural network. Acta Astronautica 66(5): 769–779
- Nagashio, T., Kida, T. S. (2009) Robust control of flexible mechanical systems by utilizing symmetry and its application to large space structures. IEEE Transactions on Control Systems Technology 17(3): 671–680
- Jin, E., Sun, Z. W. (2010) Passivity-based control for a flexible spacecraft in the presence of disturbances. International Journal of Non-Linear Mechanics 45(4): 348–356
- 264. Wang, W., Menon, P. P., Bates, D. G., Bennani, S. (2010) Robustness analysis of attitude and orbit control systems for flexible satellites. IET Control Theory and Applications 4(12): 2958–2970
- Meng, Q., Zhang, T., Song, J. Y. (2013) Modified model-based fault-tolerant time-varying attitude tracking control of uncertain flexible satellites. Proceedings of the Institution of Mechanical Engineers, Part G: Journal of Aerospace Engineering 227(11): 1827–1841
- Sales, T. P., Rade, D. A., de Souza, L. C. G. (2013) Passive vibration control of flexible spacecraft using shunted piezoelectric transducers. Aerospace Science and Technology 29(1): 403–412
- Lim, T. W. (2014) Thruster attitude control system design and performance for tactical satellite 4 maneuvers. Journal of Guidance, Control, and Dynamics 37(2): 403–412
- Pukdeboon, C., Jitpattanakul, A. (2017) Anti-unwinding attitude control with fixed-time convergence for a flexible spacecraft. International Journal of Aerospace Engineering 2017: 1–13
- Chen, C. C., Xu, S. S. D., Liang, Y. W. (2016) Study of nonlinear integral sliding mode fault-tolerant control. IEEE/ASME Transactions on Mechatronics 21(2): 1160–1168

 Bang, H., Ha, C. K., Kim, J. H. (2005) Flexible spacecraft attitude maneuver by application of sliding mode control. Acta Astronautica 57(11): 841–850

- Lu, K. F., Xia, Y. Q. (2015) Finite-time attitude stabilization for rigid spacecraft. International Journal of Robust and Nonlinear Control, 25(1): 32–51
- 272. Jing, C., Xu, H., Niu, X., Song, X. (2019) Adaptive nonsingular terminal sliding mode control for attitude tracking of spacecraft with actuator faults. IEEE Access 7: 31485–31493
- Zhu, Z., Xia, Y., Fu, M. (2011) Attitude stabilization of rigid spacecraft with finite-time convergence. International Journal of Robust and Nonlinear Control 21(6): 686–702
- 274. Zhou, N., Xia, Y., Wang, M., Fu, M. (2015) Finite-time attitude control of multiple rigid spacecraft using terminal sliding mode. International Journal of Robust and Nonlinear Control 25(12): 1862–1876
- Zhong, C., Wu, L., Guo, J., Guo, Y., Chen, Z. (2018) Robust adaptive attitude manoeuvre control with finite-time convergence for a flexible spacecraft. Transactions of the Institute of Measurement and Control 40(2): 425–435
- Tiwari, P. M., Janardhanan, S., Nabi, M. (2016) Attitude control using higher order sliding mode. Aerospace Science and Technology 54: 108–113
- Lu, K., Xia, Y. (2013) Adaptive attitude tracking control for rigid spacecraft with finite-time convergence. Automatica 49(12): 3591–3599
- Lu, K., Xia, Y., Fu, M., Yu, C. (2016) Adaptive finite-time attitude stabilization for rigid spacecraft with actuator faults and saturation constraints. International Journal of Robust and Nonlinear Control 26(1): 28–46
- 279. Zou, A. M., Kumar, K. D. (2019) Finite-time attitude control for rigid spacecraft subject to actuator saturation. Nonlinear Dynamics 96(2): 1017–1035
- 280. Smaeilzadeh, S. M., Golestani, M. (2019) A finite-time adaptive robust control for a spacecraft attitude control considering actuator fault and saturation with reduced steady-state error. Transactions of the Institute of Measurement and Control 41(4): 1002–1009
- Nunes, E. V. L., Hsu, L., Lizarralde, F. (2009) Global exact tracking for uncertain systems using output-feedback sliding mode control. IEEE Transactions on Automatic Control 54(5): 1141–1147
- Aouaouda, S., Chadli, M., Boukhnifer, M., Karimi, H.R. (2015) Robust fault tolerant tracking controller design for vehicle dynamics: A descriptor approach. Mechatronics 30: 316–326
- 283. Yin, S., Gao, H., Qiu, J., Kaynak, O. (2017) Descriptor reduced-order sliding mode observers design for switched systems with sensor and actuator faults. Automatica 76: 282–292
- Yin, S., Xiao, B. (2017) Tracking control of surface ships with disturbance and uncertainties rejection capability. IEEE/ASME Transactions on Mechatronics 22(3): 1154–1162
- Choi, Y. C., Ahn, H. S. (2015) Nonlinear control of quadrotor for point tracking: Actual implementation and experimental tests. IEEE/ASME Transactions on Mechatronics 20(3): 1179–1192
- 286. Wang, Y., Gu, L., Xu, Y., Cao, X. (2016) Practical tracking control of robot manipulators with continuous fractional-order nonsingular terminal sliding mode. IEEE Transactions on Industrial Electronics 63(10): 6194–6204
- Tanaka, M., Tanaka, K., Matsuno, F. (2015) Approximate path-tracking control of snake robot joints with switching constraints. IEEE/ASME Transactions on Mechatronics 20(4): 1633–1641
- Eielsen, A. A., Vagia, M., Gravdahl, J. T., Pettersen, K. Y. (2014) Damping and tracking control schemes for nanopositioning. IEEE/ASME Transactions on Mechatronics 19(2): 432–444

# Chapter 2 Preliminaries



#### 2.1 Introduction

Since the terminology used in the field of satellite attitude control and stability analysis of nonlinear systems is not unique and differs among authors, this chapter starts with brief notations and expressions frequently used throughout the book. Following that, some mathematical lemmas and definitions are introduced to facilitate theoretical analysis in the rest of this book. The attitude control system of rigid or flexible satellites is then modeled. This chapter finishes with the testbeds used to verify the effectiveness of the subsequent modeling error compensation-based attitude control approaches.

#### 2.2 Notation

The notation in this book is fairly standard. Let  $\mathbb{R}$  be the set of the real numbers and  $\mathbb{R}_+$  be the set of the positive real numbers. The set of m by n real matrices is denoted as  $\mathbb{R}^{m\times n}$ . For the sets  $\mathcal{S}_1\subseteq\mathbb{R}^n$  and  $\mathcal{S}_2\subseteq\mathbb{R}^n$ ,  $\mathcal{S}_1\backslash\mathcal{S}_2$  denotes the set  $\{x\in\mathbb{R}^n:x\in\mathcal{S}_1,x\notin\mathcal{S}_2\}$ .  $I_n\in\mathbb{R}^{n\times n}$  is the  $n\times n$  identity matrix.  $\mathbf{0}$  is a zero vector or matrix having an appropriate dimension. For any matrix  $A\in\mathbb{R}^{m\times n}$ ,  $A^T$  denotes its transpose,  $A^\dagger$  represents its pseudo inverse,  $A^{-1}$  is its left inverse if A has full column rank, and  $A^2=A^TA$ .  $||\cdot||$  stands for the Euclidean norm for vectors or the induced matrix norm for matrices.  $\det(\cdot)$  denotes the determinant of a square matrix. The space of all signals which are globally bounded and square-integrable on  $[0,t_f)$ ,  $t_f\in\mathbb{R}_+$  or  $t_f=+\infty$ , are denoted by  $\mathcal{L}_\infty[0,t_f)$  and  $\mathcal{L}_2[0,t_f)$ , respectively.  $\lambda_{\min}(A)$  and  $\lambda_{\max}(A)$  are the minimum and the maximum eigenvalue of  $A\in\mathbb{R}^{m\times m}$ , respectively.  $\ln(\cdot)$ ,  $\exp(\cdot)$ ,  $\tanh(\cdot)$ ,  $\operatorname{sech}(\cdot)$ ,  $\cosh(\cdot)$ , and  $\operatorname{sgn}(\cdot)$  are the logarithmic, the exponential, the hyperbolic tangent, the hyperbolic secant, the hyperbolic cosine, and the sign function, respectively.

36 2 Preliminaries

For two given vectors  $\mathbf{x} = [x_1, x_2, \dots, x_n]^T \in \mathbb{R}^n$  and  $\mathbf{y} = [y_1, y_2, \dots, x_n]^T \in \mathbb{R}^n$  and a given positive scalar  $\ell \in \mathbb{R}_+$ ,  $\mathbf{x}^\ell \in \mathbb{R}^n$ ,  $\sqrt{\mathbf{x}} \in \mathbb{R}^n$ ,  $\frac{\mathbf{x}}{\mathbf{y}} \in \mathbb{R}^n$ ,  $\lfloor \mathbf{x} \rfloor^m \in \mathbb{R}^n$ , and  $|\mathbf{x}| \in \mathbb{R}^n$  are five vectors defined as  $\mathbf{x}^\ell = [x_1^\ell, x_2^\ell, \dots, x_n^\ell]^T$ ,  $\sqrt{\mathbf{x}} = [\sqrt{x_1}, \sqrt{x_2}, \dots, \sqrt{x_n}]^T$ ,  $\frac{\mathbf{x}}{\mathbf{y}} = [\frac{x_1}{y_1}, \frac{x_2}{y_2}, \dots, \frac{x_n}{y_n}]^T$ ,  $\lfloor \mathbf{x} \rfloor^\ell = [|x_1|^\ell \operatorname{sgn}(x_1), |x_2|^\ell \operatorname{sgn}(x_2), \dots, |x_n|^\ell \operatorname{sgn}(x_n)|]^T$ , and  $|\mathbf{x}| = [|x_1|, |x_2|, \dots, |x_n|]^T$ , respectively; the partial differential of scalar function  $h(\mathbf{x}) \in \mathbb{R}$  with regard to  $\mathbf{x}$  is defined as  $\nabla_{\mathbf{x}} h(\mathbf{x}) \in \mathbb{R}^n$ ; the partial differential of a set of functions  $h(\mathbf{x}) \in \mathbb{R}^\ell$  with respect to  $\mathbf{x}$  is given as  $\nabla_{\mathbf{x}} h(\mathbf{x}) \in \mathbb{R}^{\ell \times n}$ ; the ball  $\mathcal{B}_\ell(\mathbf{x}) = \{\mathbf{y} \in \mathbb{R}^n : ||\mathbf{y} - \mathbf{x}|| < \ell\}$  is also defined;  $\mathbf{x} \leq \mathbf{y}$  means that  $x_i \leq y_i$  holds for all  $i = 1, 2, \dots, n$ . diag $(\mathbf{x}) \in \mathbb{R}^{n \times n}$  denotes a diagonal matrix with  $\mathbf{x}$  as the vector of diagonal entries of such a matrix.  $\operatorname{sgn}(\mathbf{x}) \in \mathbb{R}^n$ ,  $\operatorname{ln}(\mathbf{x}) \in \mathbb{R}^n$ , and  $\operatorname{tanh}(\mathbf{x}) \in \mathbb{R}^n$  are defined with their ith argument given by  $\operatorname{sgn}(x_i)$ ,  $\operatorname{ln}(x_i)$ ,  $\operatorname{cosh}(x_i)$ , and  $\operatorname{tanh}(x_i)$ , respetively,  $i = 1, 2, \dots, n$ . Two matrices  $\operatorname{Sech}(\mathbf{x}) = \operatorname{diag}([\operatorname{sech}(x_1), \operatorname{sech}(x_2), \dots, \operatorname{sech}(x_n)]^T) \in \mathbb{R}^{n \times n}$  and  $\operatorname{Cosh}(\mathbf{x}) = \operatorname{diag}([\operatorname{cosh}(x_1), \operatorname{cosh}(x_2), \dots, \operatorname{cosh}(x_n)]^T) \in \mathbb{R}^{n \times n}$  are also defined.  $\operatorname{sat}(\mathbf{x}, \ell_{\max}) \in \mathbb{R}^n$  is a vector-valued saturation function as  $\operatorname{sat}(\mathbf{x}, \ell_{\max}) = [\operatorname{sat}(x_1), \operatorname{sat}(x_2), \dots, \operatorname{sat}(x_n)]^T$ ,  $\ell_{\max} \in \mathbb{R}_+$ , where

$$\operatorname{sat}(x_i) = \begin{cases} \ell_{\max}, & \text{if } x_i > \ell_{\max} \\ x_i, & \text{if } -\ell_{\max} \le x_i \le \ell_{\max} \\ -\ell_{\max}, & \text{if } x_i < -\ell_{\max} \end{cases}$$
 (2.1)

Moreover, for any given vector  $\boldsymbol{v} = [v_1, v_2, v_3]^T \in \mathbb{R}^3, \boldsymbol{v}^{\times} \in \mathbb{R}^{3\times 3}$  denotes the skew-symmetric matrix defined as

$$\boldsymbol{v}^{\times} = \begin{bmatrix} 0 & -\upsilon_3 & \upsilon_2 \\ \upsilon_3 & 0 & -\upsilon_1 \\ -\upsilon_2 & \upsilon_1 & 0 \end{bmatrix}$$
 (2.2)

#### 2.3 Mathematical Definition

Consider a nonlinear system

$$\dot{x} = f(x, d, t), x(0) = x_0$$
 (2.3)

where  $x \in \mathbb{R}^n$  is the system state,  $f : \mathbb{R}^n \times \mathbb{R}^m \times \mathbb{R}_+ \to \mathbb{R}^n$  is a nonlinear function and piecewise continuous in t, and  $d \in \mathbb{R}^m$  is the modeling error or external disturbance. The solution of (2.3) which starts from the point  $x_0$  at t = 0 is denoted as  $x(t, x_0)$ . Moreover, the origin x = 0 is the unique equilibrium point of (2.3).

#### **Definition 2.1** The origin of (2.3) is

- Lyapunov stable: there is  $\delta > 0$  such that for any  $\mathbf{x}_0 \in \mathbb{R}^n$ , if  $\mathbf{x}_0 \in \mathcal{B}_{\delta}(\mathbf{0})$  then  $\mathbf{x}(t, \mathbf{x}_0) \in \mathcal{B}_{\delta}(\mathbf{0})$  for all  $t \geq 0$ .
- *Asymptotically stable*: if it is Lyapunov stable and  $\lim_{t\to\infty} \mathbf{x}(t, \mathbf{x}_0) = \mathbf{0}$  for any  $\mathbf{x}_0 \in \mathbb{R}^n$ .
- Globally exponentially stable: if  $||\mathbf{x}(t, \mathbf{x}_0)|| \le k||\mathbf{x}_0||e^{-\alpha t}$  is satisfied for any  $\mathbf{x}_0 \in \mathbb{R}^n$ ,  $k \in \mathbb{R}_+$ ,  $\alpha \in \mathbb{R}_+$ .
- Uniformly ultimately bounded stable: if exists a ball  $\mathcal{B}_{\delta}(\mathbf{0})$  such that for all  $\mathbf{x}_0 \in \mathcal{B}_{\delta}(\mathbf{0})$ , there is a constant  $\varsigma \in \mathbb{R}_+$  and a constant  $T(\varsigma) \in \mathbb{R}_+$  satisfying  $||\mathbf{x}(t, \mathbf{x}_0)|| \leq \varsigma$  for all  $t \geq T(\varsigma)$ .
- *Finite-time stable*: if it is Lyapunov stable and for any  $x_0 \in \mathbb{R}^n$  there exists  $0 < t_T < \infty$  such that  $x(t, x_0) = \mathbf{0}$  for all  $t > t_T$ . The function  $T(x_0) = \inf\{t_T \ge 0 : x(t, x_0) = \mathbf{0}, \forall t \ge t_T\}$  is called the *settling-time function* of (2.3).
- *Fixed-time stable*: if it is finite-time stable and the settling-time function of (2.3),  $T(\mathbf{x}_0)$ , is bounded on  $\mathbb{R}^n$ , i.e., there exists  $T_{\max}$  satisfying  $\sup_{\mathbf{x}_0 \in \mathbb{R}^n} T(\mathbf{x}_0) \le T_{\max} < \infty$ .

**Definition 2.2** [1] The origin of (2.3) is *practically fixed-time stable*, if it is Lyapunov stable and there exists a bounded set  $\mathcal{D}_1 \subseteq \mathbb{R}^n$  and a scalar  $T_f \in \mathbb{R}_+$  such that for any  $r \in \mathbb{R}_+$  and any state starting within the ball  $\mathcal{B}_r(\mathbf{0})$  converges to  $\mathcal{D}_1$  in the time  $T_f$  and stays in  $\mathcal{D}_1$  thereafter.

**Definition 2.3** [2] The origin of (2.3) is *practically exponentially stable* if there exists  $r \in \mathbb{R}_+$ ,  $\gamma_1 \in \mathbb{R}_+$ , and  $\gamma_2 \in \mathbb{R}_+$  such that  $||x(t, x_0)|| \le r + \gamma_2 ||x_0|| e^{-\gamma_1 t}$ .

**Definition 2.4** [3] Let  $\gamma \in \mathbb{R}_+$  be a given constant, then the origin of (2.3) is said to be stabilized with  $\mathcal{L}_2$  gain disturbance attenuation level of  $\gamma$  from the disturbance d to the state x, if the following inequality holds for any  $\mu \in \mathbb{R}_+$ .

$$\int_{0}^{T} ||\boldsymbol{x}(t, \boldsymbol{x}_{0})||^{2} dt \leq \gamma^{2} \int_{0}^{T} ||\boldsymbol{d}||^{2} dt + \mu, \forall \boldsymbol{d} \in \mathcal{L}_{2}[0, T), \forall T \in \mathbb{R}$$
 (2.4)

# 2.4 Preliminary Lemmas

**Lemma 2.1** For a given vector  $\mathbf{x} = [x_1, x_2, \dots, x_n]^T \in \mathbb{R}^n$ , it follows that  $\frac{1}{2} \tanh^2(x_i) \leq \ln(\cosh(x_i))$ ,  $||\mathbf{Sech}^2(\mathbf{x})|| = 1$ , and  $\tanh^T(\mathbf{x}) \tanh(\mathbf{x}) \leq \mathbf{x}^T \tanh^T(\mathbf{x})$ ,  $i = 1, 2, \dots, n$ .

38 2 Preliminaries

**Lemma 2.2** [4] For a given vector  $\mathbf{x} = [x_1, x_2, ..., x_n]^T \in \mathbb{R}^n$  and any two positive constants statisfying  $0 < c_1 \le 1$  as well as  $c_2 > 1$ , then

$$\left(\sum_{i=1}^{n} |x_i|\right)^{c_1} \le \sum_{i=1}^{n} |x_i|^{c_1}, \left(\sum_{i=1}^{n} |x_i|\right)^{c_2} \le n^{c_2 - 1} \sum_{i=1}^{n} |x_i|^{c_2}$$
(2.5)

**Lemma 2.3** [5] Let v and  $\rho$  be real-value functions defined in  $\mathbb{R}_+$ , and let b and c be positive constants. If they satisfy the differential inequality

$$\dot{\upsilon} < -c\upsilon + b\rho(t)^2, \upsilon(0) > 0 \tag{2.6}$$

then the following inequality holds:

(i) If  $\rho \in \mathcal{L}_{\infty}[0, +\infty)$ , then  $\upsilon \in \mathcal{L}_{\infty}[0, +\infty)$  and

$$\upsilon(t) \le \upsilon(0) \exp(-ct) + \frac{b}{c} ||\rho||_{\infty}^{2}$$
(2.7)

(ii) If  $\rho \in \mathcal{L}_2[0, +\infty)$ , then  $\upsilon \in \mathcal{L}_\infty[0, +\infty)$  and

$$v(t) \le v(0) \exp(-ct) + b||\rho||_2^2$$
 (2.8)

**Lemma 2.4** [6] The origin of (2.3) is practically fixed-time stable, if there is a positive function  $V(x) \in \mathbb{R}$  satisfying

$$\dot{V}(x) \le -\alpha_0 V^{r_1}(x) - \beta_0 V^{r_2}(x) + \rho \tag{2.9}$$

where  $\alpha_0 \in \mathbb{R}_+$ ,  $\beta_0 \in \mathbb{R}_+$ ,  $r_1 > 1$ ,  $0 < r_2 < 1$ , and  $\rho \in \mathbb{R}_+$  are positive constants. Moreover, the state  $\mathbf{x}(t, \mathbf{x}_0)$  converges into the residual set:

$$\mathcal{D}_1 = \left\{ \boldsymbol{x}(t, \boldsymbol{x}_0) : V(\boldsymbol{x}) \le \min \left\{ \left( \frac{l}{\alpha_0} \right)^{\frac{1}{r_1}}, \left( \frac{l}{\beta_0} \right)^{\frac{1}{r_2}} \right\} \right\}$$
 (2.10)

with  $l = \frac{\rho}{1-\theta}$  and the constant  $0 < \theta < 1$ . The finite-time  $T_{max} \in \mathbb{R}_+$  required to reach into  $\mathcal{D}_1$  is bounded by

$$T_{\text{max}} \le \frac{1}{\alpha_0(r_1 - 1)} + \frac{1}{\beta_0(1 - r_2)}, \forall \mathbf{x}_0 \in \mathbb{R}^n$$
 (2.11)

#### 2.5 Definition of Reference Frames

This section describes different reference frames for representing the satellite's position and attitude. Those reference frames are shown in Fig. 2.1.

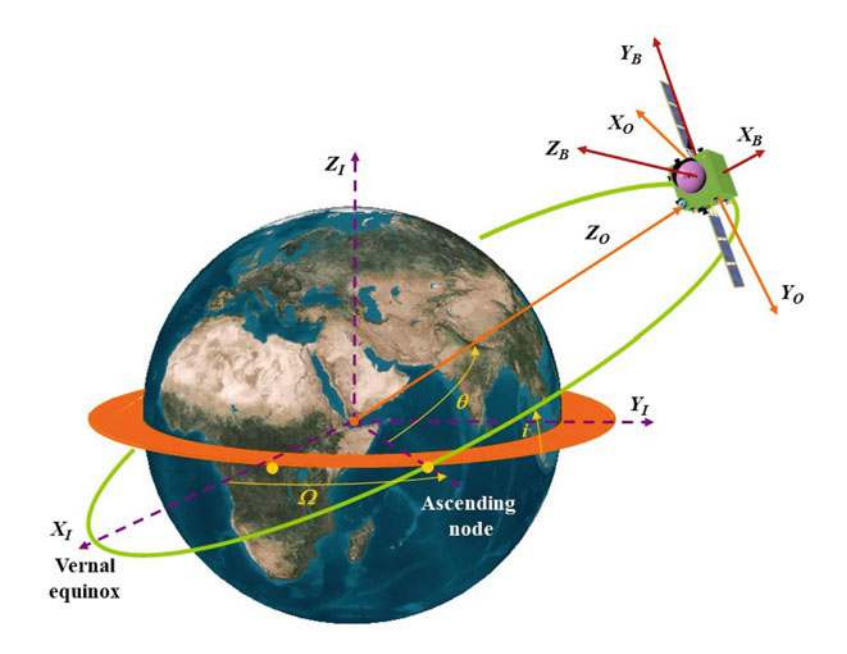


Fig. 2.1 The Earth-centered inertial, the body, and the orbit reference frames

#### 2.5.1 Earth-Centered Inertial Frame

The Earth-centered inertial frame  $\mathcal{F}_I$  is an inertial frame for terrestrial navigation. The frame is fixed in space. This means that it is a non-accelerated reference frame in which Newton's Laws are valid. The origin of this frame is oriented at the center of Earth. The x-axis points toward the point where the plane of the Earth's orbit toward the Sun, crosses the Equator going from South to North. z-axis points toward the North pole. y-axis completes the right-hand Cartesian coordinate system. This defines a right-handed orthogonal body coordinate frame  $(X_I, Y_I, Z_I)$ .

#### 2.5.2 Orbit Frame

The orbit frame  $\mathcal{F}_O$  rotates relative to the Earth-centered inertial frame, with an orbital rate depending on the altitude of the satellite. The origin O is at the center of the mass of the satellite. The x-axis is toward the direction of motion tangentially to the orbit. The tangent is only perpendicular to the radius vector in the circular orbit and does not align with the velocity vector of the satellite in elliptical orbits. The z-axis points toward the center of Earth. The y-axis is perpendicular to the orbital plane and completes the right-hand system  $(X_O, Y_O, Z_O)$ .

40 2 Preliminaries

# 2.5.3 Body Frame

This frame  $\mathcal{F}_B$  is a moving reference frame fixed on the satellite. The orientation of the satellite is determined relative to the orbit frame. The angular velocity is expressed in the body frame. The *x*-axis is forward and the *z*-axis is downward. The *y*-axis completes the right hand orthogonal system  $(X_B, Y_B, Z_B)$ . The origin O is at the center of the mass of the satellite. Its axes are fixed in the satellite body and coincide with the principal axis of inertia.

# 2.6 Attitude Representation

# 2.6.1 Euler Angles

The Euler angles are an intuitive way to represent satellite attitude with explicit physical meanings. The foundation of Euler angles is the Euler theorem, that is the rotation of a rigid body around one fixed point can be regarded as the composition of several finite rotations around the fixed point [7].

The orientation of the satellite's body-fixed frame  $\mathcal{F}_B$  with respect to  $\mathcal{F}_O$  involves three successive Euler angles rotations. In practical aerospace missions, it is possible to bring a rigid body into an arbitrary orientation by performing three successive rotations that involve the axes fixed in the Earth-centered inertial frame [8, 9]. As shown in Fig. 2.2,  $\mathcal{F}_B$  is first transformed into the intermediate frame 1 via a rotation about the  $Z_B$  axis by the angle  $\psi$ . This is followed by a rotation about the new  $X_1$  axis by an angle  $\phi$ . Finally, the satellite's pitch angle,  $\theta$ , defines the rotation about the new  $Y_2$ . Figure 2.3 shows a 3D representation of the Euler angles describing the orientation of the body-fixed frame  $\mathcal{F}_B$  with respect to the orbit frame  $\mathcal{F}_O$ . According to the preceding rotation, the physical meanings of the three Euler angles are presented as follows.

• The yaw angle  $\psi \in \mathbb{R}$ : It is the angle between the axis  $OX_O$  in the frame  $\mathcal{F}_O$  and the projection on the local level of the  $OX_B$  axis in the frame  $\mathcal{F}_B$ .

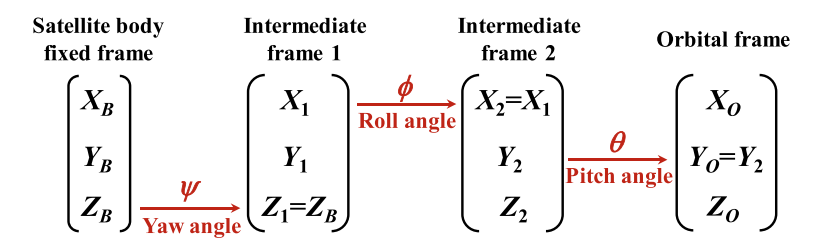


Fig. 2.2 Euler angles

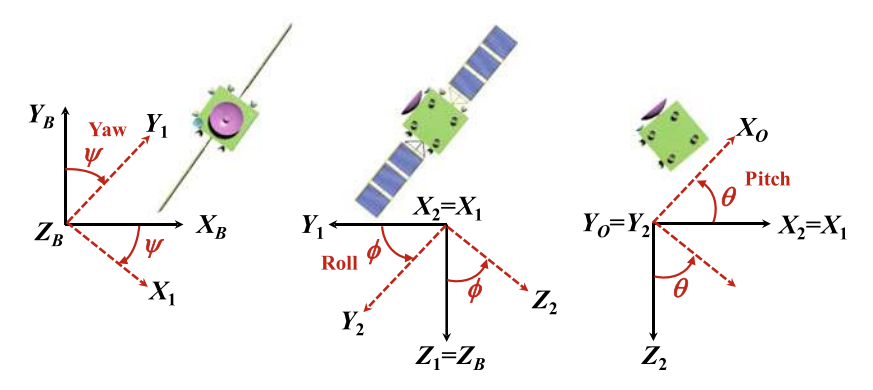


Fig. 2.3 Euler rotation

- The roll angle  $\phi \in \mathbb{R}$ : It is the angle between the pitch axis  $OY_B$  in the frame  $\mathcal{F}_B$  and its projection on the local level.
- The pitch angle  $\theta \in \mathbb{R}$ : It is the angle between the roll axis  $OX_B$  in the frame  $\mathcal{F}_B$  and its projection on the local level.

# 2.6.2 Unit Quaternion

According to [8, 9], the unit quaternion is another widely utilized method to represent the satellite attitude. On the basis of the Euler theorem, four attitude parameters composed by the Euler axis/angles can be presented in the form of

$$\mathbf{Q} = [q_0, \mathbf{q}^{\mathrm{T}}]^{\mathrm{T}} = [q_0, q_1, q_2, q_3]^{\mathrm{T}} = \left[\cos\frac{\Phi}{2}, e_x \sin\frac{\Phi}{2}, e_y \sin\frac{\Phi}{2}, e_z \sin\frac{\Phi}{2}\right]^{\mathrm{T}}$$
(2.12)

where  $\bar{\boldsymbol{e}} = [e_x, e_y, e_z]^{\mathrm{T}} \in \mathbb{R}^3$  is the Euler rotation axis satisfying  $e_x^2 + e_y^2 + e_z^2 = 1$ ,  $\Phi \in \mathbb{R}$  is the rotation angle around the Euler rotation axis,  $\boldsymbol{q} = [q_1, q_2, q_3]^{\mathrm{T}} \in \mathbb{R}^3$ , and  $q_0^2 + q_1^2 + q_2^2 + q_3^2 = 1$ .

# 2.6.3 Modified Rodrigues Parameters

According to [9], the modified Rodrigues parameters (MRPs) based attitude presentation is a three-parameter and non-redundant attitude description method. Given a Euler rotation angle  $\Phi \in \mathbb{R}$  about the Euler principal axis  $n \in \mathbb{R}^3$ , the attitude orientation of the satellite in  $\mathcal{F}_B$  with respect to  $\mathcal{F}_I$  can be represented by the MRPs vector  $\boldsymbol{\sigma} = [\sigma_1, \sigma_2, \sigma_3]^T$  and

42 2 Preliminaries

$$\sigma = n \tan\left(\frac{\Phi}{4}\right), \, \Phi \in [0^\circ, 360^\circ) \tag{2.13}$$

Moreover, the mathematical relationship between the MRPs  $\sigma$  and the unit quaternion Q defined in (2.13) is given by

$$\sigma_i = \frac{q_i}{1+q_0}, i = 1, 2, 3$$
 (2.14)

# 2.7 Modeling of Satellite Attitude Control System

The mathematical model of the attitude control system of any satellite consists of two parts. One is the attitude kinematics and the other is the attitude dynamics.

#### 2.7.1 Attitude Kinematics

In this section, the attitude kinematics of the satellite is modeled by using the Euler angles, the unit quaternion, and the modified Rodrigues parameters.

#### A Attitude Kinematics via Euler Angles

When the Euler angles are used to represent the attitude of the satellite, its attitude kinematics can be described as [10]

$$\dot{\mathbf{\Theta}} = \mathbf{R}^{-1}(\mathbf{\Theta})(\boldsymbol{\omega} + \boldsymbol{\omega}_c(\mathbf{\Theta})) \tag{2.15}$$

where  $\boldsymbol{\Theta} = [\theta, \phi, \psi]^T$  is the attitude Euler angles vector of the satellite with respect to the orbit frame  $\mathcal{F}_O$  obtained by a yaw-pitch-roll  $(\psi - \phi - \theta)$  sequence of rotations.  $\boldsymbol{\omega} = [\omega_1, \omega_2, \omega_3]^T \in \mathbb{R}^3$  is the satellite's angular velocity with respect to  $\mathcal{F}_I$  and expressed in the body-fixed frame  $\mathcal{F}_B$ .  $\boldsymbol{R}(\boldsymbol{\Theta}) \in \mathbb{R}^{3 \times 3}$  and  $\boldsymbol{\omega}_c(\boldsymbol{\Theta}) \in \mathbb{R}^3$  are defined as

$$\mathbf{R}(\mathbf{\Theta}) = \begin{bmatrix} 1 & 0 & -\sin\phi \\ 0 & \cos\theta & \cos\phi\sin\theta \\ 0 - \sin\theta\cos\phi\cos\phi \end{bmatrix}$$
(2.16)

$$\boldsymbol{\omega}_{c}(\boldsymbol{\Theta}) = \omega_{0} \begin{bmatrix} \sin \psi \cos \phi \\ \cos \psi \cos \theta + \sin \psi \sin \theta \sin \phi \\ -\cos \psi \sin \theta + \sin \psi \cos \theta \sin \phi \end{bmatrix}$$
(2.17)

where  $\omega_0 \in \mathbb{R}_+$  is the satellite's orbital rate. It can be calculated by  $\omega_0 = \sqrt{\frac{\mu_e}{a_c^3}}$  is satellite orbital rate,  $a_c \in \mathbb{R}_+$  is the distance from the center of Earth to the satellite's

center of mass, and  $\mu_e \in \mathbb{R}_+$  is the gravitational parameter of Earth. The term  $\boldsymbol{\omega}_b = [\omega_{b1}, \omega_{b2}, \omega_{b3}]^T = \boldsymbol{R}(\boldsymbol{\Theta})\dot{\boldsymbol{\Theta}}$  actually is the satellite angular velocity with respect to  $\mathcal{F}_O$ .

**Remark 2.1** It is obtained from (2.16) that  $det(\mathbf{R}(\mathbf{\Theta})) = \cos \phi$ . Hence, the following equation should be met such that  $\mathbf{R}(\mathbf{\Theta})$  is invertible, and then the attitude kinematics (2.15) remains valid for  $t \ge 0$ ,

$$\phi(t) \neq \frac{N\pi}{2}, \forall t \ge 0 \tag{2.18}$$

where N is an odd integer. To ensure (2.18), the initial pitch angle  $\phi(0)$  can be restricted such that  $-\frac{\pi}{2} < \phi(0) < \frac{\pi}{2}$ , and then the controller should be designed to achieve  $-\frac{\pi}{2} < \phi(t) < \frac{\pi}{2}$  for t > 0. The restriction on  $\phi(0)$  is a mild condition, which is satisfied in practice. That is because the attitude stabilization maneuver is usually performed before the attitude tracking maneuvering in aerospace engineering. After the attitude stabilization maneuver, the satellite attitude will be stabilized with small attitude angles deviation, that is,  $-\frac{\pi}{2} < \theta < \frac{\pi}{2}$ ,  $-\frac{\pi}{2} < \phi < \frac{\pi}{2}$ , and  $-\frac{\pi}{2} < \psi < \frac{\pi}{2}$  can be guaranteed.

**Remark 2.2** In addition to the Euler angles (EAs), the unit quaternion (UO), the rotation matrix (RM), and the Rodriguez parameters (RPs), as well as its modified version (MRPs), can also be applied to represent the attitude. Each attitude representation method has its advantages and disadvantages. For example, the unwinding phenomena will occur in the satellite attitude system design if its attitude is represented by using the UO. In comparison with UO, RM, RPs, and MRPs, the EAs can explicitly provide the attitude control designer with a satellite's physical orientation angles in space. This is the reason that the Euler attitude angles representation is widely applied in satellite attitude control engineering. Additionally, it is easily obtained that only a restriction  $-\frac{\pi}{2} < \phi(t) < \frac{\pi}{2}$ ,  $t \ge 0$  is imposed, and there is not any restriction on the roll and the yaw attitude angles. The roll attitude angle and the yaw attitude angle can be  $-\pi < \theta < \pi$  and  $-\pi < \psi < \pi$ , respectively. For practical aerospace engineering, the pitch attitude angle satisfying  $-\frac{\pi}{2} < \phi(t) < \frac{\pi}{2}$  is quite large for the tracking missions. Therefore, based on the aforementioned analysis, the Euler attitude angle representation is confirmed to be appropriate for the large-angle attitude maneuver.

#### **B** Attitude Kinematics via Unit Quaternion

When the unit quaternion is adopted to represent the attitude of the satellite, its attitude kinematics can be modeled as

$$\dot{\boldsymbol{q}} = \frac{1}{2} (\boldsymbol{q}^{\times} + q_0 \boldsymbol{I}_3) \boldsymbol{\omega} \tag{2.19}$$

$$\dot{q}_0 = -\frac{1}{2} \boldsymbol{q}^{\mathrm{T}} \boldsymbol{\omega} \tag{2.20}$$

44 2 Preliminaries

where  $\boldsymbol{\omega} = [\omega_1, \omega_2, \omega_3]^T$  represents the angular velocity of the body with respect to the frame  $\mathcal{F}_I$  and expressed in body-fixed frame  $\mathcal{F}_B$ . The unit quaternion  $\boldsymbol{Q} = [q_0, \boldsymbol{q}^T]^T \in \mathbb{R} \times \mathbb{R}^3$  describes the attitude orientation of the satellite in frame  $\mathcal{F}_B$  with respect to the Earth-centered inertial frame  $\mathcal{F}_I$  with  $\boldsymbol{q}^T\boldsymbol{q} + q_0^2 = 1$  satisfied.

#### C Attitude Kinematics via MRPs

When the MRPs are used to represent the attitude of the satellite, its attitude kinematics can be modeled as [11]

$$\dot{\sigma} = G(\sigma)\omega \tag{2.21}$$

where the matrix  $G(\sigma) \in \mathbb{R}^{3\times 3}$  is given as

$$G(\sigma) = \frac{1}{4}((1 - \sigma^{\mathsf{T}}\sigma)I_3 + 2\sigma^{\mathsf{X}} + 2\sigma\sigma^{\mathsf{T}})$$
 (2.22)

**Property 2.1** The matrix  $G(\sigma)$  satisfies

$$\boldsymbol{G}^{\mathrm{T}}(\boldsymbol{\sigma})\boldsymbol{G}(\boldsymbol{\sigma}) = \left(\frac{1+\boldsymbol{\sigma}^{\mathrm{T}}\boldsymbol{\sigma}}{4}\right)^{2}\boldsymbol{I}_{3}, \boldsymbol{G}^{-1}(\boldsymbol{\sigma}) = \frac{16}{(1+\boldsymbol{\sigma}^{\mathrm{T}}\boldsymbol{\sigma})}\boldsymbol{G}^{\mathrm{T}}(\boldsymbol{\sigma})$$
(2.23)

**Remark 2.3** As a complete revolution is performed, this particular MRPs set goes singular. As shown in [12], the original MRPs vector and its corresponding shadow counterpart  $\sigma^s = -\frac{\sigma}{\sigma^T \sigma}$  could be used to represent satellite's attitude rotation to avoid the singularity problem.

# 2.7.2 Attitude Dynamics

In aerospace engineering, the satellite having large flexible appendages is called flexible satellite. Otherwise, it is named as rigid satellite. The attitude dynamics for both types of satellite is modeled in this section.

#### A Attitude Dynamics of Rigid Satellite

The attitude dynamics of a rigid satellite can be described by [10]

$$J\dot{\omega} = -S(\omega)J\omega + u + u_d \tag{2.24}$$

where  $\boldsymbol{u} = [u_1, u_2, u_3]^{\mathrm{T}} \in \mathbb{R}^3$  is the total control torque generated by actuators and applied to the satellite. The positive-definite matrix  $\boldsymbol{J} \in \mathbb{R}^{3 \times 3}$  is the total inertia of such rigid satellite.  $\boldsymbol{u}_d = [u_{d1}, u_{d2}, u_{d3}]^{\mathrm{T}} \in \mathbb{R}^3$  is the unknown torque generated by the modeling error in the dynamics of such rigid satellite.

#### **B** Attitude Dynamics of Flexible Satellite

The attitude dynamics of a flexible satellite can be found from the Euler-Lagrange analysis. It is described as [10, 13]

$$J\dot{\omega} = -\omega^{\times}(J\omega + \delta\dot{\eta}) - \delta\ddot{\eta} + u + u_d \tag{2.25}$$

$$\ddot{\boldsymbol{\eta}} + \boldsymbol{\Xi}\dot{\boldsymbol{\eta}} + \boldsymbol{\Lambda}^2 \boldsymbol{\eta} + \boldsymbol{\delta}^{\mathrm{T}}\dot{\boldsymbol{\omega}} = \mathbf{0}$$
 (2.26)

where the matrix  $\boldsymbol{J} \in \mathbb{R}^{3 \times 3}$  is positive-definite and denotes the total inertia of such flexible satellite,  $\boldsymbol{\delta} \in \mathbb{R}^{3 \times N}$  is the coupling matrix between the elastic structures and rigid dynamics,  $\boldsymbol{\eta} \in \mathbb{R}^N$  is the modal coordinate vector relative to the main body.  $\boldsymbol{\Xi} = \operatorname{diag}([2\Xi_1\Lambda_1, 2\Xi_2\Lambda_2, \ldots, 2\Xi_N\Lambda_N]^T) \in \mathbb{R}^{N \times N}$  is the modal damping matrix,  $\boldsymbol{\Lambda}^2 = \operatorname{diag}([\Lambda_1^2, \Lambda_2^2, \ldots, \Lambda_N^2]^T) \in \mathbb{R}^{N \times N}$  is the stiffness matrix, and  $N \in \mathbb{R}_+$  is the number of elastic modes considered, where  $\Xi_i \in \mathbb{R}$  is the damping ratio, and  $\Lambda_i \in \mathbb{R}$  is the modal frequency,  $i = 1, 2, \ldots, N$ .  $\boldsymbol{u}_d = [u_{d1}, u_{d2}, u_{d3}]^T \in \mathbb{R}^3$  is the uncertain torque generated by the modeling error in the dynamics of such flexible satellite.  $\boldsymbol{u} = [u_1, u_2, u_3]^T \in \mathbb{R}^3$  is the total control torque generated by all actuators.

Remark 2.4 The attitude dynamics (2.25) and (2.26) are established by computing the kinetic and the potential energies and then applying the Lagrange equations. The elastic displacement of the flexible appendages is assumed to be small. Note that (2.25) and (2.26) are quite standard and precise to describe the dynamics of the rigid and the flexible part of the satellite. When investigating flexible satellite attitude control problem, almost all the existing controllers were designed based on (2.25) and (2.26).

#### 2.8 Attitude Control Testbed for Satellite

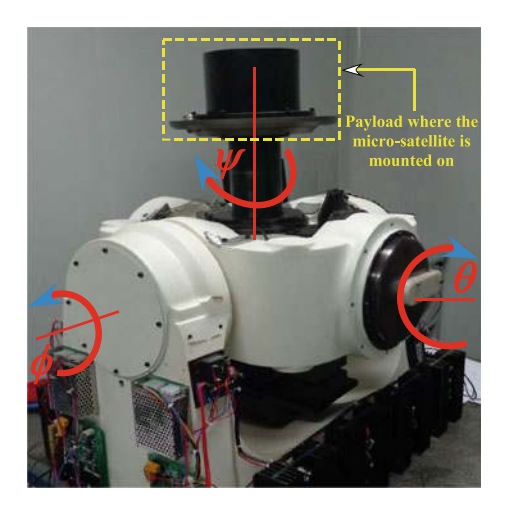
A simulation study is not enough for attitude control verification. Hardware-in-loop tests on the ground are further requested to verify the performance of attitude controllers. At this time, experimental testbeds are necessitated. Currently such testbeds are classified into non-air-bearing and air-bearing. Three types of testbeds applied to test the controllers in this book are introduced in this section.

# 2.8.1 Three-Axis Non-Air-Bearing Simulator

Figure 2.4 shows a three-degrees-of-freedom simulator for attitude control testing. Each degree of freedom is actuated by SGMAH servomotors manufactured by Yaskawa Electric. The encoder mounted to each servomotor is RON786C from HEIDENHAIN, Inc. Each encoder has 3600 lines, which yields a resolution of 14400 pulses/rev after the A and B signals from the encoder have been processed by Interpo-

46 2 Preliminaries

**Fig. 2.4** The non-air-bearing three-degrees-of-freedom testbed



lation and Digitizing Electronics IBV 600 from HEIDENHAIN, Inc. The controller core of the simulator is a TMS320F2812 digital signal processor that obtains position information, calculates control algorithms, and sends control efforts to the regulated current converter through a 12-bit digital-to-analog converter and some analog signal processing circuits. The sampling period is 0.25 seconds. In the experimental system, a personal computer was used to develop the control program written in C language, to compile it, to download the resulting code into the digital signal processor for execution, and to acquire experimental data. When carrying out tests, the considered satellite will be mounted on the payload.

# 2.8.2 Single-Axis Air-Bearing Testbed

Figure 2.5 shows a single-axis air-bearing suspending rotary testbed to verify the validity of the attitude controllers. This testbed consists of an air-bearing simulator, a flexible beam made from a slender aluminum beam, and some measuring and control instruments. The rigid hub and the flexible beam are suspended by air-bearing to simulate the state of zero gravity in space. The vibrations of the flexible beam are measured by an accelerometer installed on the tip of the beam. The rotary angle of the table is measured by combination of an inductosyn with an angle digital display meter. The system uses thruster and reaction wheels as actuators. The maximum torque that can be generated by the reaction wheel is 0.15 N·m. An optical fiber rate gyro is used to measure rotation angular velocity. In the experimental system, a personal xPC-based computer was used to develop the control program written in C language, to compile it, to download the resulting code into the core controller for execution, and to acquire experimental data.

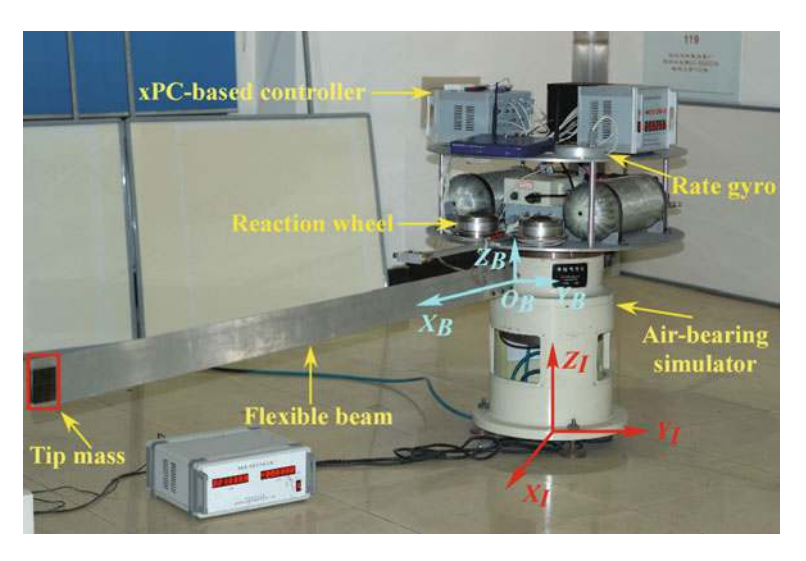


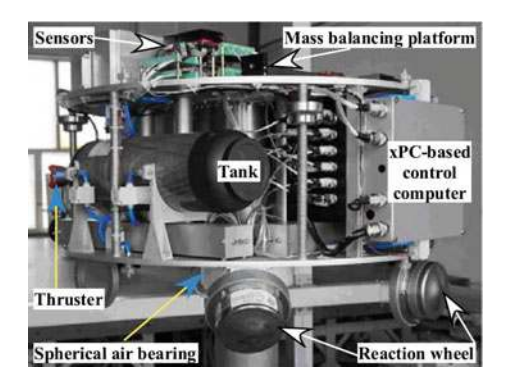
Fig. 2.5 The single-axis attitude air-bearing testbed

# 2.8.3 Three-Axis Air-Bearing Testbed

Figure 2.6 shows a scaling satellite three-axis attitude dynamics and control simulator. This simulator is a three-degrees-of-freedom experimental testbed for validation of guidance, navigation, and control (GNC) schemes for satellites. It can ensure full freedom in the yaw axis,  $\pm 30$  degrees in the pitch axis, and  $\pm 20$  degrees in the roll axis. The simulator includes a three-axis spherical air bearing to simulate the zero-gravity laboratory environment. Three reaction wheels are fixed on each axis, respectively, to achieve attitude control. Six cold-gas thrusters with a compressed air tank for thruster air supply are distributed about the simulator to provide rotational motion around the roll, the pitch, and the yaw axis. The simulator's center of gravity is maintained by using a mass balancing platform a triad of linear actuators. In the simulator, there are three orthogonally mounted single-axis rate gyros, a threeaxis magnetometer, and three-axis accelerator, to achieve attitude determination. At the core of the simulator is an xPC-based control computer. The developed attitude control system runs entirely on this computer with the hardware-in-the-loop. The power needed by the testbed is supplied by a battery charger located off the simulator. A desktop computer is also located off of the testbed. It communicates with the computer on the simulator for data acquisition and display.

48 2 Preliminaries

**Fig. 2.6** The three-axis attitude air-bearing testbed



# 2.9 Summary

This is a preliminary chapter. Mathematical notations, some basic definitions, and mathematical lemmas related to nonlinear system stability were presented, which are useful to the development and theoretical analysis of attitude control approaches to be developed in the rest of this book. The reference frames used to represent satellite's attitude were introduced. The mathematical model of the satellite's attitude control system was then given. At last, three types of testbeds applied to test the attitude control approaches were elaborated.

#### References

- Tian, B., Zuo, Z., Yan, X., Wang, H. (2017) A fixed-time output feedback control scheme for double integrator systems. Automatica 80: 17–24
- Benabdallah, A., Ellouze, I., Hammami, M. A. (2009) Practical stability of nonlinear timevarying cascade systems. Journal of Dynamical and Control Systems 15(1): 45–62
- 3. Schaft, A. V. D. (2000) L<sub>2</sub>-gain and passivity techniques in nonlinear control. London: Springer
- Zuo, Z. Y. (2015) Nonsingular fixed-time consensus tracking for second-order multi-agent networks. Automatica 54: 305–309
- Krstic, M., Kanellakopoulos, I., Kokotovic, P. V. (1995) Nonlinear and adaptive control design. NewYork: John Wiley
- Polyakov, A. (2012) Nonlinear feedback design for fixed-time stabilization of linear control systems. IEEE Transactions on Automatic Control 57(8): 2106–2110
- 7. Quan, Q. (2017) Introduction to multicopter design and control. Singapore: Springer Nature
- 8. Wie, B. (2008) Space vehicle dynamics and control. USA, AIAA
- 9. Hu, Q. L., Li, B., Xiao, B., Zhang, Y. M. (2021) Control allocation for spacecraft under actuator faults. Singapore: Springer Nature
- Xiao, B., Hu, Q. L., Zhang, Y. M. (2012) Adaptive sliding mode fault tolerant attitude tracking control for flexible spacecraft under actuator saturation. IEEE Transactions on Control Systems Technology 20(6): 1605–1612
- Zou, A. M., Kumar, K. D. (2010) Adaptive attitude control of spacecraft without velocity measurements using chebyshev neural network. Acta Astronautica 66(5): 769–779

 Schaub, H., Akella, M. R., Junkins, J. L. (2001) Adaptive control of nonlinear attitude motions realizing linear closed loop dynamics. Journal of Guidance, Control, and Dynamics 24(1): 95–100

13. Yu, Y. N., Meng, X. Y., Li, K. Y., Xiong, F. F. (2014) Robust control of flexible spacecraft during large-angle attitude maneuver. Journal of Guidance, Control, and Dynamics 37(3): 1027–1033

# Part II Modeling Error Robust Compensation Attitude Control

# Chapter 3 Observer-Free Output Feedback Attitude Control



#### 3.1 Introduction

Most aerospace tasks require satellites to perform large-angle attitude tracking maneuvers [1, 2]. Many investigations on large-angle attitude controller design have been reported to accomplish these maneuvers. The work in [3] was an earlier attempt to achieve this objective. An adaptive attitude controller was presented. However, modeling error was not handled; moreover, a linearized model was used, even though this model may not fully and well characterize the satellite dynamics. A simple controller demanding minimum onboard computations was presented in [4] for large pitch-angle maneuver without considering any modeling error. To address the problem of fast and large-angle attitude control, a robust control law was developed for flexible satellites [5]. In [6], the robust large-angle attitude control problem with modeling error due to external disturbance and delayed control inputs was investigated. In [7], a model predictive controller was designed for satellites to perform the large-angle attitude maneuvers with input-to-state stability ensured. To the authors' best knowledge, few studies have been seen on angular velocity observer-free attitude control design for satellites with modeling error due to external disturbances [8]. Although this was achieved in [9] with the attitude stabilized with good accuracy, the structure of the controller was complicated.

Motivated by addressing the preceding challenges and drawbacks, this chapter mainly focuses on designing a practical engineering approach to achieve a large-angle attitude tracking maneuver for rigid satellites. It only requires the attitude output for feedback. This chapter is the extension of [10]. Unlike [10], the linearization error and the modeling error due to external disturbances are considered when presenting the mathematical model. Moreover, experimental tests are conducted. The main contributions of this chapter are listed as follows.

Unlike the angular velocity observer-based attitude control strategies, the presented
control framework does not need any observer for the unmeasured angular velocity. The controller has a simple structure to achieve a large-angle attitude tracking
maneuver. In comparison with the conventional intelligent attitude control strate-

gies such as the neural-network-based controllers and the fuzzy theory-based controllers, the proposed scheme demands inexpensive onboard computations. Hence, this approach shows more practical application potential.

- This proposed angular velocity observer-free attitude control is an improvement over the existing observer-free attitude output feedback control schemes [11], because the controller in this chapter is developed with modeling error induced by external disturbance explicitly considered. Applying the result in [11], the attitude tracking maneuver and practical stability may be accomplished in the presence of external disturbances by providing sufficiently large control gains to dominate the disturbance through knowledge of an upper limit. However, when the external disturbances are considered, rigorous stability analysis is not presented in [11]. In contrast, the stability of the closed-loop system from the designed approach is rigorously theoretically proved despite external disturbances; moreover, high control accuracy is ensured by the synthesized velocity-free controller despite such modeling error.
- Although the main result of this chapter is developed on the basis of the linearized attitude system, in comparison with the Proportional-Integral-Derivative (PID) control law for the linearized attitude system, the proposed control approach does not ignore the linearization error. Therefore, it renders the presented scheme more practically suitable for large-angle attitude tracking maneuvers.

# 3.2 Transformed Open-Loop Attitude System

In this chapter, rigid satellite is considered with its products of inertia ignored. Only the principal moment of inertia is considered. Moreover, the attitude is represented by the Euler angles. Then, the rigid satellite's inertia matrix can be denoted as  $J = \text{diag}([J_1, J_2, J_3]^T) \in \mathbb{R}^{3\times 3}$ . Like the conventional attitude control design in practical engineering, a linearized vector is first introduced as

$$\boldsymbol{a} = [\dot{\theta} - \omega_0 \psi, \dot{\phi} - \omega_0, \dot{\psi} + \omega_0 \theta]^{\mathrm{T}}$$
(3.1)

Based on (3.1), one can rewrite the attitude kinematics (2.15) as

$$\boldsymbol{\omega} = \boldsymbol{a} + \Delta \boldsymbol{f}_1(\boldsymbol{\Theta}, \dot{\boldsymbol{\Theta}}) \tag{3.2}$$

where  $\Delta f_1(\mathbf{\Theta}, \dot{\mathbf{\Theta}}) = \mathbf{R}(\mathbf{\Theta})\dot{\mathbf{\Theta}} - \boldsymbol{\omega}_c(\mathbf{\Theta}) - \boldsymbol{a}$  is the linearization error.

**Remark 3.1** Although a linearized term (3.1) is introduced to transform the attitude kinematics into (3.2), it is different from the traditional method [12, 13] to linearize the attitude kinematics. That is because the linearization error,  $\Delta f_1$ , is not ignored in (3.2). The results in [12] and [13] were presented by assuming that the satellite has only a small attitude deviation from the orientation of  $\mathcal{F}_0$  and, hence, the linearization error  $\Delta f_1$  is ignored.

3.3 Problem Statement 55

From (3.2), the attitude dynamics (2.24) of the rigid satellite can be rewritten into an open-loop system given by

$$J\ddot{\Theta} + M\dot{\Theta} + N\Theta = u + u_d + \Delta f_2 + \Delta f_3$$
 (3.3)

where  $N = \omega_0^2 \text{diag}([J_2 - J_3, 0, J_2 - J_1]^T)$ , and

$$\mathbf{M} = -\omega_0(J_1 + J_3 - J_2) \begin{bmatrix} 0 & 0 & 1 \\ 0 & 0 & 0 \\ -1 & 0 & 0 \end{bmatrix}$$
(3.4)

$$\Delta \boldsymbol{f}_{2} = -(\Delta \boldsymbol{f}_{1})^{\times} \boldsymbol{J} (\boldsymbol{a} + \Delta \boldsymbol{f}_{1}) - \boldsymbol{a}^{\times} \boldsymbol{J} \Delta \boldsymbol{f}_{1} - \boldsymbol{J} \frac{d(\Delta \boldsymbol{f}_{1})}{dt}$$
(3.5)

$$\Delta \mathbf{f}_{3} = \begin{bmatrix} (J_{2} - J_{3})\dot{\phi}(\dot{\psi} + \omega_{0}\theta) \\ (J_{3} - J_{1})(\dot{\theta}\dot{\psi} + \omega_{0}\theta\dot{\theta} - \omega_{0}\psi\dot{\psi} - \omega_{0}^{2}\theta\psi) \\ (J_{1} - J_{2})\dot{\phi}(\dot{\theta} - \omega_{0}\dot{\psi}) \end{bmatrix}$$
(3.6)

It can be inferred from (3.3) that  $\Delta f_2$  and  $\Delta f_3$  are induced by the linearization error  $\Delta f_1$ . These two items explicitly appear in the transformed dynamics (3.3). They may deteriorate the attitude control accuracy especially when the large-angle attitude tracking maneuver is being performed. Hence, the linearization error should be fully considered in attitude controller design.

#### 3.3 Problem Statement

In this chapter, the environment disturbance torques are considered only in the modeling error. This means that the inertia J is known. Let  $\Theta_d = [\theta_d, \phi_d, \psi_d]^{\rm T} \in \mathbb{R}^3$  (known, while  $\dot{\Theta}_d$  and  $\ddot{\Theta}_d$  are bounded and continuous) with  $-\frac{\pi}{2} < \phi_d < \frac{\pi}{2}$  be the planned attitude trajectory to be followed, given any angular velocity and the initial attitude such that  $-\frac{\pi}{2} < \phi(0) < \frac{\pi}{2}$ , the control problem can be stated as: For rigid satellites with their attitude system described by (2.15) and (2.24), using the attitude feedback  $\Theta$  only to design an observer-free controller for u to maneuver the large-angle attitude tracking. The trajectory  $\Theta_d$  is followed with high accuracy.  $-\frac{\pi}{2} < \phi(t) < \frac{\pi}{2}$  is ensured for  $t \geq 0$  by choosing appropriate gains for the designed controller. Moreover, the controller should be synthesized without angular velocity measurements and also without any observer for the unmeasured angular velocity.

# 3.4 Angular Velocity-Free Robust Controller

Let  $\Theta_e = \Theta - \Theta_d$  be the attitude tracking error and  $\omega_e = \dot{\Theta} - \dot{\Theta}_d$  be the velocity tracking error. The modeling errors  $\Delta f_2$ ,  $\Delta f_3$ , and the external disturbance  $u_d$  are lumped as a system uncertainty  $d \in \mathbb{R}^3$ , that is

$$d = u_d + \Delta f_2 + \Delta f_3 \tag{3.7}$$

Then, the transformed open-loop system (3.3) can be reformed as

$$J\ddot{\Theta} + M\dot{\Theta} + N\Theta = u + d \tag{3.8}$$

To this end, the main solution to the large-angle attitude tracking problem with attitude output feedback only is given in the following theorem, while the measurements of angular velocity are not needed.

**Theorem 3.1** Consider the rigid satellites with their attitude model described by (2.15) and (2.24), let an angular velocity-free robust controller be developed as

$$\boldsymbol{u} = -k_p \boldsymbol{\Theta}_e - k_d \boldsymbol{v}_e + \boldsymbol{J} \ddot{\boldsymbol{\Theta}}_d + \boldsymbol{M} \dot{\boldsymbol{\Theta}}_d + \boldsymbol{N} \boldsymbol{\Theta}$$
 (3.9)

and  $\mathbf{v}_e \in \mathbb{R}^3$  is synthesized as  $\mathbf{v}_e = \mathbf{\Theta}_c + \kappa \mathbf{\Theta}_e$ ,  $\mathbf{\Theta}_c$  satisfies

$$\dot{\mathbf{\Theta}}_c = -k_f(\mathbf{\Theta}_c + \kappa \mathbf{\Theta}_e) \tag{3.10}$$

where  $k_p \in \mathbb{R}_+$ ,  $k_d \in \mathbb{R}_+$ ,  $k_f \in \mathbb{R}_+$ , and  $\kappa \in \mathbb{R}_+$  are four scalars. If these four gains are selected to satisfy

$$k_p > 4\delta_1^2 \|\boldsymbol{J}\| \tag{3.11}$$

$$k_d > 4\kappa \delta_2^2 \|\boldsymbol{J}\| \tag{3.12}$$

$$\delta_2 k_p \kappa \lambda_{\min}(\boldsymbol{J}) \ge 4\delta_1 \|\boldsymbol{M}\|^2 \tag{3.13}$$

$$k_d k_p k_f \delta_1 \ge 4\kappa (k_d \delta_1 + k_p \delta_2)^2 \tag{3.14}$$

$$k_d k_f \lambda_{\min}(\boldsymbol{J}) \ge 4\delta_2 (k_f \|\boldsymbol{J}\| + ||\boldsymbol{M}||)^2$$
 (3.15)

$$2\delta_1 k_p - 1 > 0 (3.16)$$

$$\frac{k_d k_f}{2\kappa} - k_d \delta_2 - \frac{1}{4} > 0 \tag{3.17}$$

$$2\delta_2 \kappa \lambda_{\min}(\boldsymbol{J}) - 4\delta_1 \lambda_{\max}(\boldsymbol{J}) - 4\|\boldsymbol{M}\| - 1 > 0$$
 (3.18)

with  $\delta_1 \in \mathbb{R}_+$  and  $\delta_2 \in \mathbb{R}_+$  being two constants such that  $0 < \delta_1 < 1$ ,  $0 < \delta_2 < 1$ , respectively; then it follows that:

(R1): The  $\mathcal{L}_2$ -gain disturbance attenuation with a level of  $\gamma$  is achieved if  $\mathbf{d} \in \mathcal{L}_2[0, T)$ , where  $\gamma = \sqrt{\frac{\delta_1^2 + \delta_2^2 + 1}{\rho}}$ , and

$$\rho = \min \left\{ \frac{\frac{\delta_1 k_p}{2} - \frac{1}{4}}{\lambda_{\max}(\boldsymbol{D}_1)}, \frac{\frac{k_d k_f}{2\kappa} - k_d \delta_2 - \frac{1}{4}}{\lambda_{\max}(\boldsymbol{D}_2)}, \frac{\frac{\delta_2 \kappa \lambda_{\min}(\boldsymbol{J})}{2} - \delta_1 \lambda_{\max}(\boldsymbol{J}) - \|\boldsymbol{M}\| - \frac{1}{4}}{\lambda_{\max}(\boldsymbol{D}_1) + \lambda_{\max}(\boldsymbol{D}_2)} \right\}$$
(3.19)

where  $D_1$  and  $D_2$  are two constants matrices given by

$$\boldsymbol{D}_{1} = \begin{bmatrix} k_{p} \boldsymbol{I}_{3} & 2\delta_{1} \boldsymbol{J} \\ 2\delta_{1} \boldsymbol{J}^{\mathrm{T}} & \boldsymbol{J} \end{bmatrix}$$
 (3.20)

$$\boldsymbol{D}_2 = \begin{bmatrix} \frac{k_d}{\kappa} \boldsymbol{I}_3 & -2\delta_2 \boldsymbol{J} \\ -2\delta_2 \boldsymbol{J}^{\mathrm{T}} & \boldsymbol{J} \end{bmatrix}$$
(3.21)

(R2): The tracking errors  $\Theta_e$  and  $\omega_e$  are uniformly ultimately bounded if  $d \in \mathcal{L}_{\infty}[0, \infty)$ .

**Remark 3.2** From (3.10) and the definition of  $v_e$ , it follows that that the transfer function between  $v_e$  and  $\Theta_e$  satisfies

$$\mathbf{v}_e(s) = \mathbf{T}(s)\mathbf{\Theta}_e(s), \mathbf{T}(s) = \frac{\kappa s}{s + k_f}$$
 (3.22)

which implies that (3.22) is not an observer, because it does not have control input directly acting on (3.22). Hence, it can be obtained from Theorem 3.1 that the developed control law obviates the use of any observer to the estimation of the unmeasurable angular velocity. The velocity-free attitude control objective with no observer to estimate the unmeasurable velocity is achieved.

**Remark 3.3** Although the linearization technique is applied to obtain the transformed kinematics (3.2) and dynamics (3.3), the linearization errors  $\Delta f_1(\omega_0, \Theta, \dot{\Theta})$ ,  $\Delta f_2$ , and  $\Delta f_3$  are not ignored. Hence, although the controller (3.9) is developed based on the transformed model (3.3), it essentially considers the model uncertainties and linearization errors for the original model (2.15) and (2.24). Based on Remark 2.2 and compared with the control law in [14], the presented scheme is efficient for performing a large-angle attitude maneuver. That is because the controller in [14] was synthesized by assuming a small attitude deviation. However, the controller (3.9) inherently has a simple structure without complicate online computation. Then, it is summarized from these two advantages that the developed control scheme is practically implementation-efficient and is suitable for satellites to perform large-angle attitude maneuvers.

## 3.5 Stability Proof

The Lyapunov stability theory can be applied to prove Theorem 3.1 with the proof organized as: A candidate Lyapunov function is first defined, and then the stability analysis is conducted.

## 3.5.1 Candidate Lyapunov Function

Select a candidate Lyapunov function as  $V = V_1 + V_2$  for the model (2.15) and (2.24), where  $V_1$  and  $V_2$  are defined as

$$V_1 = \frac{1}{2} \boldsymbol{\omega}_e^{\mathrm{T}} \boldsymbol{J} \boldsymbol{\omega}_e + \frac{k_p}{2} \boldsymbol{\Theta}_e^{\mathrm{T}} \boldsymbol{\Theta}_e + \frac{k_d}{2\kappa} \boldsymbol{v}_e^{\mathrm{T}} \boldsymbol{v}_e$$
 (3.23)

$$V_2 = (\delta_1 \mathbf{\Theta}_e - \delta_2 \mathbf{v}_e)^{\mathrm{T}} \boldsymbol{J} \boldsymbol{\omega}_e \tag{3.24}$$

It can be found that

$$V \ge \frac{1}{4} \begin{bmatrix} \mathbf{\Theta}_e \\ \mathbf{\omega}_e \end{bmatrix}^{\mathsf{T}} \mathbf{D}_1 \begin{bmatrix} \mathbf{\Theta}_e \\ \mathbf{\omega}_e \end{bmatrix} + \frac{1}{4} \begin{bmatrix} \mathbf{v}_e \\ \mathbf{\omega}_e \end{bmatrix}^{\mathsf{T}} \mathbf{D}_2 \begin{bmatrix} \mathbf{v}_e \\ \mathbf{\omega}_e \end{bmatrix}$$
(3.25)

$$V \leq \begin{bmatrix} \mathbf{\Theta}_e \\ \mathbf{\omega}_e \end{bmatrix}^{\mathrm{T}} \mathbf{D}_1 \begin{bmatrix} \mathbf{\Theta}_e \\ \mathbf{\omega}_e \end{bmatrix} + \begin{bmatrix} \mathbf{v}_e \\ \mathbf{\omega}_e \end{bmatrix}^{\mathrm{T}} \mathbf{D}_2 \begin{bmatrix} \mathbf{v}_e \\ \mathbf{\omega}_e \end{bmatrix}$$
(3.26)

With the choices of the gains given in (3.11) and (3.12),  $D_1$  and  $D_2$  are ensured to be positive definite. Then, V > 0 always holds for the state  $\mathbf{x} = [\boldsymbol{\Theta}_e^{\mathrm{T}}, \boldsymbol{v}_e^{\mathrm{T}}, \boldsymbol{\omega}_e^{\mathrm{T}}]^{\mathrm{T}} \neq \mathbf{0}$ . Hence, V is proved to be continuously differentiable and positive definite. With respect to the states  $\boldsymbol{\Theta}_e$ ,  $\boldsymbol{v}_e$ , and  $\boldsymbol{\omega}_e$ , V is radically unbounded.

# 3.5.2 Stability Analysis

Inserting the control law (3.9) into the transformed system (3.8) leads to

$$J\ddot{\mathbf{\Theta}}_e + M\omega_e = -k_p\mathbf{\Theta}_e - k_d\mathbf{v}_e + \mathbf{d}$$
 (3.27)

Applying the definition of  $v_e$  and (3.10), one has

$$\dot{\mathbf{v}}_e = -k_f \mathbf{v}_e + \kappa \mathbf{\omega}_e \tag{3.28}$$

3.5 Stability Proof 59

From (3.27) and (3.28), it yields

$$\dot{V}_{1} = \boldsymbol{\omega}_{e}^{\mathrm{T}} \boldsymbol{J} \dot{\boldsymbol{\omega}}_{e} + k_{p} \boldsymbol{\Theta}_{e}^{\mathrm{T}} \dot{\boldsymbol{\Theta}}_{e} + \frac{k_{d}}{\kappa} \boldsymbol{v}_{e}^{\mathrm{T}} \dot{\boldsymbol{v}}_{e} 
= \boldsymbol{\omega}_{e}^{\mathrm{T}} \boldsymbol{d} - \frac{k_{d} k_{f}}{\kappa} \boldsymbol{v}_{e}^{\mathrm{T}} \boldsymbol{v}_{e} - \boldsymbol{\omega}_{e}^{\mathrm{T}} \boldsymbol{M} \boldsymbol{\omega}_{e}$$
(3.29)

$$\dot{V}_{2} = (\delta_{1}\dot{\boldsymbol{\Theta}}_{e} - \delta_{2}\dot{\boldsymbol{v}}_{e})^{\mathrm{T}}\boldsymbol{J}\boldsymbol{\omega}_{e} + (\delta_{1}\boldsymbol{\Theta}_{e} - \delta_{2}\boldsymbol{v}_{e})^{\mathrm{T}}\boldsymbol{J}\dot{\boldsymbol{\omega}}_{e} 
= -\delta_{1}k_{p}\boldsymbol{\Theta}_{e}^{\mathrm{T}}\boldsymbol{\Theta}_{e} - k_{d}\delta_{1}\boldsymbol{\Theta}_{e}^{\mathrm{T}}\boldsymbol{v}_{e} - \delta_{1}\boldsymbol{\Theta}_{e}^{\mathrm{T}}\boldsymbol{M}\boldsymbol{\omega}_{e} + \delta_{1}\boldsymbol{\Theta}_{e}^{\mathrm{T}}\boldsymbol{d} 
+ \delta_{1}\boldsymbol{\omega}_{e}^{\mathrm{T}}\boldsymbol{J}\boldsymbol{\omega}_{e} + k_{p}\delta_{2}\boldsymbol{v}_{e}^{\mathrm{T}}\boldsymbol{\Theta}_{e} + k_{d}\delta_{2}\boldsymbol{v}_{e}^{\mathrm{T}}\boldsymbol{v}_{e} + \delta_{2}\boldsymbol{v}_{e}^{\mathrm{T}}\boldsymbol{M}\boldsymbol{\omega}_{e} 
- \delta_{2}\boldsymbol{v}_{e}^{\mathrm{T}}\boldsymbol{d} - \delta_{2}(-k_{f}\boldsymbol{v}_{e} + \kappa\boldsymbol{\omega}_{e})^{\mathrm{T}}\boldsymbol{J}\boldsymbol{\omega}_{e}$$
(3.30)

Combining (3.29) with (3.30) leads to

$$\dot{\mathbf{V}} \leq -\frac{\delta_{1}k_{p}}{2} \|\mathbf{\Theta}_{e}\|^{2} - \left(\frac{k_{d}k_{f}}{2\kappa} - k_{d}\delta_{2}\right) \|\mathbf{v}_{e}\|^{2} + \delta_{1}\mathbf{\Theta}_{e}^{\mathsf{T}}\mathbf{d} - \delta_{2}\mathbf{v}_{e}^{\mathsf{T}}\mathbf{d} 
- \left(\frac{\delta_{2}\kappa\lambda_{\min}(\mathbf{J})}{2} - \delta_{1}\lambda_{\max}(\mathbf{J}) - \|\mathbf{M}\|\right) \|\boldsymbol{\omega}_{e}\|^{2} + \boldsymbol{\omega}_{e}^{\mathsf{T}}\mathbf{d} 
- \frac{1}{2} \begin{bmatrix} \|\mathbf{\Theta}_{e}\| \\ \|\boldsymbol{\omega}_{e}\| \end{bmatrix}^{\mathsf{T}} \mathbf{D}_{3} \begin{bmatrix} \|\mathbf{\Theta}_{e}\| \\ \|\boldsymbol{\omega}_{e}\| \end{bmatrix} - \frac{1}{2} \begin{bmatrix} \|\mathbf{\Theta}_{e}\| \\ \|\mathbf{v}_{e}\| \end{bmatrix}^{\mathsf{T}} \mathbf{D}_{4} \begin{bmatrix} \|\mathbf{\Theta}_{e}\| \\ \|\mathbf{v}_{e}\| \end{bmatrix} 
- \frac{1}{2} \begin{bmatrix} \|\boldsymbol{\omega}_{e}\| \\ \|\mathbf{v}_{e}\| \end{bmatrix}^{\mathsf{T}} \mathbf{D}_{5} \begin{bmatrix} \|\boldsymbol{\omega}_{e}\| \\ \|\mathbf{v}_{e}\| \end{bmatrix}$$
(3.31)

where

$$\boldsymbol{D}_{3} = \begin{bmatrix} \frac{\delta_{1}k_{p}}{2} & -\delta_{1} \|\boldsymbol{M}\| \\ -\delta_{1} \|\boldsymbol{M}\| & \frac{\delta_{2}\kappa\lambda_{\min}(\boldsymbol{J})}{2} \end{bmatrix}$$
(3.32)

$$\mathbf{D}_{4} = \begin{bmatrix} \frac{\delta_{1}k_{p}}{2} & -k_{d}\delta_{1} - k_{p}\delta_{2} \\ -k_{d}\delta_{1} - k_{p}\delta_{2} & \frac{k_{d}k_{f}}{2\kappa} \end{bmatrix}$$
(3.33)

$$\boldsymbol{D}_{5} = \begin{bmatrix} \frac{\delta_{2}\kappa\lambda_{\min}(\boldsymbol{J})}{2} & -\delta_{2}(k_{f}\|\boldsymbol{J}\| + \|\boldsymbol{M}\|) \\ -\delta_{2}(k_{f}\|\boldsymbol{J}\| + \|\boldsymbol{M}\|) & \frac{k_{d}k_{f}}{2\kappa} \end{bmatrix}$$
(3.34)

Furthermore, applying Young's inequality leads to

$$4\delta_1 \mathbf{\Theta}_e^{\mathsf{T}} d \le \|\mathbf{\Theta}_e\|^2 + 4\delta_1^2 \|d\|^2 \tag{3.35}$$

$$-4\delta_2 \mathbf{v}_e^{\mathrm{T}} \mathbf{d} \le \|\mathbf{v}_e\|^2 + 4\delta_2^2 \|\mathbf{d}\|^2 \tag{3.36}$$

$$4\boldsymbol{\omega}_{e}^{\mathrm{T}}\boldsymbol{d} \leq \|\boldsymbol{\omega}_{e}\|^{2} + 4\|\boldsymbol{d}\|^{2} \tag{3.37}$$

The matrices  $D_3$ ,  $D_4$ , and  $D_5$  are also ensured to be positive definite due to the gains choices in (3.13)–(3.15). Then, (3.31) can be simplified as follows by inserting (3.35)–(3.37)

$$\dot{\mathbf{V}} \leq -\left(\frac{\delta_{1}k_{p}}{2} - \frac{1}{4}\right) \|\mathbf{\Theta}_{e}\|^{2} - \left(\frac{k_{d}k_{f}}{2\kappa} - k_{d}\delta_{2} - \frac{1}{4}\right) \|\mathbf{v}_{e}\|^{2} - \left(\frac{\delta_{2}\kappa\lambda_{\min}(\mathbf{J})}{2} - \delta_{1}\lambda_{\max}(\mathbf{J}) - \|\mathbf{M}\| - \frac{1}{4}\right) \|\boldsymbol{\omega}_{e}\|^{2} + (\delta_{1}^{2} + \delta_{2}^{2} + 1)\|\mathbf{d}\|^{2}$$
(3.38)

In addition, the following can be obtained from (3.26).

$$V \le \lambda_{\max}(\mathbf{D}_1) \|\mathbf{\Theta}_e\|^2 + (\lambda_{\max}(\mathbf{D}_1) + \lambda_{\max}(\mathbf{D}_2)) \|\mathbf{\omega}_e\|^2 + \lambda_{\max}(\mathbf{D}_2) \|\mathbf{v}_e\|^2 \quad (3.39)$$

Because all the control gains are chosen to satisfy (3.16)–(3.18), it follows from (3.19) and (3.39) that

$$\dot{V} \le -\rho \|\boldsymbol{x}\|^2 + (\delta_1^2 + \delta_2^2 + 1) \|\boldsymbol{d}\|^2 \tag{3.40}$$

Based on the preceding analysis, it can be established by the following.

(1) If  $d \in \mathcal{L}_2[0, T)$ , integrating (3.40) from t = 0 to t = T yields

$$\int_{0}^{T} \|\boldsymbol{\Theta}_{e}\|^{2} dt \le \int_{0}^{T} \|\boldsymbol{x}\|^{2} dt \le \frac{V(0)}{\rho} + \gamma^{2} \int_{0}^{T} \|\boldsymbol{d}\|^{2} dt \tag{3.41}$$

Then, using Definition 2.4, (3.41) shows that the closed-loop attitude system is stabilized with  $\mathcal{L}_2$ -gain disturbance attenuation level of  $\gamma$  from the lumped system uncertainty d to the tracking errors  $\Theta_e$  and  $\omega_e$ .

(2) In the case of  $d \in \mathcal{L}_{\infty}[0, \infty)$ , there will have a positive scalar  $d_{\max} \in \mathbb{R}_+$  such that  $\|d\| \le d_{\max}$ . Then, it can be found that (3.40) will be further bounded by

$$\dot{V} \le -\rho \|\mathbf{x}\|^2 + (\delta_1^2 + \delta_2^2 + 1)d_{\text{max}}^2 \tag{3.42}$$

Hence, one has  $\dot{V}<0$  when  ${\bf x}$  is outside of the ball  $\mathcal{B}_{\varepsilon}({\bf 0})$ , where  $\varepsilon=d_{\max}\gamma$ . That is to say, V will decrease monotonically when the state  ${\bf x}$  is not within the ball  $\mathcal{B}_{\varepsilon}({\bf 0})$ . Then, all the signals in the closed-loop system are ensured to be bounded. More specifically, there is a scalar  $T_0\in\mathbb{R}_+$  such that  $\|{\bf \Theta}_e\|\leq \varepsilon, \|{\bf v}_e\|\leq \varepsilon$ , and  $\|{\bf \omega}_e\|\leq \varepsilon$  for  $t\geq T_0$ . Using Definition 2.1,  ${\bf \Theta}_e$  and  ${\bf \omega}_e$  are proved to be uniformly ultimately bounded stable.

#### 3.5.3 Discussions

For any on-orbital satellite, the external disturbances acting on it are bounded practically. Otherwise, the satellite will be out of control. Hence, it should have  $u_d \in \mathcal{L}_{\infty}[0,\infty)$  at least. In addition, the attitude stabilization maneuver is usually performed before the attitude tracking maneuvering in practice. When the attitude stabilization maneuver is finished, the attitude and the rotation velocity  $(\dot{\theta}, \dot{\phi},$  and  $\dot{\psi}$ ) are stabilized with small deviation, that is,  $-\frac{\pi}{2} < \theta < \frac{\pi}{2}, -\frac{\pi}{2} < \phi < \frac{\pi}{2}$  and  $-\frac{\pi}{2} < \psi < \frac{\pi}{2}$  are achieved. Then, the satellite is at least with  $\Theta \in \mathcal{L}_{\infty}[0,\infty)$  and  $\dot{\Theta} \in \mathcal{L}_{\infty}[0,\infty)$  after attitude stabilization maneuvering. Meanwhile, it is seen from the definition of  $\Delta f_1$  that  $\Delta f_1$  is a function of variables  $\Theta$  and  $\dot{\Theta}$ . Hence, one has  $\Delta f_1 \in \mathcal{L}_{\infty}[0,\infty)$  because **J** is also bounded. Moreover, it can be obtained from (3.5) and (3.6) that  $\Delta f_2$  and  $\Delta f_3$  are two functions of the attitude angle  $\Theta$ , the rotation velocity  $\dot{\Theta}$ , and the attitude acceleration  $\ddot{\Theta}$ , which also belongs to  $\mathcal{L}_{\infty}[0,\infty)$  for any on-orbital satellite; otherwise, the satellite's attitude will be uncontrollable. To this end, it follows that  $\Delta f_2 \in \mathcal{L}_{\infty}[0, \infty)$  and  $\Delta f_3 \in \mathcal{L}_{\infty}[0, \infty)$ . Based on these analyses,  $d \in \mathcal{L}_{\infty}[0, \infty)$  can be obtained from (3.7). Therefore, applying (R2) in Theorem 3.1 can conclude that the closed-loop system ensured by the controller (3.9) is at least uniformly ultimately bounded stable.

It is seen from (3.41) that when  $d \in \mathcal{L}_2[0,T)$ , the external disturbance attenuation capability can be improved by choosing appropriate gains to ensure a smaller value for  $\gamma$ . In the case of  $d \in \mathcal{L}_{\infty}[0,\infty)$ , it is known from (3.42) that the control accuracy depends on  $\gamma$ . Smaller  $\gamma$  ensures better attitude tracking accuracy. Hence, from the definition of  $\gamma$  and Theorem 3.1, the following procedures can be followed to select the control gains.

- Step #1: Calculate  $\lambda_{\min}(\boldsymbol{J})$ ,  $\lambda_{\max}(\boldsymbol{J})$ ,  $\|\boldsymbol{M}\|$ , and  $\|\boldsymbol{J}\|$ .
- Step #2: Select small values for  $\delta_1$  and  $\delta_2$  such that  $0 < \delta_2 < 1$  and  $0 < \delta_2 < 1$ . Smaller  $\delta_1$  and  $\delta_2$  will accordingly lead to a smaller  $\gamma$ .
- Step #3: Choose a positive gain  $\kappa$  with (3.18) satisfied.
- Step #4: Select the gain  $k_p$  by satisfying (3.11), (3.13), and (3.16).
- Step #5: Choose positive control gains  $k_d$  and  $k_f$  satisfying (3.12), (3.14), (3.15), and (3.17).
- Step #6: Based on Step #3-#5, tune k<sub>p</sub>, k<sub>d</sub>, κ, and k<sub>f</sub> to have a smaller γ until the
  requirements imposed by the aerospace tasks on the attitude tracking accuracy is
  met.

#### 3.6 Simulation Results

Having proved in Sect. 3.5 that, the developed tracking control framework is capable of maneuvering the large-angle attitude with good control performance, this section will apply a currently being developed satellite example to validate this effectiveness.

This satellite has a circular orbit with its altitude 650 km. The inclination of the satellite's orbit is 92.5 degrees. In accordance, the orbital rate of this satellite is  $\omega_0 = 0.0011$  rad/s. The satellite's inertia is  $J_1 = 50$  kg·m<sup>2</sup>,  $J_2 = 45$  kg·m<sup>2</sup>, and  $J_3 = 55$  kg·m<sup>2</sup>. The maximum torques generated by the actuators in the roll, pitch, and yaw axis, are 0.1 N·m, 0.1 N·m, and 0.1 N·m, respectively.

One on-orbital task of this satellite is to take high-resolution images of some hot districts by using its payload, that is, camera. This task requires the satellite attitude control system to follow a desired attitude trajectory planned as

$$\mathbf{\Theta}_d = [\theta_d, \phi_d, \psi_d]^{\mathrm{T}} = \begin{bmatrix} -40\sin(0.05t - \frac{\pi}{10}) \\ 60\cos(0.02t - \frac{\pi}{4}) \\ 40\sin(0.01t - \frac{\pi}{6}) \end{bmatrix} \text{ degrees}$$
(3.43)

To validate the superior attitude tracking control performance of the designed controller with angular velocity measurement obviated, the following two cases of external disturbances are considered.

- Case #1: A practical disturbance for any on-orbital satellite is considered. The external disturbance  $u_d$  consists of the earth magnetic torque  $u_{dm}$ , the gravity gradient torque  $u_{dg}$ , the solar radiation torque  $u_{ds}$ , and the aerodynamic torque  $u_{da}$ , that is,  $u_d = u_{\#1} = u_{dg} + u_{da} + u_{dm} + u_{ds}$ . These four torques are calculated as in [12]. According to the orbital and the physical parameters of the satellite, it is obtained from [12] that  $u_d$  and the lumped disturbance d are such that  $u_d \in \mathcal{L}_2[0, T)$  and  $d \in \mathcal{L}_2[0, T)$  for all T > 0.
- Case #2: A severe disturbance is assumed with  $\mathbf{u}_d = [-0.01, -0.005, 0.01]^T$  N·m. Then, one has  $\mathbf{u}_d \in \mathcal{L}_{\infty}[0, \infty)$  and  $\mathbf{d} \in \mathcal{L}_{\infty}[0, \infty)$  from the analysis in Sect. 3.5.

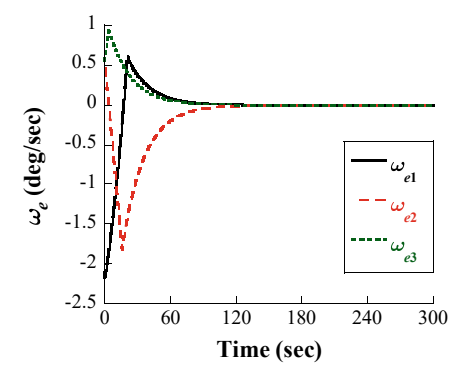
When conducting all simulations, the control gains are chosen according to the steps in Sect. 3.5 by trial-and-error until the expected attitude pointing accuracy and attitude stability were achieved, and they are finally selected as:  $\delta_1 = 0.5$ ,  $\delta_2 = 0.5$ ,  $k_p = 300$ ,  $k_d = 1500$ ,  $k_f = 8$ , and  $\kappa = 4$ . The satellite's initial states are  $\Theta(0) = [4, -4, 2]^T$  degrees and  $\omega(0) = [0.18, 0.22, -0.22]^T$  deg/s or  $\dot{\Theta}(0) = [0.2, 0.3, -0.2]^T$  deg/s.

# 3.6.1 Results of Case #1

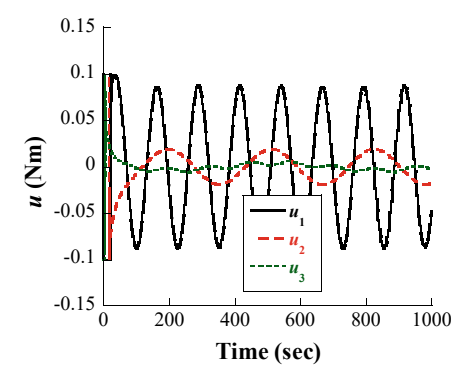
When the angular velocity-free robust controller (3.9) is applied for case #1, the resulting error of the attitude tracking is presented in Fig. 3.1. The tracking error  $\Theta_e = [\theta_e, \phi_e, \psi_e]^T$  of the attitude is stabilized after about 160 s. Although the satellite considered is not capable of measuring the angular velocity, the velocity tracking error in this case is still shown. This is seen in Fig. 3.2. Almost the same as the attitude tracking error, it requires 160 s to stabilize the velocity tracking error. The control torque consumed to provide the satellite with such tracking performance is illustrated

Fig. 3.1 The attitude tracking error of the controller (3.9) for  $u_d$  in  $C_{0.00}$  #1

Fig. 3.2 The angular velocity tracking error of the controller (3.9) for  $u_d$  in Case #1



in Fig. 3.3. The steady-state behavior of the state's tracking error is observed with the solid line in Figs. 3.4 and 3.5, respectively. The attitude tracking errors in the roll, the pitch, and the yaw axis are seen to be  $|\theta_e| \leq 3.0 \times 10^{-5}$  degrees,  $|\phi_e| \leq 2.0 \times 10^{-5}$  degrees, and  $|\psi_e| \leq 3.0 \times 10^{-5}$  degrees. The velocity tracking error  $\omega_e = [\omega_{e1}, \omega_{e2}, \omega_{e3}]^{\rm T}$  is with  $|\omega_{ei}| \leq 2.0 \times 10^{-7}$  deg/s, i = 1, 2, 3. These results verify that the designed scheme can provide the attitude tracking maneuver with high control accuracy. The desired task is accomplished after about 160 s.



**Fig. 3.3** The input torque of the controller (3.9) for  $u_d$  in Case #1

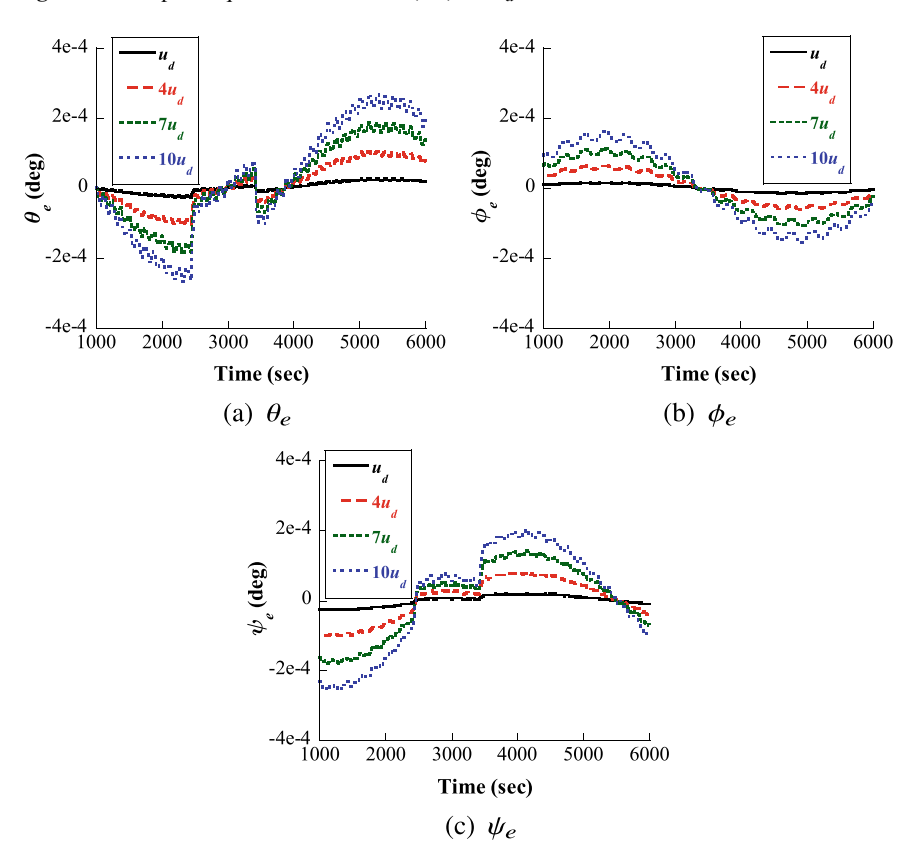


Fig. 3.4 The steady-state behavior of the attitude tracking error from the controller (3.9) in Case #1

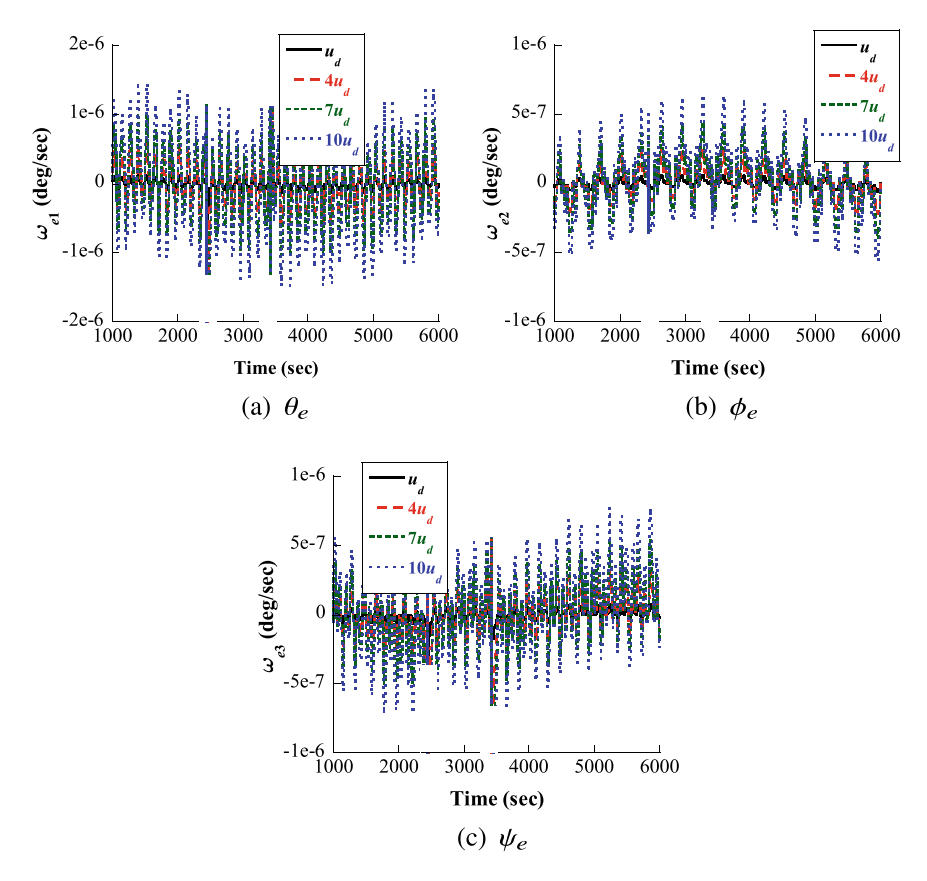


Fig. 3.5 The steady-state behavior of the angular velocity tracking error ensured by the controller (3.9) for  $u_d$ ,  $4u_d$ ,  $7u_d$ , and  $10u_d$  in Case #1

to  $u_{\#1}$ ,  $4u_d$ ,  $7u_d$ , and  $10u_d$ . The corresponding control effort in case of  $u_{\#1}$ ,  $4u_d$ ,  $7u_d$  and  $10u_d$  can be seen in Fig. 3.6. Their steady-state behavior shows that only minor differences exist in the control torque. This is induced by the different attitude and angular velocity tracking errors. The conclusion (R1) in Theorem 3.1 is well validated.

## 3.6.2 Results of Case #2

For case #2, when the developed control scheme is implemented in the satellite, it can be found from Figs. 3.7 and 3.8 that although the satellite is under the effect of severe external disturbance and without any angular velocity measurements for feedback, the planned attitude maneuvering is still accomplished. It is seen in Fig. 3.7a that the desired trajectory can be tracked after 160 s. Moreover, it is seen in Fig. 3.7b that the tracking control accuracy of the attitude is  $|\theta_e| \le 0.00190$  degrees,

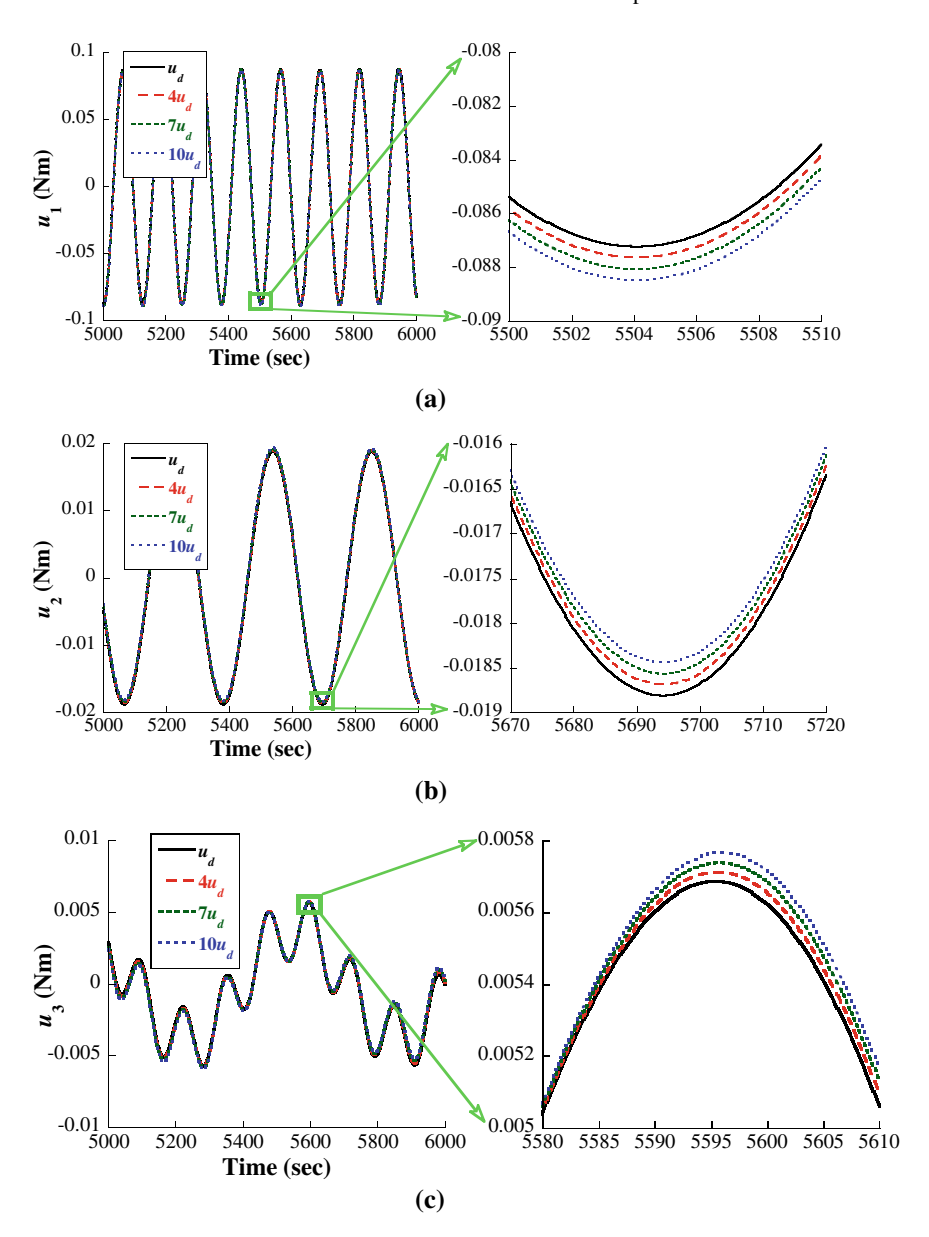


Fig. 3.6 The steady-state behavior of the control torque in the presence of  $u_d$ ,  $4u_d$ ,  $7u_d$  and  $10u_d$  in Case #1

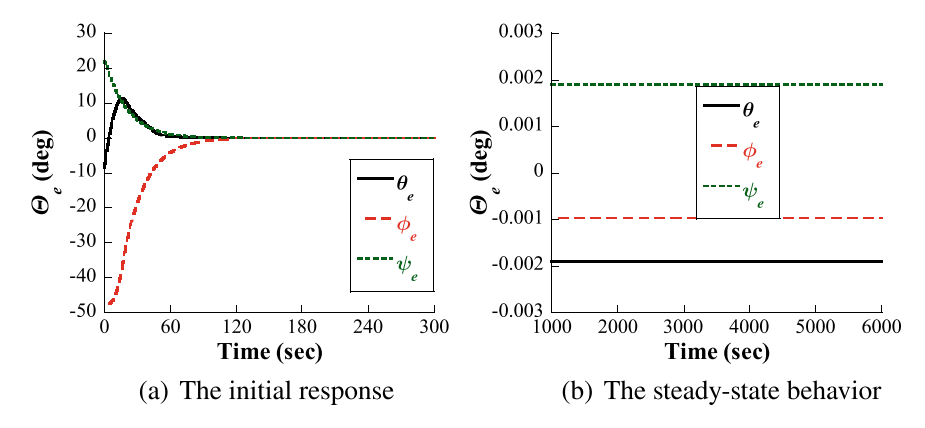


Fig. 3.7 The attitude tracking error ensured by the controller (3.9) in Case #2

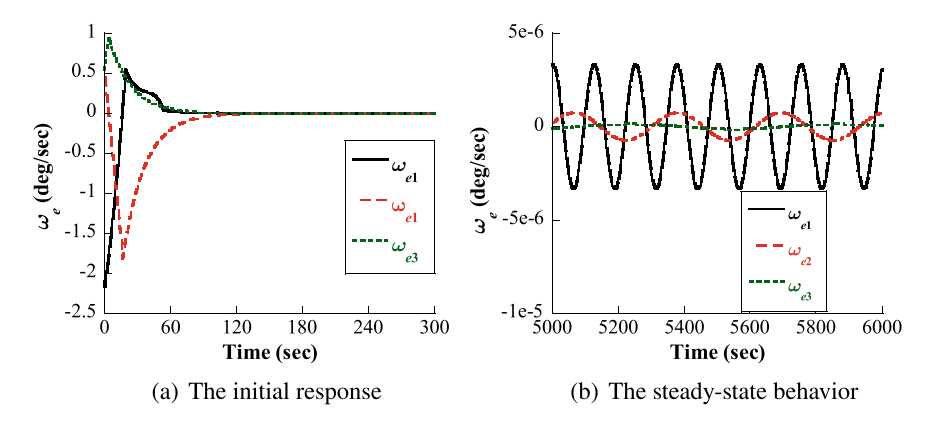


Fig. 3.8 The angular velocity tracking error from the controller (3.9) in Case #2

 $|\phi_e| \leq 0.00095$  degrees, and  $|\psi_e| \leq 0.00190$  degrees. The steady-state behavior in Fig. 3.8b shows that the velocity tracking error  $\omega_e$  is subject to  $|\omega_{ei}| \leq 5.0 \times 10^{-6}$  deg/s, i=1,2,3. The achieved high attitude-pointing accuracy is promising. The stringent requirement demanded by the onboard camera can also be satisfied in order for the camera to work properly. The planned task can thus be accomplished despite severe disturbance. The result (R2) in Theorem 3.1 is verified.

# 3.6.3 Quantitative Analysis

To quantitatively evaluate the proposed angular velocity observer-free tracking control (AVOFTC), the attitude pointing accuracy and the attitude stability are used as two performance indexes. The resulting tracking performance from AVOFTC for case #1 and case #2 are listed in Tables 3.1 and 3.2. Moreover, in comparison with

Simulation scenarios		Controller	Controller Attitude pointing accuracy (d		
			$ \theta_e $	$ \phi_e $	$ \psi_e $
Case #1	<i>u</i> #1	AVOFTC	$2.2 \times 10^{-5}$	$1.7 \times 10^{-5}$	$2.51 \times 10^{-5}$
		UQFTC	0.05	0.03	0.07
	4u#1	AVOFTC	$9.0 \times 10^{-5}$	$7.0 \times 10^{-5}$	$1.05 \times 10^{-4}$
		UQFTC	0.06	0.09	0.08
	7u <sub>#1</sub>	AVOFTC	$1.8 \times 10^{-4}$	$1.1 \times 10^{-4}$	$1.7 \times 10^{-4}$
		UQFTC	0.1	0.1	$2.3 \times 10^{-6}$
	10u#1	AVOFTC	$2.6 \times 10^{-5}$	$1.6 \times 10^{-4}$	$2.55 \times 10^{-4}$
		UQFTC	0.12	0.10	0.12
Case #2	·	AVOFTC	0.0019	$9.5 \times 10^{-4}$	0.0019
		UQFTC	0.2	0.15	0.3

Table 3.1 The attitude control accuracy comparison between AVOFTC and UQFTC

Table 3.2 The attitude stability comparison between AVOFTC and UQFTC

Simulation scenarios		Controller	Attitude stability (deg/s)		
			$ \omega_{e1} $	$ \omega_{e2} $	$ \omega_{e3} $
Case #1	<i>u</i> #1	AVOFTC	$1.45 \times 10^{-7}$	$7.0 \times 10^{-8}$	$8.0 \times 10^{-8}$
		UQFTC	$1.25 \times 10^{-7}$	$6.0 \times 10^{-8}$	$7.2 \times 10^{-8}$
	4u#1	AVOFTC	$6.0 \times 10^{-7}$	$2.8 \times 10^{-7}$	$3.4 \times 10^{-7}$
		UQFTC	$7.5 \times 10^{-7}$	$4.2 \times 10^{-7}$	$3.1 \times 10^{-7}$
	7u <sub>#1</sub>	AVOFTC	$1.1 \times 10^{-6}$	$3.2 \times 10^{-7}$	$5.9 \times 10^{-7}$
		UQFTC	$2.6 \times 10^{-7}$	$6.4 \times 10^{-7}$	
	10u#1	AVOFTC	$1.5 \times 10^{-6}$	$6.0 \times 10^{-7}$	$7.2 \times 10^{-7}$
		UQFTC	$4.8 \times 10^{-6}$	$5.7 \times 10^{-7}$	$9.8 \times 10^{-7}$
Case #2		AVOFTC	$3.6 \times 10^{-6}$	$8.0 \times 10^{-7}$	$2.2 \times 10^{-7}$
		UQFTC	$6.7 \times 10^{-6}$	$7.4 \times 10^{-7}$	$5.9 \times 10^{-7}$

the unit-quaternion feedback tracking control (UQFTC) presented in [11] is carried out. It is seen in Tables 3.1 and 3.2 that, a desirable attitude-pointing accuracy is ensured by AVOFTC for any case of external disturbance, and the corresponding attitude stability is very high. Although the UQFTC control is implemented without angular velocity measurements, its tracking performance is not accepted. That is because UQFTC is not capable of handling external disturbance.

# 3.7 Experimental Tests

In this section, the practical application of the designed angular velocity observer-free control approach will be verified on the testbed shown in Fig. 2.6. When conducting

all experimental tests, the testbed's initial states are set at  $\Theta(0) = [0, 0, 0]^T$  degrees and  $\dot{\Theta}(0) = [0, 0, 0]^T$  deg/s. The desired attitude is planned as follows

$$\mathbf{\Theta}_d = [\theta_d, \phi_d, \psi_d]^{\mathrm{T}} = \begin{bmatrix} -20\sin(0.05t - \frac{\pi}{10}) \\ 10\cos(0.02t - \frac{\pi}{4}) \\ 10\sin(0.01t - \frac{\pi}{6}) \end{bmatrix} \text{ degrees}$$
(3.44)

The inertia matrix and the maximum control torque of this testbed and the microsatellite in Sect. 3.6 are almost the same. When conducting experimental tests, only the planned trajectory (3.44) has a difference in the magnitude when compared with the desired trajectory (3.43) in simulation. In fact, due to mechanical limits, the test-bed cannot provide  $\pm 60$  degrees attitude maneuver in the pitch axis and  $\pm 40$  degrees attitude maneuver in the roll axis as given in (3.43).

#### 3.7.1 Experimental Test #1

In this test, only the reaction wheels ran, while the thrusters were not commanded to operate. This test aims to validate the capability of the presented framework to handle the external disturbance  $u_d = u_{\#1}$  in case #1. This disturbance was numerically introduced and injected into the attitude control system. Once the torque u was determined from the controller,  $u + u_{\#1}$  was then calculated and sent to the controller of reaction wheels. By this, the external disturbance in case #1 was simulated in this simulator.

With the developed controller applied to carry out this test, the obtained attitude tracking result was observed in Fig. 3.9. The desired trajectory (3.44) was successfully followed. The error of the angular velocity tracking resulting from the controller was illustrated in Fig. 3.10. The torque demanded to achieve that control performance was shown in Fig. 3.11. The proposed controller ensured the attitude tracking accuracy to be  $|\theta_e| \leq 0.0310$  degrees,  $|\phi_e| \leq 0.0233$  degrees, and  $|\psi_e| \leq 0.0222$  degrees. The ensured attitude stability or the angular tracking accuracy was such that  $|\omega_{e1}| \leq 0.0027927$  deg/s,  $|\omega_{e2}| \leq 0.0035262$  deg/s, and  $|\omega_{e3}| \leq 0.023132$  deg/s. These results verified the controller's effectiveness in ensuring  $\mathcal{L}_2$ -gain disturbance attenuation.

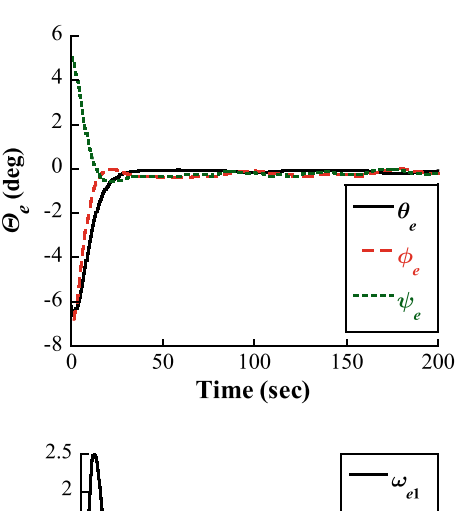
## 3.7.2 Experimental Test #2

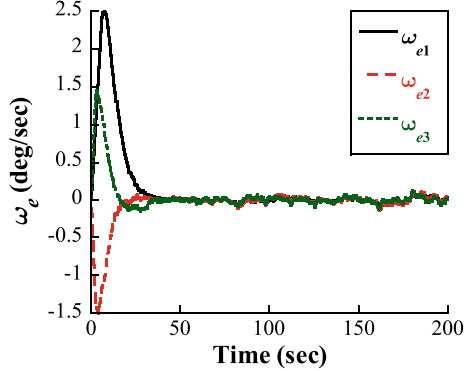
To experimentally verify the capability of the designed tracking control approach to tackle with bounded external disturbance considered in case #2, another test was carried out. In this test, as the same as Test #1, reaction wheels operated as the actuator for the simulator. However, six thrusters ran and randomly generated a constant but unknown minor torque in each axis. This torque acted on the simulator as an external

**Fig. 3.9** The tracking error of the attitude from the controller (3.9) in Test #1

**Fig. 3.10** The angular velocity tracking error from the controller (3.9) in Test #1

**Fig. 3.11** The input torque demanded by the controller (3.9) in Test #1





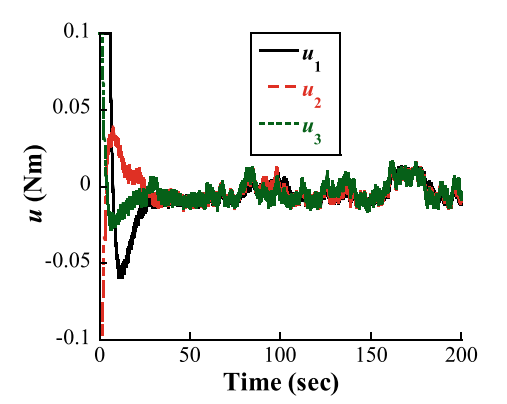
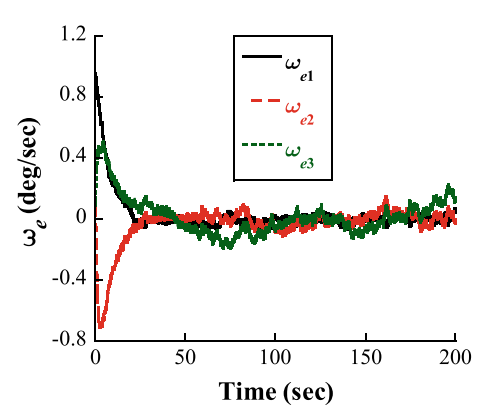


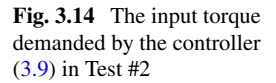
**Fig. 3.12** The tracking error of the attitude from the controller (3.9) in Test #2

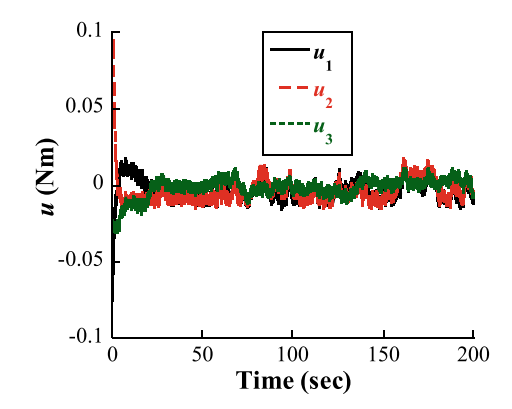
**Fig. 3.13** The angular velocity tracking error from the controller (3.9) in Test #2



disturbance. Although the magnitude of this disturbance torque was not the same as the values in case #2, their disturbance types are the same, that is, both belong to  $\mathcal{L}_{\infty}[0,\infty)$ .

After finishing Test #2, the data of the errors of the attitude tracking and the angular velocity tracking acquired were shown in Figs. 3.12 and 3.13, respectively; while the consumed control effort was illustrated in Fig. 3.14. From Figs. 3.12 and 3.13, it was seen that the planned tracking maneuver was accomplished via the proposed output feedback controller. The desired trajectory (3.44) was successfully followed after about 180 s with the attitude tracking accuracy satisfying  $|\theta_e| \le 0.090332$  degrees,  $|\phi_e| \le 0.16441$  degrees, and  $|\psi_e| \le 0.20480$  degrees. Moreover, the controller governed the velocity tracking accuracy such that  $|\omega_{e1}| \le 0.055838$  deg/s,  $|\omega_{e2}| \le 0.018145$  deg/s, and  $|\omega_{e3}| \le 0.12923$  deg/s. The tracking errors of the satellite states were ensured to be uniformly ultimately bounded despite the external disturbance generated by thrusters in this test. The conclusion (R2) in Theorem 3.1 is thus experimentally validated.





## 3.7.3 Quantitative Analysis

From the experimental results of Tests #1 and #2 and comparing them with the simulation results in Sect. 3.6, although there are discrepancies in the tracking performance between the experimental results and the simulation results, the designed controller's performance was experimentally validated. In addition, that discrepancy is owing to that the accuracy of attitude measurement sensors used on the testbed is not as high as the accuracy in simulation; actually, an ideal attitude measurement, that is., the attitude can be perfectly measured without sensor noise, etc, is assumed in Sect. 3.6. On the other hand, for the experimental Tests #1 and #2, the achieved attitude pointing accuracy is both superior to 0.05 degrees. The requirement on the attitude pointing accuracy imposed by the planned task is satisfied. However, the resulting angular velocity tracking accuracy in Test #1 and #2 are both inferior to 0.001 deg/s. This is owing to sensor noises and environmental noise on the ground. In ground tests, it is hard and even impossible to achieve the attitude stability of 0.001 deg/s.

Moreover, Test #1 and Test #2 were further carried out by using the UQFTC. The resulting attitude tracking accuracy and the velocity tracking accuracy of test #1 were  $|\theta_e|=0.52$  degrees,  $|\phi_e|=0.76$  degrees,  $|\psi_e|=1.04$  degrees, and  $|\omega_{ei}|\leq0.432$  deg/s, i=1,2,3. For Test #2, the tracking control accuracy of the attitude and the angular velocity were  $|\theta_e|=2.5146$  degrees,  $|\phi_e|=3.0973$  degrees,  $|\psi_e|=5.3650$  degrees, and  $|\omega_{ei}|\leq2.7221$  deg/s, i=1,2,3. This experimental attitude tracking performance was inferior to the performance ensured by the proposed approach.

From the above results, the practical application potential of the presented observer-free robust attitude control has been verified.

References 73

## 3.8 Summary

The difficult problem of large-angle attitude tracking control for satellites without angular velocity measurements was addressed. An efficient and practical angular velocity-free control strategy with a simple, yet efficient structure was proposed. The attitude tracking maneuver was accomplished with the desired attitude pointing accuracy ensured despite the modeling error due to external disturbances. Compared with the existing observer-based velocity-free schemes, no observer was embedded into the control scheme. The developed approach can be implemented online and in real-time. It does not require expensive online computation, enabling its convenient application to practical large-angle attitude tracking maneuvers.

#### References

- Singh, S. N., Yim, W. S. (1996) Feedback linearization and solar pressure satellite attitude control. IEEE Transactions on Aerospace and Electronic Systems 32(2): 732–741
- Yang, C. C., Wu, C. J. (2007) Optimal large-angle attitude control of rigid spacecraft by momentum transfer. IET Control Theory and Applications 1(3): 657–664
- Parlos, A. G., Sunkel, J. W. (1992) Adaptive attitude control and momentum management for large-angle spacecraft maneuvers. Journal of Guidance, Control, and Dynamics 15(4): 1018– 1028
- Venkatachalam, R. (1993) Large-angle pitch attitude maneuver of a satellite using solar radiation pressure. IEEE Transactions on Aerospace and Electronic Systems 29(4): 1164–1169
- 5. Yu, Y. N., Meng, X. Y., Li, K. Y., Xiong, F. F. (2014) Robust control of flexible spacecraft during large-angle attitude maneuver. Journal of Guidance, Control, and Dynamics 37(3): 1027–1033
- Safa, A., Baradaran-nia, M., Kharrati, H., Khanmohammadi, S. (2015) Large angle attitude maneuver control for rigid spacecraft with delayed inputs and disturbances. In: 2015 23rd Iranian Conference on Electrical Engineering, Tehran, Iran, pp 905–910
- Sakamoto, A., Ikeda, Y., Yamaguchi, I., Kida, T. (2016) Nonlinear model predictive control for large angle attitude maneuver of spacecraft with RW and RCS. In: IEEE 55th Conference on Decision and Control, Las Vegas, NV, USA, pp 3202–3209
- 8. Ye, D., Xiao, Y. (2018) Robust output feedback attitude tracking control for rigid-flexible coupling spacecraft. Journal of the Franklin Institute 355(18): 9209–9223
- 9. Jiang, B. Y., Li, C. J., Ma, G. F. (2017) Finite-time output feedback attitude control for spacecraft using "adding a power integrator" technique. Aerospace Science and Technology 66: 342–354
- Xiao, B., Fu, Z. Z., Guo, Y. N. (2017) Attitude output feedback tracking control of satellites without angular velocity observers. In: 43rd Annual Conference of the IEEE Industrial Electronics Society, Beijing, China, pp 6544

  –6548
- Tayebi, A. (2008) Unit quaternion-based output feedback for the attitude tracking problem. IEEE Transactions on Automatic Control 53(6): 1516–1520
- 12. Yang, C. D., Sun, Y. P. (2002) Mixed  $\mathcal{H}_2/\mathcal{H}_\infty$  state-feedback design for microsatellite attitude control. Control Engineering Practice 10(9): 951–970
- Gao, Z. F., Jiang, B., Shi, P., Cheng, Y. H. (2010) Sensor fault estimation and compensation for microsatellite attitude control systems. International Journal of Control Automation and Systems 8(2): 228–237
- 14. Mayhew, C. G., Sanfelice, R. G., Teel, A. R. (2011) Quaternion-based hybrid control for robust global attitude tracking. IEEE Transactions on Automatic Control 56(11): 2555–2566

# Chapter 4 Velocity-Free Attitude Control with Actuator Constraint



#### 4.1 Introduction

In addition to the interest in ensuring attitude control with high performance based on "velocity-free" output feedback, there is a practical motivation in introducing control input constraints nested into the closed loop. From the viewpoint of control law design, due to physical limitations, momentum exchange devices and/or thrusters as actuators for the satellite attitude control fail to render infinite control torque, and thus the actuator outputs are constantly bounded or constrained. Once the actuator reaches its constraints, the efforts to further increase the actuator output would not result in any variation in the output, and then this usually deteriorates the system performance or even results in system instability. Hence, it is very necessary to take actuator constraints into account during attitude controller design.

In the past decades, the actuator constraint problem has received more and more attention [1–7]. For the linear system, predictive control [8] and optimal control [9] have been applied to treat with actuator constraints problem. However, the control system must be determined prior and no disturbances are considered. The problem of input constraints for aerospace application was considered in [10]. An anti-windup control scheme has been proposed for the large angel attitude control of satellites with actuator constraint. In [11], a back-stepping technique was applied to the nonlinear flight system in the absence of input constraint first, and then a command filter was employed to compensate for the effect of the control signal rate constraint. In [12], a robust variable structure controller was designed to control the satellite attitude under actuator constraint. However, its control scheme lacks generality to the nonlinear systems.

Note that few results in satellite attitude control without angular velocity measurement in the presence of modeling error and actuator constraint were seen in the literature. With a view to tackle this challenge, this chapter focuses on developing a structure-simple control scheme that can achieve attitude tracking or stabilization with high performance even in the presence of uncertainties, disturbances, actuator constraints, and the unavailability of angular velocity. The resulting closed-loop sys-

tem is proved to be uniformly ultimate bounded stable. To the best of our knowledge, there are few works with all these issues considered simultaneously in the literature.

#### 4.2 Attitude Uniformly Ultimately Bounded Control

In this section, the satellite considered is flexible. The task to be accomplished is the attitude tracking maneuver. Moreover, the attitude kinematics (2.19)–(2.20) and the attitude dynamics (2.25)–(2.26) are used to describe the flexible satellite attitude control system.

#### 4.2.1 Flexible Satellite Attitude Tracking System

Let the unit quaternion  $Q_d = [q_{d0}, q_d^T] \in \mathbb{R}^4, q_d = [q_{d1}, q_{d2}, q_{d3}]^T \in \mathbb{R}^3$ , denote the desired attitude of the satellite and described in a desired  $\mathcal{F}_D$  with respect to the Earth-centered inertial frame  $\mathcal{F}_I$ .  $\omega_d = [\omega_{d1}, \omega_{d2}, \omega_{d3}]^T \in \mathbb{R}^3$  is the desired angular velocity. Then, the desired attitude  $Q_d$  satisfies the following kinematics:

$$\dot{\boldsymbol{q}}_d = \frac{1}{2} (\boldsymbol{q}_d^{\times} + q_{d0} \boldsymbol{I}_3) \boldsymbol{\omega}_d \tag{4.1}$$

$$\dot{q}_{d0} = -\frac{1}{2} \boldsymbol{q}_d^{\times} \boldsymbol{\omega}_d \tag{4.2}$$

Define  $Q_e = [q_{e0}, q_e^{\mathrm{T}}]^{\mathrm{T}} \in \mathbb{R}^4$ ,  $q_e = [q_{e1}, q_{e2}, q_{e3}]^{\mathrm{T}}$  as the attitude tracking error between the satellite's actual attitude Q and the desired attitude  $Q_d$ , then one has  $Q_e = Q_d^{-1} \otimes Q$ , where  $\otimes$ " denotes the quaternion multiplication. According to [13] and the attitude kinematics (2.19)–(2.20), it follows that the kinematics of the attitude tracking error  $Q_e$  satisfies

$$\dot{\boldsymbol{q}}_e = \frac{1}{2} (\boldsymbol{q}_e^{\times} + q_{e0} \boldsymbol{I}_3) \boldsymbol{\omega}_e \tag{4.3}$$

$$\dot{\boldsymbol{q}}_{e0} = -\frac{1}{2} \boldsymbol{q}_e^{\mathrm{T}} \boldsymbol{\omega}_e \tag{4.4}$$

where

$$\boldsymbol{\omega}_e = \boldsymbol{\omega} - \boldsymbol{R}(\boldsymbol{Q}_e)\boldsymbol{\omega}_d \tag{4.5}$$

denotes the angular velocity tracking error, and  $R(Q_e) \in \mathbb{R}^{3\times 3}$  denotes the rotation matrix that brings  $\mathcal{F}_D$  onto  $\mathcal{F}_B$ , i.e.,

$$\mathbf{R}(\mathbf{Q}_e) = (q_e^2 - \mathbf{q}_e^{\mathrm{T}} \mathbf{q}_e) \mathbf{I}_3 + 2\mathbf{q}_e \mathbf{q}_e^{\mathrm{T}} - 2q_{e0} \mathbf{q}_e^{\times}$$
(4.6)

From the attitude dynamics (2.25)–(2.26) and (4.5), the attitude tracking error dynamics can be obtained as

$$J\dot{\omega}_{e} + (\omega_{e} + R(Q_{e})\omega_{d})^{\times}J(\omega_{e} + R(Q_{e})\omega_{d}) - J\omega_{e}^{\times}R(Q_{e})\omega_{d} + JR(Q_{e})\dot{\omega}_{d} + ((\omega_{e} + R(Q_{e})\omega_{d})^{\times}\delta\dot{\eta} + \delta\ddot{\eta}) = u + u_{d}$$

$$(4.7)$$

Based on the preceding analysis, when the unit quaternion is adopted to represent the attitude of the flexible satellite, then its attitude tracking system can be mathematically modeled by (4.3), (4.4), and (4.7).

#### 4.2.2 Problem Formulation

In practice, the control torque u generated by all the actuators is constrained and bounded. Suppose that it is bounded by a known constant  $u_{\text{max}} \in \mathbb{R}_+$ , i.e.,

$$|u_i| \le u_{\text{max}}, i = 1, 2, 3$$
 (4.8)

Moreover, only the environmental disturbance torque is considered in the modeling error in this section. Then,  $u_d$  in (4.7) is bounded by a positive but unknown constant  $\bar{d}_i \in \mathbb{R}_+$ , i = 1, 2, 3, i.e.,

$$|u_{di}| \le \bar{d}_i \tag{4.9}$$

To this end, the control objective in this section can be stated as: Consider the attitude tracking system described by (4.3), (4.4), and (4.7), design a velocity-free control law  $\boldsymbol{u}$  to accomplish the attitude tracking maneuver with the tracking error  $\boldsymbol{Q}_e$  governed to be as small as possible even in the presence of the modeling error satisfying (4.9) and the actuator constraint (4.8).

# 4.2.3 Transformed Attitude Tracking System

Let  $\mathbf{F} = (0.5(\mathbf{q}_e^{\times} + q_{e0}\mathbf{I}_3))^{-1}$ , then it can be obtained from (4.3) and (4.7) that

$$J^*\ddot{q}_e + F^*\dot{q}_e + M^* + E^* = u^* + d^*$$
(4.10)

where 
$$\boldsymbol{u}^* = [u_1^*, u_2^*, u_3^*]^T = \boldsymbol{F}^T \boldsymbol{u}, \boldsymbol{d}^* = [d_1^*, d_2^*, d_3^*]^T = \boldsymbol{F}^T \boldsymbol{u}_d, \boldsymbol{J}^* = \boldsymbol{F}^T \boldsymbol{J} \boldsymbol{F}, \boldsymbol{F}^* = -\boldsymbol{J}^* \dot{\boldsymbol{F}}^{-1} \boldsymbol{F} - \boldsymbol{F}^T (\boldsymbol{J} \boldsymbol{F} \dot{\boldsymbol{Q}}_e)^{\times} \boldsymbol{F}, \boldsymbol{E}^* = \boldsymbol{F}^T ((\boldsymbol{R} (\boldsymbol{Q}_e) \boldsymbol{\omega}_d)^{\times} \delta \dot{\boldsymbol{\eta}} + \delta \ddot{\boldsymbol{\eta}}), \text{ and}$$

$$M^* = F^{\mathrm{T}}(F\dot{q}_e)^{\times} JR(Q_e)\omega_d + F^{\mathrm{T}}(R(Q_e)\omega_d)^{\times} JF\dot{q}_e$$

$$+ F^{\mathrm{T}}(R(Q_e)\omega_d)^{\times} JR(Q_e)\omega_d + F^{\mathrm{T}}(F\dot{q}_e)^{\times}\delta\dot{\eta}$$

$$- F^{\mathrm{T}}J((F\dot{q}_e)^{\times}R(Q_e)\omega_d - R(Q_e)\dot{\omega}_d)$$
(4.11)

**Remark 4.1** To avoid the singularity of F that will occur at  $q_{e0} = 0$ , let the attitude error of the satellite be restricted in the workspace W [14], then the attitude tracking model (4.3), (4.4), and (4.7) can be rewritten into (4.10).

$$W = \left\{ F: ||q_e|| \le e_m < 1, q_{e0} \ge \sqrt{1 - e_m^2} > 0 \right\}$$
 (4.12)

**Property 4.1** If each element  $u_i^*$  of  $u^*$  is bounded by  $\bar{u}_{max} = \frac{2}{3}u_{max}$ , i.e.,  $|u_i^*| \leq \bar{u}_{max}$ , i = 1, 2, 3, then the actuator constraint (4.8) can be met.

**Proof** If  $|u_i^*| \leq \bar{u}_{\text{max}}$  is satisfied, then it follows from  $u^* = F^T u$  that

$$\mathbf{u} = (\mathbf{F}^{\mathrm{T}})^{-1} \mathbf{u}^* = \frac{1}{2} (\mathbf{q}_e^{\times} + q_{e0} \mathbf{I}_3)^{\mathrm{T}} \mathbf{u}^*$$
 (4.13)

Applying  $|q_{ej}| \le 1$ , j = 0, 1, 2, 3, leads to

$$|u_i| \le \frac{1}{2} \sum_{i=1}^{j=3} |u_j^*| \le \frac{3}{2} \bar{u}_{\text{max}} = u_{\text{max}}$$
 (4.14)

Thereby, the conclusion in Property 4.1 is proved.

**Property 4.2** The lumped disturbance  $d^*$  is bounded. More specifically, one has

$$|d_i^*| \le \bar{\delta}_i, i = 1, 2, 3 \tag{4.15}$$

where  $\bar{\delta}_i \in \mathbb{R}_+$  is an unknown constant.

**Property 4.3**  $J^* = F^T J F$  is symmetric and positive-definite.

**Property 4.4** The matrix  $\dot{J}^* - 2F^*$  is skew-symmetric [15], where  $\dot{J}^*$  is the time-derivative of  $J^*$ .

#### 4.2.4 Command Filter

To achieve the control objective without the measurements of the angular velocity, a pseudo velocity filter [7] is first introduced and given by

$$\boldsymbol{\alpha}_F = [\alpha_{F1}, \alpha_{F2}, \alpha_{F3}]^{\mathrm{T}} = -\boldsymbol{K}_F \boldsymbol{q}_e + \boldsymbol{v}_F \tag{4.16}$$

where

$$\dot{v}_F = -(L_F + K_F)v_F + (K_F^2 + K_F L_F - K_F)q_e$$
 (4.17)

with  $L_F = \text{diag}([l_{1F}, l_{2F}, l_{3F}]^T)$ , and  $K_F = \text{diag}([k_{1F}, k_{2F}, k_{3F}]^T)$ .  $l_{iF} \in \mathbb{R}_+$  and  $k_{iF} > 1$  are constants chosen by the designer, i = 1, 2, 3.

Define a filtered tracking error as

$$\mathbf{r}_F = \dot{\mathbf{q}}_e + \mathbf{q}_e + \mathbf{\alpha}_F \tag{4.18}$$

In view of (4.16), it follows that

$$\dot{\alpha}_F = -L_F \alpha_F - K_F r_F \tag{4.19}$$

From (4.16), the time-derivative of (4.18) can be obtained as

$$\dot{\boldsymbol{r}}_F = \ddot{\boldsymbol{q}}_e + \dot{\boldsymbol{q}}_e + \dot{\boldsymbol{\alpha}}_F = \ddot{\boldsymbol{q}}_e + \boldsymbol{r}_F - \boldsymbol{q}_e - (\boldsymbol{I}_3 + \boldsymbol{L}_F)\boldsymbol{\alpha}_F - \boldsymbol{K}_F \boldsymbol{r}_F \tag{4.20}$$

Multiplying both side of (4.20) by  $J^*$  yields

$$J^*\dot{r}_F = -F^*r_F + d^* + u^* - (K_F - I_3)J^*r_F - E^* + \varphi_F$$
 (4.21)

where  $\varphi_F$  denotes the lumped modeling error and given by

$$\varphi_F = -M^* + F^*(q_e + \alpha_F) - J^*q_e - (L_F + I_3)J^*\alpha_F$$
 (4.22)

**Remark 4.2** Although the second time-derivative of  $q_e$  is involved in (4.20), it is just applied to derive the final attitude tracking model (4.21). In the subsequent controller design,  $\ddot{q}_e$  will not be involved.

# 4.2.5 Velocity-Free Neural Network Controller

Due to the advantages of neural network for approximating unknown system dynamics and its powerful representation capabilities for nonlinear function [16], the single layer neural network approximation technique is applied to represent the uncertainty  $\varphi_F$ . Then,  $\varphi_F$  can be viewed as the output of the single neural network given by

$$\boldsymbol{\varphi}_F = \boldsymbol{W}^T \boldsymbol{X} (\boldsymbol{q}_d, \dot{\boldsymbol{q}}_d, \ddot{\boldsymbol{q}}_d) \tag{4.23}$$

where  $X(q_d, \dot{q}_d, \ddot{q}_d) = [X_1, X_2, \dots, X_n]^T \in \mathbb{R}^n$  is the bias function of the neural network and  $W \in \mathbb{R}^n$  is its weight.

Let  $\phi_F^*$  be the optimal function approximation using an ideal neural network approximator, then one has

$$\boldsymbol{\varphi}_F = \boldsymbol{\varphi}_F^* + \boldsymbol{\varepsilon}_F = (\boldsymbol{W}^*)^{\mathrm{T}} \boldsymbol{X} + \boldsymbol{\varepsilon}_F \tag{4.24}$$

where  $W^*$  is the optimal approximation weight, and  $\varepsilon_F$  denotes the approximation error and is supposed to be bounded by  $|\varepsilon_F| \le \varepsilon_F^*$ , in which  $\varepsilon_F^* \in \mathbb{R}_+$  is a positive constant. Because the optimal weight needed for the best approximation of the  $\varphi_F$  is difficult to determine, its estimate function can be defined as

$$\hat{\boldsymbol{\varphi}}_F = [\hat{\varphi}_{F1}, \hat{\varphi}_{F2}, \hat{\varphi}_{F3}]^{\mathrm{T}} = \hat{\boldsymbol{W}}^{\mathrm{T}} \boldsymbol{X}$$
 (4.25)

where  $\hat{W} \in \mathbb{R}^n$  is the estimate of  $W^*$ .

Suppose that  $d^*$  and  $E^*$  are considered as the lumped disturbances for the attitude tracking error system, then (4.21) can be transformed into

$$J^*\dot{r}_F = -F^*r_F + \underline{d}^* + u^* - (L_F - I_3)J^*r_F + \varphi_F$$
 (4.26)

where  $d^* = d^* - E^*$ .

**Remark 4.3** For practical flexible satellite attitude tracking control, there always exists damping, even small, in the flexible structures, such that the magnitudes of elastic vibration and its rate are bounded. Hence,  $E^*$  is bounded. Moreover, the neural network reconstruction error  $\varepsilon_F$  and the disturbance  $d^*$  are bounded in the tracking error system. Therefore,  $d^* + \varepsilon_F$  is always bounded for all the time, i.e.,

$$||\boldsymbol{d}^* + \boldsymbol{\varepsilon}_F|| \le e_{m1} \tag{4.27}$$

where  $e_{m1} \in \mathbb{R}_+$  is a positive constant.

**Theorem 4.1** Consider the flexible satellite attitude tracking control system modeled by (4.3), (4.4), and (4.7), let a velocity-free neural network controller be developed as  $\mathbf{u} = (\mathbf{F}^{\mathrm{T}})^{-1}\mathbf{u}^*$  with

$$\boldsymbol{u}^* = \boldsymbol{K}_F \tanh(\lambda_F \boldsymbol{\alpha}_F) - \hat{\boldsymbol{\varphi}}_F \tag{4.28}$$

where  $\hat{\boldsymbol{\varphi}}_F$  is determined by (4.25) and its weight  $\hat{\boldsymbol{W}}$  updated by

$$\hat{\boldsymbol{W}} = \gamma_F \int_0^t (\boldsymbol{X} \boldsymbol{q}_e^{\mathrm{T}}(\ell) + \boldsymbol{X} \boldsymbol{\alpha}_F^{\mathrm{T}}(\ell) - \dot{\boldsymbol{X}} \boldsymbol{q}_e^{\mathrm{T}}(\ell)) d\ell + \gamma_F \boldsymbol{X} \boldsymbol{q}_e^{\mathrm{T}}$$

$$- \pi_F \gamma_F \int_0^t ||\boldsymbol{\alpha}_F|| \hat{\boldsymbol{W}}(\ell) d\ell$$
(4.29)

where  $\lambda_F \in \mathbb{R}_+$ ,  $\gamma_F \in \mathbb{R}_+$ , and  $\pi_F \in \mathbb{R}_+$  are positive control gains. Then, the uniform ultimate bounded stability of the filtered tracking error  $\mathbf{r}_F$  is achieved. The actuator constraints is satisfied by choosing appropriate  $\mathbf{K}_F$ .

**Proof** Applying (4.29), one has

$$\dot{\hat{\boldsymbol{W}}} = \gamma_F \boldsymbol{X} \boldsymbol{r}_F^{\mathrm{T}} - \pi_F \gamma_F \|\boldsymbol{\alpha}_F\| \, \hat{\boldsymbol{W}} \tag{4.30}$$

Consider a candidate Lyapunov function as

$$V_{1} = \frac{1}{2} \boldsymbol{r}_{F}^{\mathrm{T}} \boldsymbol{J}^{*} \boldsymbol{r}_{F} + \frac{\tilde{\boldsymbol{W}}^{\mathrm{T}} \tilde{\boldsymbol{W}}}{2 \gamma_{F}} + (\sqrt{\ln(\cosh(\lambda_{F} \boldsymbol{\alpha}_{F}))})^{\mathrm{T}} \boldsymbol{\Gamma}_{F}^{-1} \sqrt{\ln(\cosh(\lambda_{F} \boldsymbol{\alpha}_{F}))}$$
(4.31)

where  $\tilde{W} = W^* - \hat{W}$  and  $\Gamma_F = \text{diag}([\lambda_F, \lambda_F, \lambda_F]^T)$ . From (4.26), one can obtain that

$$\dot{V}_{1} = \mathbf{r}_{F}^{T} \mathbf{J}^{*} \dot{\mathbf{r}}_{F} + \frac{1}{2} \mathbf{r}_{F}^{T} \dot{\mathbf{J}}^{*} \mathbf{r}_{F} - \frac{1}{\gamma_{F}} \tilde{\mathbf{W}}^{T} \tilde{\mathbf{W}} 
+ (\sqrt{\ln(\cosh(\lambda_{F}\alpha_{F}))})^{T} \mathbf{\Gamma}_{F}^{-1} \frac{\operatorname{diag}(\tanh(\lambda_{F}\alpha_{F}))(\lambda_{F}\alpha_{F})}{2\sqrt{\ln(\cosh(\lambda_{F}\alpha_{F}))}} 
= \mathbf{r}_{F}^{T} (-\mathbf{F}^{*} \mathbf{r}_{F} + \mathbf{u}^{*} - (\mathbf{K}_{F} - \mathbf{I}_{3}) \mathbf{J}^{*} \mathbf{r}_{F} + \underline{\mathbf{d}}^{*} + \boldsymbol{\varphi}_{F}) + \frac{1}{2} \mathbf{r}_{F}^{T} \dot{\mathbf{J}}^{*} \mathbf{r}_{F} 
- \frac{1}{\gamma_{F}} \tilde{\mathbf{W}}^{T} \tilde{\mathbf{W}} + \dot{\boldsymbol{\alpha}}_{F}^{T} \tanh(\lambda_{F}\alpha_{F})$$
(4.32)

Substituting (4.28) into (4.32) yields

$$\dot{V}_{1} = \boldsymbol{r}_{F}^{T} (\boldsymbol{K}_{F} \boldsymbol{tanh} (\lambda_{F} \boldsymbol{\alpha}_{F}) + \tilde{\boldsymbol{W}}^{T} \boldsymbol{X} + \boldsymbol{\varepsilon}_{F} - (\boldsymbol{K}_{F} - \boldsymbol{I}_{3}) \boldsymbol{J}^{*} \boldsymbol{r}_{F} + \underline{\boldsymbol{d}}^{*}) 
- \frac{1}{\gamma_{F}} \tilde{\boldsymbol{W}}^{T} \dot{\hat{\boldsymbol{W}}} + \dot{\boldsymbol{\alpha}}_{F}^{T} \boldsymbol{tanh} (\lambda_{F} \boldsymbol{\alpha}_{F}) 
= -\boldsymbol{\alpha}_{F}^{T} \boldsymbol{L}_{F} \boldsymbol{tanh} (\lambda_{F} \boldsymbol{\alpha}_{F}) + \boldsymbol{r}_{F}^{T} (\boldsymbol{\varepsilon}_{F} + \underline{\boldsymbol{d}}^{*}) - \boldsymbol{r}_{F}^{T} (\boldsymbol{K}_{F} - \boldsymbol{I}_{3}) \boldsymbol{J}^{*} \boldsymbol{r}_{F} 
+ \pi_{F} \|\boldsymbol{\alpha}_{F}\| \tilde{\boldsymbol{W}}^{T} \hat{\boldsymbol{W}} \tag{4.33}$$

Note that

$$\tilde{\boldsymbol{W}}^{T}\hat{\boldsymbol{W}} = \tilde{\boldsymbol{W}}^{T}(\boldsymbol{W}^{*} - \tilde{\boldsymbol{W}}) \leq -\tilde{\boldsymbol{W}}^{T}\tilde{\boldsymbol{W}} + ||\tilde{\boldsymbol{W}}||||\boldsymbol{W}^{*}||$$

$$\leq -\frac{1}{2}\tilde{\boldsymbol{W}}^{T}\tilde{\boldsymbol{W}} + \frac{1}{2}\|\boldsymbol{W}^{*}\|^{2}$$
(4.34)

Additionally, the optimal approximation weight  $W^*$  is bounded by a known positive constant  $e_{m2} \in \mathbb{R}_+$ , i.e.,  $\frac{1}{2} \|W^*\|^2 \le e_{m2}$ . Then, it follows

$$\dot{V}_{1} = -\alpha_{F}^{T} L_{F} \tanh(\lambda_{F} \alpha_{F}) + r_{F}^{T} (\boldsymbol{\varepsilon}_{F} + \underline{\boldsymbol{d}}^{*}) - r_{F}^{T} (\boldsymbol{K}_{F} - \boldsymbol{I}_{3}) \boldsymbol{J}^{*} \boldsymbol{r}_{F} 
+ \pi_{F} \|\boldsymbol{\alpha}_{F}\| \tilde{\boldsymbol{W}}^{T} \hat{\boldsymbol{W}} 
\leq -l_{\min} \|\boldsymbol{\alpha}_{F}\| \|\tanh(\lambda_{F} \alpha_{F})\| + e_{m1} \|\boldsymbol{r}_{F}\| - \underline{l} \|\boldsymbol{r}_{F}\|^{2} + \pi_{F} e_{m2} \|\boldsymbol{\alpha}_{F}\| 
= -\|\boldsymbol{\alpha}_{F}\| (l_{\min} \|\tanh(\lambda_{F} \alpha_{F})\| - \pi_{F} e_{m2}) - \|\boldsymbol{r}_{F}\| (\underline{l} \|\boldsymbol{r}_{F}\| - e_{m1})$$
(4.35)

where  $l_{\min} = \min_{i=1,2,3} l_{iF}$  and  $\underline{l} = \lambda_{\min}((\boldsymbol{K}_F - \boldsymbol{I}_3)\boldsymbol{J}^*)$ . It is seen from (4.35) that  $\dot{V}_1 < 0$  when  $[\boldsymbol{\alpha}_F^T, \boldsymbol{r}_F^T]^T$  are outside the set

$$S_{1} = \left\{ ([\boldsymbol{\alpha}_{F}^{\mathsf{T}}, \boldsymbol{r}_{F}^{\mathsf{T}}]^{\mathsf{T}} : \|\mathbf{tanh}(\lambda_{F}\boldsymbol{\alpha}_{F})\| \leqslant \frac{\pi_{F}e_{m2}}{l_{\min}}, \|\boldsymbol{r}_{F}\| \leqslant \frac{e_{m1}}{\underline{l}} \right\}$$
(4.36)

which is a small set containing the origin  $[\boldsymbol{\alpha}_F^{\mathrm{T}}, \boldsymbol{r}_F^{\mathrm{T}}]^{\mathrm{T}} = \mathbf{0}$ . Hence, applying Definition 2.1 can prove that the filtered tracking error is uniformly ultimately bounded stable with

$$\lim_{t \to \infty} ||\boldsymbol{r}_F|| \in \mathcal{S}_1, \lim_{t \to \infty} ||\boldsymbol{\alpha}_F|| \in \mathcal{S}_1 \tag{4.37}$$

This implies that larger  $l_{\min}$  and  $\underline{l}$  or smaller  $\pi_F$  will yield better attitude tracking control performance. This completes the proof.

**Remark 4.4** With the pseudo velocity filter (4.16), it is seen that the control law (4.28) and the updating law (4.29) are independent of the measurement of the angular velocity. Hence, the developed controller does not rely on the angular velocity measurement.

**Remark 4.5** From the updating law (4.29), it can be assumed that  $|\hat{\varphi}_{Fi}| \leq \chi_{Fi}$ , i = 1, 2, 3. Hence, if  $k_{iF}$  are selected appropriately to satisfy  $k_{iF} < \bar{u}_{\max} - \chi_{Fi}$ , then  $|u_i^*| \leq k_{iF} |\tanh(\lambda_F \alpha_i)| + |\hat{\varphi}_{Fi}| \leq k_{iF} + \chi_{Fi \leq \bar{u}_{\max}}$  can be got from (4.28). Therefore, actuator constraints are satisfied.

## 4.2.6 Numerical Example

To verify the effectiveness of the proposed control scheme, numerical simulation is carried out by using the flexible satellite system in (2.19)–(2.20) and (2.25)–(2.26) in conjunction with the controller (4.28). The physical parameters of this satellite are given by  $u_{\text{max}} = 5 \text{ N} \cdot \text{m}$  and

$$J = \begin{bmatrix} 607.4 & -15.4 & -0.9 \\ -15.4 & 1560.8 & 25.4 \\ -0.9 & 25.4 & 1462.3 \end{bmatrix} \text{kg} \cdot \text{m}^2$$
 (4.38)

$$\boldsymbol{\delta} = \begin{bmatrix} 6.45637 & 1.27814 & 2.15629 \\ -1.25819 & 0.91756 & -1.67264 \\ 1.11687 & 2.48901 & -0.83674 \end{bmatrix} kg^{\frac{1}{2}} \cdot m$$
 (4.39)

Three elastic modes (i.e., N=3) are considered with natural frequencies  $\Lambda_1=0.7681$ ,  $\Lambda_2=1.1038$ ,  $\Lambda_3=1.8733$  rad/s and damping  $\Xi_1=0.003$ ,  $\Xi_2=0.003$  as well as  $\Xi_3=0.003$ . The desired attitude trajectory is planned as  $\boldsymbol{q}_d(t)=\frac{1}{10}[7\sqrt{2},\cos(0.5t),\sin(0.5t)]^T$ . The external disturbance torque acting on the flexible satellite is chosen from [17]

$$\mathbf{u}_d = (\|\boldsymbol{\omega}\|^2 + 0.5)[\sin 0.8t, \cos 0.5t, \cos 0.3t]^{\mathrm{T}} \,\mathrm{N} \cdot \mathrm{m}$$
 (4.40)

Control scheme	Maximum value of vibration	Settling time of vibration (s)	Settling time of tracking (s)
The controller (4.28)	0.6	80	75
PID+Anti-windup control	0.3	800	1000
ANOFC [18]	0.005	150	300

**Table 4.1** The performance comparisons for the controller (4.28), ANOFC, and PID+Anti-windup control

To implement the neural network controller (4.28), the control gains are chosen as  $\gamma_F = 25$ ,  $\pi_F = 0.15$ ,  $\lambda_F = 7.5$ ,  $l_{iF} = 10$ , and  $k_{iF} = 45$ , i = 1, 2, 3. Moreover, X in (4.28) are chosen as Gaussian-type functions [19]:

$$X_i = \exp\left(-\frac{\|\mathbf{x} - \mathbf{c}_i\|^2}{\ell_i^2}\right), i = 1, 2, \dots, n$$
 (4.41)

where  $\mathbf{x} = [\mathbf{q}_d^{\mathrm{T}}, \dot{\mathbf{q}}_d^{\mathrm{T}}, \ddot{\mathbf{q}}_d^{\mathrm{T}}]^{\mathrm{T}}$ ,  $\ell_i = \sqrt{15}$ , n = 10, and  $c_i$  denotes the vector having the same dimension as  $\mathbf{x}$  with its element randomly chosen between -1 and 1. In the simulation, the initial attitude of the flexible satellite is set as  $\mathbf{q}(0) = [0.2, -0.15, 0.3571]^{\mathrm{T}}$ . The initial angular velocity is supposed to be  $\boldsymbol{\omega}(0) = [0.28, -0.138, 0.138]^{\mathrm{T}}$  rad/s. The initial modal displacements are  $\eta_i(0) = 0.001$  and  $\dot{\eta}_i(0) = 0.0005$ , i = 1, 2, 3.

When the neural network controller (4.28) is applied, the attitude tracking maneuver is successfully accomplished. The attitude tracking error and angular velocity error signals will converge to zero in around 75 s. The control torque of each axis in this case is less than the required maximum bound. No terrible elastic oscillation is induced. When using the PID controller for the attitude tracking maneuver with the actuator constraints considered, to compensate for the effect of actuator saturation, the so-called anti-windup approach [10] is introduced to the PID. Under the action of PID plus anti-windup control, it almost takes 1000 s to achieve the objective of attitude tracking after the occurrence of actuator constraints. In addition, when the PID and the anti-windup control are applied, its control performance is much worse than our proposed control. For the purpose of further comparison, the attitude tracking maneuver is also accomplished by using the adaptive nonlinear output feedback control (ANOFC) with quaternion measurement only as designed in [20]. The simulation results show that no severe vibration is observed from the ANOFC. the tracking objective can only be achieved after 300 s. The bad control performance is observed in comparison with our proposed controller (4.28). However, the tracking performance obtained from the ANOFC is better than the PID plus anti-windup control. Further, extensive simulations were also done using different control parameters and even disturbance inputs. The overall results on maximum control torque, maximum vibration displacement and settling time of vibration and tracking are also summarized in Table 4.1.

## 4.3 $\mathcal{L}_2$ -gain Disturbance Attenuation Attitude Control

In this section, the satellite considered is rigid with the attitude represented by the modified Rodrigues parameters. The task to be accomplished is the attitude stabilization maneuver. Moreover, the attitude kinematics (2.21) and the attitude dynamics (2.24) are used to describe the rigid satellite attitude control system.

Introducing  $P = G^{-1}(\sigma)$ , then the kinematics (2.21) and the attitude dynamics (2.24) can be combined to form second-order nonlinear equation

$$\boldsymbol{J}^*(\boldsymbol{\sigma})\ddot{\boldsymbol{\sigma}} + \boldsymbol{C}(\boldsymbol{\sigma}, \dot{\boldsymbol{\sigma}})\dot{\boldsymbol{\sigma}} = \boldsymbol{P}^{\mathrm{T}}(\boldsymbol{\sigma})\boldsymbol{u} + \boldsymbol{P}^{\mathrm{T}}(\boldsymbol{\sigma})\boldsymbol{u}_d \tag{4.42}$$

where  $J^*(\sigma) = P^T J P$  and  $C(\sigma, \dot{\sigma}) = -P^T (J P \dot{G} + (J P \dot{\sigma})^{\times}) P$ .

The transformed attitude control system (4.42) is characterized by the following three properties.

**Property 4.5** The matrix  $J^*(\sigma)$  is positive-definite and bounded by two constants  $J_{\min} \in \mathbb{R}_+$  and  $J_{\max} \in \mathbb{R}_+$  such that

$$J_{\min} \|\boldsymbol{x}\|^2 < \boldsymbol{x}^{\mathrm{T}} \boldsymbol{J}^*(\boldsymbol{\sigma}) \boldsymbol{x} < J_{\max} \|\boldsymbol{x}\|^2, \forall \boldsymbol{x} \in \mathbb{R}^3, \forall \boldsymbol{\sigma} \in \mathbb{R}^3$$
 (4.43)

**Property 4.6** The matrix  $\dot{J}^*(\sigma) - 2C(\sigma, \dot{\sigma})$  is skew-symmetric, i.e., for given vectors  $x \in \mathbb{R}^3$ ,  $\sigma \in \mathbb{R}^3$ , one has

$$\boldsymbol{x}^{\mathrm{T}}(\dot{\boldsymbol{J}}^{*}(\boldsymbol{\sigma}) - 2\boldsymbol{C}(\boldsymbol{\sigma}, \dot{\boldsymbol{\sigma}}))\boldsymbol{x} = 0 \tag{4.44}$$

**Property 4.7** The matrix  $C(\sigma, \dot{\sigma})$  is bounded with respect to  $\sigma$  and linear with respect to  $\dot{\sigma}$ . There exists a positive constant  $C_{\text{max}} \in \mathbb{R}_+$  satisfying [21]

$$\|\boldsymbol{C}(\boldsymbol{\sigma}, \dot{\boldsymbol{\sigma}})\| \le C_{\text{max}} \|\dot{\boldsymbol{\sigma}}\|, \forall \boldsymbol{\sigma} \in \mathbb{R}^3$$
 (4.45)

#### 4.3.1 Problem Statement

The control objective is to find a control law u to guarantee that the attitude  $\sigma$  converges to an arbitrary small set, i.e.,  $\|\sigma(t)\| \le \varepsilon_0$  for  $t \ge T$  and external disturbance attenuation is ensured in the  $\mathcal{L}_2$  gain sense. Moreover, this objective is achieved even in the presence of no angular velocity measurements, actuator constraint (4.8), i.e.,  $|u_i| \le u_{\max}$ , i = 1, 2, 3, where  $u_{\max} \in \mathbb{R}_+$  is a positive constant decided by actuator physical property, and the modeling error induced by uncertain inertia as well as external disturbances.

#### 4.3.2 Velocity-Free Filter

Since direct or accurate measurements of satellite angular velocity may be unavailable, a passivity filter is first introduced and defined by

$$\dot{\boldsymbol{p}} = -l_1 \boldsymbol{p} + l_1 l_2 \boldsymbol{\sigma} \tag{4.46}$$

where  $\mathbf{p} = [p_1, p_2, p_3]^T \in \mathbb{R}^3$  can be viewed as an estimate of  $\boldsymbol{\omega}$ .  $l_1 \in \mathbb{R}_+$  and  $l_2 \in \mathbb{R}_+$  are two positive filter gains.

The output of the filter (4.46) is given by

$$\boldsymbol{\sigma}_f = [\sigma_{f1}, \sigma_{f2}, \sigma_{f3}]^{\mathrm{T}} = \boldsymbol{p} - l_2 \boldsymbol{\sigma}$$
 (4.47)

Then, it follow from (4.46) and (4.47) that

$$\dot{\boldsymbol{\sigma}}_f = \dot{\boldsymbol{p}} - l_2 \dot{\boldsymbol{\sigma}} = -l_1 \boldsymbol{\sigma}_f - l_2 \dot{\boldsymbol{\sigma}} \tag{4.48}$$

## 4.3.3 L<sub>2</sub>-gain Disturbance Attenuation Controller

**Theorem 4.2** Consider the rigid satellite attitude system described by (2.21) and (2.24) in the disturbance-free case, i.e.,  $\mathbf{u}_d(t) \equiv \mathbf{0}$ , if the following controller is implemented

$$\mathbf{u} = (\mathbf{P}^{\mathrm{T}}(\boldsymbol{\sigma}))^{-1} (k_{I} \tanh(\boldsymbol{\chi}) - k_{D} \tanh(\boldsymbol{\sigma}) + k_{d} \tanh(\boldsymbol{\sigma}_{f}) + k_{W} \boldsymbol{\sigma}_{f})$$
(4.49)

where  $\mathbf{\chi} = [\chi_1, \chi_2, \chi_3]^{\mathrm{T}} = -\gamma^2 \boldsymbol{\sigma} - \gamma \int_0^t \tanh(\boldsymbol{\sigma}(s)) ds, \gamma \in \mathbb{R}_+, \eta \in \mathbb{R}_+, k_p \in \mathbb{R}_+, k_l \in \mathbb{R}_+, k_d \in \mathbb{R}_+, and k_W \in \mathbb{R}_+ are control gains chosen to satisfy that$ 

$$\frac{k_p}{4} - \frac{1}{\gamma^2} J_{\text{max}} > 0 \tag{4.50}$$

$$m_1 = \frac{3l_2k_W}{4l_1} - \left(\frac{3K_W}{2l_1}\right)^2 \eta - \frac{1}{\gamma}(\sqrt{3}C_{\text{max}} + J_{\text{max}}) > 0$$
 (4.51)

$$m_2 = \frac{1}{\gamma} k_p - \frac{1}{4\gamma} k_d - \frac{l_2 k_W}{l_1 \gamma^2} > 0$$
 (4.52)

$$m_4 = \frac{k_d}{2\gamma} \left( \frac{2\gamma l_1}{l_2} - 1 \right) > 0$$
 (4.53)

$$m_3 = \frac{3k_W}{4l_1l_2} - \frac{1}{4\eta} > 0 \tag{4.54}$$

then it follows that  $\lim_{t\to\infty} \sigma(t) = 0$  and  $\lim_{t\to\infty} \omega(t) = 0$ .

**Proof** Consider a Lyapunov function candidate

$$V_{2} = \left(\frac{1}{2}\dot{\boldsymbol{\sigma}}^{\mathrm{T}} + \frac{1}{\gamma}\tanh(\boldsymbol{\sigma})\right)^{\mathrm{T}}\boldsymbol{J}^{*}\dot{\boldsymbol{\sigma}} + \frac{k_{d}}{l_{2}}\sum_{i=1}^{3}\ln(\cosh(\sigma_{fi}))$$

$$+ k_{p}\sum_{i=1}^{3}\ln(\cosh(\sigma_{i})) + \frac{k_{W}}{2l_{2}}\boldsymbol{\sigma}_{f}^{\mathrm{T}}\boldsymbol{\sigma}_{f} + \frac{k_{I}}{\gamma^{2}}\int_{0}^{\tanh(\chi)}s^{\mathrm{T}}\mathbf{Cosh}^{2}(\chi)ds$$

$$(4.55)$$

where

$$\int_0^{\tanh(\chi)} s^{\mathrm{T}} \mathbf{Cosh}^2(\chi) ds = \sum_{i=1}^3 \int_0^{\tanh(\chi_i)} \cosh^2(\chi_i) s_i ds_i > 0$$
 (4.56)

Applying (4.50), Lemma 2.1, and Property 4.5, one can prove that

$$\frac{1}{4}\dot{\boldsymbol{\sigma}}^{\mathrm{T}}\boldsymbol{J}^{*}\dot{\boldsymbol{\sigma}} + \frac{1}{\gamma}(\tanh(\boldsymbol{\sigma}))^{\mathrm{T}}\boldsymbol{J}^{*}\dot{\boldsymbol{\sigma}} + \frac{k_{p}}{2}\sum_{i=1}^{3}\ln(\cosh(\sigma_{i}))$$

$$\geq \frac{k_{p}}{2}\sum_{i=1}^{3}\ln(\cosh(\sigma_{i})) - \frac{1}{\gamma^{2}}(\tanh(\boldsymbol{\sigma}))^{\mathrm{T}}\boldsymbol{J}^{*}\tanh(\boldsymbol{\sigma})$$

$$\geq \sum_{i=1}^{3}(\frac{k_{p}}{4} - \frac{J_{\max}}{\gamma^{2}})\tanh^{2}(\sigma_{i}) > 0$$
(4.57)

In view of (4.56) and (4.57), it yields

$$V_{2} \geq \frac{1}{4}\dot{\boldsymbol{\sigma}}^{\mathrm{T}}\boldsymbol{J}^{*}\dot{\boldsymbol{\sigma}} + \frac{k_{d}}{2l_{2}}\sum_{i=1}^{3}\tanh^{2}(\sigma_{f_{i}}) + \frac{k_{p}}{4}\sum_{i=1}^{3}\tanh^{2}(\sigma_{i}) + \frac{k_{I}}{\gamma^{2}}\int_{0}^{\tanh(\chi)}s^{\mathrm{T}}\mathbf{Cosh}^{2}(\chi)ds + \frac{k_{W}}{2l_{2}}\boldsymbol{\sigma}_{f}^{\mathrm{T}}\boldsymbol{\sigma}_{f} > 0$$

$$(4.58)$$

Hence, the Lyapunov function candidate  $V_2$  can be concluded to be globally positive and radically unbounded.

When the considered rigid satellite is disturbance-free, note that  $\|\mathbf{tanh}(\boldsymbol{\sigma})\| \leq \sqrt{3}$  and

$$(\tanh(\sigma))^{\mathrm{T}}\tanh(\sigma_f) \le \frac{1}{4} \|\tanh(\sigma)\|^2 + \|\tanh(\sigma_f)\|^2$$
 (4.59)

Using Property 4.6, Property 4.7, (4.42), and the controller (4.49), the time-derivative of  $V_2$  can be simplified as

$$\dot{V}_{2} = \frac{1}{\gamma} \left( \mathbf{tanh}(\boldsymbol{\sigma})^{\mathrm{T}} \boldsymbol{C}(\boldsymbol{\sigma}, \dot{\boldsymbol{\sigma}}) + (\mathbf{Sech}^{2}(\boldsymbol{\sigma})\dot{\boldsymbol{\sigma}})^{\mathrm{T}} \right) \dot{\boldsymbol{\sigma}} + \left( k_{W} \dot{\boldsymbol{\sigma}}^{\mathrm{T}} + \frac{k_{W}}{l_{2}} \dot{\boldsymbol{\sigma}}_{f}^{\mathrm{T}} \right) \boldsymbol{\sigma}_{f} \\
+ (\mathbf{tanh}(\boldsymbol{\sigma}))^{\mathrm{T}} \left( \frac{k_{d}}{\gamma} \mathbf{tanh}(\boldsymbol{\sigma}_{f}) - \frac{k_{p}}{\gamma} \mathbf{tanh}(\boldsymbol{\sigma}) + \frac{k_{W}}{\gamma} \right) \boldsymbol{\sigma}_{f} \\
- \frac{k_{d} l_{1}}{l_{2}} \boldsymbol{\sigma}_{f}^{\mathrm{T}} \mathbf{tanh}(\boldsymbol{\sigma}_{f}) \\
\leq \frac{1}{\gamma} (\sqrt{3} C_{\max} + J_{\max}) \|\dot{\boldsymbol{\sigma}}\|^{2} - \left( \frac{k_{p}}{\gamma} - \frac{k_{d}}{4\gamma} \right) \|\mathbf{tanh}(\boldsymbol{\sigma})\|^{2} \\
- \frac{1}{2\gamma} \left( \frac{2\gamma l_{1} k_{d}}{l_{2}} - k_{d} \right) \|\mathbf{tanh}(\boldsymbol{\sigma}_{f})\|^{2} + \left( k_{W} \dot{\boldsymbol{\sigma}}^{\mathrm{T}} + \frac{k_{W}}{l_{2}} \dot{\boldsymbol{\sigma}}_{f}^{\mathrm{T}} \right) \boldsymbol{\sigma}_{f} \\
+ \frac{k_{W}}{\gamma} (\mathbf{tanh}(\boldsymbol{\sigma}))^{\mathrm{T}} \boldsymbol{\sigma}_{f} \tag{4.60}$$

In particular, using Young's inequality, the last three items on the right hand of (4.60) have the following result

$$\frac{k_{W}}{\gamma}(\mathbf{tanh}(\boldsymbol{\sigma}))^{\mathrm{T}}\boldsymbol{\sigma}_{f} + k_{W}\dot{\boldsymbol{\sigma}}^{\mathrm{T}}\boldsymbol{\sigma}_{f} + \frac{k_{W}}{l_{2}}\dot{\boldsymbol{\sigma}}_{f}^{\mathrm{T}}\boldsymbol{\sigma}_{f} 
\leq \frac{l_{2}k_{W}}{l_{1}\gamma^{2}}\|\mathbf{tanh}(\boldsymbol{\sigma})\|^{2} - \frac{3l_{1}k_{W}}{4l_{2}}\left(\frac{\dot{\boldsymbol{\sigma}}_{f} + l_{2}\dot{\boldsymbol{\sigma}}}{l_{1}}\right)^{\mathrm{T}}\dot{\boldsymbol{\sigma}}_{f} + l_{2}\dot{\boldsymbol{\sigma}} 
\leq \frac{l_{2}k_{W}}{l_{1}\gamma^{2}}\|\mathbf{tanh}(\boldsymbol{\sigma})\|^{2} - \left(\frac{3l_{2}k_{W}}{4l_{1}} - \left(\frac{3k_{W}}{2l_{1}}\right)^{2}\eta\right)\|\dot{\boldsymbol{\sigma}}\|^{2} - \left(\frac{3k_{W}}{4l_{1}l_{2}} - \frac{1}{4\eta}\right)\|\dot{\boldsymbol{\sigma}}_{f}\|^{2} 
(4.61)$$

From (4.60)–(4.61), it can be found that

$$\dot{V}_2 \le -m_1 \|\dot{\boldsymbol{\sigma}}\|^2 - m_2 \|\tanh(\boldsymbol{\sigma})\|^2 - m_3 \|\dot{\boldsymbol{\sigma}}_f\|^2 - m_4 \|\tanh(\boldsymbol{\sigma}_f)\|^2 \tag{4.62}$$

With the control gains given in (4.50)–(4.54), it leads (4.62) to  $\dot{V}_2 \leq 0$ . This implies that  $\lim_{t\to\infty} V_2(t) = V_2(\infty)$  exists. Then, it shows from the Barbalat's lemma that

$$\lim_{t \to \infty} \|\dot{\boldsymbol{\sigma}}\| = \lim_{t \to \infty} \|\tanh(\boldsymbol{\sigma})\| = \mathbf{0} \tag{4.63}$$

and

$$\lim_{t \to \infty} \dot{\boldsymbol{\sigma}}(t) = \lim_{t \to \infty} \boldsymbol{\sigma}(t) = \mathbf{0}$$
 (4.64)

Consequently, one can conclude that  $\lim_{t\to\infty} \omega(t) = 0$  from (2.21).

**Remark 4.6** The attitude controller (4.49) involves the computation of the filter output  $\sigma_f$  and the attitude orientation  $\sigma$  only. Hence, it is rigorously independent of the angular velocity measurement  $\omega$ .

**Remark 4.7** The design of the controller (4.49) does not require any information on the satellite's inertia matrix J. Hence, from the standpoint of uncertainties rejection, the derived controller has great stability and robustness.

In the next, a practical problem is solved, namely, the external disturbance effect on attitude control performance. The corresponding stability analysis can be stated by the following theorem.

**Theorem 4.3** Consider the rigid satellite attitude control system described by (2.21) and (2.24) in the presence of the modeling error induced by the uncertain inertia and external disturbance, with the application of the controller (4.49), if the control gains are chosen to satisfy (4.50), (4.53)–(4.54), and

$$\bar{m}_1 = \frac{3l_2k_W}{4l_1} - \left(\frac{3k_W}{2l_1}\right)^2 \eta - \frac{1}{\gamma}(\sqrt{3}C_{\text{max}} + J_{\text{max}}) - \frac{1}{4\beta_1} > 0$$
 (4.65)

$$\bar{m}_2 = \frac{1}{\gamma} k_P - \frac{1}{4\gamma} k_d - \frac{l_2 k_W}{l_1 \gamma^2} - \frac{1}{4\gamma^2 \beta_2} > 0 \tag{4.66}$$

where  $\beta_i \in \mathbb{R}_+$ , i = 1, 2, are positive constants, then the control objective stated in Sect. 4.3.1 can be met.

**Proof** When the external disturbance  $u_d$  is considered, the right-hand of (4.60) should be added by new items  $\dot{\sigma}^T u_d$  and  $\frac{1}{\gamma} (\tanh(\sigma))^T u_d$ , respectively. Applying the following inequalities

$$\dot{\boldsymbol{\sigma}}^{\mathrm{T}}\boldsymbol{u}_{d} \leq \frac{1}{4\beta_{1}}\dot{\boldsymbol{\sigma}}^{\mathrm{T}}\dot{\boldsymbol{\sigma}} + \beta_{1}\boldsymbol{u}_{d}^{\mathrm{T}}\boldsymbol{u}_{d} \tag{4.67}$$

$$\frac{1}{\gamma}(\tanh(\sigma))^{\mathrm{T}}\boldsymbol{u}_{d} \leq \frac{1}{4\gamma^{2}\beta_{2}}\|\tanh(\sigma)\|^{2} + \beta_{2}\boldsymbol{u}_{d}^{\mathrm{T}}\boldsymbol{u}_{d} \tag{4.68}$$

and calculating the time-derivative of  $V_2$  in (4.55) gives

$$\dot{V}_{2} \leq (\beta_{1} + \beta_{2}) \|\boldsymbol{u}_{d}\|^{2} - \bar{m}_{1} \|\dot{\boldsymbol{\sigma}}\|^{2} - m_{3} ||\dot{\boldsymbol{\sigma}}_{f}||^{2} 
- \bar{m}_{2} \|\mathbf{tanh}(\boldsymbol{\sigma})\|^{2} - m_{4} ||\mathbf{tanh}(\boldsymbol{\sigma}_{f})||^{2}$$
(4.69)

From (4.53)–(4.54) and (4.65)–(4.66), one has

$$\dot{V}_2 < (\beta_1 + \beta_2) ||\boldsymbol{u}_d||^2 - \bar{m}_1 ||\dot{\boldsymbol{\sigma}}||^2 - \bar{m}_2 ||\boldsymbol{\tanh}(\boldsymbol{\sigma})||^2$$
(4.70)

It is seen from (4.70) that  $\dot{V}_2 < 0$  when  $[\boldsymbol{\sigma}^T, \dot{\boldsymbol{\sigma}}^T]^T$  are outside of the set

$$S_2 = \left\{ [\boldsymbol{\sigma}^{\mathrm{T}}, \dot{\boldsymbol{\sigma}}^{\mathrm{T}}]^{\mathrm{T}} : ||\mathbf{tanh}(\boldsymbol{\sigma})|| \le \frac{\bar{\beta}||\boldsymbol{u}_d||}{\sqrt{\bar{m}_2}}, ||\dot{\boldsymbol{\sigma}}|| \le \frac{\bar{\beta}||\boldsymbol{u}_d||}{\sqrt{\bar{m}_1}} \right\}$$
(4.71)

where  $\bar{\beta} = \sqrt{\beta_1 + \beta_2}$ .

It is proved from (4.70) that  $V_2$  decreases monotonically outside the set  $S_2$ . Hence, all the signal in the resulting closed-loop attitude system are bounded ultimately. Moreover, it can be obtained that

$$\lim_{t \to \infty} [||\mathbf{tanh}(\boldsymbol{\sigma})||, ||\dot{\boldsymbol{\sigma}}||]^{\mathrm{T}} \in \mathcal{S}_2$$
 (4.72)

Integrating both sides of (4.70) from the initial time  $t_0$  to T yields

$$V_2(T) - V_2(t_0) \le (\beta_1 + \beta_2) \int_{t_0}^T ||\boldsymbol{u}_d(s)||^2 ds - \bar{m}_2 \int_{t_0}^T ||\boldsymbol{\tanh}(\boldsymbol{\sigma}(s))||^2 ds \quad (4.73)$$

Since  $V_2(t)$  is a non-negative function and from the property of hyperbolic tangent function, it yields

$$\int_{t_0}^{T} ||\sigma(s)||^2 ds \approx \int_{t_0}^{T} ||\tanh(\sigma(s))||^2 ds \le \varepsilon_0 \int_{t_0}^{T} ||u_d(s)||^2 ds \tag{4.74}$$

with  $\varepsilon_0 = \frac{\beta_1 + \beta_2}{\bar{m}_2}$ . In the term of the above inequality and Definition 2.4, it can be proved that  $\mathcal{L}_2$ -gain of the disturbance attenuation is achieved to be a given small value by adjusting  $\varepsilon_0$ , thereby completing the proof of achieving the control objective as stated in Sect. 4.3.1.

## 4.3.4 Control Input Upper Bound Analysis

From (4.46), one has

$$\dot{p} \le -l_1 p + l_1 l_2 |\sigma|, p(0) \ge 0$$
 (4.75)

Using Lemma 2.3, solving (4.75) yields

$$p_i(t) \le p_i(0)\exp(-l_1t) + l_1l_2 \int_0^t \exp(-l_1(t-\ell)) |\sigma_i(\ell)| d\ell, i = 1, 2, 3 \quad (4.76)$$

Applying the switching between MRPs and the shadow MRPs sets stated in Remark 2.3,  $|\sigma_i| \le ||\sigma|| \le 1$  always holds. Hence, by choosing p(0) = 0, one has  $||p(t)|| \le \sqrt{3}l_2$ . To this end, according to Property 2.1, direct calculation shows that  $G(\sigma)$  in (2.21) satisfies

$$||(\mathbf{P}^{\mathrm{T}}(\boldsymbol{\sigma}))^{-1}|| = ||\mathbf{G}(\boldsymbol{\sigma})|| = \frac{1 + \boldsymbol{\sigma}^{\mathrm{T}}\boldsymbol{\sigma}}{4} \le \frac{1}{2}$$
 (4.77)

**Theorem 4.4** For the developed attitude controller (4.49), if the control gains are chosen to satisfy (4.50), (4.53)–(4.54), (4.65)–(4.66), and

$$\frac{1}{2}(\sqrt{3}(k_p + k_I + k_d) + (\sqrt{3} + 1)k_W l_2) \le u_{\text{max}}$$
(4.78)

then the control input of each actuator rigorously enforces the actuator magnitude constraints, i.e.,  $|u_i| \le u_{\text{max}}$ , i = 1, 2, 3, is always met for  $\forall t \ge 0$ .

**Proof** Combining (4.49) and (4.78), for i = 1, 2, 3, it leaves  $u_i$  as

$$|u_{i}| \leq \|\mathbf{u}\|$$

$$\leq \|(\mathbf{P}^{\mathrm{T}}(\boldsymbol{\sigma}))^{-1}\| \|k_{I} \tanh(\boldsymbol{\chi}) - k_{p} \tanh(\boldsymbol{\sigma}) + k_{d} \tanh(\boldsymbol{\sigma}_{f}) + k_{W} \boldsymbol{\sigma}_{f}\|$$

$$\leq \frac{1}{2} (\sqrt{3}(k_{p} + k_{I} + k_{d}) + k_{W} ||\boldsymbol{\sigma}_{f}||)$$

$$(4.79)$$

In addition, it can be proved from (4.47) that  $\sigma_f$  is bounded by

$$||\sigma_f|| \le ||p|| + l_2||\sigma|| \le (\sqrt{3} + 1)l_2$$
 (4.80)

This last result together with (4.78) can be used in (4.79) to demonstrate that

$$|u_i| \le \frac{1}{2}(\sqrt{3}(k_p + k_I + k_d) + (\sqrt{3} + 1)k_W l_2) \le u_{\text{max}}$$
 (4.81)

Hence, the attitude controller (4.49) is proved to be within the actuator constraint.  $\square$ 

## 4.3.5 Numerical Study

To verify the effectiveness of the proposed control approach, the detailed response is numerically simulated using the rigid satellite control system governed by (2.21) and (2.24) in conjunction with the controller (4.49). The satellite is activated by six thrusters distributed symmetrically on three axes of the body frame of the satellite with a maximum thrust of  $u_{\text{max}} = 5 \text{ N·m}$ . The nominal inertia matrix is specified by  $J_0 = \text{diag}([20, 20, 30]^T) \text{ kg·m}^2$ . A time-varying moment inertia matrix as stated in [22] is incorporated as modeling error. Moreover, the external disturbance  $u_d$  is also taken into account, which is given as same as in [22].

In simulation, the proposed controller (4.49) (LAFC), the unit quaternion output feedback controller (UQOF) developed in [23], and the nonlinear Proportional-Integral control design without angular velocity (NPIC) designed in [20] are compared while the satellite attitude is maneuvering. The control gains for those three controllers are listed in Table 4.2. The initial orientation of satellite is  $\sigma(0) = [0.2499, -0.8837, -0.2901]^T$  with a zero initial body angular velocity.

Controller	Control gains
LAFC (4.49)	$k_p = 1.4, k_I = 0.015, k_d = 1.2, k_W = 0.1,$ $l_1 = l_2 = 20, \beta_i = 2, \eta = 0.0017, \gamma = 1000$
UQOF	$\alpha_1 = 2.5, \alpha_2 = 2.5,$ $\Gamma_1 = \text{diag}([0.75, 0.75, 0.75]^T)$
NPIC	$k_x = 2, k_i = 0.01, k_p = 5$

Table 4.2 The controller gains chosen for numerical study

We first present the simulation results when applying LAFC. We see the solid line in Figs. 4.1, 4.2, 4.3, 4.4 and 4.5, the controller managed to stabilize the origin equilibrium point in 30 s with great pointing accuracy. Indeed, since the knowledge of the satellite's inertia was not required and an implicit integral item was incorporated in the control law design, the external disturbance's effect on the attitude

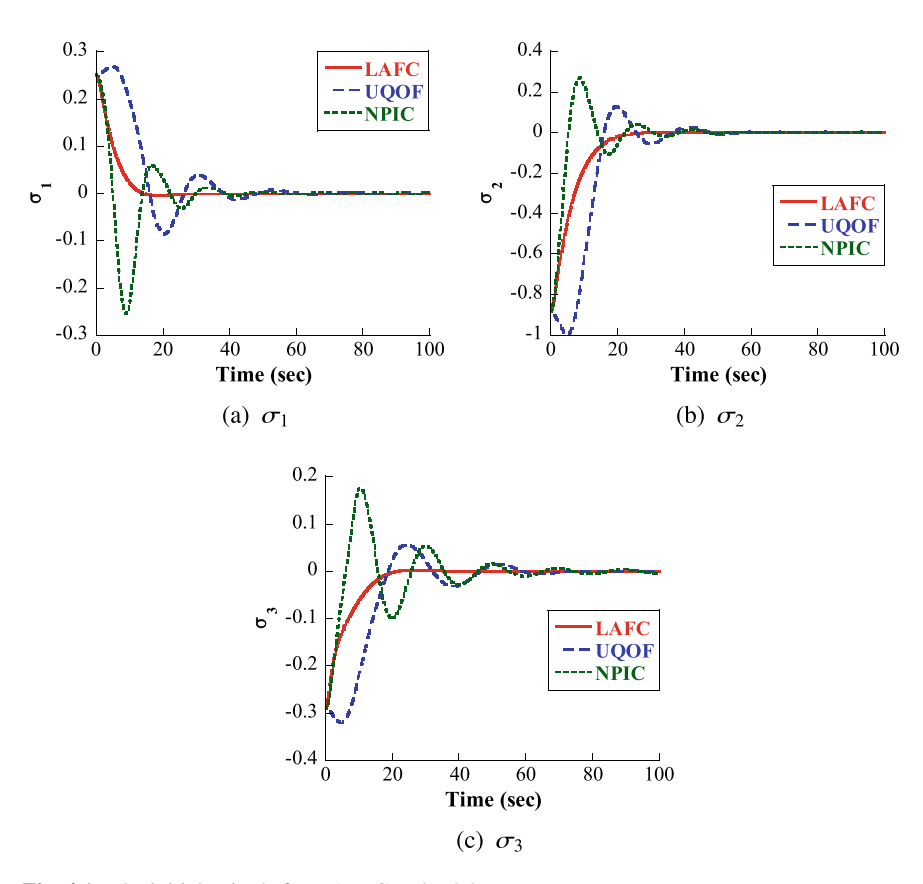


Fig. 4.1 The initial attitude from AVFC and UQOF

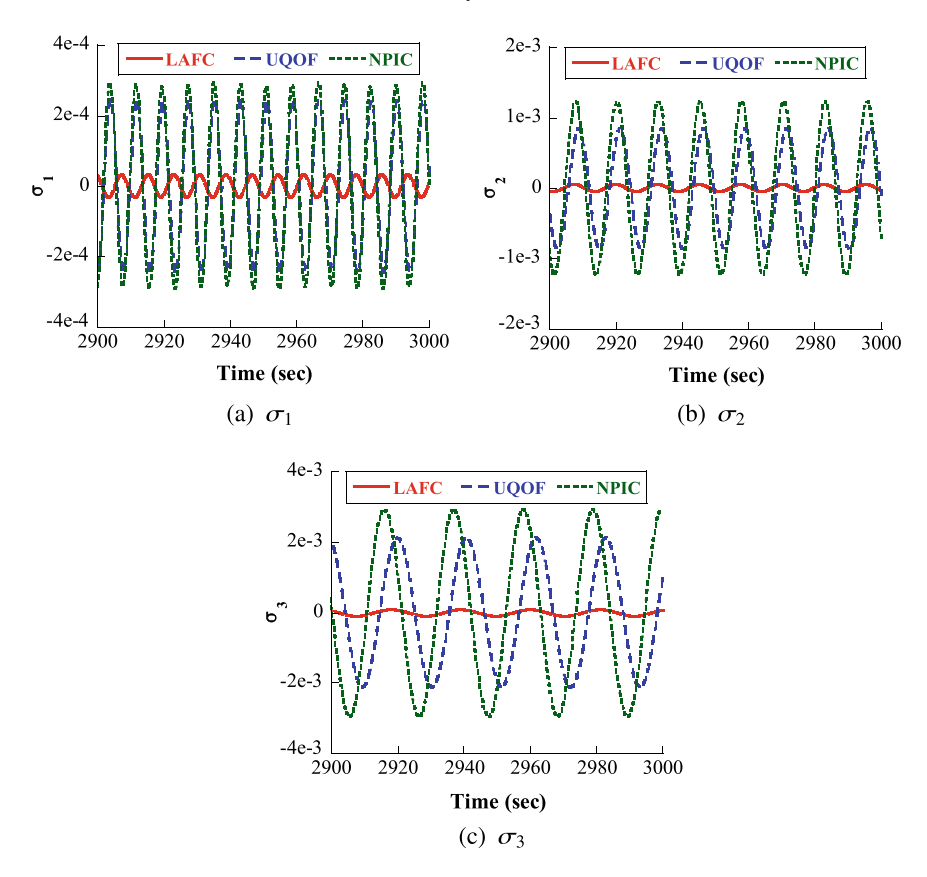


Fig. 4.2 The steady-state attitude from LAFC and UQOF

control performance can be compensated efficiently, and also great robustness to system uncertainties can be guaranteed. It is also interesting to note that the control output of each thruster can rigorously enforce its magnitude constraints, as shown in Fig. 4.5 (solid line). For the case of UQOF, as expected, we see the dashed line clearly in Figs. 4.1, 4.2, 4.3, 4.4 and 4.5 that UQOF can achieve the objective of attitude stabilization. However, due to the inherent properties of UQOF that there does not exist any robustness to the unknown inertia parameters and the external disturbances, a relatively lower pointing accuracy and slew rate accuracy response is observed. The application of NPIC leads to the attitude and the angular velocity shown by the dotted line in Fig. 4.1–4.4. As pointed out in [20] that this control law is only efficient for tackling nonzero constant external disturbance. Therefore, when time-varying disturbance given in [22] is considered, bad control performance is obtained although the attitude stabilization maneuver can be accomplished with angular velocity measurements eliminated. Moreover, note that, to guarantee that the actual output of thruster is less its upper bound, the control gains in NPIC were selected smaller. Consequently, terrible oscillations in attitude, velocity and control

4.4 Summary 93

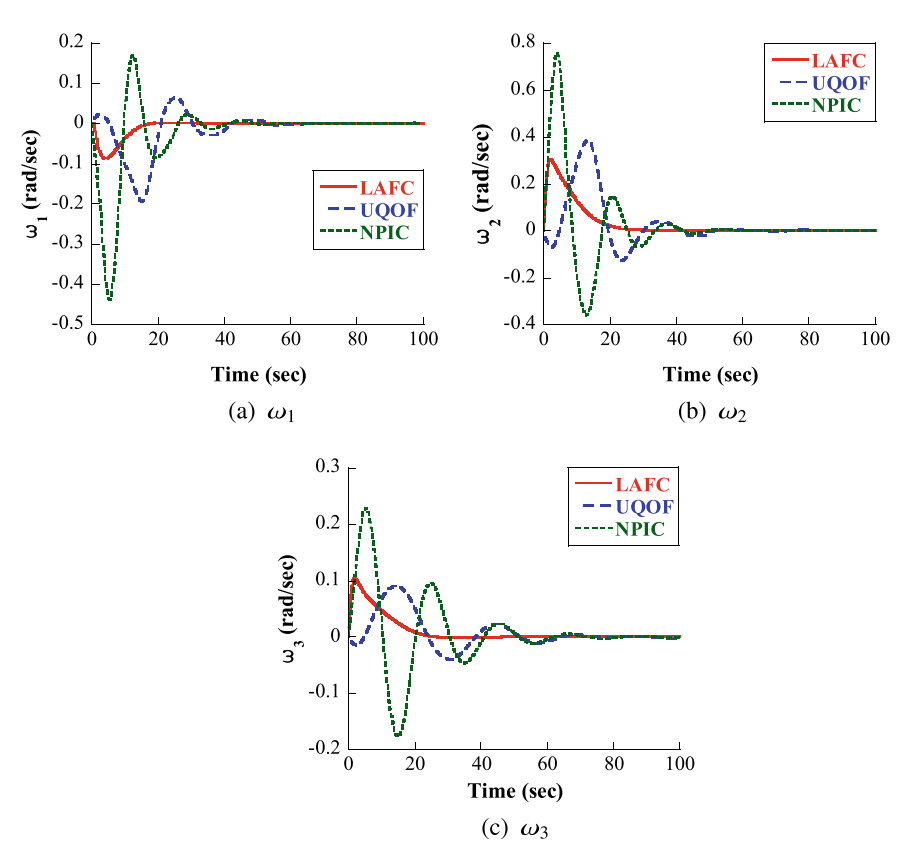


Fig. 4.3 The initial angular velocity from LAFC and UQOF

input are induced. Despite the fact that there still exists some room for improvement with different design control parameter sets, there is not much improvement in the control input response.

Comparison with [23] and [20] shows that the solution (4.49) provides a faster response and higher pointing accuracy. The steady-state stabilization errors for LAFC, UQOF, and NPIC are summarized in Table 4.3.

# 4.4 Summary

The adaptive attitude tracking control problem of flexible satellites with modeling error induced by uncertainty and external disturbance was first studied in this chapter. A neural network-based tracking controller was presented to guarantee the uniformly ultimate boundedness of the attitude tracking error. This controller was free of the angular velocity measurement. The controller rigorously enforces the actuator constraint. The main feature of this controller was that it establishes a straightforward

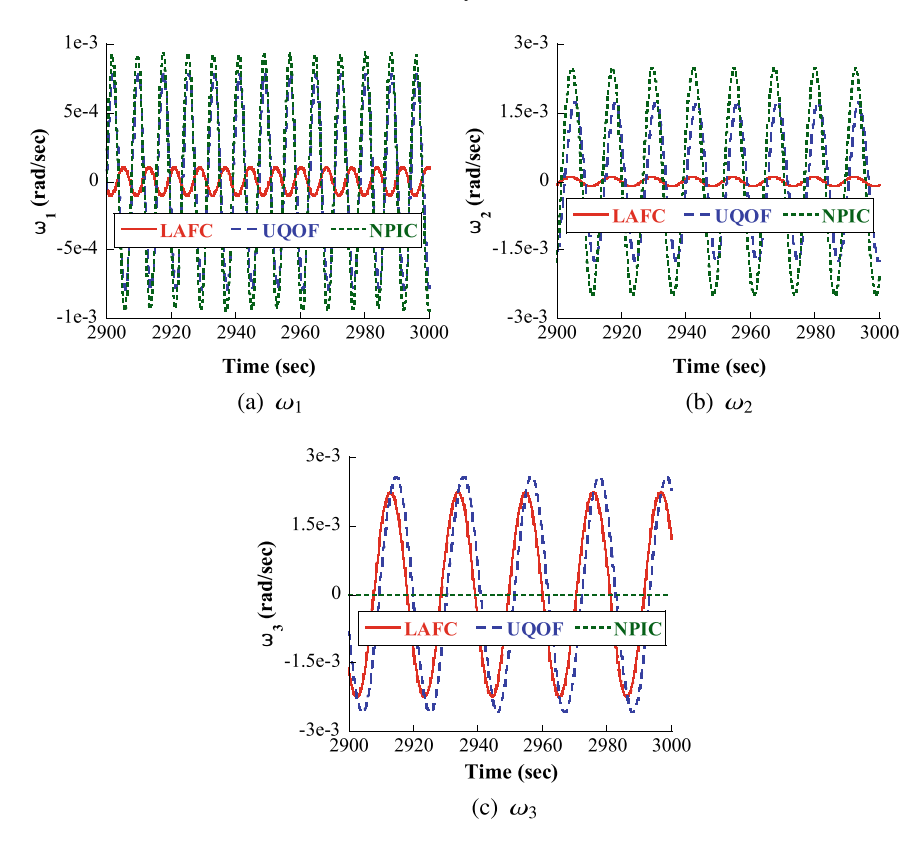


Fig. 4.4 The steady-state angular velocity from LAFC and UQOF

relationship between the magnitudes of the available control inputs and those of the desired trajectories and disturbances. Another problem solved in this chapter is the angular velocity-free attitude stabilization control of rigid satellites with actuator constraint and modeling error due to uncertain inertia and external disturbance. The proposed control law was inertia-independent with angular velocity eliminated and allowed  $\mathcal{L}_2$ -gain of the closed-loop attitude system to be chosen arbitrarily small to achieve any level of  $\mathcal{L}_2$ -gain external disturbance attenuation. The developed scheme has a simple design procedure, structure, and inexpensive computation cost, and thus demands much less onboard resources during its implementation.

4.4 Summary 95

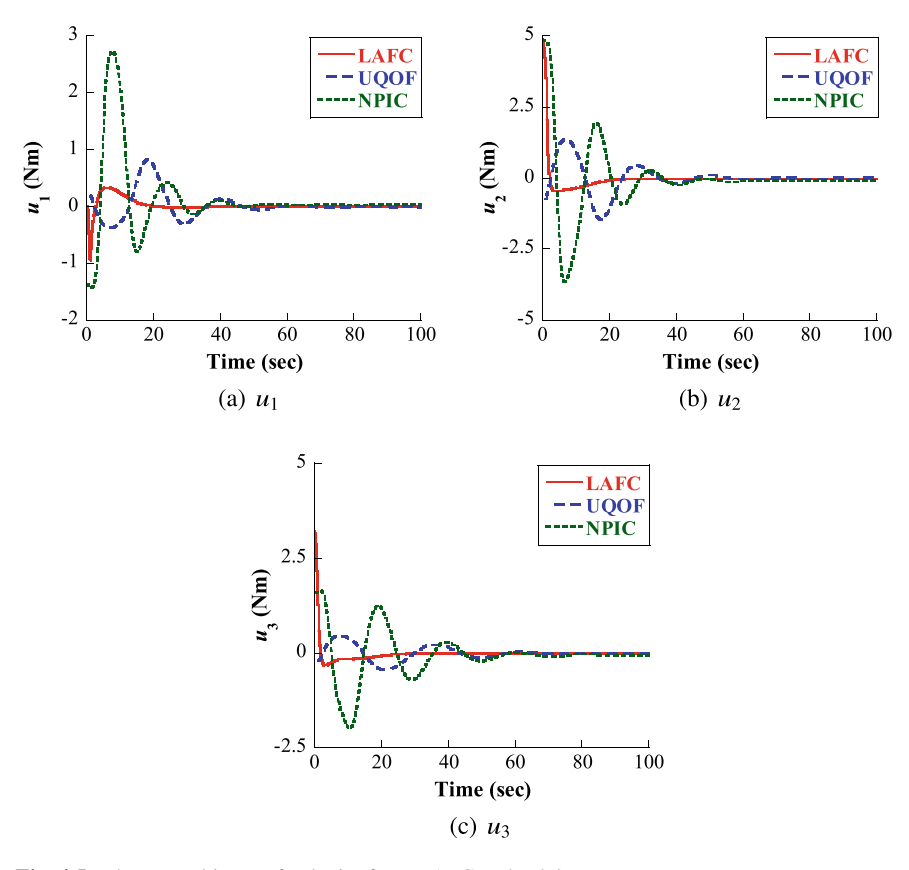


Fig. 4.5 The control input of velocity from LAFC and UQOF

**Table 4.3** The control performance for the controller (4.49), UQOF, and NPIC

Performance	Axis	Controller		
		LAFC	UQOF	NPIC
Pointing accuracy (rad)	Roll	$2.0 \times 10^{-5}$	$2.5 \times 10^{-4}$	$3.0 \times 10^{-4}$
	Pitch		$1.5 \times 10^{-3}$	
	Yaw	$2.0 \times 10^{-5}$	$2.5 \times 10^{-3}$	$3.0 \times 10^{-3}$
Slew rate accuracy (rad/s)	Roll	$7.0 \times 10^{-5}$	$8.0 \times 10^{-4}$	$1.0 \times 10^{-3}$
	Pitch		$2.0 \times 10^{-3}$	
	Yaw	$2.5 \times 10^{-5}$	$3.0 \times 10^{-3}$	$3.5 \times 10^{-3}$
Attitude stabilization	time (s)	30	100	75

#### References

- Farrell, J., Polycarpou, M., Sharma, M. (2003) Adaptive backstepping with magnitude, rate, and bandwidth constraints: Aircraft longitude control. In Proceedings of the Annual American Control Conference, Denver, Colorado Denver: 3898–3904
- He, P. G., Jagannathan, S. (2007) Reinforcement learning neural-network-based controller for nonlinear discrete-time systems with input constraints. IEEE Transactions on Systems Man and Cybernetics Part B: Cybernetics 37(2): 425–436
- 3. Hu, Q. (2008) Adaptive output feedback sliding-mode manoeuvring and vibration control of flexible spacecraft with input saturation. IET Control Theory and Applications 2(6): 467–478
- Graichen, K., Zeitz, M. (2008) Feedforward control design for finite-time transition problems of nonlinear systems with input and output constraints. IEEE Transactions on Automatic Control 53(5): 1273–1278
- Leonessa, A., Haddad, W. M., Hayakawa, T., Morel, Y. (2009) Adaptive control for nonlinear uncertain systems with actuator amplitude and rate saturation constraints. International Journal of Adaptive Control and Signal Processing 23(1): 73–96
- Kulkarni, A., Purwar, S. (2009) Wavelet based adaptive backstepping controller for a class of nonregular systems with input constraints. Expert Systems with Applications 36(3): 6686–6696
- Purwar, S., Kar, I. N., Jha, A. N. (2008) Adaptive output feedback tracking control of robot manipulators using position measurements only. Expert Systems with Applications 34(4): 2789–2798
- Famularo, D., Martino, D., Mattei, M. (2008) Constrained control strategies to improve safety and comfort on aircraft. Journal of Guidance, Control, and Dynamics 31(6): 1782–1792
- 9. Luo, Y. H., Zhang, H. G. (2008) Approximate optimal control for a class of nonlinear discrete-time systems with saturating actuators. Progress in Natural Science 18(8): 1023–1029
- Bang, H., Tahk, M. J., Choi, H. D. (2003) Large angle attitude control of spacecraft with actuator saturation. Control Engineering Practice 11(9): 989–997
- 11. Sonneveldt, L., Chu, Q. P., Mulder, J. A. (2007) Nonlinear flight control design using constrained adaptive backstepping. Journal of Guidance, Control, and Dynamics 30(2): 322–336
- Boskovic, J. D., Li, S. M., Mehra, R. K. (2001) Robust adaptive variable structure control of spacecraft under control input saturation. Journal of Guidance, Control, and Dynamics 24(1): 14–22
- 13. Cai, W. C., Liao, X. H., Song, Y. D. (2008) Indirect robust adaptive fault-tolerant control for attitude tracking of spacecraft. Journal of Guidance, Control, and Dynamics 31(5): 1456–1463
- Lo, S. C., Chen, Y. P. (1995) Smooth sliding mode control for spacecraft attitude tracking maneuvers. Journal of Guidance, Control, and Dynamics 18(6): 1345–1349
- Kristiansen, R., Nicklasson, P. J., Gravdahl, J. T. (2009) Satellite attitude control by quaternionbased backstepping. IEEE Transactions on Control Systems Technology 17(1): 227–232
- Chen, P. C., Huang, A. C. (2005) Adaptive multiple-surface sliding control of hydraulic active suspension systems based on the function approximation technique. Journal of Vibration and Control 11(5): 685–706
- 17. Leeghim, H., Choi, Y., Bang, H. (2009) Adaptive attitude control of spacecraft using neural networks. Acta Astronautica 64(7-8): 778–786
- 18. Chen, F., Jiang, R., Zhang, K., Jiang, B., Tao, G. (2016) Robust backstepping sliding-mode control and observer-based fault estimation for a quadrotor uav. IEEE Transactions on Industral Electronics 63(8): 5044–5056
- Zhou, J., Er, M. J., Zhou, Y. (2006) Adaptive neural network control of uncertain nonlinear systems in the presence of input saturation. In: Proceedings of the 9th International Conference on Control, Automation, Robotics and Vision, pp 1–5
- Subbarao, K., Akella, M. R. (2004) Differentiator-free nonlinear proportional-integral controllers for rigid-body attitude stabilization. Journal of Guidance, Control, and Dynamics 27(6): 1092–1096

References 97

21. Nicosia, S., Tomei, P. (1992) Nonlinear observer and output feedback attitude control of space-craft. IEEE Transactions on Aerospace and Electronic Systems 28(4): 970–977

- 22. Song, Y. D., Cai, W. C. (2009) Quaternion observer-based model-independent attitude tracking control of spacecraft. Journal of Guidance, Control, and Dynamics 32(5): 1476–1482
- 23. Tayebi, A. (2008) Unit quaternion-based output feedback for the attitude tracking problem. IEEE Transactions on Automatic Control 53(6): 1516–1520

# Chapter 5 Velocity-Free Attitude Fault-Tolerant Control



#### 5.1 Introduction

The analysis of recent spacecraft accident statistics shows that a significant portion of such is attributed to actuator fault in attitude control system [1]. In December 1983, faulty reaction wheels of satellite GPS BI-05 led to mission failure. A recent accident occurred with GPS BII-07, a spacecraft in the NAVSTAR GPS constellation developed by the U.S. Department of Defense. It suffered a reaction wheel failure that led to three-axis stabilization failure and a total loss of the spacecraft [2]. Those accidents justify the development of fault tolerant control (FTC). It aims to ensure proper operation even in the presence of component faults. Up to date, a variety of FTC approaches have been proposed [3–5]. Because spacecraft attitude dynamics is inherent with nonlinearity, external disturbance, and uncertainty, designing FTC for spacecraft is becoming much more difficult. Active FTC is an approach characterized by a Fault Detection and Isolation (FDI) mechanism to detect and identify fault online. Many efforts on active FDI together with methods for reconfiguring control systems have been conducted for satellites [6–10].

An alternative active FTC is the so-called passive approach. It applies the robust control technique to ensure system stability without FDI even in the presence of fault. So far several passive FTC algorithms have been developed and applied to satellites [11, 12]. The problem of automated attitude recovery for rigid and flexible LAFC was discussed based on feedback linearization control [13]. A variable structure FTC controller was synthesized to perform attitude stabilization maneuver [14]. Attitude tracking control of a rigid satellite was investigated by designing a passive fault-tolerant controller [15]. Two types of faults in the reaction wheel were accommodated by applying SMC [16]. A terminal sliding mode-based FTC was developed to perform rest-to-rest on a satellite system [17].

The implementation of the preceding FTC or FDI schemes necessitates full state feedback. This may be not satisfied in practice. For instance, the angular velocity measurement would not be available. Although many approaches have been proposed to handle actuator faults and unmeasured angular velocity, few results are seen to

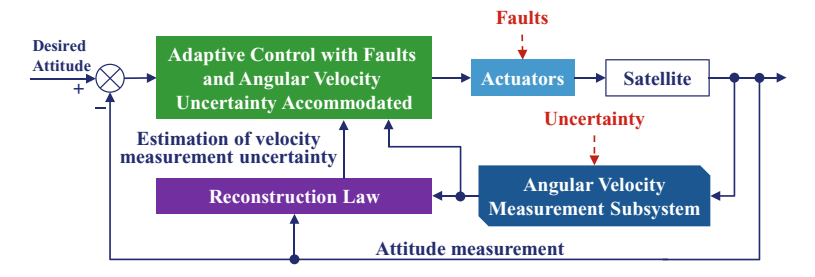


Fig. 5.1 The full control architecture of VFAFTTC with actuator faults and angular velocity measurement uncertainty

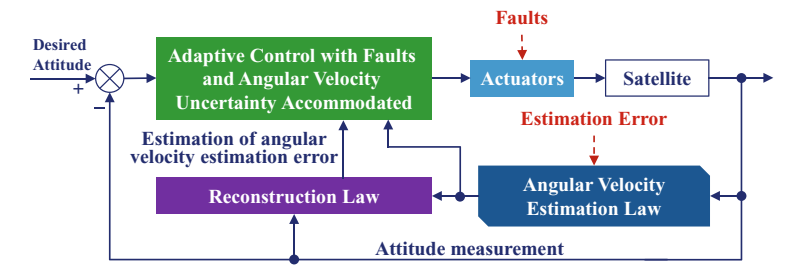


Fig. 5.2 The full control architecture of VFAFTTC with actuator faults and no measurement of angular velocity

address these two problems simultaneously. Motivated by simultaneously addressing the problems including actuator faults, angular velocity measurement uncertainty, uncertain dynamics, and external disturbance, a novel robust velocity-free attitude fault-tolerant tracking control scheme (VFAFTTC) is developed. It consists of a reconstruction law developed in [23] and a novel robust adaptive control law. When angular velocity measurement is available, the full control architecture of the proposed scheme is shown in Fig. 5.1, wherein the reconstruction law is to estimate the angular velocity measurement uncertainty. For the case that there is no angular velocity measurement, the full control architecture of the proposed approach is illustrated in Fig. 5.2. In Fig. 5.2, the angular velocity estimation law is to estimate the angular velocity by using the attitude measurement. The main novelty of this proposed control approach is listed as follows.

- The proposed solution can accomplish the attitude tracking control task for satellites with uncertain dynamics due to uncertain parameters, external disturbance, actuator faults, and angular velocity measurement uncertainty. The attitude tracking error is governed to be uniformly ultimately bounded. The control framework is shown in Fig. 5.1.
- Compared with the state-of-the-art approaches to handle actuator faults for satellites, the proposed strategy does require any prior knowledge of the actuator faults.

Moreover, this scheme is practically implementable without any angular velocity sensors, and the resulting closed-loop system is shown in Fig. 5.2.

• The proposed control approach does not necessitate the dynamic model of the actuators when handling actuator faults.

#### **5.2** Reaction Wheel Faults

Reaction wheel is a type of actuator widely used in satellite attitude control. It consists of a flywheel driven by an electric motor and the associated bearing and drive electronics. It is vulnerable to two main sources of faults [18]:

- (F1) Decreased reaction torque: It is induced by increased friction between stator and rotor, marginal failure of bearings, and decreased motor torque and current drive. These issues affect the rate of change of the wheel speed and consequently decrease the generated reaction torque.
- (F2) Increased bias torque: When the external disturbance is negated and the demanded reaction torque is zero, the reaction wheel should hold its speed and generate no torque. Incipient faults can occur based on changes in friction due to aging, time-varying temperature, etc., that may accelerate or decelerate the wheel, thereby generating a bias torque, even when the commanded torque is zero.

These two faults can be mathematically modeled as

$$\boldsymbol{u} = (\boldsymbol{I}_n - \boldsymbol{E})\boldsymbol{\tau} + \bar{\boldsymbol{u}} \tag{5.1}$$

where  $\boldsymbol{\tau} = [\tau_1, \tau_2, \tau_3]^T \in \mathbb{R}^3$  is the control torque commanded by attitude controller,  $\boldsymbol{E} = \mathrm{diag}([l_{11}(t), l_{22}(t), l_{33}(t)]^T) \in \mathbb{R}^{3 \times 3}$  with  $0\% \leq l_{ii}(t) \leq 100\%$ , i = 1, 2, 3 is the healthy and time-varying indicator matrix due to fault F1, and  $\bar{\boldsymbol{u}} = [\bar{u}_1, \bar{u}_2, \bar{u}_3]^T \in \mathbb{R}^3$  is the fault entering the satellite in an additive way due to the increased bias torque. For example, if the ith actuator operates normally, then it has  $l_{ii} = 0\%$  and  $\bar{u}_i = 0$ . The case in which  $l_{ii} = 30\%$  implies that the ith actuator loses 30% control torque.

**Remark 5.1** In this chapter, only the bias torque fault and the partial loss of actuator effectiveness are considered. The total loss fault, i.e.,  $l_{ii} = 100\%$  and the lock-in-place fault, i.e.,  $\bar{u}_i$  has a constant value are not investigated. If some actuator undergoes the total loss fault or the lock-in-place fault, then the satellite dynamics will be underactuated. The controller design for the underactuated system is not the main issue investigated in this book.

#### 5.3 Angular Velocity Measurement Uncertainty

When implementing any feedback controller to satellites, the attitude feedback  $\sigma$  or q can be supplied and measured by attitude sensors. However, in practical applications,

the availability of the angular velocity measurement  $\dot{\sigma}$ ,  $\omega$ , or  $\dot{q}$  is not always satisfied because of either cost limitations or implementation constraints. This issue should be solved. Let  $\mathbf{v}_m = [v_{m1}, v_{m2}, v_{m3}]^T \in \mathbb{R}^3$  be the angular velocity estimation, and  $\mathbf{v}_u \in \mathbb{R}^3$  denote the angular velocity estimation error or the angular velocity measurement uncertainty, the following can be established as

$$\mathbf{v}_m = \dot{\mathbf{\sigma}} + \mathbf{v}_u \tag{5.2}$$

$$\mathbf{v}_m = \dot{\mathbf{q}} + \mathbf{v}_u \tag{5.3}$$

$$\mathbf{v}_m = \mathbf{\omega} + \mathbf{v}_u \tag{5.4}$$

**Remark 5.2** For the satellites with angular velocity or rate sensors such as the gyroscope,  $v_u$  in (5.2)–(5.4) can be viewed as the angular velocity sensor faults.

#### 5.4 Problem Formulation

The modeling error considered in this chapter consists of the environmental disturbance torque, uncertain inertia, and the reaction wheel faults (5.1). Moreover, the satellite considered is rigid with the attitude represented by the modified Rodrigues parameters  $\sigma$ . According to (4.42), the following second-order nonlinear equation can describe the rigid satellite attitude system.

$$\boldsymbol{M}_{0}(\boldsymbol{\sigma})\ddot{\boldsymbol{\sigma}} + \boldsymbol{C}_{0}(\boldsymbol{\sigma}, \dot{\boldsymbol{\sigma}})\dot{\boldsymbol{\sigma}} + \Delta\boldsymbol{h}(\boldsymbol{\sigma}, \dot{\boldsymbol{\sigma}}, \ddot{\boldsymbol{\sigma}}) = \boldsymbol{P}^{\mathrm{T}}(\boldsymbol{\sigma})\boldsymbol{u} + \boldsymbol{P}^{\mathrm{T}}(\boldsymbol{\sigma})\boldsymbol{u}_{d}$$
 (5.5)

where  $M_0(\sigma) = P^T J_0 P$ ,  $C_0(\sigma, \dot{\sigma}) = -P^T (J_0 P \dot{\sigma} + (J_0 P \dot{\sigma})^{\times}) P$ , and  $\Delta h(\sigma, \dot{\sigma}, \ddot{\sigma}) = P^T \Delta J P - P^T (\Delta J P \dot{\sigma} + (\Delta J P \dot{\sigma})^{\times}) P$ .  $J_0$  is the nominal inertia parameters.  $\Delta J$  is the uncertain inertia.  $\Delta h(\sigma, \dot{\sigma}, \ddot{\sigma})$  denote the uncertain dynamics introduced by the uncertain inertia of the satellite.

**Remark 5.3** For the attitude system (5.5),  $M_0(\sigma)$  and  $C_0(\sigma, \dot{\sigma})$  satisfy Property 4.5, Property 4.6, and Property 4.7 with different values of  $J_{\min}$ ,  $J_{\max}$ , and  $C_{\max}$ .

Let  $\sigma_d = [\sigma_{d1}, \sigma_{d2}, \sigma_{d3}]^{\mathrm{T}} \in \mathbb{R}^3$  be the desired trajectory to be followed.  $\dot{\sigma}_d$  and  $\ddot{\sigma}_d$  are continuous and bounded, respectively, i.e.,  $||\dot{\sigma}_d|| \leq \dot{\sigma}_d^{\max}$ , where  $\dot{\sigma}_d^{\max} \in \mathbb{R}_+$  is a positive scalar. The control problem of this chapter can be stated as: For the satellite with its dynamics described by (5.5), applying the available measurement  $\sigma$  and estimated angular velocity  $v_m$  only to design a controller to ensure that the desired trajectory  $\sigma_d$  can be followed despite the reaction wheel faults (5.1), the angular velocity measurement uncertainty (5.2), the uncertain inertia  $\Delta J$ , and the external disturbance  $u_d$ .

#### 5.5 Transformed System with Reaction Wheel Fault

Two new variables  $\mathbf{x}_1 = [x_{11}, x_{12}, x_{13}]^T = \boldsymbol{\sigma}$  and  $\mathbf{x}_2 = [x_{21}, x_{22}, x_{23}]^T = \dot{\boldsymbol{\sigma}}$  are first introduced. Then, the attitude system (5.5) with the reaction wheel faults (5.1) and the angular velocity uncertainty (5.2) can be rewritten as

$$\dot{\boldsymbol{x}}_1 = \boldsymbol{v}_m - \boldsymbol{v}_u \tag{5.6}$$

$$M_{0}(x_{1})\dot{x}_{2} + C_{0}(x_{1}, x_{2})x_{2} = P^{T}(x_{1})(I_{n} - E)\tau + P^{T}(x_{1})\bar{u} + P^{T}(x_{1})u_{d} - \Delta h(\sigma, \dot{\sigma}, \ddot{\sigma})$$
(5.7)

#### 5.6 Terminal Sliding-Mode Observer

From (5.2), the following equation will always hold

$$\dot{\boldsymbol{v}}_m = \ddot{\boldsymbol{\sigma}} + \dot{\boldsymbol{v}}_u \tag{5.8}$$

Because  $\mathbf{v}_m$  is the estimation of the angular velocity,  $\dot{\mathbf{v}}_m$  represents the estimated measurement of the angular acceleration.  $\ddot{\boldsymbol{v}}_u = [\dot{v}_{u1}, \dot{v}_{u2}, \dot{v}_{u3}]^{\mathrm{T}} \in \mathbb{R}^3$  denotes the measurement error/uncertainty in the angular acceleration.

In satellite engineering, the rate damping control and the attitude acquisition are performed by thrusters before attitude stabilization or tracking maneuvering. After rate damping and attitude acquisition, the angular acceleration is maintained to be within a certain value. Let this certain value be denoted as  $\ddot{\sigma}_{i_{max}} \in \mathbb{R}_+$ , i = 1, 2, 3, then it follows that  $|\ddot{\sigma}_i(t)| \leq \ddot{\sigma}_{i_{max}}$  for  $t \geq 0$ .

**Assumption 5.1**  $\dot{v}_u$  is bounded and satisfies  $|\dot{v}_{ui}| \leq \ddot{\sigma}_{i_{\max}}$ , i = 1, 2, 3.

Based on Assumption 5.1, one has

$$||\dot{\boldsymbol{v}}_{u}|| \leq \sqrt{\sum_{i=1}^{3} \ddot{\sigma}_{i_{\max}}^{2}} = \gamma \tag{5.9}$$

As a stepping stone, an auxiliary system is introduced as

$$\dot{\boldsymbol{x}}_a = \boldsymbol{v}_m - k_r \boldsymbol{x}_e \tag{5.10}$$

where  $k_r \in \mathbb{R}_+$  is a constant,  $\mathbf{x}_a \in \mathbb{R}^3$  is the auxiliary system's state, and  $\mathbf{x}_e = \mathbf{x}_a - \mathbf{x}_1$ .

From (5.6), (5.8), and (5.10), it leaves the dynamics of  $x_e$  as the following linear system with unknown input:

$$\begin{cases}
\begin{bmatrix} \dot{x}_e \\ \dot{v}_u \end{bmatrix} = \begin{bmatrix} -k_r I_n I_n \\ \mathbf{0} & \mathbf{0} \end{bmatrix} \begin{bmatrix} x_e \\ v_u \end{bmatrix} + \begin{bmatrix} \mathbf{0} \\ \dot{v}_u \end{bmatrix} \\
y = x_e
\end{cases} (5.11)$$

where  $[\boldsymbol{x}_e^{\mathrm{T}}, \boldsymbol{v}_u^{\mathrm{T}}]^{\mathrm{T}} \in \mathbb{R}^6$  is the state of this system, and  $\boldsymbol{y} \in \mathbb{R}^3$  is the system output. Based on (5.10) and the definition of  $\boldsymbol{x}_e$ , it follows that

$$\dot{\boldsymbol{x}}_a = -k_r \boldsymbol{x}_a + k_r \boldsymbol{x}_1 + \boldsymbol{v}_m \tag{5.12}$$

Because  $x_1$  and  $v_m$  are available,  $x_a$  can be calculated by solving (5.12). Then,  $y = x_e = x_a - x_1$  can be obtained by using the available  $x_a$  and  $x_1$ . The output y is, thus, available.

To this end, the work of reconstructing  $v_u$  is changed into estimating the state of the system (5.11) by using the output y only. To solve this problem, the following terminal sliding-mode observer is designed

$$\begin{cases} \dot{\hat{x}}_e = -k_r \hat{x}_e + \hat{v}_u - \eta_1 \operatorname{sgn}(e_1) - \eta_2 e_1 \\ \dot{\hat{v}}_u = -\eta_3 e_1 - \eta_4 \lfloor e_v \rfloor^{\frac{a}{b}} - \eta_5 \operatorname{sgn}(e_v) \end{cases}$$
(5.13)

where  $\hat{x}_e$  is the estimation of  $x_e$ ,  $\hat{v}_u$  is the estimation of  $v_u$ ,  $e_v = \eta_1 \operatorname{sgn}(e_1)$ ,  $e_1 = \hat{x}_e - y$ , and  $\eta_i \in \mathbb{R}_+$ , i = 1, 2, 3, 4, 5, are the observer gains.  $a \in \mathbb{R}_+$  and  $b \in \mathbb{R}_+$  are two odd integers satisfying a < b.

**Lemma 5.1** When the terminal sliding-mode observer (5.13) is applied to estimate the angular velocity estimation error or the measurement uncertainty  $\mathbf{v}_u$  satisfying Assumption 5.1, the estimation error  $\mathbf{e} = [\mathbf{e}_1^T, \mathbf{e}_2^T]^T$  is ensured to have  $||\mathbf{e}(t)|| \le \varepsilon_0$  for all  $t \ge 0$ , where  $\mathbf{e}_2 = \hat{\mathbf{v}}_u - \mathbf{v}_u = [e_{21}, e_{22}, e_{23}]^T$  is the reconstruction error of  $\mathbf{v}_u$  and

$$\varepsilon_0 = \max\{\frac{\sqrt{3}\eta_4(\eta_1)^{\frac{a}{b}} + \sqrt{3}\eta_5 + \gamma}{\lambda_{\min}(\mathbf{Q})}, ||\mathbf{e}(0)||\}$$
 (5.14)

with the positive-definite constant matrix Q given by

$$Q = \begin{bmatrix} (k_r + \eta_2)I_n & -I_n \\ \eta_3 I_n & \mathbf{0} \end{bmatrix}$$
 (5.15)

**Proof** From (5.11) and (5.13), one has

$$\dot{\mathbf{e}}_1 = -k_r \mathbf{e}_1 + \mathbf{e}_2 - \eta_1 \text{sgn}(\mathbf{e}_1) - \eta_2 \mathbf{e}_1 \tag{5.16}$$

$$\dot{\boldsymbol{e}}_{2} = -\eta_{3}\boldsymbol{e}_{1} - \eta_{4} \lfloor \boldsymbol{e}_{v} \rfloor^{\frac{a}{b}} - \eta_{5} \operatorname{sgn}(\boldsymbol{e}_{v}) - \dot{\boldsymbol{v}}_{u}$$
 (5.17)

Consider a candidate Lyapunov function  $V_0 = \frac{1}{2}e^T e$ , applying (5.9) and (5.16)–(5.17) result in

$$\dot{V}_{0} = -k_{r} \boldsymbol{e}_{1}^{\mathsf{T}} \boldsymbol{e}_{1} + \boldsymbol{e}_{1}^{\mathsf{T}} \boldsymbol{e}_{2} - \eta_{1} \boldsymbol{e}_{1}^{\mathsf{T}} \mathbf{sgn}(\boldsymbol{e}_{1}) - \eta_{2} \boldsymbol{e}_{1}^{\mathsf{T}} \boldsymbol{e}_{1} - \eta_{3} \boldsymbol{e}_{2}^{\mathsf{T}} \boldsymbol{e}_{1} 
- \eta_{4} \boldsymbol{e}_{2}^{\mathsf{T}} \lfloor \boldsymbol{e}_{v} \rfloor^{\frac{a}{b}} - \eta_{5} \boldsymbol{e}_{2}^{\mathsf{T}} \mathbf{sgn}(\boldsymbol{e}_{v}) - \boldsymbol{e}_{2}^{\mathsf{T}} \dot{\boldsymbol{v}}_{u} 
\leq -\boldsymbol{e}^{\mathsf{T}} \boldsymbol{Q} \boldsymbol{e} - \eta_{1} \|\boldsymbol{e}_{1}\| + \left(\sqrt{3} \eta_{4} (\eta_{1})^{\frac{a}{b}} + \sqrt{3} \eta_{5} + \gamma\right) \|\boldsymbol{e}\| 
\leq -||\boldsymbol{e}|| \left(\lambda_{\min}(\boldsymbol{Q})||\boldsymbol{e}|| - \left(\sqrt{3} \eta_{4} (\eta_{1})^{\frac{a}{b}} + \sqrt{3} \eta_{5} + \gamma\right)\right)$$
(5.18)

Hence,  $\dot{V}_0 < 0$  if  $||e|| > \frac{\sqrt{3}\eta_4(\eta_1)^{\frac{d}{b}} + \sqrt{3}\eta_5 + \gamma}{\lambda_{\min}(\mathcal{Q})}$ . This implies that if e is outside the compact set  $\mathcal{D}_1 = \{e|||e|| \le \frac{\sqrt{3}\eta_4(\eta_1)^{\frac{d}{b}} + \sqrt{3}\eta_5 + \gamma}{\lambda_{\min}(\mathcal{Q})}\}$ , then  $\dot{V}_0 < 0$ ; and hence, ||e|| decreases monotonically with respect to t. A decreasing value of  $V_0$  eventually drives e into the set  $\mathcal{D}_1$  and, then, it will never go out of  $\mathcal{D}_1$ . The set  $\mathcal{D}_1$  is, thus, attractive. Therefore, it can be proved that  $||e|| \le \varepsilon_0$ ,  $t \ge 0$ .

**Lemma 5.2** For the angular velocity estimation error or the measurement uncertainty  $\mathbf{v}_u$  satisfying Assumption 5.1, applying the terminal sliding-mode observer (5.13), let  $k_r$  and the observer gains and initial estimation states be chosen such that

$$\eta_1 > \max \left\{ \left( \frac{\sqrt{3}\eta_4 + \sqrt{3}\eta_5 + \gamma}{\lambda_{\min}(\boldsymbol{Q})} + \varsigma_0 \right)^{\frac{b}{b-a}}, 1 \right\}$$
(5.19)

$$\eta_5 - \gamma > 0 \tag{5.20}$$

where  $\varsigma_0 \in \mathbb{R}_+$  is a scalar. Then,  $\mathbf{v}_u$  can be precisely reconstructed  $\hat{\mathbf{v}}_u$ .  $\mathbf{e}_2(t) \equiv \mathbf{0}$  is guaranteed for  $t > t_1 = \frac{b(\mathbf{e}_2(t_0))^{\frac{b-a}{2b}}}{(b-a)\eta_4} + t_0$ ,  $t_0 = \frac{\|\mathbf{e}_1(0)\|}{\varsigma_0}$ .

**Proof** See [23] for the reason that the observer gains should be chosen to satisfy (5.19)–(5.20).

**Remark 5.4** It is seen in Lemma 5.1 that in comparison with the existing Luenberger-type state observers [25–27] and other observers such as the globally convergent velocity observer [28], the proposed terminal sliding-mode observer (5.13) ensures the reconstruction error to be finite-time stable. Hence, a faster estimation for the angular velocity measurement uncertainty  $v_u$  is achieved. This is the main motivation of presenting the terminal sliding-mode observer (5.13) in this chapter.

#### 5.7 Velocity-Free Fault-Tolerant Attitude Controller

It is inferred from (5.1) that  $0 < \mu = ||E|| = \max_{i=1,2,3} \{|l_{ii}|\} < 1$ . However,  $\mu$  is unknown. Although there may exist bias torque fault  $\bar{u}$  in actuators, it is bounded.

Conservatively, the bias torque in the ith reaction wheel actuator should be smaller than the maximum torque  $u_{i_{-}\max} \in \mathbb{R}_{+}$  of the ith reaction wheel actuator, i.e.,  $\bar{u}_{i} \leq u_{i_{-}\max}$ , i=1,2,3.  $\Delta h(\sigma,\dot{\sigma},\ddot{\sigma})$  and  $u_{d}$  should also be bounded, i.e., there exist two unknown scalars  $d_{\max_{-1}} \in \mathbb{R}_{+}$  and  $d_{\max_{-2}} \in \mathbb{R}_{+}$  such that  $||\Delta h(\sigma,\dot{\sigma},\ddot{\sigma})|| \leq d_{\max_{-2}}$  and  $||u_{d}|| \leq d_{\max_{-1}}$ . If  $\Delta h(\sigma,\dot{\sigma},\ddot{\sigma})$  and  $u_{d}$  are not bounded, then the maximum torque generated by actuators will be unable to attenuate  $\Delta h(\sigma,\dot{\sigma},\ddot{\sigma})$  and  $u_{d}$ . In this case, the satellite will be uncontrollable. This makes the attitude controller design without any sense. Therefore,  $||\Delta h(\sigma,\dot{\sigma},\ddot{\sigma})|| \leq d_{\max_{-2}}$  and  $||u_{d}|| \leq d_{\max_{-1}}$  and reasonable. On the other hand, it is also obtained from Property 2.1 that  $||G(\sigma)|| \leq 0.5$  and  $||P(x_1)|| = \frac{16||G(\sigma)||}{(1+\sigma^{\top}\sigma)^2} \leq 8$ . As a consequence, one has

$$||\boldsymbol{P}^{\mathrm{T}}(\boldsymbol{x}_{1})\boldsymbol{\bar{u}} + \boldsymbol{P}^{\mathrm{T}}(\boldsymbol{x}_{1})\boldsymbol{u}_{d} - \Delta\boldsymbol{h}(\boldsymbol{\sigma}, \dot{\boldsymbol{\sigma}}, \ddot{\boldsymbol{\sigma}})|| \leq 8d_{\max} + d_{\max} + 4d_{\max} + 8\sqrt{\sum_{i=1}^{3} u_{i_{-}\max}^{2}} = \rho$$
(5.21)

where the constant  $\rho \in \mathbb{R}$  is positive but unknown.

Let  $z_1 = [z_{11}, z_{12}, z_{13}]^T = \boldsymbol{\sigma} - \boldsymbol{\sigma}_d$  denote the attitude tracking error of the satellite, and introduce another new variable as  $z_2 = \boldsymbol{v}_m - \dot{\boldsymbol{\sigma}}_d + k_{c1}z_1 - \hat{\boldsymbol{v}}_u$ , where  $k_{c1} \in \mathbb{R}_+$  is a scalar. From Lemma 5.2, it is known that  $z_1$  and  $z_2$  are available for feedback when designing an attitude tracking controller.

**Theorem 5.1** For the satellite dynamics (5.5) with external disturbances, uncertain inertia  $\Delta J$ , reaction wheel actuator faults (5.1), and angular velocity measurement uncertainty (5.2) satisfying Assumption 5.1, applying the estimation law (5.13) for the angular velocity measurement uncertainty, let a velocity-free fault-tolerant attitude controller be developed as

$$\tau = G^{T}(x_1)(\tau_{\text{nor}} + \tau_{\text{com}\_1} + \tau_{\text{com}\_2})$$
 (5.22)

with

$$\tau_{\text{nor}} = -z_1 - k_{c2}z_2 + C_0(x_1, z_2 + \dot{\sigma}_d - k_{c1}z_1)(k_{c1}z_1 - \dot{\sigma}_d) - M_0(x_1)(-\ddot{\sigma}_d + k_{c1}(z_2 - k_{c1}z_1))$$
(5.23)

$$\tau_{\text{com}_{-}1} = -(\hat{\mu}_0 - 1)||\tau_{\text{nor}} + \tau_{\text{com}_{-}2}||\mathbf{sgn}(z_2)|$$
 (5.24)

$$\tau_{\text{com}_2} = -\hat{\rho} \text{sgn}(z_2) \tag{5.25}$$

where  $k_{c2} \in \mathbb{R}_+$  is the control gain,  $\hat{\rho} \in \mathbb{R}$  is the estimation of the scalar  $\rho$ ,  $\hat{\mu}_0 \in \mathbb{R}$  is the estimation of the constant  $\mu_0 = \frac{1}{1-\mu}$ ,  $\mu_0 \ge 1$ ;  $\hat{\mu}_0$  and  $\hat{\rho}$  are updated by

$$\dot{\hat{\mu}}_0 = -k_{c3}\hat{\mu}_0 + k_{c3}||\boldsymbol{\tau}_{\text{nor}} + \boldsymbol{\tau}_{\text{com},2}||||z_2||, \, \hat{\mu}_0(0) \ge 1$$
 (5.26)

$$\dot{\hat{\rho}} = -k_{c4}\hat{\rho} + k_{c4}||z_2||, \, \hat{\rho}(0) > 0 \tag{5.27}$$

with two gains  $k_{c3} \in \mathbb{R}_+$  and  $k_{c4} \in \mathbb{R}_+$ . If the observer gains  $k_r$ ,  $\eta_i$ , i = 1, 2, 3, 4, 5, and the control gains are chosen with (5.19), (5.20), and

$$2k_{c1} > 3$$
 (5.28)

$$k_{c2} - 2 - ((k_{c1}C_{\text{max}}\varepsilon_0)^2 + C_{\text{max}}\varepsilon_0) > 0$$
 (5.29)

satisfied, then, the closed-loop system is stable in that all the signals are uniformly ultimately bounded.

**Proof** Differentiating  $z_1$  by using inserting (5.8) results in

$$\dot{z}_1 = z_2 - k_{c1}z_1 + \hat{\mathbf{v}}_u - \mathbf{v}_u = z_2 - k_{c1}z_1 + \mathbf{e}_2$$
 (5.30)

Applying Property 4.5, (5.7), (5.8), (5.22), (5.23), and (5.30), it follows that

$$M_{0}(\mathbf{x}_{1})\dot{\mathbf{z}}_{2} = M_{0}(\mathbf{x}_{1})(\dot{\mathbf{v}}_{m} - \ddot{\boldsymbol{\sigma}}_{d} + k_{c1}\dot{\mathbf{z}}_{1} - \dot{\hat{\mathbf{v}}}_{u})$$

$$= -\mathbf{z}_{1} - k_{c2}\mathbf{z}_{2} + \boldsymbol{\tau}_{\text{com}\_1} + \boldsymbol{\tau}_{\text{com}\_2} - \boldsymbol{E}\boldsymbol{\tau}$$

$$+ \boldsymbol{P}^{T}(\mathbf{x}_{1})\bar{\boldsymbol{u}} + \boldsymbol{P}^{T}(\mathbf{x}_{1})\boldsymbol{u}_{d} - \Delta\boldsymbol{h}(\boldsymbol{\sigma}, \dot{\boldsymbol{\sigma}}, \ddot{\boldsymbol{\sigma}})$$

$$- \boldsymbol{C}_{0}(\mathbf{x}_{1}, \mathbf{x}_{2})\boldsymbol{x}_{2} - M_{0}(\mathbf{x}_{1})(\dot{\boldsymbol{e}}_{2} + k_{c1}\boldsymbol{e}_{2})$$

$$- \boldsymbol{C}_{0}(\mathbf{x}_{1}, \mathbf{z}_{2} + \dot{\boldsymbol{\sigma}}_{d} - k_{c1}\mathbf{z}_{1})(k_{c1}\mathbf{z}_{1} - \dot{\boldsymbol{\sigma}}_{d})$$

$$(5.31)$$

Using Property 4.7, it leads to

$$-C_{0}(x_{1}, x_{2})x_{2} + C_{0}(x_{1}, x_{2})z_{2} = C_{0}(x_{1}, z_{2} - x_{2})x_{2}$$

$$= C_{0}(x_{1}, k_{c1}z_{1} - \dot{\sigma}_{d} - e_{2})(z_{2} + \dot{\sigma}_{d} - k_{c1}z_{1} + e_{2})$$

$$= C_{0}(x_{1}, z_{2} + \dot{\sigma}_{d} - k_{c1}z_{1})(k_{c1}z_{1} - \dot{\sigma}_{d}) + C_{0}(x_{1}, k_{c1}z_{1} - \dot{\sigma}_{d})e_{2}$$

$$- C_{0}(x_{1}, e_{2})e_{2} - C_{0}(x_{1}, z_{2} + \dot{\sigma}_{d} - k_{c1}z_{1})e_{2}$$

$$(5.32)$$

For the dynamics (5.5), select a Lyapunov candidate function as

$$V_1 = \frac{1}{2} \mathbf{z}_1^{\mathrm{T}} \mathbf{z}_1 + \frac{1}{2} \mathbf{z}_2^{\mathrm{T}} \mathbf{M}_0(\mathbf{x}_1) \mathbf{z}_2 + \frac{1}{2k_{c3}} (1 - \mu) \tilde{\mu}_0^2 + \frac{1}{2k_{c4}} \tilde{\rho}^2$$
 (5.33)

where  $\tilde{\rho} = \rho - \hat{\rho}$  and  $\tilde{\mu}_0 = \mu_0 - \hat{\mu}_0$  are the estimation error of  $\rho$  and  $\mu_0$ , respectively. Using 4.5, it is seen from (5.33) that

$$K_1||X||^2 \le V_1 \tag{5.34}$$

with  $X = [z_1^T, z_2^T, z_1^T, \tilde{\mu}_0, \tilde{\rho}]^T$  and  $K_1 = \min \left\{ \frac{1}{2}, \frac{\lambda_2}{2}, \frac{1-\mu}{2k_{c3}}, \frac{1}{2k_{c4}} \right\} > 0$ . Differentiating  $V_1$  with (5.30)–(5.32) and 4.6 applied, one has

$$\dot{V}_{1} = z_{1}^{T} \dot{z}_{1} + \frac{z_{2}^{T} \dot{M}_{0}(x_{1})z_{2}}{2} + z_{2}^{T} M_{0}(x_{1}) \dot{z}_{2} - \frac{(1-\mu)}{k_{c3}} \tilde{\mu}_{0} \dot{\hat{\mu}}_{0} - \frac{\tilde{\rho} \dot{\hat{\rho}}}{k_{c4}}$$

$$= -k_{c1} ||z_{1}||^{2} - k_{c2}||z_{2}||^{2} + z_{1}^{T} e_{2} - \tilde{\rho}(||z_{2}|| - \hat{\rho}) + z_{2}^{T} (\tau_{\text{com\_1}} + \tau_{\text{com\_2}})$$

$$- E \tau + P^{T}(x_{1}) \bar{u} + P^{T}(x_{1}) u_{d} - \Delta h(\sigma, \dot{\sigma}, \ddot{\sigma}) - M_{0}(x_{1}) (\dot{e}_{2} + k_{c1} e_{2})$$

$$+ C_{0}(x_{1}, k_{c1} z_{1} - \dot{\sigma}_{d}) e_{2} C_{0}(x_{1}, e_{2}) e_{2} - C_{0}(x_{1}, z_{2} + \dot{\sigma}_{d} - k_{c1} z_{1}) e_{2})$$

$$- (1 - \mu) \tilde{\mu}_{0}(||u_{\text{nor}} + \tau_{\text{com\_2}}||||z_{2}|| - \hat{\mu}_{0})$$
(5.35)

On the other hand, it can be obtained from (5.24) and (5.25) that

$$z_{2}^{\mathrm{T}}(\boldsymbol{\tau}_{\text{com}_{2}} + \boldsymbol{P}^{\mathrm{T}}(\boldsymbol{x}_{1})(\bar{\boldsymbol{u}} + \boldsymbol{u}_{d}) - \Delta \boldsymbol{h}(\boldsymbol{\sigma}, \dot{\boldsymbol{\sigma}}, \ddot{\boldsymbol{\sigma}})) \leq -\hat{\rho}||z_{2}|| + \rho||z_{2}||$$

$$= \tilde{\rho}||z_{2}||$$
(5.36)

$$\mathbf{z}_{2}^{\mathrm{T}}(\boldsymbol{\tau}_{\mathrm{com}_{-}1} - \boldsymbol{E}\boldsymbol{\tau}) \le (1 - \mu)\tilde{\mu}_{0}||\boldsymbol{\tau}_{\mathrm{nor}} + \boldsymbol{\tau}_{\mathrm{com}_{-}2}||||\boldsymbol{z}_{2}||$$
 (5.37)

Using (5.36)–(5.37) and (5.26)–(5.27), (5.35) can be further simplified as

$$\dot{V}_{1} \leq -k_{c1}||z_{1}||^{2} - k_{c2}||z_{2}||^{2} + z_{1}^{T}\boldsymbol{e}_{2} + \tilde{\rho}\hat{\rho} + (1-\mu)\tilde{\mu}_{0}\hat{\mu}_{0} 
+ z_{2}^{T}(-\boldsymbol{M}_{0}(\boldsymbol{x}_{1})(\dot{\boldsymbol{e}}_{2} + k_{c1}\boldsymbol{e}_{2}) + \boldsymbol{C}_{0}(\boldsymbol{x}_{1}, k_{c1}\boldsymbol{z}_{1} - \dot{\boldsymbol{\sigma}}_{d})\boldsymbol{e}_{2} 
- \boldsymbol{C}_{0}(\boldsymbol{x}_{1}, \boldsymbol{e}_{2})\boldsymbol{e}_{2} - \boldsymbol{C}_{0}(\boldsymbol{x}_{1}, z_{2} + \dot{\boldsymbol{\sigma}}_{d} - k_{c1}\boldsymbol{z}_{1})\boldsymbol{e}_{2})$$
(5.38)

From Lemma 5.1,  $||e(t)|| \le \varepsilon_0$  is seen for  $t \ge 0$  and regardless of the controller. Hence, one has  $||e_1(t)|| \le \varepsilon_0$  and  $||e_2(t)|| \le \varepsilon_0$ ,  $t \ge 0$ . Then, it follows from (5.17) and Assumption 5.1 that

$$||\dot{\boldsymbol{e}}_{2}|| \leq \eta_{3}||\boldsymbol{e}_{1}|| + \eta_{4}||\boldsymbol{e}_{v}|^{\frac{a}{b}}|| + \eta_{5}||\mathbf{sgn}(\boldsymbol{e}_{v})|| + ||\dot{\boldsymbol{v}}_{u}||$$

$$\leq \eta_{3}\varepsilon_{0} + \sqrt{3}\eta_{4}\eta_{1}^{\frac{a}{b}} + \sqrt{3}\eta_{5} + \gamma = l_{0}$$

$$(5.39)$$

Invoking (5.39), Property 4.5, and Property 4.7, the following inequalities hold for  $t \ge 0$ 

$$-z_{2}^{T} \boldsymbol{M}_{0}(\boldsymbol{x}_{1}) (\dot{\boldsymbol{e}}_{2} + k_{c1} \boldsymbol{e}_{2}) \leq \lambda_{1} ||z_{2}|| ||\boldsymbol{M}_{0}(\boldsymbol{x}_{1})|| (||\dot{\boldsymbol{e}}_{2}|| + k_{c1}||\boldsymbol{e}_{2}||)$$

$$\leq \lambda_{1} (l_{0} + k_{c1} \varepsilon_{0}) ||z_{2}||$$

$$\leq 0.5 ||z_{2}||^{2} + 0.5 (\lambda_{1} (l_{0} + k_{c1} \varepsilon_{0}))^{2}$$

$$(5.40)$$

$$z_{2}^{T}C_{0}(\mathbf{x}_{1}, k_{c1}\mathbf{z}_{1} - \dot{\boldsymbol{\sigma}}_{d})\boldsymbol{e}_{2} \leq C_{\max}||\mathbf{z}_{2}|| ||k_{c1}\mathbf{z}_{1} - \dot{\boldsymbol{\sigma}}_{d}||||\boldsymbol{e}_{2}|| \\ \leq C_{\max}\varepsilon_{0}||\mathbf{z}_{2}||(k_{c1}||\mathbf{z}_{1}|| + \dot{\boldsymbol{\sigma}}_{d}^{\max}) \\ \leq \frac{1}{2}||\mathbf{z}_{2}||^{2} + \frac{1}{2}(C_{\max}\varepsilon_{0}\dot{\boldsymbol{\sigma}}_{d}^{\max})^{2} \\ + \frac{1}{2}||\mathbf{z}_{1}||^{2} + \frac{(k_{c1}C_{\max}\varepsilon_{0})^{2}}{2}||\mathbf{z}_{2}||^{2}$$

$$(5.41)$$

$$z_{2}^{T}C_{0}(\mathbf{x}_{1}, \mathbf{e}_{2}) \mathbf{e}_{2} \leq C_{\max}||\mathbf{z}_{2}||||\mathbf{e}_{2}||^{2} \leq C_{\max}\varepsilon_{0}^{2}||\mathbf{z}_{2}||$$

$$\leq 0.5||\mathbf{z}_{2}||^{2} + 0.5(C_{\max}\varepsilon_{0}^{2})^{2}$$
(5.42)

$$\begin{split} z_{2}^{\mathrm{T}}C_{0}(\boldsymbol{x}_{1}, z_{2} + \dot{\boldsymbol{\sigma}}_{d} - k_{c1}z_{1})\boldsymbol{e}_{2} &\leq C_{\max}||z_{2}||||z_{2} + \dot{\boldsymbol{\sigma}}_{d} - k_{c1}z_{1}||||\boldsymbol{e}_{2}|| \\ &\leq C_{\max}\varepsilon_{0}||z_{2}||(||z_{2}|| + k_{c1}||z_{1}|| + \dot{\boldsymbol{\sigma}}_{d}^{\max}) \\ &\leq 0.5||z_{2}||^{2} + 0.5(C_{\max}\varepsilon_{0}\dot{\boldsymbol{\sigma}}_{d}^{\max})^{2} + 0.5||z_{1}||^{2} \\ &+ 0.5(k_{c1}C_{\max}\varepsilon_{0})^{2}||z_{2}||^{2} + C_{\max}\varepsilon_{0}||z_{2}||^{2} \end{split}$$

$$(5.43)$$

Then, one can simplify (5.38) as follows by using (5.40)–(5.43):

$$\dot{V}_{1} \leq -\left(k_{c2} - 2 - ((k_{c1}C_{\max}\varepsilon_{0})^{2} + C_{\max}\varepsilon_{0})\right)||z_{2}||^{2} + \varepsilon_{0}||z_{1}|| 
- (k_{c1} - 1)||z_{1}||^{2} + \tilde{\rho}(\rho - \tilde{\rho}) + (1 - \mu)\tilde{\mu}_{0}(\mu_{0} - \tilde{\mu}_{0}) 
+ \frac{(\lambda_{1}(l_{0} + k_{c1}\varepsilon_{0}))^{2}}{2} + \frac{(C_{\max}\varepsilon_{0}^{2})^{2}}{2} + (C_{\max}\varepsilon_{0}\dot{\sigma}_{d}^{\max})^{2} 
\leq -\left(k_{c2} - 2 - ((k_{c1}C_{\max}\varepsilon_{0})^{2} + C_{\max}\varepsilon_{0})\right)||z_{2}||^{2} - 0.5\tilde{\rho}^{2} 
- \left(k_{c1} - \frac{3}{2}\right)||z_{1}||^{2} + \frac{1}{2}\rho^{2} - \frac{(1 - \mu)}{2}\tilde{\mu}_{0}^{2} + \frac{(1 - \mu)}{2}\mu_{0}^{2} 
+ \frac{(\lambda_{1}(l_{0} + k_{c1}\varepsilon_{0}))^{2}}{2} + \frac{(C_{\max}\varepsilon_{0}^{2})^{2}}{2} + (C_{\max}\varepsilon_{0}\dot{\sigma}_{d}^{\max})^{2} + \frac{\varepsilon_{0}^{2}}{2}$$
(5.44)

To this end, the following two parts are given to analyze the stability of the closed-loop attitude tracking control system.

(1) Stability analysis of the closed-loop attitude tracking system for  $t \ge 0$ : With  $0 < \mu < 1$  and the gain choice in (5.28) and (5.29), one can rewrite (5.44) as

$$\dot{V}_1 < -K_2 V_1 + \varepsilon_1, t > 0 \tag{5.45}$$

where

$$K_2 = \min\left\{2k_{c1} - 3, \frac{2(k_{c2} - 2 - ((k_{c1}C_{\max}\varepsilon_0)^2 + C_{\max}\varepsilon_0))}{\lambda_1}, k_{c3}, k_{c4}\right\} > 0$$
(5.46)

$$\varepsilon_{1} = \frac{\rho^{2} + \mu_{0}^{2} + \lambda_{1}^{2}(l_{0} + k_{c1}\varepsilon_{0})^{2} + \left(C_{\max}\varepsilon_{0}^{2}\right)^{2} + \varepsilon_{0}^{2}}{2} + \left(C_{\max}\varepsilon_{0}\dot{\sigma}_{d}^{\max}\right)^{2} > 0 \quad (5.47)$$

Solving (5.45) results in

$$0 \le V_1(t) \le \left(V_1(0) - \frac{\varepsilon_1}{K_2}\right) \exp(-K_2 t) + \frac{\varepsilon_1}{K_2} \le \varepsilon_2, t \ge 0 \tag{5.48}$$

with  $\varepsilon_2 = \max\{V_1(0), \frac{\varepsilon_1}{K_2}\}$ . It follows from (5.34) and (5.48) that

$$||X|| \le \sqrt{\frac{\varepsilon_2}{K_1}}, t \ge 0 \tag{5.49}$$

which implies that  $z_1$ ,  $z_2$ ,  $\tilde{\mu}_0$ , and  $\tilde{\rho}$  are bounded for all  $t \geq 0$ . Because  $\ddot{\sigma}_d$ ,  $\rho$ , and  $\mu$  are bounded, using (5.22)–(5.25), one can conclude that  $\hat{\mu}_0$ ,  $\hat{\rho}$ , and  $u_c$  are bounded. Therefore, it is proved that the closed-loop attitude tracking control system is stable in that all the signals are bounded.

(2) Convergence property of  $z_1$  and  $z_1$  for  $t \ge t_1$ : Because of the reconstruction law (5.13) when implementing the controller (5.22),  $e_2(t) \equiv \mathbf{0}$  and  $\dot{e}_2(t) \equiv \mathbf{0}$  for  $t \ge t_1$  are obtained from Lemma 5.2. Inserting  $e_2(t) \equiv \mathbf{0}$  and  $\dot{e}_2(t) \equiv \mathbf{0}$  into (5.38), for  $t \ge t_1$ , it leaves (5.38) as

$$\dot{V}_{1} \leq -k_{c1}||z_{1}||^{2} - k_{c2}||z_{2}||^{2} + \tilde{\rho}\hat{\rho} + (1-\mu)\tilde{\mu}_{0}\hat{\mu}_{0}$$

$$\leq -k_{c1}||z_{1}||^{2} - k_{c2}||z_{2}||^{2} - \frac{(1-\mu)}{2}\tilde{\mu}_{0}^{2} - \frac{\tilde{\rho}^{2}}{2} + \frac{\rho^{2}}{2} + \frac{\mu_{0}^{2}}{2}$$

$$\leq -K_{3}V_{1} + \varepsilon_{3}$$
(5.50)

where  $K_3 = \min\{2k_{c1}, \frac{2k_{c2}}{\lambda_1}, k_{c3}, k_{c4}\} > 0$  and  $\varepsilon_3 = \frac{\rho^2 + \mu_0^2}{2} > 0$ . Solving (5.50) yields

$$0 \le V_1(t) \le V_1(t_1) \exp(-K_3(t-t_1)) + \varepsilon_3 \int_{t_1}^t \exp(-K_3(t-s)) ds$$
  
=  $V_1(t_1) \exp(-K_3(t-t_1)) + \frac{\varepsilon_3}{K_3} (1 - \exp(-K_3(t-t_1)))$  (5.51)

Therefore, using (5.34), it is proved that the state X is bounded ultimately as

$$0 \le V_1(t) \le \max \left\{ 2V_1(t_1) \exp(-K_3(t-t_1)), \frac{2\varepsilon_3}{K_3} \right\}, t \ge t_1$$
 (5.52)

$$0 \le ||X|| \le \max \left\{ \sqrt{\frac{2V_1(t_1)}{K_1}} \exp(-\frac{K_3(t-t_1)}{2}), \sqrt{\frac{2\varepsilon_3}{K_1K_3}} \right\}, t \ge t_1$$
 (5.53)

$$0 \le ||z_1|| \le ||X|| \le \max\left\{\sqrt{\frac{2V_1(t_1)}{K_1}} \exp(-\frac{K_3(t-t_1)}{2}), \sqrt{\frac{2\varepsilon_3}{K_1K_3}}\right\}, t \ge t_1$$
(5.54)

From (5.54), using Definition 2.1, it can be concluded that  $z_1$ ,  $z_2$ ,  $\tilde{\mu}_0$  and  $\tilde{\rho}$  are ultimately uniformly bounded.  $\ddot{\sigma}_d$ ,  $\rho$ , and  $\mu$  are bounded, using (5.22)–(5.25), one can further conclude that  $\hat{\mu}_0$ ,  $\hat{\rho}$ , and  $\boldsymbol{u}_c$  are bounded.

It is seen in the proof of Theorem 5.1 that uniformly ultimately bounded stability of the attitude tracking error  $z_1$  is ensured despite the angular velocity uncertainty  $v_u$ , the disturbances d, the actuator faults (5.1), and the uncertain inertia  $\Delta J$ . This is owing to the control efforts  $\tau_{\text{com}\_1}$  and  $\tau_{\text{com}\_2}$  in the controller (5.22). The control effort (5.23) is used to govern the stability of the nominal system (i.e., the satellite dynamics is free of actuator faults, unknown dynamics, and external disturbance). The control power (5.24) is applied to compensate for the reaction wheel actuator faults (5.1). The control effort (5.25) is to compensate for the disturbance d and uncertain dynamics  $\Delta h(\sigma, \dot{\sigma}, \ddot{\sigma})$ . Moreover, this approach does not necessitate the exact knowledge of the actuator faults. It is independent of when, where, and how the actuator faults occur. In addition, the designed controller does not require any identification process to reconstruct the external disturbance and the uncertain dynamics. Therefore, the presented scheme is essentially a robust control method. The tracking performance is ensured to be robust to the external disturbance, the actuator faults, and the uncertain dynamics.

It is also found in Lemma 5.2 and Theorem 5.1 that, if there are angular velocity sensors, then the proposed approach can accomplish the attitude tracking task despite actuator faults and angular velocity measurement uncertainty. If there is not any rate sensor to supply angular velocity measurements, then the proposed scheme can still guarantee that the desired attitude is followed even in the case of actuator faults. This is achieved by providing an estimated angular velocity to replace the angular velocity.

**Remark 5.5** From the proof of Lemma 5.2 and Theorem 5.1, it is known that a faster convergence of the reconstruction error for the angular velocity measurement uncertainty and the attitude tracking error is ensured by choosing gains. Moreover, it is seen in (5.54) that larger  $K_3$  (i.e., larger  $k_{ci}$ , i = 1, 2, 3, 4) will lead to a smaller  $||z_1||$ . Higher tracking accuracy is achieved. Therefore, the observer gains and the control gains can be selected based on the following procedures to ensure better estimation performance and better tracking control accuracy for the satellite attitude control system.

- Step #1: Determine the value of  $\gamma$  according to (5.9) and the maximum acceleration velocity.
- Step #2: Choose a positive  $\varsigma_0$ . A larger  $\varsigma_0$  will lead to a smaller  $t_0$ .
- Step #3: Select positive observer gains  $k_r$ , a, and b satisfying a < b to ensure a smaller  $t_1$ . Then, a faster estimation of  $v_u$  is achieved.
- Step #4: Choose positive observer gains  $\eta_1$ ,  $\eta_2$ ,  $\eta_3$ ,  $\eta_4$ , and  $\eta_5$  such that (5.19) and (5.20).
- Step #5: Determine the value of  $C_{\text{max}}$  by using the physical parameters.
- Step #6: Select positive control gains  $k_{c1}$ ,  $k_{c2}$ ,  $k_{c3}$ , and  $k_{c4}$  with (5.28)–(5.29) satisfied. Larger  $k_{c1}$ ,  $k_{c2}$ ,  $k_{c3}$ , and  $k_{c4}$  will result in faster convergence of  $\hat{\mu}_0$ , $\hat{\rho}$ , and smaller attitude tracking error  $z_1$ .

#### 5.8 Numerical Example

To demonstrate the effectiveness of the proposed control scheme incorporated with the angular velocity observer in this chapter, a rigid satellite is numerically simulated. The orbit of the satellite is circular, with an altitude of 500 km and an inclination of 89 degrees. The nominal inertia matrix  $J_0$  of this satellite is

$$\boldsymbol{J}_0 = \begin{bmatrix} 20 & 0 & 0.9 \\ 0 & 17 & 0 \\ 0.9 & 0 & 15 \end{bmatrix} \text{ kg} \cdot \text{m}^2$$
 (5.55)

Due to the onboard payload motion, the mass properties of the satellite may vary. Thus, a time-varying moment inertia matrix is considered [20] with

$$\Delta \mathbf{J} = \text{diag}([3, 2, 1]^{T})(1 + \exp(-0.1t) + 2\vartheta(t - 10) - 4\vartheta(t - 20))\text{kg} \cdot \text{m}^{2} \quad (5.56)$$

where  $\vartheta(\cdot)$  is defined as  $\vartheta(t \ge 0) = 1$  and  $\vartheta(t < 0) = 0$ . The external disturbance  $u_d$  is assumed as

$$\mathbf{u}_{d} = \begin{bmatrix} 2\cos(6\xi_{d}t) + 1.3\sin(2\xi_{d}t) - 1\\ 3.5\cos(9\xi_{d}t) - 2\sin(5\xi_{d}t) + 6\\ 2.5\cos(6\xi_{d}t) - 5\sin(3\xi_{d}t) + 4 \end{bmatrix} \times 10^{-3} \text{ N} \cdot \text{m}$$
 (5.57)

with  $\xi_d = \|\boldsymbol{\omega}\| + 0.001$  and  $\boldsymbol{\omega}(0) = [-0.1984, 0.3998, -0.321]^T$  rad/s.

To validate the proposed approach, simulation was conducted with the desired attitude planned as  $\sigma_d = [0.6321, -0.08562, 0.212]^T$ . The designed controller (5.22) was implemented with its gains and its initial observer states selected as  $k_r = 0.001$ ,  $\eta_1 = 120$ ,  $\eta_2 = 0.0001$ ,  $\eta_3 = 0.0001$ ,  $\eta_4 = 0.001$ ,  $\eta_5 = 20$ , a = 1, b = 2,  $k_{c1} = 0.38$ ,  $k_{c2} = 200$ ,  $k_{c3} = 0.5$ ,  $k_{c4} = 0.001$ ,  $\hat{x}_e(0) = y(0)$ ,  $x_a(0) = 0$ , and  $\hat{v}_u(0) = v_u(0) - \dot{\sigma}(0)$ . The initial attitude of the satellite was  $\sigma(0) = [0.8172, 0.8562, 0.8562]^T \times 10^{-3}$ . Moreover, the following ad hoc numerical differentiation of the measurement provided by attitude sensors was employed to estimate the angular velocity  $\dot{\sigma}$  in the numerical simulation.

$$v_m = \frac{\sigma\left((N+1)\Delta t\right) - \sigma(N\Delta t)}{\Delta t} \tag{5.58}$$

where  $\Delta t \in \mathbb{R}_+$  was the sampling time, and  $N = 0, 1, 2, \dots$ , was the sampling point. At this time, the reconstruction law in Fig. 5.2 is to estimate the angular velocity estimation error  $v_u$ .

The nominal inverse dynamics control law which is widely applied was also tested for comparison. This law is given by [24]

$$\boldsymbol{\tau}_{\text{nor}} = \boldsymbol{G}^{\text{T}}(\boldsymbol{M}_{0}(\boldsymbol{\sigma})(-k_{d}(\dot{\boldsymbol{\sigma}} - \dot{\boldsymbol{\sigma}}_{d}) - k_{p}z_{1} + \ddot{\boldsymbol{\sigma}}_{d}) + \boldsymbol{C}_{0}(\boldsymbol{\sigma}, \dot{\boldsymbol{\sigma}})\dot{\boldsymbol{\sigma}})$$
(5.59)

where  $k_p \in \mathbb{R}_+$  and  $k_c \in \mathbb{R}_+$  are two control gains. From [24], it is known that the control law (5.59) can stabilize the nominal attitude tracking system (i.e., the satellite is free of disturbance, uncertainty, and actuator fault). However, the implementation of the nominal controller (5.59) necessitates the exact value of  $\dot{\sigma}$ . Note that  $\dot{\sigma}$  may be not accurately measured in practice. Instead, it is feedback by (5.58). Hence, the nominal inverse dynamics control was practically implemented as

$$\tau_{\text{nor}} = \mathbf{G}^{T}(\mathbf{M}_{0}(\sigma)(-k_{d}(\mathbf{v}_{m} - \dot{\sigma}_{d}) - k_{p}z_{1} + \ddot{\sigma}_{d}) + \mathbf{C}_{0}(\sigma, \mathbf{v}_{m})\mathbf{v}_{m})$$
(5.60)

Here, the control law (5.60) is called the practical inverse dynamics controller.

#### 5.8.1 Reaction Wheel Fault Scenarios

To investigate the fault tolerant control performance of the controller (5.22), the reaction wheels are assumed to experience the following faults.

- The reaction wheel mounted in line with the  $X_B$  axis of  $\mathcal{F}_B$  loses 20% of its normal power after 10 s. An increased bias torque  $-0.001 \text{ N} \cdot \text{m}$  occurs for all the time.
- The actuator fixed in line with the  $Y_B$  axis of  $\mathcal{F}_B$  loses its power of 40% after 10 s. An increased bias torque 0.001 N · m occurs once the attitude tracking maneuver was started.
- The reaction wheel mounted in line with  $Z_B$  axis of  $\mathcal{F}_B$  undergoes 50% loss of effectiveness after 10 s, and an increased bias torque  $-0.001 \text{ N} \cdot \text{m}$  occurs for all the time.

#### 5.8.2 Simulation Results

When the practical inverse dynamics controller (5.60) was applied to the satellite attitude system, the angular velocity measurement uncertainty introduced by the ad hoc numerical differentiation (5.58) was relatively large. It led the practical inverse dynamics controller (5.60) to achieve an inferior tracking result. However, once the designed scheme, i.e., VFAFTTC, was applied in the satellite attitude system, the resulting tracking error of the planned attitude was shown in Fig. 5.3. As expected, the tracking task was accomplished by the proposed scheme. As we can see in Fig. 5.3a, the planned trajectory was followed after 16 s. The tracking accuracy of  $|z_{11}| \le 4.0 \times 10^{-4}$ ,  $|z_{12}| \le 8.0 \times 10^{-4}$ , and  $|z_{13}| \le 8.0 \times 10^{-4}$  were found in Fig. 5.3b. This accuracy is superior enough to guarantee the accomplishment of the planned tasks despite the actuator faults, the angular velocity measurement uncertainty, the external disturbance, and the uncertain inertia. This superior trajectory tracking property is owing to the effect of the incorporated estimation law for the angular velocity

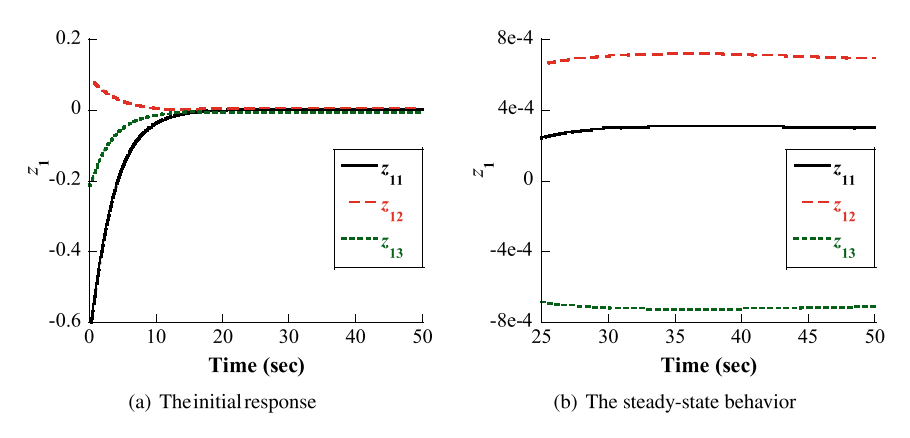


**Fig. 5.3** The attitude tracking error  $z_1$  from VFAFTTC

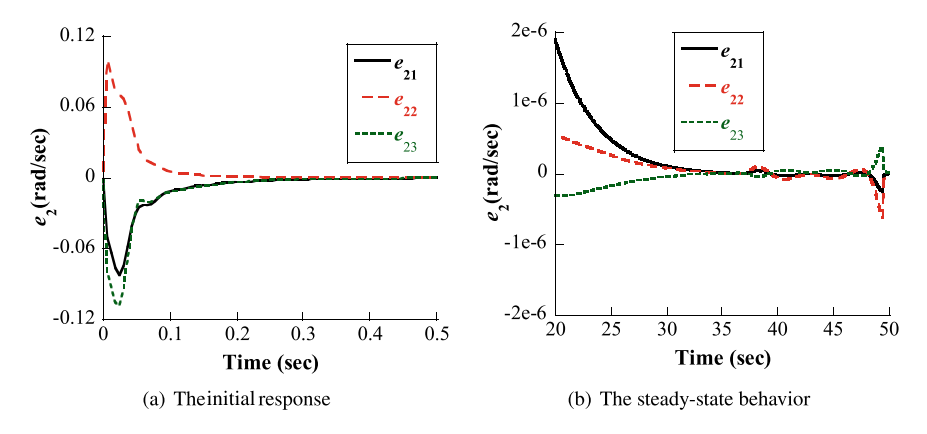
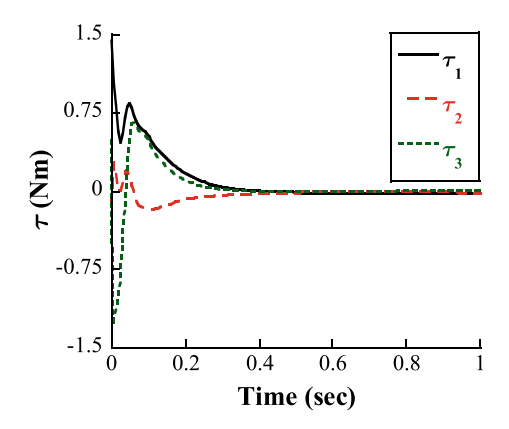


Fig. 5.4 The angular velocity estimation error  $e_2$  from VFAFTTC

measurement uncertainty. It was observed in Fig. 5.4 that the estimation of the angular velocity measurement uncertainty was achieved after a period of short time, i.e., 0.3 s. Moreover, high-precision estimation was ensured by this estimation law. As illustrated in Fig. 5.4b, the estimation accuracy was superior to  $2.0 \times 10^{-6}$  rad/s. Finally, due to the adaptive control parts  $\tau_{\rm com\_1}$  and  $\tau_{\rm com\_2}$  in the controller (5.22), the external disturbance, the actuator faults (F1-F2), and the uncertain dynamics  $\Delta h(\sigma, \dot{\sigma}, \ddot{\sigma})$  were adaptively compensated. Those simulation results coincided with Theorem 5.1 well. The control torque commanded by the proposed VFAFTTC to accomplish the attitude tracking task is shown in Fig. 5.5.

**Fig. 5.5** The commanded control torque from VFAFTTC



#### 5.8.3 Quantitative Analysis

More simulations were further carried out for the following two testing scenarios by applying the nominal inverse dynamics controller (5.59), the practical inverse dynamics control law (5.60), the controller (5.60) with the reconstruction law (5.13), the proposed control approach, and the proposed controller (5.22) in conjunction with a globally convergent velocity observer (GCVO) [28].

- Case #1: The satellite was free of external disturbance, actuator faults, and uncertain inertia.
- Case #2: The external force, the uncertain inertia, and the actuator faults F1-F2 in Sect. 5.8 were considered.

To quantitatively evaluate the above five control schemes, two performance indices were used: first, *the tracking accuracy*, i.e., the absolute value of the steady behavior of the attitude tracking errors  $|z_{1i}|$ , i = 1, 2, 3, and second, *the system settling-time*  $t_s$ , i.e., the time after which  $z_{1i}$  have a steady-state behavior, respectively.

The control gains in the controllers (5.59) and (5.60) were chosen by trial and error until a good tracking performance was achieved. After carrying out 2000 times numerical simulations for Case #1 and Case #2 by using those five controllers with different  $\sigma_d$ , respectively, the tracking performance was listed in Tables 5.1 and 5.2, respectively.

(C1) It was seen in Table 5.1 that except for the practical inverse dynamics controller, the other four approaches achieved almost the same tracking performance for Case #1. However, the nominal inverse dynamics controller (5.59), the practical inverse dynamics controller (5.60), and the controller (5.60) with the reconstruction law (5.13) failed to perform the tracking task in Case #2. That is because those three controllers are not capable of handling external disturbances, actuator faults, and uncertain dynamics.

(C2) As listed in Table 5.1, the proposed control approach and the approach with the controller (5.22) and the GCVO applied ensured almost the same tracking accuracy for Case #1 and Case #2. That is because the GCVO and the presented

Control schemes	The averag	ge tracking acc	curacy			
senemes	z11		z <sub>12</sub>		z <sub>13</sub>	
	Case #1	Case #2	Case #1	Case #2	Case #1	Case #2
Controller (5.59)	$2.74 \times 10^{-6}$	×	3.68 × 10 <sup>-4</sup>	×	4.30 × 10 <sup>-4</sup>	×
Controller (5.60)	×	×	×	×	×	×
Controller (5.60) + estimation law (5.13)	2.77 × 10 <sup>-4</sup>	×	3.79 × 10 <sup>-4</sup>	×	4.27 × 10 <sup>-4</sup>	×
Controller (5.22) + GCVO	2.82 × 10 <sup>-4</sup>	4.27 × 10 <sup>-4</sup>	3.63 × 10 <sup>-4</sup>	7.92 × 10 <sup>-4</sup>	4.31 × 10 <sup>-4</sup>	$7.84 \times 10^{-4}$
The proposed controller	$2.76 \times 10^{-4}$	4.15 × 10 <sup>-4</sup>	3.65 × 10 <sup>-4</sup>	7.85 × 10 <sup>-4</sup>	4.04 × 10 <sup>-4</sup>	7.93 × 10 <sup>-4</sup>

**Table 5.1** The comparison of the average attitude tracking accuracy of 2000 times simulations ("×" denotes that the corresponding approach fails to accomplish the attitude tracking task)

**Table 5.2** The comparison of the average settling time  $t_s$  of 2000 times simulations ("×" denotes that the corresponding approach fails to perform the attitude tracking task)

Control schemes	The average settling time $t_s$ (see	c)
como senemes	Case #1	Case #2
Controller (5.59)	24.6	×
Controller (5.60)	×	×
Controller (5.60) + estimation law (5.13)	36.1	×
Controller (5.22) + GCVO	22.4	39.3
The proposed controller	10.2	16.5

estimation law (5.13) can both provide the unmeasured joint velocity with precise estimation information. However, as we can see in Table 5.2, the developed approach guaranteed a shorter settling time for both cases. This is because the estimation law (5.13) can provide the estimation error with a finite-time convergence, while the GCVO can guarantee an asymptotic estimation only. Hence, the effect of the velocity estimation error was eliminated within a shorter period by the proposed control approach.

In the above quantitative analysis, the trajectory tracking performance was evaluated only. The performance of the estimation law (5.13) was not shown. To evaluate its estimation performance, another two performance indices were adopted: first, the estimation accuracy, i.e., the steady-state behavior of the estimation error  $||e_2||$ , and second, the estimation time  $t_{se}$ , i.e., the time after which  $||e_2||$  has a steady-state behavior. The estimation performance obtained from 2000 times tests was listed in Table 5.3. For Case #1 and Case #2, although almost the same estimation accuracy

Table 5.3 The comparison of the estimation performance from different observers

Observers for estimating angular velocity	The estimation performance			
	The average estimation accuracy $  e_2  $ (rad/s)	$  e_2  $ (rad/s)	The average estimation time $t_{se}$ (sec)	e (sec)
	Case #1	Case #2	Case #1	Case #2
GCVO [28]	$1.82 \times 10^{-6}$	$1.91 \times 10^{-6}$	6.508	12.677
The proposed estimation law (5.13)	1.74 × $10^{-6}$	$1.98 \times 10^{-6}$	0.242	0.281

was achieved for both observers, the GCVO achieved a slower estimation than the estimation law (5.13). That is since the GCVO can govern the estimation error to be asymptotically stable only, while the estimation law (5.13) can ensure finite-time convergence for  $||e_2||$ .

Through the above results and analysis, the effectiveness of the developed attitude tracking control architecture has been validated.

#### 5.9 Summary

Considering angular velocity measurement uncertainty and modeling error including reaction wheel actuator faults, external disturbance, and uncertain inertia, simultaneously, a novel robust velocity-free fault tolerant attitude tracking control approach was presented for satellites. An observer-based reconstruction law was incorporated into this architecture to provide an exact reconstruction of that angular velocity measurement uncertainty after a finite time. With the application of this approach, the attitude tracking task was accomplished. The attitude tracking error was governed to be uniformly ultimately bounded, even when the satellite does not have any velocity sensor. The key advantage of this methodology is that actual angular velocity and any prior knowledge of reaction wheel actuator faults are not required. Moreover, the proposed control did not require any online or offline fault detection and isolation mechanism.

#### References

- 1. Tafazoli, M. (2009) A study of on-orbit spacecraft failures. Acta Astronautica 64(2-3): 195-205
- 2. Robertson, B., Stoneking, E. (2003) Satellite GN&C anomaly trends. vol 113, pp 531–542
- 3. Blanke, M., IzadiZamanabadi, R., Bogh, S. A., Lunau, C. P. (1997) Fault-tolerant control systems: A holistic view. Control Engineering Practice 5(5): 693–702
- 4. Patton, R. J. (1997) Fault-tolerant control systems: The 1997 situation. pp 1033–1054
- Yang, H., Staroswiecki, M., Jiang, B., Liu, J. Y. (2011) Fault tolerant: Cooperative control for a class of nonlinear multi-agent systems. Systems & Control Letters 60(4): 271–277
- Boskovic, J. D., Bergstrom, S. E., Mehra, R. K. (2005) Robust integrated flight control-design under failures, damage, and state-dependent disturbances. Journal of Guidance, Control, and Dynamics 28(5): 902–917
- Chen, W., Saif, M. (2007) Observer-based fault diagnosis of satellite systems subject to timevarying thruster faults. Transactions of the ASME Journal of Dynamic Systems Measurement and Control 129(3): 352–356
- 8. Henry, D. (2008) Fault diagnosis of microscope satellite thrusters using  $\mathcal{H}_{\infty}/\mathcal{H}_{\perp}$  filters. Journal of Guidance, Control, and Dynamics 31(3): 699–711
- 9. Hou, Q., Cheng, Y. H., Lu, N. Y., Jiang, B. (2008) Study on FDD and FTC of satellite attitude control system based on the effectiveness factor. In: 2008 2nd International Symposium on Systems and Control in Aerospace and Astronautic, pp 1086–1101
- Williamson, W. R., Speyer, J. L., Dang, V. T., Sharp, J. (2009) Fault detection and isolation for deep space satellites. Journal of Guidance, Control, and Dynamics 32(5): 1570–1584

References 119

 Lam, Q. M., Xin, M. (2010) Robustness evaluation of Θ-D technique for spacecraft attitude control subject to reaction wheel failures. In: AIAA Guidance, Navigation, and Control Conference, pp 8302–8319

- 12. De Ruiter, A. (2011) A fault-tolerant magnetic spin stabilizing controller for the jc2sat-ff mission. Acta Astronautica 68(1–2): 160–171
- Tafazoli, S., Khorasani, K. (2006) Nonlinear control and stability analysis of spacecraft attitude recovery. IEEE Transactions on Aerospace and Electronic Systems 42(3): 825–845
- Liang, Y. W., Xu, S. D., Tsai, C. L. (2007) Study of VSC reliable designs with application to spacecraft attitude stabilization. IEEE Transactions on Control Systems Technology 15(2): 332–338
- 15. Jin, J. Y., Ko, S. H., Ryoo, C. K. (2008) Fault tolerant control for satellites with four reaction wheels. Control Engineering Practice 16(10): 1250–1258
- Jiang, Y., Hu, Q. L., Ma, G. F. (2010) Adaptive backstepping fault-tolerant control for flexible spacecraft with unknown bounded disturbances and actuator failures. ISA Transactions 49(1): 57–69
- Lee, H., Kim, Y. (2010) Fault-tolerant control scheme for satellite attitude control system. IET Control Theory and Applications 4(8): 1436–1450
- 18. Murugesan, S., Goel, P. S. (1987) Fault tolerant spacecraft attitude control system. Sadhana 11(1&2): 232–261
- 19. Khalil, H. K. (2002) Nonlinear systems. Prentice Hall
- Song, Y. D., Cai, W. C. (2009) Quaternion observer-based model-independent attitude tracking control of spacecraft. Journal of Guidance, Control, and Dynamics 32(5): 1476–1482
- 21. Sidi, M. J. (1997) Spacecraft dynamics and control. Cambridge University Press
- Tayebi, A. (2008) Unit quaternion-based output feedback for the attitude tracking problem. IEEE Transactions on Automatic Control 53(6): 1516–1520
- 23. Hu, Q. L and Xiao, B. and Shi, P.,(2015) Tracking control of uncertain Euler-Lagrange systems with finite-time convergence, International Journal of Robust and Nonlinear Control,25(17) 3299–3315.
- 24. Spong, M. W and Hutchinson, S. and Vidyasagar, M.,(2006) Robot modeling and control, New York: John Wiley.
- 25. Qiao, J. Z. and Li, Z. X. and Xu, J. W. and Yu, X., (2020), Composite nonsingular terminal sliding mode attitude controller for spacecraft with actuator dynamics under matched and mismatched disturbances, IEEE Transactions on Industrial Informatics, 16(2),1153–1162.
- Xu, J. W. and Yu, X. and Qiao, J. Z., (2021) Hybrid disturbance observer-based anti-disturbance composite control with applications to mars landing mission, IEEE Transactions on Systems Man Cybernetics: Systems, 51(5),2885–2893.
- 27. Wu, C. W and Liu, J. X. and Xiong, Y. Y. and Wu, L. G.,(2018) Observer-based adaptive fault-tolerant tracking control of nonlinear nonstrict-feedback systems, IEEE Transactions on Neural Networks and Learning Systems, 29(7), 3022–3033.
- 28. Namvar, M. (2009) A class of globally convergent velocity observers for robotic manipulators, IEEE Transactions on Automatic Control, 54(8), 1956–1961.

### Part III Modeling Error Adaptive Compensation Attitude Control

## **Chapter 6 Adaptive Attitude Stabilization Control**



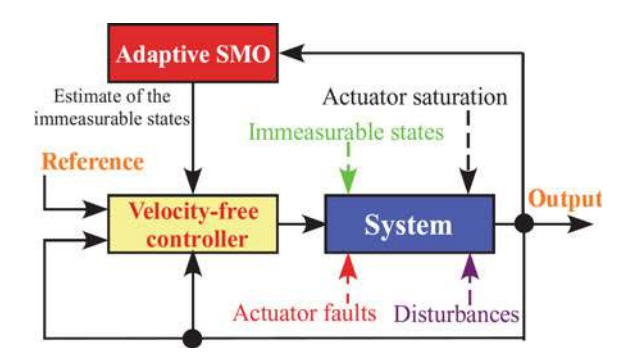
#### 6.1 Introduction

Although many observers, sliding mode observer (SMO), or even finite-time observer for state estimation, and observer-based output feedback control approaches have been reported, those schemes are characterized by two drawbacks: (1) they are designed based on the assumption that all actuators operate normally, i.e., actuator faults never occur; and (2) a practical issue, i.e., actuator constraint is not investigated. Challenging operating conditions increase the possibility of malfunctions in sensors, actuators, and controllers.

With an effort to tackle the above two drawbacks, this chapter investigates the feasibility of partial-state feedback control design for a class of multi-input multi-output systems with actuator faults, system uncertainties, external disturbances, immeasurable states, and actuator constraints explicitly addressed simultaneously. The main result to be achieved is to extend previous work on partial-state feedback control [1] while approaching the challenging case of output feedback control for a general type of nonlinear systems subject to the above five issues rather than only the satellite attitude control system. However, the approach in [1] was not able to handle system uncertainties, it can only be applied to satellites and would be ineffective when applied to other nonlinear systems. An adaptive SMO-based velocity-free fault-tolerant and uncertainties attenuation control scheme is proposed for such as solution, as shown in Fig. 6.1. The controller is designed using the measurable output and the estimated value for the adaptive SMO only. The main contributions of this chapter, relative to the existing works, can be outlined as follows.

• In terms of theoretical contribution: Compared with the state observer even finite-time observer-based control schemes such as [2–4] which can only handle three issues including system uncertainties, external disturbances, and immeasurable states, this chapter presents a general solution for the integrated design to address not only those three issues but also actuator faults and actuator input saturation simultaneously. Hence, the proposed control scheme will have an extra fault-tolerant capability to handle actuator faults. Actually, simply combing the existing

**Fig. 6.1** The structure of the adaptive SMO-based velocity-free control



state observer-based control [2–4] with FTC such as [5] cannot solve those five problems simultaneously, because those five issues are highly coupled. Hence, the design of the approach to them is complex and multidimensional, it needs adequate techniques.

• In terms of engineering application: The proposed approach is able to achieve not only the FTC for actuator faults but also the attenuation control for disturbances and system uncertainties. Moreover, that is implemented with output feedback only. It means that sensors for measuring system output are requested only to be equipped, while the sensors for obtaining system states' measurements are not needed. A low-cost reliable control design is achieved. This leads to the great potential application of the approach to achieve economic control system design.

#### 6.2 Euler-Lagrange System

Consider a multi-input-multi-output nonlinear system represented by the Euler-Lagrange equation of the form [6]

$$H(x)\ddot{x} + C(x, \dot{x})\dot{x} + g(x) = u + d + f(x, \dot{x}, t)$$
 (6.1)

where  $x \in \mathbb{R}^n$  is the generalized coordinates,  $\dot{x} \in \mathbb{R}^n$  is the generalized velocity,  $u \in \mathbb{R}^n$  is the control force,  $H(x) \in \mathbb{R}^{n \times n}$  denotes the symmetric positive-definite inertia,  $C(x, \dot{x}) \in \mathbb{R}^{n \times n}$  is the matrix of Coriolis and centrifugal force,  $f(x, \dot{x}, t) \in \mathbb{R}^n$  is the system uncertainty,  $d \in \mathbb{R}^n$  is the external disturbance, and  $g(x) \in \mathbb{R}^n$  represents the gravitational force. Moreover, this Euler-Lagrange system has the following properties.

**Property 6.1** The matrix H(x) is bounded by  $0 < l_{\min}||y||^2 \le y^T H(x) y \le l_{\max}||y||^2$  for  $\forall y \in \mathbb{R}^n$  and  $\forall x \in \mathbb{R}^n$ , where  $l_{\min} \in \mathbb{R}_+$  and  $l_{\max} \in \mathbb{R}_+$  are two scalars.

**Property 6.2** The matrix  $\dot{\mathbf{H}}(\mathbf{x}) - 2\mathbf{C}(\mathbf{x}, \dot{\mathbf{x}})$  is skew-symmetric for all  $\mathbf{x} \in \mathbb{R}^n$ . There has  $\mathbf{y}^{\mathrm{T}}(\dot{\mathbf{H}}(\mathbf{x}) - 2\mathbf{C}(\mathbf{x}, \dot{\mathbf{x}}))\mathbf{y} = 0$ ,  $\forall \mathbf{x} \in \mathbb{R}^n$  and  $\forall \mathbf{y} \in \mathbb{R}^n$ .

**Property 6.3** The matrix  $C(x, \dot{x})$  is bounded with respect to x and linear with respect to  $\dot{x}$ . It exists a scalar  $c_{\text{max}} \in \mathbb{R}_+$  such that  $||C(x, \dot{x})|| \leq c_{\text{max}}||\dot{x}||, \forall x \in \mathbb{R}^n$ .

**Remark 6.1** The Euler-Lagrange system (6.1) can be adopted to describe the dynamics of many industrial systems, such as robotic manipulators, satellites, twin-lift helicopters, hypersonic flight vehicles, and marine vehicle. In addition, the external disturbance acting on this system is usually bounded in practice. The following assumption is thus made reasonably.

**Assumption 6.1** The external disturbance in (6.1) is bounded. There always exist a constant  $d_{\text{max}} \in \mathbb{R}_+$  such that  $||\boldsymbol{d}|| \le d_{\text{max}}$  for all  $t \ge 0$ .

#### 6.3 General Model of Actuator Faults

The nonlinear system (6.1) is presented in the absence of actuator fault. However, actuator faults may occur. Because a minor fault in the actuator may lead to an unsatisfactory performance or even system instability, actuator fault should be investigated. Actuator fault is commonly categorized into four major types: (F1) *Locked-in-place*, (F2) *Loss of effectiveness*, (F3) *Hard cover*, and (F4) *Floating around trim*. These faults are illustrated in Fig. 6.2, where  $\tau_{\text{max}}$  and  $-\tau_{\text{max}}$ ,  $\tau_{\text{max}} \in \mathbb{R}_+$ , represent, respectively, the upper bound and lower bound of the actuator response;  $t_F$  denotes the time when fault occurs.

Assume that the Euler-Lagrange system (6.1) is controlled by  $N \in \mathbb{R}_+$  actuators. After characterizing the fault types, the fault generated F1–F4 can be modeled for each actuator as [7].

$$\tau_{ai} = l_i(t)\tau_{ci} + \bar{\tau}_{ci}, i = 1, 2, ..., N$$
 (6.2)

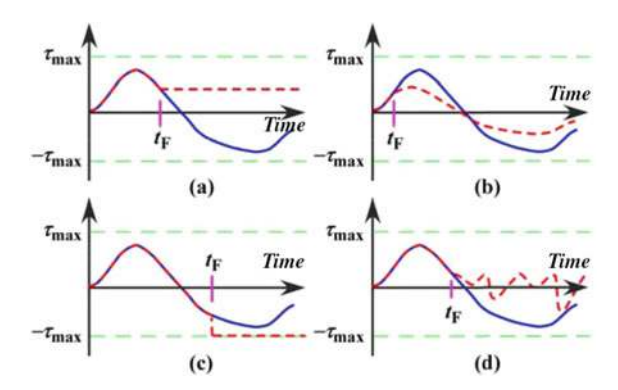


Fig. 6.2 Four types of actuator faults: a F1; b F2; c F3; and d F4 (the solid line denotes the commanded control of the actuator, while the dashed line denotes the applied control of the actuator)

where  $l_i(t) \in \mathbb{R}_+$ ,  $i \in 1, 2, ..., N$  is the actuator fault indicator represented by a quantitative value in the range of 0–1, i.e.,  $0 \le l_i(t) \le 1$ ;  $\bar{\tau}_{ci} \in \mathbb{R}$ , i = 1, 2, ..., N with  $|\bar{\tau}_{ci}| \le \tau_{\max}$  denotes the uncertain actuator failure.  $\tau_{ci} \in \mathbb{R}$ , i = 1, 2, ..., N is the desired control force commanded by the controller.  $\tau_{ai} \in \mathbb{R}$ , i = 1, 2, ..., N is the actual control generated by the actuator.

- No fault:  $\tau_{ai} = \tau_{ci}$ ,  $l_i(t) = 1$ , and  $\bar{\tau}_{ci} = 0$ .
- Locked-in-place fault:  $l_i(t) = 0$ , and  $\tau_{ci}$  is to a constant value at which the actuator has frozen leading to  $\tau_{ai} = \bar{\tau}_{ci}$ .
- Loss of effectiveness fault: In this case, if it is assumed that there is 50% degradation in the control actuation,  $l_i(t)$  will take a value of 0.5, and  $\bar{\tau}_{ci} = 0$ .
- Floating around trim fault: Float-type failure can be accounted for, with  $l_i(t) = 1$  and  $\bar{\tau}_{ci} \neq 0$ .
- Hard-cover fault:  $l_i(t) = 0$  and  $\bar{\tau}_{ci} = \tau_{\text{max}}$ .

Suppose that all actuators of the Euler-Lagrange system (6.1) are configured with an actuator matrix  $D \in \mathbb{R}^{n \times N}$ . For full control of this system, redundant actuators are usually mounted, i.e.,  $n \leq N$ . As a result, D is available and it is generally made full-row rank. The relationship between u in (6.1) and the commanded control of the actuator can be established as

$$\boldsymbol{u} = \boldsymbol{D}\boldsymbol{\tau}_a = \boldsymbol{D}\boldsymbol{E}(t)\boldsymbol{\tau}_c + \boldsymbol{D}\bar{\boldsymbol{\tau}}_c \tag{6.3}$$

where  $\boldsymbol{\tau}_a = [\tau_{a1}, \tau_{a2}, \dots, \tau_{aN}]^{\mathrm{T}}$  is the applied control by N actuators,  $\boldsymbol{\tau}_c = [\tau_{c1}, \tau_{c2}, \dots, \tau_{cN}]^{\mathrm{T}}$  is the control input commanded by the system controller,  $\bar{\boldsymbol{\tau}}_c = [\bar{\tau}_{c1}, \bar{\tau}_{c2}, \dots, \bar{\tau}_{cN}]^{\mathrm{T}}$  is the uncertain fault, and  $\boldsymbol{E}(t) = \mathrm{diag}([l_1(t), l_2(t), \dots, l_N(t)]^{\mathrm{T}}) \in \mathbb{R}^{N \times N}$  is the actuation effectiveness matrix.

#### **6.4 Problem Statement**

The objective is to design an observer for the Euler-Lagrange system (6.1) with only the available measurement x. The resulting observation error asymptotically converges to zero, or an arbitrary small set containing the origin with finite-time convergence. Then, based on the measurement x and the states of the observer, a controller is designed to guarantee that all states in the closed-loop system are uniformly ultimately bounded in the presence of input constraint, i.e.,  $|\tau_{ci}| \leq \tau_{\text{max}}$ , i = 1, 2, ..., N and modeling error consisting of external disturbance  $u_d$ , system uncertainty  $f(x, \dot{x}, t)$ , and actuator fault (6.3).

#### 6.5 Observer-Based State Estimation

#### 6.5.1 Adaptive State Observer

In this section, the Euler-Lagrange system is assumed to have no system uncertainty. That is  $f(x, \dot{x}, t) = 0$ . Given that the matrices H(x),  $C(x, \dot{x})$ , and g(x) in (6.1) are known. An SMO will be developed for the estimation of x and  $\dot{x}$  with only the available measurement x. Define  $x_1 = x$ ,  $x_2 = \dot{x}$ , and system output y = x. Consider actuator fault (6.3), (6.1) can be rewritten as

$$\dot{x}_1 = x_2 \tag{6.4}$$

$$H(y)\dot{x}_2 = -C(y, x_2)x_2 - g(y) + DE(t)\tau_c + D\bar{\tau}_c + d$$
 (6.5)

Let  $\hat{x}_1$  and  $\hat{x}_2$  denote the estimate of  $x_1$  and  $x_2$ , respectively. Define the observation error  $e_1 = [e_{11}, e_{12}, \dots, e_{1n}]^T = \hat{x}_1 - x_1$ ,  $e_2 = [e_{21}, e_{22}, \dots, e_{2n}]^T = \hat{x}_2 - x_2$ , the following terminal SMO is designed:

$$\dot{\hat{\boldsymbol{x}}}_1 = \hat{\boldsymbol{x}}_2 - \boldsymbol{x}_{\nu} \tag{6.6}$$

$$H(y)\dot{\hat{x}}_{2} = -C(y, \hat{x}_{2})\hat{x}_{2} - \frac{k_{3}}{(k_{1})^{\frac{\gamma}{\beta}}} \left[x_{\nu}\right]^{\frac{\gamma}{\beta}} - \frac{k_{2}}{k_{1}}x_{\nu} - g(y) - k_{4}\hat{x}_{2} + D\tau_{c} \quad (6.7)$$

where  $\mathbf{x}_{v} = [x_{v1}, x_{v2}, \dots, x_{vn}]^{\mathrm{T}} = k_{1} \mathbf{sgn}(\mathbf{e}_{1}), k_{i} \in \mathbb{R}_{+}, i = 1, 2, 3, 4$  are observer gains,  $\gamma \in \mathbb{R}_{+}$  and  $\beta \in \mathbb{R}_{+}$  are two odd integers such that  $\gamma < \beta$ .

Combining (6.4) and (6.5) with the observer (6.6) and (6.7), the observation error dynamics is obtained as

$$\dot{\boldsymbol{e}}_1 = \boldsymbol{e}_2 - \boldsymbol{x}_{\nu} \tag{6.8}$$

$$H(y)\dot{e}_{2} = -C(y,\hat{x}_{2})\hat{x}_{2} + C(y,x_{2})x_{2} + D(I_{N} - E(t))\tau_{c}$$

$$-\frac{k_{2}}{k_{1}}x_{v} - \frac{k_{3}}{(k_{1})^{\frac{\gamma}{\beta}}} \left[x_{v}\right]^{\frac{\gamma}{\beta}} - k_{4}\hat{x}_{2} - D\bar{\tau}_{c} - d$$
(6.9)

Note that, we assume that the state  $\dot{x}$  is bounded, i.e.,  $||\dot{x}|| \leq Q_0$ . That is a reasonable assumption, because for most rigid bodies represented by (6.1),  $\dot{x}$  stands for velocity,  $\dot{x}$  is bounded due to the physical limitation of mechanical. However, this assumption will not be required when the observer is used in connection with the controller design, as discussed in Sect. 6.6 (Theorem 6.3).

**Lemma 6.1** With the SMO (6.6)–(6.7), select the observer gains satisfying

$$\frac{Q_2}{(1-\pi_1)\eta_1} < \frac{k_4}{c_{\text{max}}} - Q_0 \tag{6.10}$$

where  $Q_1 = 2\sqrt{N}||D||\tau_{\text{max}} + d_{\text{max}} + k_4Q_0$ ,  $\eta_1 \in \mathbb{R}_+$  and  $0 < \pi_1 < 1$  are two positive scalars, while  $Q_2 = Q_1 + \sqrt{n}(k_2 + k_3)$ . If  $||\dot{x}|| \le Q_0$  is satisfied, and  $\hat{x}_2(0)$  is chosen such that  $||e_2(0)|| \le \frac{k_4}{c_{\text{max}}} - Q_0$ , then the error  $e_2$  will be always bounded by  $\frac{k_4}{c_{\text{max}}} - Q_0$ , i.e.,  $||e_2(t)|| \le \frac{k_4}{c_{\text{max}}} - Q_0$  for  $t \ge 0$ .

**Proof** Applying the linear property of  $C(x, \dot{x})$  in Property 6.3, one has

$$C(y, x_2)x_2 - C(y, \hat{x}_2)\hat{x}_2 = -C(y, x_2)e_2 - C(y, e_2)\hat{x}_2$$
 (6.11)

Choose a Lyapunov candidate function  $V_0 = \frac{1}{2} e_2^T H(y) e_2$  for the error dynamics (6.8), (6.9), it is obtained from Assumption 6.1 and Property 6.2 that

$$\dot{V}_{0} = \mathbf{e}_{2}^{\mathrm{T}} \left( \mathbf{D} (\mathbf{I}_{N} - \mathbf{E}(t)) \mathbf{\tau}_{c} - \mathbf{C}(\mathbf{y}, \mathbf{e}_{2}) \hat{\mathbf{x}}_{2} - \mathbf{D} \bar{\mathbf{\tau}}_{c} - \mathbf{d} - \frac{k_{2}}{k_{1}} \mathbf{x}_{v} \right) \\
- \frac{k_{3}}{(k_{1})^{\frac{\gamma}{\beta}}} |\mathbf{x}_{v}|^{\frac{\gamma}{\beta}} - k_{4} \hat{\mathbf{x}}_{2} \right) \\
\leq Q_{1} ||\mathbf{e}_{2}|| - (k_{4} - c_{\max}(||\mathbf{e}_{2}|| + Q_{0}))||\mathbf{e}_{2}||^{2} - k_{2} \mathbf{e}_{2}^{\mathrm{T}} \mathbf{sgn}(\mathbf{e}_{1}) \\
- k_{3} \mathbf{e}_{2}^{\mathrm{T}} \mathrm{diag}(|\mathbf{sgn}(\mathbf{e}_{1})|^{\frac{\gamma}{\beta}}) \mathbf{sgn}(\mathbf{x}_{v}) \\
\leq -(k_{4} - c_{\max}(||\mathbf{e}_{2}|| + Q_{0}))||\mathbf{e}_{2}||^{2} + (Q_{1} + \sqrt{n}k_{2} + \sqrt{n}k_{3})||\mathbf{e}_{2}|| \\
= -(k_{4} - c_{\max}(||\mathbf{e}_{2}|| + Q_{0}))||\mathbf{e}_{2}||^{2} + Q_{2}||\mathbf{e}_{2}||$$
(6.12)

where  $e_2^{\mathrm{T}}(\boldsymbol{D}(\boldsymbol{I}_N-\boldsymbol{E}(t))\boldsymbol{\tau}_c-\boldsymbol{D}\bar{\boldsymbol{\tau}}_c-\boldsymbol{d}) \leq Q_1||\boldsymbol{e}_2||$  is used. As a consequence, if  $||\boldsymbol{e}_2|| < \frac{k_4}{c_{\max}} - Q_0$ , then there will exist an positive scalar  $\frac{\eta_1}{c_{\max}}$  such that  $c_{\max}(||\boldsymbol{e}_2||+Q_0)+\eta_1=k_4$ . The inequality (6.12) becomes

$$\dot{V}_0 \le -\eta_1 ||\mathbf{e}_2||^2 + Q_2 ||\mathbf{e}_2|| 
= -\eta_1 \pi_1 ||\mathbf{e}_2||^2 + (Q_2 - (1 - \pi_1)\eta_1 ||\mathbf{e}_2||) ||\mathbf{e}_2||$$
(6.13)

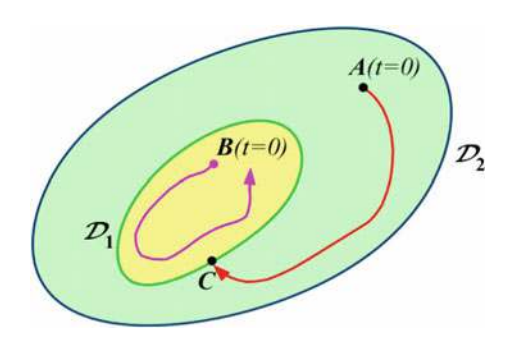
It thus leads to

$$\dot{V}_0 \le -\eta_1 \pi_1 ||\boldsymbol{e}_2||^2 \le -\frac{2\eta_1 \pi_1}{l_{\text{max}}} V_0$$
 (6.14)

when  $e_2$  is outside of the set  $\mathcal{D}_1 = \left\{ e_2 : ||e_2|| \le \frac{\mathcal{Q}_2}{(1-\pi)\eta_1} \right\}$ ; here, the inequality  $V_0 \le \frac{\mathcal{Q}_2}{(1-\pi)\eta_1}$  $0.5l_{\text{max}}||\boldsymbol{e}_2||^2$  from Property 6.1 is used.

From (6.14), it can be concluded that  $V_0$  will decrease monotonically for  $e_2 \notin \mathcal{D}_1$ . Then, it is got to know from the definition of  $V_0$  that  $e_2$  will decrease monotonically once  $e_2$  is outside the set  $\mathcal{D}_1$ , while  $||e_2|| < \frac{k_4}{c_{\max}} - Q_0$  is satisfied. That means that,  $\mathcal{D}_1$  is a region of attraction for  $||e_2|| < \frac{k_4}{c_{\text{max}}} - Q_0$ . Furthermore, because the estimate  $\hat{x}_2(0)$  is chosen such that  $||e_2|| < \frac{k_4}{c_{\text{max}}} - Q_0$ , using the above analysis and the observer gains chosen according to (6.10), it can be concluded that  $||e_2(t)|| < \frac{k_4}{c_{\text{max}}} - Q_0$  for all  $t \ge 0$ . The proof is completed. 

**Fig. 6.3** The geometric representation of sets in the proof of Lemma 6.1



**Remark 6.2** The proof process of Lemma 6.1 can be illustrated by Fig. 6.3.  $k_4$  should be chosen large enough to guarantee that  $e_2(0)$  is within the set  $\mathcal{D}_2 = \left\{e_2 : ||e_2|| \le \frac{k_4}{c_{\max}} - \mathcal{Q}_0\right\}$ . If  $e_2(0)$  starts with A which is within the set  $\mathcal{D}_2 \setminus \mathcal{D}_1$ , the error state  $e_2$  will move in  $\mathcal{D}_1$ . Once inside the set  $\mathcal{D}_1$ ,  $e_2(t)$  cannot get out. If  $e_2(0)$  starts with B in the set  $\mathcal{D}_1$ , the state  $e_2(t)$  will never move out of the set  $\mathcal{D}_1$ , as shown by the analysis in the proof of Lemma 6.1. Hence, it can be concluded that  $\mathcal{D}_1$  is a region of attraction. It also ensures  $e_2 \in \mathcal{D}_2$  for all  $t \ge 0$ ; this means that  $e_2$  is always bounded.

**Theorem 6.1** Consider the Euler-Lagrange system (6.1) in combination with the SMO (6.6), (6.7). Given the initial estimate  $\hat{x}_2(0)$  chosen such that  $||e_2(0)|| \leq \frac{k_4}{c_{\text{max}}} - Q_0$ , choose  $\beta$ ,  $\gamma$ , and the observer gains  $k_i$ , i = 1, 2, 3, 4 such that (6.10) and

$$k_1 > \frac{k_4}{c_{\text{max}}} - Q_0 \tag{6.15}$$

$$\frac{k_3}{k_1^{\gamma/\beta}} - \kappa_1 - Q_1 \left(\frac{k_4}{c_{\text{max}}} - Q_0\right)^{-\frac{\gamma}{\beta}} > 0$$
 (6.16)

$$\frac{k_2}{k_1} - 2k_4 > 0 (6.17)$$

where  $\lambda_1 \in \mathbb{R}_+$  and  $\kappa_1 \in \mathbb{R}_+$  are two scalars. Then, whether the actuator fault (6.3) occurs or not, the observer errors  $\mathbf{e}_1$  and  $\mathbf{e}_2$  are finite time stable, i.e.,  $\mathbf{e}_1(t) \equiv 0$  for  $t \geq T_0 = \frac{||\mathbf{e}_1(0)||}{\lambda_1}$  and  $\mathbf{e}_2(t) \equiv 0$  for  $t \geq T_1 = T_0 + \frac{\beta 2^{\frac{\beta-\gamma}{2\beta}}(l_{\max})^{\frac{\beta+\gamma}{2\beta}}(V_0)^{\frac{\beta-\gamma}{2\beta}}(T_0)}{\kappa_1(\beta-\gamma)}$ , where  $\lambda_1 \in \mathbb{R}_+$  is a constant such that  $\lambda_1 + \left(\frac{k_4}{c_{\max}} - Q_0\right) \leq k_1$ .

**Proof** To prove Theorem 6.1, the Lyapunov's direct method is adopted, and it can be divided into the following two parts.

• Stability analysis of the estimation error  $e_1$ :

It can be obtained from (6.15) that there exists a constant  $\lambda_1 \in \mathbb{R}_+$  such that  $\lambda_1 + (\frac{k_4}{c_{\max}} - Q_0) \le k_1$ . Then, consider an candidate Lyapunov function as  $V_1 = 0.5e_1^Te_1$ , applying Lemma 6.1 yields

$$\dot{V}_1 = \mathbf{e}_1^{\mathrm{T}}(\mathbf{e}_2 - k_1 \mathbf{sgn}(\mathbf{e}_1)) \le -||\mathbf{e}_1||(k_1 - ||\mathbf{e}_2||) \le -\lambda_1||\mathbf{e}_1|| = -\lambda_1 \sqrt{2V_1} \quad (6.18)$$

Solving (6.18) yields  $V_1(t) \equiv 0$  for  $t \geq T_0$ , i.e.,  $||e_1(t)|| \equiv 0$  for that  $t \geq T_0$ . The observation error  $e_1$  is thus finite-time stable by using Definition 2.1. Sliding motion takes place on  $e_1 = \dot{e}_1 = \mathbf{0}$  by  $t = T_0$ , then solving for equivalent output injection yields  $[x_v]_{eq} = e_2$ ; here, the subscript "eq" denotes the equivalent state on the sliding surface  $e_1 = \dot{e}_1 = \mathbf{0}$  in the sense of sliding-mode control theory.

• Stability analysis of the estimation error  $e_2$ :

Once the sliding motion  $(e_1 = \dot{e}_1 = 0)$  is achieved after the finite time  $T_0$ , using  $[x_v]_{eq} = e_2$ , the error dynamics has the form

$$H(y)\dot{e}_{2} = -C(y,\hat{x}_{2})\hat{x}_{2} + C(y,x_{2})x_{2} + D(I_{N} - E(t))\tau_{c}$$

$$-\frac{k_{2}}{k_{1}}e_{2} - \frac{k_{3}}{(k_{1})^{\frac{\gamma}{\beta}}} \left[x_{\nu}\right]^{\frac{\gamma}{\beta}} - k_{4}\hat{x}_{2} - D\bar{\tau}_{c} - d$$
(6.19)

From Lemma 6.1, it follows that  $||e_2|| < \frac{k_4}{c_{\text{max}}} - Q_0$  for that  $t \ge 0$ . Then, further differentiating  $V_0$ , applying (6.11), Property 6.2, Property 6.3, and the gain choice in (6.16), (6.17) yield

$$\dot{V}_{0} = \boldsymbol{e}_{2}^{T} \left( \boldsymbol{D} (\boldsymbol{I}_{N} - \boldsymbol{E}(t)) \boldsymbol{\tau}_{c} - \boldsymbol{C}(\boldsymbol{y}, \boldsymbol{e}_{2}) \hat{\boldsymbol{x}}_{2} - \frac{k_{2} \boldsymbol{e}_{2}}{k_{1}} - \frac{k_{3} \left[\boldsymbol{x}_{v}\right]^{\frac{\gamma}{\beta}}}{(k_{1})^{\frac{\gamma}{\beta}}} - k_{4} \hat{\boldsymbol{x}}_{2} - \boldsymbol{D} \bar{\boldsymbol{\tau}}_{c} - \boldsymbol{d} \right) \\
\leq Q_{1} ||\boldsymbol{e}_{2}|| - \left( \frac{k_{2}}{k_{1}} - (c_{\max}(||\boldsymbol{e}_{2}|| + Q_{0}) + k_{4}) \right) ||\boldsymbol{e}_{2}||^{2} - \frac{k_{3} ||\boldsymbol{e}_{2}||^{1 + \frac{\gamma}{\beta}}}{(k_{1})^{\frac{\gamma}{\beta}}} \\
= -\kappa_{1} ||\boldsymbol{e}_{2}||^{1 + \frac{\gamma}{\beta}} - \left( \frac{k_{3}}{(k_{1})^{\frac{\gamma}{\beta}}} - \kappa_{1} - Q_{1} \left( \frac{k_{4}}{c_{\max}} - Q_{0} \right)^{-\frac{\gamma}{\beta}} \right) ||\boldsymbol{e}_{2}||^{1 + \frac{\gamma}{\beta}} - \left( \frac{k_{2}}{k_{1}} - 2k_{4} \right) ||\boldsymbol{e}_{2}||^{2} \\
\leq -\kappa_{1} ||\boldsymbol{e}_{2}||^{1 + \frac{\gamma}{\beta}} \\
\leq -\kappa_{1} \left( \frac{2V_{0}}{l_{\max}} \right)^{\frac{\beta + \gamma}{2\beta}} \tag{6.20}$$

Because the above stability analysis for  $e_2$  starts with the time  $T_0$ , one can integrate both sides of (6.20) from  $T_0$  to t, and solve (6.20) to obtain  $V_0(t) \equiv 0$  for all  $t \geq T_1$ . According to the definition of  $V_0$  and the positive definiteness of H(y), it follows that  $e_2(t) \equiv 0$  for all  $t \geq T_1$ , i.e., the observer error  $e_2$  is thus finite time stable by using Definition 2.1. Thereby, the proof is completed here.

**Remark 6.3** It should be pointed out that, the value of  $T_0$  cannot be explicitly determined. That is because  $\lambda_1$  is only used to theoretically analyze the finite-time convergence of  $e_1$ . It is only proven that  $\lambda_1$  does indeed exist according to (6.15). However, its exact value would be unknown. It is also not necessary to choose  $\lambda_1$  in the implementation of the approach.

#### 6.5.2 Effect of System Uncertainties

Limit to finite system modeling techniques, mathematical model could not be exactly established. The Euler-Lagrange system (6.1) will be subject to modeling error  $f(x, \dot{x}, t)$ . Generally,  $f(x, \dot{x}, t)$  is represented by  $f(x, \dot{x}, t) = \xi(x, \dot{x}, t)\Phi$  with  $\Phi \in \mathbb{R}^{l_1}$  a constant but unknown parameter vector, and  $\xi(x, \dot{x}, t) \in \mathbb{R}^{n \times l_1}$  a bounded function such that

$$||\boldsymbol{\xi}(\boldsymbol{x}_1, \dot{\boldsymbol{x}}_1, t)\boldsymbol{\Phi} - \boldsymbol{\xi}(\boldsymbol{x}_2, \dot{\boldsymbol{x}}_2, t)\boldsymbol{\Phi}|| \le c_q ||\dot{\boldsymbol{x}}_1 - \dot{\boldsymbol{x}}_2|| + c_p ||\boldsymbol{x}_1 - \boldsymbol{x}_2||$$
(6.21)

for  $x_1 \in \mathbb{R}^n$ ,  $x_2 \in \mathbb{R}^n$ ,  $c_p \in \mathbb{R}_+$  and  $c_q \in \mathbb{R}_+$  are bounded but possibly time-varying positive scalars. Uncertainty  $f(x, \dot{x}, t)$  includes, for example, uncertainty in Coriolis-Centrifugal forces, gravity forces, and viscous frictions. For a manipulator with revolute joints and with bounded joint velocities, due to the dependency of dynamics to joint angles, the representation  $f(x, \dot{x}, t) = \xi(x, \dot{x}, t) \Phi$  is always possible [8].

In the sequel, we denote  $\hat{\Phi} \in \mathbb{R}^{l_1}$  as the estimate of  $\Phi$  and present the following adaptive observer design approach with system uncertainties considered.

**Theorem 6.2** Consider the terminal SMO given in Sect. 6.5.1, an except that (6.7) is replaced by

$$H(y)\dot{\hat{x}}_{2} = -C(y, \hat{x}_{2})\hat{x}_{2} - g(y) + D\tau_{c} - \frac{k_{2}}{k_{1}}x_{v} - k_{4}\hat{x}_{2} - \frac{k_{3}}{(k_{1})^{\frac{\gamma}{\beta}}} \left[ x_{v} \right]^{\frac{\gamma}{\beta}} + \xi(y, \hat{x}_{2}, t)\hat{\Phi}$$
(6.22)

where  $\hat{\Phi}$  is adaptively updated by

$$\hat{\mathbf{\Phi}} = \Gamma \mathbf{\xi}^{\mathrm{T}}(\mathbf{y}, \hat{\mathbf{x}}_2, t) \mathbf{y} - \mathbf{\Gamma} \boldsymbol{\varphi}$$
 (6.23)

$$\dot{\boldsymbol{\varphi}} = \frac{d\boldsymbol{\xi}^{\mathrm{T}}(\boldsymbol{y}, \hat{\boldsymbol{x}}_{2}, t)}{dt} \boldsymbol{y} + \boldsymbol{\xi}^{\mathrm{T}}(\boldsymbol{y}, \hat{\boldsymbol{x}}_{2}, t) \hat{\boldsymbol{x}}_{2} + \delta_{1} \hat{\boldsymbol{\Phi}}$$
(6.24)

and  $\delta_1 \in \mathbb{R}_+$  is a constant,  $\Gamma \in \mathbb{R}^{l_1 \times l_1}$  is a positive-definite constant matrix. Choose the initial state  $\hat{\Phi}(0)$  and the observer gains to satisfy

$$k_1 > \frac{Q_2}{(1 - \pi_1)\eta_1} \tag{6.25}$$

$$\sqrt{\frac{2\ell_0 V_2(0) + 2\rho}{l_{\min}\ell_0}} < \frac{Q_2}{(1 - \pi_1)\eta_1} < \frac{k_4 - c_q}{c_{\max}} - Q_0$$
 (6.26)

where  $V_2(0)=0.5\boldsymbol{e}_2^T(0)\boldsymbol{H}(\boldsymbol{y}(0))\boldsymbol{e}_2(0)+0.5\tilde{\boldsymbol{\Phi}}^T(0)\boldsymbol{\Gamma}^{-1}\tilde{\boldsymbol{\Phi}}(0), \tilde{\boldsymbol{\Phi}}(0)=\hat{\boldsymbol{\Phi}}(0)-\boldsymbol{\Phi}(0),$   $\rho=0.5\delta_1\delta_2||\boldsymbol{\Phi}||^2;\;\lambda_1\in\mathbb{R}_+,\;\delta_1\in\mathbb{R}_+,\;and\;\delta_2>0.5$  are three positive constants,  $\ell_0=\min\left\{(\frac{2\eta_1\pi_1}{l_{max}},\frac{\delta_1(2\delta_2-1)}{\delta_2\pi_{max}}\right\},$  while  $\pi_{max}$  is the maximum eigenvalue of the matrix  $\boldsymbol{\Gamma}$ . Suppose that the initial estimate  $\hat{\boldsymbol{x}}_2(0)$  is chosen such that  $||\boldsymbol{e}_2(0)||\leq \frac{Q_2}{(1-\pi_1)\eta_1}$ , then the observer error  $\boldsymbol{e}_1$  will be finite time stable with finite-time  $T_0$ , i.e.,  $\boldsymbol{e}_1(t)\equiv \boldsymbol{0}$  for  $t\geq T_0=\frac{||\boldsymbol{e}_1(0)||}{\lambda_1}$  with  $\lambda_1\in\mathbb{R}_+$  being a constant such that  $\lambda_1+\frac{Q_2}{(1-\pi_1)\eta_1}\leq k_1$  and the observer error  $\boldsymbol{e}_2$  is ultimately uniformly bounded.

**Proof** Like the proof of Theorem 6.1, the proof of Theorem 6.2 can be divided into the following two parts.

• Stability analysis of the estimation error  $e_2$ :

With the replaced estimation (6.22) for  $x_2$ , one has

$$H(y)\dot{e}_{2} = -C(y,\hat{x}_{2})\hat{x}_{2} + C(y,x_{2})x_{2} + D(I_{N} - E(t))\tau_{c}$$

$$-\frac{k_{2}}{k_{1}}x_{v} - \frac{k_{3}}{(k_{1})^{\frac{\gamma}{\beta}}} \left[x_{v}\right]^{\frac{\gamma}{\beta}} - k_{4}\hat{x}_{2} + \xi(y,\hat{x}_{2},t)\hat{\Phi}$$

$$-\xi(x,\dot{x},t)\Phi - D\bar{\tau}_{c} - d$$
(6.27)

Note that

$$\xi(y, \hat{x}_{2}, t)\hat{\Phi} - \xi(x, \dot{x}, t)\Phi = \xi(y, \hat{x}_{2}, t)\hat{\Phi} - \xi(x_{1}, x_{2}, t)\Phi 
= -\xi(y, \hat{x}_{2}, t)\tilde{\Phi} + \tilde{\xi}\Phi$$
(6.28)

where  $\tilde{\boldsymbol{\xi}} = \boldsymbol{\xi}(\boldsymbol{y}, \hat{\boldsymbol{x}}_2, t) - \boldsymbol{\xi}(\boldsymbol{x}_1, \boldsymbol{x}_2, t)$ . It thus results (6.23) in

$$\dot{\hat{\mathbf{\Phi}}} = -\mathbf{\Gamma} \boldsymbol{\xi}^{\mathrm{T}}(\mathbf{y}, \hat{\mathbf{x}}_{2}, t) \boldsymbol{e}_{2} - \delta_{1} \mathbf{\Gamma} \hat{\mathbf{\Phi}}$$
 (6.29)

With (6.21), one has  $||\tilde{\boldsymbol{\xi}}\boldsymbol{\Phi}|| = ||\boldsymbol{\xi}(\boldsymbol{y},\hat{\boldsymbol{x}}_2,t)\boldsymbol{\Phi} - \boldsymbol{\xi}(\boldsymbol{x}_1,\boldsymbol{x}_2,t)\boldsymbol{\Phi}|| \leq c_q ||\boldsymbol{e}_2||$ . Choosing another candidate Laypunov function  $V_2 = \frac{e_1^T H(\boldsymbol{y})\boldsymbol{e}_2}{2} + \frac{\tilde{\boldsymbol{\Phi}}^T \boldsymbol{\Gamma}^{-1} \tilde{\boldsymbol{\Phi}}}{2}$  with  $\tilde{\boldsymbol{\Phi}} = \boldsymbol{\Phi} - \hat{\boldsymbol{\Phi}}$ , differentiating  $V_2$  and substituting (6.28) and (6.29) lead to

$$\dot{V}_{0} = \mathbf{e}_{2}^{\mathrm{T}} \left( \mathbf{D} (\mathbf{I}_{N} - \mathbf{E}(t)) \mathbf{\tau}_{c} - \mathbf{C}(\mathbf{y}, \mathbf{e}_{2}) \hat{\mathbf{x}}_{2} - \mathbf{D} \mathbf{\tau}_{c} - \frac{k_{2}}{k_{1}} \mathbf{x}_{v} - \frac{k_{3}}{(k_{1})^{\frac{\gamma}{\beta}}} \left[ \mathbf{x}_{v} \right]^{\frac{\gamma}{\beta}} \right) \\
-k_{4} \hat{\mathbf{x}}_{2} - \mathbf{d} + \mathbf{\xi}(\mathbf{y}, \hat{\mathbf{x}}_{2}, t) \hat{\mathbf{\Phi}} - \mathbf{\xi}(\mathbf{q}, \dot{\mathbf{q}}, t) \mathbf{\Phi} - \tilde{\mathbf{\Phi}}^{\mathrm{T}} \mathbf{\Gamma}^{-1} \dot{\hat{\mathbf{\Phi}}} \\
\leq Q_{1} ||\mathbf{e}_{2}|| - (k_{4} - c_{\max}(||\mathbf{e}_{2}|| + Q_{0}) - c_{q}) ||\mathbf{e}_{2}||^{2} + \delta_{1} \tilde{\mathbf{\Phi}}^{\mathrm{T}} \hat{\mathbf{\Phi}} \\
- k_{2} \mathbf{e}_{2}^{\mathrm{T}} \mathbf{sgn}(\mathbf{e}_{1}) - k_{3} \mathbf{e}_{2}^{\mathrm{T}} \mathrm{diag}(|\mathbf{sgn}(\mathbf{e}_{1})|^{\frac{\gamma}{\beta}}) \mathbf{sgn}(\mathbf{x}_{v}) \\
\leq \delta_{1} \tilde{\mathbf{\Phi}}^{\mathrm{T}} \hat{\mathbf{\Phi}} - (k_{4} - c_{\max}(||\mathbf{e}_{2}|| + Q_{0}) - c_{q}) ||\mathbf{e}_{2}||^{2} \\
+ (Q_{1} + \sqrt{n}k_{2} + \sqrt{n}k_{3}) ||\mathbf{e}_{2}|| \\
= \delta_{1} \tilde{\mathbf{\Phi}}^{\mathrm{T}} \hat{\mathbf{\Phi}} - (k_{4} - c_{\max}(||\mathbf{e}_{2}|| + Q_{0}) - c_{q}) ||\mathbf{e}_{2}||^{2} + Q_{2} ||\mathbf{e}_{2}|| \\$$

As the proof of Lemma 6.1, if  $||e_2|| < \frac{k_4 - c_q}{c_{\max}} - Q_0$ , then there will still exist an positive scalar  $\frac{\eta_1}{c_{\max}}$  such that  $c_{\max}(||e_2|| + Q_0) + \eta_1 = k_4 - c_q$ . This leads (6.30) to

$$\dot{V}_{2} \leq -\eta_{1}||\mathbf{e}_{2}||^{2} + Q_{2}||\mathbf{e}_{2}|| + \delta_{1}\tilde{\mathbf{\Phi}}^{T}\hat{\mathbf{\Phi}} 
= -\eta_{1}\pi_{1}||\mathbf{e}_{2}||^{2} + (Q_{2} - (1 - \pi_{1})\eta_{1}||\mathbf{e}_{2}||)||\mathbf{e}_{2}|| + \delta_{1}\mathbf{\Phi}^{T}\hat{\mathbf{\Phi}}$$
(6.31)

At this time, when  $e_2$  is outside of the set  $\mathcal{D}_1$ , we get

$$\dot{V}_{2} \leq -\eta_{1}\pi_{1}||\boldsymbol{e}_{2}||^{2} + \delta_{1}\tilde{\boldsymbol{\Phi}}^{T}\hat{\boldsymbol{\Phi}}$$

$$\leq -\ell_{0}\left(\frac{\boldsymbol{e}_{2}^{T}\boldsymbol{H}(\boldsymbol{y})\boldsymbol{e}_{2}}{2} + \frac{\tilde{\boldsymbol{\Phi}}^{T}\boldsymbol{\Gamma}^{-1}\tilde{\boldsymbol{\Phi}}}{2}\right) + \frac{\delta_{1}(2\delta_{2} - 1)\tilde{\boldsymbol{\Phi}}^{T}\boldsymbol{\Gamma}^{-1}\tilde{\boldsymbol{\Phi}}}{2\delta_{2}\pi_{\max}} + \delta_{1}\tilde{\boldsymbol{\Phi}}^{T}\hat{\boldsymbol{\Phi}}^{T}\hat{\boldsymbol{\Phi}} \tag{6.32}$$

Define  $\frac{\delta_1(2\delta_2-1)\tilde{\pmb{\Phi}}^T\Gamma^{-1}\tilde{\pmb{\Phi}}}{2\delta_2\pi_{\max}}=\tilde{\Phi}\in\mathbb{R}_+$ , it leaves (6.32) as  $\dot{V}_2\leq -\ell_0V_2+\tilde{\Phi}+\delta_1\tilde{\pmb{\Phi}}^T\hat{\pmb{\Phi}}$ . Using the completion of squares, the following equation can be calculated:

$$\delta_{1}\tilde{\boldsymbol{\Phi}}^{T}\hat{\boldsymbol{\Phi}} = \delta_{1}\tilde{\boldsymbol{\Phi}}^{T}(\boldsymbol{\Phi} - \tilde{\boldsymbol{\Phi}}) \leq \delta_{1}\left(\frac{1}{2\delta_{2}}||\tilde{\boldsymbol{\Phi}}||^{2} + \frac{\delta_{2}}{2}||\boldsymbol{\Phi}||^{2} - ||\tilde{\boldsymbol{\Phi}}||^{2}\right) \\
= -\frac{\delta_{1}(2\delta_{2} - 1)}{2\delta_{2}}||\tilde{\boldsymbol{\Phi}}||^{2} + \frac{\delta_{1}\delta_{2}}{2}||\boldsymbol{\Phi}||^{2} \tag{6.33}$$

From (6.33), one can apply the definition of  $\bar{\Phi}$  to obtain

$$\bar{\boldsymbol{\Phi}} + \delta_1 \tilde{\boldsymbol{\Phi}}^T \hat{\boldsymbol{\Phi}} \leq \bar{\boldsymbol{\Phi}} - \frac{\delta_1 (2\delta_2 - 1)}{2\delta_2} ||\tilde{\boldsymbol{\Phi}}||^2 + \frac{\delta_1 \delta_2}{2} ||\boldsymbol{\Phi}||^2$$

$$\leq \frac{\delta_1 \delta_2}{2} ||\boldsymbol{\Phi}||^2 = \rho$$
(6.34)

Then, one has

$$\dot{V}_2 \le -\ell_0 V_2 + \rho \tag{6.35}$$

Solving this inequality yields  $V_2(t) \leq V_2(0) + \frac{\rho}{\ell_0}$ . Using  $0.5l_{\min}||\boldsymbol{e}_2||^2 \leq V_2$  for all  $\boldsymbol{e}_2 \in \mathbb{R}^n$ , one can get  $||\boldsymbol{e}_2|| \leq \varepsilon$  for all  $t \geq 0$ , where  $\varepsilon = \sqrt{\frac{2\ell_0 V_2(0) + 2\rho}{l_{\min}\ell_0}}$ . From the above analysis, it can be concluded from the gains' choice (6.26) and

From the above analysis, it can be concluded from the gains' choice (6.26) and the chosen initial values  $\hat{x}_2(0)$  and  $\hat{\Phi}(0)$  that the inequality  $||e_2|| \le \varepsilon$  will always hold for all  $t \ge 0$ . That is to say,  $e_2$  is ultimately uniformly bounded by Definition 2.1.

• Stability analysis of the estimation error  $e_1$ :

The stability analysis of the estimation error  $e_1$  is as same as in the proof of Theorem 6.1.

Summarizing the above analysis, Theorem 6.2 is thus proved.

**Remark 6.4** From the proof of Theorem 6.2, it can be known that once the initial values of  $\hat{x}_1(0)$ ,  $\hat{x}_2(0)$ , and  $\hat{\Phi}(0)$  are chosen, the observation or estimation accuracy for  $e_2$  highly depends on the choice of the observer gains. A smaller value of  $\delta_1$ ,  $\pi_{\text{max}}$ , and  $\delta_2$ , or a larger value of  $\eta_1$ ,  $\pi_1$  will result in a smaller value of  $\varepsilon$ . Consequently, the accuracy of the observation for  $x_2$  is much higher.

# 6.6 Adaptive State Observer-Based Controller

A velocity-free fault-tolerant and modeling error compensation control scheme is proposed for the Euler-Lagrange system (6.1) based on the observer proposed. The controller is designed as

$$\boldsymbol{\tau}_c = \mathbf{sat}(\boldsymbol{D}^{\dagger} \boldsymbol{v}_c, \tau_{\text{max}}) \tag{6.36}$$

where  $v_c = [v_{c1}, v_{c2}, \dots, v_{cN}]^T \in \mathbb{R}^n$  denotes the input of the controller. For convenience of input constraint effect analysis, the following auxiliary system is introduced

$$\dot{x}_a = -k_a x_a - \frac{||\Delta \tau_c||^2}{||x_a||^2} x_a - \Delta \tau_c$$
 (6.37)

where  $k_a \in \mathbb{R}_+$ ,  $\boldsymbol{x}_a \in \mathbb{R}^n$  is the state of the auxiliary system, and  $\Delta \boldsymbol{\tau}_c = \boldsymbol{D}(\boldsymbol{\tau}_c - \boldsymbol{D}^{\dagger} \boldsymbol{v}_c)$ .

Introducing coordinate change  $z_2 = \hat{x}_2 + \rho_1 \hat{x}_1$  with the scalar  $\rho_1 \in \mathbb{R}_+$  the stability of the closed-loop system with the control (6.36) can be summarized in the following theorem.

**Theorem 6.3** Consider the Euler-Lagrange system given by (6.1) with the modeling error induced by actuator fault (6.3) and uncertainties  $f(q, \dot{q}, t)$  satisfying (6.21). Application of the adaptive SMO (6.6) and (6.22), if the controller (6.36) is implemented with the input signal  $v_c$  designed by

$$v_{c} = \mathbf{g}(\mathbf{y}) + \frac{k_{2}\mathbf{x}_{v}}{k_{1}} + \frac{k_{3}}{(k_{1})^{\frac{\gamma}{\beta}}} \left[ \mathbf{x}_{v} \right]^{\frac{\gamma}{\beta}} + k_{4}\hat{\mathbf{x}}_{2} - \rho_{2}\mathbf{z}_{2} - \rho_{3}\mathbf{x}_{a}$$

$$- \boldsymbol{\xi}(\mathbf{y}, \hat{\mathbf{x}}_{2}, t)\hat{\boldsymbol{\Phi}} - \hat{\mathbf{x}}_{1} - \rho_{1}\boldsymbol{H}(\mathbf{y})(\mathbf{z}_{2} - \rho_{1}\hat{\mathbf{x}}_{1}) - \rho_{1}\boldsymbol{C}(\mathbf{y}, \hat{\mathbf{x}}_{2})\hat{\mathbf{x}}_{1} - \boldsymbol{\Pi}_{0}$$

$$(6.38)$$

where  $\rho_2 \in \mathbb{R}_+$ ,  $\rho_3 \in \mathbb{R}_+$  are the control gains, and  $\Pi_0 = \frac{\rho_1}{2}(c_{\max}^2||z_2||^2 + ||\boldsymbol{H}(\boldsymbol{y})||^2)z_2$ . Suppose that the control gains are chosen such that  $k_a - 0.5\rho_3^2 - 0.5 > 0$  and  $\rho_2 - 1 > 0$ , then all the states of the closed-loop system, i.e.,  $\boldsymbol{q}$  and  $\dot{\boldsymbol{q}}$ , are ultimately uniformly bounded. The modeling error consisting of external disturbances, actuator fault, and system uncertainty is attenuated and compensated.

**Proof** With application of the controller (6.36), it results in

$$D\tau_c = D\text{sat}(D^{\dagger}v_c, \tau_{\text{max}}) = \Delta\tau_c + v_c \tag{6.39}$$

Using the definition of  $z_2$ , inserting (6.38) into the adaptive SMO (6.22) yields

$$H(y)\dot{z}_2 = \Delta \tau_c - C(y, \hat{x}_2)z_2 - \rho_1 H(y)x_y - \hat{x}_1 - \rho_2 z_2 - \rho_3 x_a - \Pi_0. \quad (6.40)$$

Consider a candidate Lyapunov function as  $V_3 = \frac{1}{2}(\hat{x}_1^T\hat{x}_1 + z_2^T H(y)z_2 + x_a^T x_a)$ . Using Property 6.2, the linearity property in Property 6.3, combining (6.6), (6.37), and (6.40) results in

$$\dot{V}_{3} = -\rho_{1}||\hat{\boldsymbol{x}}_{1}||^{2} - \boldsymbol{x}_{v}\hat{\boldsymbol{x}}_{1}^{T} - \boldsymbol{x}_{a}^{T}\Delta\boldsymbol{\tau}_{c} + \boldsymbol{z}_{2}^{T}(-\boldsymbol{C}(\boldsymbol{y}, \boldsymbol{e}_{2})\boldsymbol{z}_{2} + \Delta\boldsymbol{\tau}_{c} - \rho_{1}\boldsymbol{H}(\boldsymbol{y})\boldsymbol{x}_{v} - \rho_{2}\boldsymbol{z}_{2} - \rho_{3}\boldsymbol{x}_{a} - \boldsymbol{\Pi}_{0}) - k_{a}||\boldsymbol{x}_{a}||^{2} - ||\Delta\boldsymbol{\tau}_{c}||^{2}$$
(6.41)

Because  $||x_v|| \le \sqrt{nk_1}$  holds due to  $x_v = k_1 \text{sgn}(e_1)$ , it can be obtained from Property 6.3 that

$$z_{2}^{\mathrm{T}}(-\boldsymbol{C}(\boldsymbol{y},\boldsymbol{e}_{2})z_{2} - \rho_{1}\boldsymbol{H}(\boldsymbol{y})\boldsymbol{x}_{v}) \leq c_{\max}||\boldsymbol{e}_{2}||||z_{2}||^{2} + \rho_{1}\|\boldsymbol{H}(\boldsymbol{y})\|\|z_{2}\|\sqrt{n}k_{1}$$

$$\leq \frac{\rho_{1}c_{\max}^{2}\|z_{2}\|^{4}}{2} + \frac{\|\boldsymbol{e}_{2}\|^{2}}{2\rho_{1}}$$

$$+ \frac{\rho_{1}}{2}\|\boldsymbol{H}(\boldsymbol{y})\|^{2}\|z_{2}\|^{2} + \frac{nk_{1}^{2}}{2\rho_{1}}$$

$$(6.42)$$

Using Young's inequalities  $-\boldsymbol{x}_{v}\hat{\boldsymbol{x}}_{1}^{\mathrm{T}} \leq \frac{\rho_{1}||\hat{\boldsymbol{x}}_{1}||^{2}}{2} + \frac{nk_{1}^{2}}{2\rho_{1}}, \quad \boldsymbol{z}_{2}^{\mathrm{T}}\Delta\boldsymbol{\tau}_{c} \leq \frac{||\Delta\boldsymbol{\tau}_{c}||^{2} + ||\boldsymbol{z}_{2}||^{2}}{2}, \\ -\rho_{3}\boldsymbol{z}_{2}^{\mathrm{T}}\boldsymbol{x}_{a} \leq \frac{||\boldsymbol{z}_{2}||^{2} + \rho_{3}^{2}||\boldsymbol{x}_{a}||^{2}}{2}, -\boldsymbol{x}_{a}^{\mathrm{T}}\Delta\boldsymbol{\tau}_{c} \leq \frac{||\Delta\boldsymbol{\tau}_{c}||^{2} + ||\boldsymbol{x}_{a}||^{2}}{2}, \text{ and imposing (6.42), then (6.41)}$  will be bounded by

$$\dot{V}_{3} \leq -\frac{\rho_{1}}{2} \|\hat{\boldsymbol{x}}_{1}\|^{2} - (\rho_{2} - 1) \|\boldsymbol{z}_{2}\|^{2} - \left(k_{a} - \frac{\rho_{3}^{2}}{2} - \frac{1}{2}\right) \|\boldsymbol{x}_{a}\|^{2} + \frac{\|\boldsymbol{e}_{2}\|^{2}}{2\rho_{1}} + \frac{nk_{1}^{2}}{\rho_{1}}$$
(6.43)

It is known from the proof of Theorem 6.2 that,  $||e_2(t)|| \le \varepsilon$  holds for all  $t \ge 0$ . It follows from (6.43) that

$$\dot{V}_3 \le -2\lambda_0 V_3 + \frac{\|\varepsilon\|^2}{2\rho_1} + \frac{nk_1^2}{\rho_1} \tag{6.44}$$

where  $\lambda_0 = \min\{0.5\rho_1, \frac{\rho_2-1}{l_{\max}}, k_a-0.5\rho_3^2-0.5\}$ . That means that  $V_3$  is ultimately uniformly bounded together with the states  $\hat{\boldsymbol{x}}_1, \boldsymbol{z}_2$ , and  $\boldsymbol{x}_a$ . More specifically, there exists a finite-time  $t_f$  such that  $||\hat{\boldsymbol{x}}_1|| < \bar{\varepsilon}$  and  $||\boldsymbol{z}_2|| < \bar{\varepsilon}$  for  $\forall \bar{\varepsilon} > \sqrt{\frac{1}{2\lambda_0\rho_1}(\frac{||\varepsilon||^2}{2} + nk_1^2)}$  and  $\forall t > t_f$ .

Because  $e_1(t)$  is finite time stable in  $T_0$  and  $e_2(t)$  is ultimately uniformly bounded with  $||e_2(t)|| \le \varepsilon$ , for all  $t > \bar{t}_f = \max\{t_f, T_0\}$ , it follows that

$$||x|| = ||\hat{x}_1 - e_1|| \le ||\hat{x}_1|| + ||e_1|| < \bar{\varepsilon}$$
(6.45)

and

$$||\dot{\mathbf{x}}|| = ||\mathbf{x}_2|| \le ||\hat{\mathbf{x}}_2|| + ||\mathbf{e}_2|| \le ||\mathbf{z}_2|| + ||\rho_1\hat{\mathbf{x}}_1|| + ||\mathbf{e}_2|| < \varepsilon^*$$
(6.46)

where  $\varepsilon^* = \bar{\varepsilon} + \rho_1 \bar{\varepsilon} + \varepsilon$ . It is thus concluded from (6.45), (6.46), and Definition 2.1 that the states of the closed-loop system, i.e., x and  $\dot{x}$  are ultimately uniformly bounded. The proof is hence completed here.

It can be summarized from the proof of Theorem 6.3 that, only the system output, the states of the observer, and the state of the auxiliary system (6.37) are feedback to the controller (6.36). Hence, the controller is rigorously independent on the measurements  $\dot{x}$ . Moreover, the assumption, i.e.,  $||\dot{x}|| \leq Q_0$  is also not required in the controller design.

Summarizing the analyses in the proof of Theorem 6.3 and Remark 6.4, all the gains of the observer and the controller can be chosen according to the following procedures when implementing the proposed approach.

- Step #1: Determine the observation/estimation accuracy accuracy  $\varepsilon$  for  $e_2$ .
- Step #2: It is seen in the proof of Theorem 6.2 that  $\boldsymbol{\varepsilon} = \sqrt{\frac{2\ell_0 V_2(0) + 2\rho}{l_{\min}\ell_0}}$ , then once can choose  $\eta_1, 0 < \pi_1 < 1, \delta_1, \delta_2 > 0.5$ ,  $\boldsymbol{\Gamma}, \hat{\boldsymbol{x}}_2(0)$ , and  $\hat{\boldsymbol{\Phi}}(0)$  to satisfy this equation.
- Step #3: Select  $k_1$ ,  $k_2$ ,  $k_3$ ,  $k_4$ ,  $\beta$ , and  $\gamma$  to satisfy inequalities (6.25), (6.26).
- Step #4: Choose a positive  $\bar{\epsilon}$  according to the set of requirements (such as control accuracy) imposed by the mission. It is known from (6.45) that if smaller  $\bar{\epsilon}$  is selected, then higher accuracy will be achieved.
- selected, then higher accuracy will be achieved.

   Step #5: Based on the inequality  $\bar{\varepsilon} > \sqrt{\frac{0.5||\varepsilon||^2 + nk_1^2}{2\lambda_0 \rho_1}}$  in the proof of Theorem 6.3 and the value of  $\varepsilon$  determined in Step 1, choose  $\rho_1$ ,  $\rho_2 > 1$ ,  $\rho_3$ , and  $k_a$  such that  $\bar{\varepsilon} > \sqrt{\frac{0.5||\varepsilon||^2 + nk_1^2}{2\lambda_0 \rho_1}}$  and  $k_a 0.5\rho_3^2 0.5 > 0$ . However, a smaller  $\rho_1$  will lead to a high-accuracy control of  $\dot{x}$  according to (6.46).

# 6.7 Application to Microsatellite Attitude Control

Having shown that, for proper choices of the gains for the observer and the controller as given in Sects. 6.5 and 6.6, the system states x and  $\dot{x}$  will be ultimately uniformly bounded, this section will apply the proposed control to the problem of rigid satellite attitude stabilization control through along with accompanying simulation and experimental results.

Consider a microsatellite controlled by using four reaction wheels with the maximum torque  $\tau_{\text{max}} = 0.1 \text{ N} \cdot \text{m}$ . The corresponding actuator matrix is  $D^* = [1, 0, 0, \frac{1}{\sqrt{3}}; 0, 1, 0, \frac{1}{\sqrt{3}}; 0, 0, 1, \frac{1}{\sqrt{3}}]$ . Assuming that only the satellite attitude  $\sigma$  is measurable, while its angular velocity  $\omega$  is immeasurable, i.e.,  $\dot{\sigma} = [\omega_1, \omega_2, \omega_3]^T$  is immeasurable. Because  $J^*(\sigma)$  in (4.42) is a known function of  $\sigma$ , considering reaction wheel faults, the transformed rigid satellite attitude system (4.42) in Sect. 4.3 can be put into the Euler-Lagrange system (6.1) with g(y) = 0, by introducing the change of variables  $y = \sigma$ ,  $x_1 = \sigma$ ,  $x_2 = \dot{\sigma}$ ,  $D = (P(\sigma))^T D^*$ , and  $d = (P(\sigma))^T u_d$ . Hence, the proposed observer-based velocity-free control approach in this chapter is applicable to the rigid satellite attitude control problem.

To this end, the control objective of that considered rigid satellite attitude system to be achieved can be stated as: Consider the rigid satellite attitude system described by (4.42) for given any initial attitude and angular velocity, design a velocity-free (i.e.,  $\dot{\sigma}$  is not required) control law u to accomplish attitude stabilization maneuver, i.e., the closed-loop attitude control system can be stabilized with the attitude  $\sigma$  converging to zero or a small set containing the origin. Moreover, the control objective should be met in the presence of external disturbance  $u_d$ , actuator fault, actuator constraint, and system uncertainties.

#### 6.7.1 Simulation Results

The external disturbance for  $u_d$  in (4.42) is calculated as in [9], and the following fault scenarios are introduced and simulated.

- The actuator mounted in line with  $+X_B$ -axis loses 50% of its normal power after 3 s.
- The actuator mounted in line with  $+Y_B$ -axis loses its power of 10% in the time interval from 5 to 10 s; this wheel gets locked-in place at a value of  $-0.01 \text{ N} \cdot \text{m}$  after 10 s.
- The actuator fixed in line with  $+Z_B$  -axis experiences 0.005 N·m of floating around trim fault after 7 s, i.e.,  $e_3(t) = 1$  for all  $t \ge 0$ , and  $\bar{\tau}_{c3} = 0.005$  N·m when t > 7.
- The fourth actuator is always healthy.

For the considered rigid satellite, the uncertainties in its attitude control system are mainly induced by uncertain inertia. The mass properties of rigid may be uncer-

tain due to onboard payload motion, rotation of solar arrays, or fuel consumptions, making J time-varying and even uncertain. Therefore, the simulation is carried out under the condition that the moment inertia matrix  $J = J_0 + \Delta J$  is unknown and time varying. Here,  $J_0 = \text{diag}([16, 18, 23.5]^T) \text{ kg} \cdot \text{m}^2$  is the nominal part, and the following uncertain  $\Delta J$  is considered in simulation.

$$\Delta \mathbf{J} = (1 + \exp(-0.1t) + 2\mathbf{v}(t - 10) - 1.5\mathbf{v}(t - 20))\operatorname{diag}([3, 2, 1]^{\mathrm{T}})\operatorname{kg} \cdot \operatorname{m}^{2}$$
 (6.47)

where  $v(\cdot)$  is defined as v(t > 0) = 1 and v(t < 0) = 0.

Based on Remark 6.4 and the procedures of choosing the controller and observer parameters as stated in Sects. 6.5 and 6.6, the control gains for the controller (6.36) are chosen as  $k_a = 5$ ,  $\rho_1 = 2.2$ ,  $\rho_2 = 2.05$ , and  $\rho_3 = 2.75$ . The gains of the observer are chosen as  $\gamma = 7$ ,  $\beta = 19$ ,  $k_1 = 0.15$ ,  $k_2 = 9$ ,  $k_3 = 16$ ,  $k_4 = 0.0005$ ,  $\Gamma = \text{diag}([2, 2, 3, 3, 3, 4]^T)$ , and  $\delta_1 = 0.001$ . The initial states of the satellite are  $\sigma(0) = [0.4, -0.25, 0.3]^T$  and  $\dot{\sigma}(0) = [0, 0, 0]^T$  rad/s.

Figures 6.4 and 6.5 show the observer error states obtained from the SMO (6.6) and (6.22) incorporated in the controller (6.36). It is shown that sliding motion is obtained on  $e_1 = 0$  in finite time at about 3.7 s. After a short period, roughly 0.3 s, uniformly ultimately bounded stability of  $e_2$  is achieved. This convergence happens in the presence of external disturbance and actuator faults. Moreover, high observing accuracies for  $x_1$  and  $x_2$  are realized with the reconstruction error  $|e_{1i}| \le 2.0 \times 10^{-7}$ , and  $|e_{2i}| \le 1.0 \times 10^{-5}$ , i = 1, 2, 3. From the results obtained, the estimate states  $\hat{x}_1$ ,  $\hat{x}_2$  can converge to the actual states  $\sigma$ ,  $\dot{\sigma}$  with minor errors under the effect of the observer despite external disturbance and reaction wheel faults. Hence, the conclusion in Theorem 6.2 is verified.

Because the observer can precisely reconstruct the satellite attitude  $\sigma$  and its angular velocity  $\dot{\sigma}$ , the observer-based and its angular velocity-free controller (6.36) guarantees the satellite attitude and its velocity to be uniformly ultimately bounded stable in finite time roughly 65 s, as we can see in Figs. 6.6 and 6.7. The attitude stabilization maneuver is thus accomplished without angular velocity measurement, even when an actuator fault occurs. The associated commanded control is shown in Fig. 6.8. The control power of each reaction wheel is within its maximum allowable

**Fig. 6.4** The observer error  $e_1$  from the adaptive SMO

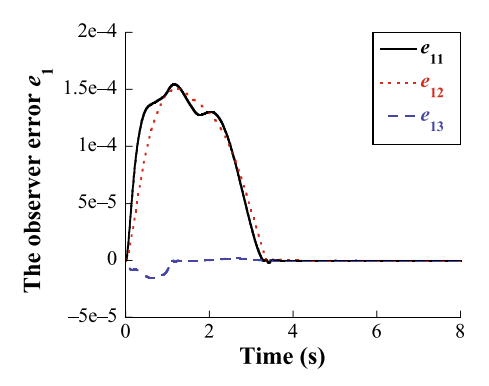


**Fig. 6.5** The observer error  $e_2$  from the adaptive SMO

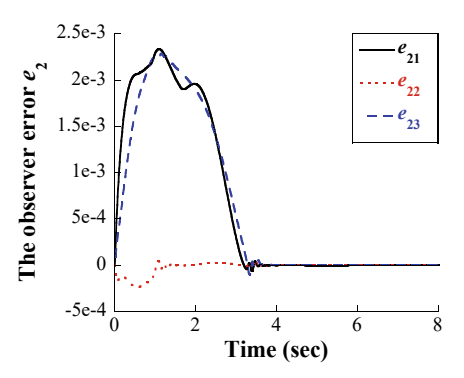


**Fig. 6.6** The attitude from the controller (6.36)

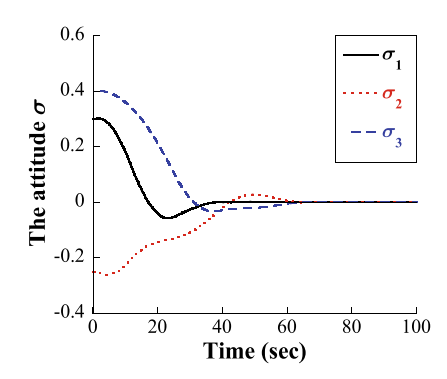
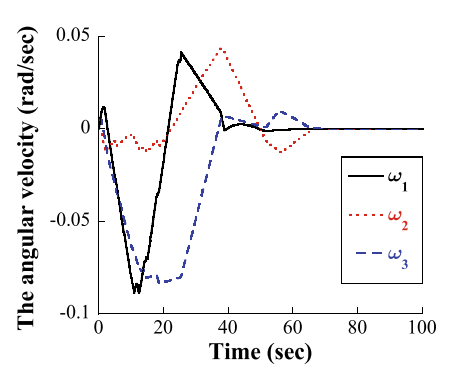


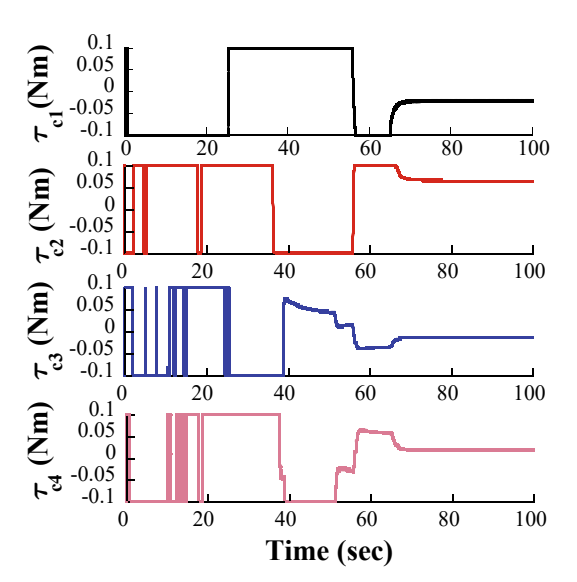
**Fig. 6.7** The angular velocity from the controller (6.36)



limit, i.e., 0.1 N·m. It is interesting to see Fig. 6.8 that the control power of each actuator will not be near zero. That is due to the fact that, extra control torque is needed to compensate for the lock-in-place fault, and the floating around trim fault occurring in the actuators in  $+Y_B$  and  $+Z_B$ .

Taking sensor noise into account, numerical simulation is further carried out to verify the realistic application of the proposed approach to engineering. For satellite, nongyroscopic sensors are equipped to measure its attitude information. In practical satellite engineering, attitude sensors are usually modeled by a zero-

**Fig. 6.8** The commanded control from the controller (6.36)



mean Gaussian white-noise process with standard deviation  $\sigma_{ST}$ . Hence, the attitude control by using the designed scheme is further simulated with  $\sigma_{ST}=35$  arcseconds, while the control and the observer gains are chosen the same as the values in the preceding simulation. Results show that, high observing accuracies for  $x_1$  and  $x_2$  are still guaranteed. The reconstruction errors are  $|e_{1i}| \leq 2.2 \times 10^{-5}$ , and  $|e_{2i}| \leq 1.6 \times 10^{-3}$ , i=1,2,3. Moreover, the attitude control accuracy is  $|\sigma_i| \leq 3.0 \times 10^{-3}$ , and  $|\omega_i| \leq 1.2 \times 10^{-3}$ , i=1,2,3. Those control performances still satisfy the stringent pointing requirements of the satellite to provide operation conditions for the payloads even in the presence of actuator faults.

# 6.7.2 Experimental Results

To test the proposed controller on the ground, the three-degrees-of-freedom simulator shown in Fig. 2.4 is used. During experimental tests, the considered microsatellite will be mounted on the payload of this simulator. When the proposed approach is applied, the experimental results are shown in Figs. 6.9 and 6.10. It is seen from Fig. 6.9a that, the attitude stabilization is accomplished within 60 s. By transforming the modified Rodrigues parameters  $\sigma$  into Euler attitude angles, it can be obtained that the attitude pointing accuracy achieved is 0.015 degrees. The resulting angular velocity is shown in Fig. 6.10. As the steady state behavior clearly shows in Fig. 6.11, attitude stability is within 0.002 deg/s. These control performances can guarantee the satellite attitude system satisfies necessary stringent requirements for accomplishing the planned mission, such as image taking and data transmission. On the other hand, it is worth mentioning that, the inertia moment cannot be precisely calculated in practice. As a result, the value of the inertia used in the implementation of the proposed

**Fig. 6.9** The experimental result of the attitude from the controller (6.36)

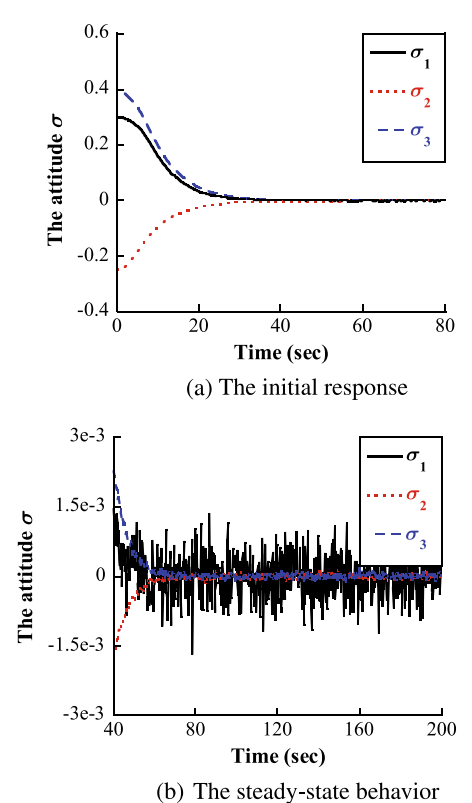
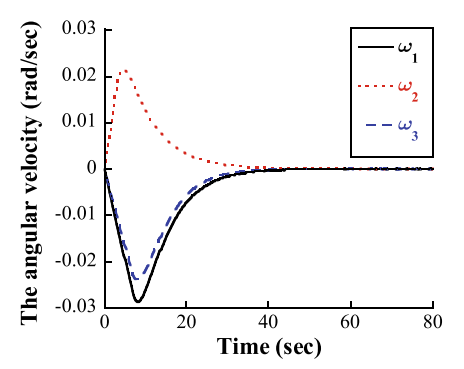


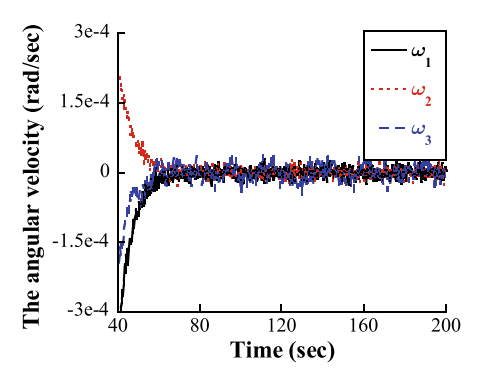
**Fig. 6.10** The initial angular velocity from the controller (6.36) in test



control is not the exact value of the real inertia. Hence, there exist uncertainties in the attitude control system during experiments.

Compared the experimental results in Figs. 6.9, 6.10 and 6.11 with the simulation results in Figs. 6.6 and 6.7, almost no overshoot is observed in experiment results. That is because, when carrying out experiments on ground and indoor, there is no external disturbance acting on the testbed. However, it can be seen that the

**Fig. 6.11** The angular velocity's steady-state from the controller (6.36) in test



experimental results match the simulation results very well, and 60 s are needed to stabilize the attitude in both results. To summarize, high-accuracy pointing control (order of  $10^{-2}$  deg) and high-accuracy attitude stability (order of  $10^{-3}$ deg/s) can high-accuracy attitude be realized through the proposed control. Hence, the easiness of implementation, high accuracy, and robustness are well verified through the experiment.

# 6.8 Summary

A velocity-free fault-tolerant and modeling error compensation control approach was proposed for a class of nonlinear systems. The SMO presented achieved precise reconstruction of unmeasured system states even in the presence of system uncertainties. The control design was carried out using the estimated states and the measurement of system output. Contrary to the existing observer-based velocity-free feedback control schemes, the controller guaranteed the uniformly ultimately boundedness of the states in the closed-loop system, despite actuator fault, actuator constraint, and external disturbance. The proposed method was applied to the attitude control of a satellite with only the measurement of attitude available.

#### References

- 1. Xiao, B., Hu, Q. L., Wang, D. W. (2015) Spacecraft attitude fault tolerant control with terminal sliding-mode observer. Journal of Aerospace Engineering 28(1): 04014055
- Li, S., Yang, J., Chen, W. H., Chen, X. (2012) Generalized extended state observer based control for systems with mismatched uncertainties. IEEE Transactions on Industrial Electronics 59(12): 4792–4802
- Zhang, J. H., Feng, G., Xia, Y. Q. (2014) Design of estimator-based sliding-mode outputfeedback controllers for discrete-time systems. IEEE Transactions on Industrial Electronics 61(5): 2432–2440

References 143

4. Chen, W. T., Saif, M. (2008) Output feedback controller design for a class of mimo nonlinear systems using high-order sliding-mode differentiators with application to a laboratory 3-d crane. IEEE Transactions on Industrial Electronics 55(11): 3985–3997

- Liang, Y. W., Ting, L. W., Lin, L. G. (2012) Study of reliable control via an integral-type sliding mode control scheme. IEEE Transactions on Industrial Electronics 59(8): 3062–3068
- Lombaerts, T. J. J., Smaili, M. H., Stroosma, O., Chu, Q. P., Mulder, J. A., Joosten, D. A. (2009) Piloted simulator evaluation results of new fault-tolerant flight control algorithm. Journal of Guidance, Control, and Dynamics 32(6): 1747–1765
- Boskovic, J. D., Bergstrom, S. E., Mehra, R. K. (2005) Robust integrated flight control-design under failures, damage, and state-dependent disturbances. Journal of Guidance, Control, and Dynamics 28(5): 902–917
- 8. Namvar, M. (2009) A class of globally convergent velocity observers for robotic manipulators. IEEE Transactions on Automatic Control 54(8): 1956–1961
- 9. Yang, C. D., Sun, Y. P. (2002) Mixed  $\mathcal{H}_2/\mathcal{H}_{\infty}$  state-feedback design for microsatellite attitude control. Control Engineering Practice 10(9): 951–970

# **Chapter 7 Fixed-Time Optimal Attitude Control**



#### 7.1 Introduction

The main feature of the existing attitude control approaches can only achieve steady-state performance. The transient control performance can not be determined or prescribed. This is an important performance index in the practical satellite mission. To achieve satellite attitude maneuvering with external disturbances, performance constraints, and actuator faults [1], an adaptive FTC law was designed via the prescribed performance control (PPC) technique. Considering actuator fault and performance constraint, a robust FTC scheme was designed by the backstepping control technique [2]. Using the fixed-time and appointed-time prescribed performance functions, a adaptive fixed-time FTC law for a mechanical system [3] and a barrier Lyapunov functions-based adaptive appointed-time FTC algorithm for a satellite [4] were presented.

Note that the optimal attitude control scheme is rarely reported to satellite attitude control system with actuator fault. That is because obtaining the solution of the Hamilton–Jacobi–Bellman (HJB) equation is intractable. Motivated by this problem, the adaptive dynamic programming (ADP) method was available [5–8]. It combines reinforcement learning (RL) and the dynamic programming method to improve control performance by learning environmental feedback. The ADP method applies the actor-critic/critic-only neural network (NN) to approximate the optimal control law. Hence, it circumvents the difficult problem of obtaining the HJB equation's analytical solution in the traditional optimal control method [9–11].

Currently, the RL-based approximate optimal control has been widely used. In [12], an optimal control policy utilizing online iterative learning was presented for a discrete-time nonlinear system. In [13], a backstepping tracking control scheme for an unmanned ship was developed by using actor-critic NN. Combining the game theory and the ADP, a distributed optimal FTC scheme was proposed for a class of nonlinear systems [14]. In [15], an RL-based optimal attitude tracking control policy was developed for satellites with uncertainties, where a critic-only NN was adopted to learn that control policy. In [16], an online learning attitude controller

via the saturated HJB error was proposed. A variable parameter was given to change the learning gain and relax the persistent excitation condition. In [17], the tracking control policy was designed by employing the ADP to accomplish a quadrotor's path following. Usually, the RL-based optimal control policy needs to satisfy the persistent excitation assumption. To relax it, a modified online learning optimal control policy with the finite excitation assumption was proposed [18, 19]. Using the simple critic-only structure [8], the estimator-based optimal control was reported to ensure the optimality and predefined behavioral metrics of an uncertain Euler–Lagrange system by combining the RL and PPC method. Using the gradient descent approach, the finite-time convergent data-based updating law for the critic weight was developed [20]. The weight estimate error can be reduced to a tiny set in finite time.

Most of the preceding RL-based optimal control can only guarantee the uniformly ultimately bounded stability of the closed-loop system. Although the closed-loop system has a good balance between the control cost and the control performance, its convergence rate may be slow. To solve this problem, a fixed-time fault tolerant optimal attitude control is presented in this chapter with its highlights listed as:

- To guarantee the prescribed attitude stabilization performance, a prescribed performance function without knowing the precise system's initial value is designed. Utilizing the error transformation method, the attitude stabilization errors restricted by the function are transformed to the unconstrained variables. On this basis, a fixed-time RL-based optimal control framework is proposed to guarantee the attitude control system's prescribed performance, optimality, and fixed-time stability even in the presence of faults and disturbances.
- The critic-only NN weight update law is presented by using the adaptive control methodology rather than the traditional gradient descent algorithm [9, 10, 18]. In particular, the proposed control scheme integrates the update law, which not only can make the weight update law independent of the persistent excitation condition, but also ensures the practical fixed-time stability of the estimation error.
- Considering the advantages of finite-time control techniques, i.e., fast convergence rate and high convergence accuracy, the fractional terms are added to the design process of the classic ADP-based optimal controller to obtain the new ADP-based fixed-time optimal controller. Compared with the traditional approximate optimal control policies [9, 10, 18], the proposed RL-based optimal control framework can guarantee the system to be fixed-time stable. It means that the controlled system's state and NN weight estimation error with the application of the presented controller have a faster convergence rate.

#### 7.2 Problem Statement

Taking actuator fault into consideration, then the rigid satellite attitude system described by (2.21) and (2.24) can be given by

7.2 Problem Statement 147

$$\begin{cases}
\dot{\sigma} = G(\sigma)\omega \\
J\dot{\omega} = -\omega^{\times}J\omega + u + \varsigma
\end{cases}$$
(7.1)

where  $\boldsymbol{\varsigma} = ((\boldsymbol{E} - \boldsymbol{I}_3)\boldsymbol{u} + \bar{\boldsymbol{u}}) + \boldsymbol{u}_d$  is the lumped term including the actuator fault  $(E - I_3)u + \bar{u}$  and the external disturbance torque  $u_d$ , where  $E = \text{diag}([l_{11}, l_{22}, l_{23}, l_$  $l_{33}$ ]<sup>T</sup>) is the fault coefficient with  $0 < l_{ii} \le 1$ , i = 1, 2, 3, and  $\bar{u} \in \mathbb{R}^3$  is the biased faulty torque. The model of the actuator faults, i.e.,  $(E - I_3)u + \bar{u}$ , considered in this chapter is directly referred from [21] and [22]. It is fully analyzed in [21] and [22] that this model is practically reasonable.

In aerospace engineering, the dynamic behavior of the attitude stabilization error is expected to be limited in the preset bounds to guarantee its transient and steady-state performance, i.e., the tracking error  $\sigma_i$ , i = 1, 2, 3 needs to satisfy  $-\rho(t) < \sigma_i < \rho(t)$ , where  $\rho(t)$  is the prescribed performance function and designed as

$$\rho(t) = \exp\left(\frac{1}{a_0 + t} - b_0 t\right) + \rho_{\infty} \tag{7.2}$$

where  $a_0 \in \mathbb{R}_+$ ,  $b_0 \in \mathbb{R}_+$ , and  $\rho_\infty \in \mathbb{R}_+$  are constants. Then, one has

$$\dot{\rho}(t) = \left(-b_0 - \frac{1}{(a_0 + t)^2}\right) \exp\left(\frac{1}{a_0 + t} - b_0 t\right) < 0 \tag{7.3}$$

The function (7.2) has the following properties: (i)  $\rho(0) > \rho_{\infty}$ , (ii)  $\lim_{a_0 \to 0} \rho(0) =$  $\infty$ , and (iii)  $\lim_{t\to\infty} \rho(t) = \rho_{\infty}$ , where  $\rho_{\infty}$  is the ultimately bound of  $|\sigma_i|$ . The property (ii) indicates that the function (7.2) does not require the system's initial states.

A new variable  $z = [z_1, z_2, z_3]^T$  is defined to transform the attitude stabilization error constrained by  $\rho(t)$  into an unconstrained variable, i.e.,

$$z_{i} = \frac{1}{2} \ln \frac{1 + \frac{\sigma_{i}}{\rho_{i}}}{1 - \frac{\sigma_{i}}{\rho_{i}}}, i = 1, 2, 3$$
(7.4)

If  $z_i$  is bounded, then  $\sigma_i$  is within the predefined bounds. The transformation process will be valid. Moreover, the time-derivative of (7.4) is given as

$$\dot{z} = \Lambda (\dot{\sigma} - \Gamma \sigma) \tag{7.5}$$

where  $\mathbf{\Lambda} = \mathrm{diag}([\frac{\rho_1}{\rho_1^2 - \sigma_1^2}, \frac{\rho_2}{\rho_2^2 - \sigma_2^2}, \frac{\rho_3}{\rho_3^2 - \sigma_3^2}]^T)$  and  $\mathbf{\Gamma} = \mathrm{diag}([\frac{\dot{\rho}_1}{\rho_1}, \frac{\dot{\rho}_2}{\rho_2}, \frac{\dot{\rho}_3}{\rho_3}]^T)$ . To this end, another state  $\mathbf{x} = [\mathbf{z}^T, \boldsymbol{\omega}^T]^T \in \mathbb{R}^6$  can be introduced to transform (7.1)

into

$$\dot{x} = f(x) + G(x)u + G(x)c \tag{7.6}$$

where  $f(x) = [(\Lambda(G(\sigma)\omega - \Gamma\sigma))^{\mathrm{T}}, -(J^{-1}\omega^{\times}J\omega^{\mathrm{T}})^{\mathrm{T}}]^{\mathrm{T}}$  and  $G(x) = [0^{\mathrm{T}}, (J^{-1})^{\mathrm{T}}]^{\mathrm{T}}$ . Using (7.4), one can obtain f(0) = 0.

The control objective of this chapter can be stated as: For the rigid satellite attitude control system (7.1) with modeling error induced by actuator fault and external disturbance, design a reinforcement learning-based fault tolerant optimal attitude controller to stabilize the attitude with performance constraint. Moreover, this attitude stabilization should be accomplished within fixed time.

**Remark 7.1** When all the actuators of the rigid satellite system are fault-free, i.e.,  $\bar{u} = 0$ ,  $E \equiv I_3$  for all  $t \geq 0$  and it is disturbance-free, the nominal system is obtained. According to (7.6), this nominal system can be written as

$$\dot{\mathbf{x}} = f(\mathbf{x}) + \mathcal{G}(\mathbf{x})\mathbf{u} \tag{7.7}$$

To stabilize this nominal system fast, an RL-based fixed-time optimal control framework is designed. It is utilized as a fundamental controller of the subsequent fault tolerant control design.

#### 7.3 Fixed-Time Optimal Stabilization Control

To guarantee the optimality of the nominal system (7.7), a control policy u is to be designed to minimize the cost function  $\Im(x)$ , i.e.,

$$\Im(\mathbf{x}) = \int_0^\infty \mathcal{U}(\mathbf{x}, \mathbf{u}) \, d\tau \tag{7.8}$$

where  $\mathcal{U}(x, u) = x^{\mathrm{T}} Q x + u^{\mathrm{T}} R u \ge 0$ ,  $\mathcal{U}(\mathbf{0}, \mathbf{0}) = 0$ ,  $Q \in \mathbb{R}^{6 \times 6}$  and  $R \in \mathbb{R}^{3 \times 3}$  are two positive-definite matrices.

Using the optimal control policy  $u^*$ , the corresponding optimal cost is given by

$$\mathfrak{I}^*(\mathbf{x}) = \int_0^\infty \mathcal{U}\left(\mathbf{x}, \mathbf{u}^*\right) d\tau \tag{7.9}$$

Taking the time-derivative for both sides of  $\mathfrak{I}^*(x)$ , the following HJB equation is obtained

$$\mathcal{H}(\mathbf{x}, \mathbf{u}^*, \nabla_{\mathbf{x}} \Im^*) = \mathcal{U}(\mathbf{x}, \mathbf{u}^*) + \nabla_{\mathbf{x}}^{\mathrm{T}} \Im^*(f(\mathbf{x}) + \mathcal{G}(\mathbf{x}) \mathbf{u}^*) = 0$$
 (7.10)

where  $\nabla_{\mathbf{r}} \mathfrak{I}^* \in \mathbb{R}^6$ .

Solving (7.10) can get the optimal control policy as

$$\boldsymbol{u}^* = -\frac{1}{2} \boldsymbol{R}^{-1} \boldsymbol{\mathcal{G}}^{\mathrm{T}}(\boldsymbol{x}) \nabla_{\boldsymbol{x}} \mathfrak{I}^* \tag{7.11}$$

Inserting  $u^*$  into (7.10), one has

$$\mathcal{H}(x, u^*, \nabla_x \Im^*) = x^{\mathrm{T}} Q x + \nabla_x^{\mathrm{T}} \Im^* f(x) - \frac{1}{4} \nabla_x^{\mathrm{T}} \Im^* \mathcal{G}(x) R^{-1} \mathcal{G}(x)^{\mathrm{T}} \nabla_x \Im^* = 0$$
(7.12)

Note that obtaining the solution to (7.12) is difficult, while the NN with sufficient basis functions compact set can reconstruct any smooth function. Therefore, the NN can be selected to approximate  $\mathfrak{I}^*(x)$ , i.e.,

$$\mathfrak{I}^*(x) = \mathbf{\Xi}^{\mathrm{T}}(x)\mathcal{W}^* + \varepsilon(x) \tag{7.13}$$

where  $\Xi(x) \in \mathbb{R}^n$  denotes the basis function,  $W^* \in \mathbb{R}^n$  is the optimal weight, and  $\varepsilon(x)$  is the NN approximation error. Then, (7.11) can be rephrased as

$$\boldsymbol{u}^* = -\frac{1}{2} \boldsymbol{R}^{-1} \boldsymbol{\mathcal{G}}^{\mathrm{T}}(\boldsymbol{x}) \left( \nabla_{\boldsymbol{x}}^{\mathrm{T}} \boldsymbol{\Xi} \boldsymbol{\mathcal{W}}^* + \nabla_{\boldsymbol{x}} \boldsymbol{\varepsilon} \right)$$
(7.14)

with  $\nabla_x \Xi \in \mathbb{R}^{n \times 6}$ . Hence, the approximation of  $\mathfrak{I}^*(x)$  is written as  $\mathfrak{I}(x) = \Xi^{\mathrm{T}}(x)\hat{W}$ .  $u^*$  is approximated by

$$\boldsymbol{u}_0 = -\frac{1}{2} \boldsymbol{R}^{-1} \boldsymbol{\mathcal{G}}^{\mathrm{T}}(\boldsymbol{x}) \nabla_{\boldsymbol{x}}^{\mathrm{T}} \boldsymbol{\Xi} \hat{\boldsymbol{W}}$$
 (7.15)

where  $\hat{W}$  is used to approximate  $W^*$ .

**Assumption 7.1** The NN approximation error satisfies  $||\nabla_x \varepsilon|| \le \varepsilon_N$  with  $\varepsilon_N$  being a positive scalar [9, 18].

**Theorem 7.1** Considering the rigid satellite's nominal attitude system (7.7) in the presence of Assumption 7.1, if the RL-based optimal control policy is designed as

$$u = u_0 - \mathcal{G}(x)^{\dagger} \left( \kappa \tanh\left(\frac{x}{c}\right) + Ax + \alpha \left\lfloor x \right\rfloor^{\frac{p}{q}} + \beta \left\lfloor x \right\rfloor^{\frac{m}{n}} \right)$$
 (7.16)

with the NN weight  $\hat{W}$  updated by

$$\dot{\hat{W}} = \frac{1}{2\gamma_1} \nabla_{\mathbf{x}} \Xi \mathcal{G}(\mathbf{x}) \mathbf{R}^{-1} \mathcal{G}(\mathbf{x})^{\mathrm{T}} \mathbf{x} - \frac{\gamma_2}{\gamma_1} \Psi(\mathbf{x}) \hat{W}$$
(7.17)

where  $\kappa \in \mathbb{R}^{6 \times 6}$  and  $A \in \mathbb{R}^{6 \times 6}$  are positive diagonal matrices, p > q and m < n are positive odd scalars,  $\alpha \in \mathbb{R}_+$ ,  $\beta \in \mathbb{R}_+$ , and  $c \in \mathbb{R}_+$  are positive constants,  $\Psi(x) = \exp(-\frac{\gamma_3}{||x||}) + \gamma_4$ ,  $\gamma_1 \in \mathbb{R}_+$ ,  $\gamma_2 \in \mathbb{R}_+$ ,  $\gamma_3 \in \mathbb{R}_+$ , and  $\gamma_4 \in \mathbb{R}_+$  are positive real numbers, then the NN weight approximation error  $\tilde{W} = W^* - \hat{W}$  and the state x are fixed-time stable.

**Proof** Let a candidate Lyapunov function be given as

$$V_1 = \frac{1}{2} \mathbf{x}^{\mathrm{T}} \mathbf{x} + \frac{1}{2} \gamma_1 \tilde{\mathbf{W}}^{\mathrm{T}} \tilde{\mathbf{W}}$$
 (7.18)

Differentiating  $V_1$  and inserting (7.7) as well as (7.16) yield

$$\dot{V}_{1} = \mathbf{x}^{\mathrm{T}} \left( f(\mathbf{x}) + \mathcal{G}(\mathbf{x}) \mathbf{u}_{0} - \mathcal{G}(\mathbf{x}) \mathbf{u}^{*} + \mathcal{G}(\mathbf{x}) \mathbf{u}^{*} - \kappa \tanh \left( \frac{\mathbf{x}}{c} \right) \right) 
- A\mathbf{x} - \alpha \left[ \mathbf{x} \right]^{\frac{p}{q}} - \beta \left[ \mathbf{x} \right]^{\frac{m}{n}} \right) - \gamma_{1} \tilde{\mathbf{W}}^{\mathrm{T}} \dot{\hat{\mathbf{W}}}$$

$$= \tilde{\mathbf{W}}^{\mathrm{T}} \left( \frac{1}{2} \nabla_{\mathbf{x}} \mathbf{\Xi} \mathcal{G}(\mathbf{x}) \mathbf{R}^{-1} \mathcal{G}(\mathbf{x})^{\mathrm{T}} \mathbf{x} - \gamma_{1} \dot{\hat{\mathbf{W}}} \right) + \mathbf{x}^{\mathrm{T}} \left( f(\mathbf{x}) \right) 
+ \frac{1}{2} \mathcal{G}(\mathbf{x}) \mathbf{R}^{-1} \mathcal{G}^{\mathrm{T}}(\mathbf{x}) \nabla_{\mathbf{x}} \varepsilon + \mathcal{G}(\mathbf{x}) \mathbf{u}^{*} - A\mathbf{x} - \alpha \left[ \mathbf{x} \right]^{\frac{p}{q}} 
- \beta \left[ \mathbf{x} \right]^{\frac{m}{n}} - \kappa \tanh \left( \frac{\mathbf{x}}{c} \right) \right)$$
(7.19)

Using (7.17),  $\tilde{W}^T\hat{W} \leq -\min(\Psi(x))\|\tilde{W}\|^2 + \max(\Psi(x))||W^*||^2$  can be obtained. Note that f(x) is locally Lipchitz function, there is a positive scalar  $L_f$  satisfying  $\|f(x)\| \leq L_f \|x\|$ . One can obtain  $||\mathcal{G}(x)|| \leq \bar{G}$ , where  $\bar{G}$  is a real number. Since  $u^*$  is the optimal control policy to enforce the states of the system (7.7) to converge to the origin, it is reasonable to assume that it has an upper bound satisfying  $||u^*|| \leq \psi$ . Consider the inequality  $|\chi| - \chi \tanh\left(\frac{\chi}{c}\right) \leq \bar{\eta}_0 c$  reported in [23], where  $\bar{\eta}_0 = 0.2785$ , c > 0, and  $\chi \in \mathbb{R}$ . Furthermore, using the fact that  $||x|| = \sum_{i=1}^6 \left(x_i^2\right)^{\frac{1}{2}} \leq \sum_{i=1}^6 |x_i|$ , one has

$$-\boldsymbol{x}^{\mathrm{T}}\boldsymbol{\kappa} \tanh\left(\frac{\boldsymbol{x}}{c}\right) \leq \lambda_{\min}(\boldsymbol{\kappa}) \left(-\sum_{i=1}^{6} |\boldsymbol{x}_{i}| + 6\bar{\eta}_{0}c\right) \leq -\lambda_{\min}(\boldsymbol{\kappa})||\boldsymbol{x}|| + \eta_{0} \quad (7.20)$$

with  $\eta_0 = 6\lambda_{\min}(\kappa)\bar{\eta}_0 c$ .

Then,  $\dot{V}_1$  is simplified as

$$\dot{V}_{1} \leq -\min\{\Psi(\mathbf{x})\}\gamma_{2}\|\tilde{\mathbf{W}}\|^{2} - \lambda_{\min}(\mathbf{A})||\mathbf{x}||^{2} + \eta_{0} 
+ \gamma_{0}||\mathbf{x}|| - \lambda_{\min}(\mathbf{\kappa})||\mathbf{x}|| + \gamma_{2}\max\{\Psi(\mathbf{x})\}||\mathbf{W}^{*}||^{2} + L_{f}||\mathbf{x}||^{2} 
\leq -\alpha_{1}V_{1} + \beta_{1}$$
(7.21)

where  $\alpha_1 = \min\{\frac{2\gamma_2\min(\Psi(x))}{\gamma_1}, 2(\lambda_{\min}(A) - L_f)\}$ ,  $\beta_1 = \eta_0 + \gamma_2\max(\Psi(x))||W^*||^2$ . If  $\lambda_{\min}(\kappa) \geq \bar{G}\psi + \frac{1}{2}\lambda_{\max}(R^{-1})\bar{G}^2\varepsilon_N$  and  $\lambda_{\min}(A) - L_f > 0$  are satisfied, one has  $V_1 \leq \left(V_1(0) - \frac{\beta_1}{\alpha_1}\right)\exp(-\alpha_1 t) + \frac{\beta_1}{\alpha_1}$ . Hence, x and  $\tilde{W}$  are bounded. One can assume that  $||\tilde{W}|| \leq k_1$ , where  $k_1 \in \mathbb{R}_+$  is a positive constant.

In addition, (7.19) can be rewritten as

$$\dot{V}_{1} = x^{\mathrm{T}} \left( f(x) - Ax + \frac{1}{2} \mathcal{G}(x) R^{-1} \mathcal{G}^{\mathrm{T}}(x) \nabla_{x} \varepsilon - \alpha \left\lfloor x \right\rfloor^{\frac{p}{q}} - \beta \left\lfloor x \right\rfloor^{\frac{m}{n}} - \kappa \tanh \left( \frac{x}{\varepsilon} \right) + \mathcal{G}(x) u^{*} \right) + \gamma_{2} \Psi(x) \tilde{W}^{\mathrm{T}} \hat{W}$$
(7.22)

where the last term of (7.22) is bounded by

$$\gamma_{2}\Psi(\mathbf{x})\tilde{W}^{T}\hat{W} = \gamma_{2}\Psi(\mathbf{x})\sum_{i=1}^{n}(\tilde{W}_{i}W_{i}^{*} - \tilde{W}_{i}^{2})$$

$$\leq -\frac{\eta_{1}}{2}\|\tilde{W}\|^{2} + \frac{\eta_{2}}{2}\|W^{*}\|^{2} - \frac{\eta_{1}}{2}(\|\tilde{W}\|^{2})^{\frac{m+n}{2n}}$$

$$-\frac{\eta_{2}}{2}(\|\tilde{W}\|^{2})^{\frac{p+q}{2q}} + \frac{\eta_{1}}{2}(\|\tilde{W}\|^{2})^{\frac{m+n}{2n}} + \frac{\eta_{2}}{2}(\|\tilde{W}\|^{2})^{\frac{p+q}{2q}}$$
(7.23)

with  $\eta_1 = \min\{\gamma_2 \Psi(\mathbf{x})\}\$  and  $\eta_2 = \max\{\gamma_2 \Psi(\mathbf{x})\}\$ .

Using the similar process in (7.21) and (7.23),  $\dot{V}_1$  in (7.22) can be simplified as

$$\dot{V}_{1} \leq \mathbf{x}^{\mathrm{T}} \left( -\alpha \left[ \mathbf{x} \right]^{\frac{p}{q}} - \beta \left[ \mathbf{x} \right]^{\frac{m}{n}} \right) + \eta_{0} + \gamma_{2} \Psi(\mathbf{x}) \tilde{W}^{\mathrm{T}} \hat{W} 
\leq -\alpha \mathbf{x}^{\mathrm{T}} \left[ \mathbf{x} \right]^{\frac{p}{q}} - \beta \mathbf{x}^{\mathrm{T}} \left[ \mathbf{x} \right]^{\frac{m}{n}} - \frac{\eta_{1}}{2} (\|\tilde{W}\|^{2})^{\frac{m+n}{2n}} - \frac{\eta_{2}}{2} (\|\tilde{W}\|^{2})^{\frac{p+q}{2q}} 
- \frac{\eta_{1}}{2} \|\tilde{W}\|^{2} + \frac{\eta_{1}}{2} (\|\tilde{W}\|^{2})^{\frac{m+n}{2n}} + \frac{\eta_{2}}{2} (\|\tilde{W}\|^{2})^{\frac{p+q}{2q}} + \eta_{0} + \frac{\eta_{2}}{2} \|W^{*}\|^{2}$$
(7.24)

If  $\|\tilde{W}\|^2 < 1$ , one has  $-\frac{\eta_1}{2} \|\tilde{W}\|^2 + \frac{\eta_1}{2} (\|\tilde{W}\|^2)^{\frac{m+n}{2n}} < \xi$ , where  $\xi = (a_0)^{\frac{a_0}{1-a_0}} - (a_0)^{\frac{1}{1-a_0}}$  and  $a_0 = \frac{m+n}{2n}$  is a positive scalar. If  $\|\tilde{W}\|^2 \ge 1$ , it leads to  $-\frac{\eta_1}{2} \|\tilde{W}\|^2 + \frac{\eta_1}{2} (\|\tilde{W}\|^2)^{\frac{m+n}{2n}} \le 0$ .

According to (7.21), there is a positive scalar  $k_1$  satisfying  $||\tilde{W}|| < k_1$ , then it can prove that

$$\dot{V}_{1} \leq -\alpha(||\mathbf{x}||^{2})^{\frac{p+q}{2q}} - \beta(||\mathbf{x}||^{2})^{\frac{m+n}{2n}} \frac{\eta_{2}}{2} (\|\tilde{\mathbf{W}}\|^{2})^{\frac{p+q}{2q}} + \frac{\eta_{1}}{2} \xi + \frac{\eta_{2}}{2} (k_{1}^{2})^{\frac{p+q}{2q}} 
+ \eta_{0} + \frac{\eta_{2}}{2} \|\mathbf{W}^{*}\|^{2} - \frac{\eta_{1}}{2} (\|\tilde{\mathbf{W}}\|^{2})^{\frac{m+n}{2n}} 
\leq -\alpha_{2} V_{1}^{\frac{p+q}{2q}} - \beta_{2} V_{1}^{\frac{m+n}{2n}} + \eta_{1}$$
(7.25)

where  $\alpha_2=2^{\frac{p-q}{2q}}\min\left\{2^{\frac{p+q}{2q}}6^{\frac{p-q}{2q}}\alpha,\frac{\eta_2}{2}(\frac{2}{\gamma_1})^{\frac{p+q}{2q}}\right\}$ ,  $\beta_2=\min\left\{2^{\frac{m+n}{2n}}\beta,\frac{\eta_1}{2}(\frac{2}{\gamma_1})^{\frac{m+n}{2n}}\right\}$ , and  $\eta_\iota=\frac{\eta_1}{2}\xi+\frac{\eta_2}{2}(k_1^2)^{\frac{p+q}{2q}}+\eta_0+\frac{\eta_2}{2}\|\mathcal{W}^*\|^2$ . According to (7.25) and Lemma 2.4, the state  $\boldsymbol{x}$  in the nominal system (7.7) and  $\tilde{\mathcal{W}}$  can converge to the corresponding small regions  $\mathcal{D}_1$  and  $\mathcal{D}_2$ 

$$\mathcal{D}_{1} = \left\{ x : \lim_{t \to T_{1}} ||x|| \le \sqrt{2} \min \left\{ \left( \frac{\eta_{l}}{\alpha_{2}(1 - \theta_{0})} \right)^{\frac{q}{p+q}}, \left( \frac{\eta_{l}}{\beta_{2}(1 - \theta_{0})} \right)^{\frac{n}{m+n}} \right\} \right\}$$
(7.26)

$$\mathcal{D}_{2} = \left\{ \boldsymbol{x} : \lim_{t \to T_{1}} ||\tilde{\mathcal{W}}|| \le \sqrt{\frac{2}{\gamma_{1}}} \min \left\{ \left( \frac{\eta_{t}}{\alpha_{2}(1 - \theta_{0})} \right)^{\frac{q}{p+q}}, \left( \frac{\eta_{t}}{\beta_{2}(1 - \theta_{0})} \right)^{\frac{n}{m+n}} \right\} \right\}$$
(7.27)

within the fixed time  $T_1$  determined by  $T_1 \leq \frac{2q}{\alpha_2\theta_0(p-q)} + \frac{2n}{\beta_2\theta_0(n-m)}$ , where  $0 < \theta_0 < 1$ . Hence, the attitude stabilization error  $\sigma$  will be restricted in the prescribed bounds

due to the boundedness of z, i.e.,  $x = [z^T, \omega^T]^T$  is bounded. The conclusion in Theorem 7.1 is thereby proved.

Because x and W are bounded by  $\mathcal{D}_1$  and  $\mathcal{D}_2$ , respectively, we can further analyze the error between the designed controller (7.16) and the optimal solution (7.14), i.e.,  $u - u^*$ . It follows that

$$u - u^* = \frac{1}{2} R^{-1} \mathcal{G}^{\mathsf{T}}(x) \left( \nabla_x^{\mathsf{T}} \Xi \tilde{\mathcal{W}} + \nabla_x \varepsilon \right) - \mathcal{G}(x)^{\dagger} \left( Ax + \kappa \tanh \left( \frac{x}{c} \right) \right)$$

$$+ \alpha \left[ x \right]^{\frac{p}{q}} + \beta \left[ x \right]^{\frac{m}{n}}$$
(7.28)

Let the radiuses of the sets  $\mathcal{D}_1$  and  $\mathcal{D}_2$  be  $r_{d1}$  and  $r_{d2}$ , respectively. Then, it follows that  $||Ax + \kappa \tanh(x/c) + \alpha \lfloor x \rfloor^{\frac{p}{q}} + \beta \lfloor x \rfloor^{\frac{m}{n}}|| \leq \Upsilon$ , where  $\Upsilon = \lambda_{\max}(A)r_{d1} + \lambda_{\max}(\kappa) + \alpha \sqrt{6}r_{d1}^{\frac{p}{q}} + \beta \sqrt{6}r_{d1}^{\frac{m}{n}}$ . Moreover, it is also reasonable to assume that  $||\nabla_x \Xi|| \leq \bar{\phi}$  and  $||\mathcal{G}(x)^{\dagger}|| \leq \bar{G}_0$ , where  $\bar{\phi} \in \mathbb{R}_+$  and  $\bar{G}_0 \in \mathbb{R}_+$  are positive scalars. Then, it can be concluded that

$$||\boldsymbol{u} - \boldsymbol{u}^*|| \le \frac{1}{2} \lambda_{\max}(\boldsymbol{R}^{-1}) \bar{G}(\bar{\phi}r_{d2} + \varepsilon_N) + \bar{G}_0 \Upsilon$$
 (7.29)

Therefore, when x and  $\tilde{W}$  converge to the small residual sets  $\mathcal{D}_1$  and  $\mathcal{D}_2$ , respectively, the control policy u can approach to the optimal control  $u^*$ . In accordance, the controller (7.16) is an approximate optimal controller.

**Remark 7.2** The approximated optimal control policy (7.16) is different from the RL-based optimal control law in [5, 18]. The development of the control law (7.16) is inspired by the concept of sliding mode control. In (7.16), the continuous robust term  $\kappa$  tanh  $\left(\frac{x}{c}\right)$  is employed to attenuate the NN approximation error, which is usually used to attenuate the bounded external disturbance in sliding mode control. The other three terms  $Ax + \alpha \lfloor x \rfloor^{\frac{p}{q}} + \beta \lfloor x \rfloor^{\frac{m}{n}}$  are designed to increase the converge rate (i.e., achieving fixed-time stability). Therefore, the fixed-time stability of the closed-loop system is achieved.

**Remark 7.3** The existing NN weight updating laws of the actor-critic/critic-only NN are designed by gradient descent algorithm and depend on the persistent/finite excitation assumptions [5, 9, 18, 24]. The weight estimation errors are uniformly ultimately bounded. Different from them, the weight updating law (7.17) not only relaxes these assumptions but also ensures that the weight estimation errors converge to a small neighborhood around zero with fixed-time convergence. Therefore, the critic-only NN can approximate the function  $\mathfrak{I}^*$  with a faster rate.

**Remark 7.4** The designed term  $\Psi(x) = \exp(-\frac{\gamma_3}{||x||}) + \gamma_4$  in weight update law (7.17) is to tune the weight  $\hat{W}$  adaptively. One can see that the term is related to the state x. For all x,  $\Psi(x) > 0$ . When the state x is far away from the origin, the value of  $\Psi(x)$  is big. When the state x is near to the origin, the value of  $\Psi(x)$  is small. This means the adjustment process of neural network weight has more self-adaptation ability compared with a single constant  $\gamma_4$ .

#### 7.4 Fixed-Time Optimal Fault-Tolerant Control

Considering the modeling error consisting of external disturbance and actuator fault, the system (7.6) can be rewritten as

$$\dot{x} = f(x) + \mathcal{G}(x)u + \varsigma_1 \tag{7.30}$$

where  $\varsigma_1 = \mathcal{G}(x)\varsigma$  is the modeling error.

In view of (7.30), an estimator will be designed to compensate for the modeling error  $\varsigma_1$ . Moreover, introducing a new variable as

$$\dot{\mathbf{x}}_a = \mathbf{f}(\mathbf{x}) + \mathbf{G}(\mathbf{x})\mathbf{u} + \beta_1 \mathbf{x}_e \tag{7.31}$$

where  $\beta_1 \in \mathbb{R}_+$  is a positive constant.

From (7.30) and (7.31),  $x_e = x - x_a$  is defined. One has  $\dot{x}_e = \varsigma_1 - \beta_1 x_e$ . Then, the following nonlinear estimator is proposed to estimate  $\varsigma_1$ .

$$\hat{\boldsymbol{\varsigma}}_1 = \beta_1 \hat{\boldsymbol{x}}_e + \dot{\boldsymbol{x}}_e \tag{7.32}$$

where  $\hat{\boldsymbol{\varsigma}}_1$  is the estimation of  $\boldsymbol{\varsigma}_1$ .

Defining  $\tilde{x}_e = x_e - \hat{x}_e$ , where  $\hat{x}_e$  is the estimation of  $x_e$  and updated by

$$\dot{\hat{\mathbf{x}}}_e = \dot{\mathbf{x}}_e + \beta_2 \tilde{\mathbf{x}}_e + b_1 \left[ \tilde{\mathbf{x}}_e \right]^{\frac{m}{n}} + b_2 \left[ \tilde{\mathbf{x}}_e \right]^{\frac{p}{q}} \tag{7.33}$$

where  $\beta_2 \in \mathbb{R}_+$ ,  $b_1 \in \mathbb{R}_+$ , and  $b_2 \in \mathbb{R}_+$  are constants. Then, it follows that

$$\dot{\tilde{x}}_e = \varsigma_1 - \beta_1 x_e - (\dot{x}_e + \beta_2 \tilde{x}_e + b_1 \lfloor \tilde{x}_e \rfloor^{\frac{m}{n}} + b_2 \lfloor \tilde{x}_e \rfloor^{\frac{p}{q}})$$

$$= -\beta_2 \tilde{x}_e - b_1 |\tilde{x}_e|^{\frac{m}{n}} - b_2 |\tilde{x}_e|^{\frac{p}{q}} \tag{7.34}$$

and the estimator error  $\tilde{\boldsymbol{\varsigma}}_1 = \boldsymbol{\varsigma}_1 - \hat{\boldsymbol{\varsigma}}_1$  satisfies

$$\tilde{\boldsymbol{\varsigma}}_1 = \boldsymbol{\varsigma}_1 - (\beta_1 \hat{\boldsymbol{x}}_e - \beta_1 \boldsymbol{x}_e + \boldsymbol{\varsigma}_1) = \beta_1 \tilde{\boldsymbol{x}}_e \tag{7.35}$$

To this end, selecting  $\bar{V}=0.5\tilde{x}_e^T\tilde{x}_e$  and differentiating it as well as inserting (7.34), one has  $\dot{\bar{V}} \leq -2^{\frac{m+n}{2n}}b_1\bar{V}^{\frac{m+n}{2n}}-2^{\frac{p+q}{2q}}6^{\frac{p-q}{2q}}b_2\bar{V}^{\frac{p+q}{2q}}$ . Using Definition 2.1, it can prove that  $\tilde{x}_e$  converges to the origin within the fixed time  $T_0$ . The estimation error  $\tilde{\zeta}_1$  can also converge to zero when  $t \geq T_0$ .

**Remark 7.5** The term  $\dot{x}$  is required in the designed observer. The sliding mode differentiator given in [25] can be applied to obtain the value of  $\dot{x}$  by inputting the value of x into that differentiator. In engineering, the attitude and the angular velocity can be measured by sensors. Hence, x is measurable. The estimator (7.32) is implementable in practice.

**Theorem 7.2** For the faulty attitude control system (7.30), applying the estimator (7.32), if the RL-based fixed-time fault-tolerant optimal control policy is synthesized as

$$\boldsymbol{u} = \boldsymbol{u}_0 - \boldsymbol{\mathcal{G}}(\boldsymbol{x})^{\dagger} \left( \kappa \tanh\left(\frac{\boldsymbol{x}}{c}\right) + A\boldsymbol{x} + \frac{\beta_1^2}{4\beta_2} \boldsymbol{x} + \alpha \left\lfloor \boldsymbol{x} \right\rfloor^{\frac{p}{q}} + \beta \left\lfloor \boldsymbol{x} \right\rfloor^{\frac{m}{n}} - \hat{\boldsymbol{\varsigma}}_1 \right)$$
(7.36)

then the system state x, the estimation error  $\tilde{\zeta}$ , and the weight estimation error  $\tilde{W}$  can be steered into the corresponding small sets within a fixed time. The prescribed performance and the optimality of the faulty system are ensured simultaneously.

**Proof** Let another Lyapunov candidate function be specified by

$$V_2 = \frac{1}{2} \mathbf{x}^{\mathrm{T}} \mathbf{x} + \frac{1}{2} \gamma_1 \tilde{\mathbf{W}}^{\mathrm{T}} \tilde{\mathbf{W}} + \frac{1}{2} \tilde{\mathbf{x}}_e^{\mathrm{T}} \tilde{\mathbf{x}}_e$$
 (7.37)

Substituting (7.30), (7.35), and (7.36) into  $\dot{V}_2$ , it yields

$$\dot{V}_{2} = x^{\mathrm{T}} (f(x) + \mathcal{G}(x)u + \varsigma_{1}) - \gamma_{1} \tilde{W}^{\mathrm{T}} \dot{\hat{W}} + \tilde{x}_{e}^{\mathrm{T}} \dot{\tilde{x}}_{e}$$

$$= x^{\mathrm{T}} \left( f(x) + \mathcal{G}(x)u_{0} - \mathcal{G}(x)u^{*} + \mathcal{G}(x)u^{*} - \hat{\varsigma}_{1} + \varsigma_{1} - \kappa \tanh\left(\frac{x}{c}\right) \right)$$

$$- Ax - \alpha \left\lfloor x \right\rfloor^{\frac{p}{q}} - \beta \left\lfloor x \right\rfloor^{\frac{m}{n}} - \frac{\beta_{1}^{2}}{4\beta_{2}} x\right) - \gamma_{1} \tilde{W}^{\mathrm{T}} \dot{\hat{W}} + \tilde{x}_{e}^{\mathrm{T}} \dot{\tilde{x}}_{e}$$

$$= x^{\mathrm{T}} \left( f(x) + \mathcal{G}(x)u_{0} - \mathcal{G}(x)u^{*} + \mathcal{G}(x)u^{*} - \kappa \tanh\left(\frac{x}{c}\right) \right)$$

$$- Ax - \alpha \left\lfloor x \right\rfloor^{\frac{p}{q}} - \beta \left\lfloor x \right\rfloor^{\frac{m}{n}} - \frac{\beta_{1}^{2}}{4\beta_{2}} x\right) + \beta_{1} x^{\mathrm{T}} \tilde{x}_{e} - \gamma_{1} \tilde{W}^{\mathrm{T}} \dot{\hat{W}} + \tilde{x}_{e}^{\mathrm{T}} \dot{\tilde{x}}_{e}$$
(7.38)

Using the definition of  $\tilde{x}_e$ ,  $\dot{V}_2$  can be written as

$$\dot{V}_{2} \leq -\left(\beta_{2}||\tilde{\boldsymbol{x}}_{e}||^{2} - \beta_{1}||\boldsymbol{x}||||\tilde{\boldsymbol{x}}_{e}|| + \frac{\beta_{1}^{2}}{4\beta_{2}}||\boldsymbol{x}||^{2}\right) - b_{1}\tilde{\boldsymbol{x}}_{e}^{T}\left[\tilde{\boldsymbol{x}}_{e}\right]^{\frac{m}{n}} - b_{2}\tilde{\boldsymbol{x}}_{e}^{T}\left[\tilde{\boldsymbol{x}}_{e}\right]^{\frac{p}{q}} \\
+ \boldsymbol{x}^{T}\left(\boldsymbol{f}(\boldsymbol{x}) + \boldsymbol{\mathcal{G}}(\boldsymbol{x})\boldsymbol{u}_{0} - \boldsymbol{\mathcal{G}}(\boldsymbol{x})\boldsymbol{u}^{*} + \boldsymbol{\mathcal{G}}(\boldsymbol{x})\boldsymbol{u}^{*} - \kappa \tanh\left(\frac{\boldsymbol{x}}{c}\right)\right) \\
- \boldsymbol{A}\boldsymbol{x} - \alpha\left[\boldsymbol{x}\right]^{\frac{p}{q}} - \beta\left[\boldsymbol{x}\right]^{\frac{m}{n}}\right) - \gamma_{1}\tilde{\boldsymbol{W}}^{T}\hat{\boldsymbol{W}}$$

$$\leq -\left(\sqrt{\beta_{2}}||\tilde{\boldsymbol{x}}_{e}|| - \frac{\beta_{1}}{2\sqrt{\beta_{2}}}||\boldsymbol{x}||\right)^{2} - b_{1}\tilde{\boldsymbol{x}}_{e}^{T}\left[\tilde{\boldsymbol{x}}_{e}\right]^{\frac{m}{n}} - b_{2}\tilde{\boldsymbol{x}}_{e}^{T}\left[\tilde{\boldsymbol{x}}_{e}\right]^{\frac{p}{q}} + \boldsymbol{x}^{T}\left(\boldsymbol{f}(\boldsymbol{x})\right) \\
+ \boldsymbol{\mathcal{G}}(\boldsymbol{x})\boldsymbol{u}_{0} - \boldsymbol{\mathcal{G}}(\boldsymbol{x})\boldsymbol{u}^{*} + \boldsymbol{\mathcal{G}}(\boldsymbol{x})\boldsymbol{u}^{*} - \kappa \tanh\left(\frac{\boldsymbol{x}}{c}\right) - \boldsymbol{A}\boldsymbol{x} - \alpha\left[\boldsymbol{x}\right]^{\frac{p}{q}} \\
- \beta\left[\boldsymbol{x}\right]^{\frac{m}{n}}\right) - \gamma_{1}\tilde{\boldsymbol{W}}^{T}\hat{\boldsymbol{W}}$$

$$(7.39)$$

According to (7.23),  $\dot{V}_2$  can be simplified as

$$\dot{V}_{2} \leq -\alpha(||\mathbf{x}||^{2})^{\frac{p+q}{2q}} - \beta(||\mathbf{x}||^{2})^{\frac{m+n}{2n}} + \frac{\eta_{2}}{2}||\mathbf{W}^{*}||^{2} - \frac{\eta_{1}}{2}(||\tilde{\mathbf{W}}||^{2})^{\frac{m+n}{2n}} - \frac{\eta_{2}}{2}(||\tilde{\mathbf{W}}||^{2})^{\frac{p+q}{2q}} - b_{1}(||\tilde{\mathbf{x}}_{e}||^{2})^{\frac{m+n}{2n}} - b_{2}(||\tilde{\mathbf{x}}_{e}||^{2})^{\frac{p+q}{2q}} - \lambda_{\min}(\mathbf{A})||\mathbf{x}||^{2} + L_{f}||\mathbf{x}||^{2} + \mathbf{x}^{T} \Big(\mathcal{G}(\mathbf{x})\mathbf{u}^{*} + \frac{1}{2}\mathcal{G}(\mathbf{x})\mathbf{R}^{-1}\mathcal{G}^{T}(\mathbf{x})\nabla_{\mathbf{x}}\varepsilon\Big) - \kappa||\mathbf{x}|| + \eta_{0} \\
\leq -\alpha_{3}V_{2}^{\frac{p+q}{2q}} - \beta_{3}V_{2}^{\frac{m+n}{2n}} + \eta_{\kappa} \tag{7.40}$$

$$\begin{split} \text{where } \beta_3 &= \min \left\{ 2^{\frac{m+n}{2n}} \beta, \frac{\eta_1}{2} (\frac{2}{\gamma_1})^{\frac{m+n}{2n}}, b_1 2^{\frac{m+n}{2n}} \right\}, \eta_{\kappa} &= \frac{\eta_1}{2} \xi + \frac{\eta_2}{2} (k_1^2)^{\frac{p+q}{2q}} + \eta_0 + \frac{\eta_2}{2} \| \mathcal{W}^* \|^2, \\ \text{and } \alpha_3 &= 3^{\frac{p-q}{2q}} \min \left\{ 2^{\frac{p+q}{2q}} 6^{\frac{p-q}{2q}} \alpha, \frac{\eta_2}{2} (\frac{2}{\gamma_1})^{\frac{p+q}{2q}}, 2^{\frac{p+q}{2q}} 6^{\frac{p-q}{2q}} b_2 \right\}. \end{split}$$

If  $\lambda_{\min}(\kappa) \geq \bar{G}\psi + \frac{1}{2}\lambda_{\max}(\mathbf{R}^{-1})\bar{G}^2\varepsilon_N$  and  $\lambda_{\min}(\mathbf{A}) - L_f > 0$  are satisfied, (7.40) will hold. Utilizing Lemma 2.4, it can prove that the system (7.30) is stable within fixed-time  $T_2$ , which is bounded by  $T_2 \leq \frac{2q}{\alpha_3\theta_0(p-q)} + \frac{2n}{\beta_3\theta_0(n-m)}$  with  $0 < \theta_0 < 1$ . After  $T_2$ ,  $\mathbf{x}$ ,  $\tilde{\mathbf{W}}$ , and  $\tilde{\mathbf{x}}_e$  will converge into the residual sets  $\mathcal{D}_3$ ,  $\mathcal{D}_4$ , and  $D_5$ , respectively. They are given by

$$\mathcal{D}_{3} = \left\{ x : ||x|| \le \sqrt{2} \min \left\{ \left( \frac{\eta_{\kappa}}{(1 - \theta_{0})\alpha_{3}} \right)^{\frac{q}{p+q}}, \left( \frac{\eta_{\kappa}}{(1 - \theta_{0})\beta_{3}} \right)^{\frac{n}{m+n}} \right\} \right\}$$
(7.41)

$$\mathcal{D}_4 = \left\{ \tilde{\mathcal{W}} : ||\tilde{\mathcal{W}}|| \le \sqrt{\frac{2}{\gamma_1}} \min\left\{ \left( \frac{\eta_{\kappa}}{(1 - \theta_0)\alpha_3} \right)^{\frac{q}{p+q}}, \left( \frac{\eta_{\kappa}}{(1 - \theta_0)\beta_3} \right)^{\frac{n}{m+n}} \right\} \right\}$$
(7.42)

$$\mathcal{D}_5 = \left\{ \tilde{\boldsymbol{x}}_e : ||\tilde{\boldsymbol{x}}_e|| \le \sqrt{2} \min\left\{ \left( \frac{\eta_{\kappa}}{(1 - \theta_0)\alpha_3} \right)^{\frac{q}{p+q}}, \left( \frac{\eta_{\kappa}}{(1 - \theta_0)\beta_3} \right)^{\frac{n}{m+n}} \right\} \right\}$$
(7.43)

Therefore, the proposed RL-based fixed-time fault-tolerant optimal controller can drive the state x converge to the small region  $\mathcal{D}_3$ . The prescribed performance of the attitude stabilization error  $\sigma$  is assured. According to (7.35) and (7.40), one can obtain that the estimation error  $\tilde{\varsigma}$  such that  $||\tilde{\varsigma}|| = \beta_1 ||\tilde{x}_e|| \le \beta_1 r_{d5}$ , where  $r_{d5}$  is the radius of  $\mathcal{D}_5$ . The proposed estimator thus precisely compensates for the modeling error.

**Remark 7.6** The Lyapunov function  $V_2$  contains the estimation error  $\tilde{x}_e$ , i.e.,  $\tilde{\zeta}_1 = \beta_1 \tilde{x}_e$ . According to (7.40),  $\tilde{x}_e$  can converge to the small set  $\mathcal{D}_5$  when  $t > T_2$ . The boundedness of the estimation error  $\tilde{\zeta}_1$  will be ensured for all t > 0. The stability proof of the overall estimator-controller closed-loop system is presented.

## 7.5 Numerical Example

In this section, Theorems 7.1 and 7.2 are examined by numerical simulation with the following two cases considered.

- (1) Case I: There is no actuator fault and no external disturbance acting on the satellite attitude system.
- (2) Case II: The satellite attitude system is subject to some actuator fault and external disturbance.

The rigid satellite's inertial matrix is  $J = [20, 0, 0.9; 0, 17, 0; 0.9, 0, 15] \, \text{kg} \cdot \text{m}^2$ . Its initial states are set as  $\Xi(0) = [0.2517, 0.388, -0.4247]^T$  and  $\omega(0) = [0, 0, 0]^T$  rad/s. The parameters of the prescribed performance function (7.2) are selected as  $a_0 = 80$ ,  $b_0 = 0.3$ , and  $\rho_{\infty} = 0.0001$ . The set of neural network basis function is selected as  $\Xi(x) = [x_1^2, x_2^2, x_3^2, x_1x_2, x_2x_3, x_1x_3]^T$ . The control gains in (7.36) are given as  $\gamma_1 = 0.008$ ,  $R = 0.2I_3$ ,  $\kappa = 0.01I_6$ ,  $A = 2I_6$ ,  $\alpha = 0.5$ ,  $\beta = 4$ ,  $\frac{p}{q} = \frac{17}{19}$ , and  $\frac{m}{n} = \frac{19}{13}$ . To show the superiority of the RL-based fixed-time optimal control scheme in reducing control cost quantitatively, the simulation results of each case will eventually be computed using a new cost function  $V_{ci}$ , i = 1, 2, i.e.,  $V_{ci} = \int_0^{\infty} (\bar{\mathbf{x}}^T Q \bar{\mathbf{x}} + \mathbf{u}^T \mathcal{R} \mathbf{u}) \mathrm{d}t$ , where  $\bar{\mathbf{x}} = [\sigma^T, \omega^T]^T$ ,  $Q = 5I_6$ , and  $\mathcal{R} = 5I_3$ .

# 7.5.1 Simulation Result of Case I

In this case, the RL-based fixed-time optimal control policy (7.16) with performance constraints (it is named as PPCADP here) and the traditional RL-based optimal control policy with critic-only NN structure (TADP) in [18] are compared. The attitude  $\sigma$  guaranteed by PPCADP and TADP is shown in the Figs. 7.1 and 7.2, respectively. It is seen in Fig. 7.1 that  $\sigma_1$ ,  $\sigma_2$ , and  $\sigma_3$  are within the pre-specified region given by the bounded functions and have a faster convergence rate. They are stable before 10s. The angular velocity is shown in Fig. 7.3. PPCADP ensures higher control accuracy and smaller stabilization time than TADP. The initial weight of  $\hat{W}$  is selected  $\hat{W}(0) = [58, 60, 56, 60, 62, 61]^{T}$ , the NN weight (i.e.,  $\hat{W}$ ) updated by (7.17) is demonstrated in Fig. 7.5. The weight  $\hat{W}$  remains at the corresponding stable value when the attitude control system is stable. The control input of the nominal system with PPCADP and TADP is presented in Fig. 7.4. The dashed line has a smaller control torque when the system is stable. To achieve a faster convergence rate and higher control accuracy, PPCADP requires a bigger initial control input. However, the lower cost of the overall spacecraft attitude control system with PPCADP can be achieved than TADP. This can be seen in the total control cost  $V_{c1}$  shown in Fig. 7.6.  $V_{c1}$  obtained from TADP in the first 40 s is larger due to it slower convergence rate.

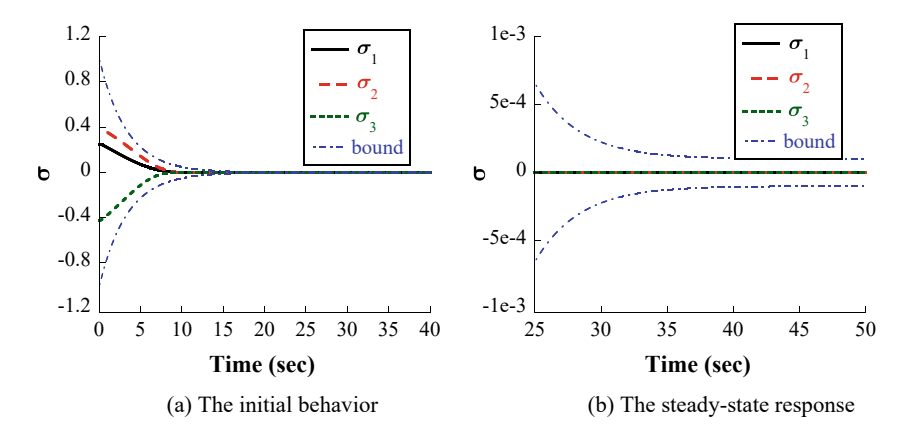


Fig. 7.1 The attitude achieved by PPCADP in Case I

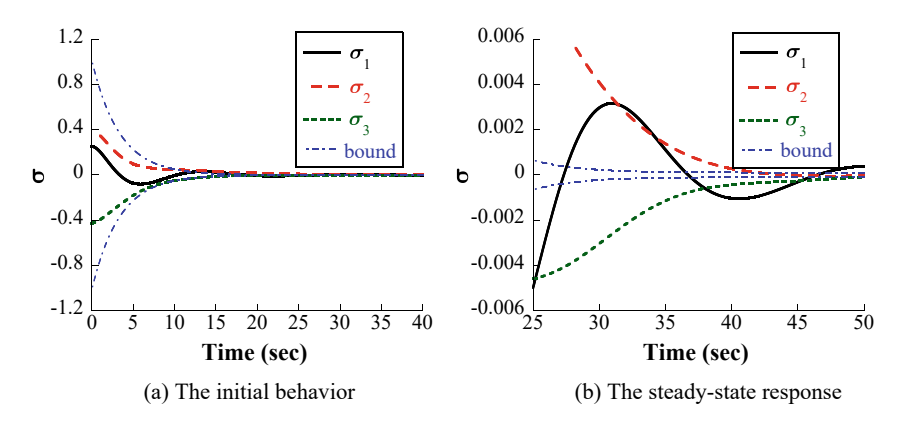


Fig. 7.2 The attitude achieved by TADP in Case I

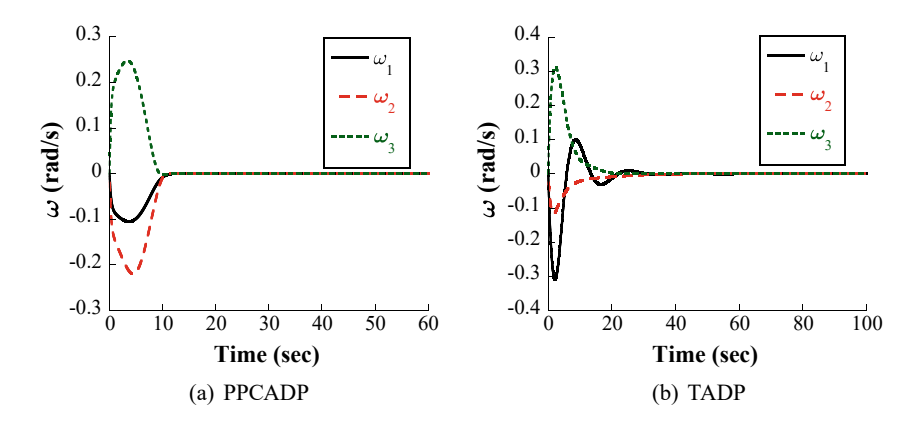


Fig. 7.3 The angular velocity achieved by PPCADP and TADP in Case I

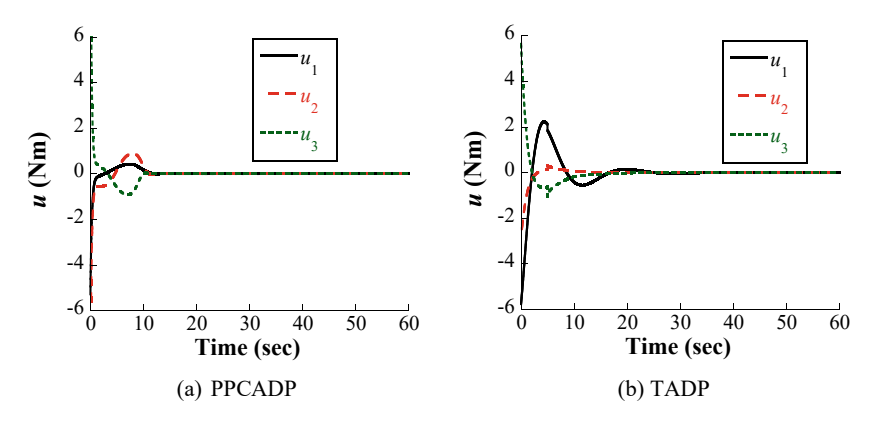
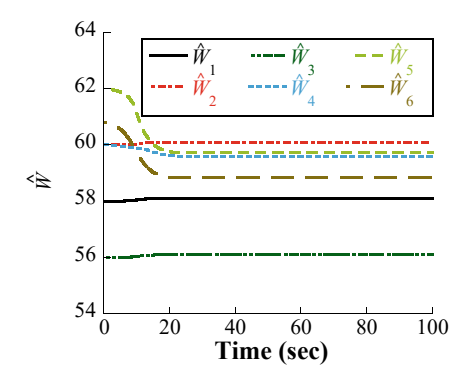
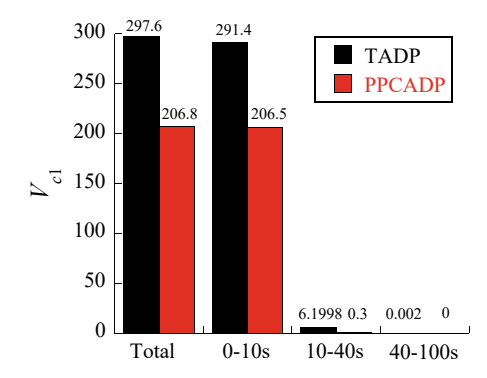


Fig. 7.4 The control achieved by PPCADP and TADP in Case I

**Fig. 7.5** The estimated weight achieved by PPCADP in Case I



**Fig. 7.6**  $V_{c1}$  achieved by PPCADP and TADP in Case I



## 7.5.2 Simulation Result of Case II

In this case, the external disturbance is supposed as

$$\mathbf{u}_{d} = \begin{bmatrix} 3\cos(0.02t) + 2.5\sin(0.01\pi t) \\ 1.5\cos(0.02\pi t) - 2\sin(0.04t) \\ 3.4\cos(0.02\pi t) - 0.5\sin(0.02t) \end{bmatrix} \times 10^{-2} \,\mathrm{N} \cdot \mathrm{m}$$
 (7.44)

The actuator fault is listed in the Table 7.1. To estimate the lumped term  $\varsigma$ , the parameters of estimator (7.32) are selected as  $b_1 = 2$ ,  $b_2 = 3$ ,  $\beta_1 = 0.2$ , and  $\beta_2 = 0.5$ .

The RL-based fixed-time fault-tolerant optimal controller (7.36) (ADPFTC) and the integral sliding mode fault-tolerant control (ISMFTC) in [26] are compared. The initial value of  $\hat{W}$  is set as  $\hat{W}(0) = [73, 74, 75, 77, 76]^T$ . The convergence performance of the attitude  $\sigma$  with the application of ADPFTC and ISMFTC are shown in Figs. 7.7 and 7.8, respectively. Although the convergence time of both control schemes is similar (i.e., they are stable before 20 s), compared with Fig. 7.8, one can find that the attitude  $\sigma_1$ ,  $\sigma_2$ , and  $\sigma_3$  in Fig. 7.7 are within the predefined bounds strictly.

The angular velocity is depicted in Fig. 7.9, ADPFTC achieves higher control accuracy and smaller convergence time than ISMFTC. The estimation error  $\tilde{\zeta}$  is shown in the Fig. 7.11. The estimation accuracy resulting from the proposed estimator  $\hat{\zeta}$  is high (i.e.,  $|\tilde{\zeta}_i| < 3 \times 10^{-5}$ , i = 1, 2, 3). The estimated weight  $\hat{W}$  is shown in Fig. 7.12, and  $\hat{W}$  remains at a stable value finally. The control torque of the faulty system with ADPFTC and ISMFTC are shown in Fig. 7.10. ADPFTC demands smaller control torque. The control cost  $V_{c2}$  is presented in Fig. 7.13. It demonstrates that the lower cost of the attitude control system with ADPFTC was achieved than ISMFTC. Furthermore,  $V_{c2}$  achieved by ADPFTC in the first 100 s is reduced by 64.77% compared with ISMFTC. To this end, the effectiveness of the RL-based control (7.35) is verified.

Table 7.1 The actuator faults in Case II			
i-	$l_{ii}$		$\bar{u}_i (N \cdot m)$
Actuator			
i = 1	$\begin{cases} 1\\ 0.9 + 0.05\sin(2\pi t) \end{cases}$	$0 < t < 15$ $0 \ge 15$	0.001
i = 2	\{0.9 \\1	$0 < t < 10$ $0 \ge 10$	0
i = 3	$\begin{cases} 0.6 + 0.1\sin(3\pi t) \\ 1 \end{cases}$	$0 < t < 20$ $0 \ge 20$	$0.05\sin(t)$

Table 7.1 The actuator faults in Case II

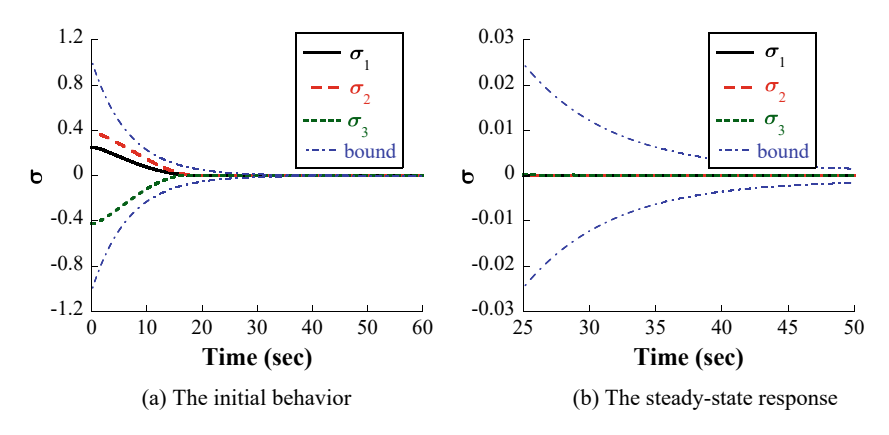


Fig. 7.7 The attitude achieved by ADPFTC in Case II

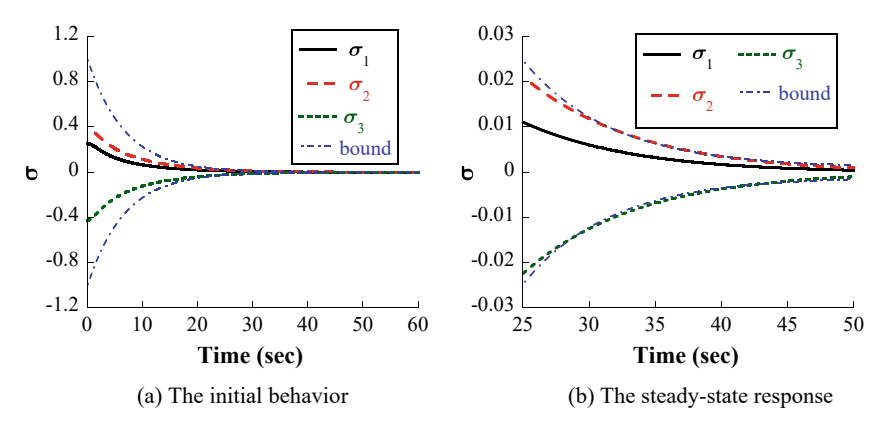


Fig. 7.8 The attitude achieved by ISMFTC in Case II

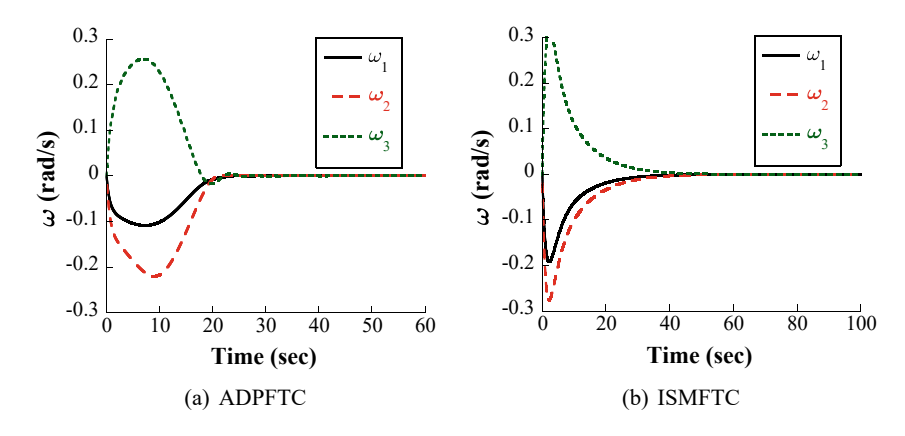


Fig. 7.9 The velocity achieved by ADPFTC and ISMFTC in Case II

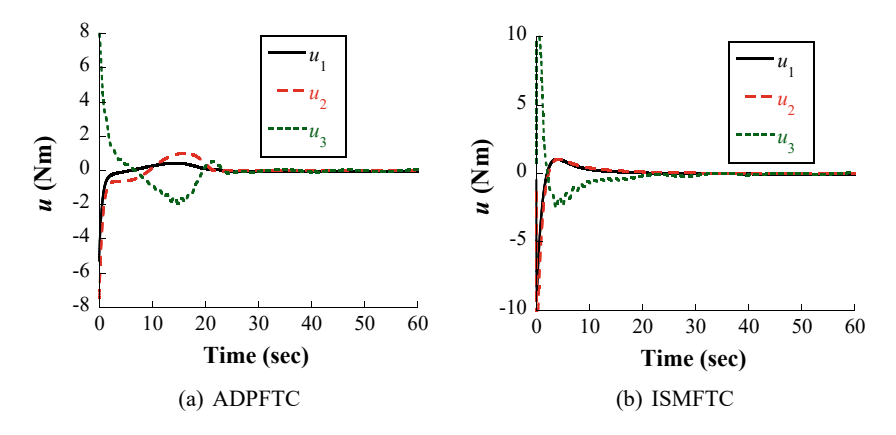
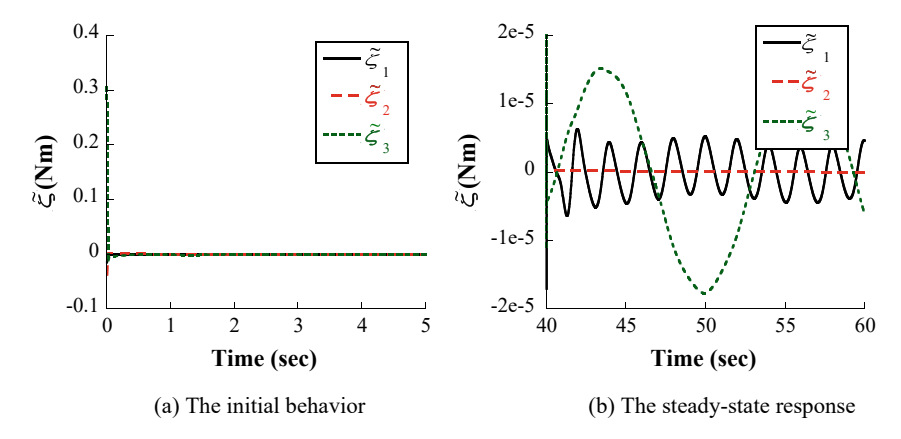
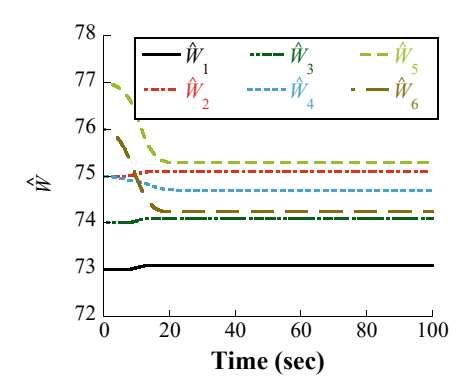


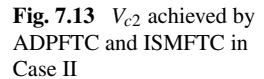
Fig. 7.10 The control achieved by ADPFTC and ISMFTC in Case II

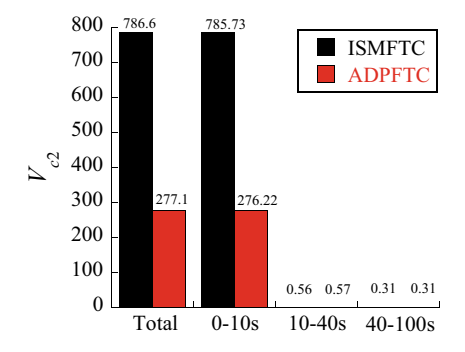


**Fig. 7.11** The estimation error of the estimator (7.32)

**Fig. 7.12** The estimated weight achieved by ADPFTC in Case II







# 7.6 Summary

An RL-based fixed-time attitude optimal control framework was presented for satellites with prescribed performance, external disturbance, and actuator fault. An NN weight update law without employing finite/persistent excitation conditions was designed. The weight estimation error can converge to a small region within a fixed time. A fixed-time estimator was introduced to address the external disturbance and actuator fault. The proposed RL-based fault-tolerant optimal control policy guaranteed that the system states, the weight estimation error, and the lumped term estimation error were fixed-time stable. This approach achieved faster stability in comparison with the uniformly ultimately bounded stability of the existing RL-based optimal control method.

#### References

- Hu, Q., Shao, X., Guo, L. (2018) Adaptive fault-tolerant attitude tracking control of spacecraft with prescribed performance. IEEE/ASME Transactions on Mechatronics 23(1): 331–341
- Shao, X., Hu, Q., Shi, Y., Jiang, B. (2020) Fault-tolerant prescribed performance attitude tracking control for spacecraft under input saturation. IEEE Transactions on Control Systems Technology 28(2): 574–582
- Yin, Z., Luo, J., Wei, C. (2019) Quasi fixed-time fault-tolerant control for nonlinear mechanical systems with enhanced performance. Applied Mathematics and Computation 352: 157–173
- Liu, M., Shao, X., Ma, G. (2019) Appointed-time fault-tolerant attitude tracking control of spacecraft with double-level guaranteed performance bounds. Aerospace Science and Technology 92: 337–346
- Yang, X., Liu, D., Wang, D. (2014) Reinforcement learning for adaptive optimal control of unknown continuous-time nonlinear systems with input constraints. International Journal of Control 87(3): 553–566
- Liu, H., Li, B., Xiao, B., Ran, D., Zhang, C. (2023) Reinforcement learning-based tracking control for a quadrotor unmanned aerial vehicle under external disturbances. International Journal of Robust and Nonlinear Control 33(17): 10360–10377

References 163

 Kong, L., He, W., Yang, C., Sun, C. (2021) Robust neurooptimal control for a robot via adaptive dynamic programming. IEEE Transactions on Neural Networks and Learning Systems 32(6): 2584–2594

- 8. Dong, H., Zhao, X., Luo, B. (2022) Optimal tracking control for uncertain nonlinear systems with prescribed performance via critic-only ADP. IEEE Transactions on Systems, Man, and Cybernetics: Systems 52(1): 561–573
- 9. Vamvoudakis, K. G., Lewis, F. L. (2010) Online actor-critic algorithm to solve the continuous-time infinite horizon optimal control problem. Automatica 46(5): 878–888
- Wang, D., Liu, D., Mu, C., Zhang, Y. (2018) Neural network learning and robust stabilization of nonlinear systems with dynamic uncertainties. IEEE Transactions on Neural Networks and Learning Systems 29(4): 1342–1351
- 11. He, W., Meng, T., He, X., Sun, C. (2019) Iterative learning control for a flapping wing micro aerial vehicle under distributed disturbances. IEEE Transactions on Cybernetics 49(4): 1524–1535
- Wei, Q., Liu, D. (2014) Adaptive dynamic programming for optimal tracking control of unknown nonlinear systems with application to coal gasification. IEEE Transactions on Automation Science and Engineering 11(4): 1020–1036
- 13. Wen, G., Ge, S. S., Chen, C. L. P., Tu, F., Wang, S. (2019) Adaptive tracking control of surface vessel using optimized backstepping technique. IEEE Transactions on Cybernetics 49(9): 3420–3431
- Xu, Y., Yang, H., Jiang, B., Polycarpou, M. M. (2022) Distributed optimal fault estimation and fault-tolerant control for interconnected systems: A Stackelberg differential graphical game approach. IEEE Transactions on Automatic Control 67(2): 926–933
- Dong, H., Zhao, X., Hu, Q., Yang, H., Qi, P. (2022) Learning-based attitude tracking control with high-performance parameter estimation. IEEE Transactions on Aerospace and Electronic Systems 58(3): 2218–2230
- Yang, H., Hu, Q., Dong, H., Zhao, X., Li, D. (2023) Optimized data-driven prescribed performance attitude control for actuator saturated spacecraft. IEEE/ASME Transactions on Mechatronics 28(3): 1616–1626
- Mu, C., Zhang, Y. (2020) Learning-based robust tracking control of quadrotor with timevarying and coupling uncertainties. IEEE Transactions on Neural Networks and Learning Systems 31(1): 259–273
- Dong, H., Zhao, X., Yang, H. (2021) Reinforcement learning-based approximate optimal control for attitude reorientation under state constraints. IEEE Transactions on Control Systems Technology 29(4): 1664–1673
- Yang, H., Hu, Q., Dong, H., Zhao, X. (2022) ADP-based spacecraft attitude control under actuator misalignment and pointing constraints. IEEE Transactions on Industrial Electronics 69(9): 9342–9352
- Kokolakis, N. M. T., Vamvoudakis, K. G. (2022) Safety-aware pursuit-evasion games in unknown environments using gaussian processes and finite-time convergent reinforcement learning. IEEE Transactions on Neural Networks and Learning Systems 35(3): 3130–3143
- 21. Murugesan, S., Goel, P. S. (1987) Fault-tolerant spacecraft attitude control system. Sadhana 11(1): 233–261
- 22. Godard (2010) Fault tolerant control of spacecraft. PhD thesis, Ryerson University (Canada)
- Polycarpou, M. M., Ioannou, P. A. (1996) A robust adaptive nonlinear control design. Automatica 32(3): 423 427
- Al-Tamimi, A., Lewis, F. L., Abu-Khalaf, M. (2008) Discrete-time nonlinear HJB solution using approximate dynamic programming: Convergence proof. IEEE Transactions on Systems, Man, and Cybernetics, Part B: Cybernetics 38(4): 943–949
- Levant, A. (2003) Higher-order sliding modes, differentiation and output-feedback control. International Journal of Control 76(9-10): 924–941
- Li, B., Hu, Q., Yang, Y., Postolache, O. A. (2019) Finite-time disturbance observer based integral sliding mode control for attitude stabilisation under actuator failure. IET Control Theory & Applications 13(1): 50–58

# Chapter 8 Faster Fixed-Time Attitude Stabilization Control



#### 8.1 Introduction

Applying the finite-time attitude controllers, the settling time cannot be precisely estimated. Some conditions should be imposed on states to obtain a desirable convergence time. The finite-time convergence depends on initial states [1]. A prior precise estimation of the settling time can not be obtained.

Unlike the finite-time stability (FTS) [2, 3], the fixed-time stability [4, 5] is efficient to guarantee a desired finite convergence time despite any initial states. Only the control gains determine the settling time. This method can obtain finite-time convergence while the settling time does not depend on initial states. Its key feature is that the bound of settling time is determined by control gains only. Hence, the convergence rate of the system states can be predefined offline. For instance, a fixedtime control approach was available for network consensus [6]. Inspired by [6], a non-singular fixed-time TMSC approach was proposed for nonlinear systems with matched uncertainties [7]. In [8], it was shown that the settling-time ensured by the NTSMC controller is not optimal, the proposed stable system achieved less convergence time than that in [6]. Another fixed-time control scheme was proposed in [9] to ensure the satellite attitude to have fixed-time convergence despite uncertainties and disturbances. In [10], the fixed-time attitude tracking problem for rigid satellites was studied with singularity avoided. The predefined convergence time of the attitude tracking error was guaranteed further. The fixed-time relative position and attitude synchronization control of satellite fly-around mission for a noncooperative target was studied in [12]. Two relative position and attitude stabilization controllers with fixed-time convergence were further presented to achieve the fly-around maneuver for a non-cooperative target [11, 13].

Motivated by providing faster attitude control capability, a novel fast fixed time but singularity-free stable system is preliminarily designed in this chapter. Applying the proposed fixed-time stable system, a continuous faster fixed-time controller is then developed for the attitude stabilization maneuvering of a flexible satellite. The main features of this chapter are highlighted as follows:

- A new fixed-time surface is preliminary presented based on a novel fixed-time stable system. Compared with the existing fixed-time stable system [6, 8], the proposed fixed-time stable system can provide a faster convergence rate.
- A novel faster fixed-time sliding mode-based attitude control framework is presented for flexible satellites. The attitude and the angular velocity are governed to be practically fixed-time stable despite uncertain inertia, disturbance, and any initial states. In comparison with the existing fixed-time approaches [9, 10, 12, 14, 15], a global faster convergence is ensured when the states are near or far from the equilibrium point.
- Compared with the adaptive attitude controllers [16–18], the designed controller is continuous and chattering free.

#### 8.2 Problem Statement

In this chapter, the satellite considered is flexible. The attitude kinematics (2.19)–(2.20) and the attitude dynamics (2.25)–(2.26) are used to describe the flexible satellite attitude control system. Moreover, the modeling error considered in this chapter consists of the disturbance torque  $u_d$  and uncertain inertia. Let the nominal inertia and the uncertain inertia be denoted by  $J_0$  (positive definite) and  $\Delta J$ , respectively it leads the total inertia J in (2.25) to be  $J = J_0 + \Delta J$ .

**Assumption 8.1**: There is a positive scalar  $a_1 \in \mathbb{R}_+$  such that  $||\Delta J|| \le a_1$ .

**Assumption 8.2**: The disturbance torque  $u_d$  is finite. A positive scalar  $a_2 \in \mathbb{R}_+$  exists such that  $||u_d|| \le a_2$ .

**Assumption 8.3**: The flexible coupling term  $\delta \ddot{\eta} + \omega^{\times} \delta \dot{\eta}$  in (2.26) satisfies  $||\delta \ddot{\eta} + \omega^{\times} \delta \dot{\eta}|| \le a_3 + a_4 ||\omega||$  with two positive constants  $a_3 \in \mathbb{R}_+$  and  $a_4 \in \mathbb{R}_+$ .

Since the flexible appendages of any on-orbital satellite have damping devices, the flexible vibration will be bounded. The damping devices will run to decrease the flexible vibration, when the vibration is large. Hence,  $\delta \ddot{\eta}$  and  $\delta \dot{\eta} = [\bar{\eta}_1, \bar{\eta}_2, \bar{\eta}_3]^T$  are bounded in practice. There exists two positive constants  $\bar{a}_3 \in \mathbb{R}_+$  and  $\bar{a}_4 \in \mathbb{R}_+$  such that  $||\delta \ddot{\eta}|| \leq \bar{a}_3$  and  $||\delta \dot{\eta}|| \leq \bar{a}_4$ . Then, one has  $||\delta \ddot{\eta} + \omega^{\times} \delta \dot{\eta}|| \leq \bar{a}_3 + a_4||\omega^{\times} \delta \dot{\eta}|| \leq \bar{a}_3 + \sqrt{3}\bar{a}_4||\omega||$ . Assumption 8-3 is thus reasonable, i.e.,  $\bar{a}_3 = a_3$  and  $a_4 = \sqrt{3}\bar{a}_4$ .

To this end, the control problem of this chapter is formulated as: Despite the modeling error induced by the uncertainty inertia  $\Delta J$  and the unknown disturbance  $u_d$ , the flexible vibration, and any initial states, develop a controller to guarantee that the flexible satellite attitude system (2.19)–(2.20) and (2.25)–(2.26) is practically fixed-time stable. Two positive scalars  $\epsilon_q \in \mathbb{R}_+$  and  $\epsilon_\omega \in \mathbb{R}_+$  exist such that  $||q(t)|| \le \epsilon_\omega$  and  $||\omega(t)|| \le \epsilon_\omega$  for  $t \ge t_s$ , where  $t_s \in \mathbb{R}_+$  is a positive constant.

#### 8.3 A New Fixed-Time Stable System

**Theorem 8.1** Let a system be designed as

$$\dot{z} = -\frac{1}{N(z)} \left( \alpha_0 \lfloor z \rfloor^{1+\gamma_0} + \beta_0 \lfloor z \rfloor^{\frac{p_1}{q_1}} \right) \tag{8.1}$$

where  $z \in \mathbb{R}$  is the system state,  $N(z) = a_1 + (1 - a_1) \exp(-b_1|z|^{c_1})$  and  $\gamma_0 = (\frac{m_1}{2n_1})(1 + sgn(|z| - 1))$ .  $\alpha_0 > 0$ ,  $\beta_0 > 0$ ,  $0 < a_1 < 1$ , and  $b_1 > 0$  are four scalars.  $c_1 > 0$  is an even integer.  $m_1 > 0$ ,  $n_1 > 0$ ,  $p_1 > 0$ , and  $q_1 > 0$  are odd integers satisfying  $m_1 > n_1$  and  $p_1 < q_1$ . Then, the system (8.1) is fixed-time stable.

**Proof** Introducing a new variable as  $y = |z|^{\frac{q_1 - p_1}{q_1}}$  and using (8.1), it follows that

$$\dot{y} = \frac{q_1 - p_1}{q_1} \left[ z \right]^{-\frac{p_1}{q_1}} \dot{z} 
= \frac{q_1 - p_1}{q_1 N \left[ z \right]^{\frac{p_1}{q_1}}} (\alpha_0 \left[ z \right]^{1 + \gamma_0} + \beta_0 \left[ z \right]^{\frac{p_1}{q_1}}) 
= \frac{q_1 - p_1}{q_1} \frac{1}{N(z)} (\alpha_0 \left| z \right|^{\frac{q_1 - p_1}{q_1}} + \gamma_0} + \beta_0) 
= \frac{q_1 - p_1}{q_1} \frac{1}{N(z)} (\alpha_0 y^{1 + \gamma_0} \frac{q_1}{q_1 - p_1} + \beta_0)$$
(8.2)

Solving (8.2), the settling-time  $T_s$  is given by

$$T_{s} = \frac{q_{1}}{q_{1} - p_{1}} \int_{0}^{y(0)} \frac{N(z)}{\alpha_{0} y^{1 + \gamma_{0}} \frac{q_{1}}{q_{1} - p_{1}} + \beta_{0}} dy$$

$$= \frac{q_{1}}{q_{1} - p_{1}} \left( \int_{1}^{y(0)} \frac{N(z)}{\alpha_{0} y^{1 + \gamma_{0}} \frac{q_{1}}{q_{1} - p_{1}} + \beta_{0}} dy + \int_{0}^{1} \frac{N(z)}{\alpha_{0} y^{1 + \gamma_{0}} \frac{q_{1}}{q_{1} - p_{1}} + \beta_{0}} dy \right)$$

$$= \frac{q_{1}}{q_{1} - p_{1}} \left( \int_{1}^{y(0)} \frac{N(z)}{\alpha_{0} y^{\rho_{1}} + \beta_{0}} dy + \int_{0}^{1} \frac{N(z)}{\alpha_{0} y + \beta_{0}} dy \right)$$

$$(8.3)$$

where  $\rho_1 = 1 + \frac{m_1 q_1}{n_1 (q_1 - p_1)}$ 

If N(z) = 1, the settling-time (8.3) can be rewritten as

$$T_s' = \frac{q_1}{q_1 - p_1} \left( \int_1^{y(0)} \frac{1}{\alpha_0 y^{\rho_1} + \beta_0} dy + \int_0^1 \frac{1}{\alpha_0 y + \beta_0} dy \right)$$
(8.4)

Since  $a_1 \le N(z) < 1$ , it is proved from (8.3) and (8.4) that  $T_s < T_s'$  is valid for any y(0). The system (8.1) is therefore fixed-time stable by using Definition 2.1. Moreover, invoking  $\rho_1 = 1 + \frac{m_1 q_1}{n_1 (q_1 - p_1)} > 1$ ,  $T_s'$  is bounded by

П

$$T_{s}' \leq \frac{q_{1}}{q_{1} - p_{1}} \left( \int_{1}^{y(0)} \frac{1}{\alpha_{0} y^{\rho_{1}}} dy + \int_{0}^{1} \frac{1}{\alpha_{0} y + \beta_{0}} dy \right)$$

$$\leq \frac{q_{1}}{q_{1} - p_{1}} \left( \frac{1 - y(0)^{1 - \rho_{1}}}{\alpha_{0} (\rho_{1} - 1)} dy + \int_{0}^{1} \frac{1}{\alpha_{0} y + \beta_{0}} dy \right)$$

$$\leq \frac{n_{1}}{\alpha_{0} m_{1}} + \frac{q_{1}}{q_{1} - p_{1}} \frac{1}{\alpha_{0}} \ln \left( 1 + \frac{\alpha_{0}}{\beta_{0}} \right)$$
(8.5)

To this end, the proof of Theorem 8.1 is completed.

In [6], a fixed-time stable system (named as FTSS1) is presented as

$$\dot{z} = -\alpha_0 z^{\frac{m_1}{n_1}} - \beta_0 z^{\frac{p_1}{q_1}} \tag{8.6}$$

Another fixed-time stable system (called as FTSS2) is also given in [8], which is

$$\dot{z} = -\alpha_0 z^{\frac{1}{2} + \frac{m_1}{2n_1} + \left(\frac{m_1}{2n_1} - \frac{1}{2}\right) \operatorname{sgn}(|z| - 1)} - \beta_0 z^{\frac{p_1}{q_1}}$$
(8.7)

For FTSS1 and FTSS2,  $\alpha_0 > 0$  and  $\beta_0 > 0$  are two scalars.  $m_1 > 0$ ,  $n_1 > 0$ ,  $p_1 > 0$ ,  $q_1 > 0$  are four odd integers such that  $m_1 > n_1$  and  $p_1 < q_1$ .

**Theorem 8.2** The convergence rate of the proposed fixed-time stable system (8.1) is faster than FTSS1 and FTSS2.

**Proof** It can be obtained from [6] and [8] that the settling time of FTSS1 and FTSS2 can be uniformly given by

$$T_F = \frac{q_1}{q_1 - p_1} \left( \int_1^{y(0)} \frac{1}{\alpha_0 y^{\xi} + \beta_0} dy + \int_0^1 \frac{1}{\alpha_0 y + \beta_0} dy \right)$$
(8.8)

where  $\xi = 1 + \frac{(m_1 - n_1)q_1}{n_1(q_1 - p_1)}$  for FTSS1 and  $\xi = 1$  for FTSS2.

Subtracting  $T_F$  from  $T_s'$  yields

$$T_{s}' - T_{F} = \frac{q_{1}}{q_{1} - p_{1}} \left( \int_{1}^{y(0)} \frac{1}{\alpha_{0} y^{\rho_{1}} + \beta_{0}} dy - \int_{1}^{y(0)} \frac{1}{\alpha_{0} y^{\xi} + \beta_{0}} dy \right)$$

$$= \frac{q_{1}}{q_{1} - p_{1}} \int_{1}^{y(0)} \frac{\alpha_{0} (y^{\xi} - y^{\rho_{1}})}{(\alpha_{0} y^{\rho_{1}} + \beta_{0})(\alpha_{0} y^{\xi} + \beta_{0})} dy$$
(8.9)

In accordance to the definition of  $\rho_1$  and  $\xi$ , one has  $\rho_1 > \xi$  and  $y^{\xi} - y^{\rho_1} < 0$ . Then,  $T_s' - T_F < 0$  can be proved from (8.9) for any initial states. As a consequence,  $T_s < T_s' < T_F$  is obtained. This implies that the convergence rate of the proposed system (8.1) is faster than FTSS1 and FTSS2.

**Remark 8.1** N(z) in (8.1) is used to tune the convergence rate. When the states are far from the equilibrium point, N(z) tends to  $a_1$  and then  $\frac{1}{N(z)}$  approaches  $\frac{1}{a_1} > 1$ . A

faster convergence is thus obtained. Once the states are near the equilibrium point, N(z) approaches 1. This means that N(z) varies between 1 and  $a_1$ . Moreover, a novel power term is also included in (8.1). As the states become smaller,  $\gamma_0$  can improve the convergence rate. According to definition of  $\gamma_0$ , when |z| < 1, the proposed fixed-time stable system (8.1) uses a linear term of z instead of  $|z|^{\frac{m}{n}}$ . As a result, the convergence speed significantly increases due to  $m_1 > n_2$ . Therefore, in combination with Theorem 8.2, it could be claimed that (8.1) is a new fast fixed-time stable system.

# 8.4 Fixed-Time Faster Sliding Mode Surface

Inspired by Theorem 8.1, a novel non-singular faster sliding mode surface (NFSMS) is presented as

$$S = \omega + \frac{1}{N(q)} (k_1 \lfloor q \rfloor^{1+\gamma_0} + k_2 S_c)$$
 (8.10)

where  $S = [S_1, S_2, S_3]^T$ ,  $\gamma_0 = \frac{m_1}{2n_1}(1 + \text{sgn}(||\boldsymbol{q}|| - 1))$ , and  $N(\boldsymbol{q}) = a_1 + (1 - a_1)$  exp $(-b_1||\boldsymbol{q}||^{c_1})$ .  $m_1 > 0$  and  $n_1 > 0$  are two odd integers such that  $m_1 > n_1$ .  $0 < a_1 < 1, b_1 > 0, k_1 > 0$ , and  $k_2 > 0$  are positive gains.  $c_1 > 0$  is an even integer.  $S_c = [S_{c1}, S_{c2}, S_{c3}]^T$  is designed

$$S_{ci} = \begin{cases} |q_i|^{\frac{p_1}{q_1}} \operatorname{sgn}(q_i), & \text{if } \bar{S}_i = 0 \text{ or } \bar{S}_i \neq 0, |q_i| \geq \bar{\phi} \\ l_1 q_i + l_2 q_i^2 \operatorname{sgn}(q_i), & \text{if } \bar{S}_i \neq 0, |q_i| < \bar{\phi} \end{cases}$$
(8.11)

with i=1,2,3 and a constant  $0<\bar{\phi}<1$ .  $p_1$  and  $q_1$  are two positive integers satisfying  $p_1< q_1$ , and

$$l_1 = \left(2 - \frac{p_1}{q_1}\right)\bar{\phi}^{\frac{p_1}{q_1} - 1} \tag{8.12}$$

$$l_2 = \left(\frac{p_1}{q_1} - 1\right) \bar{\phi}^{\frac{p_1}{q_1} - 2} \tag{8.13}$$

$$\bar{\mathbf{S}} = [\bar{S}_1, \bar{S}_2, \bar{S}_3]^{\mathrm{T}} = \boldsymbol{\omega} + \frac{1}{N(\boldsymbol{q})} \left( k_1 \lfloor \boldsymbol{q} \rfloor^{1+\gamma_0} + k_2 \lfloor \boldsymbol{q} \rfloor^{\frac{p_1}{q_1}} \right)$$
(8.14)

**Theorem 8.3** Consider the flexible satellite system described by (2.19)–(2.20) and (2.25)–(2.26), once its states reach the NFSMS (8.10), i.e.,  $S = \bar{S} = 0$ , then they will respectively converge to their stable equilibrium points  $\mathbf{q} = [1, 0, 0, 0]^T$  and  $\boldsymbol{\omega} = \mathbf{0}$  in a fixed time despite any initial attitude and angular velocity.

**Proof** Once the NFSMS (8.10) is reached, it follows that  $S = \bar{S} = 0$  and

$$\boldsymbol{\omega} = -\frac{1}{N(\boldsymbol{q})} (k_1 \lfloor \boldsymbol{q} \rfloor^{1+\gamma_0} + k_2 \boldsymbol{S_c})$$
 (8.15)

Define a Lyapunov function as  $V_1 = 0.5(\boldsymbol{q}^{\mathrm{T}}\boldsymbol{q} + (1-q_0)^2)$ , its time-derivative can be computed from (2.19)–(2.20) as

$$\dot{V}_{1} = -\frac{\boldsymbol{q}^{\mathrm{T}}}{2N(\boldsymbol{q})} \left( k_{1} \lfloor \boldsymbol{q} \rfloor^{1+\gamma_{0}} + k_{2} \lfloor \boldsymbol{q} \rfloor^{\frac{p_{1}}{q_{1}}} \right)$$
(8.16)

which can prove  $\lim_{t\to\infty} q = 0$  and  $\lim_{t\to\infty} q_0 = 1$  or -1.

Consider a new Lyapunov candidate function as  $V_2 = 0.5 q^{\mathrm{T}} q + 0.5(1 + q_0)^2$ . Differentiating  $V_2$  results in

$$\dot{V}_2 = \frac{\boldsymbol{q}^{\mathrm{T}}}{2N(\boldsymbol{q})} \left( k_1 \lfloor \boldsymbol{q} \rfloor^{1+\gamma_0} + k_2 \lfloor \boldsymbol{q} \rfloor^{\frac{\rho_1}{q_1}} \right)$$
(8.17)

It is found from (8.17) and the Lyapunov instability theorem [19] that the equilibrium point  $[\boldsymbol{q}^{\mathrm{T}}, q_0]^{\mathrm{T}} = [0, 0, 0, -1]^{\mathrm{T}}$  is not stable.  $[\boldsymbol{q}^{\mathrm{T}}, q_0]^{\mathrm{T}} = [0, 0, 0, 1]^{\mathrm{T}}$  is thus selected as the equilibrium point to be stabilized.

Since  $q_0 \to 1$ , the following inequality is satisfied.

$$(1 - q_0)^2 \le (1 - q_0)(1 + q_0) = q_1^2 + q_2^2 + q_3^2$$
(8.18)

which implies  $V_1 \le q_1^2 + q_2^2 + q_3^2$ . Therefore, one has

$$\dot{V}_1 \le -\alpha_1 V_1^{\frac{2+\gamma_0}{2}} - \beta V_1^{\frac{q_1+p_1}{2q_1}} \tag{8.19}$$

where  $\alpha_1 = \frac{3^{-0.5\gamma_0}k_1}{2N(q)}$  and  $\beta = \frac{k_2}{2N(q)}$ . Invoking Theorem 8.1, q and  $\omega$  are proved to be fixed-time stable.

**Remark 8.2** The development of the adjustable function N(q) in (8.10) is inspired by [20]. Although N(q) in (8.10) is the same as the adjustable function used in [20], and the other part of the sliding surface (8.10) is different from the sliding surface given in [20]. As proved in Theorem 8.3, a fixed-time convergence can be obtained from (8.10) despite any initial states. However, the finite convergence time obtained from [20] is dependent on the system's initial states. This article is an improvement and extension of [20].

#### 8.5 Faster Fixed-Time Attitude Controller

Using the NFSMS (8.10) and the dynamics (2.25)–(2.26), one has

$$J_0 \dot{\mathbf{S}} = \mathbf{F} + \mathbf{u} + \mathbf{\Pi} \tag{8.20}$$

where

$$F = -\boldsymbol{\omega}^{\times} \boldsymbol{J}_{0} \boldsymbol{\omega} + \frac{1}{N^{2}(\boldsymbol{q})} \boldsymbol{J}_{0} \left( \frac{1}{2} N(\boldsymbol{q}) (k_{1} \boldsymbol{P}_{1} + k_{2} \boldsymbol{P}_{2}) (q_{0} \boldsymbol{I}_{3} + \boldsymbol{q}^{\times}) \boldsymbol{\omega} \right)$$

$$- \dot{N} (\boldsymbol{q}_{v}) (k_{1} \lfloor \boldsymbol{q} \rfloor^{1+\gamma_{0}} + k_{2} \boldsymbol{S}_{c})$$
(8.21)

$$\mathbf{P}_1 = (1 + \gamma_0) \operatorname{diag}(|\mathbf{q}|^{\gamma_0}) \tag{8.22}$$

$$\mathbf{P}_2 = \text{diag}([P_{21}, P_{22}, P_{23}]^{\mathrm{T}}) \tag{8.23}$$

$$P_{2i} = \begin{cases} \frac{p_1}{q_1} |q_i|^{\frac{p_1 - q_1}{q_1}}, & \text{if } \bar{S}_i = 0 \text{ or } \bar{S}_i \neq 0, |q_i| \geq \bar{\phi}, i = 1, 2, 3\\ l_1 + 2l_2 |q_i|, & \text{if } \bar{S}_i \neq 0, |q_i| < \bar{\phi} \end{cases}$$
(8.24)

and  $\Pi = \boldsymbol{u}_d - \boldsymbol{\omega}^{\times} \boldsymbol{\delta} \dot{\boldsymbol{\eta}} - \boldsymbol{\delta} \ddot{\boldsymbol{\eta}} - \Delta \boldsymbol{J} \dot{\boldsymbol{\omega}} - \boldsymbol{\omega}^{\times} \Delta \boldsymbol{J} \boldsymbol{\omega}$ .

According to Assumption 8-1 to Assumption 8-3, one has

$$||\mathbf{\Pi}|| \le a_2 + a_3 + a_4 ||\boldsymbol{\omega}|| + a_1 ||\dot{\boldsymbol{\omega}}|| + a_1 ||\boldsymbol{\omega}||^2 \le c_1 + c_2 M \tag{8.25}$$

where  $c_1 = a_2 + a_3$  and  $c_2 = \max\{a_1, a_4\}$  are constants but unknown.  $M = ||\boldsymbol{\omega}|| + ||\dot{\boldsymbol{\omega}}|| + ||\boldsymbol{\omega}||^2$  is available by using the measurement  $\boldsymbol{\omega}$ . Therefore, it can be obtained that

$$||\mathbf{\Pi}||^2 \le (c_1 + c_2 M)(c_1 + c_2 M) = \kappa_1 + \kappa_2 M + \kappa_3 M^2$$
(8.26)

where  $\kappa_1 = c_1^2$ ,  $\kappa_2 = 2c_1c_2$ , and  $\kappa_3 = c_2^2$  are positive but unknown constants.

Let a robust adaptive fixed-time control law be designed as

$$\boldsymbol{u} = -\frac{1}{N(\boldsymbol{S})} \left( \gamma_1 \boldsymbol{S} + \gamma_2 \lfloor \boldsymbol{S} \rfloor^{1+\bar{\gamma}} + \gamma_3 \lfloor \boldsymbol{S} \rfloor^{\frac{p_2}{q_2}} \right) - \boldsymbol{F} - \boldsymbol{u}_{\text{adp}}$$
(8.27)

where  $\bar{\gamma} = \frac{m_2}{2n_2}(1 + \text{sgn}(||S|| - 1))$ .  $\gamma_1 > 0$ ,  $\gamma_2 > 0$ , and  $\gamma_3 > 0$  are constants.  $m_2 > 0$ ,  $n_2 > 0$ ,  $p_2 > 0$ , and  $q_2 > 0$  are four odd integers satisfying  $m_2 > n_2$ ,  $p_2 < q_2$ .  $u_{\text{adp}}$  is an adaptive control effort specified by

$$\boldsymbol{u}_{\text{adp}} = \frac{\boldsymbol{S}}{2\varepsilon^2} (\hat{\kappa}_1 + \hat{\kappa}_2 M + \hat{\kappa}_3 M^2)$$
 (8.28)

with  $\hat{\kappa}_i \in \mathbb{R}$  updated by

$$\dot{\hat{\kappa}}_1 = p_{11} \left( \frac{||\mathbf{S}||^2}{2\varepsilon^2} - p_{12} \hat{\kappa}_1 \right)$$
 (8.29)

$$\dot{\hat{\kappa}}_2 = p_{21} \left( \frac{||\mathbf{S}||^2 M}{2\varepsilon^2} - p_{22} \hat{\kappa}_2 \right)$$
 (8.30)

$$\dot{\hat{\kappa}}_3 = p_{31} \left( \frac{||\mathbf{S}||^2 M^2}{2\varepsilon^2} - p_{32} \hat{\kappa}_3 \right)$$
 (8.31)

where  $\varepsilon \in \mathbb{R}_+$ ,  $p_{11} \in \mathbb{R}_+$ ,  $p_{12} \in \mathbb{R}_+$ ,  $p_{21} \in \mathbb{R}_+$ ,  $p_{22} \in \mathbb{R}_+$ ,  $p_{31} \in \mathbb{R}_+$ , and  $p_{32} \in \mathbb{R}_+$  are positive gains.

**Theorem 8.4** When implementing the fixed-time attitude controller (8.27) with the adaptive update law (8.28) to the flexible satellite attitude system (2.19)–(2.20) and (2.25)–(2.26), the closed-loop system is practically fixed-time stable.

**Proof** Construct a Lyapunov function as

$$V_3 = \mathbf{S}^{\mathrm{T}} \mathbf{J}_0 \mathbf{S} + \sum_{i=1}^{3} \frac{1}{p_{i1}} \tilde{\kappa}_i^2$$
 (8.32)

where  $\tilde{\kappa}_i = \kappa_i - \hat{\kappa}_i$ . Using (8.27)–(8.31), one can differentiate  $V_3$  as

$$\dot{V}_{3} = 2S^{T}(F + u + \Pi) - \sum_{i=1}^{3} \frac{2}{p_{i1}} \tilde{\kappa}_{i} \dot{\hat{\kappa}}_{i}$$

$$= -\frac{2S^{T}}{N(S)} \left( \gamma_{1}S + \gamma_{2} \lfloor S \rfloor^{1+\bar{\gamma}} + \gamma_{3} \lfloor S \rfloor^{\frac{p_{2}}{q_{2}}} \right) - 2S^{T}(u_{\text{adp}} - \Pi) - \sum_{i=1}^{3} \frac{2}{p_{i1}} \tilde{\kappa}_{i} \dot{\hat{\kappa}}_{i}$$

$$\leq 2||S||||\Pi|| - \frac{2\gamma_{2}}{N(S)} \sum_{i=1}^{3} |S_{i}|^{2+\sigma_{2}} - \sum_{i=1}^{3} \frac{2}{p_{i1}} \tilde{\kappa}_{i} \dot{\hat{\kappa}}_{i}$$

$$- \frac{2\gamma_{3}}{N(S)} \sum_{i=1}^{3} |S_{i}|^{\frac{p_{2}}{q_{2}}+1} - 2S^{T} u_{\text{adp}} - \frac{2\gamma_{1}}{N(S)} ||S||^{2}$$

$$(8.33)$$

Using (8.26) and  $||S||||\Pi|| \le \frac{||S||^2||\Pi||^2}{2\varepsilon^2} + \frac{\varepsilon^2}{2}$ , it leaves (8.33) as

$$\dot{V}_{3} \leq \varepsilon^{2} - \frac{2\gamma_{2}}{S} \sum_{i=1}^{3} |S_{i}|^{2+\tilde{\gamma}} - \frac{2\gamma_{3}}{N(S)} \sum_{i=1}^{3} |S_{i}|^{\frac{p_{2}}{q_{2}}+1} - \sum_{i=1}^{3} \tilde{\kappa}_{i} \left(\frac{||S||^{2}M^{i-1}}{\varepsilon^{2}}\right) \\
-2p_{i2}\hat{\kappa}_{i} - \frac{2\gamma_{1}}{N(S)} ||S||^{2} \\
\leq \varepsilon^{2} - \frac{2\gamma_{1}}{N(S)} ||S||^{2} + \sum_{i=1}^{3} (p_{i2}\kappa_{i}^{2} - p_{i2}\tilde{\kappa}_{i}^{2}) \\
= -n_{1}V_{3} + \delta_{1} \tag{8.34}$$

where  $\eta_1 = \min\{\frac{2\gamma_1}{N(S)\lambda_{\max}(J_0)}, p_{11}p_{12}, p_{21}p_{22}, p_{31}p_{32}\}, \delta_1 = \sum_{i=1}^3 p_{i2}\kappa_i^2 + \varepsilon^2$ . Then, one can prove that S and  $\tilde{\kappa}_i$  are uniformly ultimately bounded. It is therefore reasonable to assume that there exist positive constants  $\zeta_i$  such that  $|\tilde{\kappa}_i| \leq \zeta_i$ , i = 1, 2, 3.

On the other hand, (8.33) can be also simplified as

$$\begin{split} \dot{V}_{3} \leq & \varepsilon^{2} - \frac{2\gamma_{2}}{N(S)} \sum_{i=1}^{3} |S_{i}|^{2+\bar{\gamma}} - \frac{2\gamma_{3}}{N(S)} \sum_{i=1}^{3} |S_{i}|^{\frac{p_{2}}{q_{2}}+1} - \sum_{i=1}^{3} \tilde{\kappa}_{i} \left( \frac{||S||^{2}M^{i-1}}{\varepsilon^{2}} - 2p_{i2}\hat{\kappa}_{i} \right) \\ & - \frac{2\gamma_{1}}{N(S)} ||S||^{2} \\ \leq & - \frac{2\gamma_{2}}{N(S)} \sum_{i=1}^{3} |S_{i}|^{2+\bar{\gamma}} - \frac{2\gamma_{3}}{N(S)} \sum_{i=1}^{3} |S_{i}|^{\frac{p_{2}}{q_{2}}+1} + 2p_{12}\kappa_{1}\tilde{\kappa}_{1} + 2p_{22}\kappa_{2}\tilde{\kappa}_{2} + 2p_{32}k_{3}\tilde{\kappa}_{3} + \varepsilon^{2} \\ \leq & - \frac{2\gamma_{2}}{N(S)} \left( \frac{1}{\lambda_{\max}(J_{0})} \right)^{\frac{2+\bar{\gamma}}{2}} (||S||)^{2+\bar{\gamma}} - \frac{2\gamma_{3}}{N(S)} \left( \frac{1}{\lambda_{\max}(J_{0})} \right)^{\frac{p_{2}+q_{2}}{2q_{2}}} (||S||)^{\frac{p_{2}+q_{2}}{q_{2}}} \\ & - \sum_{i=1}^{3} \left( \frac{\xi_{i}}{p_{i1}} \tilde{\kappa}_{i}^{2} \right)^{\frac{2+\bar{\gamma}}{2}} - \sum_{i=1}^{3} \left( \frac{\xi_{i}}{p_{i1}} \tilde{\kappa}_{i}^{2} \right)^{\frac{p_{2}+q_{2}}{2q_{2}}} + \delta_{1} \end{split}$$

where  $\tilde{\kappa}_{i}\hat{\kappa}_{i} = \tilde{\kappa}_{i}^{2} - \tilde{\kappa}_{i}\kappa_{i} \leq \frac{\chi_{i}}{2}\kappa_{i}^{2} - \frac{2\chi_{i}-1}{2\chi_{i}}\tilde{\kappa}_{i}^{2}$  is used,  $\chi_{i} \in \mathbb{R}_{+}$  is a positive scalar,  $i = 1, 2, 3, \delta_{1} = \sum_{i=1}^{3} \left(\frac{\bar{\chi}_{i}}{p_{i1}}\tilde{\kappa}_{i}^{2}\right)^{\frac{2+\bar{\gamma}}{2}} + \sum_{i=1}^{3} \left(\frac{\bar{\chi}_{i}}{p_{i1}}\tilde{\kappa}_{i}^{2}\right)^{\frac{p_{2}+q_{2}}{2q_{2}}} - \sum_{i=1}^{3} \frac{2\bar{\chi}_{i}}{p_{i1}}\tilde{\kappa}_{i}^{2} + \sum_{i=1}^{3} p_{i2}\chi_{i}\kappa_{i}^{2},$  and  $\bar{\chi}_{i} = \frac{2\chi_{i}-1}{2\chi_{i}}$ .

If  $\frac{\xi_i}{p_{i1}}\tilde{\kappa}_i^2 \geq 1$ , it has

$$\left(\frac{\xi_{i}}{p_{i1}}\tilde{\kappa}_{i}^{2}\right)^{\frac{2+\tilde{\gamma}}{2}} + \left(\frac{\xi_{i}}{p_{i1}}\tilde{\kappa}_{i}^{2}\right)^{\frac{p_{2}+q_{2}}{2q_{2}}} - \frac{2\xi_{i}}{p_{i1}}\tilde{\kappa}_{i}^{2} \le \left(\frac{\xi_{i}}{p_{i1}}\tilde{\kappa}_{i}^{2}\right)^{\frac{2+\tilde{\gamma}}{2}} - \frac{\xi_{i}}{p_{i1}}\tilde{\kappa}_{i}^{2} \tag{8.36}$$

For the case  $\frac{\xi_i}{p_{i1}}\tilde{\kappa}_i^2 < 1$ , it follows that

$$\left(\frac{\xi_{i}}{p_{i1}}\tilde{\kappa}_{i}^{2}\right)^{\frac{2+\tilde{\gamma}}{2}} + \left(\frac{\xi_{i}}{p_{i1}}\tilde{\kappa}_{i}^{2}\right)^{\frac{p_{2}+q_{2}}{2q_{2}}} - \frac{2\xi_{i}}{p_{i1}}\tilde{\kappa}_{i}^{2} \le \left(\frac{\xi_{i}}{p_{i1}}\tilde{\kappa}_{i}^{2}\right)^{\frac{p_{2}+q_{2}}{2q_{2}}} - \frac{\xi_{i}}{p_{i1}}\tilde{\kappa}_{i}^{2} \le 1 \tag{8.37}$$

Following  $|\tilde{\kappa}_i| \leq \zeta_i$ , (8.36), and (8.37), it yields

$$\left(\frac{\xi_{i}}{p_{i1}}\tilde{\kappa}_{i}^{2}\right)^{\frac{2+\tilde{\gamma}}{2}} + \left(\frac{\xi_{i}}{p_{i1}}\tilde{\kappa}_{i}^{2}\right)^{\frac{p_{2}+q_{2}}{2q_{2}}} - \frac{2\xi_{i}}{p_{i1}}\tilde{\kappa}_{i}^{2} \le \max\left\{\left(\frac{\xi_{i}}{p_{i1}}\zeta_{i}^{2}\right)^{\frac{2+\tilde{\gamma}}{2}} - 1, 1\right\} \tag{8.38}$$

Then, using Lemma 2.2, (8.35) can be rewritten as

$$\dot{V}_3 \le -\eta_2 V_3^{\frac{2+\bar{\gamma}}{2}} - \eta_3 V_3^{\frac{p_2+q_2}{2q_2}} + \delta_2 \tag{8.39}$$

where

$$\eta_2 = \min \left\{ \gamma_2 \left( \frac{1}{\lambda_{\text{max}}(\boldsymbol{J}_0)} \right)^{\frac{2+\bar{\gamma}}{2}}, \; \xi_i^{\frac{2+\bar{\gamma}}{2}} \right\}$$
 (8.40)

$$\eta_3 = \min \left\{ \gamma_3 \left( \frac{1}{\lambda_{\max}(\boldsymbol{J}_0)} \right)^{\frac{p_2 + q_2}{2q_2}}, \ \xi_i^{\frac{p_2 + q_2}{2q_2}} \right\}$$
(8.41)

$$\delta_2 = \sum_{i=1}^{3} \left( \max \left\{ \left( \frac{\xi_i}{p_{i1}} \zeta_i^2 \right)^{\frac{2+\bar{\gamma}}{2}} - 1, \ 1 \right\} + p_{i2} \chi_i \kappa_i^2 \right) + \varepsilon^2$$
 (8.42)

Invoking Lemma 2.4 and (8.39) can prove that the NFSMS (8.10) is practically fixed-time stable. The states and S will converge to the set  $\mathcal{D}_3 = \{S : ||S|| \le \epsilon_s\}$  after fixed time  $\bar{T}_1$ , where  $\epsilon_s = \min\{h_1, h_2\}$  and

$$h_1 = \left(\frac{\delta_2}{(1-\bar{\theta})\eta_2}\right)^{\frac{2}{2+\bar{\gamma}}} \tag{8.43}$$

$$h_2 = \left(\frac{\delta_2}{(1 - \bar{\theta})\eta_3}\right)^{\frac{2q_2}{p_2 + q_2}} \tag{8.44}$$

$$\bar{T}_1 < \frac{2n_2}{\eta_1 m_2} + \frac{2q_2}{q_2 - p_2} \frac{1}{\eta_1} \ln \left( 1 + \frac{\eta_2}{\eta_3} \right) \tag{8.45}$$

with a scalar  $0 < \bar{\theta} < 1$ .

Once the NFSMS (8.10) converges into the set  $\mathcal{D}_3$ , the following three cases should be analyzed.

Case 1: If  $\bar{S}_i = 0$  is reached, it implies that S = 0. Based on the Theorem 8.3,  $q_i = 0$  and  $\omega_i = 0$  will be achieved after fixed time, i = 1, 2, 3.

Case 2: If  $\bar{S}_i \neq 0$  and  $|q_i| \leq \bar{\phi}$ , according to (8.11), then one has  $\omega_i + \frac{1}{N(q)}$   $(k_1 \lfloor q_i \rfloor^{1+\gamma_0} + k_2(l_1q_i + l_2q_i^2 \operatorname{sgn}(q_i))) = S_i$ . Because the NFSMS (8.10) converges to the set  $\mathcal{D}_3 = \{S : ||S|| \leq \epsilon_s\}$  after fixed time  $\bar{T}_1$ , it follows that

$$\epsilon_{\omega} = \epsilon_s + k_1 \epsilon_q^{1+\gamma_0} + k_2 \epsilon_q^{\frac{\rho_1}{q_1}} \tag{8.46}$$

$$\epsilon_q = \max\left\{\bar{\phi}, \min\left\{\left(\frac{\epsilon_s}{k_1}\right)^{\frac{1+\gamma_0}{2}}, \left(\frac{\epsilon_s}{k_2}\right)^{\frac{p_1}{2q_2}}\right\}\right\}$$
 (8.47)

Case 3: If  $\bar{S}_i \neq 0$  and  $|q_i| \geq \bar{\phi}$ , it can be got that

$$\omega_i + \frac{1}{N(\boldsymbol{q}_n)} \left( k_1 \lfloor q_i \rfloor^{1+\gamma_0} + k_2 \lfloor q_i \rfloor^{\frac{p_1}{q_1}} \right) = S_i$$
 (8.48)

which can be rewritten as

$$\omega_i + \frac{1}{N(\boldsymbol{q}_v)} \left( k_1 - \frac{S_i}{\lfloor q_i \rfloor^{1+\gamma_0}} \right) \lfloor q_i \rfloor^{1+\gamma_0} + \frac{1}{N(\boldsymbol{q}_v)} k_2 \lfloor q_i \rfloor^{\frac{p_1}{q_1}} = 0$$
 (8.49)

$$\omega_{i} + \frac{1}{N(\boldsymbol{q}_{v})} k_{1} \lfloor q_{i} \rfloor^{1+\gamma_{0}} + \frac{1}{N(\boldsymbol{q}_{v})} \left( k_{2} - \frac{S_{i}}{|q_{i}|^{\frac{p_{1}}{q_{1}}}} \right) \lfloor q_{i} \rfloor^{\frac{p_{1}}{q_{1}}} = 0$$
 (8.50)

Choosing  $k_1$  and  $k_2$  such that  $k_1 - \frac{S_i}{\lfloor q_i \rfloor^{1+\gamma_0}} > 0$  or  $k_2 - \frac{\psi_i}{\lfloor q_i \rfloor^{p_1/q_1}} > 0$ , then it is concluded from Theorem 8.1 that the angular velocity  $\omega_i$  will converges to zero after fixed-time. At this time, based on  $\omega_i = 0$  after fixed-time, solving (8.48) leads to  $|q_i| \le \epsilon_q$  after fixed-time.

Summarizing the analysis in Case 1, Case 2, and Case 3, it can be concluded that the attitude  $q_i$  and the angular velocity  $\omega_i$  will converge into the sets  $\mathcal{D}_4 = \{q_i : |q_i| \le \epsilon_q\}$  and  $\mathcal{D}_5 = \{\omega_i : |\omega_i| \le \epsilon_\omega\}$  after fixed time, respectively. Using Definition 2.2, it is proved that the closed-loop flexible satellite attitude control system is practically fixed-time stable.

**Remark 8.3** When applying the proposed approach to perform attitude maneuvers in practice, the controller (8.27) and the adaptive control law (8.28) will be implemented and numerically computed by an embedded computer equipped in flexible satellites. The designed approach is thus implementable and applicable in practical aerospace engineering.

**Remark 8.4** The implementation of the proposed approach, the work of tuning or choosing the control gains  $k_i$ ,  $\gamma_j$ ,  $p_i$ ,  $q_i$ ,  $m_i$ ,  $n_i$ ,  $\varepsilon$ ,  $a_1$ ,  $b_1$ ,  $c_1$ , and  $\bar{\phi}$ , i=1,2, j=1,2,3, to achieve higher pointing accuracy and acceptable control effort should be carefully done. The following details should be followed when choosing gains.

- (1) The parameter  $\bar{\phi}$  has a direct effect on the converging accuracy of the system states q and  $\omega$ . It is found from (8.10) that the selection of  $\bar{\phi}$  affects the effectiveness of resolving the singularity problem. When  $\bar{\phi}=0$ , the proposed NFSMS (8.10) becomes the conventional fast terminal sliding mode manifold, which leads to the unexpected singularity problem.
- (2) Larger  $k_i$  and  $\gamma_j$  leads to a faster convergence rate. However, larger  $k_i$  and  $\gamma_j$  will result in a large overshoot and more control energy consumption.
- (3) For the purpose of accomplishing attitude control with high pointing accuracy,  $\varepsilon$  should be chosen small enough. Since  $\varepsilon$  appears in the denominator of  $u_{\rm adp}$ , a higher control input is required. Hence, a tradeoff should be considered between the control effort and the system performance. Fortunately, since the maximum torque generated by actuators is known to a designer, the gain  $\varepsilon$  should be selected to satisfy that the control torque does not exceed the maximum power.
- (4) According to the settling time expression, the parameters  $p_i$ ,  $q_i$ ,  $m_i$ , and  $n_i$  also play important roles in dominating the system convergence rate and accuracy.

When applying the proposed fixed-time attitude control approach, those control gains should be chosen appropriately to achieve the desired convergence rate and attitude control accuracy. It should be stressed that there is not a standard procedure to select out those gains. They are currently selected by trial and error until a good tracking performance is obtained.

#### **8.6 Simulation Results**

To verify the capability of the presented approach, simulation is conducted with the controller (8.29) applied to a flexible satellite with  $J_0 = [486.7, 14.9, -1.2; 14.9, 177.4, -7.3, -1.2, -7.3, 404.3] \, \text{kg} \cdot \text{m}^2$  and  $\delta = [1, 0.1, 0.1; 0.5, 0.1, 0.01; -1, 0.3, 0.01] \, \text{kg}^{\frac{1}{2}} \cdot \text{m/s}^2$ . For this satellite, the first three elastic modes are considered, i.e., N = 3. The natural frequencies of the flexible appendage are  $\Lambda_1 = 1.8912 \, \text{rad/s}$ ,  $\Lambda_2 = 2.884 \, \text{rad/s}$ , and  $\Lambda_3 = 3.4181 \, \text{rad/s}$ . The damping ratios are  $\xi_1 = 0.01$ ,  $\xi_2 = 0.01$ , and  $\xi_3 = 0.01$ . The control gains are chosen as  $\gamma_1 = 5$ ,  $\gamma_2 = \gamma_3 = 20$ ,  $k_1 = 1$ ,  $k_2 = 0.8$ ,  $p_1 = p_2 = 9$ ,  $q_1 = q_2 = 15$ ,  $m_1 = m_2 = 35$ ,  $n_1 = n_2 = 33$ ,  $a_1 = a_2 = 0.8$ ,  $b_1 = b_2 = 10$ ,  $c_1 = c_2 = 2$ ,  $\bar{\phi} = 0.001$ ,  $p_{ij} = 0.1$ , i = 1, 2, 3, j = 1, 2, and  $\kappa_1(0) = \kappa_2(0) = \kappa_3(0) = 0$ . The initial states are  $q(0) = [-0.31, 0.09, 0.41, 0.85]^T$ ,  $\omega(0) = [0.01, 0.02, -0.01]^T \, \text{rad/s}$ ,  $\eta(0) = 0$ , and  $\dot{\eta}(0) = 0$ . The uncertain inertia is assumed as  $\Delta J = 0.1 J$ . Moreover, the following external disturbance is considered

$$\mathbf{d} = \begin{bmatrix} 0.2\cos(0.2\pi t) - 0.1\cos(0.4\pi t) - 0.1\\ 0.3\sin(0.2\pi t) - 0.1\cos(0.4\pi t) + 0.2\\ 0.2\sin(0.2\pi t) - 0.2\sin(0.4\pi t) - 0.3 \end{bmatrix} \mathbf{N} \cdot \mathbf{m}.$$
(8.51)

After applying the controller (8.27) to the attitude stabilization maneuvering task, the resulting attitude and the rotation velocity are shown in Figs. 8.1, 8.2, 8.3 and 8.4, respectively. Those results verify the analysis in Sect. 8.5 well. The proposed law ensures a fast convergence. The planned attitude maneuver is accomplished after  $t_s = 12$  seconds. The attitude control accuracy is superior to  $1.2 \times 10^{-6}$ , i.e.,  $|q_i| \le 1.2 \times 10^{-6}$  is ensured for  $t \ge 12$  seconds, i = 1, 2, 3, 4. The control accuracy of the rotation velocity is better than  $1.5 \times 10^{-6}$  rad/s, i.e.,  $|\omega_i| \le 1.5 \times 10^{-6}$  rad/s is achieved for  $t \ge 12$  seconds, i = 1, 2, 3. The ensured convergence time, the pointing accuracy, and the attitude stability can provide the satellite's payload with a perfect attitude system. Hence, the planned missions can be successfully carried out. The control power requested to achieve that control performance is shown in Fig. 8.5. Moreover, the flexible vibration is illustrated in Fig. 8.6. It is seen that the flexible vibration is bounded and damped naturally. The reasonability of Assumption 8-3 is verified.

The pointing accuracy and the attitude stability are plotted in terms of the convergence time in Fig. 8.7. It shows that different requirements on the pointing accuracy and the attitude stability lead to different convergence time. For instance, if the mission requires the satellite to provide the control accuracy of  $|q_i| \le 2.2 \times 10^{-6}$  and  $|\omega_i| \le 2.2 \times 10^{-6}$  rad/s, then the convergence time is 8.8 s. It is seen that inferior control accuracy corresponds to less convergence time.

To further assess the suggested controller's performance, the following two performance indices are considered.

(1) The integral absolute errors (IAEs) of the attitude and the angular velocity described as IAE $_{q_i} = \int_0^{T_o} |q_i(t)| dt$ , IAE $_{\omega_i} = \int_0^{T_o} |\omega_i| dt$ , i = 1, 2, 3, where  $T_o \in \mathbb{R}$  is the attitude maneuvering time. A less IAE means a faster convergent rate.

8.6 Simulation Results 177

**Fig. 8.1** The initial attitude from the controller (8.27)

**Fig. 8.2** The steady-behavior of the attitude from the controller (8.27)

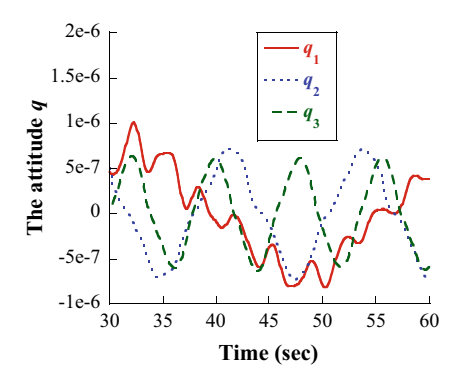
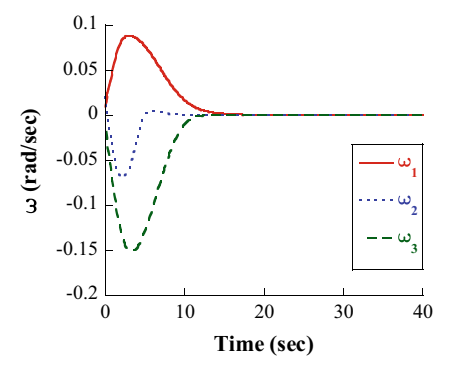


**Fig. 8.3** The initial angular velocity from the controller (8.27)

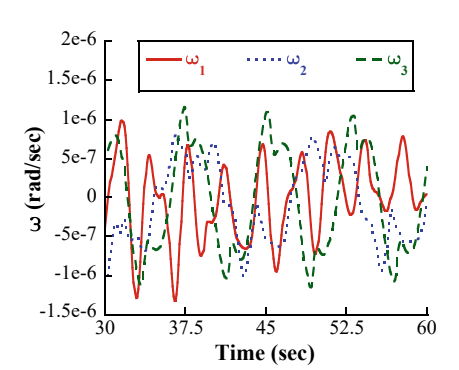


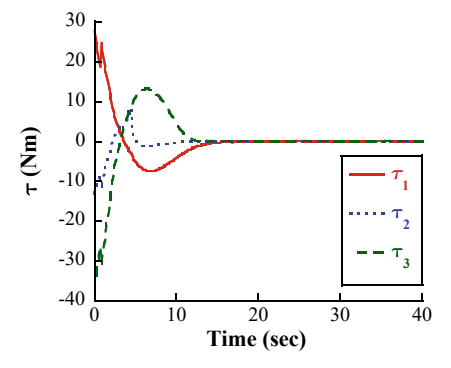
(2) The integral time-weighted absolute errors (ITAEs) defined as ITAE $_{q_i} = \int_0^{T_o} t |q_i(t)| dt$ , ITAE $_{\omega_i} = \int_0^{T_o} t |\omega_i| dt$ , i=1,2,3. The ITAE index evaluates the control accuracy of the steady-state behavior rather than the initial response. Note that the ITAE index does not evaluate the sluggish initial errors. However, the initial errors could be evaluated by the IAE index. Hence, those two performance indices should be considered simultaneously to comprehensively evaluate the attitude stabilization

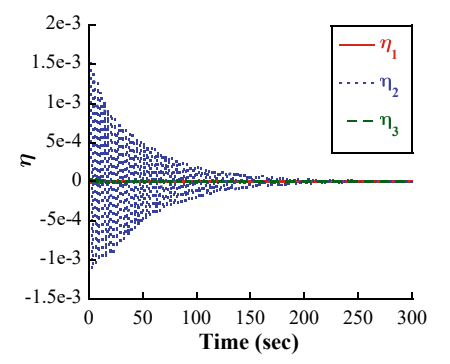
**Fig. 8.4** The steady-behavior of the velocity from the controller (8.27)

**Fig. 8.5** The input of the controller (8.27)

**Fig. 8.6** The flexible vibration from the controller (8.27)







performance of any control schemes despite system uncertainties and disturbances. Smaller IAE and ITAE mean better control performance.

With these two performance indices in mind, the fixed-time control strategies presented in [6] and [8] are also applied to the considered flexible satellite attitude system to carry out numerical simulation for the purpose of comparing their control performance with that of the designed approach. The obtained performance indices of those three controllers are listed in Table 8.1 and Table 8.2 to acquire more insights on

8.6 Simulation Results 179

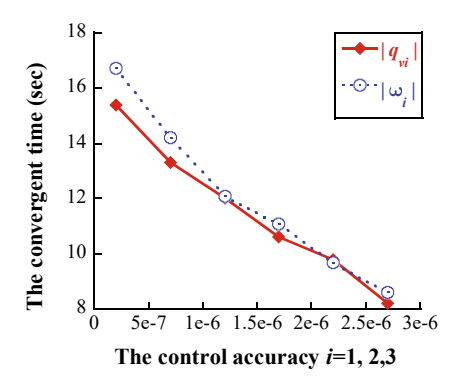


Fig. 8.7 The relation between the control accuracy and the convergence time

**Table 8.1** The IAE performance comparison of three schemes

IAE	The controller (8.27)	The controller [8]	The controller [6]
$IAE_{q_1}$	10.3	10.52	11.3
$IAE_{q_2}$	2.6	2.9	3.1
$IAE_{q_3}$	14.6	16.1	16.9
$IAE_{\omega_1}$	6.4	9.5	10.1
$IAE_{\omega_2}$	2.6	4.1	4.2
$IAE_{\omega_3}$	8.8	13.3	13.7

**Table 8.2** The ITAE performance comparison of three schemes

IAE	The controller (8.27)	The controller [8]	The controller [6]
$IAE_{q_1}$	25.7	34.1	41.5
$IAE_{q_2}$	3.6	5.3	6.1
$IAE_{q_3}$	33.9	55.1	63.2
$IAE_{\omega_1}$	19.93	44.7	52.4
$IAE_{\omega_2}$	5.78	12.7	14.2
$IAE_{\omega_3}$	29.9	69.2	77.1

the effectiveness of the controllers. It is observed that the desired control performance was guaranteed by the controller (8.27) in the presence of the external disturbance (8.51). The convergence rate provided by the proposed controller is faster than those in [6] and [8].

To this end, it can be concluded from the abovementioned simulation results that the presented faster fixed-time control approach successfully solves the fixed-time attitude stabilization problem for flexible satellites with external disturbance and uncertainties. The proposed law obtaining an improved performance, such as fast transient and high precision compared to existing attitude controllers, is validated.

# 8.7 Summary

A new faster fixed-time attitude stabilization controller was presented for flexible satellites. Regarding any initial attitude and angular velocity, the attitude stabilization maneuvering was accomplished after a fixed convergence time despite any uncertain inertia parameters and disturbances. The attitude and the angular velocity were practically fixed-time stable. Compared with the existing fixed-time controllers, the designed approach can provide the system's states with a faster convergence rate near or far from the stable equilibrium points. The proposed controller was non-singular and chattering-free.

### References

- Tian, B., Lu, H., Zuo, Z., Wang, H. (2018) Fixed-time stabilization of high-order integrator systems with mismatched disturbances. Nonlinear Dynamics 94(4): 2889–2899
- Chen, C. C. (2019) A unified approach to finite-time stabilization of high-order nonlinear systems with and without an output constraint. International Journal of Robust and Nonlinear Control 29(2): 393

  –407
- 3. Li, B., Qin, K., Xiao, B., Yang, Y. (2019) Finite-time extended state observer based fault tolerant output feedback control for attitude stabilization. ISA Transactions 91: 11–20
- 4. Chen, C. C., Sun, Z. Y. (2018) Fixed-time stabilisation for a class of high-order non-linear systems. IET Control Theory & Applications 12(18): 2578–2587
- Polyakov, A. (2012) Nonlinear feedback design for fixed-time stabilization of linear control systems. IEEE Transactions on Automatic Control 57(8): 2106–2110
- Zuo, Z. Y. (2015) Nonsingular fixed-time consensus tracking for second-order multi-agent networks. Automatica 54: 305–309
- 7. Zuo, Z. Y. (2015) Non-singular fixed-time terminal sliding mode control of nonlinear systems. IET Control Theory & Applications 9(4): 545–552
- 8. Zhang, Y., Tang, S., Guo, J. (2018) Adaptive terminal angle constraint interception against maneuvering targets with fast fixed-time convergence. International Journal of Robust and Nonlinear Control 28(8): 2996–3014
- Gao, J., Cai, Y. (2015) Fixed-time control for spacecraft attitude tracking based on quaternion. Acta Astronautica 115: 303–313
- Shi, X. N., Zhou, Z. G., Zhou, D. (2020) Adaptive fault-tolerant attitude tracking control of rigid spacecraft on lie group with fixed-time convergence. Asian Journal of Control 22(1): 423–435
- Huang, Y., Jia, Y. (2018) Robust adaptive fixed-time tracking control of 6-DOF spacecraft fly-around mission for noncooperative target. International Journal of Robust and Nonlinear Control 28(6): 2598–2618
- Huang, Y., Jia, Y. (2019) Adaptive fixed-time six-DOF tracking control for noncooperative spacecraft fly-around mission. IEEE Transactions on Control Systems Technology 27(4): 1796– 1804
- Huang, Y., Jia, Y. (2017) Adaptive fixed-time relative position tracking and attitude synchronization control for non-cooperative target spacecraft fly-around mission. Journal of the Franklin Institute 354(18): 8461–8489
- Jiang, B. Y., Hu, Q. L., Friswell, M. I. (2016) Fixed-time attitude control for rigid spacecraft with actuator saturation and faults. IEEE Transactions on Control Systems Technology 24(5): 1892–1898

References 181

15. Jiang, B., Hu, Q., Friswell, M. I. (2016) Fixed-time rendezvous control of spacecraft with a tumbling target under loss of actuator effectiveness. IEEE Transactions on Aerospace and Electronic Systems 52(4): 1576–1586

- Zhu, Z., Xia, Y., Fu, M. (2011) Attitude stabilization of rigid spacecraft with finite-time convergence. International Journal of Robust and Nonlinear Control 21(6): 686–702
- 17. Zhou, N., Xia, Y., Wang, M., Fu, M. (2015) Finite-time attitude control of multiple rigid spacecraft using terminal sliding mode. International Journal of Robust and Nonlinear Control 25(12): 1862–1876
- Zhong, C., Wu, L., Guo, J., Guo, Y., Chen, Z. (2018) Robust adaptive attitude manoeuvre control with finite-time convergence for a flexible spacecraft. Transactions of the Institute of Measurement and Control 40(2): 425–435
- 19. Khalil, H. K. (2002) Nonlinear systems. Prentice Hall
- Fallaha, C. J., Saad, M., Kanaan, H. Y., Al-Haddad, K. (2010) Sliding-mode robot control with exponential reaching law. IEEE Transactions on Industrial Electronics 58(2): 600–610

# Part IV Observer-Based Modeling Error Compensation Attitude Control

# Chapter 9 Extended-State Observer-Based Attitude Control



#### 9.1 Introduction

Recent years have witnessed a lot of attention to the flexible satellite attitude control problem. Many control schemes have been presented [1], including the backstepping control [2], the proportional-derivative control [3], the  $\mathcal{H}_{\infty}$  control [4], the adaptive control [5], the active disturbance rejection [6], the DOB control [7], and so forth [8].

Although a number of studies have shown that robust control techniques are effective in handling flexible vibrations, most of them can only guarantee robustness rather than asymptotic stability of the closed-loop attitude system. A satisfactorily high-accuracy of attitude control would not be achieved. When using adaptive or sliding mode control techniques to design controllers for external disturbance rejection and flexible vibration attenuation, and to achieve asymptotic attitude control, the upper bound of disturbance and vibrations are usually estimated in the controller design. It results in that the controller has certain conservativeness.

In view of addressing those drawbacks, one effective but direct methodology is to estimate the disturbance and flexible vibrations as accurately as possible first, and then design the controller by using the estimated value. Therefore, inspired by the concept of fault detection and identification block [9–11] that detects and identifies faults online and reconfigures the controller online, or nonlinear observer of estimating system uncertainties [12–14], a nonlinear estimator-based control approach is presented in this chapter for a flexible satellite. An estimator is first designed to estimate the magnitude of external disturbance and unknown flexible vibrations in satellite attitude dynamics. This is achieved in finite time and with zero estimation error. A controller designed by using that estimated value is then presented. Asymptotic stability of the closed-loop system is guaranteed.

The main contribution of this chapter in comparison with the existing schemes in the literature for external disturbances rejection and vibration attenuation control is that, the proposed approach is able to achieve high-accuracy attitude control with asymptotic stability of the closed-loop system, and to guarantee no conservativeness of the developed controller.

#### 9.2 Mathematical Model

The mechanical structure of a flexible satellite considered in this chapter is shown in Fig. 9.1. The model consists of a rigid hub with radius b, which denotes the central body of the satellite, and two uniform cantilever flexible beams with the length l and the tip mass  $m_p$ , which represent antennas, solar arrays, or any other flexible structures. This model is representative of a relatively large class of spacecraft employed for communication, remote sensing, or numerous other applications. Denote w(x, t) as the flexible deformation at point x with respect to the frame  $\mathcal{F}_R$ ,  $x \in [0, l]$ .

The dynamic model of the considered flexible satellite motion can be found from Euler-Lagrange analysis and is given by the attitude kinematics (2.15) and the dynamics (2.25)–(2.26). Moreover, by using appropriate calculations, this flexible satellite attitude kinematics (2.15) and the dynamics (2.25)–(2.26) can be combined into the following two-order differential equation:

$$M(\mathbf{\Theta})\ddot{\mathbf{\Theta}} + H_1(\mathbf{\Theta}, \dot{\mathbf{\Theta}})\dot{\mathbf{\Theta}} + H_2(\mathbf{\Theta}, \dot{\mathbf{\Theta}}) = \tau - d$$
 (9.1)

where 
$$d = -R^{\mathrm{T}}(\Theta)(-\omega^{\times}\delta\dot{\eta} - \delta\ddot{\eta} + u_d)$$
,  $\tau = R^{\mathrm{T}}(\Theta)u$ ,  $M(\Theta) = R^{\mathrm{T}}(\Theta)JR(\Theta)$ ,  $H_1(\Theta, \dot{\Theta}) = R^{\mathrm{T}}(\Theta)\left(J\frac{dR(\Theta)}{dt} - \omega^{\times}JR(\Theta)\right)$ , and  $H_2(\Theta, \dot{\Theta}) = -R^{\mathrm{T}}(\Theta)\left(J\frac{d\omega_c(\Theta)}{dt} - \omega^{\times}J\omega_c(\Theta)\right)$ .

**Property 9.1** The matrix  $M(\Theta)$  is symmetric positive-definite.

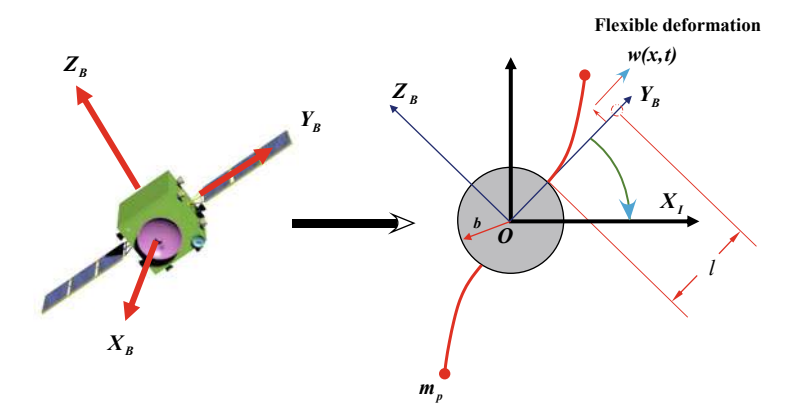


Fig. 9.1 The mechanical structure of the flexible satellite in Chap. 9

**Property 9.2**  $\dot{\mathbf{M}}(\mathbf{\Theta}) - 2\mathbf{H}_1(\mathbf{\Theta}, \dot{\mathbf{\Theta}})$  is skew-symmetric. For any  $\mathbf{x} \in \mathbb{R}^3$  and  $\mathbf{\Theta} \in \mathbb{R}^3$ ,  $\mathbf{x}^{\mathrm{T}}(\dot{\mathbf{M}}(\mathbf{\Theta}) - 2\mathbf{H}_1(\mathbf{\Theta}, \dot{\mathbf{\Theta}}))\mathbf{x} = 0$  is always valid.

### 9.3 Problem Statement

The main goal is to design a controller for the flexible satellite to accomplish attitude stabilization maneuver with high-attitude pointing accuracy and high stability. More specifically, given any initial attitude and angular velocity, consider the flexible satellite attitude system described by (2.15) and the dynamics (2.25)–(2.26) in the presence of modeling error due to external disturbances  $u_d$  and unknown flexible vibrations, design a controller u that the body-fixed frame  $\mathcal{F}_B$  is controlled to coincide with the frame  $\mathcal{F}_O$ . It can guarantee that the attitude  $\Theta$  and the angular velocity  $\omega_b$  are globally asymptotically stable, i.e.,  $\Theta \to 0$  and  $\omega_b \to 0$ .

Remark 9.1 It is worth mentioning that the flexible structures are not controlled. That is because there is no control input for the dynamics of flexible structures, as it can be seen in (2.26). This means that the controller to be developed is inherently a passive but not an active control law for suppressing the vibration of flexible structures. Only the attitude controller needs to be designed with the desired attitude maneuver accomplished, while it is not necessary to design a control law to achieve vibration suppression control of a flexible structure. Actually, if the controller is an active vibration suppression scheme, then it should have control power generated for motors, etc., to govern the flexible structure. Therefore, the aforesaid goal should be achieved even in the presence of flexible vibrations, while the flexible vibrations are attenuated under the effect of the damping incorporated in the flexible appendages.

# 9.4 Extended-State Observer for Modeling Error

It is seen in the dynamics (2.25) that the lumped modeling error  $u_d - \omega^{\times} \delta \dot{\eta} - \delta \ddot{\eta}$  is unknown, and this will significantly affect the attitude control performance. Hence, to eliminate this effect and accomplish the attitude stabilization maneuver with high accuracy, a nonlinear estimator is developed to estimate that lumped modeling error.

Introducing  $M_g(\Theta) = M(\Theta)\dot{\Theta}$  and using Property 9.2 yield  $\dot{M}_g(\Theta) = \tau - d - H_3$  with  $H_3 = H_2(\Theta, \dot{\Theta}) + (H_1(\Theta, \dot{\Theta}) - \dot{M}(\Theta))\dot{\Theta}$ . Define a new coordinate as  $\chi = k_e \int_0^t (\tau - H_3 - \chi(\ell))d\ell - k_e M_g$ , where  $k_e > 0$  is a positive constant. Then, it follows that

$$\dot{\mathbf{\chi}} = -k_e \mathbf{\chi} + k_e \mathbf{d} \tag{9.2}$$

Starting from (9.2), the problem of estimating  $u_d - \omega^{\times} \delta \dot{\eta} - \delta \ddot{\eta}$  can be formulated as that of estimating the state of a linear augmented system driven by  $\chi$  and by an

unknown input. If the unknown input d can be exactly estimated, then  $u_d - \omega^{\times} \delta \dot{\eta} - \delta \ddot{\eta}$  can be estimated by multiplying  $-(\mathbf{R}^{\mathrm{T}}(\mathbf{\Theta}))^{-1}$ .

Assume that the lumped disturbance d is described by a differentiable function with time-derivative  $\rho \in \mathbb{R}^3$ . Define two state variables as  $x_1 = \chi$ ,  $x_2 = d$ , then the following linear system can be obtained.

$$\dot{x}_1 = -k_e x_1 - k_e x_2 \tag{9.3}$$

$$\dot{\mathbf{x}}_2 = \mathbf{\rho} \tag{9.4}$$

In aerospace engineering of flexible satellites, there practically always exists damping even small in its flexible appendages. This makes the magnitudes of elastic vibrations  $||\eta||$ , its rate  $||\dot{\eta}||$ , and its acceleration  $||\ddot{\eta}||$  bounded during attitude maneuvering. On the other hand, the aerodynamic torque and the solar radiation torque are also bounded. Therefore, the following will be used in the estimator design.

**Assumption 9.1** Although the input d is unknown, its amplitude is bounded by a constant  $\mu_1 > 0$ , i.e.,  $||d|| \le \mu_1$ .

**Theorem 9.1** For the linear system given by (9.3) and (9.4) with unknown input, design a nonlinear estimator as

$$\dot{\hat{x}}_1 = -k_e \hat{x}_1 + k_e \hat{x}_2 - \ell_1 \text{sgn}(e_1) - \ell_2 e_1$$
 (9.5)

$$\dot{\hat{\mathbf{x}}}_2 = -\ell_3 \mathbf{e}_1 - \ell_4 \lfloor \mathbf{x}_v \rfloor^{\frac{m}{n}} - \ell_5 \mathbf{sgn}(\mathbf{x}_v)$$
 (9.6)

where  $\hat{\mathbf{x}}_i$  is the estimate of  $\mathbf{x}_i$ , i = 1, 2, respectively.  $\mathbf{x}_v = \ell_1 \operatorname{sgn}(\mathbf{e}_1)$ ,  $\mathbf{e}_i = \hat{\mathbf{x}}_i - \mathbf{x}_i$ ,  $\ell_j$ , j = 1, 2, ..., 5 are positive estimate gains, while  $m \in \mathbb{R}_+$  and  $n \in \mathbb{R}_+$  are positive odd integers such that m < n. Choose the gains such that

$$\ell_5 k_e - \mu_1 > 0 \tag{9.7}$$

and

$$\ell_1 > \max \left\{ \left( \frac{\sqrt{3}k_e \ell_4 + \sqrt{3}\ell_5 + \mu_1}{\lambda_{\min}(M)} + \mu_2 \right)^{\frac{n}{n-m}}, \left( \frac{k_e(\sqrt{3}\ell_5 + \mu_1) + \mu_2 \lambda_{\min}(A)}{\sqrt{3}\ell_5 + \mu_1 + \mu_2 \lambda_{\min}(A)} \right)^{\frac{n}{m}} \right\}$$
(9.8)

where  $\mu_2$  is a positive scalar, and  $\mathbf{A} = \begin{bmatrix} (k_e + \ell_2)\mathbf{I}_3 - k_e\mathbf{I}_3 \\ \ell_3\mathbf{I}_3 & \mathbf{0} \end{bmatrix}$ . Then,  $\mathbf{d}$  and  $\mathbf{u}_d - \mathbf{\omega}^\times \delta \dot{\boldsymbol{\eta}} - \delta \ddot{\boldsymbol{\eta}}$  will be estimated by  $\hat{\mathbf{x}}_2$ ,  $-(\mathbf{R}^{\mathrm{T}}(\mathbf{\Theta}))^{-1}\hat{\mathbf{x}}_2$  in finite time, respectively. Moreover, one has  $\mathbf{u}_d - \mathbf{\omega}^\times \delta \dot{\boldsymbol{\eta}} - \delta \ddot{\boldsymbol{\eta}} \equiv -(\mathbf{R}^{\mathrm{T}}(\mathbf{\Theta}))^{-1}\hat{\mathbf{x}}_2$  for all the time  $t \geq T_e = \frac{n(V_1(\bar{t}))^{\frac{n-m}{2n}}}{(n-m)\ell_4k_e^{m/n}} + \bar{t}$ , where  $V_1(\bar{t}) = (\hat{\mathbf{x}}_2(\bar{t}) - \mathbf{x}_2(\bar{t}))^2$  and  $\bar{t} = \frac{||e_1(0)||}{\mu_2}$ .

The proposed estimator can be viewed as a disturbance observer [16–19]. Although many disturbance observer design approaches are available in literature [18, 20], the proposed observer can achieve a fast and precise estimation. This can be seen in Theorem 9.1. The estimation error is guaranteed to be finite-time stable. In comparison with the existing schemes such as [13, 21], a faster and more precise reconstruction is achieved.

## 9.5 Observer-Based Attitude Controller

As discussed in [22], there is a mathematical relationship between Euler angles rotation and unit-quaternion. Because the orientation of the considered satellite in this chapter with respect to  $\mathcal{F}_O$  is obtained by a yaw-pitch-roll sequence of rotations, its corresponding unit-quaternion  $\mathbf{Q}_e = [q_{e0}, \mathbf{q}_e^{\mathsf{T}}]^{\mathsf{T}} \in \mathbb{R}^4$ ,  $\mathbf{q}_e \in \mathbb{R}^3$  can be obtained from  $\psi$ ,  $\phi$ , and  $\theta$  that

$$Q_{e} = \begin{bmatrix} \cos(\frac{\theta}{2})\cos(\frac{\phi}{2})\cos(\frac{\psi}{2}) + \sin(\frac{\theta}{2})\sin(\frac{\phi}{2})\sin(\frac{\psi}{2}) \\ \sin(\frac{\theta}{2})\cos(\frac{\phi}{2})\cos(\frac{\psi}{2}) - \cos(\frac{\theta}{2})\sin(\frac{\phi}{2})\sin(\frac{\psi}{2}) \\ \cos(\frac{\theta}{2})\sin(\frac{\phi}{2})\cos(\frac{\psi}{2}) + \sin(\frac{\theta}{2})\cos(\frac{\phi}{2})\sin(\frac{\psi}{2}) \\ -\sin(\frac{\theta}{2})\sin(\frac{\phi}{2})\cos(\frac{\psi}{2}) + \cos(\frac{\theta}{2})\cos(\frac{\phi}{2})\sin(\frac{\psi}{2}) \end{bmatrix}$$
(9.9)

It is worth mentioning that this quaternion  $Q_e$  denotes the satellite orientation between  $\mathcal{F}_B$  and  $\mathcal{F}_O$ . Hence, using this unit-quaternion representation, the flexible satellite attitude kinematics (2.15) and the dynamics (2.25) can again be given by [23]:

$$\begin{cases}
\dot{q}_{e0} = -\frac{1}{2} \boldsymbol{q}_e^{\mathrm{T}} \boldsymbol{\omega}_b \\
\dot{\boldsymbol{q}}_e = \frac{1}{2} (\boldsymbol{q}_e^{\mathrm{Y}} + q_{e0} \boldsymbol{I}_3) \boldsymbol{\omega}_b
\end{cases}$$
(9.10)

$$J\dot{\omega}_b = -(\omega_b)^{\times} J\omega_b + H_4 + \omega^{\times} \delta \dot{\eta} - \delta \ddot{\eta} + u + u_d$$
 (9.11)

where 
$$H_4 = (\omega_b)^{\times} J \omega_c(\Theta) + (\omega_c(\Theta))^{\times} J \omega + J \dot{\omega}_c(\Theta)$$

To achieve a high-accuracy attitude stabilization maneuver, the following nonlinear controller is presented:

$$\boldsymbol{u} = \boldsymbol{u}_{a \text{ N}} + \boldsymbol{u}_{a \text{ com}} \tag{9.12}$$

where  $u_{a_{-}N} \in \mathbb{R}^3$  is the normal control effort, and  $u_{a_{-}com} \in \mathbb{R}^3$  is the compensation control module added to the output of the nominal controller to compensate for disturbance and flexible vibrations. This compensation controller is designed by using the estimate of  $u_d - \omega^{\times} \delta \dot{\eta} - \delta \ddot{\eta}$  in the preceding part.

**Theorem 9.2** Consider the flexible satellite attitude system described by using the attitude kinematics (2.15) and the dynamics (2.25)–(2.26), with the application of the nonlinear estimator (9.5)–(9.6), design the nominal and the compensation control

module as

$$\boldsymbol{u}_{a_{-}N} = -k_{c1}(\boldsymbol{q}_e + k_{c2}\boldsymbol{\omega}_b) - \boldsymbol{H}_4 \tag{9.13}$$

$$\boldsymbol{u}_{a \text{ com}} = (\boldsymbol{R}^{\mathrm{T}}(\boldsymbol{\Theta}))^{-1}\hat{\boldsymbol{x}}_{2} \tag{9.14}$$

where  $k_{c1} \in \mathbb{R}_+$  and  $k_{c2} \in \mathbb{R}_+$  are two positive control gains. If these gains are chosen satisfying (9.7), (9.8) and

$$k_{c2} - \frac{k_{c3}}{k_{c1}} > 0 (9.15)$$

$$\frac{\lambda_R}{4k_{c3}k_{c1}} - (\ell_5 k_e - \mu_1) \ge 0 \tag{9.16}$$

where  $k_{c3} \in \mathbb{R}_+$  is an arbitrarily positive scalar, then the closed-loop attitude system can be guaranteed to be asymptotic stable, i.e.,  $\Theta \to 0$ ,  $\omega_b \to 0$ . The attitude stabilization maneuver is, thus, accomplished with high accuracy for the considered flexible satellite.

**Proof** Consider a radially unbounded positive definite Lyapunov function candidate for the system (9.10)–(9.11) as

$$V_2 = \frac{\boldsymbol{\omega}_b^{\mathrm{T}} \boldsymbol{J} \boldsymbol{\omega}_b}{2k_{c1}} + \boldsymbol{q}_e^{\mathrm{T}} \boldsymbol{q}_e + (1 - q_{e0})^2 + \frac{\boldsymbol{e}_1^{\mathrm{T}} \boldsymbol{e}_1}{2} + \frac{\boldsymbol{e}_2^{\mathrm{T}} \boldsymbol{e}_2}{2}$$
(9.17)

Inserting the controller (9.13)–(9.14) into (9.11) results in

$$J\dot{\boldsymbol{\omega}}_{b} = -k_{c1}(\boldsymbol{q}_{e} + k_{c2}\boldsymbol{\omega}_{b}) - S(\boldsymbol{\omega}_{b})\boldsymbol{J}\boldsymbol{\omega}_{b}$$

$$+ \boldsymbol{\omega}^{\times}\delta\dot{\boldsymbol{\eta}} - \delta\ddot{\boldsymbol{\eta}} + \boldsymbol{u}_{d} + (\boldsymbol{R}^{T}(\boldsymbol{\Theta}))^{-1}\hat{\boldsymbol{x}}_{2}$$

$$= -k_{c1}(\boldsymbol{q}_{e} + k_{c2}\boldsymbol{\omega}_{b}) - S(\boldsymbol{\omega}_{b})\boldsymbol{J}\boldsymbol{\omega}_{b} + (\boldsymbol{R}^{T}(\boldsymbol{\Theta}))^{-1}\boldsymbol{e}_{2}$$
(9.18)

Using (9.10) and (9.18), the time-derivative of the Lyapunov function  $V_2$  can be calculated as

$$\dot{V}_{2} = \frac{\boldsymbol{\omega}_{b}^{\mathrm{T}} \boldsymbol{J} \dot{\boldsymbol{\omega}}_{b}}{k_{c1}} + \boldsymbol{q}_{e}^{\mathrm{T}} (\boldsymbol{q}_{e}^{\times} + q_{e0} \boldsymbol{I}_{3}) \boldsymbol{\omega}_{b} + (1 - q_{e0}) \boldsymbol{q}_{e}^{\mathrm{T}} \boldsymbol{\omega}_{b} + \sum_{i=1}^{2} \boldsymbol{e}_{i}^{\mathrm{T}} \dot{\boldsymbol{e}}_{i}$$

$$= -k_{c2} ||\boldsymbol{\omega}_{b}||^{2} + \frac{\boldsymbol{\omega}_{b}^{\mathrm{T}} (\boldsymbol{R}^{\mathrm{T}} (\boldsymbol{\Theta}))^{-1} \boldsymbol{e}_{2}}{k_{c1}} + \sum_{i=1}^{2} \boldsymbol{e}_{i}^{\mathrm{T}} \dot{\boldsymbol{e}}_{i}$$
(9.19)

According to the proof of Theorem 9.1 in [15], it can be obtained that

$$\mathbf{e}_{1}^{\mathsf{T}}\dot{\mathbf{e}}_{1} \leq -(k_{e} + \ell_{2})||\mathbf{e}_{1}||^{2} - (\ell_{1} - k_{e}||\mathbf{e}_{2}||)||\mathbf{e}_{1}|| \tag{9.20}$$

$$\mathbf{e}_{2}^{\mathrm{T}}\dot{\mathbf{e}}_{2} \leq -\ell_{4}k_{n}^{\frac{m}{n}}||\mathbf{e}_{2}||^{\frac{m+n}{n}} - (\ell_{5}k_{e} - \mu_{1})||\mathbf{e}_{2}|| \tag{9.21}$$

and

$$||e_2|| < ||e|| < \lambda_R \tag{9.22}$$

$$\ell_1 > k_e \lambda_R + \varepsilon_0 \tag{9.23}$$

where  $\lambda_R = \frac{\sqrt{3}k_e\ell_4\ell_1^{\frac{m}{n}} + \sqrt{3}\ell_5 + \mu_1}{\lambda_{\min}(A)}$ . Then, it can be obtained from (9.20)–(9.23) that

$$\sum_{i=1}^{2} \boldsymbol{e}_{i}^{\mathsf{T}} \dot{\boldsymbol{e}}_{i} \leq -(k_{e} + \ell_{2})||\boldsymbol{e}_{1}||^{2} - \ell_{4} k_{e}^{\frac{m}{n}} ||\boldsymbol{e}_{2}||^{\frac{m+n}{m}} - (\ell_{5} k_{e} - \mu_{1})||\boldsymbol{e}_{2}|| \tag{9.24}$$

In addition, applying the Young's inequality, one has

$$\frac{\boldsymbol{\omega}_b^{\mathrm{T}}(\boldsymbol{R}^{\mathrm{T}}(\boldsymbol{\Theta}))^{-1}\boldsymbol{e}_2}{k_{c1}} \le \frac{k_{c3}||\boldsymbol{\omega}_b||^2}{k_{c1}} + \frac{||\boldsymbol{e}_2||^2}{4k_{c3}k_{c1}}$$
(9.25)

Therefore, (9.19) can be simplified as follows by using (9.20)–(9.23).

$$\dot{V}_{2} \leq -(k_{c2} - \frac{k_{c3}}{k_{c1}})||\boldsymbol{\omega}_{b}||^{2} - (k_{e} + \ell_{2})||\boldsymbol{e}_{1}||^{2} - \ell_{4}k_{e}^{\frac{m}{n}}||\boldsymbol{e}_{2}||^{\frac{m+n}{m}} \\
+ ||\boldsymbol{e}_{2}|| \left(\frac{||\boldsymbol{e}_{2}||}{4k_{c3}k_{c1}} - (\ell_{5}k_{e} - \mu_{1})\right)||\boldsymbol{e}_{2}||$$
(9.26)

Furthermore, the followings can be obtained from (9.15), (9.16), and (9.22)

$$\dot{V}_2 \le -\left(k_{c2} - \frac{k_{c3}}{k_{c1}}\right) ||\boldsymbol{\omega}_b||^2 - (k_e + \ell_2) ||\boldsymbol{e}_1||^2 - \ell_4 k_e^{\frac{m}{n}} ||\boldsymbol{e}_2||^{\frac{m+n}{m}}$$
(9.27)

By integrating (9.27) form 0 to  $\infty$ , one has

$$\int_0^\infty \dot{V}_2(\ell) d\ell \le V_2(0) - V_2(\infty) \le V_2(0) < \infty \tag{9.28}$$

Because the Lyapunov function is radially unbounded, all the signals remain bounded. Using Barbalat's lemma, it can be proved from the uniformly continuity of  $\dot{V}_2$  that  $\dot{V}_2(t) \to 0$  as  $t \to \infty$ . This further guarantee that  $\lim_{t \to \infty} \ddot{V}_2(t) = 0$  because  $\dot{V}_2$  is uniformly continuous. To this end, it can be obtained from (9.27) that  $\lim_{t \to \infty} e_1(t) = 0$ ,  $\lim_{t \to \infty} e_2(t) = 0$ ,  $\lim_{t \to \infty} \omega_b(t) = 0$ , and  $\lim_{t \to \infty} \dot{\omega}_b(t) = 0$ . Using (9.23) and  $\lim_{t \to \infty} e_2(t) = 0$ , it can be proved that  $q_e \to 0$  as  $t \to \infty$ . From the unity constraint  $q_{e0}^2 + q_e^T q_e = 1$  of the quaternion  $Q_e$ , it follows that  $q_{e0} \to \pm 1$  as  $t \to \infty$ . This strictly corresponds to  $\Theta \to 0$ . As a result, the closed-loop attitude system is asymptotic stable. High-accuracy attitude control is, hence, achieved.

Summarizing the aforesaid analysis, it is proved that  $\Theta \to 0$  and  $\omega_b \to 0$  as  $t \to \infty$ . It means that the satellite body-fixed frame  $\mathcal{F}_B$  will finally coincide with the orbit reference frame  $\mathcal{F}_O$ . High-accuracy attitude stabilization is, hence, achieved.

### 9.6 Simulation Results

As the initial step towards final experimental verification, the performance of the proposed controller should be numerically simulated first. Hence, a flexible satellite currently being developed will be simulated to test the effectiveness of the proposed control scheme. The orbit of the satellite is circular, with an altitude of 638 km and an inclination of 95.4 deg. Its orbital rate is  $\omega_0 = 0.0011$  rad/s. Its physical parameters are  $\boldsymbol{J} = [486.7, 14.9, -1.2; 14.9, 177.4, -7.3; -1.2, -7.3, 404.3]$  kg·m²,  $\boldsymbol{\delta} = [1, 0.1, 0.1; 0.5, 0.1, 0.01; -1, 0.3, 0.01]$  kg½·m/s², and the first three elastic modes have been taken into account, i.e., N = 3. The natural frequencies are  $\Delta_1 = 1.8912$  rad/s,  $\Delta_2 = 2.884$  rad/s,  $\Delta_3 = 3.4181$  rad/s, and damping ratios are  $\xi_1 = 0.01$ ,  $\xi_2 = 0.01$ , and  $\xi_3 = 0.01$ . A time-varying external disturbance is also considered. It is given by  $\boldsymbol{u}_d = (||\boldsymbol{\omega}_b||^2 + 0.05)[\sin 0.8t, \cos 0.5t, \cos 0.3t]^T$  N·m.

The gains of the estimator (9.5)–(9.6) are chosen as  $k_e = 7.5$ ,  $\ell_1 = 0.05$ ,  $\ell_2 = 0.5$ ,  $\ell_3 = 0.5$ ,  $\ell_4 = 10.5$ ,  $\ell_5 = 0.05$ , m = 17, and n = 19. The control gains for the controller (9.12) are chosen as  $k_{c1} = 15$  and  $k_{c2} = 16.7$ . The initial satellite attitude angles are  $\theta = 6$  degrees,  $\phi = -4.5$  degrees, and  $\psi = 3$  degrees, while the initial velocity is  $\omega_b(0) = [0.2, 0.1, -0.15]^T$ deg/s. The initial flexible modal displacements and velocities are given by  $\eta_i(0) = 0$  and  $\dot{\eta}_i(0) = 0$  for i = 1, 2, 3.

Denoting the actual estimation error between the magnitude of the external disturbance, the vibrations  $\mathbf{u}_d - \boldsymbol{\omega}^\times \delta \dot{\boldsymbol{\eta}} - \delta \ddot{\boldsymbol{\eta}}$  and the estimated value  $-(\mathbf{R}^T(\boldsymbol{\Theta}))^{-1}\hat{x}_2$  as  $\boldsymbol{\varepsilon}$ , i.e.,  $\boldsymbol{\varepsilon} = (\mathbf{u}_d - \boldsymbol{\omega}^\times \delta \dot{\boldsymbol{\eta}} - \delta \ddot{\boldsymbol{\eta}}) + (\mathbf{R}^T(\boldsymbol{\Theta}))^{-1}\hat{x}_2$ . When the proposed estimation-based approach is implemented to the considered flexible satellite attitude system, Fig. 9.2 shows the successful estimation using the incorporated nonlinear estimator. As shown by the steady-state behavior of the actual estimation error  $\boldsymbol{\varepsilon}$  in Fig. 9.2b, the estimation accuracy is smaller than  $1.0 \times 10^{-3} \, \mathrm{N} \cdot \mathrm{m}$ . The lumped disturbance  $\mathbf{u}_d - \boldsymbol{\omega}^\times \delta \dot{\boldsymbol{\eta}} - \delta \ddot{\boldsymbol{\eta}}$  including external disturbances and flexible vibrations is exactly reconstructed by  $-(\mathbf{R}^T(\boldsymbol{\Theta}))^{-1}\hat{x}_2$  after a short period of time, roughly  $T_e = 3.1$  seconds. This can be seen in Fig. 9.2a. That estimation result verified the conclusion in Theorem 9.1 that, the total unknown torque induced by external disturbance and flexible vibrations can be precisely estimated by  $-(\mathbf{R}^T(\boldsymbol{\Theta}))^{-1}\hat{x}_2$  in finite time  $T_e$ .

Due to the precise estimation of the external disturbances and unknown flexible vibrations torque supplied by the estimator (9.5), (9.6), the controller in (9.12) can completely compensate for the effect of external disturbance and unknown vibrations. As a result, the controller produces an asymptotic convergence of the angular velocity and the attitude angles. External disturbance rejection and robustness against unknown flexible vibrations are achieved. The attitude Euler angles are presented in

9.6 Simulation Results 193

**Fig. 9.2** The estimation error of the lumped modeling error

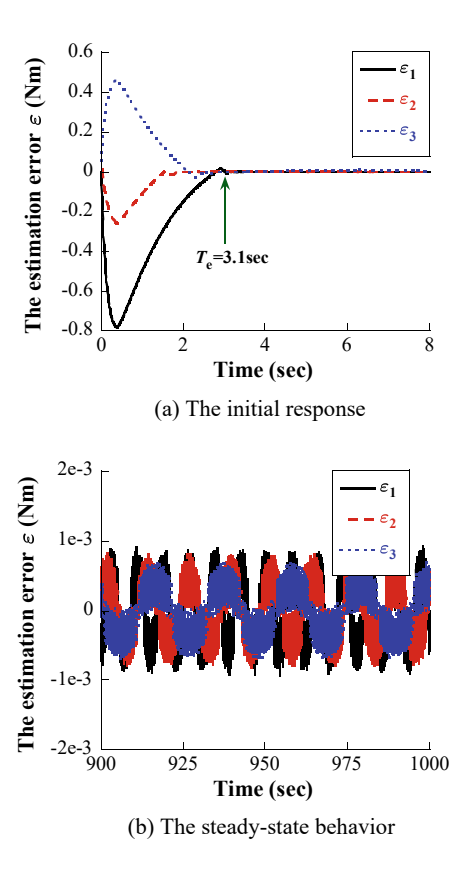
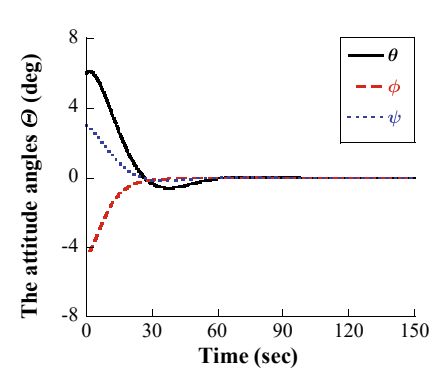


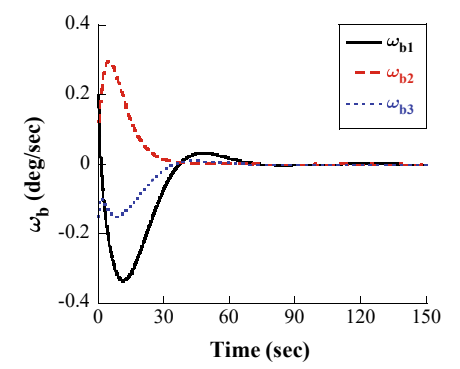
Fig. 9.3 and the attitude velocity is illustrated in Fig. 9.4. The attitude pointing accuracy is within 0.0005 degrees and attitude stability is within 0.0002 deg/sec. Those obtained attitude stability and pointing accuracy satisfy a set of stringent pointing requirements to perform the planned mission even in the face of external disturbances and unknown flexible vibrations. The vibrations of flexible appendages can be seen in Fig. 9.5. The corresponding control torque is shown in Fig. 9.6. It is interesting to see that the attenuation control of vibrations is achieved, and they will be completely suppressed after 200 s. Based on this result, one has  $-\omega^{\times}\delta\dot{\eta} - \delta\ddot{\eta} = 0$  after 200 s. That is to say, the signal estimated after 200 s is the external disturbance  $u_d$ . At this time, the control effort in (9.12) only needs to compensate for the external disturbance. That is the reason why the steady behavior of u in Fig. 9.6b is quite the same as external disturbance  $u_d$ .

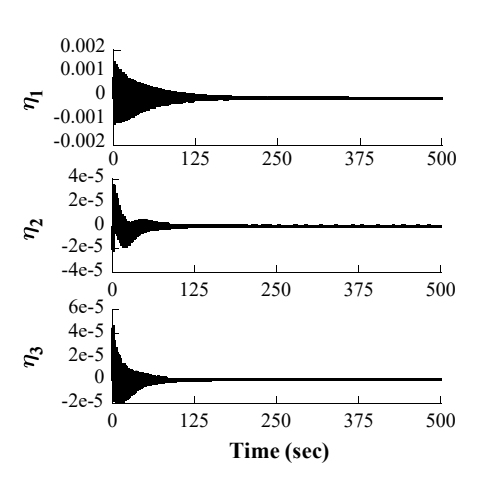
**Fig. 9.3** The attitude Euler angles from the controller (9.12)

**Fig. 9.4** The angular velocity from the controller (9.12)

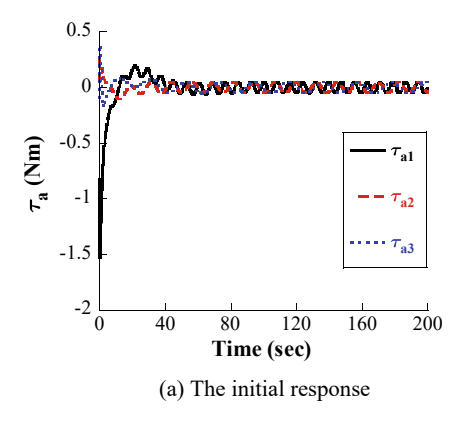
**Fig. 9.5** The flexible vibrations from the controller (9.12)

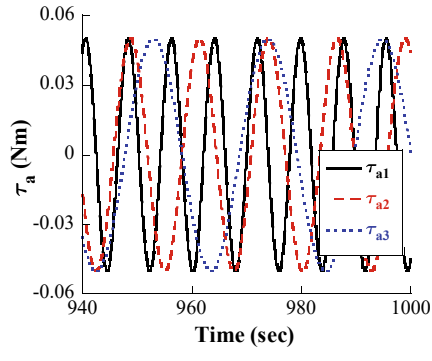






**Fig. 9.6** The control input of the controller (9.12)





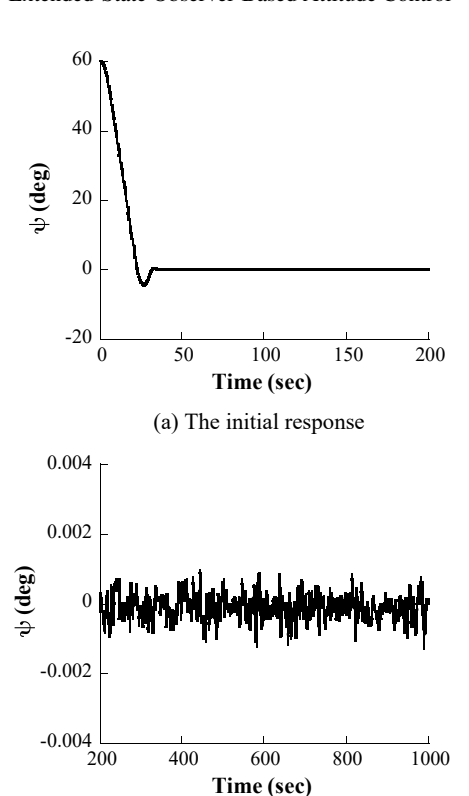
(b) The steady-state behavior

# 9.7 Experimental Study

In this section, experiments are further performed to verify the validity of the proposed approach on the single-axis air-bearing suspending rotary testbed, as shown in Fig. 2.5. In comparison with Figs. 9.1 and 2.5, it is known that this testbed can exactly simulate the attitude motion of Euler attitude yaw angle  $\psi$  rotation.

To verify the engineering application of the proposed nonlinear estimator-based attitude control approach, the experiment has been conducted by using the testbed. A large-angle attitude stabilization maneuver is performed. The initial attitude angle is  $\psi(0) = 60$  degrees, and the initial angular velocity is  $\omega_{b3}(0) = 0$  deg/s. With an application of the proposed controller, the experimental results are shown in Figs. 9.7, 9.8 and 9.9. It can be seen in Fig. 9.7a that the attitude stabilization maneuver is accomplished within 40 s. Moreover, the attitude pointing accuracy achieved is 0.002 degrees. This can be observed in the steady-state behavior of Fig. 9.7b, and hence high-accuracy control performance is guaranteed. The resulting angular velocity is shown in Fig. 9.9. As the steady-state behavior clearly shows in Fig. 9.8b, attitude

Fig. 9.7 The experimental result of the attitude from the controller (9.12)



(b) The steady-state behavior

stability is within 0.0015 deg/s. This accuracy is very high for flexible satellite. The actual control input torque is shown in Fig. 9.9.

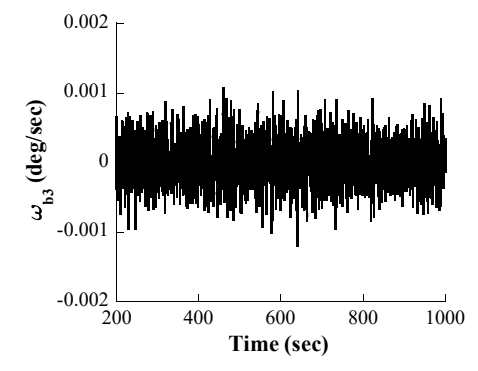
Compared the experimental results in Figs. 9.7, 9.8 and 9.9 with the simulation results in Figs. 9.3, 9.4, 9.5 and 9.6, it is interesting to see that there exists a minor difference in the attitude stabilization time. That is because the inertia parameters in the experimental testbed have a scaling factor 10% of the inertia matrix used in simulations. Moreover, the obtained attitude pointing accuracy between simulation and experimental results is also different, and the latter is almost less than the former by an order of magnitude. That is due to the fact that the actual actuator, gyro, and controller are used in experiments rather than using an ideal mathematical model in simulation. Although some differences are observed, it can be seen that the behavior (including overshoot) of experimental results matches the behavior of the simulation results well.

To summarize, high-accuracy pointing control (order of  $10^{-3}$  deg) and high-accuracy attitude stability (order of  $10^{-3}$  deg/s) can be realized through the proposed control. Hence, the ease of implementation, high accuracy, and robustness of the proposed control are well verified through the experiment.

**Fig. 9.8** The experimental result of the angular velocity from the controller (9.12)

2 1 0 0 3<sup>2</sup> -2 -3 -4 0 50 100 150 200 Time (sec)

(a) The initial response



(b) The steady-state behavior

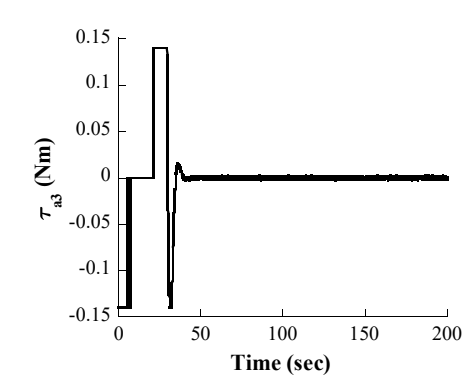


**Fig. 9.9** The experimental result of the input torque of the controller (9.12)

# 9.8 Summary

Although there have been significant investigations in robust and high-accuracy control design for flexible satellites, very few have addressed the problem of the conservativeness of the controller. In this chapter, an estimator-based methodology for flexible attitude stabilization control is presented. The scheme incorporates a nonlinear estimator for estimating the external disturbances and unknown flexible vibrations simultaneously, and a Proportional-Derivative (PD)-type controller. The estimation is achieved in finite time and with zero estimation error. The controller is designed by using the estimated value. Hence, modeling error compensation with disturbance rejection and vibration attenuation control can be achieved. The outstanding advantage of the approach is that it can achieve high-accuracy attitude control with asymptotic stability of the closed-loop system and no-conservativeness of the controller simultaneously. It has been verified through simulations and experiments that the proposed control is easily implementable with high-pointing accuracy achieved and robust against unknown flexible vibrations.

#### References

- MoradiMaryamnegari, H., Khoshnood, A. M. (2019) Robust adaptive vibration control of an underactuated flexible spacecraft. Journal of Vibration and Control 25(4): 834–850
- Miao, Y., Wang, F., Liu, M. (2018) Anti-disturbance backstepping attitude control for rigidflexible coupling spacecraft. IEEE Access 6: 50729–50736
- Liu, H., Guo, L., Zhang, Y. (2012) An anti-disturbance PD control scheme for attitude control and stabilization of flexible spacecrafts. Nonlinear Dynamics 67(3): 2081–2088
- 4. Wu, S., Chu, W., Ma, X., Radice, G., Wu, Z. (2018) Multi-objective integrated robust  $\mathcal{H}_{\infty}$  control for attitude tracking of a flexible spacecraft. Acta Astronautica 151: 80–87
- Zhang, C., Ma, G., Sun, Y., Li, C. (2019) Prescribed performance adaptive attitude tracking control for flexible spacecraft with active vibration suppression. Nonlinear Dynamics 96(3): 1909–1926
- Zhu, Y., Guo, L., Qiao, J., Li, W. (2019) An enhanced anti-disturbance attitude control law for flexible spacecrafts subject to multiple disturbances. Control Engineering Practice 84: 274–283
- 7. Zhou, C., Zhou, D. (2017) Robust dynamic surface sliding mode control for attitude tracking of flexible spacecraft with an extended state observer. Proceedings of the Institution of Mechanical Engineers, Part G: Journal of Aerospace Engineering 231(3): 533–547
- Wang, Z., Xu, M., Jia, Y., Xu, S., Tang, L. (2017) Vibration suppression-based attitude control for flexible spacecraft. Aerospace Science and Technology 70: 487–496
- 9. Yin, S., Ding, S. X., Xie, X. C., Luo, H. (2014) A review on basic data-driven approaches for industrial process monitoring. IEEE Transactions on Industrial Electronics 61(11): 6418–6428
- Yin, S., Li, X. W., Gao, H. J., Kaynak, O. (2015) Data-based techniques focused on modern industry: an overview. IEEE Transactions on Industrial Electronics 62(1): 657–667
- Yin, S., Liu, L., Hou, J. (2016) A multivariate statistical combination forecasting method for product quality evaluation. Information sciences 355: 229–236
- 12. Xiao, B., Yin, S., Wu, L. G. (2017) A structure simple controller for satellite attitude tracking maneuver. IEEE Transactions on Industrial Electronics 64(2): 1436–1446
- Cao, Y., Chen, X. B. (2014) Disturbance-observer-based sliding-mode control for a 3-DOF nanopositioning stage. IEEE/ASME Transactions on Mechatronics 19(3): 924–931

References 199

 Xiao, B., Yin, S., Kaynak, O. (2016) Tracking control of robotic manipulators with uncertain kinematics and dynamics. IEEE Transactions on Industrial Electronics 63(10): 6439–6449

- Xiao, B., Hu, Q. L., Singhose, W., Huo, X. (2013) Reaction wheel fault compensation and disturbance rejection for spacecraft attitude tracking. Journal of Guidance, Control, and Dynamics 36(6): 1565–1575
- Chen, W. H., Yang, J., Guo, L., Li, S. (2016) Disturbance-observer-based control and related methods—An overview. IEEE Transactions on Industrial Electronics 63(2): 1083–1095
- Yang, J., Su, J., Li, S., Yu, X. (2014) High-order mismatched disturbance compensation for motion control systems via a continuous dynamic sliding-mode approach. IEEE Transactions on Industrial Informatics 10(1): 604–614
- Liu, J. X., Laghrouche, S., Wack, M. (2014) Observer-based higher order sliding mode control of power factor in three-phase AC/DC converter for hybrid electric vehicle applications. International Journal of Control 87(6): 1117–1130
- Yang, J., Li, S. H., Sun, C. Y., Guo, L. (2013) Nonlinear-disturbance-observer-based robust flight control for airbreathing hypersonic vehicles. IEEE Transactions on Aerospace and Electronic Systems 49(2): 1263–1275
- 20. Rigatos, G. G. (2015) Nonlinear control and filtering using differential flatness approaches: applications to electromechanical systems. New York: Springer
- 21. De, L. A., Mattone, R. (2005) An identification scheme for robot actuator faults. In: 2005 IEEE/RSJ International Conference on Intelligent Robots and Systems, pp 1127–1131
- 22. Sidi, M. J. (1997) Spacecraft dynamics and control. Cambridge University Press
- 23. Xiao, B., Hu, Q. L., Zhang, Y. M. (2015) Finite-time attitude tracking of spacecraft with fault-tolerant capability. IEEE Transactions on Control Systems Technology 23(4): 1323–1335

# Chapter 10 Disturbance Observer-Based Attitude Control



#### 10.1 Introduction

The most existing DO requires external disturbance or modeling error to satisfy some strict conditions. For instance, most ESO are only feasible for the unknown constant disturbance  $u_d$  or the disturbance with slow variation [1–3], i.e.,  $\dot{u}_d = 0$ ,  $\dot{u}_d \approx 0$ ,  $\lim_{t\to\infty} \dot{u}_d = 0$ , or  $||\dot{u}_d|| \leq \delta_1$ , where  $\delta_1$  is positive and small scalar. When the external disturbance is treated as an extended state in ESO, the external disturbance should be differentiable. On the other hand, it usually requires the SMO or HOSMO to be upper bounded by a known value  $\delta_2$ , i.e.,  $||u_d|| \leq \delta_2$ . In practice, however, the external disturbance may not satisfy these assumptions. The class of the external disturbance handled by the existing DO is limited. Hence, it is of interest to determine observers that can release these constraints or assumptions. Although this is achieved in [2], its result is applicable to linear systems only. In this chapter, we address this problem first by deriving a novel DO-based control approach that stabilizes the rigid bodies' system despite any type of external disturbance. The main features of this control approach are listed as follows.

- A general systematic DO-based control approach is presented. The closed-loop attitude system is stabilized in the presence of external disturbances. The attitude and the angular velocity are exponentially stabilized if the external disturbance has no rate of change. When the external disturbance is time-varying, the attitude and the angular velocity are exponentially stabilized to a small set containing the origin, despite the slow-varying or fast-varying disturbances. Moreover, the controller has a simple structure. It necessitates inexpensive onboard computations.
- The proposed DO provides the disturbance estimation error with exponential rate.
   Compared with the existing DO or ESO, the designed observer can release the restrictions on the rate of change of the modeling error. The class of disturbances handled in this chapter can be much larger than the existing DO or ESO.

Note that although many investigations have been reported for satellite attitude tracking control design with modeling error and actuator uncertainties addressed, most of them have the following drawbacks: (1) Few results can handle system uncertainties and actuator uncertainties simultaneously. (2) Most of the attitude tracking schemes in literature cannot guarantee the exponential stability of the overall system. Therefore, the robustness to uncertainties is weak. Although such stability was reported in [4], actuator uncertainties were not investigated. (3) The existing approaches to actuator misalignment are only appropriate for satellites with its actuators belonging to a specific type and having a particular configuration.

Motivated by addressing the aforementioned three challenges, a new resilient control approach is then presented in this chapter for attitude tracking with practically exponential convergence ensured. This is developed in the framework of the observer-based control technique. A structure simple estimation law is preliminarily synthesized to observe the modeling error including the system uncertainties and actuator uncertainties. Based on this observer, a self-resilient controller is then synthesized. The following are the main contributions of this resilient control approach.

- The proposed resilient control approach governs the attitude tracking system to be practically exponentially stable despite the system uncertainties and the actuator uncertainties. Hence, in comparison with the existing attitude controllers that ensure asymptotic stability or ultimately uniformly bounded stability [5–8], the proposed controller has more robustness to uncertainties.
- In contrast to [4, 9, 10], the resilient control scheme has the capability of tolerating systems and actuator uncertainties, while the controllers in [4, 9, 10] can only provide exponential stability in the absence of systems uncertainties and external disturbances. Moreover, the designed controller is independent of the actuator's type and its configuration in the satellite. It has an excellent resilient capability to the actuator uncertainties in a more general way.
- The controller is designed with the satellite's attitude represented by using attitude Euler angles. Moreover, in comparison with the neural-network-based attitude controller [11], the structure of the proposed approach is simple, and its implementation does not necessitate expensive onboard computation. The presented approach has significant practical application potential.

# 10.2 Attitude Exponential Stabilization Control

#### 10.2.1 Problem Statement

In this section, the rigid satellite is considered with its attitude represented by the modified Rodrigues parameters. The control objective of this section can be stated as: For any initial states  $\sigma(0)$  and  $\omega(0)$ , the goal is to use the angular velocity and the attitude feedback to design a robust control torque u to guarantee that the closed-loop

system described by (2.21) and (2.24) is globally exponentially stabilized despite any modeling error  $u_d$ . The attitude  $\sigma$  and the angular velocity  $\omega$  are exponentially stabilized to their equilibrium points or converge to a small set around the equilibrium points with acceptable control accuracy.

## 10.2.2 Disturbance Observer

Consider a class of nonlinear systems with their model described by

$$\dot{x} = f(x) + g(x)u + d \tag{10.1}$$

where  $x \in \mathbb{R}^n$  is the measurable state of the system,  $u \in \mathbb{R}^m$  is the system's control input,  $d \in \mathbb{R}^n$  is the modeling error acting on the system. The function  $f(x) \in \mathbb{R}^n$  is known. The matrix  $g(x) \in \mathbb{R}^{n \times m}$  is known and invertible.

To estimate or observe the modeling error in the nonlinear system in (10.1), a novel but structure-simple observer will be presented in this section. A new state  $\mathbf{x}_a \in \mathbb{R}^n$  is preliminarily introduced with its dynamics satisfying

$$\dot{x}_a = f(x) + g(x)u + F_1 x_e \tag{10.2}$$

where  $x_e = x - x_a$  and  $F_1 \in \mathbb{R}^{n \times n}$  is a constant matrix determined by the designed.

**Lemma 10.1** For the nonlinear system (10.1) with the modeling error d, let an observer be designed as

$$\dot{\hat{\xi}} = -L\hat{\xi} + L(F_1 x_e - F_2(x_e)) \tag{10.3}$$

with  $F_2(x_e) = Lx_e$ ,  $L = L^T \in \mathbb{R}^{n \times n}$  is the observer gain matrix, and it is positive-definite. Applying the observer state, develop an estimation law for the modeling error d as

$$\hat{\boldsymbol{d}} = \hat{\boldsymbol{\xi}} + \boldsymbol{F}_2(\boldsymbol{x}_e) \tag{10.4}$$

where  $\hat{\boldsymbol{d}}$  is the estimation of  $\boldsymbol{d}$ . Suppose that the observer gain  $\boldsymbol{L}$  is chosen such that  $\lambda_{\min}(\boldsymbol{L}) - \frac{1}{4} > 0$ , then the following results can be achieved for all  $\boldsymbol{d}_e(\boldsymbol{0})$ .

- (R1) The disturbance estimation error  $\mathbf{d}_e = \mathbf{d} \hat{\mathbf{d}}$  is globally exponentially stable if  $\dot{\mathbf{d}} = \mathbf{0}$ .
- (R2) If  $\dot{\boldsymbol{d}} \neq \boldsymbol{0}$  and the rate of change of  $\boldsymbol{d}$  is bounded, i.e., there exists a positive scalar  $\mu \in \mathbb{R}$  such that  $||\dot{\boldsymbol{d}}(t)|| \leq \mu$  for all  $t \geq 0$ , then the disturbance estimation error  $\boldsymbol{d}_e$  converges with an exponential rate, equal to  $(1-\alpha)(\lambda_{\min}(\boldsymbol{L})-\frac{1}{4})$ , to the ball with radius  $\frac{2\mu}{\sqrt{\alpha(4\lambda_{\min}(\boldsymbol{L})-1)}}$  where  $0 < \alpha < 1$ .

**Proof** From (10.1) and (10.2), it can be obtained that the dynamics of  $x_e$  is such that

$$\dot{\mathbf{x}}_e = -\mathbf{F}_1 \mathbf{x}_e + \mathbf{d} \tag{10.5}$$

In accordance, it follows from (10.5) that the estimation error  $d_e$  is such that

$$\dot{d}_{e} = \dot{d} - \dot{\hat{d}} 
= \dot{d} + L\hat{\xi} - LF_{1}x_{e} + LF_{2}(x_{e}) - L\dot{x}_{e} 
= \dot{d} + L\hat{\xi} - LF_{1}x_{e} + LF_{2}(x_{e}) - L(-F_{1}x_{e} + d) 
= \dot{d} - Ld_{e}$$
(10.6)

Choose a Lyapunov candidate function for (10.6) as  $V_o = \frac{1}{2} \boldsymbol{d}_e^{\mathrm{T}} \boldsymbol{d}_e$ , one has

$$\dot{V}_o = \boldsymbol{d}_e^{\mathrm{T}} \dot{\boldsymbol{d}}_e = -L \boldsymbol{d}_e^{\mathrm{T}} \boldsymbol{d}_e + \boldsymbol{d}_e^{\mathrm{T}} \dot{\boldsymbol{d}}$$
 (10.7)

Then, the following two cases are discussed to analyze the stability of  $d_e$ . Case #1: If  $\dot{d} = 0$ , then (10.7) can be further simplified as

$$\dot{V}_o = -L d_o^{\mathrm{T}} d_e \le -2\lambda_{\min}(L) V_o \tag{10.8}$$

where  $\lambda_{\min}(L) > 0$ . Solving (10.8) yields  $V_o(t) \leq V_o(0) \exp(-2\lambda_{\min}(L)t)$  or

$$||\boldsymbol{d}_{e}(t)|| \le \sqrt{2V_{o}(0)} \exp(-\lambda_{\min}(\boldsymbol{L})t) \tag{10.9}$$

which implies that the observer error  $d_e(t)$  will be globally exponentially stabilized for any initial observer state, i.e.,  $\lim_{t\to\infty} ||d_e(t)|| = 0$ .

Case #2: If  $\dot{d} \neq 0$  and  $||\dot{d}(t)|| \leq \mu$ , one can get from (10.7) that

$$\dot{V}_{o} \leq -\lambda_{\min}(\mathbf{L})||\mathbf{d}_{e}||^{2} + ||\mathbf{d}_{e}||\mu \leq -(\lambda_{\min}(\mathbf{L}) - \frac{1}{4})||\mathbf{d}_{e}||^{2} + \mu^{2} 
= -(1 - \alpha)\left(\lambda_{\min}(\mathbf{L}) - \frac{1}{4}\right)||\mathbf{d}_{e}||^{2} - \alpha\left(\lambda_{\min}(\mathbf{L}) - \frac{1}{4}\right)||\mathbf{d}_{e}||^{2} + \mu^{2}$$
(10.10)

where  $0 < \alpha < 1$  is a positive constant. Therefore

$$\dot{V}_o \le -(1-\alpha) \left( \lambda_{\min}(L) - \frac{1}{4} \right) ||d_e||^2, \forall ||d_e|| \ge \frac{2\mu}{\sqrt{\alpha(4\lambda_{\min}(L) - 1)}}$$
 (10.11)

To this end, it can be concluded from (10.11) and Definition 2.1 that the estimation error  $d_e$  is globally uniformly ultimately bounded.

Moreover, solving (10.11), one has

$$V_o(t) \le V_o(0) \exp(-2(1-\alpha)(\lambda_{\min}(L) - \frac{1}{4})t), \forall ||d_e|| \ge \frac{2\mu}{\sqrt{\alpha(4\lambda_{\min}(L) - 1)}}$$
(10.12)

and

$$||d_e|| \le \sqrt{2V_o(0)} \exp(-(1-\alpha)(\lambda_{\min}(L) - \frac{1}{4})t), \forall ||d_e|| \ge \frac{2\mu}{\sqrt{\alpha(4\lambda_{\min}(L) - 1)}}$$
(10.13)

Hence

$$||d_e|| \le \sqrt{2V_o(0)} \exp(-(1-\alpha)(\lambda_{\min}(L) - \frac{1}{4})t) + \frac{2\mu}{\sqrt{\alpha(4\lambda_{\min}(L) - 1)}}, \forall t \ge 0$$
(10.14)

Then, one can conclude from Definition 2.3 that the estimation error  $d_e$  converges with an exponential rate, i.e.,  $(1-\alpha)(\lambda_{\min}(L)-\frac{1}{4})$  to the ball with radius  $\frac{2\mu}{\sqrt{\alpha(4\lambda_{\min}(L)-1)}}$  for all  $d_e(\mathbf{0})$ .

Summarizing the above analysis for those two cases, the conclusions in Lemma 10.1 are then proved.

**Remark 10.1** It is seen in Lemma 10.1 that the presented observer can achieve an exponential estimation of slow-varying and even fast-varying modeling error. It can be obtained from (10.14) that the exponential rate can be tuned to be faster and the estimation accuracy of  $d_e$  can be governed to be higher by choosing larger observer gain L.

**Remark 10.2** In comparison with the existing ESO for modeling error or external disturbance, the observer (10.3) does not require the modeling error d to satisfy  $\dot{u}_d = 0$ ,  $\dot{u}_d \approx 0$ , or  $\lim \dot{u}_d = 0$ . As a sequence, the class of the modeling error that can be handled by the proposed observer is much larger than the existing DO, ESO [1, 12, 13], and SMO [3, 14]. Although both the observer (10.3) and the disturbance observer in [2] can avoid the drawback in the existing ESO or SMO, etc. the proposed observer (10.3) is more general and more systemic than the result in [2]. That is because the observer in [2] is applicable to linear systems only, while the observer (10.3) is feasible for a more general class of nonlinear systems. The observer proposed by [2] is a special case of the observer in (10.3). From this standpoint of view, the proposed observer (10.3) has wide application potential. Compared with the existing SMO, nonlinear DO, and HOSMO which do not necessitate the rate of change of the external disturbance to be zero or almost zero, the developed observer (10.3) can ensure the estimation error to be exponentially stable; furthermore, the observer (10.3) is characterized by a simple structure, and it necessitates inexpensive onboard computations.

# 10.2.3 Estimator for Satellite's Modeling Error

Because the inertia matrix J is positive-definite, the attitude dynamics (2.24) can be rewritten as

$$\dot{\omega} = -J^{-1}S(\omega)J\omega + J^{-1}u + J^{-1}u + J^{-1}u_d$$
 (10.15)

The transformed dynamics (10.15) can be described in the form of the nonlinear system (10.1) by denoting  $\mathbf{x} = \boldsymbol{\omega}$ ,  $f(\mathbf{x}) = -\mathbf{J}^{-1}S(\boldsymbol{\omega})\boldsymbol{J}\boldsymbol{\omega}$ ,  $g(\mathbf{x}) = \boldsymbol{J}^{-1}$ , and  $d = \boldsymbol{J}^{-1}\boldsymbol{u}_d$ . Then, the result presented in Sect. 10.2.1 can be applied to get the following theorem.

**Theorem 10.1** With the application of the observer (10.3) in Lemma 10.1, develop an estimation law as

$$\hat{\boldsymbol{u}}_d = \boldsymbol{J}(\hat{\boldsymbol{\xi}} + \boldsymbol{F}_2(\boldsymbol{x}_e)), \text{ or } \hat{\boldsymbol{u}}_d = \boldsymbol{J}\hat{\boldsymbol{d}}$$
 (10.16)

Choose the observer gain **L** such that  $\lambda_{min}(\mathbf{L}) - \frac{1}{4} > 0$ , then it follows that

- (R1) The estimation error  $\mathbf{u}_e = \mathbf{u}_d \hat{\mathbf{u}}_d$  is globally exponentially stable if  $\dot{\mathbf{u}}_d = \mathbf{0}$ .
- (R2) If  $\dot{\boldsymbol{u}}_d \neq \boldsymbol{0}$  and the rate of change of  $\boldsymbol{u}_d$  is bounded, i.e., there exists a positive scalar  $\mu_1 \in \mathbb{R}$  such that  $||\dot{\boldsymbol{u}}_d(t)|| \leq \mu_1$  for  $t \geq 0$ , then the estimation error  $\boldsymbol{u}_e$  converges with an exponential rate, equal to  $(1-\alpha)(\lambda_{\min}(\boldsymbol{L})-\frac{1}{4})$ , to the ball with radius  $\frac{2||\boldsymbol{J}||||\boldsymbol{J}^{-1}||\mu_1}{\sqrt{\alpha(4\lambda_{\min}(\boldsymbol{L})-1)}}$ , where  $0 < \alpha < 1$ .

**Proof** From the above denotations, it follows that  $u_d = Jd$  and

$$u_{e} = Jd - J\hat{d} = Jd_{e} \tag{10.17}$$

On the other hand, combing  $d = J^{-1}u_d$  with  $||\dot{u}_d(t)|| \le \mu_1$ , one has

$$||\boldsymbol{d}(t)|| = ||\boldsymbol{J}^{-1}\boldsymbol{u}_d|| \le ||\boldsymbol{J}^{-1}||\mu_1|$$
 (10.18)

Then, denoting  $\mu = ||\boldsymbol{J}^{-1}||\mu_1$  and following the proof of Lemma 10.1, Theorem 10.1 can be directly proved.

# 10.2.4 Observer-Based Exponential Controller

Let introduce another two new variables as  $z_1 = \sigma$  and  $z_2 = \omega + \alpha_1$ , where  $\alpha_1 = k_1 G^{\mathsf{T}}(\sigma) z_1$  and  $k_1 \in \mathbb{R}_+$  is a positive scalar. Then, it is ready to present the main solution in the following theorem to the attitude stabilization control problem.

**Theorem 10.2** For the rigid satellite attitude system (2.21) and (2.24) with modeling error, applying the disturbance estimation law (10.16), develop a nonlinear controller as

$$\boldsymbol{u} = -k_2 \boldsymbol{z}_2 - \boldsymbol{G}^{\mathrm{T}}(\boldsymbol{\sigma}) \boldsymbol{z}_1 + \boldsymbol{\omega}^{\times} \boldsymbol{J} \boldsymbol{\omega} - \boldsymbol{J} \dot{\boldsymbol{\alpha}}_1 - \hat{\boldsymbol{u}}_d$$
 (10.19)

where  $k_2 \in \mathbb{R}_+$  is a positive control gain. Suppose that the control gains are chosen such that

$$\lambda_{\min}(L) - 4l_1 - \frac{1}{4} > 0 \tag{10.20}$$

$$k_2 - \frac{||\boldsymbol{J}||^2}{l_1} > 0 \tag{10.21}$$

with  $l_1 \in \mathbb{R}_+$  being a positive scalar, then the following can be achieved.

- (R1) The closed-loop attitude system is globally exponentially stabilized if  $\dot{\mathbf{u}}_d = \mathbf{0}$ . The estimation error  $\mathbf{u}_e$ , the attitude  $\boldsymbol{\sigma}$ , and the angular velocity  $\boldsymbol{\omega}$  are globally exponentially stabilized.
- (R2) The closed-loop attitude system is ultimately uniformly bounded if  $\mathbf{u}_d \neq \mathbf{0}$  and the rate of change of  $\mathbf{u}_d$  is bounded, i.e., there exists a positive scalar  $\mu_1 \in \mathbb{R}$  such that  $||\dot{\mathbf{u}}_d(t)|| \leq \mu_1$  for all  $t \geq 0$ . More specifically, the attitude  $\boldsymbol{\sigma}$ , the estimation error  $\mathbf{u}_e$ , and the angular velocity  $\boldsymbol{\omega}$  converges with an exponential rate, equal to  $\kappa(1-\alpha)$ , to the ball with radius  $\frac{||J^{-1}||\mu_1|}{\sqrt{2\kappa\alpha}}$  where  $0 < \alpha < 1$  is a positive constant, and

$$\kappa = \min \left\{ \lambda_{\min}(\mathbf{L}) - 4l_1 - \frac{1}{4}, \frac{k_1}{16}, \frac{1}{\lambda_{\max}(\mathbf{J})} \left( k_2 - \frac{||\mathbf{J}||^2}{l_1} \right) \right\} > 0$$
 (10.22)

Remark 10.3 Because the proposed controller (10.19) can ensure the exponential stability of the closed-loop system in the presence of any type of modeling error, it can guarantee that the attitude control performance is more robust to modeling error. Moreover, for slow-varying or even fast-varying modeling error, it can be obtained from (10.22) that the attitude control accuracy can be ensured to be as high as possible by selecting appropriate gains. Larger  $\kappa$  will lead to a higher attitude stabilization accuracy. On the other hand, it is seen that the controller (10.19) is with a simple structure. It does not involve expensive computation. The controller (10.19) is actually a compensation control scheme. The included term  $-\hat{\boldsymbol{u}}_d$  is applied to compensate for the modeling error online and in real-time. Hence, this controller has less conservativeness in comparison with the existing robust modeling error attenuation/rejection controller for rigid satellites.

**Remark 10.4** For any rigid satellite in practice, its inertia J is bounded, and its varying rate  $\dot{J}$  is also bounded. The modeling error  $u_d$  acting on it is bounded practically. Moreover,  $\dot{u}_d$  is bounded at least. Otherwise, the rigid satellite will be out of control. Hence,  $\dot{d}$  is bounded for practical rigid satellites. The equation  $||\dot{u}_d(t)|| \le \mu_1$  is satisfied at least in practical engineering. Therefore, applying (R2) in Theorem 10.1 leads to the conclusion that all the signals involved in the closed-loop attitude system, with the developed controller, are uniformly ultimately bounded at least.

**Proof** Based upon the definition of  $z_1$  and  $z_2$ , it follows from (2.21) and Property 2.1 that

$$\dot{z}_1 = G(\sigma)(z_2 - \alpha_1) = -k_1 G(\sigma) G^{\mathrm{T}}(\sigma) z_1 + G(\sigma) z_2 
= -k_1 \left(\frac{1 + \sigma^{\mathrm{T}} \sigma}{4}\right)^2 z_1 + G(\sigma) z_2$$
(10.23)

For the attitude system (2.21)–(2.24), select a Lyapunov candidate function as  $V = V_o + V_1$ , where

$$V_1 = \frac{1}{2} z_1^{\mathrm{T}} z_1 + \frac{1}{2} z_2^{\mathrm{T}} J z_2 \tag{10.24}$$

Applying (2.24) and (10.23), differentiating (10.24) and inserting the control law (10.19) yield

$$\dot{V}_{1} = -k_{1}z_{1}^{\mathrm{T}} \left(\frac{1+\boldsymbol{\sigma}^{\mathrm{T}}\boldsymbol{\sigma}}{4}\right)^{2} z_{1} + z_{1}^{\mathrm{T}}\boldsymbol{G}(\boldsymbol{\sigma}) z_{2} + z_{2}^{\mathrm{T}}\boldsymbol{J}(\dot{\boldsymbol{\omega}} + \dot{\boldsymbol{\alpha}}_{1}) 
\leq -\frac{k_{1}}{16}||z_{1}||^{2} - k_{2}||z_{2}||^{2} + z_{2}^{\mathrm{T}}\boldsymbol{u}_{e}$$
(10.25)

Moreover, it can be obtained from (10.7) and (10.17) that the time derivative of V can be calculated as

$$\dot{V} \le -L d_e^{\mathrm{T}} d_e + d_e^{\mathrm{T}} \dot{d} - \frac{k_1}{16} ||z_1||^2 - k_2 ||z_2||^2 + z_2^{\mathrm{T}} J d_e$$
 (10.26)

Then, the following two cases are discussed to analyze the stability of  $d_e$ .

Case #1: If  $\dot{u}_d = 0$ , then it follows that  $\dot{d} = 0$ . At this time, one can further simplify (10.26) as

$$\dot{V} \leq -\lambda_{\min}(\boldsymbol{L})||\boldsymbol{d}_{e}||^{2} - \frac{k_{1}}{16}||\boldsymbol{z}_{1}||^{2} - k_{2}||\boldsymbol{z}_{2}||^{2} + \boldsymbol{z}_{2}^{T}\boldsymbol{J}\boldsymbol{d}_{e}$$

$$\leq -(\lambda_{\min}(\boldsymbol{L}) - 4l_{1})||\boldsymbol{d}_{e}||^{2} - \frac{k_{1}}{16}||\boldsymbol{z}_{1}||^{2} - \left(k_{2} - \frac{||\boldsymbol{J}||^{2}}{l_{1}}\right)||\boldsymbol{z}_{2}||^{2} \qquad (10.27)$$

$$\leq -2\gamma V$$

where  $\gamma = \min \left\{ \lambda_{\min}(L) - 4l_1, \frac{k_1}{16}, \frac{1}{\lambda_{\max}(J)} \left( k_2 - \frac{||J||^2}{l_1} \right) \right\} > 0$ . Then, using (10.17) and solving (10.27) yields  $V(t) \leq V(0)e^{-2\gamma t}$  or

$$||d_e(t)|| \le \sqrt{2V(0)} \exp(-\gamma t), ||u_e(t)|| \le \sqrt{2V(0)} \exp(-\gamma t)$$
 (10.28)

$$||z_1(t)|| \le \sqrt{2V(0)} \exp(-\gamma t), ||z_2(t)|| \le \sqrt{\frac{2V(0)}{\lambda_{\min}(J)}} \exp(-\gamma t)$$
 (10.29)

Hence, it can be concluded from (10.28) and (10.29) that the disturbance estimation error  $u_e(t)$ , the attitude  $\sigma$ , and the angular velocity  $\omega$  are globally exponentially stabilized, i.e.,  $\lim_{t\to\infty} ||\boldsymbol{u}_e(t)|| = 0$ ,  $\lim_{t\to\infty} ||\boldsymbol{\sigma}(t)|| = 0$ , and  $\lim_{t\to\infty} ||\boldsymbol{\omega}(t)|| = 0$ . Case #2: If  $\dot{\boldsymbol{u}}_d = 0$  and  $||\dot{\boldsymbol{u}}_d(t)|| \le \mu_1$ , then using the proof of Theorem 10.1 leads

(10.26) to be

$$\dot{V} \leq -(\lambda_{\min}(\boldsymbol{L}) - 4l_1)||\boldsymbol{d}_e||^2 + ||\boldsymbol{d}_e||||\boldsymbol{J}^{-1}||\mu_1 - \frac{k_1}{16}||z_1||^2 - \left(k_2 - \frac{||\boldsymbol{J}||^2}{l_1}\right)||z_2||^2 
\leq -\left(\lambda_{\min}(\boldsymbol{L}) - 4l_1 - \frac{1}{4}\right)||\boldsymbol{d}_e||^2 - \frac{k_1}{16}||z_1||^2 - \left(k_2 - \frac{||\boldsymbol{J}||^2}{l_1}\right)||z_2||^2 + ||\boldsymbol{J}^{-1}||^2\mu_1^2 
\leq -2\kappa V + ||\boldsymbol{J}^{-1}||^2\mu_1^2 
= -2\kappa (1 - \alpha)V - 2\kappa\alpha V + ||\boldsymbol{J}^{-1}||^2\mu_1^2$$
(10.30)

Then, it leads to

$$\dot{V} \le -2\kappa (1 - \alpha)V, \forall ||V(t)|| \ge \frac{||\boldsymbol{J}^{-1}||\mu_1|}{\sqrt{2\kappa\alpha}}$$
(10.31)

To this end, it can be concluded from (10.31) and Definition 2.1 that the closed-loop system is globally uniformly ultimately bounded.

Moreover, solving (10.31) results in

$$V(t) \le V(0) \exp(-2\kappa(1-\alpha)t), \forall ||V(t)|| \ge \frac{||J^{-1}||\mu_1|}{\sqrt{2\kappa\alpha}}$$
 (10.32)

and for all  $||V(t)|| \ge ||\boldsymbol{J}^{-1}||_{\sqrt{2\kappa\alpha}}$ , it can be got that

$$||\boldsymbol{d}_{e}(t)|| \leq \sqrt{2V(0)} \exp(-\kappa(1-\alpha)t), ||\boldsymbol{u}_{e}(t)|| = ||\boldsymbol{J}||\sqrt{2V(0)} \exp(-\kappa(1-\alpha)t)$$

$$(10.33)$$

$$||z_{1}(t)|| \leq \sqrt{2V(0)} \exp(-\kappa(1-\alpha)t), ||z_{2}(t)|| \leq \sqrt{\frac{2V(0)}{\lambda_{\min}(\boldsymbol{J})}} \exp(-\kappa(1-\alpha)t)$$

$$(10.34)$$

Applying Property 2.1 the definition of  $z_2$ , it follows that the following holds for all  $||V(t)|| \ge ||J^{-1}|| \frac{\mu_1}{\sqrt{2\kappa \alpha}}$ 

$$||\boldsymbol{\omega}|| = ||z_{2}|| + ||\boldsymbol{\alpha}_{1}|| \le ||z_{2}|| + k_{1}||\boldsymbol{G}(\boldsymbol{\sigma})||||z_{1}||$$

$$\le ||z_{2}|| + \frac{k_{1}}{4}||z_{1}|| \le \left(\sqrt{\frac{2V(0)}{\lambda_{\min}(\boldsymbol{J})}} + \frac{k_{1}}{4}\sqrt{2V(0)}\right) \exp(-\kappa(1-\alpha)t)$$
(10.35)

From (10.33)–(10.35), it can be proved that,

$$||\boldsymbol{u}_{e}(t)|| \le \beta_{1}||\boldsymbol{J}|| \exp(-\kappa(1-\alpha)t) + \zeta, \forall t \ge 0$$
 (10.36)

$$||\boldsymbol{\sigma}(t)|| \le \beta_1 \exp(-\kappa (1 - \alpha)t) + \zeta, \forall t \ge 0$$
 (10.37)

$$||\boldsymbol{\omega}(t)|| \le \beta \exp(-\kappa (1 - \alpha)t) + \zeta, \forall t \ge 0$$
 (10.38)

where  $\beta = \frac{\beta_1}{\sqrt{\lambda_{\min}(J)}} + \frac{k_1\beta_1}{4}$ ,  $\beta_1 = \sqrt{2V(0)}$ , and  $\varsigma = \frac{||J^{-1}||\mu_1|}{\sqrt{2\kappa\alpha}}$ . Then, it can be concluded from Definition 2.3 and (10.36)–(10.38) that the estimation error  $\boldsymbol{u}_e$ , the attitude  $\boldsymbol{\sigma}$ , and the angular velocity  $\boldsymbol{\omega}$  converge with an exponential rate (i.e.,  $\kappa(1-\alpha)$ ) to the ball with radius  $\varsigma = \frac{||J^{-1}||\mu_1|}{\sqrt{2\kappa\alpha}}$  for all the initial states. Summarizing the above analysis for those two cases, the conclusions in Theorem

Summarizing the above analysis for those two cases, the conclusions in Theorem 10.2 are then proved.

# 10.2.5 Rigid Microsatellite Example

Having shown in Sect. 10.2.4 that, the presented DO-based control scheme can accomplish the attitude stabilization maneuver with the desired control performance guaranteed, this section will present a numerical example of a currently being developed rigid satellite to validate that effectiveness in Theorems 10.1 and 10.2. This satellite is in a circular orbit. The altitude and the inclination of its orbit are designed to be 670 km and 90.5 degrees, respectively. This satellite's moment of inertia is  $J = [32, 1.1, -0.3; 1.1, 30, 0.8; -0.3, 0.8, 31] \, \text{kg} \cdot \text{m}^2$ . To validate the superior attitude stabilization performance of the designed controller despite the modeling error, simulations are carried out with the following two cases of modeling error considered, respectively.

- Case #1: An external disturbance having constant value is considered by assuming  $u_d = [0.01, 0.005, -0.008]^T \text{ N} \cdot \text{m}$ .
- Case #2: In this case, the satellite is assumed to be under the effect of the following time-varying external disturbance:

$$\mathbf{u}_d = [u_{d1}, u_{d2}, u_{d3}]^{\mathrm{T}} \,\mathrm{N} \cdot \mathrm{m}, u_{di} = \sin(\mu_i t + \eta_i)$$
 (10.39)

where 
$$\mu_1 = 80$$
,  $\mu_2 = 50$ ,  $\mu_3 = 20$ ,  $\eta_1 = 0.5$ ,  $\eta_2 = 0.3$ , and  $\eta_3 = 0.9$ .

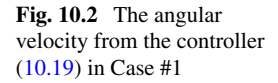
When conducting all simulations, the mathematical model (2.21) and (2.24) are applied in conjunction with the DO-based controller (10.19). The control gains are chosen as  $k_1 = 15$ ,  $k_2 = 14.5$ ,  $l_1 = 75$ ,  $L = \text{diag}([305, 305, 305]^T)$ ,  $F_1 = 250I_3$ , and  $\alpha = 0.5$ . The initial attitude of this rigid satellite is  $\sigma(0) = [0.4, -0.3, -0.5]^T$  with its initial angular velocity set as  $\omega(0) = [0, 0, 0]^T$  rad/s.

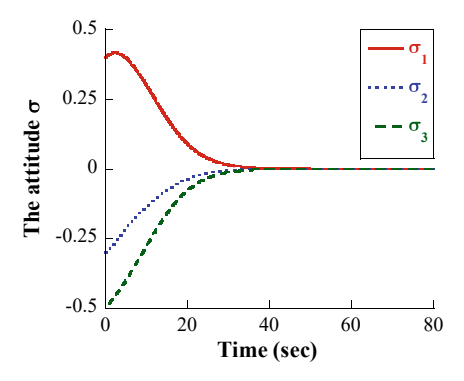
### A Simulation Results of Case #1

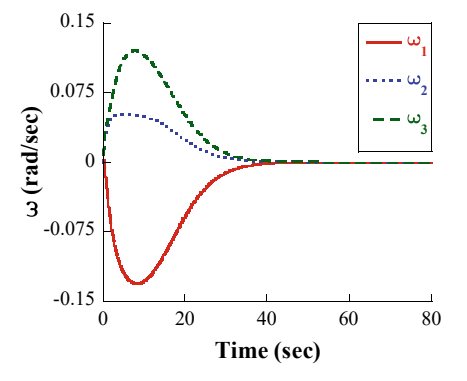
In this case, the attitude stabilization results by the presented controller (10.19) can be seen in Figs. 10.1 and 10.2. The attitude and the angular velocity are successfully stabilized after about 50 s. Moreover, after going to see the steady-state behavior of the attitude and the angular velocity, the control accuracy with  $|\sigma_i| \leq 10^{-10}$  and  $|\omega_i| \leq 10^{-10}$  rad/s, i=1,2,3 can be observed. The convergence of the attitude and the angular velocity are illustrated in Figs. 10.3 and 10.4, respectively. The inequality (10.29) is verified. The exponential stability of the closed-loop attitude system is seen despite the constant external disturbance. The conclusion (R1) in the Theorem 10.3 is validated. The control torque required to ensure that perfect attitude stabilization performance is shown in Fig. 10.4.

The above attitude stabilization result with exponential convergence is owing to the incorporated DO (10.16). When the controller (10.19) is applied to this case, the estimation error of the constant external disturbance is shown in Fig. 10.5. It is seen that the disturbance is precisely estimated after 50 s. More specifically, it is seen in Fig. 10.6 that the inequality (10.28) is strictly satisfied. The conclusion that the estimation error is exponentially stable in the presence of constant disturbance is validated.

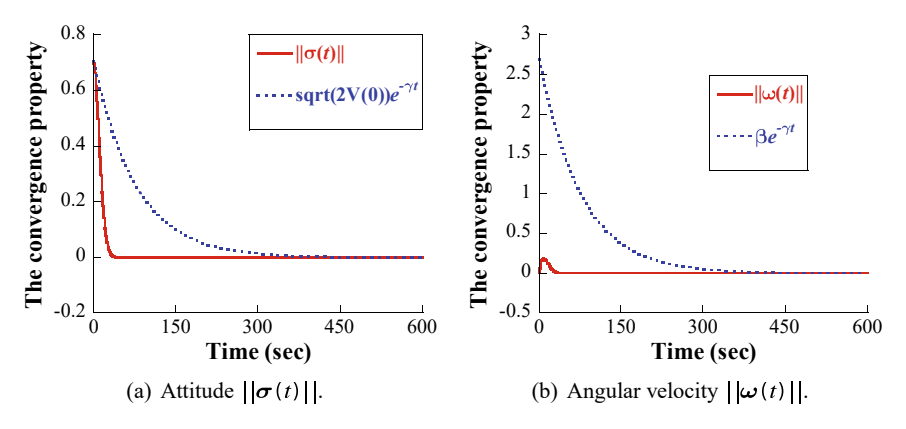
**Fig. 10.1** The attitude from the controller (10.19) in Case #1

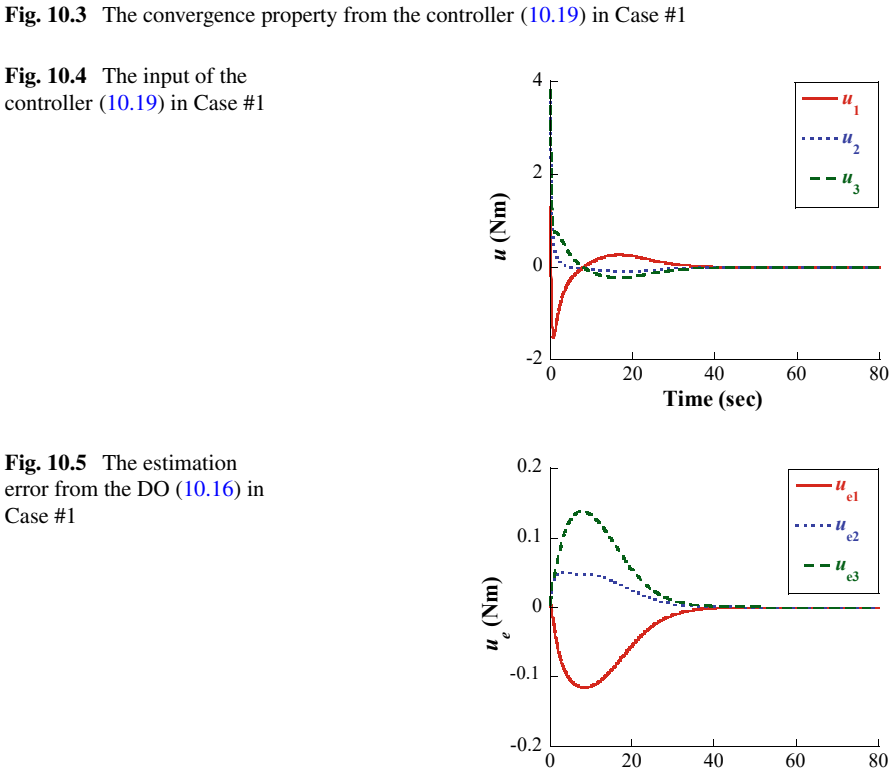






Time (sec)





### **B** Simulation Results of Case #2

When the time-varying external disturbance (10.39) is considered in this case, applying the developed DOB control law (10.19) to the satellite's attitude system, it is found that the attitude stabilization maneuver can be still accomplished. This can

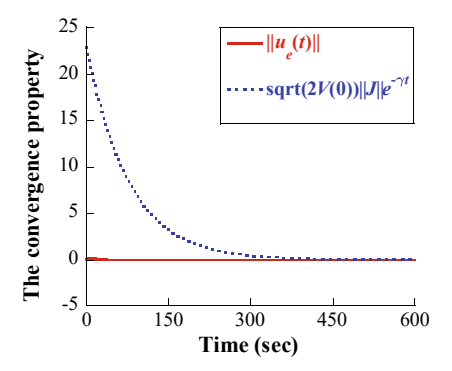


Fig. 10.6 The convergence property of the DO (10.16) in Case #1

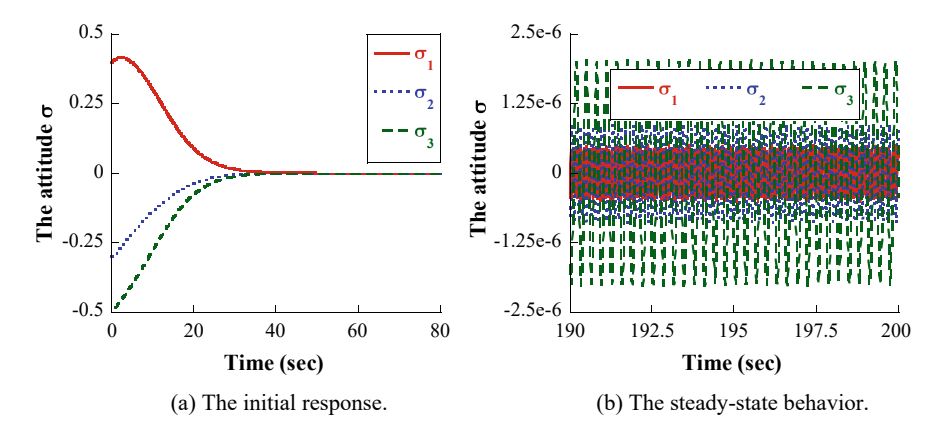


Fig. 10.7 The attitude from the controller (10.19) in Case #2

be verified by the results shown in Figs. 10.7 and 10.8. The attitude and the angular velocity are stabilized within 50 s. Moreover, it can be obtained from Fig. 10.7b that the attitude control accuracy is governed to be  $|\sigma_i| \leq 2.5 \times 10^{-6}$ , i=1,2,3. The steady-state behavior in Fig. 10.8b shows that the controller leads the angular velocity, i.e., the attitude stability, to be  $|\omega_i| \leq 1.7 \times 10^{-4}$  rad/s, i=1,2,3. These attitude pointing accuracy and attitude stability are very high even in the presence of a time-varying external disturbance (10.39). It can satisfy the stringent requirements of the attitude control system to accomplish the planned missions. Figure 10.9 shows the estimation error achieved by the incorporated DO (10.16). The external disturbance (10.39) is precisely estimated by the  $\hat{\boldsymbol{u}}_d$  in (10.16) after about 50 s. Moreover, it can be seen from its steady-state behavior in Fig. 10.9b that the estimation accuracy of the disturbance is  $|u_{ei}| \leq 3.0 \times 10^{-4} \mathrm{N} \cdot \mathrm{m}$ , i=1,2,3.

The convergence behavior of  $||u_e(t)||$ ,  $||\sigma(t)||$ , and  $||\omega(t)||$  are illustrated in Figs. 10.10, 10.11 and 10.12, respectively. In addition, it can be got from (10.39) that  $\mu_1 = 96.4365$ . Using the chosen control gains, one has  $\varsigma = 0.033078$ . Then, the

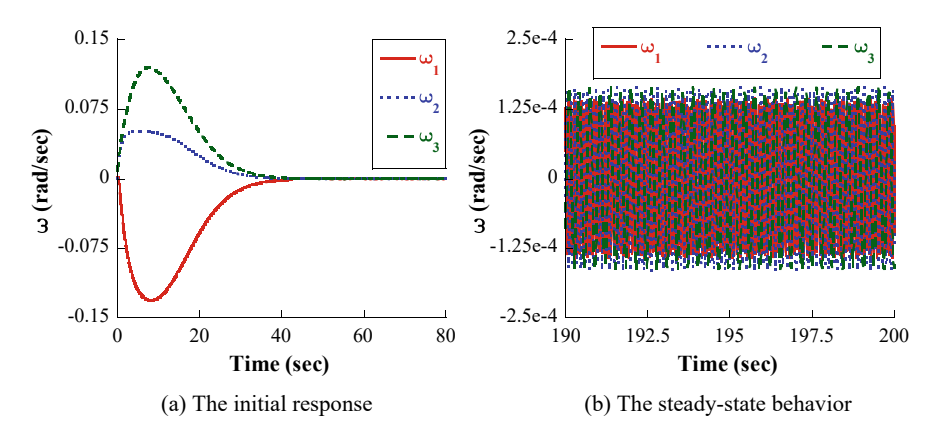


Fig. 10.8 The angular velocity from the controller (10.19) in Case #2

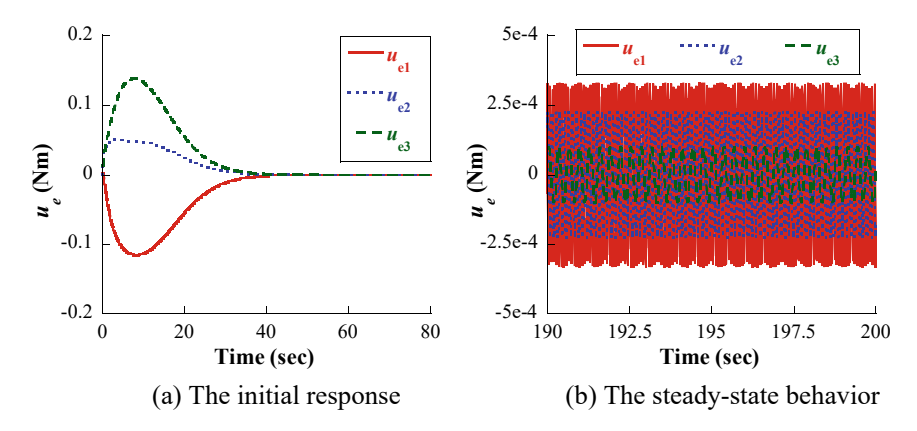


Fig. 10.9 The estimation error from the DO (10.16) in Case #2

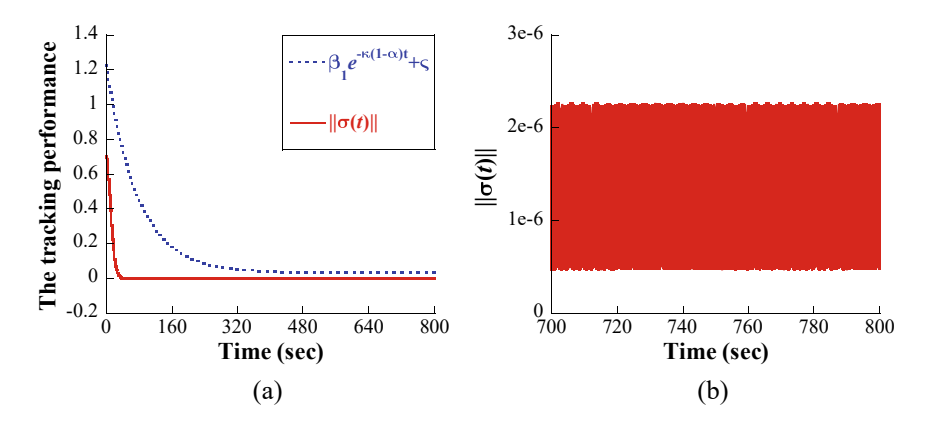


Fig. 10.10 The convergence of the attitude from the controller (10.19) in Case #2

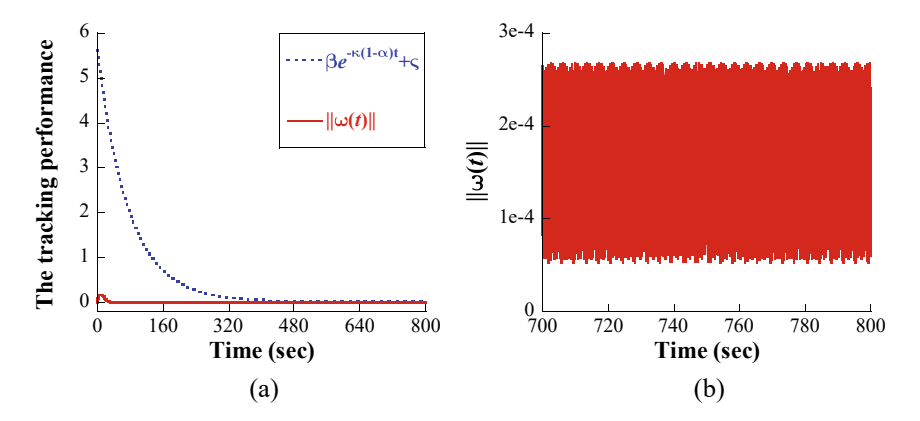


Fig. 10.11 The convergence of the angular velocity from the controller (10.19) in Case #2

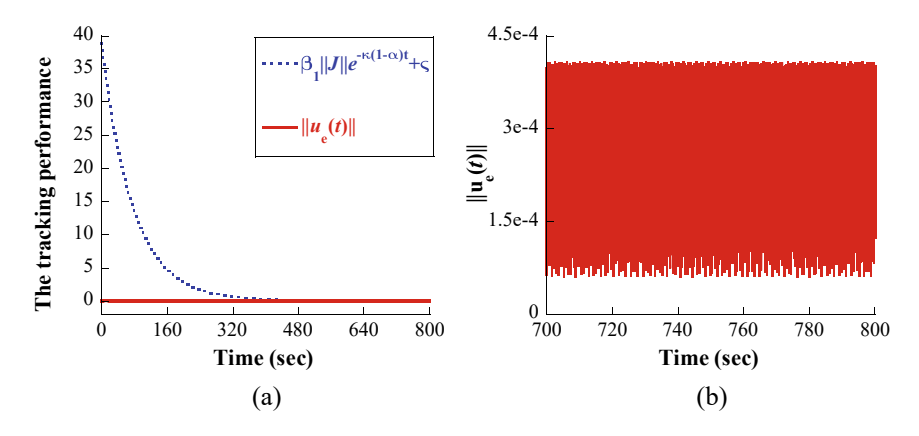


Fig. 10.12 The convergence property of the DO (10.16) in Case #2

inequalities (10.36)–(10.38) can be validated. To this end, it can be summarized from the above results that the attitude and the angular velocity are exponentially stabilized to a residual set around the equilibrium points with a radius  $\varsigma$ . The conclusion (R2) in the Theorem 10.1 is hence verified. The control torque consumed to achieve this exponential stability is shown in Fig. 10.13. It is seen in Fig. 10.13b that the control input is not zero when the attitude is stabilized. That is, because extra control torque, i.e., the term  $-\hat{\boldsymbol{u}}_d$  in (10.19), should be functional to compensate for the external disturbance.

### **C** Discussion

To quantitatively evaluate the proposed DOB control approach, the attitude pointing accuracy, and the attitude stability are used as two control performance indexes.

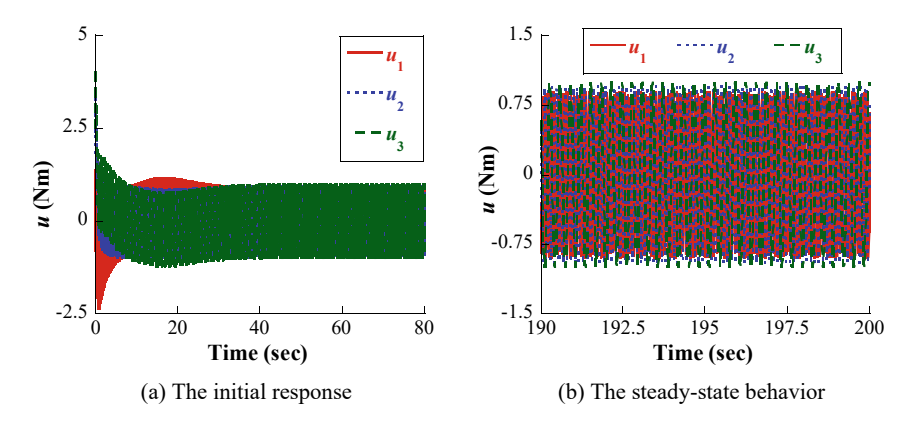


Fig. 10.13 The input of the controller (10.19) in Case #2

Moreover, the estimation accuracy of the disturbance is adopted as a performance index to evaluate the estimation performance of the proposed observer. On the other hand, to verify the sensitivity of the proposed approach to sensor noise, more simulations are carried out for case #1 and case #2 with measurement noise considered. The attitude and the angular velocity sensor noises are assumed to be a zero-mean Gaussian random variable with a variance of 0.0001, respectively. For case #1 and case #2, in the presence of measurement noises, the convergence behavior of the attitude  $\sigma$ , the angular velocity  $\omega$ , and the disturbance estimation error  $u_{\ell}$  are the same as the results when the measurement noises are not considered, respectively. The only difference is that the control accuracy and the estimation accuracy in the presence of noises are inferior to the accuracy in the absence of measurement noises. The obtained attitude control performance and the disturbance estimation performance are listed in Table 10.1. It is observed that although the measurement noise will deteriorate the attitude control performance and the external disturbance estimation performance, the estimation accuracy, the attitude pointing accuracy, and the angular velocity control accuracy still satisfy (10.36)–(10.38), respectively. The exponential stability is still achieved despite sensor noise. Hence, the proposed control approach has great application potential for engineering.

## 10.3 Attitude Exponential Tracking Control

# 10.3.1 Modeling of Actuator Uncertainties

In practical aerospace engineering, the actuators fixed in the satellite usually have uncertainties. More specifically, the actuator misalignment due to finite manufacturing technique and the actuator faults due to component aging are the widely known uncertainties in satellite actuators. It is known from [15] that the actuator faults of

The performance	Simulation condition				
indexes	Without measurement noise		With measurement noise		
	Case #1	Case #2	Case #1	Case #2	
The attitude control accuracy $ \sigma_i $ , $i = 1, 2, 3$	$7.0 \times 10^{-19}$	$2.5 \times 10^{-6}$	$4.0 \times 10^{-6}$	$1.2 \times 10^{-4}$	
The attitude stability $ \omega_i $ (rad/s), $i = 1, 2, 3$	$3.0 \times 10^{-22}$	$1.7 \times 10^{-4}$	$1.5 \times 10^{-4}$	$3.8 \times 10^{-4}$	
The disturbance estimation accuracy $ u_{ei} (N \cdot m), i = 1, 2, 3$	$3.5 \times 10^{-12}$	$3.0 \times 10^{-4}$	$2.7 \times 10^{-5}$	$1.4 \times 10^{-3}$	

Table 10.1 Comparison of the control performance from the controller (10.19)

satellite can be mathematically modeled as

$$\boldsymbol{\tau}_o = (\boldsymbol{I}_N - \boldsymbol{E})\boldsymbol{\tau} + \Delta \boldsymbol{\tau} \tag{10.40}$$

where  $\boldsymbol{\tau} = [\tau_1, \tau_2, \ldots, \tau_N]^T \in \mathbb{R}^n$  is the commanded torque of actuator's controller,  $\boldsymbol{\tau}_o \in \mathbb{R}^n$  is the actual output torque of actuators,  $\boldsymbol{I}_N$  is an  $N \times N$  identity matrix, the diagonal matrix  $\boldsymbol{E} = \text{diag}([e_1, e_2, \ldots, e_N]^T) \in \mathbb{R}^{N \times N}$  with  $0\% \le e_i \le 100\%$  denotes the effectiveness of all the actuators, i = 1, 2, ..., N,  $\Delta \boldsymbol{\tau} = [\Delta \tau_1, \Delta \tau_2, \ldots, \Delta \tau_N]^T \in \mathbb{R}^n$  is the bias fault vector of the actuators, and  $N \ge 3$  is the total number of actuators fixed in the satellite to perform attitude maneuvers.

Let  $\boldsymbol{D}_0 \in \mathbb{R}^{3 \times N}$  and  $\Delta \boldsymbol{D} \in \mathbb{R}^{3 \times N}$  be the nominal alignment and the corresponding misalignment matrix of actuators, respectively; the actuator uncertainties including the misalignment and faults can be mathematically modeled as

$$\boldsymbol{u} = (\boldsymbol{D}_0 + \Delta \boldsymbol{D})\boldsymbol{\tau}_o = (\boldsymbol{D}_0 + \Delta \boldsymbol{D})((\boldsymbol{I}_N - \boldsymbol{E})\boldsymbol{\tau} + \Delta \boldsymbol{\tau}) \tag{10.41}$$

It is seen that  $\tau_o$  in (10.41) is the actual torque generated by the faulty actuators. Hence,  $D_0\tau_o$  denotes the nominal three-axis control torque acting on the satellite,  $\Delta D\tau_o$  is the generated error torque due to the actuator misalignment, while  $\tau_o = (I_N - E)\tau + \Delta \tau$  is the actual output torque generated by the faulty actuators.

Because the actuators have misalignment, the inertia matrix J will be unknown. Let the positive-definite constant matrix  $J_0 \in \mathbb{R}^{3\times 3}$  denote the nominal inertia of satellite, and let the unknown and even time-varying matrix  $\Delta J \in \mathbb{R}^{3\times 3}$  be the uncertain inertia induced by actuator misalignment and fuel consumption, etc. Then, one has  $J = J_0 + \Delta J$ .

## 10.3.2 Problem Description

The problem of attitude tracking will be investigated in this section. Let the desired attitude trajectory be determined as  $\mathbf{\Theta}_d = [\phi_d, \theta_d, \psi_d]^{\mathrm{T}} \in \mathbb{R}^3$  with  $-\frac{\pi}{2} < \theta_d < \frac{\pi}{2}$ . Then, the problem description of this section can be formulated as: For the rigid satellites with their attitude system described by (2.15) and (2.24), suppose that the initial attitude of the satellite is such that  $-\frac{\pi}{2} < \theta(0) < \frac{\pi}{2}$ , then develop a control law  $\tau$  for attitude tracking maneuvering. The controller should have the self-resilient control capability of accommodating the modeling error due to external disturbance, actuator uncertainties, and uncertainties in the inertia.  $\mathbf{\Theta}_d$  is ensured to be followed by  $\mathbf{\Theta}$  with the tracking error  $\mathbf{\Theta}_e = [\phi_e, \theta_e, \psi_e]^{\mathrm{T}} = \mathbf{\Theta}_d - \mathbf{\Theta}$  practically exponentially stabilized, while  $-\frac{\pi}{2} < \theta(t) < \frac{\pi}{2}$  is guaranteed for  $t \geq 0$  by choosing appropriate control gains.

## 10.3.3 System Transformation

Taking the actuator uncertainties (10.41), the disturbance, and the uncertain inertia  $\Delta J$  into consideration, the rigid satellite attitude system (2.15) and (2.24) can be rewritten as

$$\dot{\mathbf{\Theta}} = \boldsymbol{\omega} + \Delta \boldsymbol{f}_1(\mathbf{\Theta}, \dot{\mathbf{\Theta}}) \tag{10.42}$$

$$\boldsymbol{J}_0 \dot{\boldsymbol{\omega}} = -\boldsymbol{\omega}^{\times} \boldsymbol{J}_0 \boldsymbol{\omega} + \boldsymbol{D}_0 \boldsymbol{\tau} + \Delta \boldsymbol{f}_2(t, \boldsymbol{\omega}, \dot{\boldsymbol{\omega}})$$
 (10.43)

where  $\Delta f_1(\mathbf{\Theta}, \dot{\mathbf{\Theta}}) = -(\mathbf{R}(\mathbf{\Theta}) - \mathbf{I}_3)\dot{\mathbf{\Theta}} - \boldsymbol{\omega}_c(\mathbf{\Theta})$  and

$$\Delta f_2(t, \boldsymbol{\omega}, \dot{\boldsymbol{\omega}}) = \boldsymbol{u}_d - \boldsymbol{\omega}^{\times} \Delta \boldsymbol{J} \boldsymbol{\omega} - \boldsymbol{D}_0 \boldsymbol{E} \boldsymbol{\tau} + \boldsymbol{D}_0 \Delta \boldsymbol{\tau} + \Delta \boldsymbol{D} ((\boldsymbol{I}_N - \boldsymbol{E}) \boldsymbol{\tau} + \Delta \boldsymbol{\tau}) - \Delta \boldsymbol{J} \dot{\boldsymbol{\omega}}$$
(10.44)

Here,  $\Delta f_1(\Theta, \dot{\Theta})$  can be viewed as the uncertainty in the attitude kinematics.  $\Delta f_2(t, \omega, \dot{\omega})$  denotes the uncertainty in the attitude dynamics, which is induced by the disturbance  $u_d$ , the actuator uncertainties, and the uncertain inertia  $\Delta J$ .

Let introduce a new variable as  $x = [\boldsymbol{\Theta}^{T}, \boldsymbol{\omega}^{T}]^{T}$ , then one can rewrite (10.42) and (10.43) as

$$A\dot{x} = f(x) + U + \Delta f \tag{10.45}$$

where 
$$\pmb{A} = \begin{bmatrix} \pmb{I}_3 & \pmb{0} \\ \pmb{0} & \pmb{J}_0 \end{bmatrix}, \pmb{f}(\pmb{x}) = \begin{bmatrix} \pmb{\omega} \\ -\pmb{\omega}^{\times} \pmb{J}_0 \pmb{\omega} \end{bmatrix}, \pmb{U} = \begin{bmatrix} \pmb{0} \\ \pmb{D}_0 \pmb{\tau} \end{bmatrix}, \Delta \pmb{f} = \begin{bmatrix} \Delta \pmb{f}_1(\pmb{\Theta}, \dot{\pmb{\Theta}}) \\ \Delta \pmb{f}_2(t, \pmb{\omega}, \dot{\pmb{\omega}}) \end{bmatrix}.$$

In (10.45), the vector f(x) is known, and the vector  $\Delta f$  can be viewed as the system uncertainties. To guarantee the successful maneuver of attitude tracking, in combination with the transformed system (10.45), a novel observer-based practically exponential and resilient control approach will be developed in this section. The architecture of this resilient control in the attitude system is illustrated in Fig. 10.14.

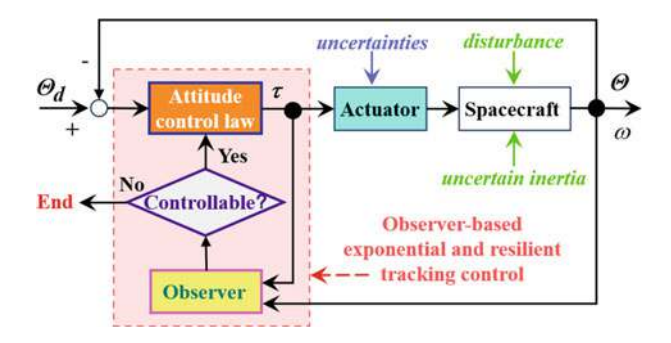


Fig. 10.14 The attitude tracking system ensured by the observer-based practically exponential and resilient control approach

For this control scheme, a novel observer is preliminarily synthesized to reconstruct the lumped uncertainties  $\Delta f$ . The output of the observer is then applied to evaluate whether the rigid satellite attitude system is controllable or not. If the evaluation result is positive, then the output of the observer and the system measurements will be feedback to synthesize a resilient control law to ensure that the overall attitude tracking system is exponentially stabilized. Otherwise, the satellite attitude will not be resilient. The attitude tracking maneuver should be ended.

## 10.3.4 Disturbance Observer for Uncertainties

Using the definition of  $\Delta \dot{f}_1(\Theta, \dot{\Theta})$ , it can be obtained that

$$\Delta \dot{\mathbf{f}}_{1}(\mathbf{\Theta}, \dot{\mathbf{\Theta}}) = -\frac{d\mathbf{R}(\mathbf{\Theta})}{dt}\dot{\mathbf{\Theta}} - (\mathbf{R}(\mathbf{\Theta}) - \mathbf{I}_{3})\ddot{\mathbf{\Theta}} - \frac{d\boldsymbol{\omega}_{c}(\mathbf{\Theta})}{dt}$$
(10.46)

In practice, the angular velocity and the angular jerk-acceleration of the satellite are bounded, i.e.,  $\dot{\Theta}$  and  $\ddot{\Theta}$  are bounded. Hence,  $\Delta \dot{f}_1(\Theta, \dot{\Theta})$  will be bounded. There exists a positive constant  $l_1 \in \mathbb{R}_+$  such that

$$||\Delta \dot{\boldsymbol{f}}_{1}(\boldsymbol{\Theta}, \dot{\boldsymbol{\Theta}})|| \le l_{1} \tag{10.47}$$

Because  $\Delta f_2(t, \omega, \dot{\omega})$  denotes the uncertain torque acting on the attitude dynamics,  $\Delta \dot{f}_2(t, \omega, \dot{\omega})$  should be also be bounded. Otherwise,  $\Delta f_2(t, \omega, \dot{\omega})$  will be not bounded, and the attitude of the satellite will be out of control. Therefore, a positive scalar  $l_2 \in \mathbb{R}$  will also exist to satisfy

$$||\Delta \dot{\boldsymbol{f}}_2(t, \boldsymbol{\omega}, \dot{\boldsymbol{\omega}})|| \le l_2 \tag{10.48}$$

From (10.47) and (10.48), it yields

$$||\Delta \dot{f}|| = \sqrt{\sum_{i=1}^{2} ||\Delta \dot{f}_i||} \le l = \sqrt{l_1^2 + l_2^2}$$
 (10.49)

Based on the above analysis, it is ready to present the following estimation law to precisely estimate the total uncertainties  $\Delta f$ 

$$\Delta f_O = \xi + k_o A x \tag{10.50}$$

where  $k_o \in \mathbb{R}$  is a positive scalar,  $\Delta f_O = [\Delta f_{O1}^T, \Delta f_{O2}^T]^T \in \mathbb{R}^6$  is the estimation of  $\Delta f$ , and  $\xi \in \mathbb{R}^6$  is the following observer's output:

$$\dot{\hat{\xi}} = -k_o \hat{\xi} + k_o (-f(x) - U - k_o A x)$$
 (10.51)

**Theorem 10.3** For the system (10.45), choose the estimation gain such that  $2k_o - 1 > 0$ , then the estimation law (10.50) can govern the estimation error  $\Delta f_e = [\Delta f_{e1}^T, \Delta f_{e2}^T]^T = \Delta f - \Delta f_O$  to converge with an exponential rate, equal to  $0.5(1 - \eta_1)(2k_o - 1)$ , to the ball with radius  $\frac{1}{\sqrt{\eta_1(2k_o - 1)}}$ , where  $0 < \eta_1 < 1$  is a positive scalar.

**Proof** From (10.45), (10.50), and (10.51), it can be obtained that the dynamics of  $x_e$  is such that

$$\Delta \dot{f}_{e} = \Delta \dot{f} - \Delta \dot{f}_{o} = \Delta \dot{f} - \dot{\xi} - k_{o} A \dot{x} = -k_{o} \Delta f_{e} + \Delta \dot{f}$$
 (10.52)

Choose a Lyapunov function for (10.52) as  $V_3 = \frac{1}{2} \Delta f_e^T \Delta f_e$ , applying (10.49) leads to

$$\dot{V}_{3} = -k_{o}||\Delta f_{e}||^{2} + \Delta f_{e}^{T} \Delta \dot{f} \leq -k_{o}||\Delta f_{e}||^{2} + l||\Delta f_{e}|| 
\leq -(k_{o} - \frac{1}{2})||\Delta f_{e}||^{2} + \frac{1}{2}l^{2} 
= -(1 - \eta_{1})(k_{o} - 0.5)||\Delta f_{e}||^{2} - \eta_{1}(k_{o} - 0.5)||\Delta f_{e}||^{2} + 0.5l^{2}$$
(10.53)

Then, it follows that

$$\dot{V}_3 \le -(1 - \eta_1) \left( k_o - \frac{1}{2} \right) ||\Delta f_e||^2, \, \forall ||\Delta f_e|| \ge \frac{l}{\sqrt{\eta_1 (2k_o - 1)}}$$
 (10.54)

Moreover, solving inequality (10.54) results in

$$||\Delta f_e|| \le \sqrt{2V_3(0)} \exp(-\frac{(1-\eta_1)(2k_o-1)}{2}t), \forall ||\Delta f_e|| \ge \frac{l}{\sqrt{\eta_1(2k_o-1)}}$$

Hence,

$$||\Delta f_e|| \le \sqrt{2V_3(0)} \exp(-\frac{(1-\eta_1)(2k_o-1)}{2}t) + \frac{l}{\sqrt{\eta_1(2k_o-1)}}, \forall t \ge 0 \quad (10.56)$$

This proves that the estimation error  $\Delta f_e$  of the uncertainties converges with an exponential rate (i.e.,  $0.5(1-\eta_1)(2k_o-1)$ ) to the ball with a radius  $\frac{l}{\sqrt{\eta_1(2k_o-1)}}$  for all  $\Delta f_e(\mathbf{0})$ .

It is seen in (10.56) that larger  $k_o$  leads to smaller  $||\Delta f_e||$ . It means that the estimation accuracy of  $||\Delta f_e||$  will be increased by tuning large  $k_o$ . Moreover, larger  $k_o$  also results in a faster convergence rate of the estimation error  $||\Delta f_e||$ . In addition, it can be obtained from (10.56) that

$$||\Delta f_{e2}|| \le \sqrt{2V_3(0)} \exp(-\frac{(1-\eta_1)(2k_o-1)}{2}t) + \frac{l}{\sqrt{\eta_1(2k_o-1)}}, \forall t \ge 0$$
(10.57)

Therefore, choosing larger  $k_o$  can ensure  $||\Delta f_{e2}|| \approx 0$  and  $||\Delta f_2(t, \boldsymbol{\omega}, \dot{\boldsymbol{\omega}})|| \approx ||\Delta f_{O2}||$ . Then, it is ready to design the following controllability determination mechanism for the three-axis attitude control system.

Controllability determination mechanism: If  $||\Delta f_{O2}|| < ||D_0\tau||$ , then the satellite is three-axis attitude controllable. Otherwise, the attitude is out of out.

**Remark 10.5** In fact,  $||\Delta f_{O2}|| < ||D_0\tau||$  means that the uncertain torque induced by disturbance, actuator uncertainty, and uncertain inertia, is smaller than the remaining control power supplied by actuators. Then, the uncertain torque can be compensated. Otherwise, the uncertain torque will lead to the instability of the closed-loop system, because the open-loop system is unstable.

## 10.3.5 Observer-Based Resilient Controller

Introduce another new variable as  $z_1 = \dot{\mathbf{\Theta}}_d - \boldsymbol{\omega} + k_{c1} \mathbf{\Theta}_e - \Delta f_{O1}$ , where  $k_{c1} \in \mathbb{R}_+$  is a positive gain. For the nominal inertia  $J_0$ . Then, the main solution to the attitude tracking problem of satellite with actuator uncertainties, disturbances, and uncertain inertia is presented as follows.

**Theorem 10.4** Consider a rigid satellite with its attitude system described by (2.15) and (2.24), with the application of the estimation law (10.50), and let the attitude controller be designed as

$$\boldsymbol{\tau} = (\boldsymbol{D}_0)^{\dagger} (\boldsymbol{J}_0 \ddot{\boldsymbol{\Theta}}_d + k_{c1} \boldsymbol{J}_0 \dot{\boldsymbol{\Theta}}_e + \boldsymbol{\omega}^{\times} \boldsymbol{J}_0 \boldsymbol{\omega} - \Delta \boldsymbol{f}_{O2} + \boldsymbol{\Theta}_e + k_{c2} \boldsymbol{z}_1)$$
(10.58)

where  $k_{c2} \in \mathbb{R}_+$  is a positive constant. If the gains of the estimation law and the controller are selected such that

$$k_o > 3, k_{c1} > 1, k_{c2} > 0.5k_o||\boldsymbol{J}_0||^2$$
 (10.59)

Then, the closed-loop system will be practically exponentially stable. The estimation error  $\Delta f_e$ , the attitude tracking error  $\Theta_e$ , and the tracking error  $\dot{\Theta}_e$  of the velocity will converge with an exponential rate, equal to  $\kappa(1-\eta_2)$ , to the ball with a radius  $\varepsilon = \frac{1}{2\sqrt{\kappa\eta_2}}$ , where  $0 < \eta_2 < 1$  is a positive scalar, and

$$\kappa = \min \left\{ \frac{k_o - 3}{2}, k_{c1} - 1, \frac{1}{\lambda_{\text{max}}(\boldsymbol{J})} \left( k_{c2} - \frac{k_o}{2} ||\boldsymbol{J}_0||^2 \right) \right\} > 0$$
 (10.60)

Remark 10.6 It is seen in Theorem 10.4 that the controller (10.58) practically exponentially stabilize the closed-loop tracking system. In comparison with the existing approaches ensuring asymptotic stability or ultimately uniformly stability, the controller (10.58) can ensure the attitude tracking performance is more robust and self-resilient to the disturbances, the uncertain inertia parameters, and the actuator uncertainties.

**Remark 10.7** It can be seen in Theorems 10.3 and 10.4 that the gains' selection of the observer (10.50) and the controller (10.26)) are independent of the upper bound l of the uncertainty  $\Delta f$ . The term l is mathematically denoted to establish the formula for the estimation accuracy  $\frac{l}{\sqrt{\eta_1(2k_o-1)}}$ , and the control accuracy  $\frac{l}{2\sqrt{\kappa\eta_2}}$ . The implementation of the observer (10.50) and the controller (10.58) do not necessitate the value of l.

From Theorem 10.3 and the presented *controllability determination mechanism*, it is known that:

- Case #1: If the uncertain torque  $||\Delta f_2||$  is less than the remaining control power  $||D_0\tau||$ , then  $\Delta f_2$  will be precisely estimated by  $\Delta f_{O2}$ . Meanwhile, the term  $-\Delta f_{O2}$  in the controller (10.58) will compensate for the uncertainty  $\Delta f_2$ , and then the closed-loop system will be stabilized even in the presence of system uncertainty and actuator uncertainties. The actuator misalignment torque  $D\tau_o$ , the actuator faults  $\tau_o$ , the external disturbance  $u_d$ , and the system uncertainty induced by  $\Delta J$  are precisely estimated and compensated by the proposed scheme.
- Case #2: When  $||\Delta f_2||$  is larger than the remaining control effort  $||D_0\tau||$ , then it can be detected by the observer that the attitude system is out of control.

Moreover, the above two cases are handled by the proposed approach automatically without any other interface. From this standpoint of view, it can be claimed that the proposed controller (10.58) has great self-resilient control capability of handling these uncertainties.

# 10.3.6 Stability Analysis

The Lyapunov stability theory can be applied to prove Theorem 10.4 with the proof organized as follows.

**Proof** Based upon (10.42) and the definition of  $\Theta_e$  and  $z_1$ , it has

$$\dot{\mathbf{\Theta}}_{e} = \dot{\mathbf{\Theta}}_{d} - \boldsymbol{\omega} - \Delta f_{1}(\mathbf{\Theta}, \dot{\mathbf{\Theta}}) = z_{1} - k_{c1}\mathbf{\Theta}_{e} - \Delta f_{e1}$$
(10.61)

It can be further obtained from (10.43) that

$$J_0 \dot{z}_1 = J_0 (\ddot{\boldsymbol{\Theta}}_d - \dot{\boldsymbol{\omega}} + k_{c1} \dot{\boldsymbol{\Theta}}_e - \Delta \dot{\boldsymbol{f}}_{O1})$$

$$= J_0 \ddot{\boldsymbol{\Theta}}_d + k_{c1} J_0 \dot{\boldsymbol{\Theta}}_e + \boldsymbol{\omega}^{\times} J_0 \boldsymbol{\omega} - \boldsymbol{D}_0 \boldsymbol{\tau} - J_0 \Delta \dot{\boldsymbol{f}}_{O1} - \Delta \boldsymbol{f}_2$$
(10.62)

Inserting the controller (10.58) into (10.62), (10.62) can be simplified as

$$J_0 \dot{z}_1 = -\Theta_e - k_{c2} z_1 - J_0 \Delta \dot{f}_{O1} - \Delta f_{e2}$$
 (10.63)

To this end, let a Lyapunov candidate function be chosen as

$$V_4 = \frac{1}{2} \Delta \boldsymbol{f}_e^{\mathrm{T}} \Delta \boldsymbol{f}_e + \frac{1}{2} \boldsymbol{\Theta}_e^{\mathrm{T}} \boldsymbol{\Theta}_e + \frac{1}{2} \boldsymbol{z}_1^{\mathrm{T}} \boldsymbol{J}_0 \boldsymbol{z}_1$$
 (10.64)

Differentiating (10.64) and inserting (10.58), (10.61), as well as (10.63) lead to

$$\dot{V}_{4} = \Delta \boldsymbol{f}_{e}^{\mathrm{T}} \Delta \dot{\boldsymbol{f}}_{e} + \boldsymbol{\Theta}_{e}^{\mathrm{T}} \dot{\boldsymbol{\Theta}}_{e} + \boldsymbol{z}_{1}^{\mathrm{T}} \boldsymbol{J}_{0} \dot{\boldsymbol{z}}_{1}$$

$$= -k_{o} ||\Delta \boldsymbol{f}_{e}||^{2} - k_{c1} ||\boldsymbol{\Theta}_{e}||^{2} - k_{c2} ||\boldsymbol{z}_{1}||^{2}$$

$$+ \Delta \boldsymbol{f}_{e} \Delta \dot{\boldsymbol{f}} - \boldsymbol{\Theta}_{e}^{\mathrm{T}} \Delta \boldsymbol{f}_{e1} - \boldsymbol{z}_{1}^{\mathrm{T}} \Delta \boldsymbol{f}_{e2} - \boldsymbol{z}_{1}^{\mathrm{T}} \boldsymbol{J}_{0} \Delta \dot{\boldsymbol{f}}_{O1}$$
(10.65)

Moreover, it can be obtained from (10.50)–(10.52) that

$$\Delta \dot{\boldsymbol{f}}_{O1} = -k_o \Delta \boldsymbol{f}_{e1} \tag{10.66}$$

Then, it leaves (10.55) from (10.56) as

$$\dot{V}_{4} = -k_{o}||\Delta f_{e}||^{2} - k_{c1}||\Theta_{e}||^{2} - k_{c2}||z_{1}||^{2} 
+ \Delta f_{e}\Delta \dot{f} - \Theta_{e}^{T}\Delta f_{e1} - z_{1}^{T}\Delta f_{e2} + k_{o}z_{1}^{T}J_{0}\Delta f_{e1}$$
(10.67)

Using Young's inequality and (10.49), one has

$$2\Delta f_{e} \Delta \dot{f} \le ||\Delta f_{e}||^{2} + ||\Delta \dot{f}||^{2} \le ||\Delta f_{e}||^{2} + l^{2} \tag{10.68}$$

$$-2\mathbf{\Theta}_{e}^{\mathsf{T}}\Delta f_{e1} \le ||\mathbf{\Theta}_{e}||^{2} + ||\Delta f_{e1}||^{2} \le ||\mathbf{\Theta}_{e}||^{2} + ||\Delta f_{e}||^{2}$$
(10.69)

$$-2z_1^{\mathsf{T}}\Delta f_{e2} \le ||z_1||^2 + ||\Delta f_{e2}||^2 \le ||\Theta_e||^2 + ||\Delta f_e||^2 \tag{10.70}$$

$$k_o \mathbf{z}_1^{\mathrm{T}} \mathbf{J}_0 \Delta \mathbf{f}_{e1} \le \frac{k_o}{2} ||\mathbf{J}_0||^2 ||\mathbf{z}_1||^2 + \frac{1}{2} ||\Delta \mathbf{f}_e||^2$$
 (10.71)

Applying (10.68)–(10.71), it can simplify (10.67) as

$$\dot{V}_{4} \leq -\frac{k_{o} - 3}{2} ||\Delta f_{e}||^{2} - (k_{c1} - 1)||\Theta_{e}||^{2} - \left(k_{c2} - \frac{k_{o}}{2}||J_{0}||^{2}\right) ||z_{1}||^{2} + 0.5l^{2} 
\leq -2\kappa V + 0.5l^{2} = -2\kappa (1 - \eta_{2})V_{4} - 2\kappa \eta_{2}V_{4} + 0.5l^{2}$$
(10.72)

Solving the inequality (10.72) results in

$$V_4 \le V(0) \exp(-2\kappa (1 - \eta_2)t), \forall V_4 \ge \frac{l}{2\sqrt{\kappa \eta_2}}$$
 (10.73)

From (10.61), (10.64), and (10.73), the following inequalities hold for  $V_4 \ge \frac{l}{2\sqrt{\kappa \eta_2}}$ :

$$||\Delta f_e|| \le \sqrt{2V_4(0)} \exp(-\kappa (1 - \eta_2)t)$$
 (10.74)

$$||\Theta_e|| \le \sqrt{2V_4(0)} \exp(-\kappa (1 - \eta_2)t)$$
 (10.75)

$$||z_1|| \le \sqrt{\frac{2V_4(0)}{J_m}} \exp(-\kappa (1 - \eta_2)t)$$
 (10.76)

$$||\dot{\mathbf{\Theta}}_e|| \le \left(\frac{1}{\sqrt{\lambda_{\min}(\mathbf{J})}} + k_{c1} + 1\right) \sqrt{2V_4(0)} \exp(-\kappa(1 - \eta_2)t)$$
 (10.77)

Then, it is ready to conclude from (10.74)–(10.77) that

$$||\Delta \mathbf{f}_e|| \le \sqrt{2V_4(0)} \exp(-\kappa (1 - \eta_2)t) + \varepsilon \tag{10.78}$$

$$||\Theta_{\varepsilon}|| \le \sqrt{2V_4(0)} \exp(-\kappa (1 - \eta_2)t) + \varepsilon \tag{10.79}$$

$$||z_1|| \le \sqrt{\frac{2V_4(0)}{J_m}} \exp(-\kappa (1 - \eta_2)t) + \varepsilon$$
 (10.80)

$$||\dot{\Theta}_e|| \le \left(\frac{1}{\sqrt{J_m}} + k_{c1} + 1\right) \sqrt{2V_4(0)} \exp(-\kappa (1 - \eta_2)t) + \varepsilon$$
 (10.81)

where  $\varepsilon = \frac{1}{2\sqrt{\kappa\eta_2}}$ . Based on (10.78)–(10.81) and using Definition 2.3, it can be proved that the closed-loop attitude system is practically exponentially stable. The estimation error  $\Delta f_e$ , the attitude tracking error  $\Theta_e$ , and the velocity tracking error  $\dot{\Theta}_e$  are practically exponentially stable. They practically exponentially converge within a ball with radius  $\varepsilon$ , while the exponential convergence rate is  $\kappa(1 - \eta_2)$ .

It is seen from (10.78)–(10.81) that larger  $\kappa$  leads to a faster convergence rate  $\kappa(1-\eta_2)$  and higher estimation and control accuracy  $\varepsilon$ . Then, based on the defini-

tion of  $\varepsilon$  in (10.60), it can be obtained that larger  $k_o$ ,  $k_{c1}$ , and  $k_{c2}$  will lead to a faster exponential convergence rate, higher estimation accuracy, and higher tracking accuracy. Therefore, the following procedures can be obeyed to obtain a better estimation and control performance:

- Step #1: Calculate the nominal values for  $||J_0||$  and  $J_M$ .
- Step #2: Choose  $k_o$  such that  $k_o > 3$ .
- Step #3: Select  $k_{c1}$  to satisfy  $k_{c1} > 1$ .
- Step #4: Based on Step 1 and Step 2, choose  $k_{c2}$  to satisfy  $k_{c2} > 0.5k_o||\boldsymbol{J}_o||^2$ .
- Step #5: If the desired estimation accuracy and the control accuracy are not met, then repeat Step #2  $\sim$  #4 by choosing larger  $k_a$ ,  $k_{c1}$ , and  $k_{c2}$ .

## 10.3.7 Simulation Example

As presented in Sect. 10.3.6, the resilient controller (10.58) can accomplish the attitude tracking maneuvering with exponential convergence, an example of a currently being developed rigid satellite is presented in this section to validate the conclusion in Theorems 10.3 and 10.4. This satellite is in a circular orbit. The altitude and the inclination of its orbit are designed to be 660 km and 90.5 degrees, respectively; correspondingly, the satellite's orbital rate is  $\omega_0 = 0.0011$  rad/s. Its nominal inertia is  $J_0 = [30, 0.1, -0.2; 0.1, 25, 0.4; -0.2, 0.4, 30]$  kg·m². For a specific aerospace task, the following trajectory is planned for the satellite to provide its payloads with the desired attitude

$$\mathbf{\Theta}_d = [\phi_d, \theta_d, \psi_d]^{\mathrm{T}} = \begin{bmatrix} -5\sin(0.02t - \frac{\pi}{8}) \\ 3\cos(0.02t - \frac{\pi}{10}) \\ 5\sin(0.03t - \frac{\pi}{8}) \end{bmatrix}$$
 degrees (10.82)

Four reaction wheels (RWs) are fixed in the satellite as the actuators to produce torque for attitude tracking maneuvering. The nominal configuration of those four RWs is  $D_0 = [1, 0, 0, \frac{1}{\sqrt{3}}; 0, 1, 0, \frac{1}{\sqrt{3}}; 0, 0, 1, \frac{1}{\sqrt{3}}]$ . Due to misalignment, the actual configuration is  $D = [D_1, D_2]$ , where

$$\boldsymbol{D}_{1} = \begin{bmatrix} \cos \Delta \alpha_{1} & \sin \Delta \alpha_{2} \sin \Delta \beta_{2} & \sin \Delta \alpha_{3} \cos \Delta \beta_{3} \\ \sin \Delta \alpha_{1} \cos \Delta \beta_{1} & \cos \Delta \alpha_{2} & \sin \Delta \alpha_{3} \sin \Delta \beta_{3} \\ \sin \Delta \alpha_{1} \sin \Delta \beta_{1} & \sin \Delta \alpha_{2} \cos \Delta \beta_{2} & \cos \Delta \alpha_{3} \end{bmatrix}$$
(10.83)

$$\boldsymbol{D}_{2} = \begin{bmatrix} \cos(\alpha_{4} + \Delta\alpha_{4})\cos(\beta_{4} + \Delta\beta_{4}) \\ \cos(\alpha_{4} + \Delta\alpha_{4})\sin(\beta_{4} + \Delta\beta_{4}) \\ \sin(\alpha_{4} + \Delta\alpha_{4}) \end{bmatrix}$$
(10.84)

Here,  $\beta_4 = \frac{\pi}{4}$  rad, and  $\alpha_4 = \arcsin(\frac{1}{\sqrt{3}})$  rad;  $-\pi < \Delta\beta_j < \pi$ ,  $j \in \{1, 2, 3\}$ , and small angles  $-\frac{\pi}{2} < \Delta\alpha_i < \frac{\pi}{2}$ ,  $-\frac{\pi}{2} < \Delta\beta_i < \frac{\pi}{2}$ , i = 1, 2, 3, 4 are the misalignment angles of those four RWs.

### A Simulation Result

In the simulation, the uncertain inertia is assumed to be  $\Delta J = 10\% J_0$ . The misalignment angles of the four RWs are randomly chosen as  $\Delta\alpha_1 = 0.1638$  rad,  $\Delta\alpha_2 = 0.2125$  rad,  $\Delta\alpha_3 = -0.1953$  rad,  $\Delta\alpha_4 = -0.2164$  rad,  $\Delta\beta_1 = -2.5287$  rad,  $\Delta\beta_2 = -1.3917$  rad,  $\Delta\beta_3 = 0.2946$  rad, and  $\Delta\beta_4 = 0.0693$  rad. The actuator faults in the four RWs are assumed to be

$$e_1 = \begin{cases} 0, & t \le 2 \\ 0.4, & t > 2 \end{cases}, e_2 = \begin{cases} 0, & t \le 4 \\ 0.7, & t > 4 \end{cases}$$
 (10.85)

$$e_3 = \begin{cases} 0, & t \le 3 \\ 0.2, & t > 3 \end{cases}, e_4 = \begin{cases} 0, & t \le 5 \\ 1, & t > 5 \end{cases}$$
 (10.86)

$$\Delta \tau_1 \equiv 0, \quad \Delta \tau_2 \equiv 0, \quad \Delta \tau_3 = \begin{cases} 0, & t \le 3 \\ 0.001, & t > 3 \end{cases}, \quad \Delta \tau_4 \equiv 0$$
 (10.87)

Moreover, the external disturbance acting on the satellite mainly includes the gravity-gradient torque, the aerodynamic torque, and the Earth magnetic torque. By using the physical and the orbital parameters of the satellite, the external disturbance is calculated and assumed as follows. It could approximate the real disturbance value of the satellite

$$u_{di} = \kappa_i \sin(\mu_i t + \eta_i) \tag{10.88}$$

where  $\kappa_1 = 0.002$ ,  $\kappa_2 = -0.003$ ,  $\kappa_3 = 0.004$ ,  $\mu_1 = 0.8$ ,  $\mu_2 = 0.5$ ,  $\mu_3 = 0.2$ ,  $\eta_1 = 0.5$ ,  $\eta_2 = 0.3$ , and  $\eta_3 = 0.9$ .

When carrying out simulations, the gains of the proposed resilient control strategy are selected as  $k_{c1} = 10.5$ ,  $k_{c2} = 5000$ , and  $k_o = 25$ . The initial states of the satellite are  $\phi(0) = -0.02$  degrees,  $\theta(0) = 0.02$  degrees,  $\psi(0) = 0.01$  degrees, and  $\omega(0) = [0.001, 0.001, 0.001]^T$  rad/s.

Based on the above-listed satellite physical parameters and the selected gains, the proposed resilient control scheme is applied to conduct simulation through Matlab/Simulink. Figures 10.15 and 10.16 show the estimation result of the incorporated observer to estimate uncertainties. From Fig. 10.15a, it is known that the term  $\Delta f_1(\Theta, \dot{\Theta})$  is estimated after about 0.05 s. Its estimation accuracy is superior to 2.0e-7, which is shown in Fig. 10.15b. As we can see in Fig. 10.16a, the uncertainty  $\Delta f_2$  can be estimated or reconstructed by  $\Delta f_{02}$  within the same period required for  $\Delta f_{01}$  to estimate  $\Delta f_1$ . Figure 10.16b shows that the corresponding estimation accuracy of  $\Delta f_2$  is better than 8.0e-4 N·m. The estimation accuracy of  $\Delta f_1$  and  $\Delta f_2$  is very superior. Moreover, exponential convergence behaviors of the estimation

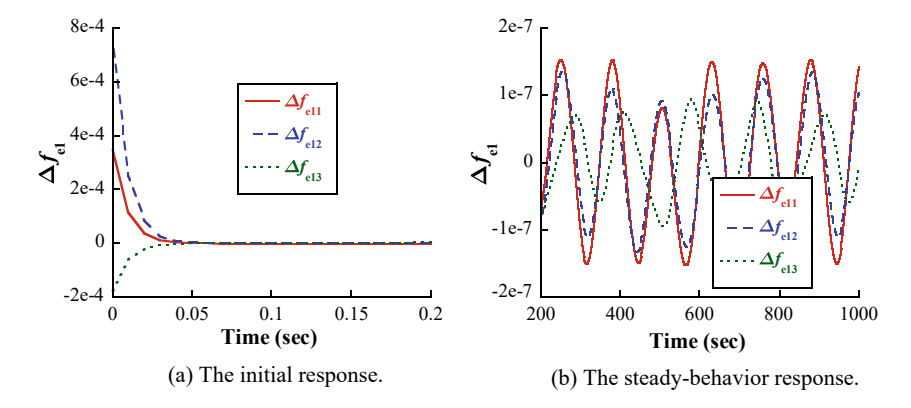


**Fig. 10.15** The estimation error  $\Delta f_{e1}$  from the estimator (10.50)

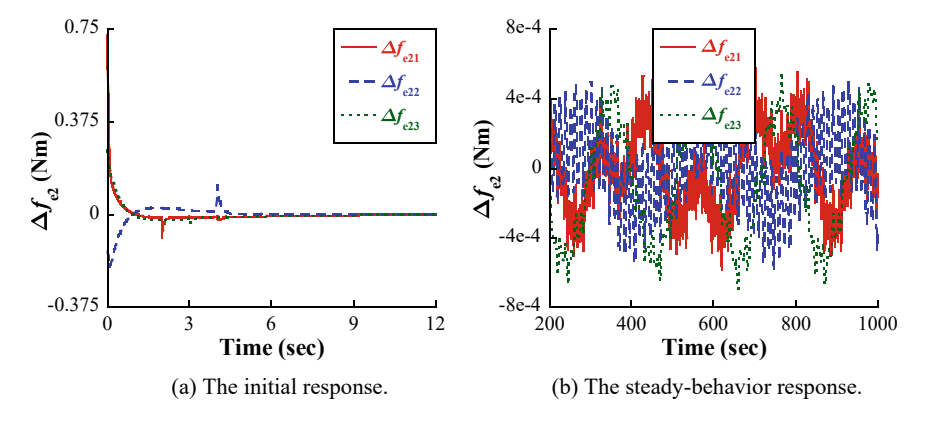


**Fig. 10.16** The estimation error  $\Delta f_{e2}$  from the estimator (10.50)

errors  $\Delta f_{e1}$  and  $\Delta f_{e2}$  are seen in Figs. 10.17 and 10.18. These results successfully verify the conclusion in Theorem 10.3.

Figures 10.19a and 10.20a show the attitude tracking result under the effect of the presented resilient control approach. It is found in Fig. 10.19b that the planned attitude trajectory (10.82) is followed with the attitude pointing accuracy being 1.2e-4 degrees.  $|\phi_e| \leq 1.2$ e-4 degrees, and  $|\psi_e| \leq 1.1$ e-4 degrees are achieved after about 10 seconds. In addition, Fig. 10.20b shows that the attitude stability is ensured by the resilient controller (10.58) to be better than 4.0e-5 deg/s. Such attitude stability is very high. More specifically, the resulting tracking error of the velocity is  $|\dot{\phi}_e| \leq 3.0$ e-5 degrees,  $|\dot{\theta}_e| \leq 3.8$ e-5 degrees, and  $|\dot{\psi}_e| \leq 1.2$ e-5 degrees. Based on the above tracking performance, it is seen that the maneuvering of attitude tracking is successfully performed after about 15 seconds. The planned aerospace task is then accomplished despite system uncertainties and actuator uncertainties. This is owing to the effect of the observer (10.50) in the approach. Because

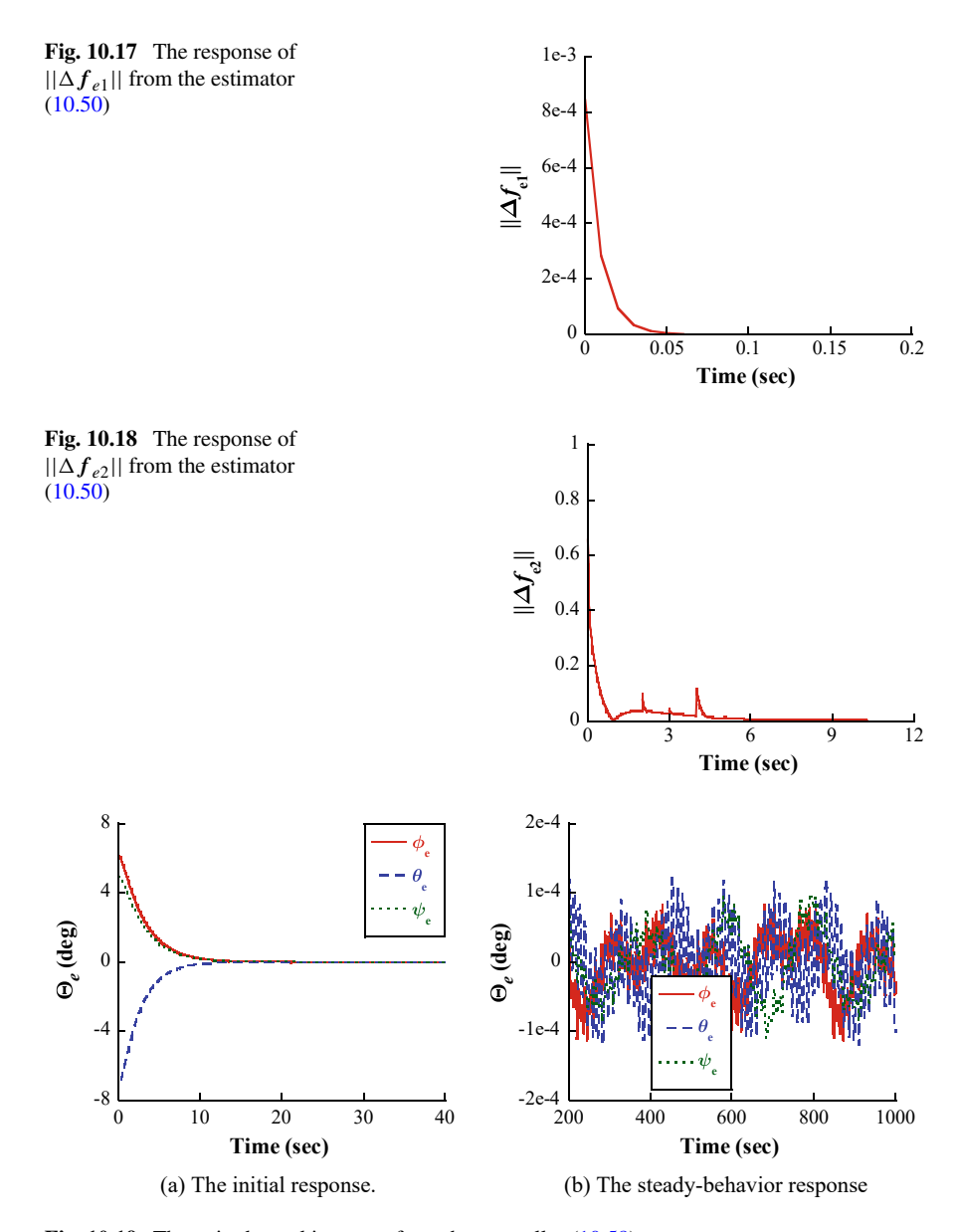


Fig. 10.19 The attitude tracking error from the controller (10.58)

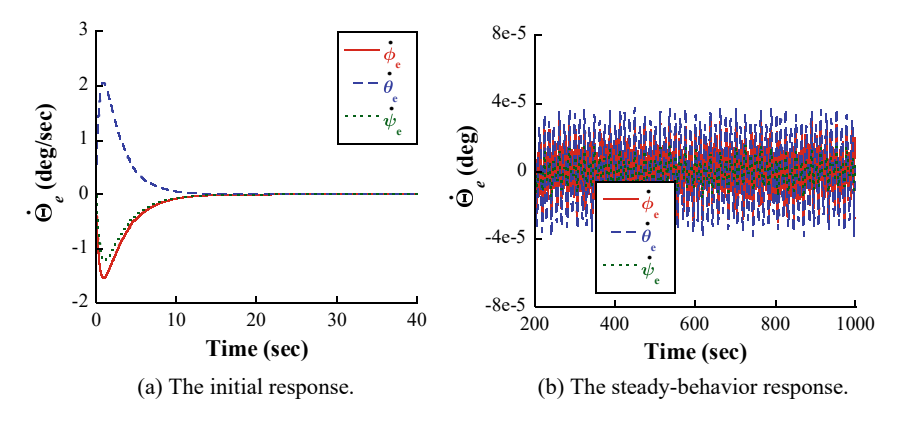
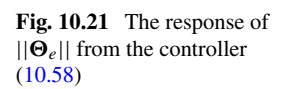
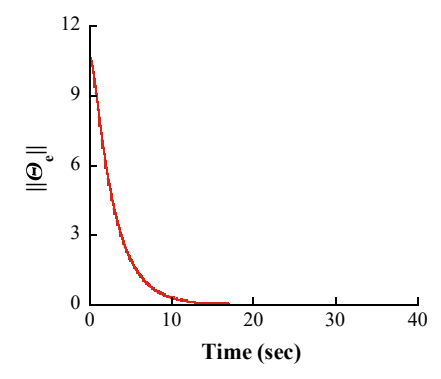
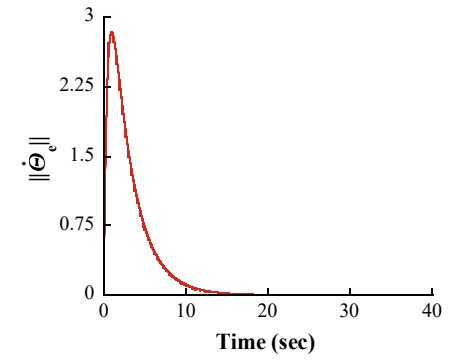


Fig. 10.20 The angular velocity tracking error from the controller (10.58)





**Fig. 10.22** The response of  $||\Theta_e||$  from the controller (10.58)



the uncertainties in the system and the actuators can be precisely estimated by the observer (10.50), then the estimation values  $\Delta f_{O1}$  and  $\Delta f_{O2}$  in the resilient controller (10.58) can compensate for the uncertainties. Moreover, the results in Figs. 10.21 and 10.22 show that the tracking errors of the attitude and the velocity

are exponentially converging. Hence, it is successful to validate the conclusion in Theorem 10.4.

### **B** Experimental Result

In this section, the practical application of the designed control approach was verified on the scaling satellite three-axis attitude dynamics and control simulator, as we can see in Fig. 2.6. During tests, because all the actuators were healthy, the actuator faults (10.85)–(10.87) were numerically injected. The six thrusters were commanded to generate torque with its value being the same as (10.88). This torque was viewed as an external disturbance. Due to the finite manufacturing technique, the real actuator configuration and the real inertia of the testbed were not the same as the designed values. Hence, the testbed was with uncertain inertia and actuator configuration. To this end, the testbed was subject to system uncertainties and actuator uncertainties were simulated. This testbed was appropriate for testing the effectiveness of the presented resilient control.

The experimental results were shown in Figs. 10.23 and 10.24. It was seen in Figs. 10.23a and 10.19a that the experimental attitude tracking response matched the simulation results well. More specifically, it is shown in Fig. 10.24b that the attitude pointing accuracy ensured by the resilient controller was superior to 0.035 degrees, i.e.,  $|\phi_e| \leq 0.034$  degrees,  $|\theta_e| \leq 0.031$  degrees, and  $|\psi_e| \leq 0.033$  degrees. The tracking error of the angular velocity was superior to 0.14°/s. This was observed in Fig. 10.24b. Hence, the attitude tracking maneuver was successfully performed despite the system uncertainties and the actuator uncertainties. Moreover, this attitude maneuvering was achieved after about 20 s, as illustrated in Figs. 10.23a and 10.24a. The difference between the initial response of the angular velocity tracking error in Figs. 10.20a and 10.24a was because the initial angular velocity of the testbed was not set as the values in the simulation. It should be pointed out that compared with the high control accuracy in Figs. 10.19 and 10.20 obtained from the simulation, a lower

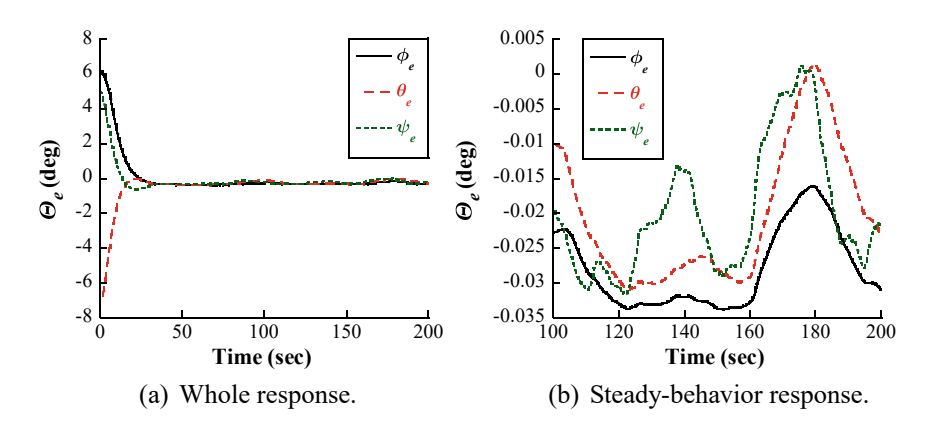


Fig. 10.23 The attitude tracking error from the controller (10.58) in test

10.4 Summary 231

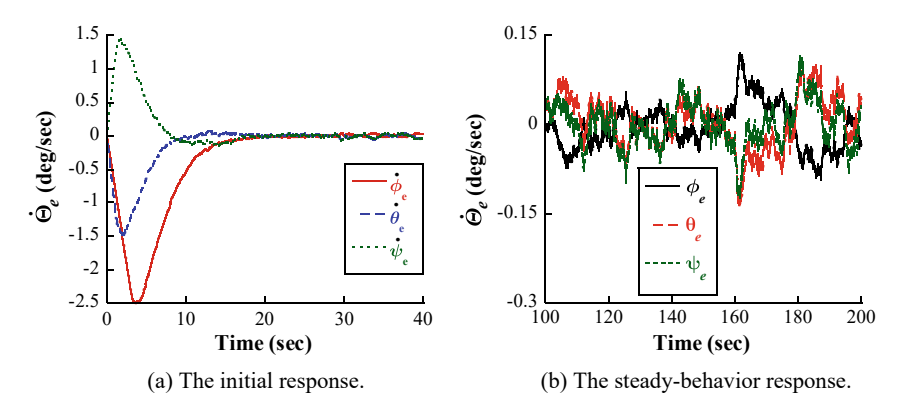


Fig. 10.24 The angular velocity tracking error from the controller (10.58) in test

control accuracy of the attitude and the angular velocity was seen in Figs. 10.23 and 10.24 for the experimental tests. This is because the measurement accuracy of the testbed is not very high. Nevertheless, the obtained attitude pointing accuracy, attitude stability, and system convergence time were desirable for practical application. To this end, the experimental verification of the Theorem 10.3 and the practical application of the proposed resilient control law was done.

# 10.4 Summary

In this chapter, an exponential attitude stabilization control approach was presented for rigid satellite with modeling error. A DO-based controller was developed. Despite the modeling error, the controller can exponentially stabilize the attitude, the angular velocity, and the DO error to be within a radius arbitrarily small set. It did not require the assumption that the rate of change of the external disturbances should be zero or almost zero. Hence, the proposed approach was capable of handling a large range of external disturbances. Disturbance attenuation control was achieved. Moreover, the controller has a simple structure without complicated computation. More robustness to external disturbance was guaranteed. Then, the practically exponential attitude tracking problem of rigid satellites with modeling error due to external disturbance, uncertain inertia parameters, actuator faults, and actuator misalignment was addressed. An observer-based resilient control solution was designed. This approach guaranteed that the desired attitude trajectory was followed with the attitude and the angular velocity tracking error practically exponentially converging to a radius arbitrary small region. The scheme was developed based on the attitude system of the satellite with its attitude represented by Euler angles. Moreover, the controller was independent of the actuator type and its configuration. Another feature of the

controller was its simple structure and less onboard computation. Hence, it lets the proposed solution have superior practical application potential for satellite engineering.

## References

- Gao, Z., Liu, X., Chen, M. Z. Q (2016) Unknown input observer-based robust fault estimation for systems corrupted by partially decoupled disturbances. IEEE Transactions on Industral Electronics 63(4): 2537–2547
- Zhang, J., Liu, X., Xia, Y., Zuo, Z., Wang, Y. (2016) Disturbance observer-based integral sliding-mode control for systems with mismatched disturbances. IEEE Transactions on Industrial Electronics 63(11): 7040–7048
- 3. Yang, J., Li, S., Yu, X. (2013) Sliding-mode control for systems with mismatched uncertainties via a disturbance observer. IEEE Transactions on Industral Electronics 60(1): 160–169
- 4. Liu, Y., Zhang, T., Li, C., Lian, B. (2017) Robust attitude tracking with exponential convergence. IET Control Theory and Applications 11(18): 3388–3395
- Zhao, L., Yu, J., Yu, H. (2018) Adaptive finite-time attitude tracking control for spacecraft with disturbances. IEEE Transactions on Aerospace and Electronic Systems 54(3): 1297–1305
- Xiao, B., Hu, Q., Wang, D., Poh, E. K. (2013) Attitude tracking control of rigid spacecraft with actuator misalignment and fault. IEEE Transactions on Control Systems Technology 21(6): 2360–2366
- Hu, Q., Li, B., Huo, X., Shi, Z. (2013) Spacecraft attitude tracking control under actuator magnitude deviation and misalignment. Aerospace Science and Technology 28(1): 266–280
- 8. Hu, Q., Li, B., Zhang, A. (2013) Robust finite-time control allocation in spacecraft attitude stabilization under actuator misalignment. Nonlinear Dynamics 73(1-2): 53–71
- 9. Berkane, S., Abdessameud, A., Tayebi, A. (2017) Hybrid global exponential stabilization on so (3). Automatica 81: 279–285
- Berkane, S., Abdessameud, A., Tayebi, A. (2018) Hybrid output feedback for attitude tracking on so(3). IEEE Transactions on Automatic Control 63(11): 3956–3963
- 11. Zhong, R., Xu, S. (2018) Neural network based terminal sliding-mode control for thrust regulation of a tethered space-tug. Astrodynamics 2(2): 175–185
- 12. Ginoya, D., Shendge, P. D., Phadke, S. B. (2014) Sliding mode control for mismatched uncertain systems using an extended disturbance observer. IEEE Transactions on Industral Electronics 61(4): 1983–1992
- 13. Pu, Z., Yuan, R., Yi, J., Tan, X. (2015) A class of adaptive extended state observers for nonlinear disturbed systems. IEEE Transactions on Industral Electronics 62(9): 5858–5869
- Liu, J.X., Laghrouche, S., Wack, M. (2014) Observer-based higher order sliding mode control of power factor in three-phase AC/DC converter for hybrid electric vehicle applications. International Journal of Control 87(6): 1117–1130
- 15. Godard (2011) Fault tolerant control of spacecraft. PhD thesis, Ryerson University (Canada)

# Chapter 11 Unknow Input Observer-Based Attitude Control



## 11.1 Introduction

Considering modeling error or disturbance as an unknown input, employing the unknown input observer (UIO) [1] to estimate modeling error or disturbance is another solution to design an attitude controller with high pointing accuracy. The development of a UIO-based attitude controller for satellite was discussed in [2]. Motivated by the advantages of UIO-based control, this chapter first presents a UIO-based robust control approach for flexible satellite's attitude stabilization maneuvers with fixed convergence time. The main features of this approach are highlighted as:

- The conventional fixed-time stability theorem [3] is extended in this chapter to decrease the settling time. A new stable system, based on which the main result of the chapter is presented, is developed with its settling time shorter than [4].
- Inspired by [5], a fixed-time nonlinear observer to reconstruct the lumped uncertainties is developed. Any prior knowledge of the total uncertainties is not required. Unlike the existing disturbance observers [6], the restrictions on the uncertainties are relaxed. Moreover, another feature of this observer is that the estimation error is finite-time stable regardless of initial estimation errors.
- By designing a novel fixed-time terminal sliding surface, a robust attitude control law is proposed for flexible satellites with external disturbance, uncertainties in inertia parameters and actuators accommodated.

It should be pointed out that most of the preceding observer-based schemes are able only to guarantee the closed-loop tracking system stability to be stable, while they do not take control performance such as overshoot into consideration. To solve these challenges, a novel UIO-based tracking control framework is further presented in this chapter. The main contributions are as follows.

 A more general class of uncertain systems with lossless second-order mechanical systems or Lagrangian systems included in the model has been investigated. The proposed approach is, thus, applicable for trajectory following control of modern industrial systems such as robotic manipulators, etc.

- A general tracking control architecture is presented. This is designed by using
  the UIO technique. In comparison with the existing ESO-based approaches, it can
  remove the need that the uncertainty/disturbance should be with no variation or
  slow variation. When compared with the SMO-/HOSMO-based controllers, the
  proposed scheme can eliminate the assumption that the uncertainty/disturbance
  should be upper bounded by a known scalar.
- The proposed control approach can achieve trajectory tracking control with exponential convergence. A perfect tracking performance without overshoot can be guaranteed even in face of system uncertainty and external disturbance. It lets this proposed scheme with significant application potential.
- A fast estimation of the disturbance and uncertainty can be achieved by the proposed estimator. Finite-time stability of the estimation error is further guaranteed.

### 11.2 UIO-Based Attitude Stabilization Control

In this section, the satellite considered is flexible with its attitude system described by (2.15), (2.25) and, (2.26). The modeling error consists of actuator uncertainty, external disturbance, and uncertain inertia. Let  $J_0 \in \mathbb{R}^{3\times 3}$  and  $\Delta J \in \mathbb{R}^{3\times 3}$  be the nominal and the uncertain inertia. Then, it has  $J = J_0 + \Delta J$ .

## 11.2.1 General Model of Actuator Uncertainty

In practice, a satellite's actuator may have uncertainty [7]. Nonnominal behavior may be seen in the actuator. This uncertainty would yield performance deterioration or system instability. Let the commanded/nominal torque of the actuator be denoted as  $\boldsymbol{u}_A = [u_{A1}, u_{A2}, u_{A3}]^T \in \mathbb{R}^3$ .  $\boldsymbol{u}_F \in \mathbb{R}^3$  represents the uncertainty torque. Then, the relationship between the commanded torque  $\boldsymbol{\tau}_A$  and the actual control torque  $\boldsymbol{u}$  can be mathematically modeled as

$$\boldsymbol{u} = \boldsymbol{u}_A + \boldsymbol{u}_F \tag{11.1}$$

### 11.2.2 Problem Formulation

Suppose that the considered flexible satellite has an attitude sensor and gyros to measure the attitude  $\Theta$  and the angular velocity  $\omega$ . Then, the control problem of this section can be formulated as: Applying the feedback of states' measurement  $\Theta$  and  $\omega$ , design a control law for  $u_A$  to ensure that the attitude angles  $\Theta$  is stabilized to  $\mathbf{0}$  after a fixed-time  $t_F \in \mathbb{R}_+$  even in the presence of the external disturbance  $u_d$ ,

the uncertain inertia  $\Delta J$ , and the actuator uncertainty  $u_F$ , i.e.,  $\Theta(t) \equiv 0$  for  $t \geq t_F$ . Moreover,  $t_F$  should be independent of the initial attitude and angular velocity.

The flexible satellite's attitude control system (2.15), (2.25), and (2.26) with actuator uncertainty (11.1) can be combined as

$$M(\mathbf{\Theta})\ddot{\mathbf{\Theta}} + C_1(\mathbf{\Theta}, \dot{\mathbf{\Theta}})\dot{\mathbf{\Theta}} + C_2(\mathbf{\Theta}, \dot{\mathbf{\Theta}}) = \bar{u} + \bar{d}$$
 (11.2)

where 
$$\bar{d} = R^{\mathrm{T}}(\Theta)(u_d + u_F - \Delta J\dot{\omega} - \omega^{\times}\Delta J\omega - \omega^{\times}\delta^{\mathrm{T}}\dot{\eta} - \delta^{\mathrm{T}}\ddot{\eta}), \bar{u} = R^{\mathrm{T}}(\Theta)u_A,$$

$$M(\Theta) = R^{\mathrm{T}}(\Theta)J_0R(\Theta), \quad C_1(\Theta,\dot{\Theta}) = R^{\mathrm{T}}(\Theta)\left(J_0\frac{dR(\Theta)}{dt} - \omega^{\times}J_0)R(\Theta)\right), \quad \text{and}$$

$$C_2(\Theta,\dot{\Theta}) = -R^{\mathrm{T}}(\Theta)\left(J_0\frac{d\omega_c(\Theta)}{dt} - \omega^{\times}J_0\omega_c(\Theta)\right).$$

Defining  $x_1 = [x_{11}, x_{12}, x_{13}]^T = \mathbf{\Theta}$  and  $x_2 = [x_{21}, x_{22}, x_{23}]^T = \dot{\mathbf{\Theta}}$ , the system (11.2) can be transformed into

$$\begin{cases} \dot{x}_1 = x_2 \\ \dot{x}_2 = \tau + d - M^{-1}(x_1)(C_1(x_1, x_2)x_2 + C_2(x_1, x_2)) \end{cases}$$
(11.3)

where  $x_1$  and  $x_2$  are the system states,  $d = M^{-1}(\Theta)\bar{d}$  denotes the lumped uncertainty, and  $\tau = M^{-1}(\Theta)\bar{u}$  is the transformed control input.

**Remark 11.1** Because the attitude  $\Theta$  and the angular velocity  $\omega$  are measurable, it can be obtained that the states  $x_1$  and  $x_2$  of the transformed system (11.3) are measurable.

## 11.2.3 Main Result

In this section, an observer-based fixed-time control framework is presented for a flexible satellite attitude system to improve the convergence rate and the pointing accuracy. This control framework is developed by using the measurements of the attitude  $\Theta$  and the angular velocity  $\omega$  or  $\dot{\Theta}$ . Moreover, it consists of a fixed-time observer and a robust fixed-time attitude stabilization controller. The fixed-time observer is to estimate the lumped uncertainty d. The states measurements and the estimated information  $d_{\rm est}$  are feedback to develop the robust fixed-time attitude stabilization controller to achieve the closed-loop system's fixed-time stability. The closed-loop attitude stabilization system resulting from this control framework is shown in Fig. 11.1.

### A A Faster Fixed-Time Stable System

Before the observer-based attitude control design, a fixed-time stable system is developed as

$$\dot{y} = -\xi(y)(\alpha y^p + \beta y^{\lambda})^k, y \in \mathbb{R}, y_0 = y(0)$$
 (11.4)

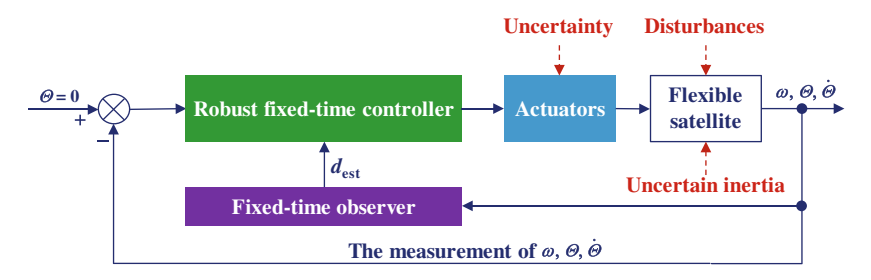


Fig. 11.1 The closed-loop system from the proposed control in this Chapter

where a > 1,  $b \in \mathbb{R}_+$ ,  $c \in \mathbb{R}_+$ ,  $\alpha \in \mathbb{R}_+$ ,  $\beta \in \mathbb{R}_+$ ,  $\bar{p} \in \mathbb{R}_+$ ,  $\bar{q} \in \mathbb{R}_+$ , and  $k \in \mathbb{R}_+$ are scalars.  $\bar{p}k < 1, \bar{q}k > 1, \xi(y) = a + (1-a)\exp(-b||y||^c)$ , and  $\lambda = \frac{1}{2k} + \frac{1}{2}\bar{q} + \frac{1}{2}\bar{q}$  $\left(\frac{1}{2}\bar{q} - \frac{1}{2k}\right) \operatorname{sgn}(||y|| - 1).$ 

**Lemma 11.1** For any initial value  $y_0$ , the system (11.4) is fixed-time stable, and its settling-time is  $T_1 \in \mathbb{R}_+$ , i.e.,  $y(t) \equiv 0$  for  $t \geq T_1$ , where  $T_1$  is bounded as

$$T_1 < \frac{1}{\beta^k (\bar{q}k - 1)} + \frac{1}{\beta^k (1 - \bar{p}k)} \ln \left( 1 + \left( \frac{\beta}{\alpha} \right)^k \right)$$
 (11.5)

Moreover, the convergence rate is faster than the fixed-time stable system proposed in [3].

**Proof** Defining a new variable  $W = y^{1-\bar{p}k}$ , it can be obtained from (11.4) that

$$\dot{W} = -(1 - \bar{p}k)y^{-\bar{p}k} \left( \xi(y)^{\frac{1}{k}} \alpha y^{\bar{p}} + \xi(y)^{\frac{1}{k}} \beta y^{\lambda} \right)^{k} 
= -(1 - \bar{p}k) \left( \xi(y)^{\frac{1}{k}} \alpha + \xi(y)^{\frac{1}{k}} \beta W^{\bar{\eta}} \right)^{k}$$
(11.6)

where  $\bar{\eta} = \frac{\lambda - \bar{p}}{1 - \bar{p}k}$ . Since 1 - pk > 0 and  $\xi(y) > 1$ , it follows from (11.6) that

$$\dot{W} \le -(1 - \bar{p}k)(\alpha + \beta W^{\bar{\eta}})^k \tag{11.7}$$

Applying the result in [3], Definition 2.1, and Lemma 2.3, it can be proved from (11.7) that W is fixed-time stable. Moreover, solving (11.7), one can get the settling-time

$$T_{1} = \frac{1}{(1 - \bar{p}k)} \int_{0}^{W_{0}} \frac{1}{\left(\xi (y)^{\frac{1}{k}} \alpha + \xi (y)^{\frac{1}{k}} \beta W^{\bar{\eta}}\right)^{k}} dW$$

$$= \frac{1}{(1 - \bar{p}k)} \left( \int_{1}^{W_{0}} \frac{1}{\xi (y)(\alpha + \beta W^{\hat{\eta}})^{k}} dW + \int_{0}^{1} \frac{1}{\xi (y)(\alpha + \beta W^{\frac{1}{k}})^{k}} dW \right)$$
where  $\hat{\eta} = \frac{\bar{q} - \bar{p}}{1 - \bar{p}k}$  and  $W_{0} = (y(0))^{1 - \bar{p}k}$ . (11.8)

 $\frac{1-p\kappa}{1-p\kappa}$ 

If  $\xi(y) = 1$ , then one has

$$T_1' = \frac{1}{(1 - \bar{p}k)} \left( \int_1^{W_0} \frac{1}{(\alpha + \beta W^{\hat{\eta}})^k} dW + \int_0^1 \frac{1}{(\alpha + \beta W^{\frac{1}{k}})^k} dW \right)$$
(11.9)

Since  $1 \le \xi(y) \le a$ , then  $\frac{1}{a} \le \frac{1}{\xi(y)} \le 1$ . Hence, for all  $W_0$ , it is concluded that

$$T_1 < T_1' \tag{11.10}$$

On the other hand,  $T'_1$  is also the settling time of the fixed-time system given in [3]. To this end, one can prove that the settling time provided by the proposed system (11.4) is less than [3]. The convergence rate of the system (11.4) is faster than [3]. From (11.9), it be proved that  $T'_1$  is bounded as

$$T_{1}' \leq \frac{1}{(1 - \bar{p}k)} \left( \int_{1}^{W_{0}} \frac{1}{\beta^{k} W^{\hat{\eta}k}} dW + \int_{0}^{1} \frac{1}{\alpha^{k} + \beta^{k} W} dW \right)$$

$$\leq \frac{1}{(1 - \bar{p}k)} \left( \frac{1 - W_{0}^{1 - \hat{\eta}k}}{\beta^{k} (\hat{\eta}k - 1)} + \frac{1}{\beta^{k}} \ln \left( 1 + \left( \frac{\beta}{\alpha} \right)^{k} \right) \right)$$
(11.11)

Since  $\hat{\eta}k > 1$  and  $W_0 > 0$ , one has

$$T_1' \le \frac{1}{\beta^k (\bar{q}k - 1)} + \frac{1}{\beta^k (1 - \bar{p}k)} \ln \left( 1 + \left( \frac{\beta}{\alpha} \right)^k \right) \tag{11.12}$$

which does not depend on the initial condition.

Lemma 11.1 is fundamental to the development of the subsequent observer and controller. The subsequent fixed-time observer, sliding surface, and attitude controller are developed based on it; moreover, the system stability will be analyzed by using Lemma 11.1. Indeed, this fixed-time stable system introduces a time-varying gain to significantly improve convergence speed near and even far away from the origin. Thus, it is expected that the observer-based attitude control possesses fast and fixed-time convergence properties.

### B Fixed-Time Unknown Input Observer

The transformed system (11.3) can be rewritten as

$$\dot{x}_2 = -l_1 x_2 + d_l + \tau \tag{11.13}$$

where  $d_l = -M^{-1}(x_1)(C_1(x_1, x_2)x_2 + C_2(x_1, x_2)) + l_1x_2 + d$  and  $l_1 \in \mathbb{R}^+$  is a positive gain.

For (11.13), an auxiliary system is introduced as

$$\dot{\mathbf{x}}_a = -l_1 \mathbf{x}_a + \mathbf{\tau} \tag{11.14}$$

where  $\mathbf{x}_a \in \mathbb{R}^3$  represents the state of this auxiliary system.

Let the error between  $x_2$  and  $x_a$  be defined as  $z = x_2 - x_a$ , it leaves the dynamics of the error be the following linear system.

$$\begin{cases} \dot{z} = -l_1 z + d_l \\ \mathbf{y} = l_2 z \end{cases} \tag{11.15}$$

where  $l_2 \in \mathbb{R}_+$  is a positive constant, z is the system's state,  $y \in \mathbb{R}^3$  is the system's output, and  $d_l$  is the unknown input of this system.

Let the fixed-time unknown input observer for the lumped uncertainty be designed as

$$\dot{\hat{z}} = \frac{\dot{y}}{l_2} + l_3 y - l_2 l_3 \hat{z} + \xi(\mathbf{e})^{\frac{1}{k_1}} \left( \alpha_1 \lfloor \mathbf{e} \rfloor^{\frac{2p_1 k_1 - 1}{k_1}} - \beta_1 \lfloor \mathbf{e} \rfloor^{\frac{2\lambda_1 k_1 - 1}{k_1}} \right)^{k_1}$$
(11.16)

where  $l_3 \in \mathbb{R}_+$ ,  $\alpha_1 \in \mathbb{R}_+$ ,  $\beta_1 \in \mathbb{R}_+$ ,  $p_1 \in \mathbb{R}_+$ ,  $\bar{q}_1 \in \mathbb{R}_+$ ,  $a_1 \geq 1$ ,  $b_1 \in \mathbb{R}_+$ ,  $c_1 \in \mathbb{R}_+$ , and  $k_1 \in \mathbb{R}_+$  are observer gains.  $\xi(\boldsymbol{e}) = a_1 + (1 - a_1) \exp(-b_1 ||\boldsymbol{e}||^{c_1})$ ,  $\lambda_1 = \frac{1}{2k_1} + \frac{1}{2}\bar{q}_1 + \left(\frac{1}{2}\bar{q}_1 - \frac{1}{2k_1}\right) \operatorname{sgn}(||\boldsymbol{e}|| - 1)$ ,  $\hat{\boldsymbol{z}}$  is the estimation of  $\boldsymbol{z}$ , and  $\boldsymbol{e} = \boldsymbol{z} - \hat{\boldsymbol{z}}$  is the estimation error. Moreover,  $\dot{\boldsymbol{y}}$  is the time derivative of  $\boldsymbol{y}$ .

**Theorem 11.1** The proposed observer (11.4) ensures the estimation error e to be fixed-time stable, i.e.,  $e(t) \equiv 0$  for  $t \geq T_e$ , where  $T_e$  satisfies

$$T_e < \frac{1}{\mu_2^{k_1}(\bar{q}_1 k_1 - 1)} + \frac{1}{\mu_2^{k_1}(1 - p_1 k_1)} \ln \left( 1 + \left( \frac{\mu_2}{\mu_1} \right)^{k_1} \right)$$
 (11.17)

where  $\mu_1 = 2^{p_1} \alpha_1$  and  $\mu_2 = 2^{\lambda_1} \beta_1$ .

**Proof** It is obtained from (11.15) and (11.16) that the estimation error of the observer satisfies

$$\dot{\mathbf{e}} = \dot{\mathbf{z}} - \dot{\hat{\mathbf{z}}} = \dot{\mathbf{z}} + l_2 l_3 \hat{\mathbf{z}} - \frac{1}{l_2} \dot{\mathbf{y}} - l_3 \mathbf{y} 
- \left( \xi(\mathbf{e})^{\frac{1}{k_1}} \alpha_1 \lfloor \mathbf{e} \rfloor^{\frac{2p_1 k_1 - 1}{k_1}} + \xi(\mathbf{e})^{\frac{1}{k_1}} \beta_1 \lfloor \mathbf{e} \rfloor^{\frac{2\lambda_1 k_1 - 1}{k_1}} \right)^{k_1} 
= - l_2 l_3 \mathbf{e} - \left( \xi(\mathbf{e})^{\frac{1}{k_1}} \alpha_1 \lfloor \mathbf{e} \rfloor^{\frac{2p_1 k_1 - 1}{k_1}} + \xi(\mathbf{e})^{\frac{1}{k_1}} \beta_1 \lfloor \mathbf{e} \rfloor^{\frac{2\lambda_1 k_1 - 1}{k_1}} \right)^{k_1}$$
(11.18)

Define a Lyapunov candidate function as  $V_1 = \frac{1}{2}e^T e$ , it leaves its time derivative as

$$\dot{V}_{1} = e^{\mathrm{T}} \dot{e} \leq -e^{\mathrm{T}} \left( \xi(e)^{\frac{1}{k_{1}}} \alpha_{1} \lfloor e \rfloor^{\frac{2p_{1}k_{1}-1}{k_{1}}} + \xi(e)^{\frac{1}{k_{1}}} \beta_{1} \lfloor e \rfloor^{\frac{2\lambda_{1}k_{1}-1}{k_{1}}} \right)^{k_{1}} \\
\leq -\sum_{i=1}^{3} \left( \xi(e)^{\frac{1}{k_{1}}} \alpha_{1} |e_{i}|^{\frac{2p_{1}k_{1}-1}{k_{1}}} + \frac{1}{k_{1}} + \xi(e)^{\frac{1}{k_{1}}} \beta_{1} |e_{i}|^{\frac{2\lambda_{1}k_{1}-1}{k_{1}}} + \frac{1}{k_{1}} \right)^{k_{1}} \\
\leq -\left( \xi^{\frac{1}{k_{1}}} \mu_{1} V_{1}^{p_{1}} + \xi^{\frac{1}{k_{1}}} \mu_{2} V_{1}^{\lambda_{1}} \right)^{k_{1}} \tag{11.19}$$

Applying Lemmas 11.1 and 2.3, it is concluded that  $V_1(e) \equiv 0$  is met for  $t \geq T_e$ , where the settling-time  $T_e$  satisfies (11.17).

**Theorem 11.2** Let an estimation law  $d_{est}$  be designed as

$$\mathbf{d}_{\text{est}} = \hat{\mathbf{d}}_l - l_1 \mathbf{x}_2 + \mathbf{M}^{-1}(\mathbf{x}_1) (\mathbf{C}_1(\mathbf{x}_1, \mathbf{x}_2) \mathbf{x}_2 + \mathbf{C}_2(\mathbf{x}_1, \mathbf{x}_2))$$
(11.20)

where

$$\hat{\mathbf{d}}_{l} = \frac{l_{1}l_{2}\hat{\mathbf{z}} + \dot{\mathbf{y}}}{l_{2}} \tag{11.21}$$

Then, the lumped uncertainty  $\mathbf{d}$  is precisely estimated by  $\mathbf{d}_{est}$  within a fixed time  $T_e$ . The estimation error  $\mathbf{d}_e = \mathbf{d} - \mathbf{d}_{est}$  is such that  $\mathbf{d}_e(t) \equiv \mathbf{0}$  for  $t \geq T_e$ .

**Proof** From (11.16) and (11.21), it follows that

$$d_{e} = d_{l} - l_{1}x_{2} + M^{-1}(x_{1})(C_{1}(x_{1}, x_{2})x_{2} + C_{2}(x_{1}, x_{2}))$$

$$- \hat{d}_{l} + l_{1}x_{2} - M^{-1}(x_{1})(C_{1}(x_{1}, x_{2})x_{2} + C_{2}(x_{1}, x_{2}))$$

$$= d_{l} - \hat{d}_{l}$$
(11.22)

Substituting (11.21) in (11.22) gives

$$\mathbf{d}_{e} = \mathbf{d}_{l} - \frac{l_{1}l_{2}\hat{\mathbf{z}} + \dot{\mathbf{y}}}{l_{2}} = \mathbf{d}_{l} - \frac{l_{1}l_{2}\hat{\mathbf{z}} - l_{1}l_{2}\mathbf{z} + l_{2}\mathbf{d}_{l}}{l_{2}} = l_{1}\mathbf{e}$$
(11.23)

Because  $e(t) \equiv \mathbf{0}$  is achieved from Theorem 11.1 for  $t \geq T_e$ ,  $d_e(t) = \mathbf{0}$  is achieved for  $t \geq T_e$ . It is inferred that d is estimated utilizing  $d_{\text{est}}$  after  $T_e$ .

**Remark 11.2** It is seen in Theorems 11.1 and 11.2 that  $\dot{y}$  is required to implement the proposed control approach in practice. To satisfy this requirement, the high-order sliding-mode differentiators (HOSMDs) [8] can be applied to obtain  $\dot{y}$ . That is because the HOSMDs can achieve an exact and finite-time estimation of the required  $\dot{y}$  by inputting the signal value y into the differentiator. It is seen in [8] that a Kth-order sliding-mode differentiator (K > 2) has a form of

$$\begin{cases}
\dot{\bar{\boldsymbol{v}}}_{0} &= \boldsymbol{v}_{0}, \boldsymbol{v}_{0} = \bar{\boldsymbol{v}}_{1} - \kappa_{0} || \bar{\boldsymbol{v}}_{0} - \boldsymbol{h} || \frac{\kappa}{K+1} || \bar{\boldsymbol{v}}_{0} - \boldsymbol{h} ||^{0} \\
\dot{\bar{\boldsymbol{v}}}_{j} &= \boldsymbol{v}_{j}, \boldsymbol{v}_{j} = \bar{\boldsymbol{v}}_{j+1} - \kappa_{j} || \bar{\boldsymbol{v}}_{j} - \boldsymbol{v}_{j-1} || \frac{\kappa-j}{K+1-j} || \bar{\boldsymbol{v}}_{j} - \boldsymbol{v}_{j-1} ||^{0} \\
\vdots & \vdots & \vdots \\
\dot{\boldsymbol{j}} &= 1, 2, \dots, K-1 \\
\dot{\bar{\boldsymbol{v}}}_{K} &= -\kappa_{K} || \bar{\boldsymbol{v}}_{K} - \boldsymbol{v}_{K-1} ||^{0}
\end{cases}$$
(11.24)

where  $\kappa_j \in \mathbb{R}_+$  is positive gains,  $\bar{\boldsymbol{v}}_j \in \mathbb{R}^r$  is the state of this differentiator,  $j = 1, 2, \ldots, K$ ,  $\boldsymbol{h} \in \mathbb{R}^r$  is the input signal. Following [8],  $\dot{\boldsymbol{h}} = \boldsymbol{v}_0$  is achieved after a finite time. Hence, when applying the differentiator (11.24) to calculate  $\dot{\boldsymbol{y}}$ ,  $\boldsymbol{y}$  should be chosen as the input signal  $\boldsymbol{h}$ , i.e.,  $\boldsymbol{h} = \boldsymbol{y}$ , and  $\bar{\boldsymbol{v}}_j \in \mathbb{R}^3$ ,  $j = 1, 2, \ldots, K$ . Then, it follows that  $\dot{\boldsymbol{y}} = \boldsymbol{v}_0$ .

**Remark 11.3** It is seen in Remark 11.1 that  $\Theta$ ,  $\omega$ ,  $\dot{\Theta}$ ,  $x_1$ , and  $x_2$  are measurable via the sensors fixed in considered satellite. Moreover,  $x_a$  can be obtained by solving (11.14) for any u. Then, z can be numerically obtained, and  $\hat{z}$  is available from (11.16). Therefore, the unknown input observer (11.16) is available for practical implementation. In addition, it is known from the paragraph below (11.2) and the nominal inertia  $J_0$  that  $M^{-1}(x_1)$ ,  $C_1(x_1, x_2)$ ,  $C_2(x_1, x_2)$  are available. Consequently, it can be obtained from Remark 11.2 and (11.21) that the estimation  $d_{\text{est}}$  is also available.

### C A Fixed-Time Sliding Manifold

The following fixed-time sliding manifold S (FTSM) is synthesized in this part to circumvent the singularity issue and provide the system states with fast fixed-time convergence.

$$S = H(x_1)x_1 + |x_2|^{\gamma} \tag{11.25}$$

with  $\mathbf{H}(\mathbf{x}_1) = \text{diag}([h(x_{11}), h(x_{12}), h(x_{13})]^T)$  and

$$h(x_{1i}) = \left(\xi(\boldsymbol{x}_1)^{\frac{1}{k_2}} \alpha_2 |x_{1i}|^{p_2 - \frac{1}{k_2 \gamma}} + \xi(\boldsymbol{x}_1)^{\frac{1}{k_2}} \beta_2 |x_{1i}|^{\lambda_2 - \frac{1}{k_2 \gamma}}\right)^{k_2 \gamma}, \ i = 1, 2, 3 \quad (11.26)$$

where  $\alpha_2 \geq 1$ ,  $\alpha_2 \in \mathbb{R}_+$ ,  $\beta_2 \in \mathbb{R}_+$ ,  $p_2 \in \mathbb{R}_+$ ,  $\bar{q}_2 \in \mathbb{R}_+$ ,  $k_2 \in \mathbb{R}_+$ ,  $\gamma > 1$ ,  $b_2 \in \mathbb{R}_+$ , and  $c_2 \in \mathbb{R}_+$  are constants.  $\frac{1}{\gamma} < p_2 k_2 < 1$ ,  $\bar{q}_2 k_2 > 1$ ,  $\lambda_2 = \frac{1}{2k_2} + \frac{1}{2} \bar{q}_2 + \left(\frac{1}{2} \bar{q}_2 - \frac{1}{2k_2}\right) \operatorname{sgn}(||\boldsymbol{x}_1|| - 1)$ , and  $\xi(\boldsymbol{x}_1) = a_2 + (1 - a_2) \exp(-b_2 ||\boldsymbol{x}_1||^{c_2})$ .

**Theorem 11.3** If a control law can be presented to govern the states of the attitude system to reach  $S = \mathbf{0}$  and stay in thereafter, then the system states converge to  $\mathbf{0}$  after a fixed time  $T_s \in \mathbb{R}_+$ , which does not depend on the initial conditions. Moreover,  $T_s$  is bounded as

$$T_s < \frac{1}{\beta_2^{k_2}(\bar{q}_2k_2 - 1)} + \frac{1}{\beta_2^{k_2}(1 - p_2k_2)} \ln\left(1 + \left(\frac{\beta_2}{\alpha_2}\right)^{k_2}\right)$$
 (11.27)

**Proof** When S = 0 is reached, from (11.25), one has

$$\dot{x}_{1i} = -\left(h(x_{1i})\right)^{\frac{1}{\gamma}} \lfloor x_{1i} \rfloor^{\frac{1}{\gamma}} 
= -\left(\xi(x_1)^{\frac{1}{k_2}} \alpha_1 |x_{1i}|^{p_2 - \frac{1}{k_2\gamma}} - \xi(x_1)^{\frac{1}{k_2}} \beta_2 |x_{1i}|^{\lambda_2 - \frac{1}{k_2\gamma}}\right)^{k_2} \lfloor x_{1i} \rfloor^{\frac{1}{\gamma}} 
= -\left(\xi(x_1)^{\frac{1}{k_2}} \alpha_2 |x_{1i}|^{p_2} - \xi(x_1)^{\frac{1}{k_2}} \beta_2 |x_{1i}|^{\lambda_2}\right)^{k_2} \operatorname{sgn}(x_{1i})$$
(11.28)

Defining a new variable  $\bar{\Xi}_i = |x_{1i}|^{1-p_2k_2}$ , (11.28) is expressed as

$$\dot{\bar{\Xi}}_{i} = -(1 - p_{2}k_{2})\dot{x}_{1i}|x_{1i}|^{-p_{2}k_{2}}\operatorname{sgn}(x_{1i})$$

$$= -(1 - p_{2}k_{2})|x_{1i}|^{-p_{2}k_{2}}\left(\xi(\mathbf{x}_{1})^{\frac{1}{k_{2}}}\alpha_{2}|x_{1i}|^{p_{2}} + \xi(\mathbf{x}_{1})^{\frac{1}{k_{2}}}\beta_{2}|x_{1i}|^{\lambda_{2}}\right)^{k_{2}}$$

$$= -(1 - p_{2}k_{2})\left(\xi(\mathbf{x}_{1})^{\frac{1}{k_{2}}}\alpha_{2} + \xi(\mathbf{x}_{1})^{\frac{1}{k_{2}}}\beta_{2}\bar{\Xi}_{i}^{\bar{\eta}_{2}}\right)^{k_{2}}$$
(11.29)

where  $\bar{\eta}_2 = \frac{\lambda_2 - p_2}{1 - p_2 k_2}$ . Similar to Lemma 11.1, the system state converges to zero after a fixed time given by (11.27).

**Remark 11.4** In [9, 10], a fixed-time sliding manifold has been presented as (11.25) in which  $h(x_{1i})$  is expressed as

$$h(x_{1i}) = \left(\alpha_2 |x_{1i}|^{p_2 - \frac{1}{k_2 \gamma}} + \beta_2 |x_{1i}|^{\bar{q}_2 - \frac{1}{k_2 \gamma}}\right)^{k_2 \gamma}$$
(11.30)

The fixed time ensured by [9, 10] is bounded by  $\bar{T}_x \leq \frac{1}{\beta_2^{k_2}(\bar{q}_2k_2-1)} + \frac{1}{\alpha_2^{k_2}(1-p_2k_2)}$ . Since  $\ln\left(1+\left(\frac{\beta_2}{\alpha_2}\right)^{k_2}\right) \leq \left(\frac{\beta_2}{\alpha_2}\right)^{k_2}$  always holds, the proposed FTSM of this chapter obtains faster convergence rate than the FTSM presented by [10].

### D Robust Fixed-Time Attitude Controller

Let the robust fixed-time attitude stabilization controller be synthesized as

$$u_{A} = (\mathbf{R}^{\mathrm{T}}(\mathbf{\Theta}))^{-1} \mathbf{M}(\mathbf{\Theta}) (\mathbf{M}^{-1}(\mathbf{x}_{1}) (\mathbf{C}_{1}(\mathbf{x}_{1}, \mathbf{x}_{2}) \mathbf{x}_{2}$$

$$+ \mathbf{C}_{2}(\mathbf{x}_{1}, \mathbf{x}_{2})) - \frac{1}{\gamma} (\tilde{\mathbf{M}}(\mathbf{x}_{1}) + \mathbf{M}(\mathbf{x}_{1})) [\mathbf{x}_{1}]^{2-\gamma}$$

$$- \mathbf{d}_{\text{est}} - \frac{1}{\rho_{0} \gamma} \bar{\mathbf{P}}(\mathbf{x}_{2}) \left( \xi(\mathbf{S})^{\frac{1}{k_{3}}} \alpha_{3} [\mathbf{S}]^{\frac{2\rho_{3}k_{3}-1}{k_{3}}} + \xi(\mathbf{S})^{\frac{1}{k_{3}}} \beta_{3} [\mathbf{S}]^{\frac{2\lambda_{3}k_{3}-1}{k_{3}}} \right)^{k_{3}}$$

$$(11.31)$$

with  $\bar{P}(\mathbf{x}_2) = \text{diag}([\bar{P}_1, \bar{P}_2, \bar{P}_3]^T)$ ,  $\bar{P}_i = \mu_{\bar{\sigma}}(|x_{2i}|^{\gamma-1})|x_{2i}|^{\gamma-1}$ ,  $i = 1, 2, 3, k_3 > 1$ ,  $\alpha_3 \in \mathbb{R}_+$ ,  $\beta_3 \in \mathbb{R}_+$ , and  $\rho_0 = \frac{\pi}{2\bar{\sigma}}$  are control gains.  $p_3k_3 < 1$ ,  $\bar{q}_3k_3 > 1$ , and  $\tilde{\mathbf{M}}(\mathbf{x}_1) = \text{diag}([\tilde{h}(x_{11}), \tilde{h}(x_{12}), \tilde{h}(x_{13})]^T$ , i = 1, 2, 3,

$$\tilde{h}(x_{1i}) = k_1 \gamma \left( \xi(\mathbf{x}_1)^{\frac{1}{k_2}} \alpha_2 |x_{1i}|^{p_2 - \frac{1}{k_2 \gamma}} + \xi(\mathbf{x}_1)^{\frac{1}{k_2}} \beta_2 |x_{1i}|^{\lambda_2 - \frac{1}{k_2 \gamma}} \right)^{k_2 \gamma - 1}$$

$$\times \left( \xi(\mathbf{x}_1)^{\frac{1}{k_2}} \alpha_2 \left( p_2 - \frac{1}{k_2 \gamma} \right) |x_{1i}|^{p_2 - \frac{1}{k_2 \gamma}} \right)$$

$$+ \xi(\mathbf{x}_1)^{\frac{1}{k_2}} \beta_2 \left( \lambda_2 - \frac{1}{k_2 \gamma} \right) |x_{1i}|^{\lambda_2 - \frac{1}{k_2 \gamma}} \right)$$

$$(11.32)$$

Moreover, the function  $\mu_{\bar{\sigma}}$  is

$$\mu_{\bar{\sigma}}(x) = \begin{cases} \sin\left(\frac{0.5\pi x}{\bar{\sigma}}\right), & |x| \le \bar{\sigma} \\ 1, & |x| > \bar{\sigma} \end{cases}$$
 (11.33)

**Theorem 11.4** For the flexible satellite with modeling error induced by  $\mathbf{u}_d$ , the uncertain inertia  $\Delta \mathbf{J}$ , and the actuator uncertainty  $\mathbf{u}_F$ , applying the estimation law (11.16) and the fixed-time attitude controller (11.31), then the attitude Euler angles and the rotation velocity are fixed-time stable with the settling time  $T_c$  satisfying  $T_c < T_s + T_1$ , where  $T_1$  is bounded by

$$T_1 < \frac{1}{\mu_A^{k_3}(\bar{q}_3 k_3 - 1)} + \frac{1}{\mu_A^{k_3}(1 - p_3 k_3)} \ln \left( 1 + \left( \frac{\mu_4^{k_3}}{\mu_3} \right) \right)$$
 (11.34)

where 
$$\mu_3 = \alpha_3(\rho_0)^{-\frac{1}{k_3}} (\mu_{\tilde{\sigma}}(|x_{2i}|^{\gamma-1}))^{\frac{1}{k_3}}$$
 and  $\mu_4 = \beta_3(\rho_0)^{-\frac{1}{k_3}} (\mu_{\tilde{\sigma}}(|x_{2i}|^{\gamma-1}))^{\frac{1}{k_3}}$ .

**Proof** Select another Lyapunov candidate function  $V_s = S^T S$ . Applying (11.25), one can calculate the time derivative of  $V_s$  as

$$\dot{V}_{s} = 2S^{T}(\dot{H}(x_{1})x_{1} + H(x_{1})\dot{x}_{1}) 
+ 2S^{T}\gamma \operatorname{diag}(|x_{2}|^{\gamma-1})(\tau + d - M^{-1}(x_{1})(C_{1}(x_{1}, x_{2})x_{2} + C_{2}(x_{1}, x_{2}))) 
(11.35)$$

Let  $\mu_{\bar{\sigma}} = [\mu_{\bar{\sigma}}(|x_{21}|^{\gamma-1}), \mu_{\bar{\sigma}}(|x_{22}|^{\gamma-1}), \mu_{\bar{\sigma}}(|x_{23}|^{\gamma-1})]^T$  be defined, then substituting the controller (11.31) into (11.35) yields

$$\dot{V}_{s} = \frac{2}{\rho_{0}} S^{T} \operatorname{diag}(\boldsymbol{\mu}_{\bar{\sigma}}) \left( \xi^{\frac{1}{k_{3}}} \alpha_{3} \lfloor S \rfloor^{\frac{2\rho_{3}k_{3}-1}{k_{3}}} + \xi^{\frac{1}{k_{3}}} \beta_{3} \lfloor S \rfloor^{\frac{2\lambda_{3}k_{3}-1}{k_{3}}} \right)^{k_{3}} 
+ \gamma S^{T} \operatorname{diag}(|\boldsymbol{x}_{2}|^{\gamma-1}) (\boldsymbol{d} - \boldsymbol{d}_{est})$$
(11.36)

Since  $d_e = d - d_{est} = 0$  for  $t > T_e$ , (11.36) can be simplified as

$$\dot{V}_{s} = \frac{2}{\rho_{0}} \mathbf{S}^{\mathrm{T}} \operatorname{diag}(\boldsymbol{\mu}_{\bar{\sigma}}) \left( \xi^{\frac{1}{k_{3}}} \alpha_{3} \lfloor \mathbf{S} \rfloor^{\frac{2\rho_{3}k_{3}-1}{k_{3}}} + \xi^{\frac{1}{k_{3}}} \beta_{3} \lfloor \mathbf{S} \rfloor^{\frac{2\lambda_{3}k_{3}-1}{k_{3}}} \right)^{k_{3}} \\
\leq - \sum_{i=1}^{3} \left( \xi^{\frac{1}{k_{3}}} \alpha_{3} (\rho_{0})^{-\frac{1}{k_{3}}} (\mu_{\bar{\sigma}} (|x_{2i}|^{\gamma-1}))^{\frac{1}{k_{3}}} |\mathbf{S}_{i}|^{\frac{2\rho_{3}k_{3}-1}{k_{3}}} + \frac{1}{k_{3}} \right)^{k_{3}} \\
+ \xi^{\frac{1}{k_{3}}} \beta_{3} (\rho_{0})^{-\frac{1}{k_{3}}} (\mu_{\bar{\sigma}} (|x_{2i}|^{\gamma-1}))^{\frac{1}{k_{3}}} |\mathbf{S}_{i}|^{\frac{2\lambda_{3}k_{3}-1}{k_{3}}} + \frac{1}{k_{3}} \right)^{k_{3}} \\
\leq - \left( \xi^{\frac{1}{k_{3}}} \mu_{3} V_{s}^{\rho_{3}} + \xi^{\frac{1}{k_{3}}} \mu_{4} V_{s}^{\lambda_{3}} \right)^{k_{3}}$$
(11.37)

Applying Lemma 2.3 and the result in Lemma 11.1, it is ready to conclude that  $V_s \equiv 0$  after the settling time  $T_1$  satisfying (11.34).

After reaching the sliding surface S = 0, it can be obtained from Theorem 10.2 that the states will be zero after the settling time  $T_s$ . Then, one can prove that the attitude Euler angles and the angular velocity are fixed-time stable with the settling time  $T_c$  satisfying  $T_c < T_s + T_1$  regardless of any initial states.

**Remark 11.5** In contrast to the existing observers, the proposed observer (11.16) provides precise estimation for the lumped uncertainty after a fixed time which does not depend on the initial estimation error. The estimation error is zero after that fixed time. Moreover, it relaxes some assumptions such as the need for the upper limit of total uncertainties to be available in advance or the time derivative of the disturbance to converge to zero. This is one of the main contributions of this work.

**Remark 11.6** When practically implement the proposed approach to perform attitude maneuvers, the controller (11.31) and the observer (11.16) will be numerically computed by the satellite's onboard embedded computer. The designed control scheme is hence implementable for in-orbital satellite. Moreover, the procedures to choose the control gains are listed in the following Remark 11.7. Hence, the controller is practically implementable for satellite system.

**Remark 11.7** When implementing the proposed approach, control gains  $\alpha_i$ ,  $\beta_i$ ,  $p_i$ ,  $q_i$ ,  $k_i$ ,  $a_j$ , and  $b_j$ , i = 1, 2, 3, j = 1, 2, should be carefully chosen and turned to achieve higher attitude accuracy and acceptable control power. Based on (11.27) and (11.34), the following procedures should be followed for choice of the control gains.

- (1) Larger  $\alpha_i$  and  $\beta_i$  lead to a faster convergence rate, but large overshoot and more control energy consumption will result. Hence, a compromise should be made between the converging rate and the overshoot.
- (2) According to (11.27) and (11.34), the gains  $p_i$ ,  $q_i$ , and  $k_i$  also important to determine the system's converging rate.
- (3) The gains  $a_j$  and  $b_j$  have profound influence on the convergence rate. If  $a_j$  is selected near 1, the effect of  $\xi$  is reduced, and vice versa. By choosing  $b_j$  large enough, the impact of  $\xi$  is highlighted.

### 11.2.4 Simulation Results

To validate the superior attitude control performance of the presented approach, numerical simulation is conducted on a flexible satellite with its structure shown in Fig. 9.1. The details of this satellite are provided in [11]. The task of this satellite is Earth observation. The satellite's orbit of the satellite is circular. Its altitude and inclination are 638 km and 95.4 degrees, respectively, i.e.,  $\omega_0 = 0.0011$  rad/s. As shown in Fig. 9.1, there are two solar paddles fixed in the  $+Y_B$  and the  $-Y_B$  axis, respectively. They are called the north and the south solar paddle, receptively. Each paddle has a dimension of 15×0.75 m. The nominal designed inertia of the satellite is  $J_0 = [487, 15, -1.2; 14.9, 177, -7.3; -1.2, -7.3, 404] \text{ kg} \cdot \text{m}^2$ . After ground testing, the coupling matrix between the rigid body and the solar paddles is calculated as  $\delta = [1, 0.1, 0.1; 0.5, 0.1, 0.01; -1, 0.3, 0.01] \text{ kg} \cdot \text{m}^2$ . Moreover, it is tested that when choosing the elastic mode number N as N=3, the flexible vibration of solar paddles can be mainly reflected. Hence, N=3 is chosen to establish the model of the attitude control system. Correspondingly, the natural frequencies are measured as  $\Lambda_1 = 1.8912 \,\text{rad/s}, \, \Lambda_2 = 2.884 \,\text{rad/s}, \, \Lambda_3 = 3.4181 \,\text{rad/s}, \, \text{respectively.}$  The damping ratios are measured on the ground as  $\xi_1 = \xi_2 = \xi_3 = 0.01$ .

For the considered satellite, the gravity-gradient torque, the aerodynamic torque, and the Earth magnetic torque are the primary external disturbances for  $\boldsymbol{u}_d$ , which will be considered in the simulation. They will be mathematically calculated according to [6] and put into the system model. Moreover, the uncertain inertia is assumed to be  $\Delta \boldsymbol{J} = 0.1 \boldsymbol{J}_0$ . When carrying out simulation, the initial attitude are  $\psi(0) = 15$  degrees,  $\phi(0) = 25$  degrees, and  $\theta(0) = -5$  degrees. The initial angular velocity is  $\boldsymbol{\omega}(0) = [0.01, -0.01, -0.02]^{\mathrm{T}}$  rad/s.

Besides the proposed observer-based fast fixed-time attitude control (named OBFFTAC), the fixed-time attitude control presented in [9] (denoted by FTAC) is also simulated under the same condition for performance comparison. For a fair comparison, the parameters of OBFFTAC are taken the same as FTAC except for the new parameters in the sliding manifold as well as the controller. The OBFFTAC parameters are chosen as  $\gamma=1.5,\ p_1=0.35,\ p_2=0.3,\ p_3=0.45,\ q_1=0.6,\ q_2=0.75,\ q_3=0.45,\ \alpha_1=0.2,\ \alpha_2=0.1,\ \alpha_3=0.4,\ \beta_1=0.08,\ \beta_2=0.06,\ \beta_3=0.1,\ k_1=2,\ k_2=2,\ k_3=2,\ l_1=0.02,\ l_2=14,\ l_3=25,\ \sigma=0.01,\ a_1=1.4,\ a_2=1.35,\ b_1=6,\ b_2=4,\ \text{and}\ c_1=c_2=1.$  Moreover, the fifth-order sliding mode differentiator (11.24) is applied to calculate  $\dot{y}$  with K=5 and  $\kappa_0=\kappa_1=\kappa_2=\kappa_3=\kappa_4=\kappa_5=1.5.$ 

### A Comparison in the Case of Normal Actuators

In the subsection, the case that all the actuators of the flexible satellite do not have any uncertainty is considered. For this case, the attitude stabilization results from the OBFFTAC and the FTAC are illustrated in Figs. 11.2, 11.3, 11.4. It is found that the OBFFTAC achieves a faster converging rate and higher pointing accuracy, while the maximum required control torques are almost identical. To

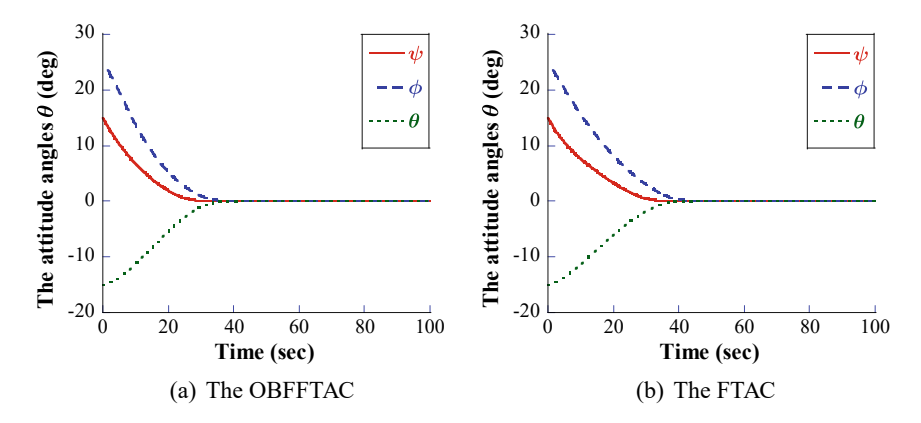


Fig. 11.2 The attitude from (11.31) with normal actuator

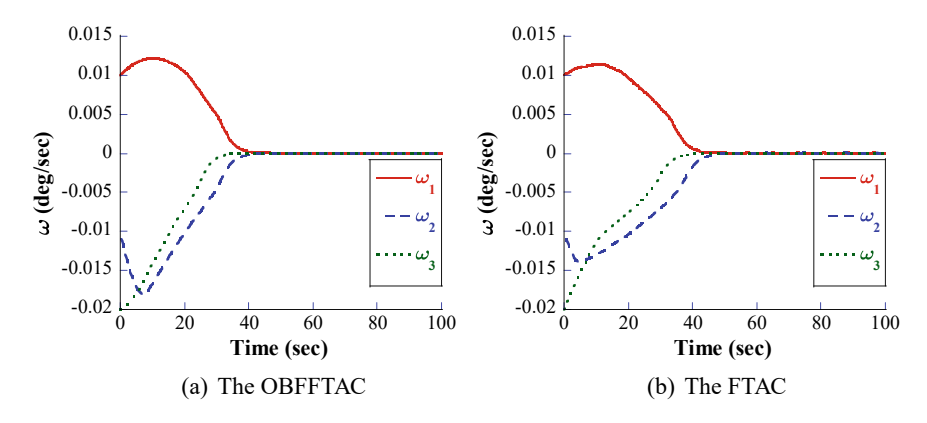


Fig. 11.3 The angular velocity from (11.31) with normal actuator

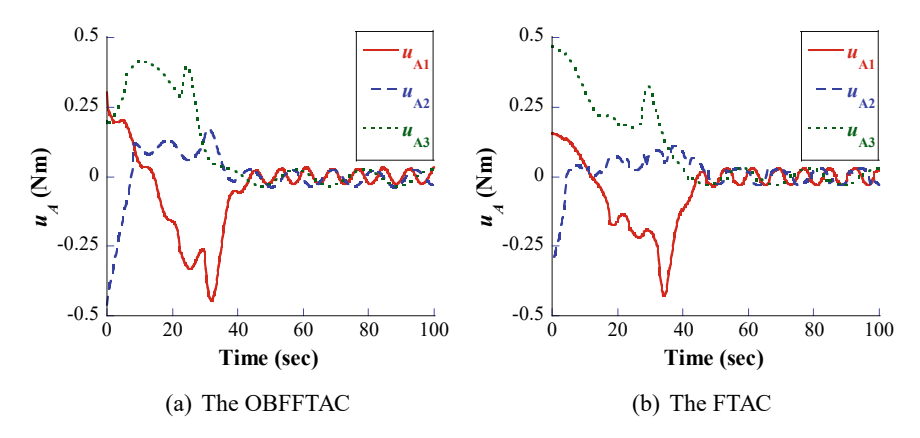


Fig. 11.4 The torque of the controller (11.31) with normal actuator

Controller	Euler angles	Angular velocity	Convergence time
OBFFTAC	$5.5 \times 10^{-6}$	$4 \times 10^{-7}$	44.6
FTAC	$4 \times 10^{-3}$	$3 \times 10^{-5}$	51.2
Improvement percentage, %	98.25	98.67	12.89

Table 11.1 The performance comparison with normal actuators

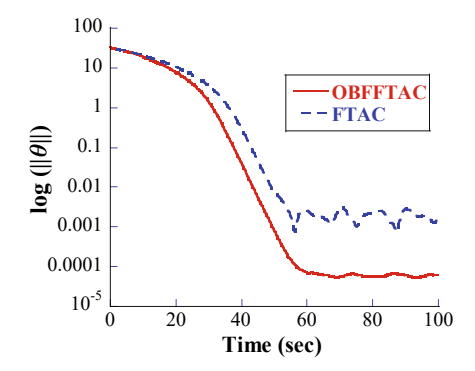


Fig. 11.5 Norm of the attitude from (11.31) with normal actuators

provide further insight into the control performance in terms of pointing accuracy as well as the convergence rate, the data analysis is given in Table 11.1. In the table, the convergence time is defined as the time after which  $||\Theta|| \le 6 \times 10^{-3}$  (deg) and  $||\omega|| \le 4 \times 10^{-5}$  (deg/s) are satisfied. It is found that the OBFFTAC provides a faster convergence rate and smaller steady-state error. The improvement percentage confirms the superior performance of OBFFTAC especially in terms of pointing accuracy. Moreover, the norm of the attitude angles and the rotation velocity are illustrated in Figs. 11.5 and 11.6, respectively. That two controllers accomplish the planned attitude maneuvering. However, the OBFFTAC provides greatly preferable control performance to the FTAC both in theory and simulation.

## B Comparison in the Case of Actuator Uncertainty

To evaluate the robust control capability of the controllers, actuator uncertainty is considered in this case. In particular, the actuator uncertainty is assumed to be the actuator fault:

$$\boldsymbol{u}_F = (\boldsymbol{E}(t) - \boldsymbol{I}_3)\boldsymbol{u}_A + \bar{\boldsymbol{u}} \tag{11.38}$$

where  $E(t) = \text{diag}([l_1, l_2, l_3]^T)$  refers to the actuator effectiveness matrix in which  $g_i$  represents fault indicator of the *i*th actuator,  $\bar{\boldsymbol{u}} = [\bar{u}_1, \bar{u}_2, \bar{u}_3]^T$  denotes the bias fault. For example,  $l_i = 1$  and  $\bar{u}_i = 0$  is associated with the case that *i*th actuator is

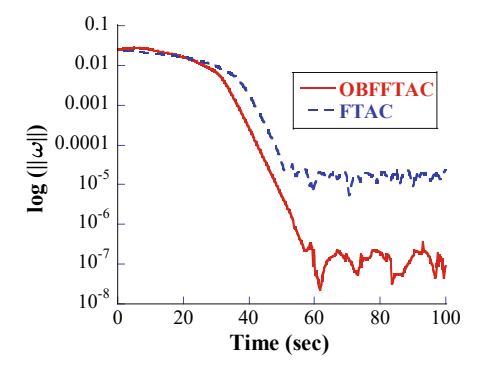


Fig. 11.6 Norm of the angular velocity from (11.31) with normal actuators

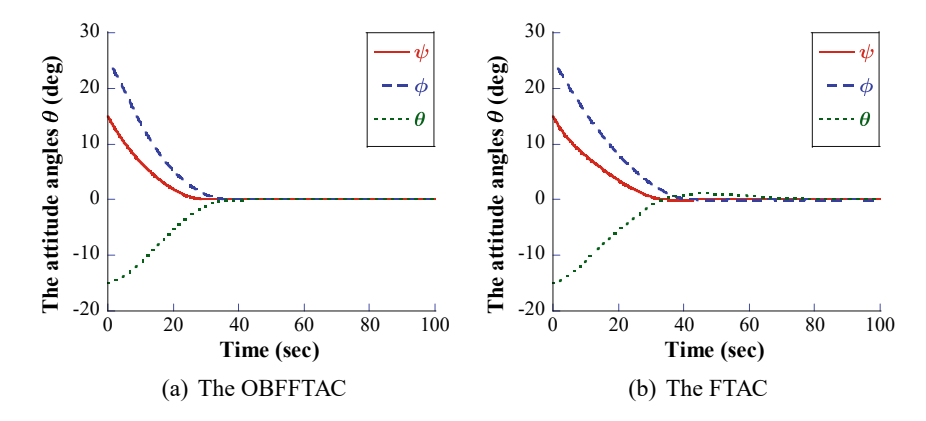


Fig. 11.7 The attitude from (11.31) with actuator uncertainty

healthy.  $0 < l_i < 1$  denotes that the *i*th actuator partially rather than totally loses its control effectiveness.

In this subsection, the fault indicator and bias faulty torque are given as  $\bar{u}_1 = 0.6\,\mathrm{N\cdot m},\ \bar{u}_2 = -0.03\,\mathrm{N\cdot m},\ \bar{u}_1 = 0.05\,\mathrm{N\cdot m},\ l_1 = \begin{cases} 1, & \text{if } t \leq 20 \\ 0.5, & \text{otherwise} \end{cases},\ l_2 = \begin{cases} 1, & \text{if } t \leq 35 \\ 0.6, & \text{otherwise} \end{cases}$  and  $l_3 = \begin{cases} 1, & \text{if } t \leq 25 \\ 0.5, & \text{otherwise} \end{cases}$ , when conducting simulation. Moreover, all the control gains are chosen the same as given in the preceding case.

Figures 11.7 and 11.8 illustrate the attitude and the rotation velocity revealing that the OBFFTAC obtains a much faster convergence rate for the case of having actuator uncertainty. The control performance is considerably degraded under the FTAC. The convergence time obtained by the FTAC significantly increases because of its longer rotation path.

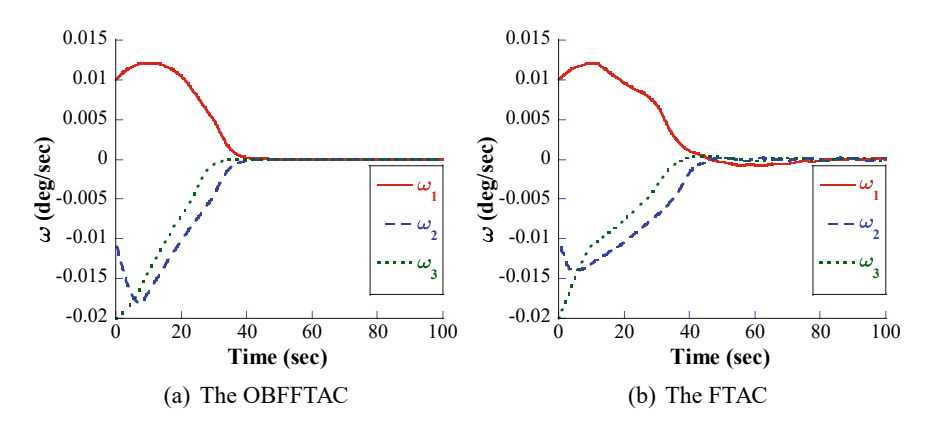


Fig. 11.8 The angular velocity from (11.31) with actuator uncertainty

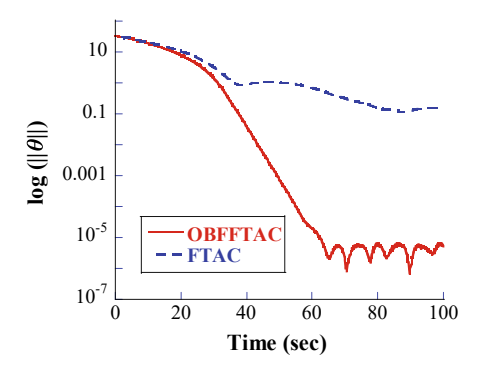


Fig. 11.9 Norm of the attitude from (11.31) with actuator uncertainty

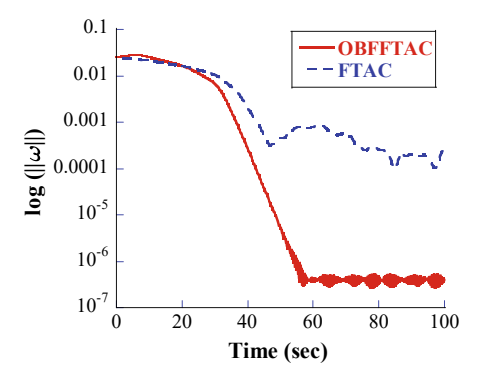


Fig. 11.10 Norm of the angular velocity from (11.31) with actuator uncertainty

According to Figs. 11.9 and 11.10, it can concluded that the OBFFTAC obtains the most accurate attitude control. This is due to the observer-based estimation law (11.16). The comparison result is listed in Table 11.2. The proposed strategy, in

Controller	Euler angles	Angular velocity	Convergence time
OBFFTAC	$7 \times 10^{-6}$	$6 \times 10^{-7}$	44.6
FTAC	0.2	$4 \times 10^{-4}$	$\infty$
Improvement percentage, %	99.99	99.85	100

Table 11.2 The performance comparison in the case of actuator uncertainty

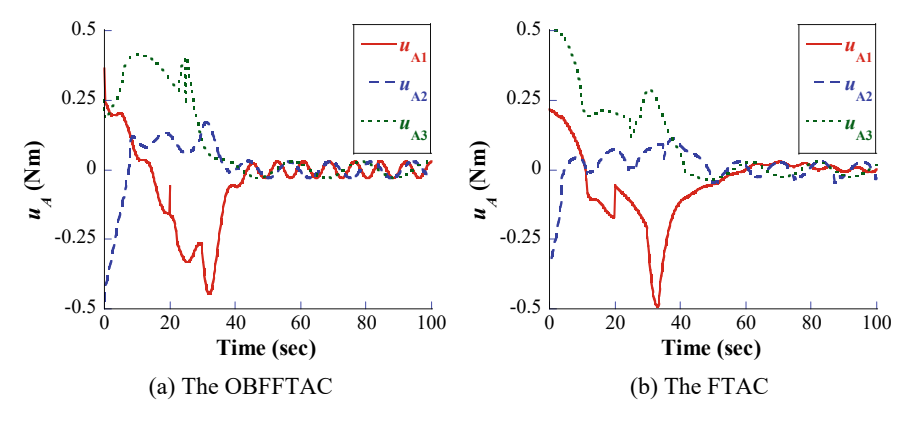


Fig. 11.11 The torque of the controller (11.31) with actuator uncertainty

contrast to the FTAC, successfully deals with the actuator uncertainty. It is confirmed that the control performance of the FTAC was significantly deteriorated while the actuators experienced uncertainty. The attitude control results of the OBFFTAC are roughly similar to that of the previous case. However, the FTAC failed to drive the attitude angles and the rotation velocity to the desired region. The superiority of the OBFFTAC over the FTAC was highlighted by this scenario.

The control power consumed is shown in Fig. 11.11. The maximum required control efforts for those two controllers are almost identical showing the superior control performance of the OBFFTAC. The lumped uncertainties along with their estimations are illustrated in Fig. 11.12. It is observed from the estimation errors in Fig. 11.13 that the total uncertainties are precisely reconstructed in a finite time, which is independent of the initial estimation errors. When a sudden actuator failure happened, the observer successfully estimated it to preserve stability and control performance. Such results confirm the claims in Theorem 11.3 that the suggested estimation law can estimate the lumped uncertainties in a fixed time. This is also the reason that superiority can be obtained from the OBFFTAC.

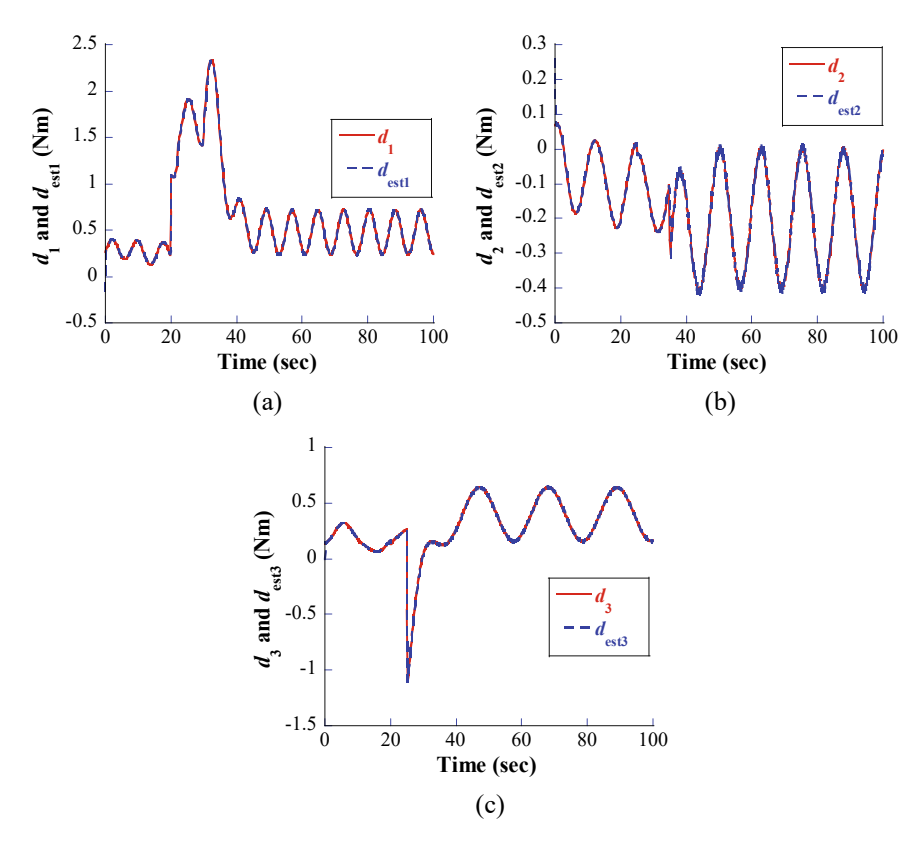
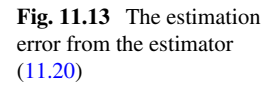
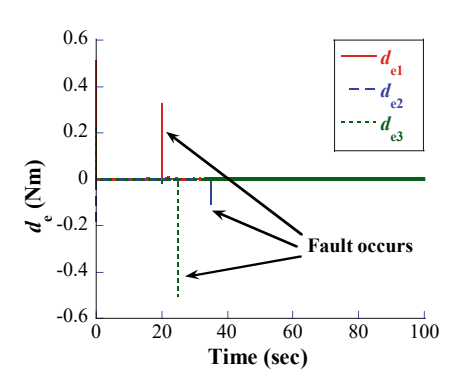


Fig. 11.12 The estimation performance of the estimator (11.20)





## 11.3 UIO-Based Attitude Tracking Control

## 11.3.1 System Description

For a general class of second-order uncertain systems with their dynamics described by

$$A_0(x)\ddot{x} + f_0(x,\dot{x}) + g_0(x) + \Delta h(x,\dot{x},\ddot{x}) = u + d$$
 (11.39)

where  $\mathbf{x} \in \mathbb{R}^n$  is the state vector,  $\mathbf{A}_0(\mathbf{x}) \in \mathbb{R}^{n \times n}$  is a nominal inertia matrix of the system,  $\mathbf{f}_0(\mathbf{x}, \dot{\mathbf{x}}) \in \mathbb{R}^n$  and  $\mathbf{g}_0(\mathbf{x}) \in \mathbb{R}^n$  denote the certain/nominal nonlinearities in the systems' dynamics,  $\mathbf{u} \in \mathbb{R}^n$  is the system input vector,  $\mathbf{d} \in \mathbb{R}^n$  is the unknown external disturbance, and the unknown vector  $\Delta \mathbf{h}(\mathbf{x}, \dot{\mathbf{x}}, \ddot{\mathbf{x}}) \in \mathbb{R}^n$  denotes the uncertain dynamics acting on the system, i.e.,

$$\Delta h(x, \dot{x}, \ddot{x}) = \Delta f(x, \dot{x}) + \Delta g(x) + \Delta A(x)\ddot{x}$$
(11.40)

in which  $\Delta A(x) \in \mathbb{R}^{n \times n}$  is the uncertain inertia,  $\Delta f(x, \dot{x}) \in \mathbb{R}^n$  and  $\Delta g(x) \in \mathbb{R}^n$  denote the system's uncertain parts of the nominal  $f_0(x, \dot{x})$  and  $g_0(x)$ , respectively.

For the considered system (11.39), it has following properties which can be adopted in the following control framework design and analysis of system's stability.

**Property 11.1** The symmetric inertia matrix  $A_0(x)$  is positive-definite. Moreover, there are two positive and known scalars  $\kappa_1 \in \mathbb{R}_+$  and  $\kappa_2 \in \mathbb{R}_+$  ensuring that the following inequality always hold for any vector  $\mathbf{a} \in \mathbb{R}^n$  and  $\mathbf{x} \in \mathbb{R}^n$ .

$$0 < \kappa_1 ||\boldsymbol{a}||^2 \le \boldsymbol{a}^{\mathrm{T}} \boldsymbol{A}_0(\boldsymbol{x}) \boldsymbol{a} \le \kappa_2 ||\boldsymbol{a}||^2$$
 (11.41)

**Remark 11.8** In comparison with another mathematical model given in (6.1) and used to describe Euler-Lagrange systems or a class of mechanical systems, the model (11.39) is more representative. It can be applied to describe the dynamics of more systems. Systems with the form (6.1) can be described by (11.39) absolutely. This is achieved by denoting  $C(q, \dot{q})\dot{q}$  as  $f_0(x, \dot{x})$ . However, systems modeled by (11.39) would be not described by (6.1). This implies that the existing second-order mechanical systems can be included in the systems described by (11.39). Hence, the mathematical model (11.39) has a more general form. To this end, it can be got to know that the model (11.39) can be adopted to describe the dynamics of many industrial systems, such as robotic manipulators, satellites, twin-lift helicopters, hypersonic flight vehicles, and marine vehicles.

**Remark 11.9** To facilitate the following tracking controller design, the model given in (11.39) can be rewritten as

$$A_0(x)\ddot{x} + f_0(x, \dot{x}) + g_0(x) = u + u_d$$
 (11.42)

where  $u_d = d - \Delta h(x, \dot{x}, \ddot{x})$ . The term  $u_d$  denotes the total modeling error acting the system.

#### 11.3.2 Problem Statement

The main problem to be investigated in this section can be formulated as: For the systems described by (11.39), design a general control framework to achieve the objective of tracking control with exponential convergence. More specifically, given any bounded desired/reference trajectory  $x_d$  (its first two time derivatives are also bounded for all time), develop a control input u to guarantee that  $x_d$  can be followed even in the presence of system uncertainty  $\Delta h(x, \dot{x}, \ddot{x})$  and external disturbance d, i.e., the trajectory tracking error  $x_e = x - x_d$  and the velocity tracking error and the velocity tracking error  $x_v = \dot{x} - \dot{x}_d$  are globally exponentially stable.

## 11.3.3 UIO-Based Exponential Tracking Controller

In this section, a general UIO-based tracking control architecture will be presented for the considered system (11.39) with exponential convergence performance guaranteed. This proposed control framework is illustrated in Fig. 11.14. It consists of two parts. One is the UIO observer-based estimator. It aims to estimate the total uncertainty precisely  $u_d$ . The other part is the control law. This law is designed by using the information supplied by the estimator. It will be applied to accomplish the planned trajectory tracking task with the total uncertainty compensated.

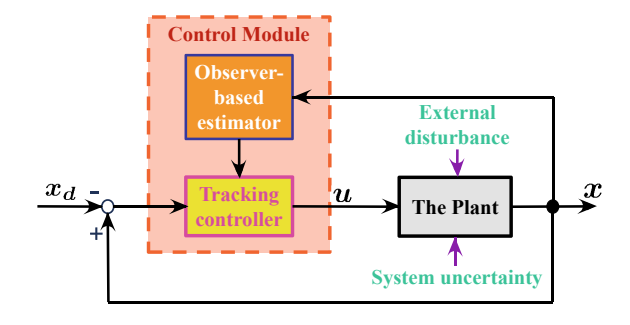
## A Unknown Input Finite-Time Observer for Modeling Error

We firstly introduce two new variables as  $\psi_1 = x$  and  $\psi_2 = \dot{x}$ . It leaves (11.42) as follows by using the Property 11.1

$$\dot{\boldsymbol{\psi}}_1 = \boldsymbol{\psi}_2 \tag{11.43}$$

$$\dot{\boldsymbol{\psi}}_{2} = -l_{1}\boldsymbol{A}_{0}^{-1}(\boldsymbol{\psi}_{1})\boldsymbol{\psi}_{2} + \boldsymbol{\zeta}(\boldsymbol{\psi}_{1},\boldsymbol{\psi}_{2}) + \boldsymbol{A}_{0}^{-1}(\boldsymbol{x})\boldsymbol{u} + \boldsymbol{A}_{0}^{-1}\boldsymbol{u}_{d}$$
(11.44)

**Fig. 11.14** The diagram of the proposed general control framework



where  $\boldsymbol{\zeta}(\boldsymbol{\psi}_1, \boldsymbol{\psi}_2) = -\boldsymbol{A}_0^{-1}(\boldsymbol{\psi}_1)(\boldsymbol{f}_0(\boldsymbol{\psi}_1, \boldsymbol{\psi}_2) + \boldsymbol{g}_0(\boldsymbol{\psi}_1) - l_1\boldsymbol{\psi}_2)$ , the positive scalar  $l_1 \in \mathbb{R}_+$  is known and determined by the designer.

For (11.44), another certain system is further introduced, which is of the form

$$\dot{\boldsymbol{\psi}}_{a} = -l_{1}\boldsymbol{A}_{0}^{-1}(\boldsymbol{\psi}_{1})\boldsymbol{\psi}_{a} + \boldsymbol{\zeta}(\boldsymbol{\psi}_{1}, \boldsymbol{\psi}_{2}) + \boldsymbol{A}_{0}^{-1}(\boldsymbol{\psi}_{1})\boldsymbol{u}$$
(11.45)

where the state  $\psi_a$  takes values in  $\mathbb{R}^n$ , and its measurement is available.

Define the error between  $\psi_2$  and  $\psi_a$  as  $\psi_e$ , i.e.,  $\psi_e = \psi_2 - \psi_a$ , and define an output signal as  $y = l_2 \psi_e$  with  $l_2 \in \mathbb{R}_+$  being a positive constant. Because the measurements of  $\psi_2$  and  $\psi_a$  are available, the signal y can be available.

On the basis of the above analysis, using the measurable output y and  $\psi_e$ , the following estimator is developed and applied to estimate the total uncertainty  $u_d$  acting on the system (11.39)

$$\hat{\boldsymbol{u}}_d = A_0(\boldsymbol{\psi}_1) \frac{l_1 l_2 A_0^{-1}(\boldsymbol{\psi}_1) \hat{\boldsymbol{\psi}}_e + \dot{\boldsymbol{y}}}{l_2}$$
 (11.46)

with  $\hat{\pmb{\psi}}_e \in \mathbb{R}^n$  being the estimate of  $\pmb{\psi}_e$  and determined by the following unknown input observer:

$$\dot{\hat{\boldsymbol{\psi}}}_{e} = -l_{2}l_{3}\hat{\boldsymbol{\psi}}_{e} + \frac{1}{l_{2}}\dot{\boldsymbol{y}} + l_{3}\boldsymbol{y} - l_{4}\lfloor\tilde{\boldsymbol{\psi}}_{e}\rfloor^{\frac{\gamma_{1}}{\gamma_{2}}}$$
(11.47)

where  $\tilde{\boldsymbol{\psi}}_e = [\tilde{\psi}_{e1}, \tilde{\psi}_{e2}, \dots, \tilde{\psi}_{en}]^{\mathrm{T}} = \hat{\boldsymbol{\psi}}_e - \boldsymbol{\psi}_e$  is the observer error between  $\boldsymbol{\psi}_e$  and  $\hat{\boldsymbol{\psi}}_e$ ;  $l_3 \in \mathbb{R}_+$  and  $l_4 \in \mathbb{R}_+$  are two observer gains with positive value;  $\gamma_1 \in \mathbb{R}_+$  and  $\gamma_2 \in \mathbb{R}_+$  are two positive odd integers such that  $\gamma_1 < \gamma_2$ .

#### **B** Exponential Tracking Controller

In addition to the defined trajectory error  $x_e$  and the velocity tracking error  $x_v$ , a new variable is defined as:

$$\boldsymbol{x}_m = \boldsymbol{x}_v + l_c \boldsymbol{x}_e \tag{11.48}$$

where  $l_c \in \mathbb{R}_+$  is a positive scalar.

Define the estimation error between  $u_d$  and  $\hat{u}_d$  as  $u_e$ , i.e.,  $u_e = u_d - \hat{u}_d$ . Then, applying the estimator proposed in (11.46), it is ready to present the main solution to the problem of asymptotic tracking control design in the following theorems.

**Theorem 11.5** Consider the uncertain systems described by (11.39), with the application of the estimator (11.46), design a controller as

$$u = -k_p x_e - k_d x_m + f_0(x, \dot{x}) + g_0(x) - \hat{u}_d + A_0(x) \ddot{x}_d - l_c A_0(x) (x_m - l_c x_e) - 0.5 \dot{A}_0(x) x_m$$
(11.49)

where  $k_p \in \mathbb{R}_+$  and  $k_d \in \mathbb{R}_+$  are two positive control gains, if the control gains are selected to satisfy

$$k_d - 0.5 > 0 (11.50)$$

$$l_2 l_3 - 0.5 > 0 ag{11.51}$$

then the estimator-based closed-loop system can be stabilized exponentially. Moreover, the total uncertainty  $\mathbf{u}_d$  can be precisely estimated by this estimator (11.46). with exponential convergence. The tracking error  $\mathbf{x}_e$ , the velocity tracking error  $\mathbf{x}_v$ , and the estimation error  $\mathbf{u}_e$ , are exponentially stable.

**Proof** Firstly, it follows from (11.44) and (11.45) that the dynamics of the observer error  $\psi_e$  is such that

$$\dot{\boldsymbol{\psi}}_{e} = -l_{1} \boldsymbol{A}_{0}^{-1}(\boldsymbol{\psi}_{1}) \boldsymbol{\psi}_{e} + \boldsymbol{A}_{0}^{-1}(\boldsymbol{\psi}_{1}) \boldsymbol{u}_{d}$$
 (11.52)

Using (11.52) and (11.46), it is able to get that  $u_e$  is such that

$$u_{e} = u_{d} - \hat{u}_{d}$$

$$= A_{0}(\psi_{1})(\dot{\psi}_{e} + l_{1}A_{0}^{-1}(\psi_{1})\psi_{e}) - \frac{1}{l_{2}}(l_{1}l_{2}\hat{\psi}_{e} + l_{2}A_{0}(\psi_{1})\dot{\psi}_{e})$$

$$= -l_{1}\tilde{\psi}_{e}$$
(11.53)

Moreover, applying the observer (11.47) and (11.52) leads to

$$\dot{\tilde{\boldsymbol{\psi}}}_{e} = \dot{\hat{\boldsymbol{\psi}}}_{e} - \dot{\boldsymbol{\psi}}_{e} = -l_{2}l_{3}\hat{\boldsymbol{\psi}}_{e} + \frac{1}{l_{2}}\dot{\boldsymbol{y}} + l_{3}\boldsymbol{y} - l_{4}\lfloor\tilde{\boldsymbol{\psi}}\rfloor^{\frac{\gamma_{1}}{\gamma_{2}}} - \dot{\boldsymbol{\psi}}_{e}$$

$$= -l_{2}l_{3}\tilde{\boldsymbol{\psi}}_{e} - l_{4}|\tilde{\boldsymbol{\psi}}_{e}|^{\frac{\gamma_{1}}{\gamma_{2}}} \tag{11.54}$$

Then, combining (11.53) and (11.54), one can find that

$$\dot{\boldsymbol{u}}_e = -l_1 \dot{\tilde{\boldsymbol{\psi}}}_e = -l_2 l_3 \boldsymbol{u}_e - l_4 \lfloor \boldsymbol{u}_e \rfloor^{\frac{\gamma_1}{\gamma_2}}$$
(11.55)

On the other hand, with the definition of  $x_e$  and (11.48), it follows that

$$\dot{\mathbf{x}}_e = \dot{\mathbf{x}} - \dot{\mathbf{x}}_d = \mathbf{x}_m - l_c \mathbf{x}_e \tag{11.56}$$

It can also be calculated by applying (11.42), the controller (11.49), and (11.56) that

$$A_{0}(\mathbf{x})\dot{\mathbf{x}}_{m} = A_{0}(\mathbf{x})(\ddot{\mathbf{x}} - \ddot{\mathbf{x}}_{d} + l_{c}(\mathbf{x}_{m} - l_{c}\mathbf{x}_{e}))$$

$$= \mathbf{u} + \mathbf{u}_{d} - \mathbf{f}_{0}(\mathbf{x}, \dot{\mathbf{x}}) - \mathbf{g}_{0}(\mathbf{x}) - A_{0}(\mathbf{x})\ddot{\mathbf{x}}_{d}$$

$$+ l_{c}A_{0}(\mathbf{x})(\mathbf{x}_{m} - l_{c}\mathbf{x}_{e})$$

$$= -k_{p}\mathbf{x}_{e} - k_{d}\mathbf{x}_{m} - \mathbf{u}_{e} - 0.5\dot{\mathbf{A}}_{0}(\mathbf{x})\mathbf{x}_{m}$$
(11.57)

Now, one can define a positive-definite Lyapunov function candidate as

$$V_{1} = \frac{1}{2} \boldsymbol{x}_{m}^{\mathrm{T}} \boldsymbol{A}_{0}(\boldsymbol{x}) \boldsymbol{x}_{m} + \frac{1}{2} k_{p} \boldsymbol{x}_{e}^{\mathrm{T}} \boldsymbol{x}_{e} + \frac{1}{2} \boldsymbol{u}_{e}^{\mathrm{T}} \boldsymbol{u}_{e}$$
(11.58)

Inserting (11.53) and (11.55)–(11.57) into the time-derivative of  $V_1$  yields

$$\dot{V}_{1} = 0.5 \boldsymbol{x}_{m}^{\mathrm{T}} \dot{\boldsymbol{A}}_{0}(x) \boldsymbol{x}_{m} + \boldsymbol{x}_{m}^{\mathrm{T}} \boldsymbol{A}_{0}(x) \dot{\boldsymbol{x}}_{m} + k_{p} \boldsymbol{x}_{e}^{\mathrm{T}} \dot{\boldsymbol{x}}_{e} + \boldsymbol{u}_{e}^{\mathrm{T}} \dot{\boldsymbol{u}}_{e} 
= \boldsymbol{x}_{m}^{\mathrm{T}} (-k_{p} \boldsymbol{x}_{e} - k_{d} \boldsymbol{x}_{m} - \boldsymbol{u}_{e}) + k_{p} \boldsymbol{x}_{e}^{\mathrm{T}} (\boldsymbol{x}_{m} - l_{c} \boldsymbol{x}_{e}) 
+ \boldsymbol{u}_{e}^{\mathrm{T}} (-l_{2} l_{3} \boldsymbol{u}_{e} - l_{4} \lfloor \boldsymbol{u}_{e} \rfloor^{\frac{r_{1}}{r_{2}}}) 
\leq - k_{p} l_{c} ||\boldsymbol{x}_{e}||^{2} - k_{d} ||\boldsymbol{x}_{m}||^{2} - \boldsymbol{x}_{m}^{\mathrm{T}} \boldsymbol{u}_{e} - l_{2} l_{3} ||\boldsymbol{u}_{e}||^{2} 
\leq - k_{p} l_{c} ||\boldsymbol{x}_{e}||^{2} - (k_{d} - 0.5) ||\boldsymbol{x}_{m}||^{2} - (l_{2} l_{3} - 0.5) ||\boldsymbol{u}_{e}||^{2}$$
(11.59)

To this end, using (11.41) in the Property 11.1 and the choice of control gains in (11.50)-(11.51), it leaves (11.59) as

$$\dot{V}_{1} \leq -k_{p}l_{c}||\boldsymbol{x}_{e}||^{2} - (k_{d} - 0.5)||\boldsymbol{x}_{m}||^{2} - (l_{2}l_{3} - 0.5)||\boldsymbol{u}_{e}||^{2} 
\leq -k_{p}l_{c}||\boldsymbol{x}_{e}||^{2} - (k_{d} - \frac{1}{2})\frac{\boldsymbol{x}_{m}^{T}\boldsymbol{A}_{0}(\boldsymbol{x})\boldsymbol{x}_{m}}{\kappa_{2}} - (l_{2}l_{3} - \frac{1}{2})||\boldsymbol{u}_{e}||^{2} 
\leq -\varepsilon V_{1}$$
(11.60)

where  $\epsilon = \min \left\{ 2l_c, \frac{2k_d - 1}{\kappa_2}, l_2 l_3 - \frac{1}{2} \right\} > 0.$ 

Solving (11.60), one has  $V_1(t) \le V_1(0) \exp(-\varepsilon t)$  for any initial states. The estimator-based closed-loop system is, thus, globally exponentially stable. Moreover, using (11.41) in the Property 11.1 and the definition of  $V_1$  in (11.58), it can be obtained that

$$||x_e|| \le \sqrt{2V_1(0)} \exp(-\frac{\varepsilon t}{2})$$
 (11.61)

$$||\boldsymbol{x}_m|| \le \sqrt{\frac{2V_1(0)}{\kappa_1}} \exp(-\frac{\varepsilon t}{2})$$
 (11.62)

$$||\boldsymbol{u}_{e}|| \le \sqrt{2V_{1}(0)} \exp(-\frac{\varepsilon t}{2}) \tag{11.63}$$

From (11.48), it further has

$$||x_v|| \le ||x_m|| + l_c||x_e|| \le \left(1 + \frac{1}{\sqrt{\kappa_1}}\right) \sqrt{2V_1(0)} \exp(-\frac{\varepsilon t}{2})$$
 (11.64)

Hence, it can be concluded from Definition 2.1 that the trajectory tracking error  $x_e$ , the velocity tracking error  $x_e$ , and the estimation error  $u_e$  are globally exponentially

stable. The desired trajectory  $x_d$  can be tracked with high accuracy and with a globally exponential rate of convergence.

**Theorem 11.6** The total uncertainty  $\mathbf{u}_d$  can not only be precisely estimated by the estimator (11.46) with the estimation error  $\mathbf{u}_d$  exponentially stabilized, but the estimation error  $\mathbf{u}_e$  will also be stabilized to zero in a period of finite time. That is, the estimation error can be finite-time stable.

**Proof** For the dynamics of the observer error given in (11.54), choose a positive-definite Lyapunov function candidate as  $V_2(t) = \frac{1}{2} \tilde{\psi}_e^T \tilde{\psi}_e$ , it can come to get from (11.54) that

$$\dot{V}_{2}(t) = \tilde{\boldsymbol{\psi}}_{e}^{\mathrm{T}}(-l_{2}l_{3}\tilde{\boldsymbol{\psi}}_{e} - l_{4}\lfloor\tilde{\boldsymbol{\psi}}_{e}\rfloor^{\frac{\gamma_{1}}{\gamma_{2}}}) \le -2l_{2}l_{3}V_{2} - 2^{\frac{\gamma_{1}+\gamma_{2}}{2\gamma_{2}}}l_{4}V_{2}^{\frac{\gamma_{1}+\gamma_{2}}{2\gamma_{2}}}$$
(11.65)

where the inequality  $\tilde{\boldsymbol{\psi}}_{e}^{\mathrm{T}} \lfloor \tilde{\boldsymbol{\psi}}_{e} \rfloor^{\frac{\gamma_{1}}{\gamma_{2}}} \geq ||\tilde{\boldsymbol{\psi}}_{e}||^{\frac{\gamma_{1}+\gamma_{2}}{\gamma_{2}}}$  is used.

Because  $\gamma_1$  and  $\gamma_2$  are two positive odd integers and are chosen to satisfy  $\gamma_1 < \gamma_2$ , one has  $0 < \frac{\gamma_1 + \gamma_2}{2\gamma_2} < 1$ . As a result, the following can be obtained from the definition of  $V_2(t)$  by solving (11.65)

$$V_2(t) \equiv 0, \, \tilde{\boldsymbol{\psi}}_e(t) \equiv \mathbf{0}, \, t \ge t_f \tag{11.66}$$

where the positive constant  $t_f \in \mathbb{R}_+$  is bounded by

$$t_f \le \frac{\gamma_2}{l_2 l_3 (\gamma_2 - \gamma_1)} \ln \left( \frac{l_2 l_3 ||\tilde{\boldsymbol{\psi}}_e(0)||^{\frac{\gamma_2 - \gamma_1}{\gamma_2}}}{l_4} + 1 \right)$$
 (11.67)

At meaning time, from (11.53) and (11.66), it is ready to get that

$$\boldsymbol{u}_e(t) \equiv \boldsymbol{0}, t \ge t_f \tag{11.68}$$

This can lead to the conclusion that the estimation error of  $u_d$  is finite-time stable [12]. The proposed estimator (11.46) is able to estimate the total uncertainty  $u_d$  with finite-time convergence. This thereby completes the proof.

It can be inferred from the proof of Theorem 11.5 that the entire controller–estimator system is globally exponentially stabilized. The tracking error is globally exponentially stable even if the system is under the effect of uncertainty and external disturbance rather than asymptotically stable [13–15] or ultimately uniformly bounded stable [16]. Consequently, the desired trajectory can be followed without any overshoot. This superior tracking performance is greatly friendly and desirable for the practical application of the proposed tracking control framework.

## 11.3.4 Rigid-Flexible Coupling Satellite Example

The effectiveness of the developed control framework will be validated in this section by applying it to a rigid-flexible satellite example. Figure 11.15 shows the mechanical diagram of this exampled satellite. It has a central rigid body with radius b and a uniform cantilever as its flexible appendage, while the length and the tip mass of the appendage are l and  $m_p$ , respectively. This type of satellite is widely launched in aerospace to accomplish missions such as communication and remote sensing, etc. Constantly, payload such as camera is fixed in the central hub, while flexible appendage such as solar arrays and antennas can be modeled as the uniform cantilever. In Fig. 11.15, the central body will rotate around the rigid point O. The cantilever beam with sectional area a, elastic modulus E, and volume density  $\rho$ , is fixed to the point  $O_B$  on the surface of the central rigid body. The coordinates applied to establish the attitude of the satellite are the inertial frame  $\mathcal{F}_I(X_I, Y_I, Z_I)$  and the floating frame  $\mathcal{F}_B(X_B, Y_B, Z_B)$ .

It is well known that the complicated dynamics of satellites coupled with large flexible appendages may best be modeled using the finite element (FE) method. Therefore, the FE model will be used to describe the flexible vibration of the rigid-coupling satellite. On the other hand, the deformation and the strain are both assumed to be minor. As a result, it can neglect small axial tension and high-order nonlinear terms. To this end, applying the first-order approximation technique and FE model, the mathematical model of this rigid-flexible satellite's attitude system can be established as follows, while the physical parameter values considered here are with all units SI.

$$(J_{mb} - \boldsymbol{p}^{\mathrm{T}}\boldsymbol{G}\boldsymbol{p})\ddot{\boldsymbol{\theta}} - \boldsymbol{U}\boldsymbol{M}_{p}^{-1}\boldsymbol{C}_{f}\dot{\boldsymbol{p}} - \boldsymbol{U}\boldsymbol{M}_{p}^{-1}(\boldsymbol{K}_{f} + \dot{\boldsymbol{\theta}}^{2}\boldsymbol{G})\boldsymbol{p} - 2\dot{\boldsymbol{\theta}}\boldsymbol{p}^{\mathrm{T}}\boldsymbol{G}\dot{\boldsymbol{p}} = T_{c} + T_{d}$$
(11.69)

$$\dot{\eta} + M_p^{-1} C_f \dot{p} + M_p^{-1} (K_f + \dot{\theta}^2 G) p = 0$$
 (11.70)

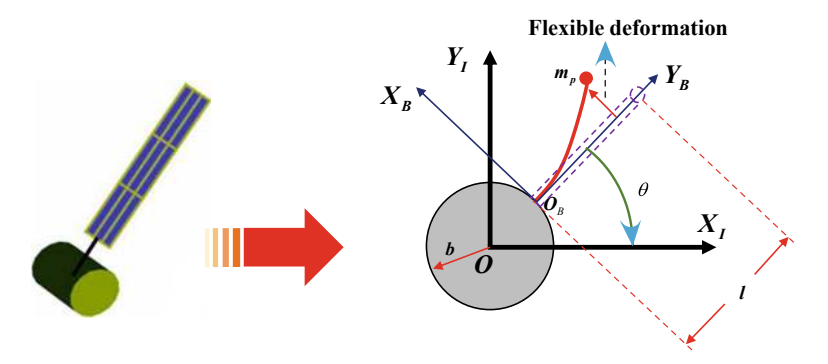


Fig. 11.15 The mechanical structure of the rigid-coupling satellite

with  $J_{mb} = J_h + J_f + J_t - UM_p^{-1}U^T > 0$ ,  $G^T = G = D - M_p$ , and  $\dot{\eta} = \dot{p} + M_p^{-1}U^T\dot{\theta}$ . The Euler angle  $\theta \in \mathbb{R}$  denotes the satellite attitude,  $T_c \in \mathbb{R}$  is the control torque,  $T_d \in \mathbb{R}$  is the disturbance torque,  $p \in \mathbb{R}^{2N}$  is the nodal displacement coordinate vector (but unknown) of the beam with N being the number of nodes when the FE method is adopted;  $J_h \in \mathbb{R}$ ,  $J_f \in \mathbb{R}$ , and  $J_t \in \mathbb{R}$  are the inertia of the central rigid body, the cantilever beam, and the tip mass, respectively.  $U \in \mathbb{R}^{2N}$  is the rigid-flexible coupling coefficients vector. The symmetric positive-definite matrices  $M_p \in \mathbb{R}^{2N \times 2N}$  and  $K_f \in \mathbb{R}^{2N \times 2N}$  are the mass matrix and the stiffness matrix of the flexible cantilever team, respectively.  $C_f \in \mathbb{R}^{2N \times 2N}$  and the symmetric positive-definite matrix  $D \in \mathbb{R}^{2N \times 2N}$  are the structural damping and the dynamic stiffness matrix of the flexible cantilever beam, respectively.  $\eta \in \mathbb{R}^{2N}$  is the modal coordinate vector relative to the rigid body. It can be seen in (11.69) that the dynamic stiffness term  $\dot{\theta}^2 G$  is added to the system stiffness term and its effect on the model is directly proportional to the square of the angular velocity. Hence, such a coupling effect can not be ignored when this rigid-flexible coupling satellite is going to perform rapid attitude maneuver.

Suppose that the desired attitude trajectory is  $\theta_d \in \mathbb{R}$  and the desired angular velocity trajectory is  $\dot{\theta}_d \in \mathbb{R}$ , the tracking control problem of this rigid-flexible coupling satellite can be formulated as: design a control law for  $T_c$  to guarantee that  $\theta_d \in \mathbb{R}$  and  $\dot{\theta}_d \in \mathbb{R}$  can be followed by  $\theta$  and  $\dot{\theta}$ , respectively. To this end, the attitude dynamics (11.69) can be written in the form of (11.1) by denoting  $\mathbf{x} = \theta$ ,  $A_0(\mathbf{x}) = J_{mb}$ ,  $\mathbf{u} = T_c$ ,  $\mathbf{d} = T_d$ ,  $\mathbf{f}_0(\mathbf{x}, \dot{\mathbf{x}}) = 0$ ,  $\mathbf{g}_0(\mathbf{x}) = 0$ , and

$$\Delta h(x, \dot{x}, \ddot{x}) = -\mathbf{p}^{\mathrm{T}} \mathbf{G} \mathbf{p} \dot{\theta} - \mathbf{U} \mathbf{M}_{p}^{-1} \mathbf{C}_{f} \dot{\mathbf{p}}$$
$$-\mathbf{U} \mathbf{M}_{p}^{-1} (\mathbf{K}_{f} + \dot{\theta}^{2} \mathbf{G}) \mathbf{p} - 2 \dot{\theta} \mathbf{p}^{\mathrm{T}} \mathbf{G} \dot{\mathbf{p}}$$
(11.71)

Consequently, the proposed control framework can be applied to perform the attitude tracking maneuver for this considered rigid-flexible satellite.

#### A Simulation Results

The effectiveness and the super tracking control performance of the presented control framework will be verified by conducting numerical simulation on a currently being developed rigid-flexible coupling satellite with its physical parameters given by:  $a = 6.5 \times 10^{-5} \,\mathrm{m}^2$ , b = 1,  $l = 20 \,\mathrm{m}$ ,  $m_p = 0.3 \,\mathrm{kg}$ ,  $J_h = 100 \,\mathrm{kg} \cdot \mathrm{m}^2$ ,  $J_t = 123 \,\mathrm{kg} \cdot \mathrm{m}^2$ ,  $J_f = 615.3 \,\mathrm{kg} \cdot \mathrm{m}^2$  and N = 30. The disturbance torque acting on the satellite is numerically assumed to be as

$$T_d = 0.2(5 + 4\sin(t) - \cos(0.4t + 2\dot{\theta}\sin(0.1t))) \,\text{N} \cdot \text{m}$$
 (11.72)

To guarantee that the payload fixed in the main body of the satellite such as the camera has appropriate attitude to accomplish the planned on-orbital missions successfully, the desired attitude trajectory should be established/planned as

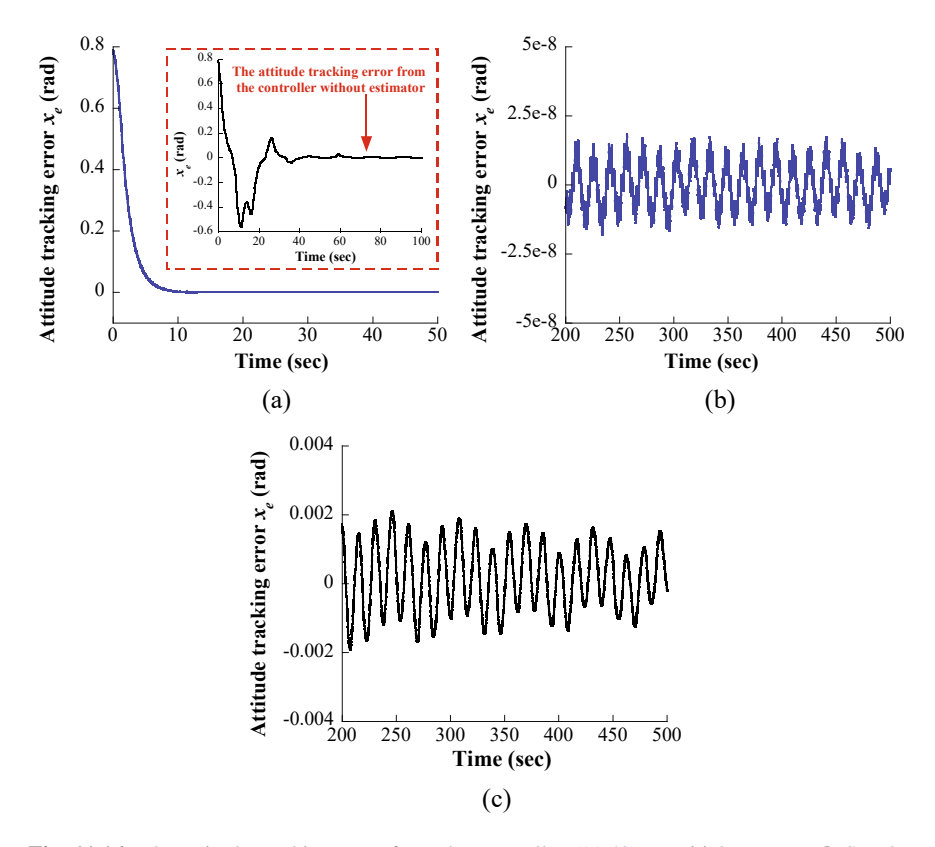


Fig. 11.16 The attitude tracking error from the controller (11.49). a Initial response. b Steady-state behavior obtained from the controller. c Steady-state behavior from the controller without the estimator

$$\theta_d = 0.3\cos\left(0.1t + \frac{\pi}{4}\right) \text{ rad} \tag{11.73}$$

When implementing the proposed control framework to the satellite attitude system, the gains of the controller (11.49) are chosen as  $l_c=160$ ,  $k_p=35$ , and  $k_d=75$ ; while the gains of the incorporated estimator (11.46) are selected as  $\ell_1=0.005$ ,  $\ell_2=7.5$ ,  $\ell_3=75$ ,  $\ell_4=145$ ,  $\ell_5=0.05$ ,  $\gamma_1=99$ , and  $\gamma_2=101$ . When performing the planned attitude tracking maneuver, the initial attitude angle and the initial angular velocity are  $\theta(0)=1$  rad and  $\dot{\theta}(0)=-0.1$  rad/s. The initial nodal displacement of the flexible cantilever beam is  $\boldsymbol{p}(0)=\boldsymbol{0}$  with  $\dot{\boldsymbol{p}}(0)=\boldsymbol{0}$ .

The attitude tracking result obtained from the proposed control is shown in Figs. 11.16 and 11.17. It can be got from Fig. 11.16a, b to know that the desired attitude trajectory is perfectly followed with the attitude pointing accuracy  $|x_e| \le 2.5 \times 10^{-8}$  rad guaranteed. The tracking error of the angular velocity can be seen in Fig. 11.17. It shows in Fig. 11.17b that the resulting attitude stability is  $|x_v| \le 2.5 \times 10^{-8}$  rad/s.

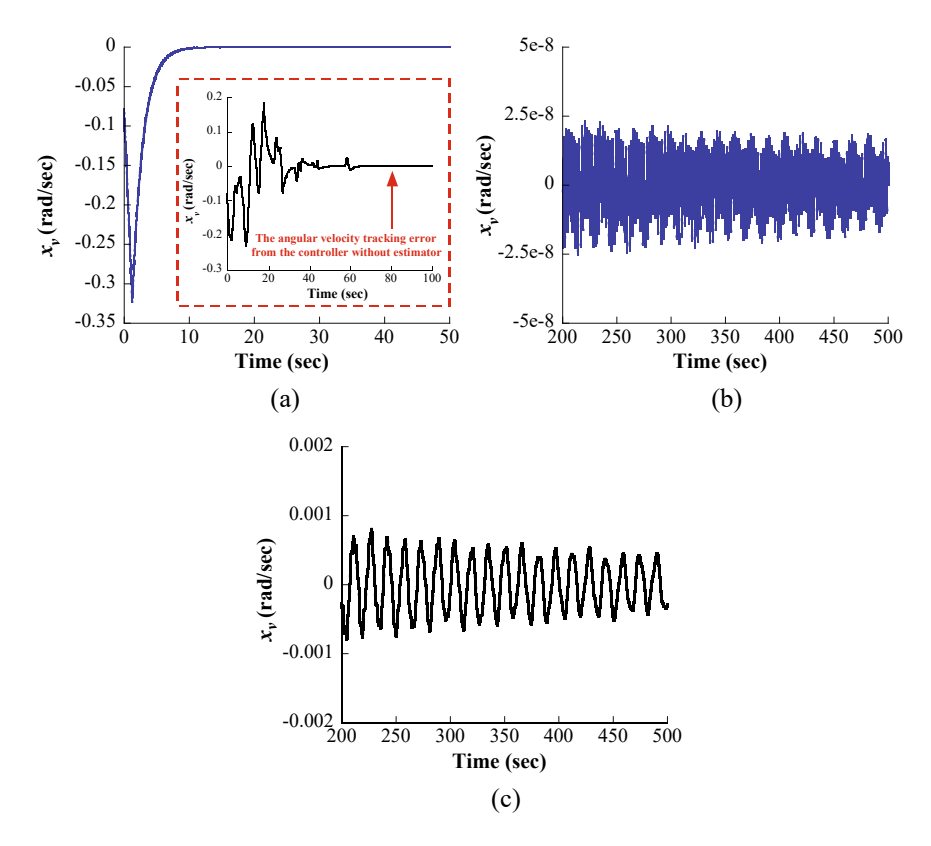


Fig. 11.17 The angular velocity tracking error from the controller (11.49). a Initial response. b Steady-state behavior obtained from the controller. c Steady-state behavior from the controller without the estimator

The pointing-accuracy and attitude stability are so significantly high that perfect attitude and angular velocity can be established for the satellite. These two can guarantee the satellite's payloads to successfully accomplish the planned missions. On the other hand, as the initial response of the attitude and the angular velocity tracking error shown in Figs. 11.16a and 11.17b, respectively, they both are with an exponential convergence. The planned attitude tracking mission is accomplished without any overshoot. It can be further found by zooming the attitude tracking error in Fig. 11.16a that, a steady-state behavior is guaranteed for the attitude tracking error after 30 s. This settling time is quite short, and hence a fast attitude tracking maneuver can be ensured. These results completely verify the conclusions in Theorem 11.6.

It should be pointed out that, the above perfect attitude tracking performance is owing to the incorporated estimator (11.46). When the proposed controller (11.49) without the estimator (11.46) is implemented to the rigid-flexible coupling satellite, the resulting tracking error can be seen in Figs. 11.16 and 11.17. It can be obtained from Fig. 11.16a and 11.17a that severe overshoot is observed. Moreover, the attitude

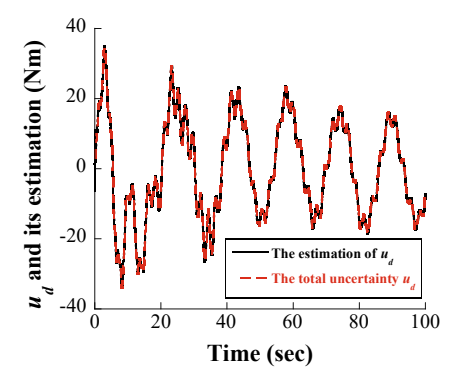
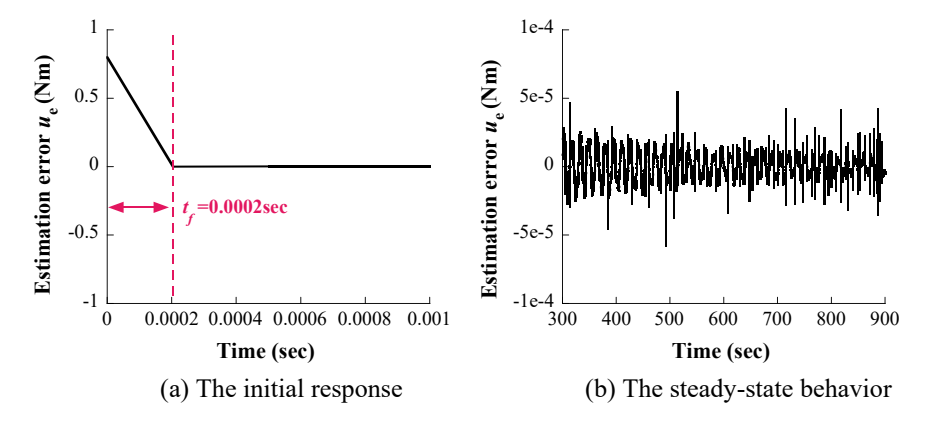


Fig. 11.18 The uncertainty estimation from the estimator (11.46)



**Fig. 11.19** The estimation error from the estimator (11.46)

pointing accuracy  $|x_e| \le 0.002$  rad and attitude stability  $|x_v| \le 0.001$  rad/s can be obtained, as we can see in Figs. 11.16c and 11.17c, respectively. These two are quite inferior. The stringent requirements of attitude pointing accuracy and attitude stability to guarantee the normal operation of the satellite's payload can not be satisfied. Hence, the planned aerospace missions would not be accomplished.

These results obtained from the controller (11.49) with the estimator (11.46) eliminated, reflect the importance of the incorporated estimator (11.46). Actually, this estimator is an important part of the proposed control framework. With the application of the estimator, the true uncertainty can be estimated. Then, the uncertainty and the external disturbance can be compensated by the term  $-\hat{u}_d$  in the controller (11.49), and hence good tracking performance is achieved. In this simulation, the total uncertainty including external disturbance and its estimation are shown in Fig. 11.18. Perfect estimation is observed. In Fig. 11.19, one can also go to its initial response to find out that the estimation error will be with a steady behavior after a short period, roughly  $t_f = 0.0002$  s; moreover, the estimation error

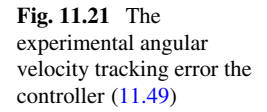
is  $|u_e| \le 6.0 \times 10^{-5} \text{ N} \cdot \text{m}$ . The conclusions in Theorem 11.6 can be demonstrated by these simulation results.

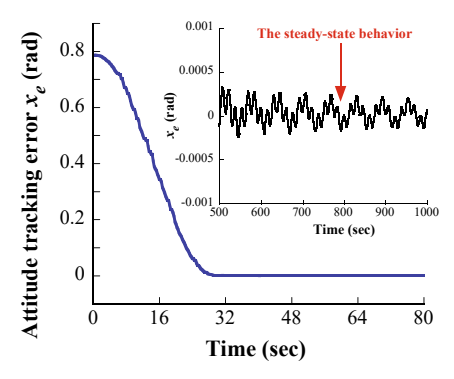
#### **B** Experimental Results

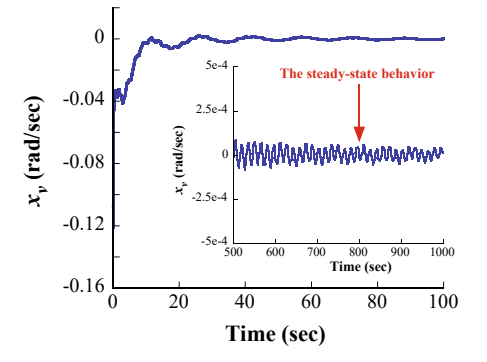
In addition to numerical simulation, any control approach to be applied in practice should be experimentally tested. Hence, experiments will be further carried out in this part to test the effectiveness of the developed tracking control framework. The tests will be conducted on a single-axis air-bearing suspending rotary testbed. This testbed is shown in Fig. 2.5. Compared Fig. 2.5 with Fig. 11.15, it is known that this testbed can exactly simulate the attitude motion of Euler attitude angle  $\theta$  rotation.

With the application of the proposed control framework to the testbed to perform the preceding planned tracking mission, the attitude tracking results are illustrated in Figs. 11.20 and 11.21. The corresponding control torque is shown in Fig. 11.22. It can be seen in Fig. 11.20 that the attitude tracking maneuver is successfully accomplished after 32 s. As shown by the steady-state behavior, the attitude pointing accuracy is guaranteed to be within 0.0005 rad. It can also been in Fig. 11.22 that the angular velocity tracking error is less than 0.00025 rad/s, i.e., the attitude stability is 0.00025 rad/s. The high attitude pointing accuracy and the high attitude stability are feasible

**Fig. 11.20** The experimental attitude tracking error from the controller (11.49)

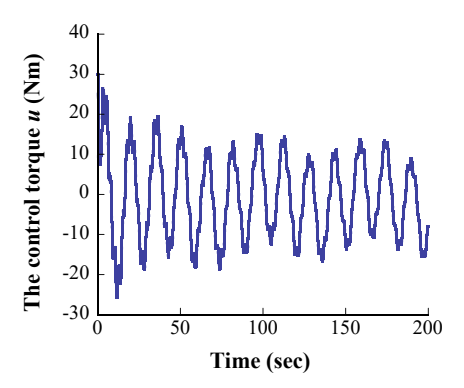






11.4 Summary 263

**Fig. 11.22** The input of the controller (11.49) in the experimental test



and perfect for the fixed payloads to perform the planned orbital missions. Moreover, it can be seen in Figs. 11.20 and 11.21 that an exponential convergence rate is ensured for both the attitude and the angular velocity tracking error. No overshoot is achieved by the proposed control framework. To that end, the performance and the effectiveness of the proposed tracking control framework are experimentally verified.

If the experimental results in Figs. 11.20 and 11.21 are further compared with the simulation results in Figs. 11.16 and 11.17, it is interesting to see that the obtained attitude pointing accuracy between simulation and experimental results is also different. The latter is almost less than the former with three-orders of magnitude. That is due to the fact that the actual actuator, gyro, and controller are used in experiments rather than using an ideal mathematical model in simulation. Moreover, noise is also with the gyro and attitude sensor. Although some differences are observed, it can be seen that the behavior of experimental results matches the behavior of the simulation results well.

From the above simulation and experimental results, it can be summarized and verified that the proposed tracking control framework is able to achieve high-accuracy tracking control with exponential convergence.

## 11.4 Summary

Although there exist several approaches regarding flexible satellite attitude control with accurate pointing, few can achieve fixed-time convergence of the system states in the face of actuator uncertainty. This chapter presented an estimation-based strategy for flexible satellite attitude stabilization maneuvering first. In particular, the control law incorporated a fast fixed-time observer for reconstructing the uncertain dynamics, and a robust fixed-time controller. This was developed via a nonsingular terminal sliding mode surface providing a faster converging rate when compared to the existing fixed-time surfaces. Then, an exponential tracking control theoretical framework was established for a general class of nonlinear systems even with modeling error. With

the application of this architecture, the closed-loop trajectory tracking system was guaranteed to be globally exponentially stable. Hence, the undesirable overshoot resulting from the existing tracking controllers can be avoided. The exponential convergence rate can be tuned to be as fast as possible by tuning the control gains. It is hence able to decrease the system settling time. With such obtained desired no overshoot and less settling time control performance, the developed control approach can be practically appealing for engineering. Moreover, the systems investigated are with a general form of mathematical model. It guarantees that the proposed control framework is applicable to a full of physical systems in practice.

#### References

- Gao, Z., Liu, X., Chen, M. Z. Q (2016) Unknown input observer-based robust fault estimation for systems corrupted by partially decoupled disturbances. IEEE Transactions on Industral Electronics 63(4): 2537–2547
- Cong, B. L., Chen, Z., Liu, X. D. (2013) Disturbance observer-based adaptive integral sliding mode control for rigid spacecraft attitude maneuvers. Proceedings of the Institution of Mechanical Engineers, Part G: Journal of Aerospace Engineering 227(10): 1660–1671
- 3. Polyakov, A. (2012) Nonlinear feedback design for fixed-time stabilization of linear control systems. IEEE Transactions on Automatic Control 57(8): 2106–2110
- Álmeida, J., Silvestre, C., Pascoal, A. (2010) Cooperative control of multiple surface vessels in the presence of ocean currents and parametric model uncertainty. International Journal of Robust and Nonlinear Control 20(14): 1549–1565
- 5. Xiao, B., Yin, S., Wu, L. G. (2017) A structure simple controller for satellite attitude tracking maneuver. IEEE Transactions on Industrial Electronics 64(2): 1436–1446
- Chen, W. H., Yang, J., Guo, L., Li, S. (2016) Disturbance-observer-based control and related methods—An overview. IEEE Transactions on Industrial Electronics 63(2): 1083–1095
- Chen, C. C., Xu, S. S. D., Liang, Y. W. (2015) Study of nonlinear integral sliding mode fault-tolerant control. IEEE/ASME Transactions on Mechatronics 21(2): 1160–1168
- 8. Levant, A. (2003) Higher-order sliding modes, differentiation and output-feedback control. International Journal of Control 76(9-10): 924–941
- Huang, Y., Jia, Y. (2018b) Robust adaptive fixed-time tracking control of 6-DOF spacecraft fly-around mission for noncooperative target. International Journal of Robust and Nonlinear Control 28(6): 2598–2618
- Huang, Y., Jia, Y. (2017) Fixed-time consensus tracking control for second-order multi-agent systems with bounded input uncertainties via NFFTSM. IET Control Theory & Applications 11(16): 2900–2909
- Xiao, B., Yin, S., Kaynak, O. (2017) Attitude stabilization control of flexible satellites with high accuracy: An estimator-based approach. IEEE/ASME Transactions on Mechatronics 22(1): 349–358
- 12. Khalil, H. K. (2002) Nonlinear systems. Prentice Hall
- 13. Wang, H. (2013) Task-space synchronization of networked robotic systems with uncertain kinematics and dynamics. IEEE Transactions on Automatic Control 58(12): 3169–3174
- Wang, H. (2017) Adaptive control of robot manipulators with uncertain kinematics and dynamics. IEEE Transactions on Automatic Control 62(2): 948–954
- Liang, X., Wang, H., Liu, Y. H., Chen, W., Hu, G., Zhao, J. (2016) Adaptive task-space cooperative tracking control of networked robotic manipulators without task-space velocity measurements. IEEE Transactions on Cybernetics 46(10): 2386–2398
- Cheng, L., Hou, Z. G., Tan, M. (2009) Adaptive neural network tracking control for manipulators with uncertain kinematics, dynamics and actuator model. Automatica 45(10): 2312–2318

# Chapter 12 Conclusion



#### 12.1 Conclusion

This book mainly investigated the attitude control problem of satellites with modeling error. To achieve this objective, motivated by the superior performance ensured by the nonlinear control theory, several advanced nonlinear compensation error approaches were developed for the satellite with its attitude controller having high performance even in the presence of other physical constraints. Those approaches were categorized into three types and presented in Part II, Part III, and Part IV, respectively. The first type was the robust compensation attitude control methods in Part II. They compensated for the modeling error in the sense that the attitude control performance has great robustness to the modeling error by tunning control gains. The second type was the adaptive compensation attitude control strategies in Part III. They adaptively estimated the severe case (i.e., the upper bound) of the modeling error and then adaptively compensated for them. The third type was the observer-based compensation attitude control approaches in Part IV. For those approaches, observers were designed first to estimate or reconstruct the modeling error, and then the attitude controllers were synthesized by using the estimation value to achieve attitude control. In general, the approaches in this book eliminated the drawbacks of most of the existing compensation control schemes. The detailed features and advantages of those developed compensation-based attitude control approaches were highlighted as follows.

The robust compensation attitude control approaches were developed in Chaps. 3–5. More specifically, an observer-free controller was presented in Chap. 3 to achieve large-angle attitude tracking with modeling error induced by external disturbance. The controller features a simpler control structure and much less computational complexity. Two robust attitude controllers were developed in Chap. 4 for attitude tracking and stabilization maneuvering of satellites with actuator constraints. The modeling error consisting of actuator fault and external disturbance was further compensated in Chap. 5 even in the presence of actuator faults and angular velocity measurement uncertainty. The controllers in Chaps. 3–5 do not require angular

266 12 Conclusion

velocity measurements. They can achieve higher control performance for attitude maneuvering by tunning their control gains.

The adaptive compensation attitude control methods were designed in Chaps. 6–8. The modeling error compensation control problem of a class of nonlinear systems with multiple actuator faults was addressed in Chap. 6. An adaptive controller was synthesized by using the output measurement only. This controller was applicable to stabilize the satellite's attitude with high performance via the attitude feedback only. The fast attitude slewing control problem of flexible satellites with modeling error due to external disturbance and uncertain inertia was solved in Chap. 7. This was achieved by presenting an adaptive sliding mode-based fixed-time controller. The closed-loop attitude control system was governed to be fixed-time stable with a faster convergence rate than the existing fixed-time controllers. The attitude stabilization control problem of satellite with actuator fault, external disturbance, and performance constraint was solved via a reinforcement learning-based fixed-time optimal control framework in Chap. 8. The closed-loop attitude system was stabilized within a fixed time. The control cost was also significantly reduced. Moreover, the persistent excitation condition that should be met in the conventional neural network weight updating laws was eliminated.

The observer-based compensation attitude control methods were designed in Chaps. 9–11. The extended-state observer-based attitude controller presented in Chap. 9 can provide asymptotical attitude control for flexible satellites with modeling error consisting of external disturbance and unknown flexible vibration precisely compensated. Two disturbance observer-based exponential attitude controllers developed in Chap. 10 were able to perform attitude stabilization and tracking maneuvers with the desired control accuracy ensured with an exponential rate. Four types of modeling error, i.e., the external disturbance, the actuator faults, the actuator misalignment, and the uncertain inertia were fully compensated. This problem was further studied in Chap. 11 by presenting an unknown-input observer-based control architecture. The fixed-time and the finite-time attitude control were achieved, respectively. Fast attitude maneuvering can be accomplished. The common feature of the controllers in Chaps. 9–11 was that they accommodated the modeling error with the modeling error completely and exactly compensated. They have no conservativeness with the energy saved during the attitude maneuvering.

All the controllers presented in this book have a certain capability of solving the challenges stated in Sect. 1.11. Unlike most of the existing attitude control methods that have capability of accommodating modeling error, two or even more than two types of modeling error can be compensated for satellite attitude control system with actuator constraint or without angular velocity measurement. Moreover, a stringent of requirements on the attitude control performance such as high pointing accuracy, better attitude stability, and fast convergence rate are met by the proposed controllers in this book. Another feature of this book was that the effectiveness of all the controllers in this book was numerically verified. In addition, some control approaches in the book were even experimentally validated. This moves a step further toward application in satellite attitude control practice.

12.2 Future Work 267

#### 12.2 Future Work

When applying the compensation control approaches in this book to satellite attitude control engineering, the following issues should be addressed further. They are also the future work to be carried out.

- The fast, the finite-time, or the fixed-time attitude control and the actuator constraint should be solved simultaneously. This may be theoretically achieved by improving the controllers in Chaps. 6–8. On the other hand, this can also be addressed by inventing new actuators that have large control torque.
- Although the observer-based compensation controllers in Chaps. 9–11 have no
  conservativeness. Their implementation necessitates angular velocity measurements. This lets them be inappropriate for the microsatellite attitude control. That
  is because sometimes the angular velocity of microsatellite may not be available.
  Hence, observer-based velocity-free compensation attitude control should be conducted in the future.
- Only the attitude controller design problem of the satellite attitude system was investigated in this book. It is known that the satellite attitude system design does not contain the controller design only. The attitude determination and the desired attitude planning are also involved. Those two works are also quite important. Therefore, those two works should be done future.
- Satellite and especially microsatellite swarm flying is becoming a new space system architecture for future complicated tasks. That is because more and more space tasks would not be carried out by using a single satellite. Hence, the extension of the compensation controllers in this book to achieve attitude coordination control of the satellite swarm is another future work.